IJACSA
WHERE WISDOM SHARES
International Journal of Advanced Computer Science and Applications

Volume 4 Issue 3

March 2013

ISSN 2156-5570(Online)
ISSN 2158-107X(Print)

SAI

www.ijacsa.thesai.org

INTERNATIONAL JOURNAL OF ADVANCED COMPUTER SCIENCE AND APPLICATIONS

THE SCIENCE AND INFORMATION ORGANIZATION

www.thesai.org | info@thesai.org

Editorial Preface

From the Desk of Managing Editor…

It is our pleasure to present to you the March 2013 Issue of International Journal of Advanced Computer Science and Applications.

Today, it is incredible to consider that in 1969 men landed on the moon using a computer with a 32-kilobyte memory that was only programmable by the use of punch cards. In 1973, Astronaut Alan Shepherd participated in the first computer "hack" while orbiting the moon in his landing vehicle, as two programmers back on Earth attempted to "hack" into the duplicate computer, to find a way for Shepherd to convince his computer that a catastrophe requiring a mission abort was not happening; the successful hack took 45 minutes to accomplish, and Shepherd went on to hit his golf ball on the moon. Today, the average computer sitting on the desk of a suburban home office has more computing power than the entire U.S. space program that put humans on another world!!

Computer science has affected the human condition in many radical ways. Throughout its history, its developers have striven to make calculation and computation easier, as well as to offer new means by which the other sciences can be advanced. Modern massively-paralleled super-computers help scientists with previously unfeasible problems such as fluid dynamics, complex function convergence, finite element analysis and real-time weather dynamics.

At IJACSA we believe in spreading the subject knowledge with effectiveness in all classes of audience. Nevertheless, the promise of increased engagement requires that we consider how this might be accomplished, delivering up-to-date and authoritative coverage of advanced computer science and applications.

Throughout our archives, new ideas and technologies have been welcomed, carefully critiqued, and discarded or accepted by qualified reviewers and associate editors. Our efforts to improve the quality of the articles published and expand their reach to the interested audience will continue, and these efforts will require critical minds and careful consideration to assess the quality, relevance, and readability of individual articles.

To summarise, the journal has offered its readership thought provoking theoretical, philosophical, and empirical ideas from some of the finest minds worldwide. We thank all our readers for their continued support and goodwill for IJACSA. We will keep you posted on updates about the new programmes launched in collaboration.

Lastly, we would like to express our gratitude to all authors, whose research results have been published in our journal, as well as our referees for their in-depth evaluations.

We hope that materials contained in this volume will satisfy your expectations and entice you to submit your own contributions in upcoming issues of IJACSA

Thank you for Sharing Wisdom!

Managing Editor
IJACSA
Volume 4 Issue 3 March 2013
ISSN 2156-5570 (Online)
ISSN 2158-107X (Print)

Associate Editors

Reviewer Board Members

- **A Kathirvel**
  Karpaga Vinayaka College of Engineering and Technology, India
- **A.V. Senthil Kumar**
  Hindusthan College of Arts and Science
- **Abbas Karimi**
  I.A.U_Arak Branch (Faculty Member) & Universiti Putra Malaysia
- **Abdel-Hameed A. Badawy**
  University of Maryland
- **Abdul Wahid**
  Gautam Buddha University
- **Abdul Hannan**
  Vivekanand College
- **Abdul Khader Jilani Saudagar**
  Al-Imam Muhammad Ibn Saud Islamic University
- **Abdur Rashid Khan**
  Gomal Unversity
- **Aderemi A. Atayero**
  Covenant University
- **Ahmed Boutejdar**
- **Dr. Ahmed Nabih Zaki Rashed**
  Menoufia University, Egypt
- **Ajantha Herath**
  University of Fiji
- **Ahmed Sabah AL-Jumaili**
  Ahlia University
- **Akbar Hossain**
- **Albert Alexander**
  Kongu Engineering College,India
- **Prof. Alcinia Zita Sampaio**
  Technical University of Lisbon
- **Amit Verma**
  Rayat & Bahra Engineering College, India
- **Ammar Mohammed Ammar**
  Department of Computer Science, University of Koblenz-Landau
- **Anand Nayyar**
  KCL Institute of Management and Technology, Jalandhar
- **Anirban Sarkar**
  National Institute of Technology, Durgapur, India
- **Arash Habibi Lashakri**
  University Technology Malaysia (UTM), Malaysia
- **Aris Skander**
  Constantine University
- **Ashraf Mohammed Iqbal**
  Dalhousie University and Capital Health
- **Asoke Nath**
  St. Xaviers College, India
- **Aung Kyaw Oo**
  Defence Services Academy
- **B R SARATH KUMAR**
  Lenora College of Engineering, India
- **Babatunde Opeoluwa Akinkunmi**
  University of Ibadan
- **Badre Bossoufi**
  University of Liege
- **Balakrushna Tripathy**
  VIT University
- **Basil Hamed**
  Islamic University of Gaza
- **Bharat Bhushan Agarwal**
  I.F.T.M.UNIVERSITY
- **Bharti Waman Gawali**
  Department of Computer Science & information
- **Bremananth Ramachandran**
  School of EEE, Nanyang Technological University
- **Brij Gupta**
  University of New Brunswick
- **Dr.C.Suresh Gnana Dhas**
  Park College of Engineering and Technology, India
- **Mr. Chakresh kumar**
  Manav Rachna International University, India
- **Chandra Mouli P.V.S.S.R**
  VIT University, India
- **Chandrashekhar Meshram**
  Chhattisgarh Swami Vivekananda Technical University
- **Chao Wang**
- **Chi-Hua Chen**
  National Chiao-Tung University
- **Constantin POPESCU**
  Department of Mathematics and Computer Science, University of Oradea
- **Prof. D. S. R. Murthy**
  SNIST, India.
- **Dana PETCU**
  West University of Timisoara
- **David Greenhalgh**

CONTENTS

Sensitivity Analysis and Validation of Refractive Index Estimation Method with Ground Based Atmospheric Polarized Radiance Measurement Data

Kohei Arai
Graduate School of Science and Engineering
Saga University
Saga City, Japan

***Abstract*—Sensitivity analysis and validation of the proposed refractive index estimation method with ground based atmospheric polarized radiance measurement data is conducted. Through the sensitivity analysis, it is found that Degree of Polarization: DP is highly dependent upon surface reflectance followed by imaginary and real part of refractive index and Junge parameter. DP at 550nm is greater than that at 870nm slightly. DP is decreased in accordance with increasing of real part and is increased with increasing of imaginary part while DP is increased with increasing of Junge parameter. It is also found that the peak of DP is appeared not only 90 degree of scattering angle but also at around 150 degree, in particular, when aerosol scattering is dominant. By using the aforementioned characteristics, it may be concluded that it is possible to estimate refractive index with ground based polarized radiance measurements**

Keywords—solar irradiance; refractive index; atmospheric polarized radiance

I. INTRODUCTION

The largest uncertainty in estimation of the effects of atmospheric aerosols on climate systems is from uncertainties in the determination of their microphysical properties, including the aerosol complex index of refraction that in turn determines their optical properties. The methods, which allow estimation of refractive indices, have being proposed so far [1]-[3]. Most of the methods use ground based direct, diffuse and aureole measurement data such as AERONET [4] and SKYNET [5]. The methodology for estimation of a complete set of vertically resolved aerosol size distribution and refractive index data, yielding the vertical distribution of aerosol optical properties required for the determination of aerosol-induced radiative flux changes is proposed [6].

The method based on the optical constants determined from the radiative transfer models of the atmosphere is also proposed [7]. Laboratory based refractive indices estimation methods with spectral extinction measurements are proposed [8],[9]. All these existing methods are based on radiance from the sun and the atmosphere. Ground based measuring instruments for solar direct, diffuse and aureole measurements are, in general, heavy and large. The method proposed here is based on the polarized radiance from the sun and the atmosphere that is measured with light and small measuring instrument. The method uses the fact that polarized radiance depends on aerosol refractive index, size distribution, molecule scattering, gaseous transmission, ozone and water vapor absorptions, etc. in the visible to near infrared wavelength region.

Through optical depth measurements with a variety of relatively transparent wavelength, it is possible to estimate size distribution, molecule scattering, gaseous transmission, ozone and water vapor absorptions, etc. so that refractive index might be estimated. In order to assess the estimation accuracy of refractive index with the proposed method, sensitivity analysis is conducted with a variety of parameters of the atmosphere.

The following section deals with the proposed method then Monte Carlo Ray Tracing: MCRT simulation is introduced followed by some experimental results on the sensitivity analysis.

II. PROPOSED METHOD

The method proposed here is based on the polarized radiance from the sun and the atmosphere that is measured with light and small measuring instrument. The method uses the fact that polarized radiance depends on aerosol refractive index, size distribution, molecule scattering, gaseous transmission, ozone and water vapor absorptions, etc. in the visible to near infrared wavelength region. Through optical depth measurements, total optical depth at the certain wavelength is known. Molecule scattering is a function of atmospheric pressure and the measured wavelength so that it is possible to estimate if the atmospheric pressure is measured. Ozone and water vapor absorption can be estimated with measured column ozone and water vapor. That is the same thing for gaseous transmission. Using MODTRAN or the other radiative transfer codes, it is estimated through a curve fitting with the measured optical depth at relatively transparent wavelength. Then aerosol optical depth is estimated.

Aerosol size distribution is also estimated under some assumption such that the distribution is followed with the power of law distribution like Junge distribution. Using measured optical depth, Angstrom exponent is calculated together with Junge parameter is calculated. The rest of atmospheric parameters, real and imaginary parts of refractive index are estimated with the measured p and s polarized

radiances from the atmosphere with the observation angle of perpendicular to the sun as shown in Figure 1.

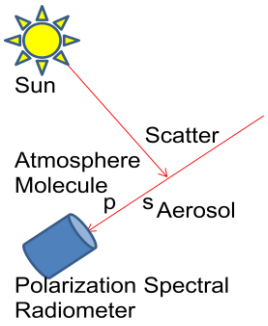

Fig.1. Observation geometry of the proposed aerosol refractive index estimation with ground based polarized spectral radiance measurements.

III. Sensitivity Analysis

Sensitivity on refractive index estimation, S is defined as follows,

$$S = \partial DP / \partial X \quad (1)$$

where DP denotes deviation of degree of polarization and X denotes R: Real part of refractive index, I: imaginary part of refractive index and J: Junge parameter. Monte Carlo simulation with 50km by 50km by 50km of cell is used for sensitivity analysis. 100 million of photons are put into the cell with selected solar azimuth and zenith angles from the top of the atmosphere.

Optical depth of molecule and aerosol are given together with surface reflectance. Wavelength is set at 550 and 870nm as an example. p and s polarization of phase functions for aerosol and molecule are calculated a prior basis. Photon counter with ± 1 degree of aperture is set in the center of the bottom of the simulation cell with the observation angle of perpendicular to the sun. As a default value of real part of refractive index is set at 1.35 as an example, also 0.02 for imaginary part together with 2.6 for the Junge parameter. Real part is varied from 1.25 to 1.45 with 0.025 steps while imaginary part is changed from 0.005 to 0.03 with 0.005 steps together with Junge parameter ranges from 2.6 to 3.6 with 0.2 steps. Meanwhile surface reflectance is changed from 0 to 1 with 0.2 steps.

The irradiance from the atmosphere pointed at perpendicular to the sun is increased in accordance with real part of refractive index. P polarized irradiance is always greater than that of s polarized irradiance. Also the Figure shows the irradiance is increased with increasing of surface reflectance. Meanwhile, the irradiance is decreased in accordance with increasing imaginary part of refractive index. Figure 2 and 3 show irradiance at the wavelength of 870 nm. These trends are same for 550nm that are not shown here, though.

It is true that the p polarized irradiance is always greater than that of the s polarized one. Also the irradiance is decreasing with increasing surface reflectance always. As the matter of fact, high surface reflectance implies that scattering in the atmosphere is likely increased so that the irradiance is increased. It is assumed that the surface is flat and Lambertian so that p polarized irradiance is always greater than that of s polarized one. Also it is true that degree of polarization increases in accordance with imaginary part of refractive index and with Junge parameter while it decreases with increasing of real part of refractive index as is shown in Figure 2.

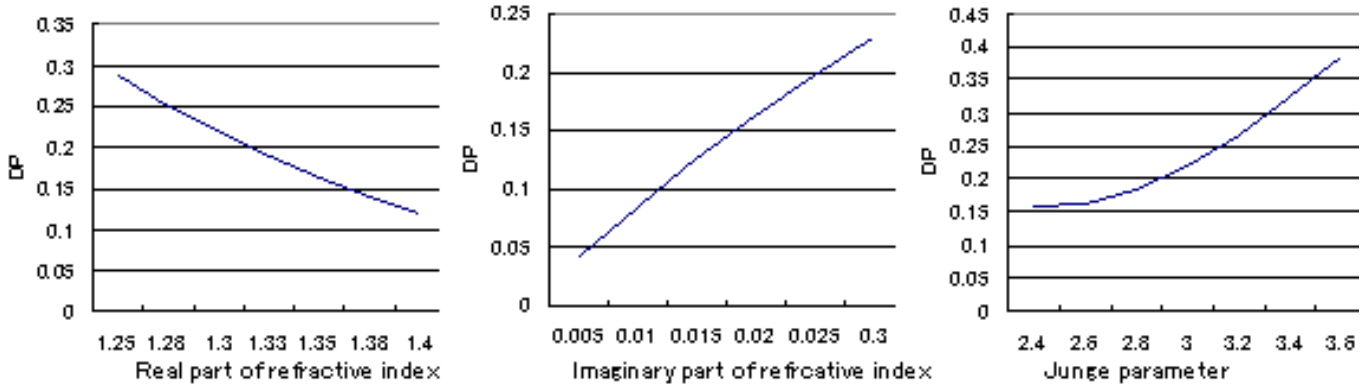

Fig.2. Trends of degree of polarization: DP with real and imaginary parts of refractive index and Junge parameter.

Using these relations, real and imaginary parts of refractive index can be estimated. Sensitivity that is defined with equation (1) then can be calculated. Figure 3 shows the sensitivities for influencing factors.

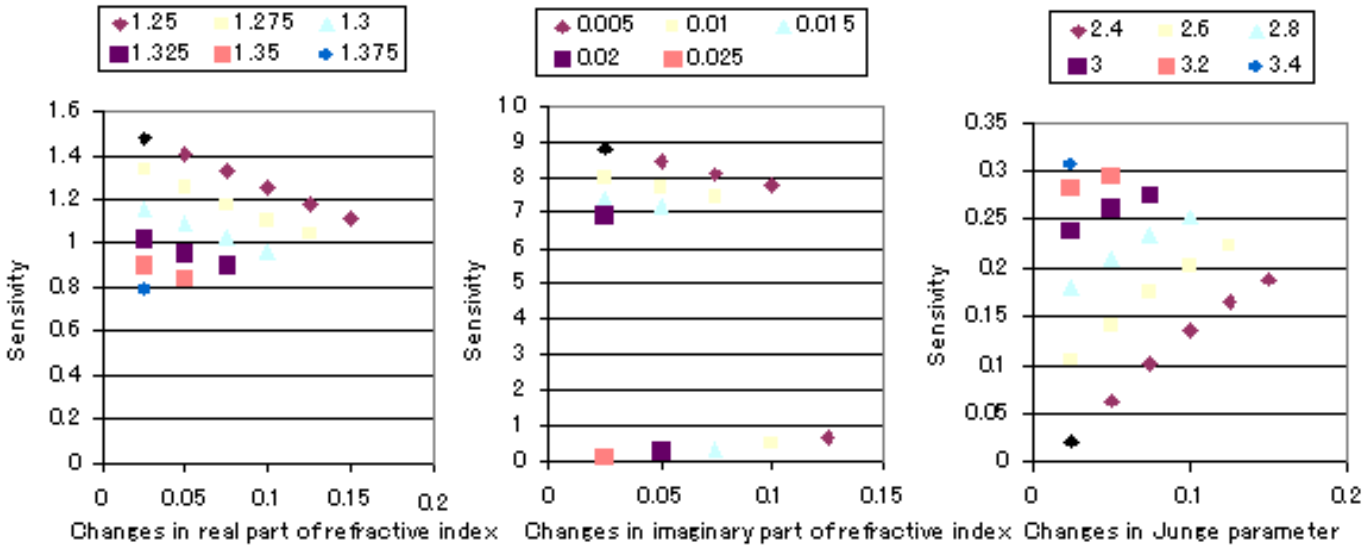

Fig.3. Sensitivity of real and imaginary parts of refractive index and Junge parameter on degree of polarization.

Consequently refractive index can be estimated with ground based polarized irradiance measurement data. This method is applied to the actual data acquired at Saga University at 2:00 GMT on November 26 2003. Measured and estimated parameters are Aerosol optical depth: 0.1191, Molecule optical depth: 0.0152, Surface reflectance: 0.45, Solar zenith angle: 70 degree, Junge parameter: 2.6. Real part of refractive index: 1.35 and Imaginary part of refractive index: 0.02 at wavelength of 870nm. The last three items are estimated based on Skyradpack with skyradiometer, POM-01 manufactured by Prede Co. Ltd. Japan. Major specification and outlook is shown in Table 1 and Figure 4, respectively.

TABLE I. MAJOR SPECIFICATION OF POM-01

Instantaneous Field of View	0.5 Degree
Minimum Scattering Angle	3 Degree
Wavelength	315, 400, 500, 675, 870, 940, 1020nm
Wavelength Selection	Filter Wheel
Detectors	Silicon Photo Diode
Measuring Range	2.5mA, 250uA, 25uA, 250nA, 25nA,2.5nA
Driving System	Pulse Motor Drive
Tracking Mode	Sun Epemeris Calculation Mode, Sun Sensor Mode
Measuring Period	Time, Air-mass
Scan Direction	Horizontal direction, Verical Direction
No. of Scattering Angle	50 in Maximum
Sun sensor	4 Elements Si Sensor
PC Interface	RS-232C
Operable Temperature Range	minus 10Deg.C toplus 45 DegC
Power Consumption	200W
Electricity	100V to 240V(2A)
Weight	23Kg

Fig.4. Outlook of POM-01

The estimated results of real and imaginary parts of refractive index based on the proposed method with measured data of p/s polarized irradiance on the ground show 1.3524 for real part while 0.01931 for imaginary part, respectively. Discrepancy between the actual (derived from skyradiometer data) and the estimated refractive index is 0.1745% for real part and 3.4278% for imaginary part of refractive index.

IV. VALIDATION

The proposed method is also validated through field campaigns. DP measured for field campaigns at Roach Lake (Nevada in U.S.A.) and Coyote Lake (California in U.S.A.) which were conducted on December 3 and 10 2008. The detailed conditions are listed in Table 2.

Phase function of DP can be measured with MS-720 of which polarization filter is attached at the optics entrance [10]. Major specification and outlook of MS-720 manufactured by Eiko Co. Ltd. is shown in Table 3 and Figure 5, respectively.

Table 4,5 shows atmospheric parameters, Otpical Depth of aerosol: Taero, Optical Depth of molecule: Tmol., Surface Reflectance of p polarization: Ref(p), Surface Reflectance of s polarization: Ref(s), Solar Zenith Angle: Sunf, and Junge Parameter: Jp for each test site.

TABLE II. DETAILED CONDITIONS OF TEST SITE

Date and time (UTM)	December 3 2008, 18:38:34	December 10 2008, 18:38:34
Solar azimuth and zenith angles	154.48, 59.84	163.92, 59.61
Location	Roach Lake(38:30:18N,115:41:29W)	Coyote Lake(35:03:53N,116:44:50W)
Air-temperature, atmospheric pressure	22.5, 933hPa	22.1, 974hPa
Junge parameter(370/870, 500/870)	2.73, 3.15	5.89, 7.21
Ozone(DU), Water vapor(g/cm^2)	284.7, 0.24	271.6, 0.46

Fig.5. Outlook of MS-720

TABLE III. MAJOR SPECIFICATION OF MS-720

Wavelength	350 to 1050nm
No. Channels	256 Ch
Wavelength Interval	3.3nm(1nm for 700 channels in PC)
Wavelength Resolution	less than 0.3nm
Half Power Width	10nm
Operable Temperature Range	minus 10 to plus 40DegC
Aparture	10, 25, 45, 180Degree
Strey Light	less than 0.15%
Measureing Time Period	0.005 to 5 sec
No.of Storable Spectral Data	900 of 256 channel data
PC Interface	USB or RS232C
Size	100x160x60
Weight	800g
Electric Poer	1.5V x 4

Figure 6 shows how Roach Lake and Coyote Lake looks like. These field campaigns are conducted under the not so bad weather condition with clear sky (partially clouded conditions as shown in Figure 7 of Terra/ASTER/VNIR images). As shown in Table 3, 4, aerosol particle size of Roach Lake is greater than that of Coyote Lake. Also aerosol optical depth of Roach Lake is greater than that of Coyote Lake.

TABLE IV. ATMOSPHERIC PARAMETERS FOR ROACH LAKE

Wave	*Taero*	*τmol*	*Refp*	*Refs*	*Sunθ*	*Jp*
500nm	0.055	0.1630	0.364	0.354	63	2.75
675nm	0.026	0.0534	0.494	0.442	63	2.75
870nm	0.042	0.0127	0.580	0.549	63	2.75

TABLE V. ATMOSPHERIC PARAMTERS FOR COYOTE LAKE

Wave	*τaero*	*Tmol*	*Refp*	*Refs*	*Sunθ*	*Jp*
500nm	0.033	0.135	0.309	0.249	63	3.14
675nm	0.011	0.0399	0.443	0.368	63	3.14
870nm	0.017	0.0143	0.430	0.309	63	3.14

(a)Roach Lake

(b)Coyote Lake

Fig.6. Test sites for field campaigns

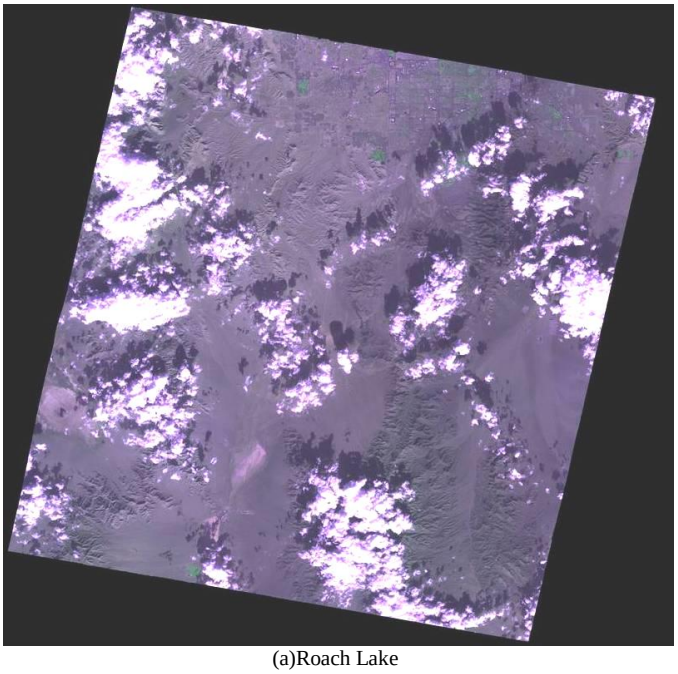

(a)Roach Lake

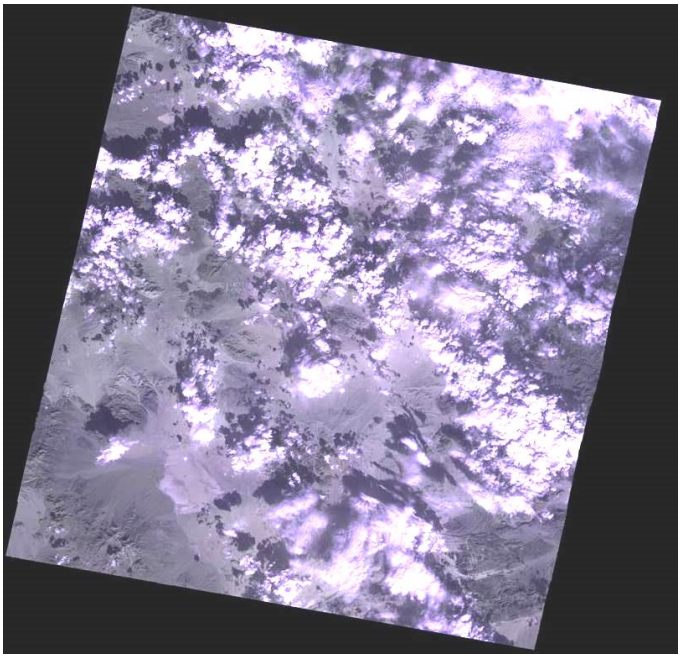

(b)Coyote Lake

Fig.7. Terra/ASTER/VNIR images for the test site

Estimated phase functions of DP with the measured p and s polarized irradiance at the test sites of Roach Lake and Coyote Lake are shown in Figure 8.

Comparison of Junge parameter and refractive index derived from skyradiometer data and DP data are also made. As shown in Table 5, both Skyradiometer derived and the proposed DP measured atmospheric irradiance data derived Junge parameter, real part and imaginary parts of aerosol refractive indices are almost same. Therefore, the proposed method does work as same as skyradiometer based method for aerosol parameter estimations.

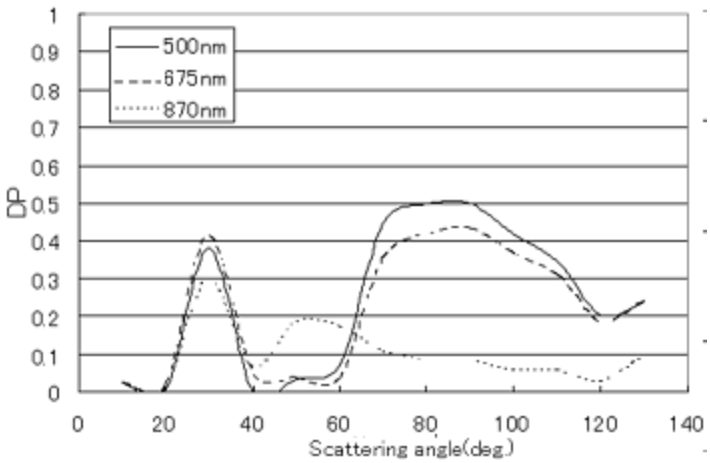

(a) Roach Lake campaign

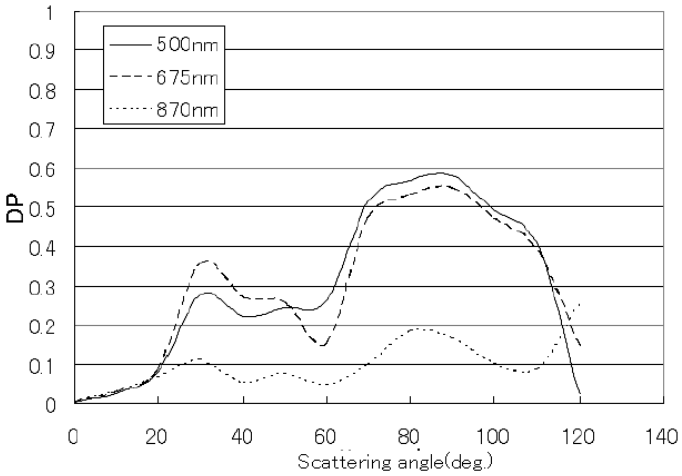

(b) Coyote Lake campaign

Fig.8. Estimated phase functions of DP with the measured p and s polarized irradiance at the test sites of Roach Lake and Coyote Lake

TABLE VI. COMPARISON OF JUNGE PARAMETER AND REFRACTIVE INDEX DERIVED FROM SKYRADIOMETER DATA AND DP DATA

	Method	Junge	Real	Imaginary
08/12/03 Roach	Skyradiometer	3.372	1.582	0.0004
	DP	3.365	1.501	0.0003
08/12/10 Coyote	Skyradiometer	5.213	1.574	0.0068
	DP	5.214	1.541	0.0066

V. CONCLUSION

Through the sensitivity analysis, it is found that Degree of Polarization: DP is highly dependent upon surface reflectance followed by imaginary and real part of refractive index and Junge parameter. DP at 550nm is greater than that at 870nm slightly. DP is decreased in accordance with increasing of real part and is increased with increasing of imaginary part while

DP is increased with increasing of Junge parameter. It is also found that the peak of DP is appeared not only 90 degree of scattering angle but also at around 150 degree, in particular, when aerosol scattering is dominant.

By using the aforementioned characteristics, it may be concluded that it is possible to estimate refractive index with ground based polarized radiance measurements

ACKNOWLEDGMENT

The author would like to thank Ms. Yui Nishimura for her contributions for conducting experiments.

REFERENCES

[1] Shaw, G.E., Error analysis of multi-wavelength sunphotometry. *Pure Appl. Geophys.*, 114, 1, 1976.

[2] Hoppel, W. A., J. W. Fitzgerald, G. M. Frick, R. E. Larson, and E. J. Mack, Aerosol size distributions and optical properties found in the marine boundary layer over the Atlantic Ocean, *J. Geophys. Res.*, 95, 3659-3686, 1990.

[3] Holben, B. N., et al., AERONET- A federated instrument network and data achieve for aerosol characterization, *Remote Sens.*, 12, 1147-1163, 1991.

[4] Holben, B.N., and Coauthors, AERONET-A federated instrument network and data archive for aerosol characterization. *Remote Sens. Environ.*, 66, 1-16. 1998.

[5] Aoki, K., T. Takamura, and T. Nakajima, Aerosol optical properties measured by SKYNET sky radiometer validation network. *Proc. of the 2nd EarthCARE Workshop*, 133-134, 2005.

[6] Redemann, R. P. Turco, K. N. Liou, P. B. Russell, R. W. Bergstrom, B. Schmid, J. M. Livingston, P. V. Hobbs, W. S. Hartley, S. Ismail, R. A. Ferrare, E. V. Browell, Retrieving the vertical structure of the effective aerosol complex index of refraction from a combination of aerosol *in situ* and remote sensing measurements during TARFOX, *J. Geophys. Res.*, 105, D8, 9949–9970, 2000.

[7] M.L.Clapp, and R.E.Miller, Complex Refractive Indices of Crystalline Hydrazine from Aerosol Extinction Spectra, Icarus, 23, 2, 396-403(8), 1996.

[8] R. Eiden, Determination of the complex index of refraction of spherical aerosol particles, *Appl. Opt*. 10, 749-757, 1971.

[9] G. E. Thomas, S. F. Bass, R. G. Grainger, and A. Lambert, Retrieval of aerosol refractive index from extinction spectra with a damped harmonic-oscillator band model, *Appl. Opt*. 44, 1332-1341, 2005.

[10] Kohei Arai, Aerosol refractive index retrievals with atmospheric polarization measuring data, Proceedings of the SPIE, 7461-06, 1-9, 2009

AUTHORS PROFILE

Kohei Arai, He received BS, MS and PhD degrees in 1972, 1974 and 1982, respectively. He was with The Institute for Industrial Science, and Technology of the University of Tokyo from 1974 to 1978 also was with National Space Development Agency of Japan (current JAXA) from 1979 to 1990. During from 1985 to 1987, he was with Canada Centre for Remote Sensing as a Post Doctoral Fellow of National Science and Engineering Research Council of Canada.

He was appointed professor at Department of Information Science, Saga University in 1990. He was appointed councilor for the Aeronautics and Space related to the Technology Committee of the Ministry of Science and Technology during from 1998 to 2000. He was also appointed councilor of Saga University from 2002 and 2003 followed by an executive councilor of the Remote Sensing Society of Japan for 2003 to 2005. He is an adjunct professor of University of Arizona, USA since 1998. He also was appointed vice chairman of the Commission "A" of ICSU/COSPAR in 2008. He wrote 30 books and published 332 journal papers

Vicarious Calibration Based Cross Calibration of Solar Reflective Channels of Radiometers Onboard Remote Sensing Satellite and Evaluation of Cross Calibration Accuracy through Band-to-Band Data Comparisons

Kohei Arai
Graduate School of Science and Engineering
Saga University
Saga City, Japan

***Abstract*—Accuracy evaluation of cross calibration through band-to-band data comparison for visible and near infrared radiometers which onboard earth observation satellites is conducted. The conventional cross calibration for visible to near infrared radiometers onboard earth observation satellites is conducted through comparisons of band-to-band data of which spectral response functions are overlapped mostly. There are the following major error sources due to observation time difference, spectral response function difference in conjunction of surface reflectance and atmospheric optical depth, observation area difference. These error sources are assessed with dataset acquired through ground measurements of surface reflectance and optical depth. Then the accuracy of the conventional cross calibration is evaluated with vicarious calibration data. The results show that cross calibration accuracy can be done more precisely if the influences due to the aforementioned three major error sources are taken into account.**

Keywords—vicarious calibration; cross calibration; visible to near infrared radiometer; earth observation satellite; remote sensing; radiative transfer equation

I. INTRODUCTION

Calibration of solar reflective wavelength coverage of mission instruments onboard remote sensing satellites is research subject for many years [1]-[17]. It is obvious that onboard calibration sources are degraded for time being as Dinguirard and Slater (1999) argued. It cannot be monitored even if onboard monitoring system is used for it because monitoring systems are degraded. Therefore, other calibrations, vicarious and cross calibrations are required. Reflectance based vicarious calibration is not accurate enough for monitoring the degradation. That is same thing for cross calibration.

Usually, the conventional cross calibration can be done through comparisons of band-to-band data of which spectral response functions are overlapped mostly. There are the following major error sources due to observation time difference, spectral response function difference in conjunction of spectral surface reflectance and spectral atmospheric optical depth, observation area difference. These error sources are assessed with dataset acquired through ground measurements of spectral surface reflectance and spectral optical depth. Then the accuracy of the conventional cross calibration is evaluated with vicarious calibration data.

Several researchers investigated cross calibration. Teillet, Fedosejevs, Thome, and Barker (2007) investigated impact of spectral response difference effect between sensors as quantitative indication using simulated data of observation [19]. The effect is called SBDE (Spectral Band Difference Effect) in this research. Twenty sensors were considered in the simulation together with some ground types, various combinations of atmospheric states and illumination geometries. They argued, overall, if spectral band difference effects (SBDEs) are not taken into account, the Railroad Valley Playa site is a 'good 'ground target for cross calibration between most but not all satellite sensors in most but not all spectral regions investigated. 'Good 'is denoted as SBDEs within 3%.

Liu, Li, Qiao, Liu, and Zhang (2004) developed a new method for cross calibration, and then applied the method to sensors Multi-channel Visible Infrared Scanning radiometers (MVIRS) and Moderate Resolution Imaging Spectro-radiometer (MODIS) [18]. They argued,"'An error analysis indicates that the calibration is accurate to within 5%, which is comparable to, or better than, the vicarious calibration method.

The method considers surface bidirectional reflectance distribution function (BRDF) mainly. BRDF indicates distribution of angle of reflection depend on an angle of incidence of illumination on the surface. In these researches, differences of SRF do not be considered. If the impact of its difference can be considered on cross calibration, differences between observed data can be explained more exactly and we can implement cross calibration by higher reliability.

ASTER/VNIR is onboard Terra satellite and is calibrated with onboard calibration sources [20], vicarious calibration data as well as cross calibration. MODIS is onboard same

platform and is calibrated with the aforementioned several types of data [21]. This situation is same thing for MISR [22] and ETM+ onboard the different platform, Landsat-7 [23].

The method proposed here is to check a reliability of the calibration sources through vicarious and cross calibrations for validations of these calibration accuracies. Namely, vicarious calibration requires spectral surface reflectance measurements and spectral optical thickness measurements. By using these ground based acquired data, cross calibration is conducted to improve a reliability of the calibration sources through comparison of vicarious calibration data. The results show that cross calibration accuracy can be done much more precisely if the influences due to the aforementioned three major error sources are taken into account.

The following section describes the proposed cross calibration method together with research background followed by some experiments. Then conclusion is described together with some discussions.

II. Proposed Cross Calibration Method

A. Research Background

The proposed cross calibration method is based on improvement of reliability of calibration accuracy through cross comparison to the vicarious calibration. The conventional cross calibration can be done with cross comparison between two visible to near infrared radiometer data. Therefore, cross calibration coefficients are essentially relative value. Cross calibration may be affected by the difference of wavelength coverage of the different visible to near infrared radiometers in conjunction with spectral surface reflectance and spectral optical depth, the difference between Instantaneous Field of View: IFOV, and the registration error between two visible to near infrared radiometer pixels and is not so good in terms calibration accuracy.

B. Example of Cross Calibration

The mission instrument in concern is VNIR: Visible to Near Infrared Radiometer of ASTER: Advanced Spectrometer for Thermal Emission and Reflectance onboard Terra satellite. Other instruments of which wavelength coverage are overlapped are onboard the same Terra satellite. Namely, the wavelength coverage of MODIS and MISR are overlapped with ASTER/VNIR. The wavelength coverage of these mission instruments are shown in Table 1 together with IFOV: Instantaneous Field of View. Other than these, the wavelength coverage of ETM+ onboard Landsat-5 is also overlapped with that of ASTER/VNIR. Therefore, cross calibration can be done between ASTER/VNIR and MODIS, MISR, ETM+. In MISR, these wavelengths are center wavelength of band. MISR bandwidth in Green, Red, and NIR are 0.028, 0.022, 0.039 *micrometer*, respectively.

Spectral response functions of these instruments are shown in Figure 1. Figure 1 (a) shows spectral responses for Green bands of the three mission instruments in concern while Figure (b) shows those for Red bands. Furthermore, Figure 1 (c) shows those for Near Infrared bands. Band width and center wavelength are different each other.

Wavelength Coverage of Visible to Near Infrared Radiometers for Cross Calibration in Unit of Micrometer Therefore, influence due to the difference of spectral response functions have to be taken into account. These data are available from the urls listed in Table 2.

Although the data acquisition time of ASTER/VNIR is totally equal to these of MISR, and MODIS because these instruments are onboard the same satellite, Terra, ETM+ onboard Landsat-5 differs from the ASTER/VNIR for about 30 minutes.

TABLE I. Major Specification of Four Radiometers in Concern for Cross Calibration Between ASTER/VNIR and the other threee Radiometrs

	ASTER (15m/px)	MISR (275m/px)	MODIS (250m/px)	ETM+ (30m/px)
Green	0.52 - 0.60 (band1)	0.558	none	0.52 - 0.60 (band2)
Red	0.63 - 0.69 (band2)	0.672	0.62 - 0.67 (band1)	0.63 - 0.69 (band3)
NIR	0.76 - 0.86 (band3N)	0.867	0.84 - 0.87 (band2)	0.75 - 0.90 (band4)

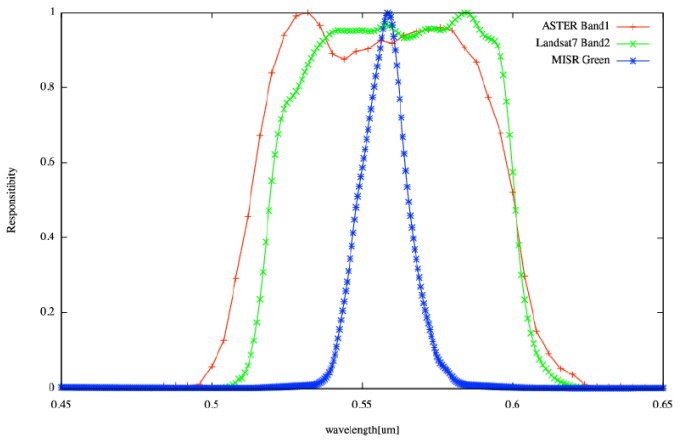

(a)Green bands

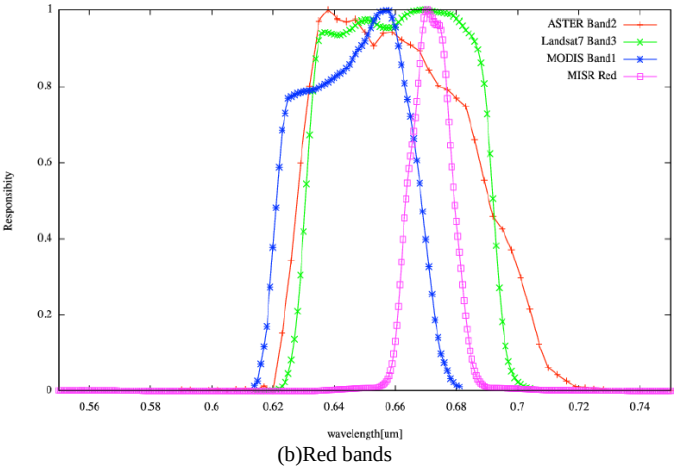

(b)Red bands

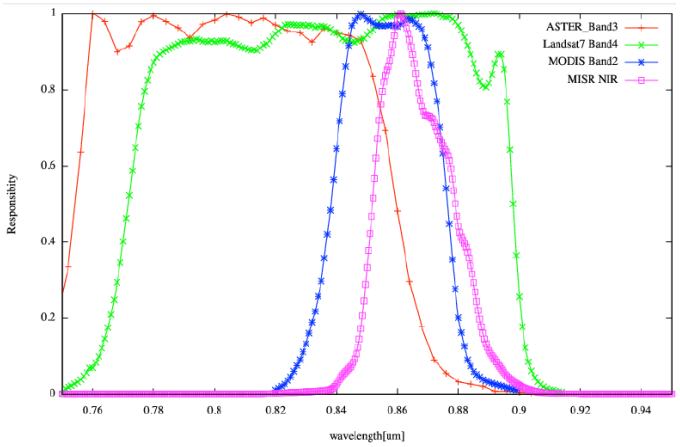

(c)Near Infrared bands

Fig.1. Comparison among the spectral response functions of ASTER/VNIR, MODIS, MISR, and ETM+

TABLE II. URLS OF WHICH VISIBLE TO NEAR INFRARED RADIOMETER DATA CAN BE DOWNLOAD

Sensor	Product name	URL
Terra/ASTER	Level 1B	http://earthexplorer.usgs.gov/
Terra/MODIS	MOD02QKM	http://ladsweb.nascom.nasa.gov/data/search.html
Terra/MISR	MI1B2T	http://l0dup05.larc.nasa.gov/MISR/cgi-bin/MISR/main.cgi
Landsat7/ETM+	Level 1T	http://earthexplorer.usgs.gov/

Other than these, registration error has to be taken into account in cross calibration. Figure 2 shows the illustrative view of the registration error between the pixels of ASTER/VNIR and the other instruments.

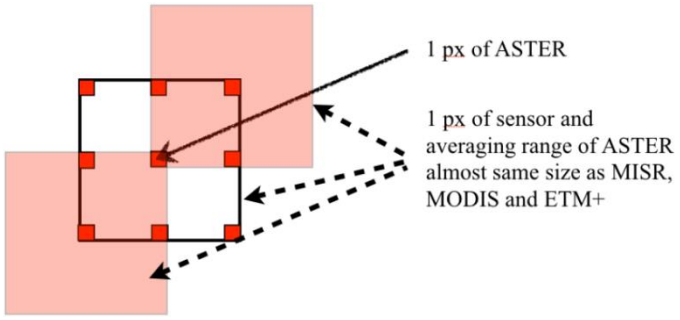

Fig.2. Registration error

Registration of the pixel of ASTER/VNIR in concern does not match perfectly to a corresponding pixel of the other mission instruments. Also, IFOV of ASTER/VNIR differs from those of the other mission instruments.

C. Coventional Cross Calibration

In the conventional cross calibration, the corresponding pixels of ASTER/VNIR are compared to those of the other instruments in unit of radiance. The difference of radiance between ASTER/VNIR and the other instruments is cross calibration coefficients for each band. It is difficult to take into account the difference of spectral response functions, the difference of acquisition time difference. Influence due to the difference of IFOV and registration error can be taken into account. Therefore, cross calibration coefficients are essentially relative values.

D. Vicarious Calibration

Vicarious calibration coefficients, on the other hand, is defined as the difference between ASTER/VNIR pixel value derived radiance and the estimated radiance derived from the radiative transfer equation with the input parameters of surface reflectance measured on the ground, refractive index and size distribution estimated with atmospheric optical depths measured on the ground at the several wavelengths for aerosol scattering and absorption, and Rayleigh scattering derived from measured atmospheric pressure. Therefore, vicarious calibration coefficients are essentially absolute values.

E. Proposed Cross Calibration

The cross calibration method proposed here provides absolute calibration coefficients with measured reflectance and optical depth which are used for vicarious calibration. Top of the atmosphere: TOA radiance is estimated with radiative transfer equation with the measured surface reflectance and optical depth through convolution with the spectral response functions of the visible to near infrared radiometers in concern. Then cross comparison is made between the estimated TOA radiance of the visible to near infrared radiometers in concern.

Vicarious calibration, on the other hand, uses measured spectral reflectance and spectral optical depth. Therefore, vicarious calibration coefficients are essentially absolute value and are comparatively good in terms calibration accuracy. The difference between the proposed cross calibration and vicarious calibration methods is comparison processes. After the vicarious calibration for different visible to near infrared radiometers, vicarious calibration coefficients of visible to near infrared radiometer are compared each other in the proposed cross calibration.

III. EXPERIMENTS

A. Experiments Conducted

Field campaigns are conducted at the following there test sites,

IV: Ivanpah Playa (35:34N, 115:24W,790m), California
AL: Alkali Lake (37:51N, 117:25W, 1463m), Nevada
RV: Railroad Valley Playa (38:30N, 115:41N, 1440m) Nevada

Table 3 shows the dates of the field campaigns. Target pixel can be identified through visual perception of blue tarp on the test sites. Thus the test site locations are precisely identified with good registration accuracy.

B. Surface Reflectance

The surface reflectance is measured at the test sites for 60 m by 60 m with 10m interval. Figure 6 shows examples of the measured spectral surface reflectance at three test sites, Ivanpah Playa on September 22 2011, Alkali Lake on September 27 2011 and Railroad Valley Playa on September

29 2011.

TABLE III. THE DATES OF THE FIELD CAMPAIGNS

IV	AL	RV
0905 06/10/2002	2159 12/16/2005	2415 07/30/2006
2184 12/11/2005	2829 09/17/2007	3199 09/21/2008
2424 08/08/2006	3197 09/19/2008	3551 09/08/2009
2536 11/28/2006	3549 09/06/2009	3935 09/27/2010
2824 09/12/2007	3935 09/25/2010	4272 08/29/2011
3192 09/14/2008	4270 08/27/2011	4656 09/16/2012
3727 12/03/2008		
3544 09/01/2009		
3928 09/20/2010		
4265 08/22/2011		
4649 09/09/2012		

The first column shows the days after launch

C. ASTER/VNIR Images

Figure 3 shows examples of the ASTER/VNIR NIR band images of three test sites. Red square shows the test site locations.

D. Atmospheric Optical Depth

The atmospheric optical depth is measured at the test sites. Figure 7 shows examples of the measured atmospheric optical depth. In the atmosphere, there are absorption due to water vapor, ozone and aerosols together with scattering due to the atmospheric molecules, aerosols. Atmospheric Optical Depth: AOD (optical thickness) in total, Optical Depth: OD due to water vapor (H_2O), ozone (O_3), molecules (MOL), aerosols (AER), and real observed OD (OBS) are plotted in Figure 7.

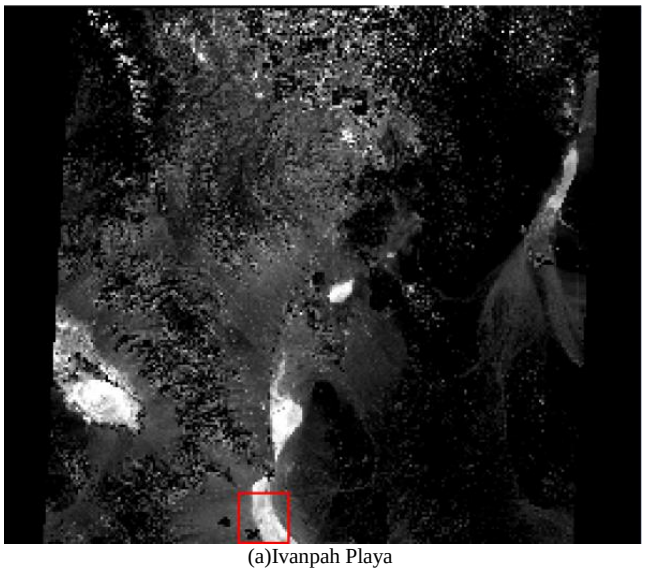

(a)Ivanpah Playa

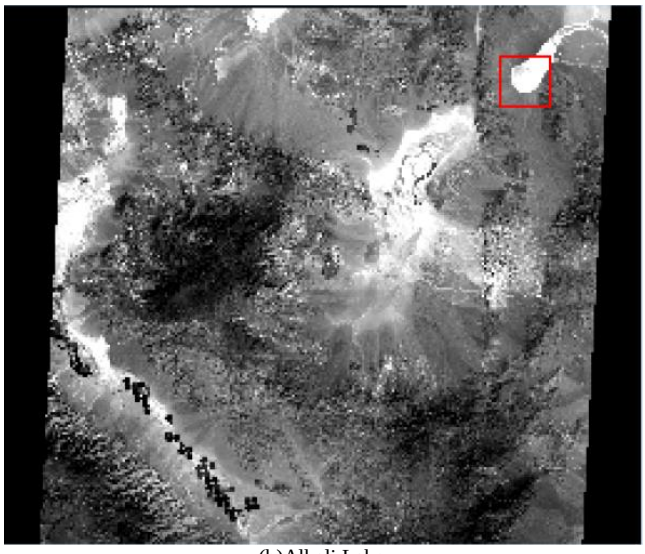

(b)Alkali Lake

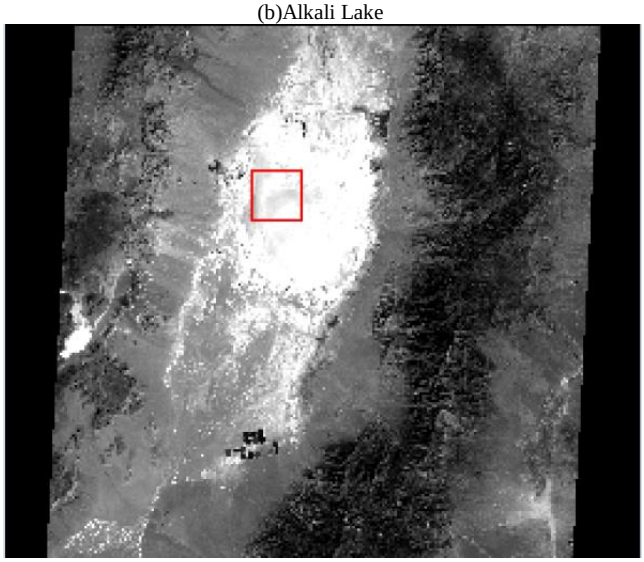

(c)Railroad Valley Playa

Figure 5 Examples of the ASTER/VNIR NIR band images of three test site

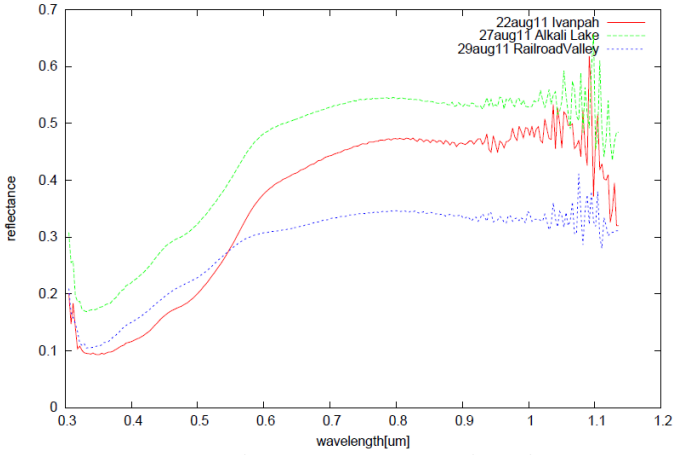

Figure 6 Examples of the measured spectral surface reflectance.

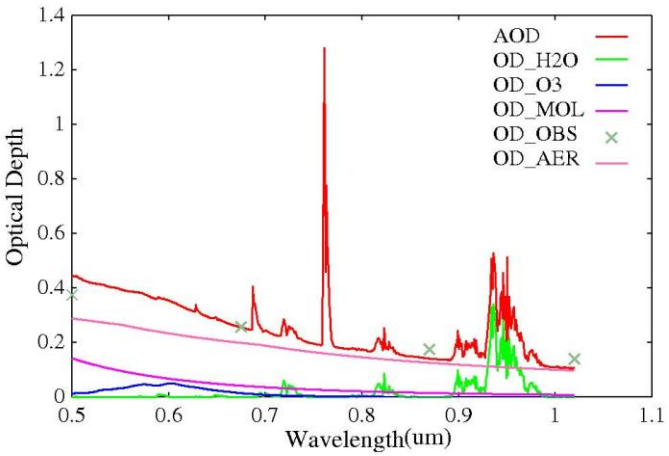

Figure 7 Example of observed atmospheric optical depth in total and the best fit curves of optical depth due to water vapor, ozone, molecules, and aerosols calculated with MODTRAN of atmospheric radiative transfer software code..

E. Vicarious Calibration

Vicarious calibration coefficients are obtained based on radiative transfer software code of MODTRAN with the field campaign data of surface reflectance, total column ozone and water vapor, as well as atmospheric pressure together with aerosol parameters; refractive index and size distribution derived from sky radiometer data and atmospheric optical depth. TOA radiance is estimated through the aforementioned procedure and then is compared to the ASTER/VNIR derived radiance results in calculation of vicarious calibration coefficients. Table 4 shows the calculated vicarious calibration data.

TABLE IV. THE VICARIOSU CALIBRATION COEFFICIENTS

(a)Ivanpah Playa

	Day	DAL	RCC_vc
Band Green	2000/06/04	169	0.89570
	2001/06/07	537	0.79536
	2002/01/17	757	0.76413
	2005/12/11	2148	0.66320
	2006/08/08	2424	0.84946
	2006/11/28	2536	0.84655
	2007/09/12	2824	0.77642
	2008/09/14	3192	0.73081
	2008/11/03	3242	0.64953
	2009/09/01	3544	0.76699
	2010/09/20	3928	0.80678
	2011/08/22	4265	0.83696
	Day	DAL	RCC_vs
Band Red	2000/06/04	169	0.93470
	2001/06/07	537	0.81293
	2002/01/17	757	0.80310
	2005/12/11	2148	0.69795
	2006/08/08	2424	0.85075
	2006/11/28	2536	0.85321
	2007/09/12	2824	0.76921
	2008/09/14	3192	0.75591
	2008/11/03	3242	0.69026
	2009/09/01	3544	0.78700
	2010/09/20	3928	0.79278
	2011/08/22	4265	0.94690
	Day	DAL	RCC_vs
Band NIR	2000/06/04	169	1.00010
	2001/06/07	537	0.87390
	2002/01/17	757	0.90067
	2005/12/11	2148	0.78288
	2006/08/08	2424	0.93711
	2006/11/28	2536	0.95591
	2007/09/12	2824	0.74768
	2008/09/14	3192	0.79275
	2008/11/03	3242	0.73340
	2009/09/01	3544	0.81375
	2010/09/20	3928	0.89448
	2011/08/22	4265	1.00322

(b)Alkali Lake

	Day	DAL	RCC_vc
Band Green	2005/12/16	2159	0.69600471
	2007/09/17	2829	0.66371092
	2008/09/19	3197	0.84800178
	2009/09/06	3549	0.774319
	2010/09/25	3933	0.67612548
	2011/08/27	4270	0.60813229
	Day	DAL	RCC_vs
Band Red	2005/12/16	2159	0.69859583
	2007/09/17	2829	0.77056662
	2008/09/19	3197	0.7507701
	2009/09/06	3549	0.79646567
	2010/09/25	3933	0.70989962
	2011/08/27	4270	0.69222309
	Day	DAL	RCC_vs
Band NIR	2005/12/16	2159	0.80871349
	2007/09/17	2829	0.81529287
	2008/09/19	3197	0.79725186
	2009/09/06	3549	0.90928185
	2010/09/25	3933	0.85319343
	2011/08/27	4270	0.85718958

(c)Railroad Valley Playa

	Day	DAL	RCC_vc
Band Green	2000/06/11	173	0.88235
	2001/06/14	541	0.80184
	2006/07/30	2415	0.94137
	2008/09/21	3199	0.76877
	2010/09/27	3935	0.74499
	2011/08/29	4272	0.70407
	Day	DAL	RCC_vs
Band Red	2000/06/11	173	0.89655
	2001/06/14	541	0.84616
	2006/07/30	2415	0.89336
	2008/09/21	3199	0.80563

	2010/09/27	3935	0.73990
	2011/08/29	4272	0.72334
Band NIR	Day	DAL	RCC_vs
	2000/06/11	173	0.97452
	2001/06/14	541	0.94041
	2006/07/30	2415	0.97833
	2008/09/21	3199	0.81471
	2010/09/27	3935	0.82571
	2011/08/29	4272	0.78299

DAL denotes the days after launch.

In accordance with the days after launch, Radiometric Calibration Coefficient: RCC is decreased as exponential function. Namely, sensitivity of ASTER/VNIR is degraded for time being. There is test site dependency and wavelength dependency. The most degraded band is band 1 followed by band 2 and band 3 depending on the corresponding wavelength. Namely, sensitivity degradation is negatively proportional to the wavelength (degradation of shorter wavelength is much greater than that of longer wavelength).

Sensitivity degradation foe the Alkali test site, on the other hand, is much significant in comparison to the other two test sites, sensitivity degradation for the other two sites indicate almost same though. One of the biggest reasons for this is sensor saturations. Due to the fact that the surface reflectance at Alkali test site is highest comparing to the others, ASTER/VNIR, in particular, band 1 and 2 are saturated. Sensitivity degradation should be same for all the test sites. Therefore, vicarious calibration coefficients for in particular band 1 and 2 derived from the Alkali test site would be better to forget.

F. Cross Calibration Coefficients

Figure 8 (a), (c), (e) shows the Radiometric Calibration Coefficient: RCC of the conventional cross calibration while Figure 8 (b), (d), (f) shows those for the proposed cross calibration. Red solid line in the figure shows RCC derived from Onboard Calibration: OBC data. OBC data derived RCC differs from both the conventional and the proposed cross calibration RCC.

These cross calibration coefficients are summarized with their averaged RCC and Standard Deviation: SD together with their Confidence Interval: CI at 95% of confidence level as shown in Table 5. Also Root Mean Square Difference: RMSD between vicarious RCC and the conventional cross calibration RCC as well as the proposed cross calibration RCC is shown in Table 6.

As shown in Table 6, RMSD between the vicarious RCC and the proposed cross calibration RCC is less than that between the vicarious RCC and the conventional cross calibration RCC.

Therefore, it is said that the proposed cross calibration method is superior to the conventional cross calibration method obviously.

Percent difference of RMSD between the conventional and the proposed cross calibration is shown in Table 7.

It may said that the proposed cross calibration method shows 6 to 89% better cross calibration accuracy in comparison to the conventional cross calibration.

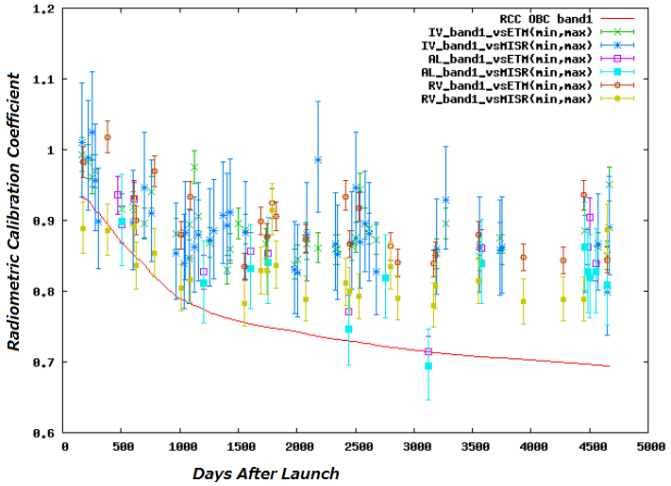

(a)Conventional Band 1

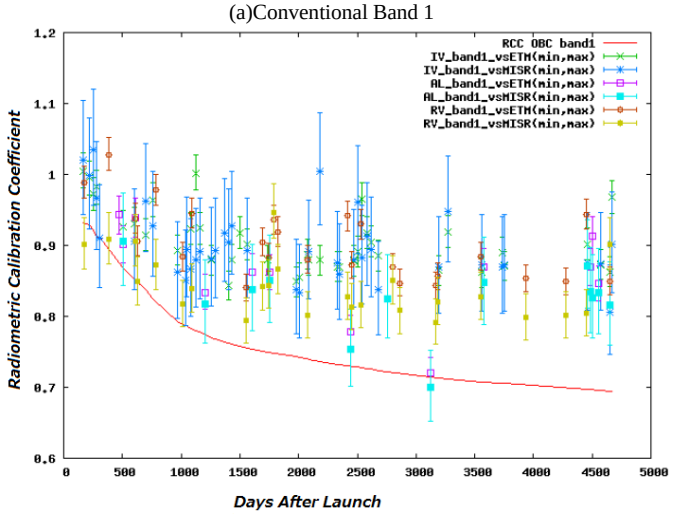

(b)Proposed Band1

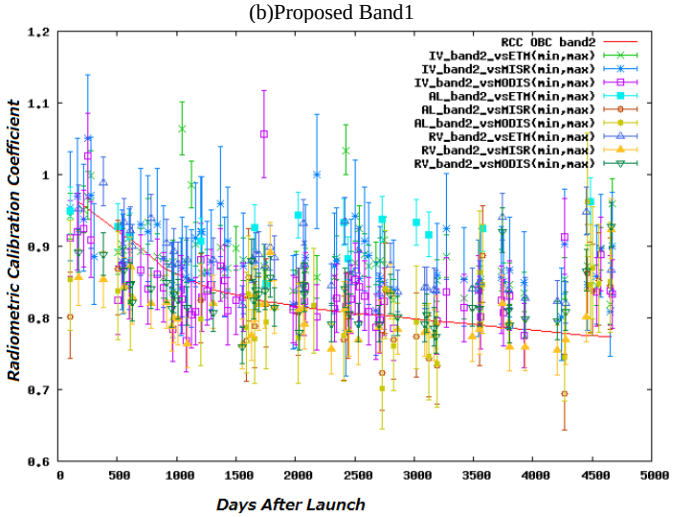

(c)Conventional Band 2

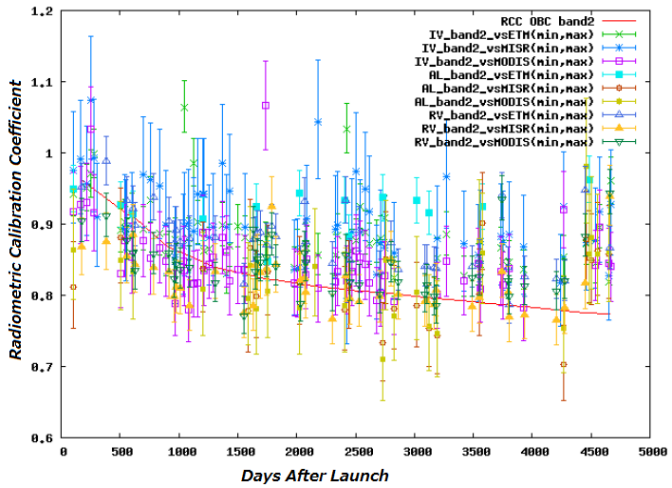

(d)Proposed Band 2

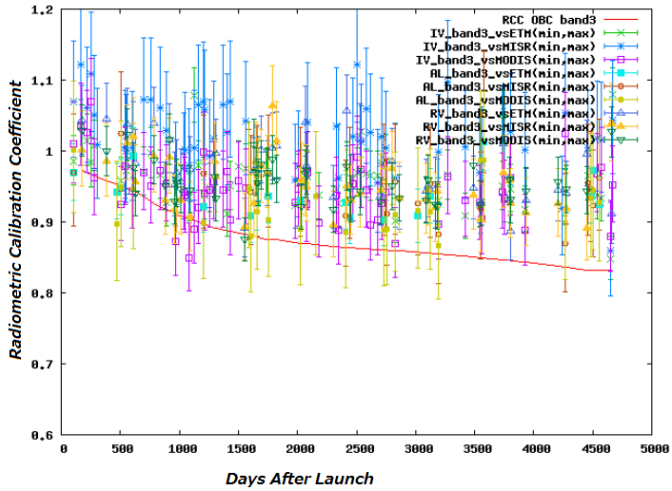

(e)Conventional Band 3

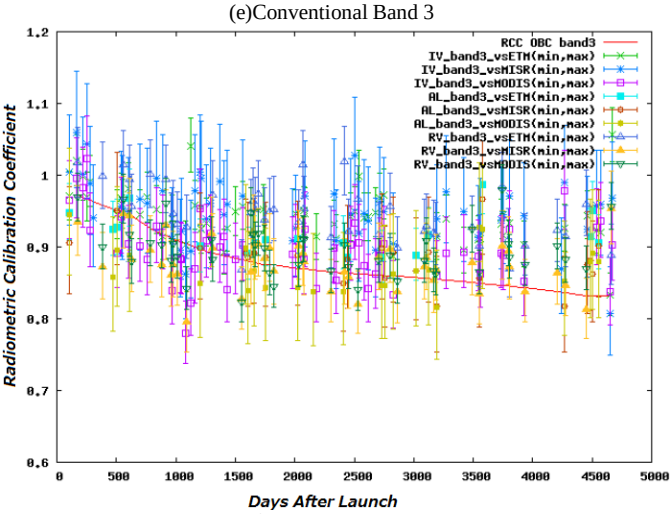

(f)Proposed Band 3

Figure 8 Comparison of cross calibration RCC between the conventional and the proposed cross calibration methods

TABLE V. SUUMARY OF CROSS CALIBRATION COEFFICIENTS

(a)Cross RCC for Green and Red bands

		Green		Red		
		vsETM	vsMISR	vsETM	vsMISR	vsMODIS
IV	average (SD)	1.80 (0.54)	1.38 (0.45)	0.03 (0.15)	3.33 (0.90)	1.15 (1.33)
	95% CI	[1.38, 2.24]	[1.02, 1.74]	[-0.09, 0.15]	[2.61, 4.04]	[0.09, 2.21]
AL	average (SD)	1.41 (0.69)	1.46 (0.58)	-0.05 (0.16)	2.47 (1.02)	2.26 (0.72)
	95% CI	[0.52, 2.31]	[0.72, 2.21]	[-0.26, 0.15]	[1.16, 3.79]	[1.33, 3.19]
RV	average (SD)	0.88 (0.11)	2.34 (0.20)	-0.08 (0.12)	2.23 (0.28)	2.12 (0.29)
	95% CI	[0.74, 1.02]	[2.09, 2.60]	[-0.23, 0.07]	[1.87, 2.59]	[1.75, 2.50]

(b)Cross RCC for NIR band

		NIR		
		vsETM	vsMISR	vsMODIS
IV (N=11)	average (SD)	-1.81 (1.14)	-6.71 (1.83)	-5.09 (1.76)
	95% CI	[-2.72, -0.90]	[-8.17, -5.25]	[-6.49, -3.69]
AL (N=6)	average (SD)	-2.80 (0.97)	-8.94 (1.62)	-7.37 (1.41)
	95% CI	[-4.06, -1.55]	[-11.04, -6.85]	[-9.19, -5.54]
RV (N=6)	average (SD)	-2.67 (0.33)	-7.96 (1.37)	-6.65 (1.14)
	95% CI	[-3.10, -2.24]	[-9.72, -6.19]	[-8.12, -5.18]

TABLE VI. AVERAGED ROOT MEAN SQUARE DIFFERENCE BETWEEN VICARIOUS CALIBRATION RCC AND CROSS CALIBRATION RCC

	Conventional			Proposed		
Site	ETM+	MISR	MODIS	ETM+	MISR	MODIS
Ivanpah	0.0733	0.0798	0.0338	0.0690	0.0645	0.0169
Alkali	0.0280	0.0625	-	0.00312	0.0387	-
Railroad	0.0889	0.0194	0.0619	0.0807	0.0031	0.0346

TABLE VII. PERCENT DIFFERENCE OF RMSD BETWEEN CONVENTIONAL AND PROPOSED CROSS RCC

	% Difference between Conventional and Proposed Cross RCC		
Site	ETM+	MISR	MODIS
Ivanpah	5.866	19.173	50.000
Alkali	88.857	38.080	-
Railroad	9.224	84.021	44.103

IV. CONCLUSION

Accuracy evaluation of cross calibration through band-to-band data comparison for visible and near infrared radiometers which onboard earth observation satellites is conducted. The conventional cross calibration for visible to near infrared radiometers onboard earth observation satellites is conducted through comparisons of band-to-band data of which spectral response functions are overlapped mostly. There are the following major error sources due to observation time difference, spectral response function difference in conjunction of surface reflectance and atmospheric optical depth, observation area difference. These error sources are assessed with dataset acquired through ground measurements of surface reflectance and optical depth. Then the accuracy of the conventional cross calibration is evaluated with vicarious calibration data.

The results show that cross calibration accuracy can be done more precisely if the influences due to the aforementioned three major error sources are taken into account.

ACKNOWLEDGMENT

The author would like to thank Dr. Satoshi Tsuchida and his colleague of The National Institute of Advanced Industrial Science and Technology (AIST), and Dr. Fumihiro Sakuma and his colleague of The Japan Space Systems: JSS people for their support to this research works. The author also would like to thank Mr. Yuichi Sarusawa of Graduate School of Saga University for his efforts to conduct cross calibration experiments.

REFERENCES

[1] Arai,K., Calibration /intercalibration of multi-sensor for satellites, Advances in Space Research, Vol.16, No.10, pp.125-128, A31-002, July 1994.

[2] P.Slater, K.Thome, A.Ono, F.Sakuma, Kohei Arai, F.Palluconi, H.Fujisada, Y.Yamaguchi and H.Kieffer, Radiometric Calibration of ASTER Data, Journal of Remote Sensing Society of Japan, Vol.15, No.2, pp.16-23, Jun.1994.

[3] A.Ono, F.Sakuma, Kohei Arai, Y.Yamaguchi, H.Fujisada, P.Slater, K.Thome, F.Palluconi and H.Kieffer, Pre-filight and In-flight Calibration Plan for ASTER, Journal of Atmospheric and Oceanic Technology, Vol.13, No.2, pp.321-335, Apr.1995.

[4] Kohei Arai, Inflight Test Site Cross Calibration Between Mission Instruments Onboard Same Platform, Advances in Space Research, Vol.19, No.9, pp.1317-1324, Jul.1997.

[5] K.Thome, K.Arai et al., ASTER Preflight and Inflight Calibration and Validation of Level 2 Products, IEEE Trans.on Geoscience and Remote Sensing, Vol.36, No.4, 1161-1172, Sep.1998.

[6] K.Thome, S.Schiller, J.Conel, K.Arai and S.Tasuchida, Results of the 1996 EOS vicarious calibration joint campaign at Lunar Lake Playa, Nevada(USA), Metrologia, Vol.35, pp.631-638, Jan.1999.

[7] K.Arai, Error budget analysis of cross calibration method between ADEOS/AVNIR and OCTS, Advances in Space Research, Vol.23, No.8, pp.1385-1388, June 1999.

[8] K.Arai, Preliminary vicarious calibration for EOS-AM1/ASTER with field campaign, Advances in Space Research, Vol.23, No.8, pp.1449-1457, June 1999.

[9] Kohei Arai and H.Tonooka, Radiometric performance evaluation of ASTER/VNIR, SWIR and TIR, IEEE Trans. on GeoScience and Remote Sensing, 43,12,2725-2732, 2005.

[10] Kohei Arai, Vicarious calibration for solar reflection channels of radiometers onboard satellites with deserted area of data, Advances in Space Research, 39, 1, 13-19, 2007.

[11] Kurtis Thome, Kohei Arai, Satoshi Tsuchida and Stuart Biggar, Vicarious calibration of ASTER via the reflectance based approach, IEEE transaction of GeoScience and Remote Sensing, 46, 10, 3285-3295, 2008.

[12] Chrysoulakis,Abrams, Feidas and Kohei Arai, Comparison of Atmospheric correction methods using ASTER data for the area of Crete, Greece, International Journal of Remote Sensing, 31,24,6347-6385,2010.

[13] Ramachandran, Justice, Abrams(Edt.),Kohei Arai et al., Land Remote Sensing and Global Environmental Changes, Part-II, Sec.5: ASTER VNIR and SWIR Radiometric Calibration and Atmospheric Correction, 83-116, Springer 2010.

[14] Arai, K., & Terayama, Y. (2000). An Experimental Study on Cross Calibration of ADEOS / AVNIR and the Visible Channels of OCTS. *Journal of Remote Sensing Society of Japan*, *20* (2), 60{68.

[15] Cachorro, V. E., Frutos, A. M. D. E., Aplicada, D. D. F., Gonzalez, M. J., & Electrica, D. D. I. (1993). Analysis of the relationships between Junge size distribution and angstrom _ turbidity parameters from spectral measurements of atmospheric aerosol extinction. *Atmospheric Environment*, *27A*(10), 1585{1591.

[16] Chandrasekhar, S. (1960). *Radiative transfer* (1st ed.). New York, US: Dover Publications, Inc.

[17] Dinguirard, M., & Slater, P. (1999). Calibration of space-multispectral imaging sensors: A review. *Remote Sensing of Environment*, *4257* (98), 194{205. Earth Remote Sensing Data Analysis Center. (2005). *ASTER User's Guid Part I General* (Ver.4.0 ed.).

[18] Liu, J.-J., Li, Z., Qiao, Y.-L., Liu, Y.-J., & Zhang, Y.-X. (2004, December). A new method for cross-calibration of two satellite sensors. *International Journal of Remote Sensing*, *25* (23), 5267{5281. Retrieved from http://www.tandfonline.com/doi/abs/10.1080/01431160412331269779 doi: 10.1080/01431160412331269779

[19] Teillet, P. M., Fedosejevs, G., Thome, K., & Barker, J. L. (2007, October). Impacts of spectral band difference effects on radiometric cross-calibration between satellite sensors in the solar-reflective spectral domain. *Remote Sensing of Environment*, *110* (3), 393{409. doi: 10.1016/j.rse.2007.03.003

[20] Tsuchida, S., Sakuma, H., & Iwasaki, A. (2004). *Equations for ASTER radiometric calibration ver.0.20.* Retrieved 2013/01/24, from http://staff.aist.go.jp/s.tsuchida/aster/cal/info/equation/index.html

[21] Xiong, X., Che, N., & Barnes, W. L. (2006). Terra MODIS On-Orbit Spectral Characterization and Performance. *IEEE transactions on Geoscience and Remote Sensing*, *44* (8), 2198{2206.

[22] C.J. Brueggc and D.J. Diner, "Instrument verification tests on the Multi-angle imaging Spectro-Radiometer (MISR)," in *Earth Observing Systems II*, SPIE 3117, San Diego, CA, 28-29 July 1997.

[23] P.M. Teillet, J.L. Barker, B.L. Markham, R.R Irish, G. Fedosejevs, J.C. Storey, Radiometric cross-calibration of the Landsat-7 ETM+ and Landsat-5 TM sensors based on tandem data sets, Remote Sensing of Environment 78 (2001) 39– 54

AUTHORS PROFILE

Kohei Aarai He received BS, MS and PhD degrees in 1972, 1974 and 1982, respectively. He was with The Institute for Industrial Science and Technology of the University of Tokyo from April 1974 to December 1978 and also was with National Space Development Agency of Japan from January, 1979 to March, 1990. During from 1985 to 1987, he was with Canada Centre for Remote Sensing as a Post Doctoral Fellow of National Science and Engineering Research Council of Canada. He moved to Saga University as a Professor in Department of Information Science on April 1990. He was a councilor for the Aeronautics and Space related to the Technology Committee of the Ministry of Science and Technology during from 1998 to 2000. He was a councilor of Saga University for 2002 and 2003. He also was an executive councilor for the Remote Sensing Society of Japan for 2003 to 2005. He is an Adjunct Professor of University of Arizona, USA since 1998. He also is Vice Chairman of the Commission-A of ICSU/COSPAR since 2008. He wrote 30 books and published 332 journal papers.

Interactive Application Development Policy Object 3D Virtual Tour History Pacitan District based Multimedia

Muga Linggar Famukhit
Informatics Faculty, University of Surakarta
Surakarta, Indonesia

Maryono
History Educational, High School Science Teacher and Education
Pacitan, Indonesia

Lies Yulianto
Pacitan, Indonesia

Bambang Eka Purnama
Informatics Faculty, University of Surakarta
Surakarta, Indonesia

***Abstract* –Pacitan has a wide range of tourism activity. One of the tourism district is Pacitan historical attractions. These objects have a history tour of the educational values, history and culture, which must be maintained and preserved as one tourism asset Kabupeten Pacitan. But the history of the current tour the rarely visited and some of the students also do not understand the history of each of these historical attractions. Hence made a information media of 3D virtual interactive applications Pacitan tour history in the form of interactive CD applications. The purpose of the creation of interactive applications is to introduce Pacitan history tours to students and the community. Creating interactive information media that can provide an overview of the history of the existing tourist sites in Pacitan The benefits of this research is the students and the public will get to know the history of historical attractions Pacitan. As a media introduction of historical attractions and as a medium of information to preserve the historical sights. Band is used in the manufacturing methods Applications 3D Virtual Interactive Attractions: History-Based Multimedia Pacitan authors used the method library, observation and interviews. Design using 3ds Max 2010, Adobe Director 11.5, Adobe Photoshop CS3 and Corel Draw. The results of this research is the creation of media interakif information that can provide knowledge about the history of Pacitan.**

Keywords–Interactive 3D Virtual Application Development Object-Based Tourism Pacitan History Multimedia

I. INTRODUCTION

Pacitan has a wide range of tourism. One of the objects Pacitan tourism is travel history. Travel history Pacitan consists of various monuments and museums. Historical sights are Jend Sudirman Monument, Monument Tumpak Rinjing Theater and Museum Buwono Keling. These objects would have historical value of education, history and culture, which should be maintained and preserved as one of the tourism assets Pacitan. (Qomaruddin Sartono, 2006).

With the development of a wide range of attractions and entertainment in Pacitan, historical tourism is increasingly less attractive and rarely visited by tourists and the community, building one of the largest and grandest monuments Pacitan received little response from the visitors. The existence of such monuments to lose competitiveness with visitors coastal resorts and shopping districts in Pacitan, it will certainly make the historical sights unnoticed by the public and students. (Mahendra Rizki, 2008). Society and current students are also many who do not understand the history of the objects that exist in the historical Pacitan. (Quesioner).

In the world of education and tourism one way to introduce a tourism object, can be presented by using a medium of information. Media information can be developed is digital information media, namely by using computer technology. Because the digital information media, information can be delivered more user friendly and very enjoyable to use. (Novitasari, 2011).

There are various types of media digital information developed at this time, one of which is a multimedia computer technology. Multimedia computer technology to make the delivery of information can be conveyed with more interactive because the reach of human senses. This is because multimedia is made up of various elements of the text, art, sound, animation and video. (Vaughan, 2004).

Virtual Reality 3D is part of the multimedia objects. Virtual reality is a 3D image in a computer or in another world (maya) that can make people feel in the real world and can perform the operation and control of real-life systems. (Daren L.I, 2009).

A. Problem Formulation

a)Starting lack of interest in the community to find out more details about the museum and the history

b) How to make technological innovations that can be used as a media introduction Pacitan historical sights?

B. Limitation Problem

a) Object of research on the history of the monument tour General Sudirman, Monuments and Museum Theater Tumpak Rinjing Keling lane.

b) Computer-based desktop

C. The Purpose

a) Creating Applications Interactive 3D Virtual Tour History Pacitan Object-Based Multimedia band is used as a means of introduction to historical sights to students and the public.

b) Creating interactive information medium that can provide an overview of historical tourist sites Pacitan.

D. BENEFITS

a) As a media introduction of the history of tourism objects that exist in Pacitan.

b) As a medium for preserving historical information to students and the public.

II. TOURISM

According to Richart Shite (2000), Tourism is travel that people do for a while, which was held from from one place to another, melinggalkan its original position, with a plan and with the intention not to seek or make a living in the places visited, but simply -eyes to enjoy pertamasyaan activities and recreation to meet the diverse activities.

A. History

According Suhartono W. Pranoto (2009) history is a science that studies and investigates the events of the past, which include science, investigation and recording. In other words, human history kelampauan include activities in the community and is unique.

Meanwhile, according to Kartikadarma Ethics (2010) is literally syajarah birth history, in the narrow sense that pedigree, origin or history.

In line with the development of knowledge, understanding sejarahpun development. Based on the shape and nature of history is divided into two terms, namely:

c) History As Events

Historical events are events that happened in the past. In other words, the history of the event is the historical process in its actuality (History as past actuality or histoire-réalité). This means the event history is objective, because the event was purely as happened.

d) History As the Story

History is the story as told in writing history (History as written / Histoire Recite) based on the results of the research. In other words, the history of the story is the reconstruction of historical events based on historical fact. The event is especially important events concerning human life in general.

B. Multimedia

Multimedia is a combination of computer and video (Rosch, 1996) or Multimedia is generally a combination of three elements, namely the sound image and text (McMormic, 1996) or multimedia is a combination of at least two media input or output image (Turban et al, 2002) or Multimedia is a tool that can create a dynamic and interactive presentations that combine text, graphics, animation, audio and video and image video (Robin and Linda, 2001).

Meanwhile, according to Ariyus Dony (2009) Multimedia derived from two words, namely multi and media. Multi means many regular and defined media tools to communicate or make something, equipment, tools introduction, a form of communication such as newspapers, magazines, or television. When linked with computer processing, multimedia is considered as a tool which displays the text, images, graphics, sound, music, and so on. Multimedia systems in question here is a technology that combines a media source such as text, graphics, sound, animation, video, etc., delivered and controlled by the interactive computer system.

C. Virtual Reality

Virtual Reality (VR) is a development of the artificial (man-made) based computer technology that can be controlled by the user using the mouse (USA, Ranang and Agustin, 2007:1). VR interactive key points lies in the hands of the user controls the enjoyment of photos by moving the mouse or by pressing the keyboard. In another sense Virtual Reality technology is also often referred to as Quick Time Virtual Reality (QTVR) is a mode to view an image as if we were in the picture and can see all the way (Vaughan, 2006:451).

D. Application Programs 3d Studio Max

According to Thabani Suyanto 3D Studio Max is a software visualization (modeling and animation) three-dimensional popular and versatile. Since its first release, 3D Studio Max to be a leader pembanggunan application of three-dimensional animation. Since the fourth version, Discreet, 3D Studio Max producers, seeking to expand its area of function that can be used to create animations for the web or movies. The latest version, version 5, has led to the expansion of the function. This is indicated by the development of the polymodeling, mapping and some revisions to the tool for animation. But of features, the most interesting features of 3D Studio Max is a reactor. Reactor is integrated with inface of 3D max and provides tools to create simulations. 3D Studio Max is often used to create models of houses or furniture. In addition, many are used in digital art or game development. (Mr. Suryanto Thabani, MM, 2004).

E. Application Program Adobe Director

Adobe Director is a software created by Macromedia and is now part of Adobe Systems. which allows users to build software in a movie metaphor, which enable users to become a film director. Originally designed to create animations, adding a powerful scripting language called Lingo made a popular choice to make CD-ROMs and standalone kiosks and web content using Adobe Shockwave. Adobe Director multimedia projects supporting both 2D and 3D. Adobe Director software is not all can. Adobe Director is software to assemble multimedia components and graphics. (Hendi Hendratman, St, 2008).

F. Program Application Adobe Photoshop

Photoshop software is used to modify images or photos in a professional manner both involve a modification of a simple object or a rumut though. Photoshop is a software that allows you to reject the bitmap-based picture, which has a high-quality tool. Completeness of existing features in Photoshop is what makes this software much akhrnya band is used by

professional graphic designers. And perhaps to this day there is still no other graphic design software to match the completeness bias features in Photoshop. (Boediman, 2005)

G. Application Program Adobe Flash

Adobe Flash CS3 is an application program professional standard authoring tool released by Adobe international company that is used to create vector and bitmap animation was amazing for the purposes of web site development, interactive and dynamic. Also this application can also be used to load animated logos, movie, game, making navigation on websites, banners, animated buttons, menus, interactive form fields, e-cards, screen server, and web site creation or production applications other web. (Suciadi, 2003: 3).

H. Program Corel Draw

Corel Draw program is a program used for applications illusion images and text quickly and easily with maximum results and satisfying. Corel Draw is also used to create vector-based graphics that the user can easily create a high-tech graphic design such as logos, caricatures, posters, brochures, calendars, labels, stickers and other free images. (Erhans, 2005).

I. Studies Library

The study was made by Latitude Yanuar Bawono Sari, Aji Widhi Wibisono and Fatra Firdaus S.Syaiful, Gunadarma University, the work was entitled "Making the Virtual Museum of Culture and Art", saying that the public interest in the preservation of cultural Indonesia has decreased, especially the younger generation, it is based on data from the department of Culture and Tourism in the year 2005-2009. Decline in public interest in the culture, because of the lack of communication media used interestingly. In that study, one solution that can be used to introduce the culture to the younger generation through a 3D virtual world that resembles a game on the computer.

Research has also been done by Heri Susanta and Gondang Riyadi in 2008, the work was entitled "3-D Model Town area of Simpang Lima for Exploration in Virtual City". Heri Susanta in the work was to provide information to the public about tourism in the virtual 3-dimensional shape. Virtual 3-dimensional model was chosen because it can increase public understanding of the tourist resorts. Virtual 3-D can also band is used for promoting the effective and efficient, because obek-object to represent the state as the original. Same thing in this study is to provide information to students and the public about the history of tourism objects in a virtual three-dimensional shape.

Based on the study conducted by Latitude Yanuar Bawono Sari and Heri Susanta, so in this study the authors want to make media information such as Application Object Interactive 3D Virtual Tour History-Based Multimedia Pacitan. Applications in the form of Virtual 3D to represent the historical sights such as the original state, so expect the students and the community more aware of the objects of historical Pacitan.

III. Historical Photo Collection Of Travel Location

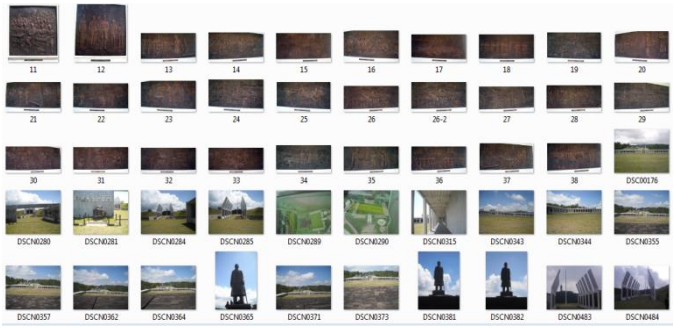

Fig. 3.1. Photo Location History Tours

A. Making History Tours Sitemap

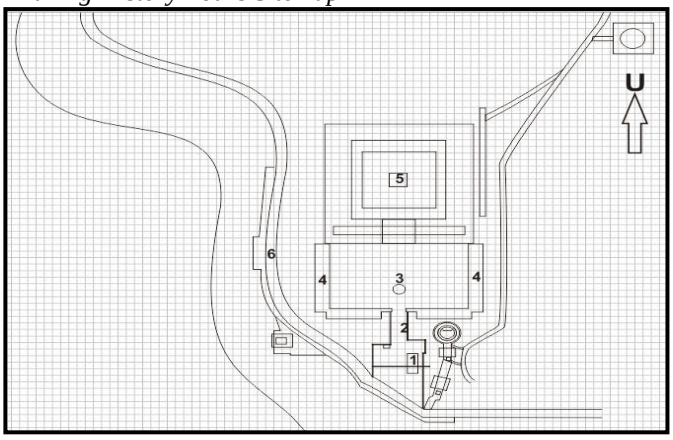

Fig.3.2. Making History Tours Sitemap

B. Import Data Plan Into 3d Max

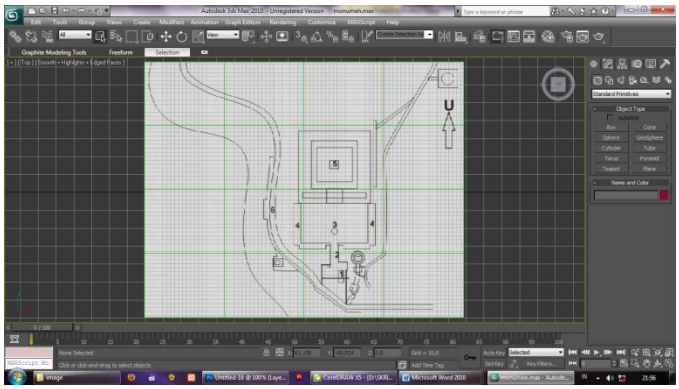

Fig.3.3. Import Data Plan In 3D Max

C. Building Making History Tours

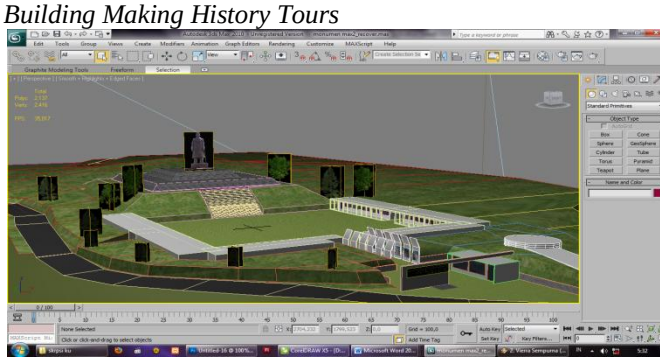

Fig.3.4. Import Data Plan In 3D Max

D. Export 3d Max File Into A Format W3d

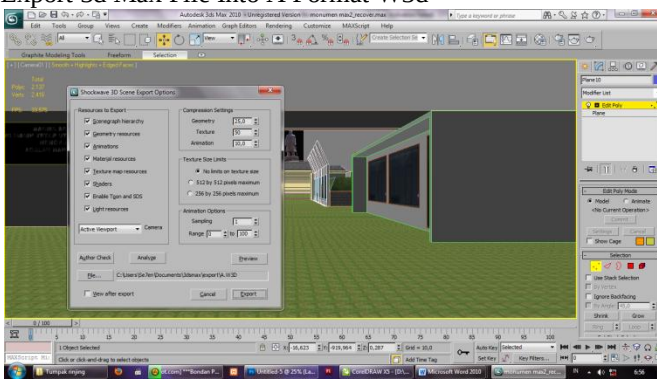

Fig.3.5. Export 3D files into the format "W3D"

E. Pengabungan Materials, Components And Export File In Shape Exe

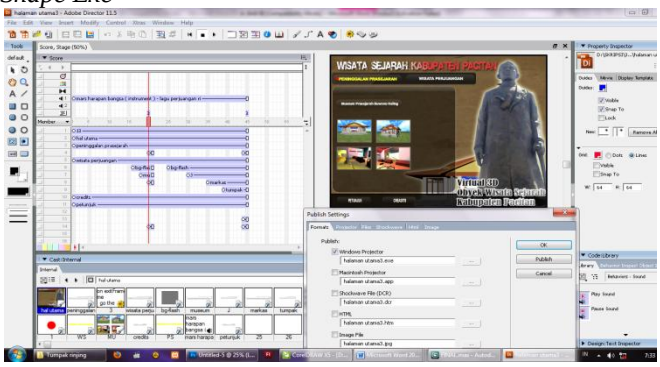

Fig.3.6. Pengabungan Materials and Components

F. Changing Icon Project With Micro Program Anggelo

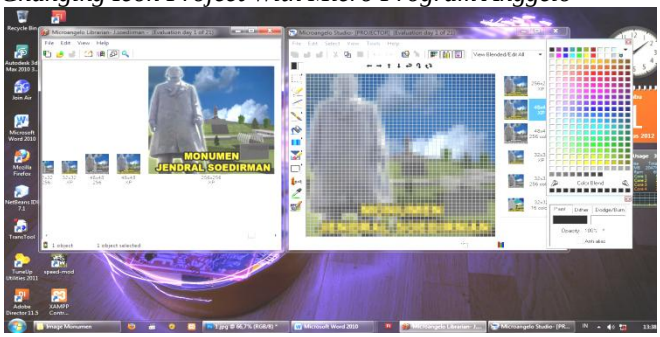

Fig.3.7. Changing Icon Project

IV. The Burning Cover Home

Fig.4.1. front cover

A. The Burning Rear Cover

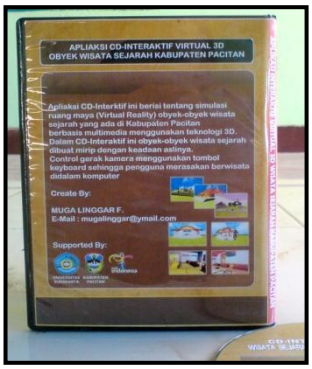

Fig. 4.2. Rear cover

B. Main Menu Display

Fig.4.3. Main menu

C. Virtual Reality Display General Sudirman Monument

Fig.4.4. Virtual Reality Monument General Sudirman

D. Monuments History Display General Sudirman

Fig. 4.5. Historical Monument General Sudirman

E. Display Location Monument Jen Sudirman

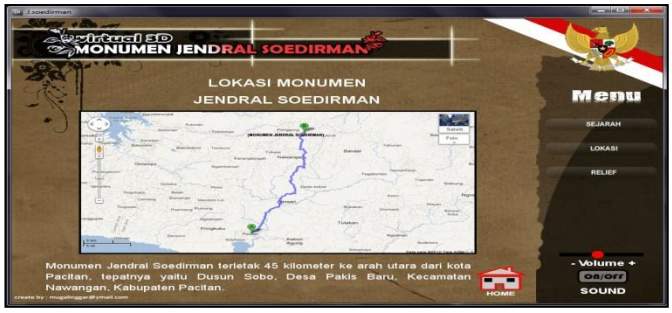

Fig.4.6. Location Monument General

F. Display Monument Relief General Sudirman

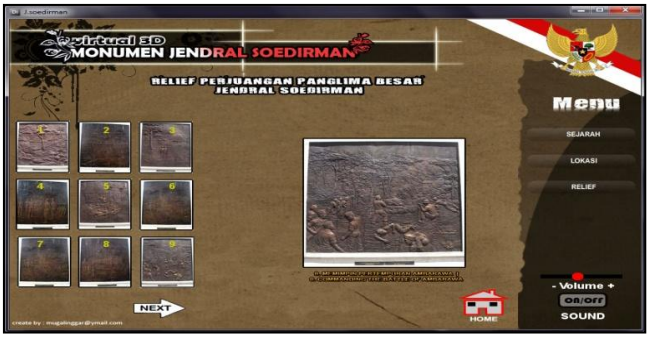

Fig. 4.7. Location Monument General

V. CONCLUSION

a) The creation of digital media information in the form Application Object Interactive 3D Virtual Tour History-Based Multimedia Pacitan difamami simple concept, easy to operate, attractive, clear and useful.

b) This application can provide knowledge about the history of the monument Pacitan General Sudirman, Tumpak Rinjing Theater Monument and Museum lane Keling.

c) This application can be used as a medium of information and the promotion of historical Pacitan to students and the public.

REFFERENCE

[1] Ariyus, Doni, Keamanan Multimedia,Penerbit Andi, 2009.

[2] Bawonosari, Lintang Yuniar, Journal,Pembuatan Museum Virtual Budaya Dan Sejarah, Universitas Gunadarma 2011.

[3] Dr. Erhans A., CorelDraw X4, PT Ercontra Rajawali, Cirebon 2005

[4] Hendratman, Hendi, The Magic Of Macromedia Director, Informatika. Bandung 2008.

[5] Hendratman, Hendi, The Magic Of 3D Studio Max, Informatika. Bandung 2011.http://pacitantourism.com diakses pada tanggal 20 mei 2012

[6] Hari Aria Soma, Animasi Kreatif Fundamental, Elex Media Komputindo. Jakarta 2007.

[7] Ir. Suryanto Thabani, Macromedia Director 8.5 Presentasi Multimedia Interaktif, Salemba. Jakarta 2008.

[8] Kartikadarma, Etika, Rancang Bangun Aplikasi E-Museum Sebagai Upaya Melestarikan Kebudayaan, Upn Veteran Yogyakarta 2011.

[9] Madcoms, Students Book Series Adobe Photoshop CS4, Yogyakarta 2009.

[10] Mulyanta, Leong Marlon, Media Pembelajaran, Universitas Atmajaya. Yogyakarta .2009

[11] Novitasari, Naskah Publikasi, Virtual Gallery Museum Gunung Merapi Sleman. Yogyakarta 2011.

[12] Riyadi Gondang, Susanta Heri, Journal, Model Kota 3 Dimensi Kawasan Simpang Lima Untuk Eksplorasi Kota Secara Virtual, Media Teknik 2008

[13] Sartono, Qomaruddin, Babad Tanah Pacitan Dan Perkembanganya, Pustaka Pacitan 2006.

[14] Setyawan Agung, Bagus Rendra, Naskah Publikasi, Perancangan Virtual Reality Sebagai Media Promosi Pada PT.Aryaguna Putra.Yogyakarta 2011.

[15] Sugianto, Mikael, Bedroom Interior Design With 3D Studio Max9, Elex Media Komputindo. Jakarta 2008.

[16] Supriadi, Yuniar, Adobe Photoshop CS3 Untuk Segala Tingkat, Elex Media Komputindo. Jakarta 2009.

[17] Susila, Candra Budi, Laporan Kerja Praktik, Media Pembelajaran Interaktif Pengenalan Huruf Hijaiyah Pada Taman Kanak-Kanak (TK) Pertiwi Kecamatan Pacitan, Surakarta 2011.

[18] Syamsudin, Deddy, Tutorial 3D max CHIP CD Indonesia. 2005-2006.

[19] Undang-Undang Republik Indonesia, No.9 Tahun 1990, Jakarta 18 Oktober 1990

[20] Vaughan, Tay, Multimedia Making It Work Edisi 6, Penerbit Andi. Yogyakarta 2006.

[21] Wiradinata, Gilang, Desain Interior Dengan 3Ds Max 2009, Penerbit Andi. Yogyakarta 2009.

[22] Gerbang Emas, Bangun Monumen Jejak Panglima Besar, Pacitan 2008

Spatial-Temporal Variations of Turbidity and Ocean Current Velocity of the Ariake Sea Area, Kyushu, Japan Through Regression Analysis with Remote Sensing Satellite Data

Kohei Arai
Graduate School of Science and Engineering
Saga University
Saga City, Japan

Yuichi Sarusawa
Graduate School of Science and Engineering
Saga University
Saga City, Japan

***Abstract*—Regression analysis based method for turbidity and ocean current velocity estimation with remote sensing satellite data is proposed. Through regressive analysis with MODIS data and measured data of turbidity and ocean current velocity, regressive equation which allows estimation of turbidity and ocean current velocity is obtained. With the regressive equation as well as long term MODIS data, turbidity and ocean current velocity trends in Ariake Sea area are clarified. It is also confirmed that the negative correlation between ocean current velocity and turbidity.**

Keywords—turbidity; ocean current; remote sensing satellite; regressive analysis

I. Introduction

There are strong scientific demands on estimation of environmental situations including water quality of the ocean. Primary productivity, ocean disaster such as red tide, ocean pollution and ocean water quality monitoring is getting much important in conjunction of global environmental issues. This paper deals with water quality, in particular, Suspended Solid: SS related turbidity and ocean current. There are some proposed methods with remote sensing satellite data for SS estimation while not so many method is proposed for ocean current velocity estimation. The method proposed here is based on regressive analysis. Regressive analysis based SS estimation method is conventional method. Also ocean current velocity estimation method proposed here is based regressive analysis.

Recently, the Ariake Sea environment is getting worth. Red tide occurrence is getting much frequent together with scale of the red tide. There are some evidences which indicate increasing of the Ariake Sea transparency. In the meantime, ocean current velocity of the Ariake Sea is decreasing. Most of these evidences are based on the measured data with research vessels. Namely, these data are obtained along with research vessels' routes. On the other hands, remote sensing satellite data derived turbidity, ocean current velocity is essentially acquired with area based measurements. Therefore, it is possible to cover almost whole Ariake Sea area at once. This is the greatest advantage of the satellite based measurements. Furthermore, it is also possible to monitor these situations repeatedly for a long time period by using remote sensing satellite data. Thus seasonal changes and long term trend of turbidity or transparency and ocean current velocity of the Ariake Sea can be clarified.

The following section describes the method for estimation of turbidity and ocean current velocity followed by some experimental data. Then conclusion is described with some discussions.

II. Regression Based Methods for Turbidity and Ocean Current Velocity Estimations

A. Regression Based Method

Regression based approach is, generally, expressed as follows,

$$Turb' = \alpha * [L_w(667)]_N + \beta \quad (1)$$

where Turb' denotes turbidity while $L_w(667)_N$ denotes water leaving radiance at 667nm of observation center wavelength of the spectral band. Atmospheric contribution is dominant for the acquired water leaving radiance so that the atmospheric corrected $L_w(667)_N$ is used for the experiments. There are MODIS Ocean Products including atmospheric corrected water leaving radiance which are provided by NASA/GSFC. On the other hands, α and β are regressive coefficients. These coefficients are obtained through regressive analysis which minimizing the following,

$$E^2 = \sum (y_i - \hat{y}_i)^2 = \sum (y_i - a - bx_i)^2 \quad (2)$$

where a and b are regressive coefficients x and y are $L_w(667)_N$ and turbidity, respectively. If the following equation can be assumed,

$$\frac{\partial E}{\partial b} = \frac{\partial E}{\partial a} = 0 \quad (3)$$

then the coefficients are determined as follows,

$$b = \frac{\sum (x_i - \bar{x})(y_i - \bar{y})}{\sum (x_i - \bar{x})^2}, a = \bar{y} - b\bar{x} \quad (4)$$

where $\bar{x}, \bar{y}$ denote means of $L_w(667)_N$ and turbidity, respectively.

B. Remote Sensing Satellite Data Used

As aforementioned, MODIS onboard Terra and Aqua satellites is the most appropriate mission instrument. The MODIS swath width is wide enough for the Ariake Sea together with Instantaneous Field of View: IFOV. Also MODIS has 36 spectral channels which are suitable for estimation of turbidity and ocean current velocity. Table 1 shows the spectral channels of MODIS.

TABLE I. SPECTRAL CHANNELS OF MODIS

Primary Use	Band	Bandwidth[1]
Land/Cloud/Aerosols Boundaries	1	620 - 670
	2	841 - 876
Land/Cloud/Aerosols Properties	3	459 - 479
	4	545 - 565
	5	1230 - 1250
	6	1628 - 1652
	7	2105 - 2155
Ocean Color/ Phytoplankton/ Biogeochemistry	8	405 - 420
	9	438 - 448
	10	483 - 493
	11	526 - 536
	12	546 - 556
	13	662 - 672
	14	673 - 683
	15	743 - 753
	16	862 - 877
Atmospheric Water Vapor	17	890 - 920
	18	931 - 941
	19	915 - 965

IFOV are different by spectral channels, 250m for channels 1 and 2, 500m for channels 3 to 7 and 1000m for the rest of channels. Therefore, all the ocean products are defined as 1000m IFOV of products. On the other hands, the size of the Ariake Sea is 30km by 100km so that 1km IFOV of ocean products would be enough.

C. Trith Data Used

Match-up data between MODIS and truth data of turbidity which are obtained at the Saga University Observation Tower which is situated at the (33.1001147 North, 130.273915 East) are collected for three months during from June to August 2010. Figure 1 shows the Google map of the Ariake Sea which is situated in Kyushu, Japan. Figure 1 also shows the location of Saga University Observation Tower. Turbidity is measured with electro-magnetic wave scattering radiance at the sea surface at the observation tower. Through a comparison with Holmagen standard liquid, the measured turbidity is calibrated. The unit of turbidity is FTU.

Table 2 shows the list of the data of the dates of turbidity measurements (Turb), the water leaving radiance in unit of $mW/cm^2/str/um$ at the four different channels which a\has the center wavelength, 412, 443, 531, and 667 nm.

Fig.1. Google map of the Ariake Sea and the location of Saga University Observation Tower

TABLE II. MATCH-UP DATA BETWEEN MODIS AND TRUTH DATA OBTANIND AT THE SAGA UNIVERSITY TOWER FOR JUST THREE MONTHS FROM JUNE TO AUGUST 2010.

Date	412	443	531	667	Turb
2010/06/02 11:00	0.5549	0.758	1.6932	0.5243	3.2
2010/06/03 12:00	0.697	0.7029	1.5953	0.5707	3
2010/06/09 11:00	0.8175	1.0853	2.0067	0.7259	7.7
2010/07/20 11:00	0.2687	0.3801	1.3053	0.5695	7
2010/07/20 14:00	0.3707	0.3684	0.7593	0.2527	4.1
2010/07/21 13:00	0.4012	0.2148	0.6054	0.1987	4.9
2010/07/22 13:00	0.7987	1.0449	1.984	0.9338	4.5
2010/07/23 13:00	1.0671	1.3122	2.3904	1.4277	10.3
2010/8/6 11:35	0.7874	0.5541	1.2454	0.5381	2.7
2010/8/6 13:10	0.5967	0.5353	1.1487	0.4942	3.1
2010/8/18 13:35	0.5477	0.513	1.0888	0.453	2.5
2010/8/19 11:00	0.6398	0.727	1.7675	0.8588	3.6
2010/8/21 10:50	0.2006	0.2884	0.936	0.2832	2.4
2010/8/21 14:00	0.3947	0.5356	0.9892	0.2442	2.4
2010/8/22 13:10	0.8374	0.8131	1.4261	0.6707	3.6
2010/8/23 13:55	0.5518	0.6825	1.5094	1.0073	11.4
2010/8/25 13:40	0.6758	0.866	1.7356	1.1435	11.9

III. EXPERIMENTS

A. Results from Regressive Analysis

The Pearson's correlation coefficient is defined as equation (5). Using the aforementioned match-up data, correlation coefficients are evaluated for the different spectral channels of MODIS. Table 3 shows the results. The correlation coefficient

of 667nm wavelength channel is greatest followed by 531, 443, and 412nm of wavelength channels as shown in Figure 2.

$$R = \frac{S_{xy}}{\sqrt{S_{xx}S_{yy}}},$$
$$S_{xx} = \sum_{i=1}^{N}(x_i - \bar{x})^2,$$
$$S_{yy} = \sum_{i=1}^{N}(y_i - \bar{y})^2,$$
$$S_{xy} = \sum_{i=1}^{N}(x_i - \bar{x})(y_i - \bar{y}) \quad (5)$$

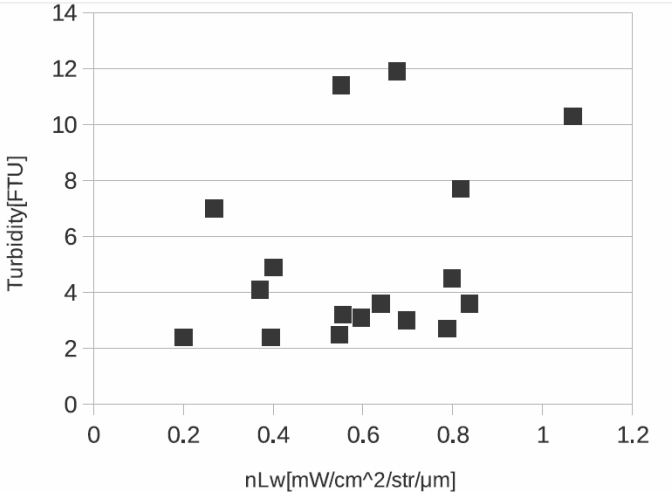

(a)412nm

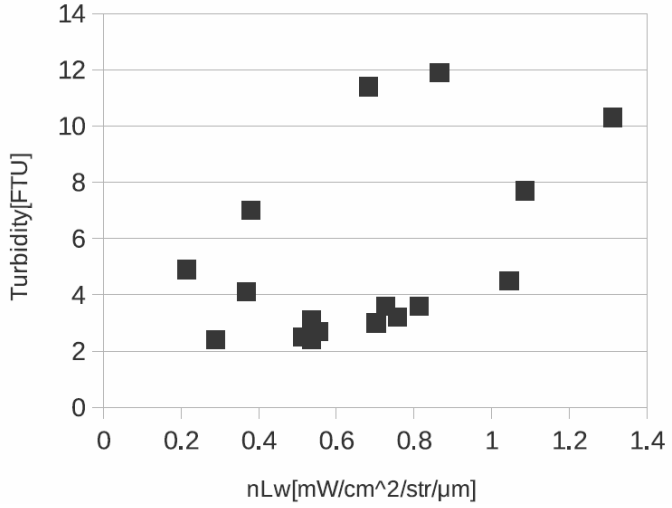

(b)443nm

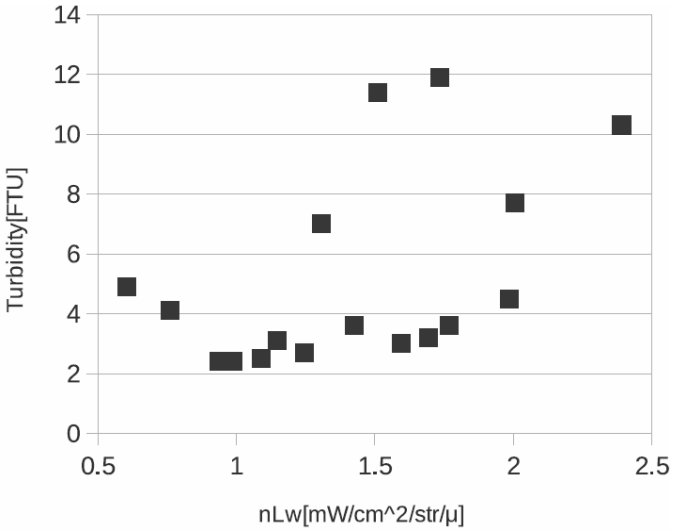

(c)531nm

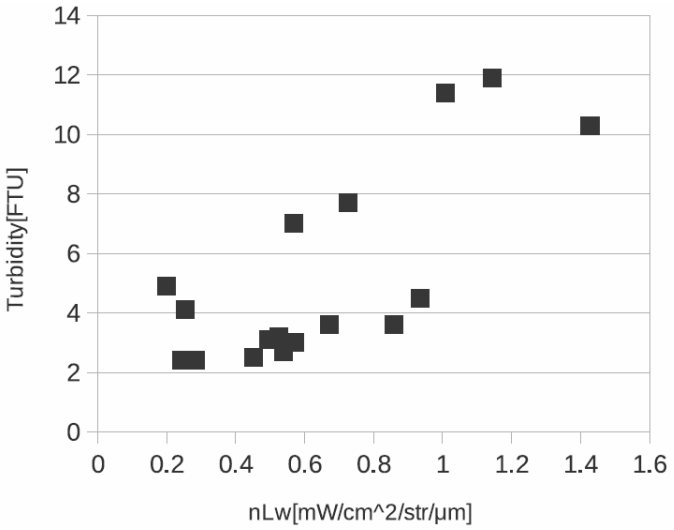

(d)667nm

Fig.2. Relations between turbidity and water leaving radiance derived from MODIS

TABLE III. CORRELATION COEFFICIENT FOR EACH WAVELENGTH BAND

	412	443	531	667
R	0.29882	0.47335	0.49884	0.74805

Therefore, regressive analysis between turbidity and water leaving radiance at 667nm is conducted based on equation (1). The result is shown in equation (6).

$$Turb' = 7.0948 * [L_w(667)]_N + 0.6463 \quad (6)$$

B. *Correlation Coefficient Between Turbidity and MODIS Based Water Leaving Radiance*

Possible reason for this is shown in Figure 3. In accordance with increasing of SS, reflectance at 667nm is decreased.

The variance of the reflectance at 667nm is greatest followed by 531, 443, and 412nm of wavelength channels.

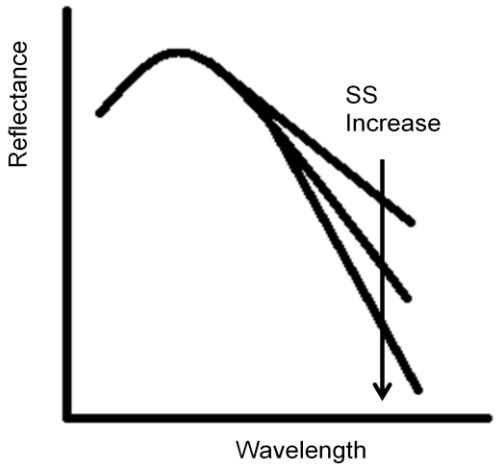

Fig.3. Illustrative view of spectral reflectance for the different suspended solid concentrations.

C. Ocean Current Velocity

In the same time as turbidity data is acquired at Saga University Observation Tower, other fundamental observation items are measured including ocean current velocity. In particular, it is known that ocean current velocity is proportional to turbidity. In order to confirm this fact, regressive analysis is made for ocean current velocity. Figure 4 shows the relation between turbidity and logarithmic function of ocean current velocity.

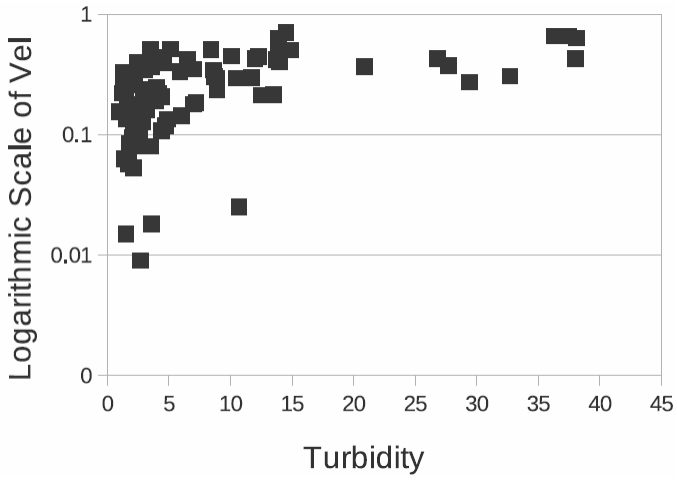

Fig.4. Relation between turbidity and logarithmic function of ocean current velocity

Positive correlation between turbidity and ocean current velocity then is confirmed. From the regressive analysis, the following equation is obtained with Root Mean Square Error: RMSE of 0.1266.

$$Vel' = 0.109095 * \ln(Turb') + 0.095643 \quad (7)$$

Thus turbidity and ocean current velocity of the Ariake Sea area can be estimated with the atmospheric corrected MODIS data.

D. Examples of Estimated turbidity and Ocean Current Velocity

Using the atmospheric corrected MODIS data of the Ariake Sea area of 2004 and 2006 (which is shown in Table 4), spatio-temporal variations of turbidity and ocean current velocity are estimated. Figure 5 shows the estimated turbidity and ocean current velocity.

TABLE IV. MODIS DATA USED FOR ESTIMATION OF TURBIDITY AND OCEAN CURRENT VELOCITY

2004-fh:Turbidity	2010-fh:Turbidity	2004-fh:Velocity	2010-fh:Velocity
T2004030021000	T2010055020500	A2004031042500	T2010026023500
T2004041015000	T2010098014500	A2004047042500	T2010055020500
T2004044022000	T2010137015000	A2004049041500	T2010098014500
T2004046021000	T2010160015500	A2004086043000	T2010137015000
A2004031042500	A2010017042000	A2004088042000	T2010154023500
A2004047042500	A2010026041000	A2004091045000	T2010160015500
A2004100044500	A2010054043500	A2004100044500	A2010017042000
A2004116044500	A2010093044000	A2004116044500	A2010026041000
A2004157044000		A2004157044000	A2010052045000
		T2004030021000	A2010054043500
		T2004041015000	
		T2004044022000	
		T2004046021000	
		T2004096015500	
		T2004119020500	

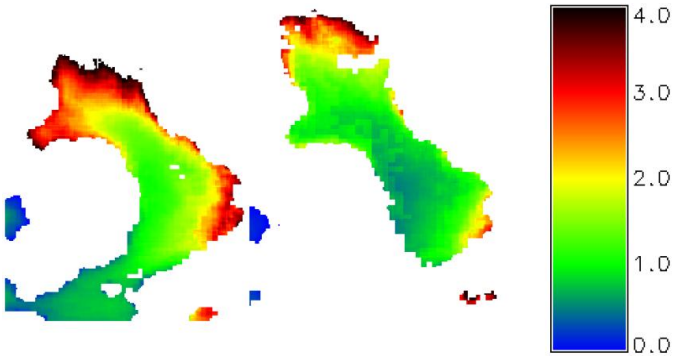

(a)Turbidity in 2004 (b)Turbidity in 2006

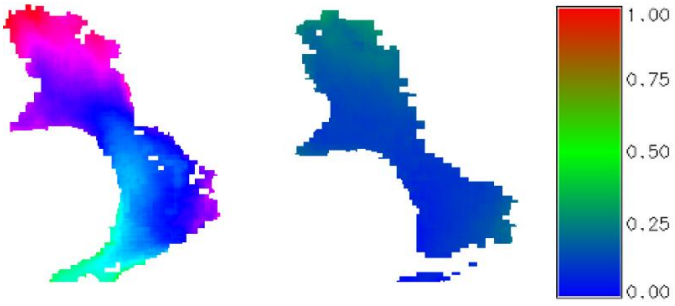

(c)Velocity in 2004 (d)Velocity in 2006

Fig.5. Example of the estimated turbidity and ocean current velocity of the Ariake Sea area in 2004 and 2006

E. Trend Analysis of Turbidity and Ocean Current Velocity

Trend analysis of turbidity and ocean current velocity, then can be done with the atmospheric corrected MODIS data. Figure 6 shows the result from the trend analysis for 12 years

starting from 2000 to 2011. Meanwhile, annual mean of turbidity is shown in Figure 7 together with its linear approximated trend in 12 years. From the trend, it is found that the linear approximation function is expressed in equation (8) with R square value of 0.58.

$$f(x) = -0.05x + 2.78 \quad (8)$$

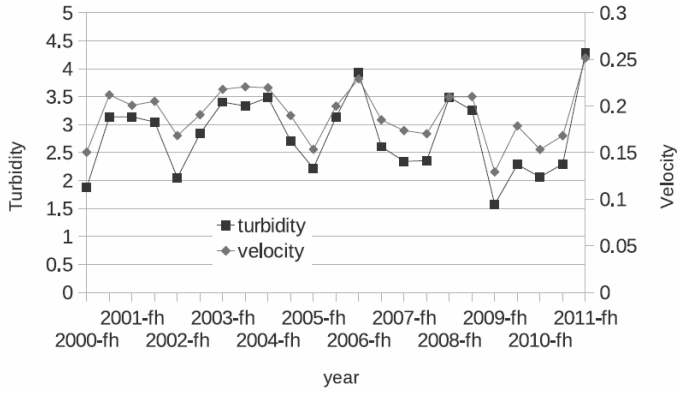

Fig.6. Result from the trend analysis for 12 years starting from 2000 to 2011

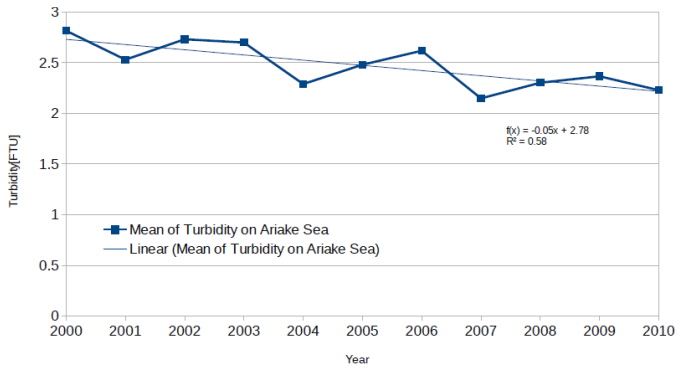

Fig.7. Annual mean of turbidity and its linear approximation function

F. Spatial Variation of Turbidity

Bi-annual mean of turbidity of the Ariake Sea during from 2000 to 2010 is shown in Figure 8. In particular, turbidity of the Shiranui Sea areas and further southern portion of areas is getting decreases during from 2000 to 2004, and gradually increased during from 2004 to 2006.

After that, it is getting decreases again during 2006 to 2010 (much severely in 2010 and the after. In other words, transparency of such areas is getting large results in photosynthesis in the Ariake Sea areas is getting much active.

In accordance with increasing of photosynthesis activity, phytoplankton is increases together with zoo plankton results in increasing of red tide occurrences. Also it is recognized that the turbidity of the areas just above the Isahaya Sea areas and northern portion of sea areas is getting decreases. Therefore, it can be said that one of the causes of the increasing red tide occurrence in the Shiranui Sea areas and the Ariake Sea areas must be decreasing of ocean current (decreasing of turbidity).

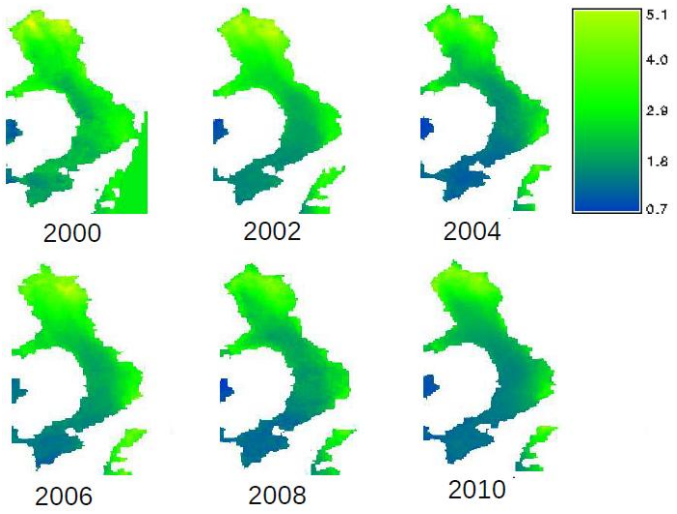

Fig.8. Bi-annual mean of turbidity of the Ariake Sea during from 2000 to 2010

IV. CONCLUSION

Regression analysis based method for turbidity and ocean current velocity estimation with remote sensing satellite data is proposed. Through regressive analysis with MODIS data and measured data of turbidity and ocean current velocity, regressive equation which allows estimation of turbidity and ocean current velocity is obtained. With the regressive equation as well as long term MODIS data, turbidity and ocean current velocity trends in Ariake Sea area are clarified. It is also confirmed that the negative correlation between ocean current velocity and turbidity

Also it is found that phytoplankton is increases together with zoo plankton results in increasing of red tide occurrences in accordance with increasing of photosynthesis activity. Also it is recognized that the turbidity of the areas just above the Isahaya Sea areas and northern portion of sea areas is getting decreases. Therefore, it can be said that one of the causes of the increasing red tide occurrence in the Shiranui Sea areas and the Ariake Sea areas must be decreasing of ocean current (decreasing of turbidity).

ACKNOWLEDGMENT

The authors would like to thank Dr. Toshiya Katano of Saga University for his great effort to provide Saga University Observation Tower's data and discussions we have had during this research.

REFERENCES

[1] S.Yamagata, K. Sakurada, N. Koyama, R. Itoyasma, Long term trend of water quality in Ariake, Yatsushiro Sea, Yusui Report, No.16, 2008.

[2] Y. Shimizu, K.Yamada, Long term transparency raising trend of Ariake Sea, and relation to red tide occurrence, Oceanography in Japan, 17, 337-356, 2008.

[3] S.Yamamoto, T.Ozu, T.Shimomai, S.Nonohara, Y.Sakuno, Estimation of turbidity distribution in Lake Shinji, Nakaumi using MODIS data, LANGUNA, 14, 57-68, 2007.

[4] Howard R. Gordon, Kenneth J. Voss,"MODIS Nor-malized

[5] Waterleaving Radiance Algorithm Theoret-ical Basis Document (MOD18) Version 5", University of Miami, 2004

[6] J. Clerk Maxwell, A Treatise on Electricity and Magnetism, 3rd ed., vol. 2. Oxford: Clarendon, 1892, pp.68–73., 2004.

AUTHORS PROFILE

Kohei Arai, He received BS, MS and PhD degrees in 1972, 1974 and 1982, respectively. He was with The Institute for Industrial Science, and Technology of the University of Tokyo from 1974 to 1978 also was with National Space Development Agency of Japan (current JAXA) from 1979 to 1990. During from 1985 to 1987, he was with Canada Centre for Remote Sensing as a Post Doctoral Fellow of National Science and Engineering Research Council of Canada. He was appointed professor at Department of Information Science, Saga University in 1990. He was appointed councilor for the Aeronautics and Space related to the Technology Committee of the Ministry of Science and Technology during from 1998 to 2000. He was also appointed councilor of Saga University from 2002 and 2003 followed by an executive councilor of the Remote Sensing Society of Japan for 2003 to 2005. He is an adjunct professor of University of Arizona, USA since 1998. He also was appointed vice chairman of the Commission "A" of ICSU/COSPAR in 2008. He wrote 30 books and published 332 journal papers

Transmission Control for Fast Recovery of Rateless Codes

Jau-Wu Huang
Department of Computer Science
National Tsing Hua University
Hsinchu, Taiwan

Kai-Chao Yang, Han-Yu Hsieh, Jia-Shung Wang
Department of Computer Science
National Tsing Hua University
Hsinchu, Taiwan

***Abstract*—Luby Transform (LT) codes are more important in communication applications due to the characteristics of fast encoding/decoding process, and low complexity. However, LT codes are optimal only when the number of input symbols is close to infinity. Some researches modified the degree distribution of LT codes to make LT codes suitable for short symbol length. In this article, we propose an optimal coding algorithm to recover all of the encoded symbols for LT codes quickly. The proposed algorithm observes the coding status of each client and increases the coding performance by changing the transmission sequence of low-degree and high-degree encoding packets. Simulation results show that the resulting decoding overhead of our algorithm are lower than the traditional LT codes, and our algorithm is very appropriate to server various clients in the broadcasting channel environment.**

Keywords*—LT codes; broadcasting channel; degree distribution

I. INTRODUCTION

Due to the rapid development of embedded system and wireless communication, smart phones and tablet computer are widely used by people. Many multimedia applications, online video and TV, are delivered in the broadcasting channel. Nevertheless, the network traffic loads are change frequently and unpredictably, the channel errors and loss are very serious. Some data acknowledgement and retransmission methods such as Automatic Repeat Request (ARQ) scheme and Forward Error Correction (FEC) codes are proposed to alleviate the problem of data packet loss. However, these methods will incur additional overhead that includes data retransmission and add redundancy into the original data. They cannot correctly decode the source data when the packet loss rate is large.

Another method, rateless codes, is proposed to solve the problem of data packet loss. Rateless codes can infinitely generate unique packets from a given set of source data. As long as the encoding packets with the size just slightly larger than the number of source blocks can be received, the original source data can be fully recovered. Rateless codes include Luby Transform (LT) codes [1], Raptor codes [2], and Online codes [3]. LT codes are the most popular full realization of rateless codes. The encoding process of LT codes is to perform XOR operations on randomly chosen d of k source data according to Robust Soliton Distribution (RSD). On the decoding side, If the original data consists of k input symbols, any encoding packet can be generated on average by $O(\ln(k/\delta))$ symbol operations. LT codes can recover k input symbols from any $k+O(\sqrt{k}\ln^2(k/\delta))$ of the encoding packets with probability $(1-\delta)$ by on average $O(k \cdot \ln(k/\delta))$ symbol operations. Therefore, the encoding and decoding processes are very simple and fast. Due to the advantages of easy implementation, low complexity, and rateless encoding, LT codes have been widely adopted, such as the Third Generation Partnership Project (3GPP) [4] and Digital Video Broadcasting (DVB) [5].

The objective of our work is to keep the features of LT codes, reduce overhead of LT codes in short block length, and serve majority of clients first to fully decode source data as soon as possible. Compare to LT codes, the proposed method has better intermediate performance and low decoding complexity than traditional LT codes. Consequently, the proposed method is more appropriate to implement on the real-time decoders, such as mobile phone with strictly delay time constrained.

The rest of the article is organized as follows. We discuss some related works in Section II. We describe our proposed method. In Section III, we describe our proposed method. Simulation results and the discussions are given in Section IV. Finally, the conclusion and future work will be given in Section V.

II. RELATED WORK

In 2006, Kamra et sl. [6] proposed growth codes that increase the data persistence of sensor network. In growth codes, the encoder gradually increases the degree of encoded packets according to z, the ratio of number of decoded symbols at the receiver to number of input symbols, such that each delivered packet has the highest probability of decoding the source symbol at the receiver. That is to say, the degree distribution is adjusted depending on the number of symbols received by the receiver. The drawback of growth codes is that the assumption requires several feedbacks from the receiver.

In 2007, Sanghavi [7] presented the first paper to solve the problem of intermediate performance of rateless codes. The author divides the percentage of received coded symbols into three regions. The first region is $z \in [0, 1/2]$ and the optimum degree distribution has degree-one packets only. The second region is $z \in [1/2, 2/3]$ and the optimum degree distribution has degree-two packets only. The optimal degree distribution for the third region $z \in [2/3, 1]$ is unknown, but the author presented an upper bound. However, the optimum degree distribution are asymptotic, they could not perform well in the practical applications with message of finite length. In 2009,

Talari et al. [8] defined the packet recovery rates at three values of *z* as the conflicting objective functions and employ NSGA-II multi-objective genetic algorithms optimization method to find several degree distributions with optimum packet recovery rates. They also propose degree distributions for both cases of message with finite and infinite (asymptotic) length.

In 2009, Kim et al. [9] proposed rateless codes that have both good intermediate performance and capacity-achievability property. Their proposed codes are generated in a similar manner as growth codes [6]; however, from a capacity-achieving degree distribution in order to be able to recover all message symbols from a minimal number of received encoding symbols. In 2011, Bioglio et al. [10] proposed Optimal Partial Decoder (OPD) that is the first optimal partial decoding algorithm for rateless codes, and furthermore analyzed its decoding complexity. OPD is an incremental decoding algorithm that spreads the decoding process during all the symbols reception and starts to decode as soon as the first coded symbol is received.

In 2010, Yang et al, [11] proposed approximate LT codes that still follow the Soliton Distribution of LT codes. The proposed codes are driven by a receiver-aware control policy, which monitors the receiving status and improves the coding performance of short data block length by rearranging low-degree and high-degree encoding packets sent to receivers. With the proposed approximate LT codes can introduce lower decoding overhead, graceful quality degradation over a wide range of channel loss rates, and unequal error protection property.

III. PROPOSED METHOD

A. LT Codes

The encoding process of LT codes contains two phases. First, a bipartite coding graph is decided. Second, encoding packets are generated by performing XOR operations. In the bipartite coding graph, one side is input symbols, and the other side is encoding packets. The edges between input symbols and encoding packets are randomly generated according to the Robust Soliton Distribution.

The Robust Soliton Distribution is based on two distributions proposed in [1]: the Ideal Soliton Distribution $\rho(1), \ldots, \rho(k)$

$$\rho(1) = 1/k$$
$$\text{For all } i = 2, \ldots, k, \ \rho(i) = 1/i(i-1).$$

and the distribution $\tau(i), \ldots, \tau(k)$

$$\tau(i) = R/ik \quad \text{for } i = 1, \ldots, k/R - 1$$
$$\tau(i) = R\ln(R/\delta)/k \quad \text{for } i = k/R$$
$$\tau(i) = 0 \quad \text{for } i = k/R + 1, \ldots, k$$

where $R = c \cdot \ln(k/\delta)\sqrt{k}$ for some suitable constant $c > 0$, and δ is the maximum decoding failure probability.

Add the Ideal Soliton Distribution $\rho(i)$ to $\tau(i)$ and normalize it, the Robust Soliton Distribution $\mu(i)$ can be obtained, and its spike is at $i = k/R$.

TABLE I. ENCODING ALGORITHM

```
Encoding algorithm (at Server):
1.  FOR i = 1 TO N
2.     Compute the numbers of received ACK1, ACK2 and
3.     Fully_Decoded respectively.
4.   IF (((NUM_ACK2 - NUM_Fully_Decoded) / (NUM_Total_Client -
5.     NUM_Fully_Decoded)) >= 0.5) OR ((Previous Mode ==
6.     Highest_Mode) AND (NUM_ACK2 - NUM_Fully_Decoded) != 0)
7.        Use Robust Soliton Distribution to generate a packet with degree
8.                        d bigger than Spike-1
9.          NUM_Highest_Mode++
10.    ELSE IF ((NUM_ACK1 - NUM_Fully_Decoded) /
11.              (NUM_Total_Client - NUM_Fully_Decoded) >= 0.5)
12.               Use Robust Soliton Distribution to generate a packet with
13.                 degree d in the range [5,Spike-1]
14.               NUM_High_Mode++
15.             ELSE
16.                  Use  Robust Soliton Distribution to generate packet
17.                  with degree d packet in the range [1,4]
18.                NUM_Low_Mode++
19.    Perform XOR operation on the packet with degree d
20.    Send the packet to all Clients
21.  END FOR
```

TABLE II. DECODING ALGORITHM

```
Decoding algorithm (at Client):
1.  WHILE receiving a new encoding packet
2.     DO the pure LT decoding process
3.        IF (number of decoded input symbols / number of input
4.           symbols) >= Low_Threshold
5.           Send ACK1 to Server
6.        IF ( number of decoded input symbols / number of input
7.           symbols)) >= High_Threshold
8.           Send ACK2 to Server
9.        IF ( number of decoded input symbols == number of input
10.          symbols)
11.          Send Fully_Decoded to Server
```

When generate the i^{th} encoding block, we first decide its degree d_i according to the Robust Soliton Distribution $\mu(i)$. Next, d_i input symbols are randomly selected. An XOR operation is performed on these d_i input symbols to generate a new encoding packet. This encoding process can be infinitely repeated to form the rateless codes.

In the decoder side, the input symbols can be recovered by using the Belief Propagation (BP) decoder. The decoder has to reconstruct the coding graph. The degree-one encoding blocks are first decoded by duplication.

Then, all edges connecting to the recovered input blocks are removed. By iteratively decoding degree-one encoding blocks and removing the edges connecting to recovered input symbols. The decoder receives $n = (1 + \varepsilon)k$ from potentially unlimited number of encoding packets can fully decode source symbols, and the constant ε is the code overhead. The number of encoding packets generated can be determined on the fly. k input symbols are used to generate $n - k$ redundant symbols for a total of n encoding symbols, and the rate of the code is k/n.

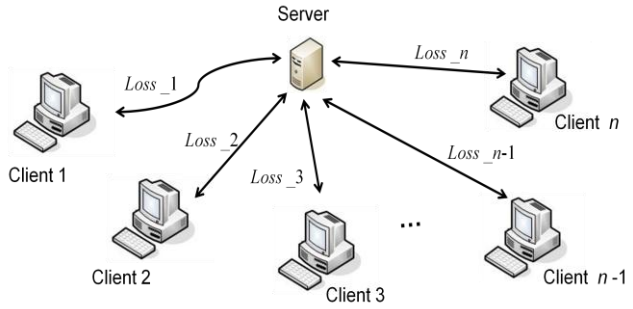

Fig. 1. The broadcasting simulation environment.

B. Rateless Control Policy

In Ideal Soliton Distribution, over 75% of encoding packets have degrees less than four. We call these packets with degree-one, degree-two, degree-three, and degree-four as "low-degree." High-degree packet includes the degree number from five to spike-1. Highest-degree packet includes the degree number more than spike, *k/R*.

Owing to the LT decoding sequence, degree-one encoding packets will be decoded earliest. Therefore, at the beginning of decoding process, low-degree encoding packets are more useful than high-degree ones, clients can easily recover most of source data. However, after most source data blocks are recovered, remaining source data blocks are more likely to be recovered from high-degree packets because high-degree packets contain more information of source data blocks. Thus low-degree packets are more important at the beginning of decoding process, but they are less important after most source data blocks have been recovered. Similarly, high-degree packets are more important than low-degree ones at the latter of decoding process.

The server tries to satisfy the need of the clients and help them to fully decode the entire source data as soon as possible. We propose a three-mode control policy that generates and transmits low-degree, high-degree and highest-degree packets depending on the client decoding conditions. In the low-degree mode, the server generates low-degree encoding packets. In high-degree mode, the server generates high-degree encoding packets.

In highest-degree mode, the server generates highest-degree encoding packets. When the client receives packets from the server, each client will send two ACKs to acknowledge the sever its current decoding status. If the client decodes over *Low_Threshold* percentage of source data, it sends an ACK1 to acknowledge the sever. If the client further decodes over *High_Threshold* percentage, it sends another ACK2 to the server. The objective of these two threshold values is to let the server know the decoding status of each client. In the broadcasting channels, the server collects the ACKs, ACK1 and ACK2, sent by clients and then decides to transmit which types of encoding packets in the next stage. If the majority of clients decodes only few source data, the server continue generate more low-degree encoding packets. If one half of the clients have already decoded over *Low_Threshold* percentage, we set to 60%, the server generates high-degree encoding packets. If one half of clients have decoded over

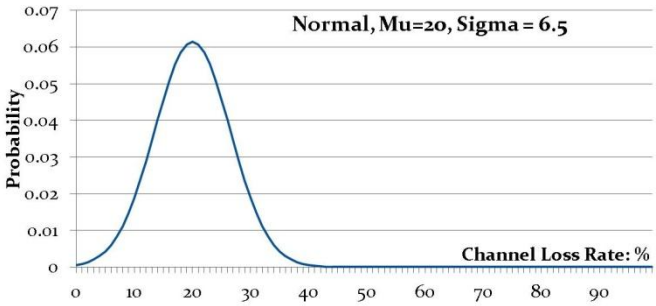

(a)

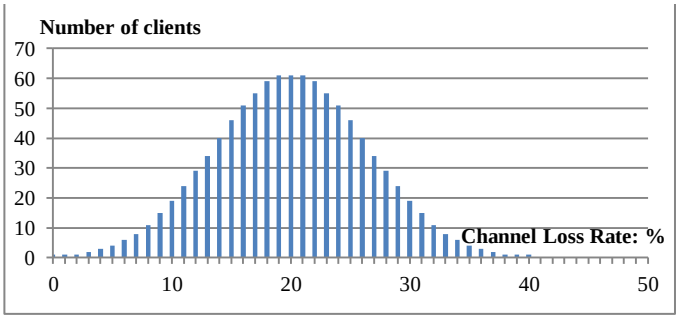

(b)

Fig. 2. (a) The probability density function of channel loss rate. (b) The number of clients for each channel loss rate.

High_Threshold percentage, we set to 90%, the server transmits highest-degree encoding packets. By doing so, the server can help the majority of clients to fully decode the entire source symbols as early as possible.

TABLE I and TABLE II show the encoding and decoding algorithms of our proposed method, respectively. Note that we assume that the number of total clients, NUM_Total_Client, is equal to 1000. In the encoding process, there are three modes, including Low_Mode, High_Mode, and Highest_Mode.

IV. Simulation Results

In this section, the performance of the proposed method is compared with LT codes.

We assume that 1000 clients are concurrently severed by a server in the broadcast channel. Fig. 1 shows the broadcasting simulation environment. The possible channel loss rate for each client can somehow be modeled by a probability density function. We adopt a Normal Distribution as shown in Fig. 2(a) to approximate the channel loss rate model, and the number of clients for each channel loss rate is as shown in Fig. 2(a). As we can see in Fig. 2(b), there is only one single client under zero loss rate channel condition, and also only one single client under 40% channel loss rate. Most of the clients are under rather moderate average 20% channel loss rate. Many applications are sensitive to delay-time-constraint so as to require short data block length in practice. We therefore apply the short data block length to evaluate the performance of proposed codes in comparison with LT codes. The length of source data k is 660, and we set the constant $c = 0.086$, $\delta = 0.5$ in Robust Soliton Distribution for LT codes. The parameters *Low_Threshold* and *High_Threshold* are set to 60% and 90%.

We consider the channel lost rate model with μ = 10%, 20%, and σ = 3.5, 6.5.

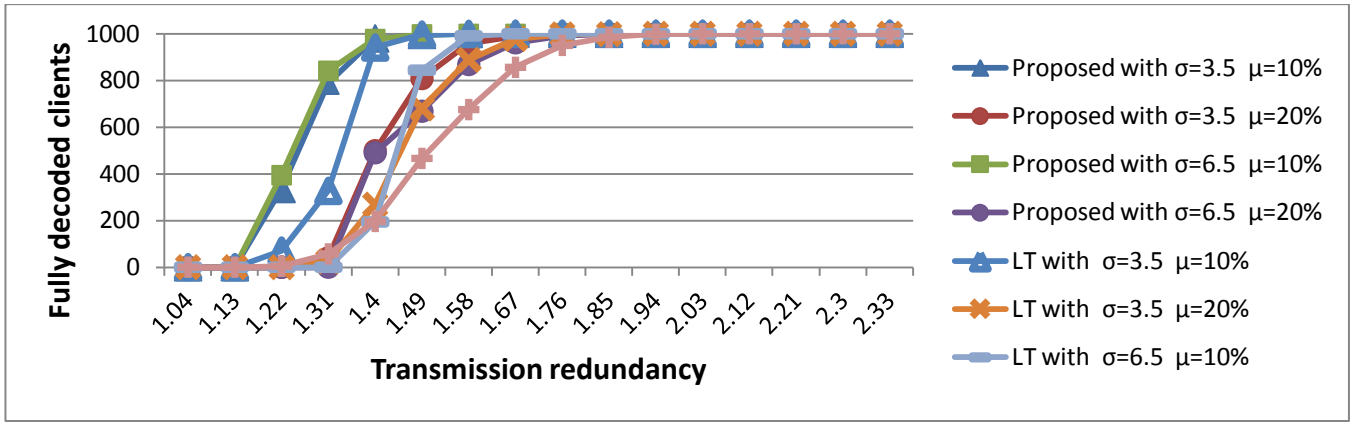

Fig. 3. Number of fully decoded clients at different transmission redundancy in broadcasting applications.

In broadcasting channel, Fig. 3 shows the number of fully decoded clients at different transmission redundancy in broadcasting applications. Transmission redundancy is denoted as the number of transmitted encoding packets divided by *k*. Simulation result reveals that our propose method overpass LT codes, we have lower transmission redundancy than LT codes. The best performance of all simulation combinations is our proposed method with μ = 10% and σ = 6.5. The less loss rate, the lower transmission redundancy. With the proposed method, we can help over 97% of clients to decode all the source data at transmission redundancy 1.40.

However, LT codes need almost double overhead to achieve these. It is because through the ACKs from clients and voting scheme, the server can be better aware of the decoding progress of the clients and always try best to serve the majority first to let them achieve fully-decoded as early as possible. The server collects the ACKs sent by clients and determines to generate low-degree, high-degree, and highest-degree encoding packets to satisfy the need of the majority of clients in the network. This is worth mentioning that LT codes are asymptotically optimal only for the number of source data tending to infinity; thus, when it comes to short source data block length, LT codes introduce higher decoding overhead.

We would like to determine the best mode-switching time according to the useless rate of the packet, hence we define the useless rate of a packet. When one client has already decoded all source data blocks, any packet that the server sent is useless.

Useless rate = number of useless packets / (number of total client – number of fully decoded client)

Fig. 4 shows that the useless rate of the packet using proposed method at μ = 10% and σ = 6.5. When the number of the transmitted encoding packets is lower than 680, the system is in low mode. Server generates and transmits the low degree packet to the client.

When the number of the transmitted encoding packets is equal to 680, over one half of clients have decoded over 60 percentages of source data, and then the system switches to high mode. Server starts to generate and transmit the high degree packet to the client. When the number of the transmitted encoding packets comes to 858, over one half of clients have decoded over 90 percentages of source data, and then the system switches to highest mode. Server starts to generate and transmit the highest degree packet to the client. When the number of the transmitted encoding packets comes to 951, the system switches back to low mode. Unfortunately, the useless rate of the transmitted packets gradually rise again, the system switches to high mode. The high useless rate is still high for some time. When the number of the transmitted encoding packets comes to 1194, the system switches to highest mode. Most of clients had decoded all of source data, so the useless rate of the transmitted encoding packets becomes almost zero. Finally, when the number of the transmitted encoding packets comes to 1253, the system switches to low mode, sever generates and sends low degree packets to the few clients that had not decoded completely. By observing the useless rate of the transmitted encoding packets, we can dynamically change mode-switching time.

In the point-to-point condition, we compare the proposed method with LT codes. Fig. 5 represents the average decoding probability of source symbols over 10,000 rounds at lost rate equaling 10% and 20%. Here decoding probability means the percentage of the source data that the client can recovered. The decoding probability increases smoothly at beginning, rapidly rises up in the middle, and again slowly increases toward one. Simulation result reveals that our propose method overpass LT codes, we have higher decoding probability than LT codes.

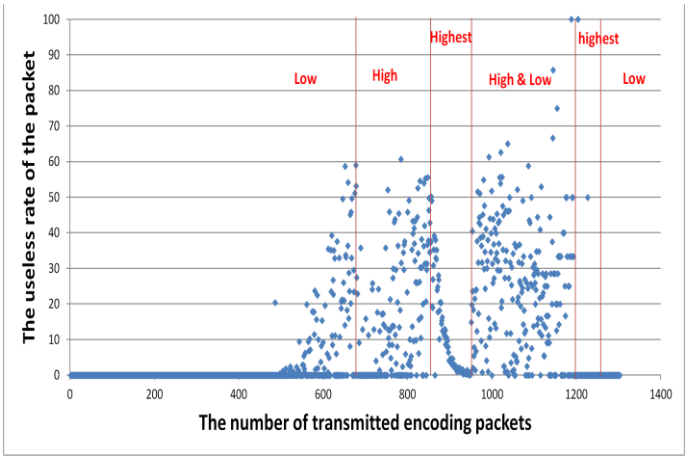

Fig. 4. The useless rate of the packet using proposed method at μ = 20% and σ = 6.5

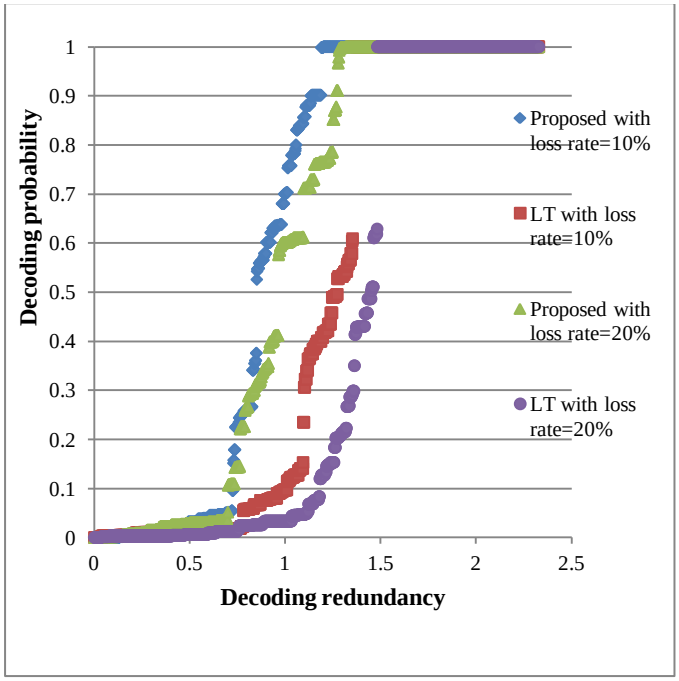

Fig. 5. Average decoding probability of a client using proposed method.

V. CONCLUSION

In this article, we proposed a three-mode control policy of rateless codes. The server can dynamically generate and transmit low-degree, high-degree and highest-degree packets to the client according to the decoding status of the client. Simulation results show that the resulting decoding overhead and useless packets rate of our proposed algorithm are lower than the traditional LT codes, and furthermore the proposed method also has better intermediate performance that LT codes. In the future, a more effective coding method and optimum degree distribution could be investigated. Besides, many multimedia applications on the handheld devices will introduce various control policies. These are worth to be further discussed and investigated.

REFERENCES

[1] M. Luby, “LT Codes,” in *Proc. of the 43rd Annual IEEE Symposium on Foundations of Computer Science* (*FOCS*), pp. 271-282, 2002.

[2] Amin Shokrollahi, "Raptor Codes," in *IEEE Transactions on Information Theory*, vol. 52, no. 6, pp. 2551-2567, 2006.

[3] P. Maymounkov, “Online codes,” NYU Technical Report TR2003-883, 2002.

[4] 3GPP TS 26.346 V6.1.0, Technical Specification Group Services and System Aspects; Multimedia Broadcast/Multicast Service; Protocols and Codecs, 2005.

[5] ETSI DVB TM-CBMS1167, IP Datacast over DVB-H: Content Delivery Protocols, Sept. 2005, draft Technical Specification, http://www.dvb.org.

[6] A. Kamra, V. Misra, J. Feldman, and D. Rubenstein, “Growth codes: Maximizing sensor network data persistence,” *ACM SIGCOMM Computer Communication Rev.*, vol. 36, no. 4, pp. 255–266, 2006.

[7] S. Sanghavi, “Intermediate performance of rateless codes,” *IEEE Information Theory Workshop*, pp. 478–482, Sep. 2007.

[8] A. Talari and N. Rahnavard, “Rateless codes with optimum intermediate performance,” *IEEE GLOBECOM* 2009, Dec. 2009.

[9] S. Kim and S. Lee, “Improved intermediate performance of rateless codes,” *ICACT* 2009, vol. 3, pp. 1682–1686, Feb. 2009.

[10] Valerio Bioglio, Marco Grangetto, Rossano Gaeta, and Matteo Sereno. An optimal partial decoding algorithm for rateless codes. *IEEE International Symposium on Information Theory*, pages 2731-2735, 2011.

[11] Kai-Chao Yang, Chun Lung Lin, Tung-Lin Wu, Jia-Shung Wang: “Service-Driven Approximate LT Codes.” *IEEE ICC* 2010: 1-5.

A Project Based CS/IS-1 Course with an Active Learning Environment

Dr. Suvineetha Herath*, Dr. Ajantha Herath*, Mr. Mohammed A.R. Siddiqui*, Mr. Khuzaima AH. El-Jallad*
*ACMSIG Teaching & Learning Group
University of Bahrain
Kingdom of Bahrain

***Abstract*—High level programming languages use system defined data types and the user defined data types in computations. We have developed a project-based CS/IS-1 course to substitute the traditional lecture based classroom to help students design and use at least two user defined data types in their computations to solve real world problems. Abstract data types and basic programming constructs are introduced efficiently to the students in an active learning environment using games. To assess and evaluate the changes made we distributed the course module among our students and other instructors. This paper describes our experience in developing the project based active learning environment.**

Keywords-I/O; arithmetic expressions; if-else and switch conditional operations; for-while iterative computation; inheritance; polymorphism; recursion; searching and sorting algorithms; IDE.

I. INTRODUCTION

The objectives of this course are to introduce computer science fundamentals using C++, provide the ability to design algorithms to solve problems and implement those using test and document programs. The course focuses on software engineering process and techniques. Student outcomes at the end of the course are shown below:

They will be able to:

1) Design, implement, test and document application programs of simple to moderate complexity that use two or more user defined types and variables, classes or abstract data types, and one main program.

2) Apply basic programming constructs such as sequence, selection, iteration, functions in complete, syntactically correct programs.

3) Communicate both technical and non-technical aspects of student's work in formal and informal settings.

4) Develop programs in multiple stages; use stubs to test the system as a whole; use drivers to carry out unit testing for functional components and for data abstractions.

5) Maintain a record of time devoted to the component tasks in the completion of programming projects.

There is both local and national need for high-quality trained programmers with the ability to learn in a short period of time and stay current with the information technology advances. Colleges can help to meet this demand by redesigning their programming courses allowing more students to succeed at the entry level. Successful application of active learning with rapidly changing technologies in the learning process is a way to remove the difficulties at entry level. Such changes will help the students to improve their skills. Consequently, both the public and private sectors will benefit with the greater number of highly-skilled trained programmers.

We identified many deficiencies in teaching a traditional lecture based CS/IS-1 class and the importance of transforming the course into a project based e-learning environment. The lecture based environment is relatively passive. In addition, we want to connect this class to other classes such as computer architecture, digital design, operating systems, security, parallel computing, and importantly the needs of industry. An effective computer programming class could provide these links. From our initial planning input we took actions to transform the course to a project based one and then collected results. Feedback from the action stage and results are used to improve the plan. We continuously improved the quality of instruction and actions while using the feedback received from the students, and took action to transform the course suitable for e-learning. A course with the features outlined above could help our students develop design skills in several different languages before their graduation.

The following sections outline the details of research model, actions taken, course plan, goals achieved, difficulties encountered, course assessment, plan for future work and summary.

II. RESEARCH MODEL

Over the years we have reviewed many textbooks and papers, and attended workshops and conferences [1-5]. We continuously improved our offerings by making changes to the course, collecting data and evaluating them, and using the feedback for further improvements. There are many good books published on C++ programming. Malik authored a very good book for this class and published the seventh edition by Cengage learning [2]. Gaddis' C++ programming with objects first, published by Pearson is also another very good book with many supplements for this class [3]. Deitel's C++ programming, published by Pearson is also another very good book with many supplements for this class [4]. Horstmann has also written a good C++ Programming book published by Wiley. Because of the simplicity and the clustered sets of programming examples and problems presented in the book we selected Liang's C++ programming second edition published by Pearson as the main text for our class [1].

At the beginning of this course we introduced number systems and simple game designs using binary numbers. Thereafter, we included random number generators and simulations with basic programming constructs as open and close project laboratories. We have integrated security-related concepts into the course. At the end, we incorporated modules to help the students understand the importance of parallelism in enhancing performance of sorting algorithms and its benefits as an application programmer, a systems programmer, an algorithm designer, and a computer architect.

Topics presented in this course include the implementation of basic programming constructs such as I/O, arithmetic expressions, if-else and switch conditional operations, for-while iterative computation controls, simple functions, classes, inheritance, polymorphism, recursion, searching and sorting algorithms. This course includes twenty eight lecture modules, fifteen hands-on project activities. Several examples of classroom activities are given below.

III. TRANSFORMATIONS-ACTIONS TAKEN

We have replaced the old text based programming style to Graphical User Interface (GUI). Students downloaded the free online and open software (FOSS) Code Blocks IDE from http://www.codeblocks.org/downloads/26/ to complete the project activities using Windows 7 operating system. [6]. The following paragraphs describe the projects assigned with sample solutions completed by the students from simple to moderate complexity.

A. Project 1:

The following code 1, depicts the first classroom project assigned to illustrate a simple vending machine. The goal of this particular activity is to introduce the concepts of cout, cin, << , >>, and simple arithmetic operations. Towards the end of the class this project is extended to demonstrate the design and the use of multiple classes.

```
#include <iostream>
using namespace std;

int main()
{
   int juice_money, cent_85, cent_1;
   cout << "This juice machine accepts Dollar bills.\n";
   cout << "How many dollars will you insert?\n";
   cin >> juice_money;

   // Find the number of 85 cent juice cans to be dispensed.
   cent_85 = 100 * juice_money / 85;

   // Find the number of pennies to be dispensed.
   cent_1 = 100 * juice_money % 85;

   //Tell the user how many juice cans they will get.
   cout << "The juice vendor will dispence:\n";
   cout << "1) " << cent_85 << " 85 cent juice cans.\n";
   cout << "2) " << cent_1  << " Pennies.\n";
   return 0;
}
```

Code 1. I/O Project

B. Project 2:

In this project students design and implement a game based on binary number to decimal conversion that is able to produce a number from 1 to 31 and hence any individual's birthday [1]. First the binary number system is introduced with binary to decimal conversions. Students were allowed to discover that any decimal number from 1 to 31 can be represented with five bits and to identify the corresponding five groups. See Code 2.

```
#include <iostream>
using namespace std;

int main()
{
   //  Initialize 6 input/output variables
   int bit1, bit2,bit3, bit4, bit5, day;

   cout << "I can guess your birthday.\n";
   cout << "Remember to put a 1 for yes and a 0 for no.\n";

   cout << "Is your birth day in set 1?\n";
   cout << "Set 1: 1, 3, 5, 7, 9, 11, 13, 15, 17, 19, 21, 23, 25, 27, 29,
31\n";
   cin >> bit1;

   cout << endl << "Is your birth day in set 2?\n";
   cout << "Set 2: 2, 3, 6, 7, 10, 11, 14, 15, 18, 19, 22, 23, 26, 27, 30,
31\n";
   cin >> bit2;

   cout << endl << "Is your birth day in set 3?\n";
   cout << "Set 3: 4, 5, 6, 7, 12, 13, 14, 15, 20, 21, 22, 23, 28, 29, 30,
31\n";
   cin >> bit3;

   cout << endl << "Is your birth day in set 4?\n";
   cout << "Set 4: 8, 9, 10, 11, 12, 13, 14, 15, 24, 25, 26, 27, 28, 29, 30,
31\n";
   cin >> bit4;

   cout << endl << "Is your birth day in set 5?\n";
   cout << "Set 5: 16, 17, 18, 19, 20, 21, 22, 23, 24, 25, 26, 27, 28, 29, 30,
31\n";
   cin >> bit5;

   day = bit5*16 + bit4*8 + bit3*4 + bit2*2 + bit1;

  cout << endl << "Your birth day is on the " << day << " day of your
birth month.";
   return 0;
}
```

Code 2. Binary to Decimal Conversion game

C. Project 3:

Conditional if else switch statements are central to writing computer programs and aimed at helping students understand and solve intractable problems. In this project students were introduced to random number generation and asked to design a game that simulates a lottery drawing [1]. They implemented the game for one, two and three digit lottery numbers, with prizes awarded to the winning numbers.

The program first invites the user to enter the number corresponding to the version of the game they are playing. Once the user inputs the numbers for their lottery ticket, the computer generates a random number and compares to see a match. At the end of the program it displays the winning award.

In the one digit game, a simple if/then statement matches the random number generated by the program for the lottery to the users guess. The random number is generated by the rand() mod 10 to ensure one digit. See Code 3.

```
#include <iostream>
#include <ctime>
#include <cstdlib>
using namespace std;

int main()
{
   srand (time(0));
   int lottery = rand() % 10, guess, prize =1;
   cout << "Would you like to play the lottery and win?\n";
   cout << "Please enter any number from 0 to 9 to find out if you
win!!\n";
   cin >> guess;
   if (lottery == guess)
         prize = 1000;
   else prize = 0;
   if (prize >0)
      cout << "Congratulations you have won " << prize << " dollars\n"
<<"The correct number was " <<lottery<< endl;
   else cout << "Sorry you have not won this time.\n" <<"The correct
number was " <<lottery<<". Please try again.";
   return 0;
}
```

Code 3. One digit game program

In the two digit game, the two numbers need to be separated from one another. There are four different winning outcomes and each will be determined by an if/then statement. The random integer, generated by the rand() mod 100 ensures two digits, from 00 to 99. The division and modulus operators are used to separate the first and second digits. See Code 4.

```
#include <iostream>
#include <ctime>
#include <cstdlib>
using namespace std;

int main()
{
   srand (time(0));
   int lottery = rand() % 100, firstdig, seconddig, guess, firstguess,
secondguess;
   int prize = 1;
   firstdig=lottery/10;
   seconddig=lottery % 10;
   cout << "Would you like to play the lottery and win?\n";
   cout << "Please enter any number from 00 to 99 to find out if you
win!!\n";
   cin >> guess;
   firstguess=guess/10;
   secondguess=guess % 10;
   if ((firstdig == firstguess) && (seconddig == secondguess))
         prize = 10000;
   else if ((firstdig == firstguess) && (seconddig != secondguess))
         prize = 5000;
   else if ((firstdig != firstguess) && (seconddig == secondguess))
         prize = 5000;
   else if ((firstdig == secondguess) && (seconddig == firstguess))
         prize = 7500;
   else prize = 0;

   if (prize >0)
      cout << "Congratulations you have won " << prize << " dollars\n"
<<"The correct number was " <<lottery<< endl;
   else cout << "Sorry you have not won this time.\n" <<"The correct
number was " <<lottery<<". Please try again.";
   return 0;
}
```

Code 4. Two digit game program

In the three digit game, the rand() mod 1000 ensures three digits, ranging from 000 to 999. The largest amount will be awarded to the users who guess all three numbers in the correct order. In this program we limited the number of matches to produce eight potential outcomes, having one number right in any of the three locations (three outcomes), having two of the numbers correct and in the proper location (three more outcomes), having all three numbers correct but in the wrong order, and having all three numbers correct in the correct order. See Code 5.

```
#include <iostream>
#include <ctime>
#include <cstdlib>
using namespace std;

int main()
{
   srand (time(0));
   int lottery = rand() % 1000, firstdig, seconddig, thirddig, guess,
firstguess, secondguess, thirdguess;
   int prize = 1;
   firstdig=lottery/100;
   seconddig=lottery % 100 / 10;
   thirddig=lottery % 100 % 10;
   cout << "Would you like to play the lottery and win?\n";
   cout << "Please enter any number from 000 to 999 to find out if you
win!!\n";
   cin >> guess;
   firstguess=guess/100;
   secondguess=guess % 100 / 10;
   thirdguess=guess % 100 % 10;
   if ((firstdig == firstguess) && (seconddig == secondguess) &&
(thirddig == thirdguess))
         prize = 100000;
   else if ((firstdig == firstguess) && (seconddig == secondguess) &&
(thirddig != thirdguess))
         prize = 4000;
   else if ((firstdig == firstguess) && (seconddig != secondguess) &&
(thirddig == thirdguess))
         prize = 4000;
   else if ((firstdig != firstguess) && (seconddig == secondguess) &&
(thirddig == thirdguess))
         prize = 4000;
   else if (((firstdig == secondguess) || (firstdig == thirdguess)) &&
((seconddig == firstguess) || (seconddig == thirdguess)) && ((thirddig ==
secondguess) || (thirddig == firstguess)))
         prize = 25000;
   else if ((firstdig == firstguess) && (seconddig != secondguess) &&
(thirddig != thirdguess))
         prize = 1000;
   else if ((firstdig != firstguess) && (seconddig == secondguess) &&
(thirddig != thirdguess))
         prize = 1000;
   else if ((firstdig != firstguess) && (seconddig != secondguess) &&
(thirddig == thirdguess))
         prize = 1000;
   if (prize >0)
      cout << "Congratulations you have won " << prize << " dollars\n"
<<"The correct number was " <<lottery<< endl;
   else cout << "Sorry you have not won this time.\n" <<"The correct
number was " <<lottery<<". Please try again.";
   return 0;
}
```

Code 5. Three digit game program

D. Project 4:

In this project students simulate a rock, paper, scissors game [1]. The program asks the user to choose one of the options to play the game. After that, the computer will determine its choice and decides the outcome of the game. A number mod 3 generates three possibilities 0, 1 or 2, with each number being assigned a value: rock, paper or scissors.

A switch will take the computer's choice and compare it to the user's choice using an if/then statement. If the two choices are the same, the game will end up tied. .

The else part will give one of the two alternative scenarios for the game in another if statement and the result of that outcome, with a final else being the result of the only other potential outcome for the scenario, since only three exist for each possibility. See Code 6.

```
#include <iostream>
    #include <ctime>
    #include <cstdlib>
    using namespace std;

    int main()
    {
       srand (time(0));
       int number = rand() % 3;
       string playerguess, cpuoption;
       cout << "Would you like to play rock/paper/scissors?\n";
       cout << "Please choose whether you would like the rock, paper, or
scissors.\n";
       cin >> playerguess;
       if (number == 0)
          cpuoption = "rock";
       else if (number == 1)
          cpuoption = "paper";
       else if (number == 2)
          cpuoption = "scissors";
       switch (number)
       {
          case 0:  if (playerguess == cpuoption)
                      cout << "You have tied.  Please play again.\n";
                      else if (playerguess == "paper" )
                      cout << "You have won.  Paper covers rock.\n";
                      else cout << "You have lost.  Rock breaks scissors.\n";
break;
          case 1: if (playerguess == cpuoption)
                      cout << "You have tied.  Please play again.\n";
                      else if (playerguess == "scissors" )
                      cout << "You have won.  Scissors cuts paper.\n";
                      else cout << "You have lost.  Paper covers rock.\n"; break;
          case 2:  if (playerguess == cpuoption)
                         cout << "You have tied.  Please play again.\n";
                         else if (playerguess == "rock" )
                         cout << "You have won.  Rock breaks scissors.\n";
                         else cout << "You have lost.  Scissors cut paper.\n";
break;
       }
       return 0;
    }
```

Code 6. Rock, Paper, Scissor

E. Project 5:

In this project students use at least three functions to design and implement a game that simulates the actions of an ATM machine, where the user initially has no money, then makes an initial deposit, and then is able to withdraw money.

The program asks the user to insert any number of quarters, dimes, nickels and pennies. Then the program tells the user the available balance. The same process will be repeated for the withdrawal, and the final balance will be displayed. There are three main functions in this program. First, is the initialization of the variables, setting the values to zero, as if this is the first time that the account is filled with money, or another programmer defines a different value other than zero that would be available for withdrawal. The second function is a deposit function to add up the coins entered into the purse that would give the user a total amount of money deposited. The third function enables withdrawal from the account. If the withdrawal exceeds the account balance the program will state that there are insufficient funds. See Code 7.

```
    #include <iostream>
    using namespace std;

    void insert(int quarters, int dimes, int nickels, int pennies, double& total);
    void withdrawl(int quarters, int dimes, int nickels, int pennies, double&
total);
    void initialize (int& quarters, int& dimes, int& nickels, int& pennies,
double& total);

    int main()
    {
       int quarters, dimes, nickels, pennies;
       double total;
       initialize(quarters, dimes, nickels, pennies, total);
       insert(quarters, dimes, nickels, pennies, total);
       withdrawl(quarters, dimes, nickels, pennies, total);
       return 0;
    }

    void insert(int quarters, int dimes, int nickels, int pennies, double& total)
    {

       cout << "Please insert how many quarters you are inserting.\n";
       cin >> quarters;
       cout << "Please insert how many dimes you are inserting.\n";
       cin >> dimes;
       cout << "Please insert how many nickels you are inserting.\n";
       cin >> nickels;
       cout << "Please insert how many pennies you are inserting.\n";
       cin >> pennies;
       total = quarters*.25+dimes * .10 + nickels * .05 + pennies * .01;
    }

    void withdrawl(int quarters, int dimes, int nickels, int pennies, double&
total)
    {

       cout << "You have $" << total << " that you can withdraw\n";
       cout << "How many quarters do you want to take out?\n";
       cin >> quarters;
       cout << "How many dimes do you want to take out?\n";
       cin >> dimes;
       cout << "How many nickels do you want to take out?\n";
       cin >> nickels;
       cout << "How many pennies do you want to take out?\n";
       cin >> pennies;
       total = total - (quarters*.25+dimes*.10+nickels*.05+pennies*.01);
       if (total>0)
          cout << "Please take your change.  Your new balance is $" <<total;
       else cout <<"You do not have enough funds.  Please try again.";
    }
```

```
    void initialize (int& quarters, int& dimes, int& nickels, int& pennies,
double& total)
    {
       quarters = 0, dimes = 0, nickels =0, pennies = 0;
       total = 0;
    }
```

Code 7. ATM Machine

F. Project 6:

In this project students define two classes and design and implement a program that simulates a juice vending machine. The program asks the user to select the juice choice from the vending machine [2]. Then the program asks for the proper amount of money for the kind of juice they selected.

The program gives the user two chances to input at least the proper amount of money before returning their money and displaying a statement asking them to try again, or outputs a thank you statement for the selection. The main menu for the vending machine then reappears after the juice has been paid for and asks the user again if he/she would like to make a selection, repeating the process until the user exits the program.

Although the system doesn't output the number of items available for each juice, the program tracks the number of juice cans, and if it runs out of one it displays a message that the item as sold out. The user defines the cashRegisterType and the dispenserType classes. The cashRegisterType acts as the user interface for the program while the dispenserType banks the information internally as the user doesn't need to know this information. See Code 8.

```
    #include <iostream>
    #include <iomanip>

    using namespace std;

    class CashRegisterType
    {
       private:
          int cashOnHand;
       public:
          CashRegisterType(int cashIn = 500); //constructor
          int getCurrentBalance() const;
          void acceptAmount(int amountIn);
    };

    CashRegisterType::CashRegisterType(int cashIn)
    : cashOnHand(cashIn)
    {

    }

    int CashRegisterType::getCurrentBalance() const
    {
       return cashOnHand;
    }

    void CashRegisterType::acceptAmount(int cashIn)
    {
       cashOnHand += cashIn;
    }

    class DispenserType
    {
       private:
          int numberOfItems;
          int cost;
       public:
          DispenserType(int noOfItems = 50, int costIn = 50);
          int getCost() const;
          void makeSale();
    };

    DispenserType::DispenserType(int noOfItems, int costIn)
    : numberOfItems(noOfItems), cost(costIn)
    {

    }

    int DispenserType::getCost() const
    {
       return cost;
    }

    void DispenserType::makeSale()
    {
       numberOfItems--;
    }

    int main()
    {

       CashRegisterType reg;
       DispenserType orange;
       DispenserType apple(50, 75);
       DispenserType mango(50, 65);
       DispenserType banana(50, 25);
       DispenserType juices(50, 125);
       int option;

       cout << "Cash in Register: $" << reg.getCurrentBalance() / 100.0 <<
endl;
       //show menu, sell items
       do
       {
          cout << "Select an Item";
          cout << "1. Orange " << orange.getCost() << " Cents." << endl;
          cout << "2. Apple " << apple.getCost() << " Cents." << endl;
          cout << "3. Mango " << mango.getCost() << " Cents." << endl;
          cout << "4. Banana " << banana.getCost() << " Cents." << endl;
          cout << "5. Juice " << juices.getCost() << " Cents." << endl;
          cout << "6. Quit." << endl;
          cout << "Enter Option: ";
          cin >> option;

          if ( option == 1 )
          {
             cout << "You bought Orange for " << orange.getCost() << "
Cents." << endl;
             reg.acceptAmount(orange.getCost());
          }
          else if ( option == 2 )
          {
             cout << "You bought Apple for " << apple.getCost() << " Cents."
<< endl;
             reg.acceptAmount(apple.getCost());
          }
          if ( option == 3 )
          {
             cout << "You bought Mango for " << mango.getCost() << "
Cents." << endl;
             reg.acceptAmount(mango.getCost());
          }
          if ( option == 4 )
          {
             cout << "You bought Banana for " << banana.getCost() << "
Cents." << endl;
             reg.acceptAmount(banana.getCost());
```

```
        }
        if ( option == 5 )
        {
           cout << "You bought Juice for " << juices.getCost() << " Cents."
<< endl;
           reg.acceptAmount(juices.getCost());
        }
      }while(option != 6);

      cout << endl;
      cout << "Cash in Register: $" << reg.getCurrentBalance() / 100.0 <<
endl;

      cin.ignore(100, '\n');
      system("pause");
      return 0;
   }
```

Code 8. Mutiple Classes

IV. Transformations, Assessment, Evaluation and Feedback

With the help of Integrated Development Environment (IDE) software, students learned how to edit-compile-run programs in their first class hour. Also, we observed that the number of assignments completed by the students both during the course and in the class hour is much more compared to a typical lecture-based programming class. The IDE helped students as designers to quickly compare alternative solutions for problems and test for correctness. Student learning was evaluated using many different methods. The background knowledge and preconception checks were performed in the form of a simple questionnaire/worksheet that the students will fill in prior to working on the project assignments. Each student explained the sample programs given in each chapter of the book to others, compiled and executed to check the correctness. The students were asked to explain the concepts they have learned and the programs so that the instructor can measure student learning. Students completed one programming assignment daily and submitted one project report per week. In larger projects, students worked together in groups. Each member turned in an evaluation of his/her own learning experiences gained by being part of a team. To reinforce the learning, a test was scheduled after the completion of each module. Excellent students performed well in all levels and had complete understanding of the subject matter. Very good students were strong in many areas but weak in some. Average students showed weaknesses in some levels. Poor students could not perform well in many areas. Classroom opinion polls and course-related self-confidence surveys were also performed to receive the feedback.

Student progress towards attaining each Student Outcome described in section 1 of this paper is measured in stages. For each stage, students complete a pre-defined set of activities in the course. Data collection processes to assess and evaluate each student outcome include exam questions, group activities, project presentations, focus groups, industrial advisory committee meetings, and other processes that are relevant and appropriate to the program. Student performance is evaluated in the course by the assessment data collection, data analysis, review and recommendations, and course outcomes. Student and Exit surveys are also used to collect data. Data collection processes for each outcome include quizzes, tests, final exams, homework, lab reports, oral presentations, and project work. The undergraduate committee and the program Chair analyze the data. The program faculty makes recommendations thereafter. The undergraduate committee approves the recommendations. The program faculty and the Chair implement those recommendations. The faculty retreat and department meeting times are used to discuss these changes.

Classroom activities were designed to reflect student-centered design and analysis processes. In general, pre project assignments helped the students explore and create on their own. They synthesized the classroom instructions with other resources to produce algorithms and then to test and to debug. In the classroom, each student provided with a computer to extend the concepts they learned in the pre project assignment. Less challenging design problems that can be solved within a given period of time were assigned as in-class closed-project assignments. A post-project assignment helped the students to analyze the use of in-class activities. More challenging and time consuming problems were assigned as post laboratories. After completing each project, students submitted a report discussing their experience. First, each student worked alone as the sole developer of the programs. Towards the end of the semester two to four students were allowed to work in a team to design, construct and complete the projects. The group was responsible for developing definitions and specification of a larger software product to solve a problem as their final project.

V. Summary

This paper described the project-based CS/IS-1 course we have developed to substitute the traditional lecture based classroom to help students design and use at least two user defined data types in a program. First we have outlined the expected student outcomes, thereafter the transformations made, data collected for evaluation and continuous improvements. For many years, we have been experimenting with methods to improve the quality of teaching programming languages for undergraduate computing students. Our goal has been and continues to be to help them become good programmers in a relatively short period of time with both theoretical understanding and practical skills so that they can enter and make an effective contribution to the profession. Traditionally, the programming lectures have been presented to a less than enthusiastic student body in a relatively passive classroom environment. In general, this lecture based instructional process consists of multiple copying stages: the instructor first copies programs from a textbook to his note book, then the instructor displays the projects onto a whiteboard, thereafter the students copy programs into their note books and then edit on a computer to compile and run after the class. Moreover, each instructor allocates considerable amount of his/her time to prepare or update the same course material in each offering. Designing a project based course with learning-by-doing modules and making it available for all the instructors on-line. It reduces the course preparation time for instructors, reduces multiple copying steps in the learning process, strengthen the abilities and increase the enthusiasm of both traditional undergraduate students as well as the adult learners. Growth of any

undergraduate computing program will largely depend on the strength of the introductory programming language courses in the curriculum. Learning takes place through creation, interaction, inspiration and effort. Thus the performance of the students can be improved by converting the traditional passive classroom into an active hands-on learning environment.

We have provided the students an efficient, rigorous and engaging learning environment with necessary tools and training to become proficient in the C++ programming language in a relatively short period of time. Also, we have enhanced the quality of the graduates by helping them to understand basic programming constructs with hands-on skills, integration and team-work. Our approaches taught the students on how to explore a programming language on their own and learn while interacting with a machine loaded with necessary tools. Our active learning environment strengthened student abilities and increase the enthusiasm of both traditional and adult learners. Our active learning modules consist of a complete programming solution to problems, partially completed programs for a given problem and tasks with no programs. We introduced one programming concept of the language at a time. Classroom activities include discussions, reading, writing, modifying and presenting programming solutions to the class. Students enjoyed program design, implementation and error correction in an active classroom.

Within our geographic area we will have opportunities to test our designs which could possibly extend to other colleges, faculty and students. We would like to compare the student retention in a project based active learning programming classes with lecture-based classes. We will continue assessing, evaluating and improving the course material continuously through faculty and student feedback for the next couple semesters. Also, we will continue to share the experience gained from this experiment with the rest of the C++ programming community.

REFERENCES

[1] Y.D. Liang, Introduction to Programming with C++, 2nd Edition, Prentice Hall, 2011

[2] D.S. Malik., C++ Programming From Problem Analysis to Program Design, 5th Edition, Cengage Learning, 2012

[3] T.Gaddis,J.Walters and G.Muganda Starting out with C++, 7th Edition, Addison Wesley,2010

[4] P.Dietel and P Dietel, C++ How to Program, 7th Edition, Addison Wesley, 2010

[5] Horstmannn, C++ For Everyone, 2nd Edition, , Wiley Publishing, ©2011

[6] http://www.codeblocks.org/downloads/26/

AUTHORS PROFILES

The first author of this paper, Dr. Suvineetha Hearth, is a faculty member of University Bahrain. She taught Information Systems, Business and Computer Science departments of Dubuque University, Richard Stockton College, and Atlantic Cape Community College in New Jersey, USA. She also worked as a teaching and research assistant at the Gifu University, and a visiting instructor at Gifu Technical College, in Japan. She received her PhD in Public Policies from the Gifu University, Japan in 1998 as a Rotary Yoneyama graduate Scholar. Also, she continued the coursework required for a second PhD in International Law at Asahi University in Japan. As an Attorney-at-Law, she serve for the Herath Foundation as the Vice President of Legal Affairs and Reforms. Her research interests include security policies, protocols for security, access control, authentication, integrity, Biometrics, Information Assurance and e-learning. She is a Life member of Sri Lanka Bar Association and senior member of the Institute of Electrical and Electronic Engineers (IEEE W) and a active member of the Association of Computer Machinery (ACM). Currently, she is leading the ACM GULF Region Teaching and Learning group and organizing IEEE Computer Society in Bahrain.

Dr. Ajantha Hearth earned his PhD from the Gifu University, Japan, in 1997. His research interests include e-commerce protocols; secure network protocols, computer forensics and algorithm transformations to cryptographic hardware. He worked as the Professor at the University of Fiji's Department of Computer Science and Information Technology in 2011. At present he is teaching at the University of Bahrain. In 1988 he received the prestigious Japanese Government Monbusho research scholarship award. In 2007 he received the Outstanding Research Award for Commitment to Excellence in Computer Forensics and Development of Student Leaders and Researchers from the IEEE–Region 2 AIAA USA. He is a senior member of the IEEE and member of ACM. In 1986, Herath brothers established the Herath Foundation to help financially needy but talented students and awarded more than 7000 scholarships to continue their higher education. He functions as the senior vice president of the Herath Foundation.

Mr. Mohammed A.R. Siddiqui is a faculty of University Bahrain. He received his MSc and B.Sc. from Osmania University, India. In 1999,,he joined UOB and also work as an adjunct faculty at Polytechnic College in Bahrain. His research interests include Visual Programming, Knowledge Base System, Database Management Systems E - Commerce and E-Learning. He is an a member of the Association of Computer Machinery (ACM.) since 2010 and an active member of ACM Gulf region Learning and Research group.

Mr. Khuzaima A.H El-Jallad is a faculty member of University Bahrain 2003. He received his MSc from Towson State University 1984, USA and B.Sc. 1982 from Point Park University, Pittsburgh,. USA. Over the past fifteen years he was working in many projects related to development of Instructional Technology and ICTs though the uses of Digital media. He is a member of the Association of Computer Machinery (ACM.) and an active member of ACM Gulf Region learning and Research group. His research interests are Programming Languages, Elearning, Quality Assurance, Multimedia, Ecommerce and Human Computer Interface.

Quadrant Based WSN Routing Technique by Shifting of Origin

Nandan Banerji, M.Tech(CSE)
Department of Computer science & Engineering,
University of Kalyani, Nadia, W.B, India

Uttam Kumar Kundu (Principal)
Bengal College of polytechnic, Bidhan Nagar
Durgapur, W.B, India

Pulak Majumder(Astt professor),
Department of Electronics and Tele-Communication Engineering, Regent Education & Research Foundation,
Barrack pore, W.B, India

Debabrata Sarddar (Asst. Professor)
Department of Computer science & Engineering,
University of Kalyani, Nadia, W.B, India

***Abstract*—A sensor is a miniaturized, low powered (basically battery powered), limited storage device which can sense the natural phenomenon or things and convert it into electrical energy or vice versa using transduction process. A Wireless Sensor Network (WSN) is such a wireless network built using sensors. The sensors communicate with each other's using wireless medium. They can be deployed in such an environment; inaccessible to human or difficult to reach. Basically there is a vast application on automated world such as robotics, avionics, oceanographic study, space, satellites etc. The routing of a packet from a source node to a destination should be efficient in such a way that must be efficient in case of energy, communication overhead, less intermediate hops. The scheme will help to route the packet with a lesser intermediate nodes as the neighbors are being selected based on their Quadrant position.**

Keywords-component; WSN; Quardent; Packet; Hops

I. INTRODUCTION

WSN is a special case of Mobile Ad-hoc NETwork (MANET) where the network topology changes very frequently with a very limited battery power. So routing in such a network is very difficult due to the dynamic network configuration. The nodes are scattered in such a manner and they are moving around the network that it is very difficult to predict the physical position of a node at a particular time.One of the related issue is that different nodes have different mobility

patterns; i.e. some nodes are heavily mobile, while some others are not. It is very difficult to predict the node movement within a WSN.

The basic characteristics of a WSN are :

1) Topology that changes dynamically.
2) Variable link capability and constraint of bandwidth of the wireless medium.
3) Optimization criteria of battery power.
4) *Physical security limitations*.

In our paper we have proposed an idea of routing in a WSN. In section-I there is a brief introduction, Section-II Related work in this domain, Section-III Idea of the proposed work & in Section-IV, V and VI the simulation, Acknowledgement, future work are briefly mentioned.

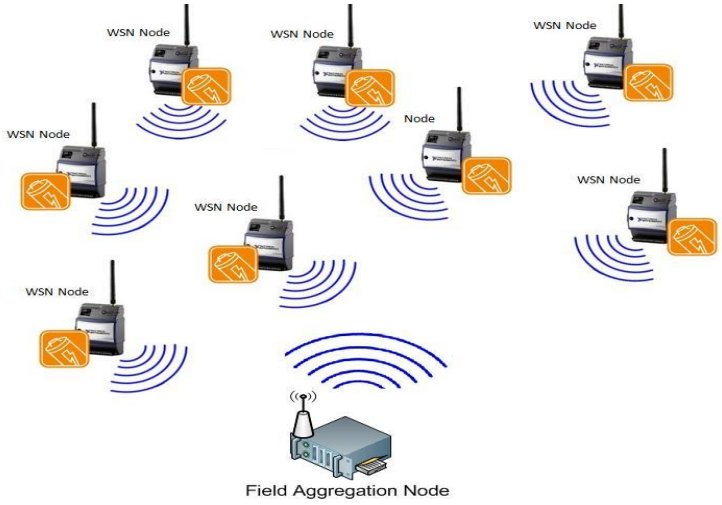

Fig.1. WSN

II. RELATED WORK:

The existing routing protocols are either proactive or reactive in nature .In proactive scheme the route is evaluated continuously hence at the time of packet forwarding time the route is known. On the other hand in reactive scheme the route is evaluated when it is demanded (sometimes it is called on demand routing). The protocols are also classified as:

- On Demand or Source initiated.
- Table Driven.

The On demand includes AODV, DSR, TORA, ASR and Table driven includes CGSR, DSDV, and WRP.

Most of the routing techniques in WSN are categorized as Geographic Routing, Hierarchical Routing, Stateless Flat Routing and Energy Aware Routing. The available schemes are of Hierarchical routing which dealing with clusters and CH (Cluster Heads). These schemes divide the network into

regions/segments and then route the traffic from one region/segment to the other. Regions can be clusters as in [1] or can be in the form of zones as in the case of adhoc routing schemes. Protocols like GPSR and GEAR which try to minimize the energy consumed by considering both energy and distance.

Geographic routing also known as localized algorithms as these algorithms use the location information and transmit the information towards the geographic direction of destination via multiple paths. In Location Aided Routing (LAR), intended to support topology-based reactive routing protocol uses location information to restrict flooding to request zone from where nodes are selected to find the routes between source and destination. ILAR (Improved Location Aided Routing) is another location based routing algorithm, selects the closet neighbor to the base line as an intermediate node.

In [11] authors suggested a load balancing factor that will help in routing with in a WSN but the load balancing factor (Θ) depends upon the energy of the sensor node . Here the energy is not a static one; hence the proposed scheme yields an average result.

III. PROPOSED WORK

The proposed scheme works over a WSN with an assumption that the network spread like a two dimensional planner square grid with equal spacing.

There are some other assumptions are:

- All the nodes are homogeneous in nature.
- The nodes can be traced by its geographical location through available GPS methods.
- The nodes are static in nature at data gathering stage.
- The homogenearity parameters of the nodes are computational power, energy constraint, limited storage and communication range.

The proposed scheme deals with the routing path between a source node to a destination node. There are a number of techniques are available but the proposed scheme highlights over a very efficient geometric technique to find the path with in a very short time.

Here each of the node with in the square grid has eight(**8**) neighbors as related in Cartesian co-ordinate system(x,y) as **N1(x,y+1),N2(x,y-1),N3(x+1,y),N4(x-1,y),N5(x+1,y+1),N6(x+1,y-1),N7(x-1,y+1),N8(x-1,y-1)**.

As the geometry suggests that each point(x, y) belongs to a particular Quadrant depending upon its (x, y) value with respect to the Origin. The proposed scheme first finds the Quadrant of Source(S) and destination(D) then the next node from S's neighbors is selected which belongs to the quadrant of D.Here the whole WSN is sub-divided into four regions based on some point (0, 0) as origin. Then the origin is shifted into the source (S) node and all the neighbors (N8) and the destination node (D) s' co-ordinates are adjusted as per geometric formula as mentioned in the figure 2.

Imagine O(0,0) is the origin and S(α,β) is the source and D(x,y) is the destination ; now if the origin is being shifted into S(α,β) the co-ordinate of D(x,y) becomes D(x',y') as per following :

$$X'=X-\alpha \quad and \quad Y'=Y-\beta$$

The quadrants are set in such a way that the Source and Destination will be in same quadrant.

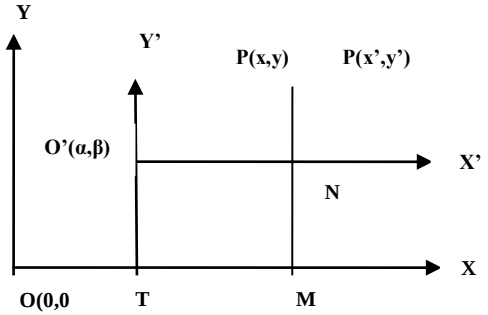

Fig.2. Geometric Origin & its Shifting

Similarly all the co-ordinates of the neighbors (N8) of source (S) are adjusted with the new origin. Now the actual process starts by filtering the N8 based on their quadrant location. The selected nodes from N8 are those whose quadrant position is similar with D. Then the perpendicular distance is calculated from that nodes to D and the smallest is selected to become the next hop towards D. Say that node is N_x ; now the N_x becomes the next Source S_x and the process goes recursively until the S_x becomes D(destination).

Flow Chart:

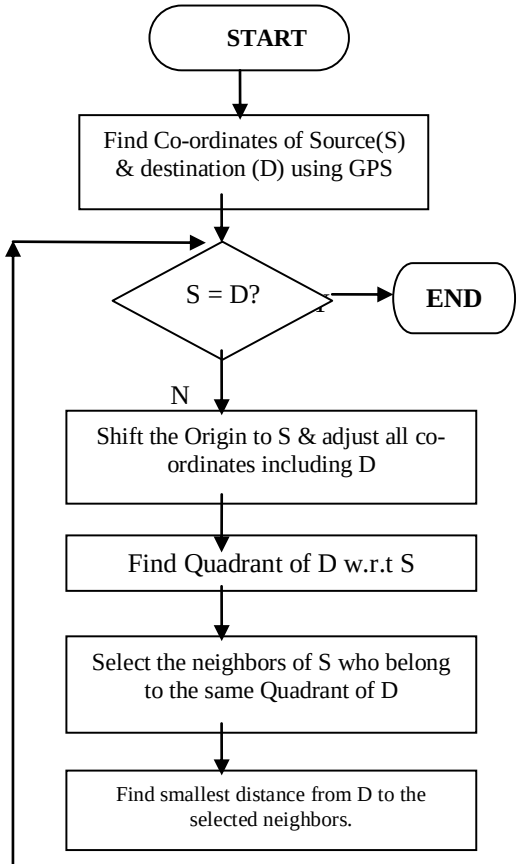

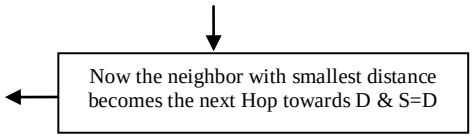

Fig.3. Flow chart of the proposed Scheme

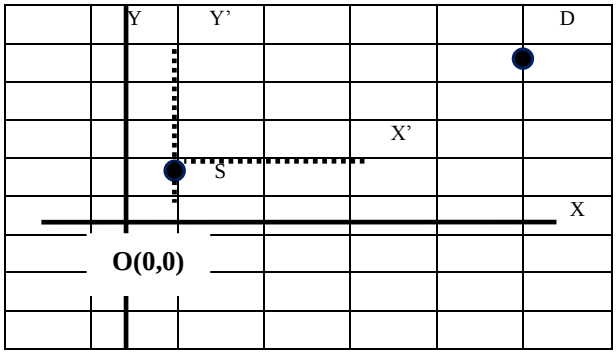

Fig.4. Grid structure with Source & Destination w.r.t Origin.

Here in the square grid initially the origin is O the it is shifted at S. Now the adjustment of co-ordinates are taken place with respect to the new origin S.

Example :

Let origin O(0,0) ,Source S(5,5) and destination D(12,9) . Now the process starts by shifting the origin into S (5, 5) hence all the neighbors of S (N8) and Destination D (12, 9) will adjust their co-ordinates based on the newer origin. Now D becomes (12-5, 9-5) = (7, 4) as adjusted co-ordinate. As D is in the first quadrant then the neighbors (from N8) only selected to become a candidate for next hop towards the destination who belongs to the same quadrant with D (here that is first quadrant).

IV. Simulation Result

Complexity: As compared to other methods here the complexity of the routing process is reduced a lot as the selection of next hop is done based on a filtering mechanism with the quadrant position of destination node. As there are four quadrants and as per proposed mechanism the selected quadrant is one the mathematically the complexity is reduced up to 25% of the total efforts.

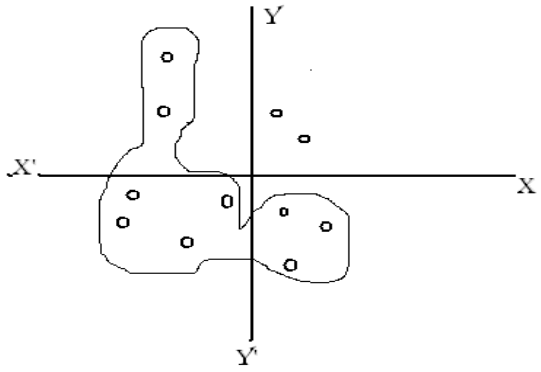

Fig.5. Proposed Schemes efficiency

The marked region is the area where the proposed algorithm does not work as it is not associated with the quadrant of D; hence only the unmarked region will take part in the process to become the next hop.

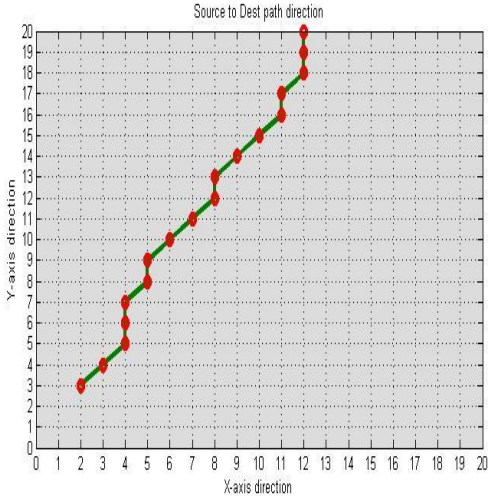

Fig.6. Output of Simulation

V. Acknowledgment

"Quadrant Based WSN Routing Technique By Shifting Of Origin" is an efficient scheme by which we can reduce the effort upto 75% of the total effort by separating the whole WSN with respect to origin and its 4 quadrants. The proposed scheme will reduce the effort as well as help to preserve battery power of the sensor node.

VI. Future Work

The proposed scheme can be extended in the context of energy or power of the sensor node. In [11] the author explained about a threshold value that can be extended in the proposed scheme to efficiently utilize the routing technique in WSN.

References

[1] Al-Karaki, J., Kamal, A.: Routing techniques in wireless sensor networks: a survey. IEEE Wireless Communications 11(6), 6–28 (2004)

[2] Blaze, M., Feigenbaum, J., Lacy, J.: Decentralized trust management. In: Proceedings of 1996 IEEE Symposium on Security and Privacy, pp. 164–173 (1996)

[3] Boukerche, A., El-Khatib, K., Xu, L., Korba, L.: A novel solution for achieving anonymity in wireless ad hoc networks. In: Proceedings of the 1st ACM international workshop on Performance 3evaluation of wireless ad hoc, sensor, and ubiquitous networks, pp. 30–38 (2004)

[4] Analysis and Improvement of the Dynamic Load Balancing of Overlay-based WSN. By Hang Qin and Zhongbo Wu.

[5] Routing Protocols in Wireless Sensor Networks. By Luis Javier García Villalba , Ana Lucila Sandoval Orozco, Alicia Triviño Cabrera and Cláudia Jacy Barenco Abbas. *Sensors* **2009**, *9*, 8399-8421; doi:10.3390/s91108399.

[6] Akkaya, K.; Younis, M. A Survey on Routing Protocols for Wireless Sensor Networks. *Ad Hoc Netw.* **2005**, *3*, 325–349.

[7] Tilak, S.; Abu-Ghazaleh, N.B.; Heinzelman, W. A Taxonomy of Wireless Micro-Sensor Network Models. *Mob. Comput. Commun. Rev.* **2002**, *6*, 28–36.

[8] Seada, K.; Helmy, A. *Geographic Protocols in Sensor Networks*; Technical Report 04-837; Computer Science Department, University of Southern California: San Diego, CA, USA, 2008.

[9] Lindsey, S.; Raghavendra, C.S. PEGASIS: Power-Efficient Gathering in Sensor Information Systems. In *Proceedings of the Aerospace Conference*, Big Sky, MT, March, 2002; pp. 1125–1130.

[10] Barenco Abbas, C.J.; González, R.; Cárdenas, N.; García Villalba, L.J. A Proposal of a Wireless Sensor Network Routing Protocol. *Telecommun. Syst.* **2008**, *38*, 61–68.

[11] Threshold Based Load Balancing Protocol

for Energy Efficient Routing in WSN. By Sohail Jabbar, Ayesha Ejaz Butt , Najm us Sahar, Abid Ali Minhas . ISBN 978-89-5519-155-4 PP. 196 Feb. 13~16, 2011 ICACT2011.

AUTHORS PROFILE

Mr. Nandan Banerji,Pursuing M.Tech(CSE) in the Department of Computer Science and Engineering, University of Kalyani, Kalyani,Nadia, West Bengal, INDIA. His research interest includes wireless and mobile system and WSN

Uttam Kumar kundu Completed his M.Tech in ECE from WBUT in 2010 and B-Tech in E.I.E from JIS College of engineering and technology under West Bengal University of Technology in 2006. His research interest includes wireless communication and satellite communication.

Pulak Mazumder received his M.Tech in Electronics & Telecommunication Engineering from WBUT, Kolkata in 2010, and his B.Tech(AMIETE) in Electronics & Telecommunication Engineering from IETE, New Delhi in 2006. At present, he is a Asst. Professor in the Department of Electronics and Tele-Communication Engineering, Regent Education & Research Foundation, Barracpore. He was earlier a lecturer in ECE dept. at Durgapur Institute of Advanced Technology, Durgapur and Calcutta Institue of Engineering and Mangement, Tollygung, Kolkata. He served Industry more than eight years as IT Network Infrastructure Management. His research interest includes wireless and mobile communication systems

Mr **Debabrata Sarddar,** Assistant Professor in the Department of Computer Science and Engineering, University of Kalyani, Kalyani,Nadia, West Bengal, INDIA. He has done PhD at Jadavpur University. He completed his M.Tech in Computer Science & Engineering from DAVV, Indore in 2006, and his B.E in Computer Science & Engineering from NIT, Durgapur in 2001. He has published more than 75 research papers in different journals and conferences. His research interest includes wireless and mobile system and WSN.

Resolution of Unsteady Navier-stokes Equations with the $C_{a,b}$ Boundary condition

Jaouad EL-Mekkaoui, Ahmed Elkhalfi
Mechanical engineering laboratory
Faculty of sciences and techniques-B.P.
2202 Route Imouzzer Fes

Abdeslam Elakkad
Department of mathematics
Regional Centre for Professions of Education and Training,
Fes, B.P: 243 Sefrou Morocco

***Abstract*—in this work, we introduce the unsteady incompressible Navier-Stokes equations with a new boundary condition, generalizes the Dirichlet and the Neumann conditions. Then we derive an adequate variational formulation of time-dependent Navier- Stokes equations. We then prove the existence theorem and a uniqueness result. A Mixed finite-element discretization is used to generate the nonlinear system corresponding to the Navier-Stokes equations. The solution of the linearized system is carried out using the GMRES method. In order to evaluate the performance of the method, the numerical results are compared with others coming from commercial code like Adina system.**

Keywords—Unsteady Navier-Stokes Equations; Mixed Finite Element Method; $C_{a,b,c}$ boundary condition; Adina system.

I. Introduction

The two firsts PDEs given in section 2 constitute the basis for computational modeling of the flow of an in compressible Newtonian fluid. For the equations, we offer a choice of two-dimensional domains on which the problem can be posed, along with boundary conditions and other aspects of the problem, and a choice of finite element discretizations on a quadrilateral element mesh, whereas the discrete Navier-Stokes equations require a method such as the generalized minimum residual method (GMRES), which is designed for non symmetric systems [9, 19]. The key for fast solution lies in the choice of effective preconditioning strategies. The package offers a range of options, including algebraic methods such as incomplete LU factorizations, as well as more sophisticated and state- of-the-art multigrid methods designed to take advantage of the structure of the discrete linearized Navier-Stokes equations. In addition, there is a choice of iterative strategies, Picard iteration or Newton method, for solving the nonlinear algebraic systems arising from the latter problem.

This paper presents the unsteady Navier-Stocks equations with a new boundary condition noted by $C_{a,b}$. This condition generalizes the known conditions, especially the conditions of Dirichlet, Neumann...

If a *and* b are the real numbers strictly positive such that

$a << b$, then $C_{a,b}$ is the Neumann boundary condition and if $a >> b$ then $C_{a,b}$ is the Dirichlet boundary condition. For that a is called the Dirichlet coefficient and b is the Neumann coefficient. So, we prove that the weak formulation of the proposed modeling has a unique solution. To calculate this latter, we use the discretization by mixed finite element method. Moreover, to compare our solution with the some previously ones, as ADINA system, some numerical results are shown.

The paper is organized as follows. Section II presents the model problem. In the section III we show the existence and uniqueness of the solution of the standard weak formulation and of semi-descretization.

In section IV we describe the approximation of the standard weak formulation using mixed finite elements and Picards nonlinear iteration and using GMRES algorithm to solve it. Numerical experiments carried out within the framework of this publication and their comparisons with other results are shown in section V.

II. Unsteady Incompressible Navier-Stokes Equations

We consider the unsteady Navier-Stokes equations for the flow with constant viscosity.

$$\begin{cases} \dfrac{\partial \vec{u}}{\partial t} - \nu \nabla^2 \vec{u} + \vec{u}.\nabla \vec{u} + \nabla p = \vec{f} \ \text{ in } \ \Omega, \\ \nabla.\vec{u} = 0 \ \text{ in } \ \Omega, \\ \vec{u}(0) = \vec{u}_0 \ \text{ in } \ \Omega. \end{cases} \tag{1}$$

Where $\nu \succ 0$ a given constant is called the kinematic viscosity. $\vec{u}$ is the fluid velocity, p is the pressure field, ∇ is the gradient and $\nabla.$ is the divergence operator.

The boundary value problem that is considered is posed on two or three-dimensional domain Ω, is defined as:

$$C_{a,b} \ : \ a\vec{u} + b(\nu \nabla \vec{u} - pI)\vec{n} = \vec{t} \ in \ \Gamma := \partial\Omega \tag{2}$$

Where $\vec{n}$ that is the usual outward-pointing normal boundary.

$\vec{t} \in H^{\frac{1}{2}}(\Gamma)$, a and b are the function nonzero continuous defined on Γ verify:
There are two strictly positive constants α_1 and β_1, such that:

$$\alpha_1 \le \frac{a(x)}{b(x)} \le \beta_1 \quad \text{for all } x \in \Gamma \qquad (3)$$

This system is the basis for computational modeling of the flow of an incompressible fluid such as air or water. The presence of the nonlinear convection term $\vec{u}\nabla\vec{u}$ means that boundary value problems associated with the Navier-Stokes equations can have more than one solution.

We define the spaces

$$h^1(\Omega) = \left\{ u : \Omega \to IR / u; \frac{\partial u}{\partial x}; \frac{\partial u}{\partial y} \in L^2(\Omega) \right\} \qquad (4)$$

$$H^1(\Omega) = \left[h^1(\Omega) \right]^2 \qquad (5)$$

$$H_N^1(\Omega) = \left\{ \vec{v} \in H^1(\Omega) / \vec{v}.\vec{n} = 0 \ \text{ on } \Gamma \right\} \qquad (6)$$

$$\xi = \left\{ \vec{v} \in D(\overline{\Omega}) / \ \nabla.\vec{v} \ \text{ and } \ \vec{v}.\vec{n} = 0 \ \text{ on } \Gamma \right\} \qquad (7)$$

$$V(\Omega) = \left\{ \vec{v} \in H_N^1(\Omega) / \nabla.\vec{v} = 0 \ \text{ on } \Gamma \right\} \qquad (8)$$

$$H = \left\{ \vec{v} \in L^2(\Omega) / \ \nabla.\vec{v} \ \text{ and } \ \vec{v}.\vec{n} = 0 \ \text{ on } \Gamma \right\} \qquad (9)$$

$L^p(0,T;X)$ is the space of strongly measurable functions $f : (0,T) \to X$ such that:

$$\| f \|_{L^p(0,T;X)} = \left[\int_0^T \| f(t) \|_X^2 \, dt \right]^{\frac{1}{2}} \prec \infty,$$

$$\| f \|_{L^\infty(0,T;X)} = \sup \operatorname{ess}_{t \in (0,T)} \| f(t) \|_X \prec \infty.$$

For $\vec{u}$, $\vec{v}$ and $\vec{w}$ in $H^1(\Omega)$ we define, as usual, the following forms:

$$a_0(\vec{u},\vec{v}) = \nu \int_\Omega \nabla\vec{u} : \nabla\vec{v} + \int_\Gamma \frac{a}{b} \vec{u}\vec{v}$$

$$b(\vec{u},q) = -\int_\Omega q \nabla.\vec{u}$$

$$d(p,q) = \int_\Omega p.q$$

$$a_1(\vec{z},\vec{u},\vec{v}) = \int_\Omega (\vec{z}\nabla\vec{u})\vec{v}$$

$$c(\vec{z},\vec{u},\vec{v}) = a_0(\vec{u},\vec{v}) + a_1(\vec{z},\vec{u},\vec{v})$$

$$l(\vec{v}) = \int_\Gamma \frac{a}{b} \vec{t}.\vec{v} + \int_\Omega \vec{f}.\vec{v}.$$

For $\vec{u}$ and $\vec{w}$ in $L^2(0,T;V)$ we consider the function

$t \to A_0\vec{u}(t)$ defined a.e. on $[0, \ T]$ by:

$$A_0\vec{u}(t) \in V', \ \ \left\langle A_0\vec{u}(t), \vec{v} \right\rangle = a_0\left(\vec{u}(t), \vec{v}\right) \ \ \forall \vec{v} \in V.$$

It can be readily checked that $t \to A_0\vec{u}(t) \in L^2(0,T;V')$.

Next, consider the mapping $t \to A_1(\vec{w}(t), \vec{u}(t))$ defined a.e On $[0, \ T]$ by:

$$\begin{cases} A_1\left(\vec{w}(t), \vec{u}(t)\right) \in V', \\ \left\langle A_1\left(\vec{w}(t), \vec{u}(t)\right), \vec{v} \right\rangle = a_1\left(\vec{w}(t), \ \vec{u}(t), \vec{v}\right) \ \ \forall \vec{v} \in V \end{cases}$$

for all $\vec{v} \in V$.

The standard weak formulation of (1), find $\vec{u} \in H_N^1(\Omega)$ and $p \in L^2(\Omega)$ such that

$$\int_\Omega \frac{\partial \vec{u}}{\partial t} \vec{v} + c(\vec{z};\vec{u},\vec{v}) + b(\vec{v},q) = \int_\Omega \vec{f}\vec{v} + \int_\Gamma \frac{a}{b} \vec{t}\vec{v}, \qquad (10)$$

$$b(\vec{u},q) = 0, \qquad (11)$$

for all $\vec{v} \in H_N^1(\Omega)$ *and* $q \in L^2(\Omega)$.

The spaces $H^1(\Omega)$, $H_N^1(\Omega)$ and V equipped with the norms

$$\| \vec{v} \|_{J,\Omega} = \left(\nu \int_\Omega \nabla\vec{v} : \nabla\vec{v} d\Omega + \int_\Gamma \frac{a}{b} \vec{v}\vec{v} d\gamma \right)^{\frac{1}{2}}$$

$$\| \vec{v} \|_{1,\Omega} = \left(|\vec{v}|_{1,\Omega}^2 + \| \vec{v} \|_{0,\Omega}^2 \right)^{\frac{1}{2}}$$

The spaces H and $L^2(\Omega)$ equipped with the norm

$$\| \vec{v} \|_{0,\Omega} = \left(\vec{v}, \vec{v} \right)^{\frac{1}{2}}$$

$C_{a,b}$ is new boundary condition, for that we need to show the existence and uniqueness theorems for this modeling.

III. Existence And Uniquness Of The Solution

A. Weak formulation

THEOREM 1. There are two strictly positive constants c_1 and c_2 such that:

$$c_1 \| \vec{v} \|_{1,\Omega} \le \| \vec{v} \|_{J,\Omega} \le c_2 \| \vec{v} \|_{1,\Omega} \quad \textit{for all } \vec{v} \in H^1(\Omega) \qquad (12)$$

PROOF. 1) The mapping $\gamma_0 : H^1(\Omega) \to L^2(\Gamma)$ is continuous

(See [6] theorem 1, 2), then there exists $c \succ 0$ such that: $\| \vec{v} \|_{0,\Gamma} \le c \| \vec{v} \|_{1,\Omega}$ for all $\vec{v} \in H^1(\Omega)$. Using this result and the result (3) give,

$$\| \vec{v} \|_{J,\Omega} \le c_2 \| \vec{v} \|_{1,\Omega} \quad \textit{for all } \ \vec{v} \in H^1(\Omega),$$

with $c_2 = \left(\beta_1 c^2 + \nu \right)^{\frac{1}{2}}$. On other hand, according to 5.55 in [1], there exists a constant $\rho \succ 0$ such that

$\| \vec{v} \|_{0,\Omega}^2 \le \rho(\| \nabla\vec{v} \|_{0,\Omega}^2 + \| \vec{v} \|_{0,\Gamma}^2), \ \forall \vec{v} \in H^1(\Omega)$, using (3) and $\| \nabla\vec{v} \|_{0,\Omega}^2 \le \| \vec{v} \|_{J,\Omega}^2$, give

$$c_1 \| \vec{v} \|_{1,\Omega} \le \| \vec{v} \|_{J,\Omega} \quad \textit{for all } \ \vec{v} \in H^1(\Omega),$$

with $c_1 = \left(\frac{\rho C}{\nu\alpha_1} + \frac{1}{\nu} \right)^{-\frac{1}{2}}$ and $C = \max\{\alpha_1; \nu\}$.

Finally $c_1 \| \vec{v} \|_{1,\Omega} \le \| \vec{v} \|_{J,\Omega} \le c_2 \| \vec{v} \|_{1,\Omega}$ for all $\vec{v} \in H^1(\Omega)$.

- $(H^1(\Omega), \|.\|_{1,\Omega})$ is a real space and $H_N^1(\Omega)$ is closed in $H^1(\Omega)$ and $\|.\|_{1,\Omega}$ and $\|.\|_{J,\Omega}$ are equivalent norms, then $(H^1(\Omega), \|.\|_{J,\Omega})$ and $(H_N^1(\Omega), \|.\|_{J,\Omega})$ are a reals Hilbert spaces.

LEMMA 2. *All* $\vec{v} \in H_0^1(\Omega)$ satisfy

$$\|\vec{v}\|_{0,4,\Omega} \le 2^{\frac{1}{4}} |\vec{v}|_{1,\Omega}^{\frac{1}{2}} \|\vec{v}\|_{0,\Omega}^{\frac{1}{2}}. \quad (13)$$

PROOF. See lemma 1.5 chapter V [2].

LEMMA 3. *All* $\vec{v} \in H^1(\Omega)$ satisfy

$$\|\vec{v}\|_{0,4,\Omega} \le 2^{\frac{1}{4}} |\vec{v}|_{1,\Omega}^{\frac{1}{2}} \|\vec{v}\|_{0,\Omega}^{\frac{1}{2}}. \quad (14)$$

PROOF. Ω is a bounded open of IR^2 with Lipschitz continuous boundary, then there exists a sequence $(\Omega_n)_{n\ge 0}$ of opens, such that

For all $n \ge 0, \Omega_n \subset \Omega$ *and* $\lim_{n\to\infty} \Omega_n = \Omega$.

Let φ_n be a function defined as:

$$\begin{cases} \varphi_n = 1 \ on \ \Omega_n, \\ \varphi_n = 1 \ on \ \Omega - \Omega_n. \end{cases} \quad (15)$$

Then for all $\vec{v} \in H^1(\Omega)$, we get $\varphi_n \vec{v} \in H_0^1(\Omega)$, for all $n \ge 0$, According to lemma 2,

$$\|\varphi_n \vec{v}\|_{0,4,\Omega} \le 2^{\frac{1}{4}} |\varphi_n \vec{v}|_{1,\Omega}^{\frac{1}{2}} \|\varphi_n \vec{v}\|_{0,\Omega}^{\frac{1}{2}}.$$

By applying dominated convergence Theorem, we get

$$\|\vec{v}\|_{0,4,\Omega} \le 2^{\frac{1}{4}} |\vec{v}|_{1,\Omega}^{\frac{1}{2}} \|\vec{v}\|_{0,\Omega}^{\frac{1}{2}}.$$

LEMMA 4. when $\vec{w}$ and $\vec{u}$ belong both to $L^2(0, T; V) \cap L^\infty(0, T; H)$ then

$$A_1(\vec{w}, \vec{u}) \in L^2(0, T; V') \quad (16)$$

PROOF. $\vec{w}, \ \vec{u}, \ \vec{v} \in V$, we have

$$\begin{aligned} a_1(\vec{w}, \vec{u}, \vec{v}) + a_1(\vec{w}, \vec{v}, \vec{u}) &= \int_\Omega \vec{w}.(\nabla \vec{u}.\vec{v} + \nabla \vec{v}.\vec{u}) \\ &= \int_\Omega \vec{w}.\nabla(\vec{u}.\vec{v}). \end{aligned}$$

Use Green's theorem to show that

$$\begin{aligned} a_1(\vec{w}, \vec{u}, \vec{v}) + a_1(\vec{w}, \vec{v}, \vec{u}) &= \int_{\partial\Omega} (\vec{z}.\vec{n})(\vec{u}.\vec{v}) - \int_\Omega div\ \vec{z}.(\vec{u}.\vec{v}) \\ &= 0. \end{aligned}$$

Then, $a_1(\vec{w}, \vec{u}, \vec{v}) = -a_1(\vec{w}, \vec{v}, \vec{u})$, and we have the upper bound:

$$a_1(\vec{w}, \vec{u}, \vec{v}) \le c_1 \|\vec{w}\|_{0,4,\Omega} \|\vec{u}\|_{0,4,\Omega} |\vec{v}|_{1,\Omega}$$

Therefore

$$\|A_1(\vec{w}(t), \vec{u}(t))\|_* \le c_1 \|\vec{w}(t)\|_{0,4,\Omega} \|\vec{u}(t)\|_{0,4,\Omega}. \quad (17)$$

We make use of lemma 2. According to (14) and (17), we have

$$\|A_1(\vec{w}(t), \vec{u}(t))\|_*^2 \le 2c_1 |\vec{w}(t)|_{1,\Omega} |\vec{u}(t)|_{1,\Omega} \|\vec{w}(t)\|_{0,\Omega} \|\vec{u}(t)\|_{0,\Omega} \quad (18)$$

Therefore,

$$\begin{aligned} &\int_0^T \|A_1(\vec{w}(t), \vec{u}(t))\|_*^2 dt \\ &\quad \le C \|\vec{w}\|_{L^\infty(0,T;H)} \|\vec{u}\|_{L^\infty(0,T;H)} \|\vec{w}\|_{L^2(0,T;V)} \|\vec{u}\|_{L^2(0,T;V)} \end{aligned}$$

This proves (16).

In the course of this proof we have shown that, if $\vec{u}$ belongs both to $L^2(0, T; V) \cap L^\infty(0, T; H)$ then

$$\|A_1(\vec{u}, \vec{u})\|_{L^2(0,T;V')} \le C \|\vec{u}\|_{L^\infty(0,T;H)} \|\vec{u}\|_{L^2(0,T;V)} \quad (19)$$

With these spaces and forms, consider the following variational formulation of problem (1)-(2).

For a given function $\vec{f} \in L^2(0, T; H^{-1}(\Omega))$ and a given element $\vec{u}_0$ of H, find $\vec{u} \in L^2(0, T; V) \cap L^\infty(0, T; H)$ Such that

$$\begin{cases} \bullet \ \dfrac{d}{dt}(\vec{u}(t), \vec{v}) + c(\vec{u}(t); \vec{u}(t), \vec{v}) = \int_\Omega \vec{f}\vec{v} + \int_\Gamma \vec{t}\vec{v}, \\ \quad \forall \vec{v} \in V, \ \text{in} \ D'(]0, T[), \\ \bullet \ \vec{u}(0) = \vec{u}_0 \quad \text{in} \ \Omega. \end{cases} \quad (20)$$

THEOREM 5. Let $\vec{u} \in L^2(0, T; V) \cap L^\infty(0, T; H)$ be solution of (20). Then $\dfrac{d\vec{u}}{dt} \in L^2(0, T; V')$.

PROOF. We have

$$c(\vec{u}(t); \vec{u}(t), \vec{v}) = \langle A_0 \ \vec{u}(t) + A_1(\vec{u}(t), \vec{u}(t)), \vec{v} \rangle$$

for all $\vec{v} \in V$.

Therefore, by Lemma 1.1 chapter V in [2], each solution $\vec{u}$ of (20) satisfies in D'(]0, T[):

$$\left\langle \frac{d\vec{u}}{dt}(t), \vec{v} \right\rangle = \int_\Omega \vec{f}\vec{v} + \int_\Gamma \frac{a}{b} \vec{t}\vec{v} - \langle A_0 \ \vec{u}(t) + A_1(\vec{u}(t), \vec{u}(t)), \vec{v} \rangle$$

for all $\vec{v} \in V$.

Now, by hypothesis

$$l : \vec{v} \to \int_\Omega \vec{f}\vec{v} + \int_\Gamma \frac{a}{b} \vec{t}\vec{v} \in L^2(0, T; V')$$

and we have mentioned previously that $A_0 \vec{u} \in L^2(0, T; V')$ when $\vec{u} \in L^2(0, T; V)$. Furthermore $A_1(\vec{u}, \vec{u}) \in L^2(0, T; V')$

Hence, $\dfrac{d\vec{u}}{dt} \in L^2(0, T; V')$.

According to Theorem 5 and Theorem 1.1 in [2] chapter V, $\vec{u} \in C^0([0,T];H)$.

In this case, it is perfectly allowable to prescribe the value of $\vec{u}$ at *t=0*. Moreover, it stems from the above proof that problem (20) can be equivalently stated as follows:

For a given function $\vec{f} \in L^2(0,T;H^{-1}(\Omega))$ and a given element $\vec{u}_0$ of H, find

$$\begin{cases} \bullet\ \vec{u} \in L^2(0,T;V) \cap L^\infty(0,T;H) \\ with\ \dfrac{d\vec{u}}{dt} \in L^2(0,T;V')\ such\ that \\ \bullet\ \dfrac{d\vec{u}}{dt} + A_0\,\vec{u} + A_1(\vec{u},\vec{u}) = L, \\ \bullet\ \vec{u}(0) = \vec{u}_0 \quad in\ \ \Omega. \end{cases} \tag{21}$$

We consider the following problem:

For a given function $\vec{f} \in L^2(0,T;H^{-1}(\Omega))$ and a given element $\vec{u}_0$ of H, find $(\vec{u}, p)$ such that

$$\begin{cases} \bullet\ \vec{u} \in L^2(0,T;V) \cap L^\infty(0,T;H) \\ with\ \dfrac{d\vec{u}}{dt} \in L^2(0,T;V')\ and\ D'(\Omega\times]0,T[) \\ \bullet\ \dfrac{\partial\vec{u}}{\partial t} - \nu\nabla^2\vec{u} + \vec{u}.\nabla\vec{u} + \nabla p = \vec{f} \quad in\ \ \Omega, \\ \bullet\ \vec{u}(0) = \vec{u}_0 \quad in\ \ \Omega. \end{cases} \tag{22}$$

THEOREM 6. Problem (21) and (22) are equivalent.

To show this Theorem we need the following lemmas

LEMMA7. Let $\vec{g} \in H^{\frac{1}{2}}(\Gamma)$ satisfies $\int_\Gamma \vec{g}\vec{n}\,d\lambda = 0$. Then there exists a function $\vec{u} \in H^1(\Omega)$ such that

$$div\,\vec{u} = 0\ and\ \vec{u} = \vec{g}\ on\ \ \Gamma.$$

PROOF. See Temam [20].

LEMMA8. The divergence operator is an isomorphism from $V^\perp$ onto $L_0^2(\Omega)$, verifies: There exists $\alpha \succ 0$ such that

$$\|div\,\vec{v}\|_{0,\Omega}^2 \geq \alpha\|\vec{v}\|_{J,\Omega}^2\ \ \forall\vec{v} \in V^\perp.$$

PROOF. Let $\vec{v} \in H_N^1(\Omega)$ By Green's formula:

$$\int_\Omega div\,\vec{v}\,dx = \int_\Gamma \vec{v}.\vec{n}\,d\lambda = 0.$$

Let q a function of $L_0^2(\Omega)$. As Ω is bounded, there exists some function $\theta \in L^2(\Omega)$ such that

$\Delta\theta = q\ in\ \ \Omega.$

We set $\vec{v}_1 = \overrightarrow{grad}\,\theta\ \ in\ \ \Omega$. Then

$div\,\vec{v}_1 = \Delta\theta = q\ \ in\ \ \Omega$; moreover, by Green's formula

$\int_\Gamma \vec{v}_1.\vec{n}\,d\lambda = \int_\Omega div\,\vec{v}_1\,dx = \int_\Omega q\,dx = 0.$

Also $\gamma_0\vec{v}_1 \in H^{\frac{1}{2}}(\Gamma)$. Therefore, we can apply Lemma 7: there exists $\vec{w}_1 \in H^1(\Omega)$ such that $div\,\vec{w}_1 = 0$ and $\gamma_0\vec{v}_1 = \gamma_0\vec{w}_1$. then $\vec{v} = \vec{v}_1 - \vec{w}_1$ is the required function since $\vec{v} \in H_0^1(\Omega)$ and $div\,\vec{v} = q$.

Finally, it follows from the open mapping Theorem (cf.Yosida [21]) that the inverse of div is continuous from $L_0^2(\Omega)$ onto $V^\perp$, therefore div is an isomorphism.

LEMMA 9. Let $\vec{l} \in H^{-1}(\Omega)$ and satisfy

$$\langle\vec{l},\vec{v}\rangle = 0,\ \forall\vec{v} \in V^\perp$$

Then there exists exactly one function φ in $L_0^2(\Omega)$ such that:

$$\langle\vec{l},\vec{v}\rangle = \int_\Omega \varphi div\vec{v}\,dx = -\langle\overrightarrow{grad}\varphi,\vec{v}\rangle. \tag{23}$$

$\forall\vec{v} \in H_N^1(\Omega).$

PROOF. Consider the following problem:

Find $\vec{u} \in V^\perp$ satisfying

$$\langle div\,\vec{u}, div\,\vec{v}\rangle = \langle\vec{l},\vec{v}\rangle, \forall\vec{v} \in V^\perp. \tag{24}$$

By the Lemma 8 and the Lax-Milgram's Theorem, (24) has a unique solution $\vec{u}$ in $V^\perp$. Then,

$$\langle div\,\vec{u}, div\,\vec{v}\rangle = \langle\vec{l},\vec{v}\rangle, \forall\vec{v} \in H_N^1(\Omega).$$

We set $\varphi = div\,\vec{u} \in L_0^2(\Omega)$ and we find (23).

It remains to prove that φ is unique in $L_0^2(\Omega)$. But clearly, if $\varphi \in L_0^2(\Omega)$ and $\langle\varphi, div\,\vec{v}\rangle = 0\ \ \forall\vec{v} \in H_N^1(\Omega)$, then $\varphi = 0$ since div maps $H_N^1(\Omega)$, onto $L_0^2(\Omega)$.

PROOF OF THEOREM 6. Clearly, if $(\vec{u}, p)$ is a solution of (22), then $\vec{u}$ satisfies (21).

Conversely, let $\vec{u} \in L^2(0,T;V) \cap L^\infty(0,T;H)$

A solution of (21) and consider the mapping defined on $H_N^1(\Omega)$, by:

$$L(\vec{v},t) = \int_0^t \left\{\langle\vec{f}(s),\vec{v}\rangle - c(\vec{u}(t);\vec{u}(t),\vec{v})\right\}ds - (\vec{u}(t),\vec{v}) + (\vec{u}_0,\vec{v})$$

For each *t*, L is a linear functional on $H_N^1(\Omega)$, that vanishes on *V*. Hence, according to Lemma 9, for each *t* there exists exactly one function $P(t) \in L_0^2(\Omega)$, such that

$$L(\vec{v},t) = -\langle\overrightarrow{grad}\,P(t),\vec{v}\rangle\ \ \forall\vec{v} \in H_N^1(\Omega).$$

In other words,

$$(P(t),\vec{v}) = \int_0^t \left\{\langle\vec{f}(s),\vec{v}\rangle - c(\vec{u}(s);\vec{u}(s),\vec{v})\right\}ds - (\vec{u}(t),\vec{v}) + (\vec{u}_0,\vec{v})$$

$$\forall\vec{v} \in H_N^1(\Omega). \tag{25}$$

By using Lemma 4, it can be checked that

$P \in C^0\left([0,T]; L_0^2(\Omega)\right)$

Next, by differentiating (25), we get:

$$\begin{aligned}&(\frac{dP(t)}{dt}, \vec{v})\\ &= \left\{\left\langle \vec{f}(s), \vec{v}\right\rangle - c(\vec{u}(s); \vec{u}(s), \vec{v})\right\} - (\frac{d\vec{u}(t)}{dt}, \vec{v}) + (\vec{u}_0, \vec{v})\\ &\qquad \forall \vec{v} \in H_N^1(\Omega). \end{aligned} \tag{26}$$

Thus, if we set $p = \frac{dP}{dt}$ in $D'(\Omega \times]0,T[)$, we find the second equation of (22).

THEOREM 10. Problem (21) has a unique solution in

$\vec{u} \in L^2(0,T;V) \cap L^\infty(0,T;H)$

PROOF. The same steps of proof of Theorem 1.5 chapter VI in [2] but the spaces *V, H,* $H_N^1(\Omega)$... are note the same. .

B. Semi-discritisation

In this paragraph, we propose to analyze a very simple one-step method in order to illustrate the type of argument that is often used when dealing with semi-discretization. Consider again the problem (20).

find $\vec{u} \in L^2(0,T;V) \cap L^\infty(0,T;H)$ Such that

$$\begin{cases} \bullet \ \dfrac{d}{dt}(\vec{u}(t), \vec{v}) + c(\vec{u}(t); \vec{u}(t), \vec{v}) = l(\vec{v}), \\ \quad \forall \vec{v} \in V, \text{ in } D'(]0,T[), \\ \bullet \ \vec{u}(0) = \vec{u}_0 \quad \text{in } \Omega. \end{cases} \tag{27}$$

Let $k = \frac{T}{N}$ and t_n the subdivisions of [0, T]: $t_n = nk$; $0 \le n \le N$.

Now, suppose that an approximation, $\vec{u}^n \in V$, of $\vec{u}(t_n)$ is available and consider the following problem:

$$\begin{cases} \bullet \ \textit{find } \vec{u}^{n+1} \in V \textit{ such that} \\ \bullet \ \dfrac{1}{k}\left(\vec{u}^{n+1} - \vec{u}^n, \vec{v}\right) + c(\vec{u}^n; \vec{u}^{n+1}, \vec{v}) \\ \qquad = \int_\Omega \vec{f}(t_{n+1})\vec{v} + \int_\Gamma \vec{t}(t_{n+1})\vec{v}, \forall \vec{v} \in V. \end{cases} \tag{28}$$

$\vec{u}^n$, $\vec{f}(t_{n+1})$ and $\vec{t}(t_{n+1})$ are given respectively in V and V', it follows that (28) can be expressed in the from:

$$\begin{cases} \bullet \ \textit{find } \vec{u}^{n+1} \in V \textit{ such that} \\ \bullet \ \left(\vec{u}^{n+1}, \vec{v}\right) + kc(\vec{u}^n; \vec{u}^{n+1}, \vec{v}) \\ = k\left[\int_\Omega \vec{f}(t_{n+1})\vec{v} + \int_\Gamma \vec{t}(t_{n+1})\vec{v},\right] + (\vec{u}_n, \vec{v}) \ \forall \vec{v} \in V. \end{cases} \tag{29}$$

Thus, we are asked to solve a linear boundary value problem associated with the bilinear form:

$$(\vec{u}, \vec{v}) \to (\vec{u}, \vec{v}) + kc(\vec{u}^n; \vec{u}, \vec{v}).$$

This form is continuous in $V \times V$ and V-elliptic since

$$(\vec{v}, \vec{v}) + kc(\vec{u}^n; \vec{v}, \vec{v}) = \|\vec{v}\|_{0,\Omega}^2 + k\|\vec{v}\|_{J,\Omega}^2$$

Therefore, by Lax-Mailgram's theorem [2], problem (29) has a unique solution $\vec{u}^{n+1}$ in *V*.

IV. DISCRETIZATION BY MIXED FINITE ELEMENTS

Our goal here is to consider the unsteady Navier-Stokes equations with $C_{a,b}$ boundary conditions in a two dimensional domain and to approximate them by a mixed finite element method.

Mixed finite element discretization of the weak formulation of the Navier- Stokes equations gives rise to a nonlinear system of algebraic equations. Two classical iterative procedures for solving this system are Newton iteration and Picard iteration

Let $T_h\ ; h \succ 0,$ be a family of rectangulations of Ω. For any $T \in T_h$.

We denote by h_T the diameter of a simplex, by h_E the diameter of a face E of T, and we set $h = \max_{T \in T_h}\{h_T\}$.

A discrete weak formulation is defined using finite dimensional spaces $X_h^1 \subset H_N^1(\Omega)$ and $M^h \subset L_0^2(\Omega)$

The discrete version of (10)-(11) is:

$$\begin{aligned} &\textit{find } \vec{u}_h \in X_h^1 \text{ and } p_h \in M^h \text{ such that:} \\ &\bullet \int_\Omega \frac{\partial \vec{u}_h}{\partial t}\vec{v}_h + \nu \int_\Omega \nabla \vec{u}_h : \nabla \vec{v}_h + \int_{\partial\Omega} \frac{a}{b}\vec{u}_h.\vec{v}_h + a_1(\vec{u}_h, \vec{u}_h, \vec{v}_h) \\ &\qquad + b(\vec{v}_h, p_h) = \int_\Omega \vec{f}\vec{v}_h + \int_\Gamma \frac{a}{b}\vec{t}\vec{v}_h \end{aligned} \tag{30}$$

$$\bullet \ b(\vec{u}_h, q_h) = 0 \tag{31}$$

$\textit{for all } \vec{v}_h \in X_h^1 \text{ and } q_h \in M^h.$

We define the appropriate bases for the finite element spaces, leading to a non linear system of algebraic equations. To define the corresponding linear algebra problem, we use a set of vector-valued basis functions $\{\vec{\varphi}_i\}_{i=1,\ldots,n_u}$ So that

$$\vec{u}_h(t,x,y) = \sum_{j=1}^{n_u} u_j(t)\vec{\varphi}_j(x,y) \tag{32}$$

We introduce a set of pressure basis functions $\{\psi_k\}_{k=1,...n_p}$ and set

$$p_h(t,x,y)=\sum_{k=1}^{n_p} p_k(t)\psi_k(x,y) \quad (33)$$

Where n_u and n_p are the numbers of velocity and pressure basis functions, respectively.

$$D\frac{dU}{dt}(t)+[N(U(t))+M]U(t)+BP(t)=L(t) \quad (34)$$

$$B^T U(t)=0 \quad (35)$$

With

$$U(t)=\left(u_1(t),u_2(t),...,u_{n_u}(t)\right)^T$$

$$P(t)=\left(p_1(t),p_2(t),...,p_{n_p}(t)\right)^T$$

$$D(d_{i,j});\ d_{i,j}=\int_\Omega \vec{\varphi}_i.\vec{\varphi}_j,$$

$$N(U(t))=(c_{i,j}),\ c_{i,j}=\sum_{k=1}^{n_u} u_k(t)\int_\Omega (\vec{\varphi}_j.\nabla\vec{\varphi}_k)\vec{\varphi}_i,$$

$$M=(m_{i,j}),\ m_{i,j}=\nu\int_\Omega \nabla\vec{\varphi}_j:\nabla\vec{\varphi}_i+\int_\Omega \frac{a}{b}\vec{\varphi}_j\vec{\varphi}_i,$$

$$M=(m_{i,j}),\ m_{i,j}=\nu\int_\Omega \nabla\vec{\varphi}_j:\nabla\vec{\varphi}_i+\int_\Omega \frac{a}{b}\vec{\varphi}_j\vec{\varphi}_i,$$

$$B=[b_{k,j}];\ b_{k,j}=-\int_\Omega \psi_k\nabla.\vec{\varphi}_j$$

$$L(t)=(l_i(t));\ l_i(t)=\int_\Omega \vec{f}(t).\vec{\varphi}_i+\int_\Gamma \frac{a}{b}\vec{t}(t)\vec{\varphi}_i$$

for $i,j=1,...,n_u$, and $k=1,...,n_p$.

Using the backward Euler method for the time derivative and substituting into (34)-(35), one obtains the following system of nonlinear equations in tensor notation:

$$U(0)=\left(u_1(0),u_2(0),...,u_{n_u}(0)\right)^T, \quad (36)$$

$$D\frac{U^{n+1}-U^n}{k}+\left[N(U^{n+1})+M\right]U^{n+1}+BP^{n+1}=L(t_{n+1}), \quad (37)$$

$$B^T U^{n+1}=0. \quad (38)$$

With $u_1(0),u_2(0),...,u_{n_u}(0)$ are the coordinates in the basis $\{\vec{\varphi}_i\}_{i=1,...n_u}$ of the approximation of $\vec{u}_0$ in X_h. Solution of the nonlinear system of equations, Eq. (34)-(35), can be carried out efficiently using Picards method, where we start with an initial guess $(U^{n,0},P^{n,0})\in IR^{n_u+n_p}$ and construct a sequence of iterates $(U^{n,m},P^{n,m})\in IR^{n_u+n_p}$ it converges to the solution of (34)-(35). In this approach we approximate the nonlinear convection term as follows:

$$\left[N(U^{n+1})+M\right]U^{n+1}\cong\left[N(U^{n+1,m})+M\right]U^{n+1,m+1}$$

For the finite-element basis functions, we chose to work with stable rectangular elements (Q2-Q1), where we use biquadratic approximation for the velocity components, bilinear approximation for the pressure, and stable triangular elements (P2-P1), where we use quadratic approximation for the velocity components and linear approximation for the pressure.

The linear system we need to solve within each iteration of Picards method has the following generic form:

$$\begin{pmatrix} A_0+N & B_0^T \\ B_0 & 0 \end{pmatrix}\begin{pmatrix} U \\ P \end{pmatrix}=\begin{pmatrix} f \\ 0 \end{pmatrix}. \quad (39)$$

We use the generalized minimum residual method (GMRES) for solving the nonsymmetric systems. Preconditioning is a technique used to enhance the convergence of an iterative method to solve a large linear system iteratively. Instead of solving a system

$Ax = b$, one solves a system $P^{-1}Ax=P^{-1}b$, where P is the preconditioned. A good preconditioned should lead to fast convergence of the Krylov method. Furthermore, systems of the form Pz = r should be easy to solve. For the Navier-Stokes equations, the objective is to design a preconditioned that increases the convergence of an iterative method independent of the Reynolds number and number of grid points. We use a least-squares commutator preconditioning [10, 11,12].

V. NUMERICAL SIMULATIONS

In this section, some numerical results of calculations with mixed finite element method and ADINA system will be presented. Using our solver, we run two traditional test problems (driven cavity flow [9, 14, 15, 16, 17], Backward-facing step problem [10, 13]) and the flow over an obstacle [9] with a number of different model parameters.

EXAMPLE 1. Driven cavity flow. It is a model of the flow in a square cavity with the lid moving from left to right. Let the computational model: $\{y=1;-1\le x\le 1/u_x=1-x^4\}$, a regularized cavity. The streamlines are computed from the velocity solution by solving the Poisson equation numerically subject to a zero Dirichlet boundary condition.

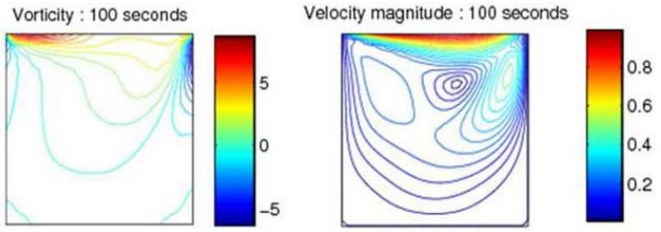

Fig.1. Vorticity (left plot), and velocity magnitude solution (right plot) using $P2-P1$ approximation a 64 × 64 square grid and Reynolds number Re =100.

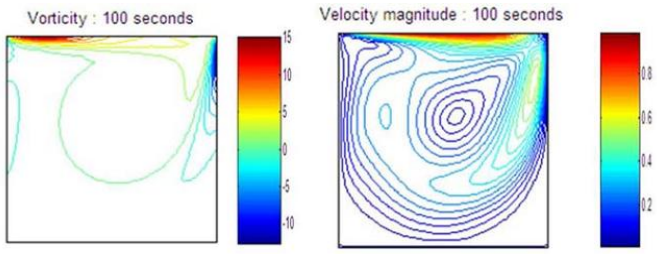

Fig.3. Vorticity (left plot), and velocity magnitude solution (right plot) using $P2 - P1$ approximation a 64 × 64 square grid and Reynolds number Re =400.

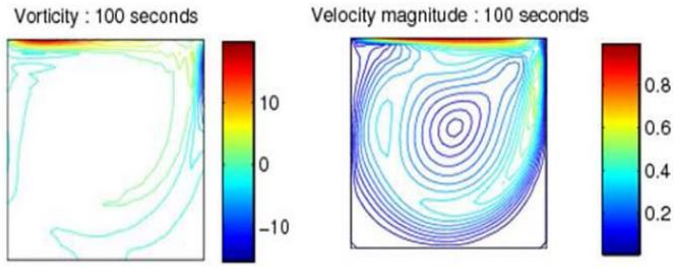

Fig.2. Vorticity (left plot), and velocity magnitude solution (right plot) using $P2 - P1$ approximation, a 64 × 64 square grid and Reynolds number Re=1000.

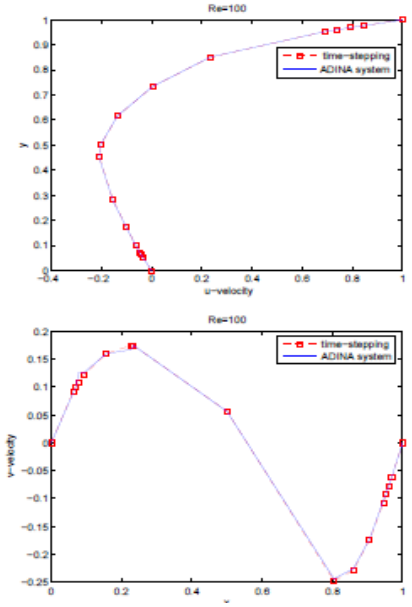

Fig.4. The velocity component u at vertical center line (left plot), and the velocity component v horizontal center line (right plot) with a 129 × 129 grid and Re=100.

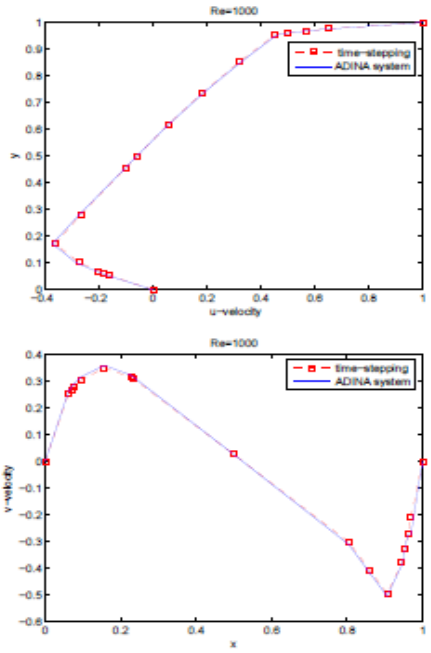

Fig.5. The velocity component u at vertical centerline (left plot), and the velocity component v at horizontal center line (right plot) with a 129 × 129 grid and Re=1000.

Figures 4 and 5 shows the velocity profiles for lines passing through the geometric center of the cavity. These features clearly demonstrate the high accuracy achieved by the proposed mixed finite element method for solving the unsteady Navier-Stokes equations in the lid-driven squared cavity.

EXAMPLE 2. L-shaped domain Ω, parabolic inflow boundary condition, natural outflow boundary condition.

This example represents flow in a rectangular duct with a sudden expansion; a Poiseuille flow profile is imposed on the inflow boundary $\{x = -1;\ 0 \le y \le 1\}$, and a no-flow (zero velocity) condition is imposed on the walls.

The Neumann condition is applied at the outflow boundary (x=5; $-1 < y < 1$) and automatically sets the mean outflow pressure to zero.

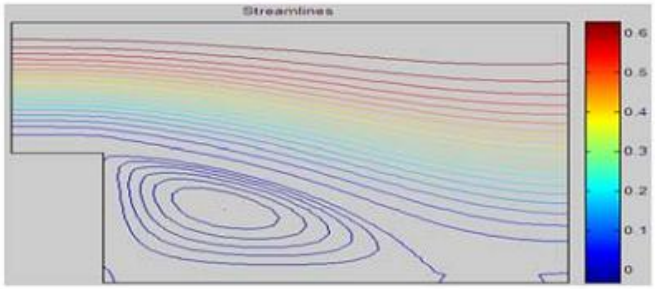

Fig.6. Equally spaced streamline plot associated with a 32 × 96 square grid, $Q_1 - P_0$ approximation and $\nu = 1/100$ (t=100 seconds).

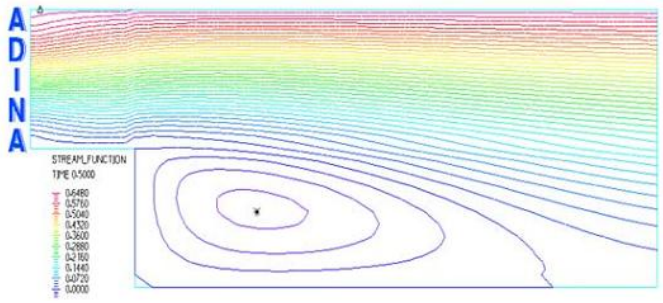

Fig.7. The solution computed with ADINA system. The plot show the streamlines associated with a 32 × 96 square grid and $\nu = 1/100$ (t=100 seconds).

The two solutions are therefore essentially identical. This is very good indication that my solver is implemented correctly.

VI. Conclusion

In this work, we were interested in the numerical solution of the partial differential equations by simulating the flow of an incompressible fluid. We introduced the unsteady Navier-Stokes equations with a new boundary condition noted Ca,b. We have shown the existence and uniqueness of the solution of the weak formulation and the solution of the semi-discretization. We used the discretization by mixed finite element method.

Numerical experiments were carried out and compared with satisfaction with other numerical results, either resulting from the literature, or resulting from calculation with commercial software like Adina system.

ACKNOWLEDGMENTS

The authors would like to express their sincere thanks for the referee for his/her helpful suggestions.

REFERENCES

[1] Alexandre Ern, Aide-m´emoire El´ements Finis, Dunod, Paris, 2005.
[2] P.A. Raviart, J. Thomas, Introduction l'analyse numerique des équations aux d´erivées partielles, Masson, Paris, 1983.
[3] R.E. Bank, B. Welfert, A posteriori error estimates for the Stokes problem, SIAM J. Numer. Anal 28, pp. 591-623, 1991.
[4] C. Carstensen, S.A. Funken. A posteriori error control in low-order finite element discretizations of incompressible stationary flow problems. Math. Comp., 70, pp. 1353-1381, 2001.
[5] R. Verfurth, A Review of A Posteriori Error Estimation and Adaptive Mesh-Refinement Techniques, Wiley-Teubner, Chichester, 1996.
[6] D.H. Wu, I.G. Currie. Analysis of a posteriori error indicator in viscous flows. Int.J.Num. Meth.Heat Fluid Flow., 12, pp. 306-327, 2001.
[7] E. Creuse, G. Kunert, S. Nicaise, A posteriori error estimation for the Stokes problem: Anisotropic and isotropic discretizations, M3AS 14, pp. 1297-1341, 2001.
[8] P. Clement, Approximation by finite element functions using local regularization, RAIRO. Anal. Numer. 2, pp. 77-84, 1975.
[9] H. Elman, D. Silvester, A. Wathen, Finite Elements and Fast Iterative Solvers: with Applications in Incompressible Fluid Dynamics, Oxford University Press, Oxford, 2005.
[10] M. ur Rehman, C. Vuik and G. Segal, A comparison of preconditioners for incompressible Navier-Stokes solvers, Int. J. Numer. Meth. Fluids, 57, pp.1731-1751,2007.
[11] H. Elman, V.E. Howle, J. Shadid, D. Silvester, and R. Tuminaro, Least squares preconditioners for stabilized discretizations of the Navier-Stokes equations. SIAM J. Sci. Comput., 30, 290-311, 2007.
[12] A. Gauthier, F. Saleri, and A. Veneziani, A fast preconditioner for the incompressible Navier-Stokes equations, Comput. Visual. Sci, 6, pp. 105 -112, 2004.
[13] P. Gresho, D. Gartling, J. Torczynski, K. Cliffe, K. Winters, T. Garratt, A. Spence, and J.Goodrich, Is the steady viscous incompressible 2d flow over a backward facing step at Re =800 stable?, Int. J. Numer. Methods Fluids, 17, pp. 501-541, 1993.
[14] S. Turek, A comparative study of some time-stepping techniques for the incompressible Navier-Stokes equations: From fully implicit nonlinear schemes to semi-implicit projection methods, Int. J. Numer. Meth. Fluids, 22, pp.987-1011, 1996.
[15] E. Erturk, T.C. Corke and C. Gokcol, Numerical solutions of 2-D steady incompressible driven cavity flow at high Reynolds numbers, Int. J. Numer. Meth. Fluids, 48, pp.747-774, 2005.
[16] S. Garcia, The Lid-Driven Square Cavity Flow: from Stationary to Time Periodic and Chaotic, Commun. Comput. Phys, 2, pp.900-932, 2007.
[17] E. Barragy and G.F. Carey, Stream function vorticity driven cavity solution using p finite elements, Comput. Fluids, 26, pp.453-468, 1997.
[18] F. Brezzi and M. Fortin, Mixed and Hybrid Finite Element Method, Springer Verlag; New York, 1991.
[19] A. Nejat, and C. Ollivier-Gooch, Effect of discretization order on preconditioning and convergence of a high-order unstructured Newton GMRES solver for the Euler equations, J. Comput. Phys. 227, pp.2366 2386.2008.
[20] R.Temam Navier-Stokes Equations. North Holland, Amsterdam,1977.
[21] K.Yosida, Functional Analysis. Spriger-Verlag, Berlin,1965.
[22] Elman, H. and Ramage, A. and Silvester, D.J. *Algorithm 866: IFISS: a* Matlab toolbox for modelling incompressible flow. ACM Transactions on Mathematical Software, 33, pp.1-18, 2007.
[23] S.Alami1, A.Elakkad, and A. Elkhalfi, A posteriori error estimation for incompressible flow problem, IJMER, 2, pp. 533-538, 2012.
[24] Mohamed S. Ebeida, Roger L. Davis† and Roland W. Freund, Unsteady Incompressible Flow Simulation Using Galerkin Finite Elements with Spatial/Temporal Adaptation, American Institute of Aeronautics and Astronautics, pp.1-11, 2007.

An Overview of Recent Machine Learning Strategies in Data Mining

Bhanu Prakash Battula
Research Scholar
Acharya Nagarjuna University
Guntur, Andhra Pradesh, India

Dr. R. Satya Prasad
Associate Professor
Acharya Nagarjuna University
Guntur, Andhra Pradesh, India

***Abstract*—Most of the existing classification techniques concentrate on learning the datasets as a single similar unit, in spite of so many differentiating attributes and complexities involved. However, traditional classification techniques, require to analysis the dataset prior to learning and for not doing so they loss their performance in terms of accuracy and AUC. To this end, many of the machine learning problems can be very easily solved just by careful observing human learning and training nature and then mimic the same in the machine learning.**

This paper presents an updated literature survey of current and novel machine learning strategies inducing models efficiently for supervised and unsupervised learning in data mining.

Keywords—Data mining; classification; supervised learning; unsupervised learning; learning strategies.

I. INTRODUCTION

One of the research hotspots in the field of machine learning is classification. There are different types of classification models such as decision trees, SVM, neural networks, Bayesian belief networks, Genetic algorithm etc. The simple structure, the wide applicability on real time problems, the high efficiency and the high accuracy are the strengths for decision trees. In recent years, many authors proposed improvements in decision trees learning strategy. A large number of classifiers build the model of dataset for classification by using the traditional learning strategies. On the other hand, the traditional learning techniques are bottle necked the performance of the datasets. However, several investigations also suggest that there are other factors that contribute to such performance degradation, for example, size of the dataset, density of the dataset, and overall complexity of the dataset. This paper presents an updated survey of various machine learning strategies. It also describes the applicability of the algorithm on real-world data.

The rest of this paper is organized as follows. Section 2 presents the basics of data mining. Section 3 describes a generic datasets and measures used for recent learning strategies. Several recent works related to different learning strategies are reviewed in Section 4. Section 5 concludes our work by presenting future scope on the topic.

II. DATA MINING

A. Basics of Data Mining

Data Mining is the analysis of (often large) observational data sets to find unsuspected relationships and to summarize the data in novel ways that are both understandable and useful to the owner [1]. There are many different data mining functionalities. A brief definition of each of these functionalities is now presented. The definitions are directly collated from [2]. Data characterization is the summarization of the general characteristics or features of a target class of data. Data Discrimination, on the other hand, is a comparison of the general features of target class data objects with the general features of objects from one or a set of contrasting classes. Association analysis is the discovery of association rules showing attribute value conditions that occur frequently together in a given set of data.

Classification is an important application area for data mining. Classification is the process of finding a set of models (or functions) that describe and distinguish data classes or concepts, for the purpose of being able to use the model to predict the class of objects whose class label is unknown. The derived model can be represented in various forms, such as classification rules, decision trees, mathematical formulae, or neural networks. Unlike classification and prediction, which analyze class-labeled data objects, clustering analyzes data objects without consulting a known class label.

Outlier Analysis attempts to find outliers or anomalies in data. A detailed discussion of these various functionalities can be found in [2]. Even an overview of the representative algorithms developed for knowledge discovery is beyond the scope of this paper. The interested person is directed to the many books which amply cover this in detail [1], [2].

B. Classificationa and Clustering Tasks

Learning how to classify objects to one of a pre-specified set of categories or classes is a characteristic of intelligence that has been of keen interest to researchers in psychology and computer science. Identifying the common ―core‖ characteristics of a set of objects that are representative of their class is of enormous use in focusing the attention of a person or computer program. For example, to determine whether an animal is a zebra, people know to look for stripes rather than examine its tail or ears. Thus, stripes figure strongly in our *concept* (generalization) of zebras. Of course stripes alone are not sufficient to form a class description for zebras as tigers have them also, but they are certainly one of the important characteristics.

The ability to perform classification and to be able to *learn* to classify gives people and computer programs the power to

make decisions. The efficacy of these decisions is affected by performance on the classification task. In machine learning, the classification task described above is commonly referred to as *supervised learning*. In supervised learning there is a specified set of classes, and example objects are labeled with the appropriate class (using the example above, the program is told what a zebra is and what is not). The goal is to generalize (form class descriptions) from the training objects that will enable novel objects to be identified as belonging to one of the classes.

In contrast to supervise learning is *unsupervised learning*. In this case the program is not told which objects are zebras. Often the goal in unsupervised learning is to decide which objects should be grouped together—in other words, the learner forms the classes itself. Of course, the success of classification learning is heavily dependent on the quality of the data provided for training—a learner has only the input to learn from. If the data is inadequate or irrelevant then the concept descriptions will reflect this and misclassification will result when they are applied to new data.

III. Datasets and Performance Evaluation Measures

A. Benchmark Datasets

Table I summarizes the benchmark datasets used in almost all the recent studies of machine learning. The details of the datasets are given in Table I. For each data set, the number of instances, missing values, numeric attributes, nominal attributes and number of classes. The complete details regarding all the datasets can be obtained from UCI Machine Learning Repository [3].

B. Evaluation Criteria

To assess the classification results. The most commonly used performance evaluation measures in machine learning are accuracy, tree size, AUC and error rate. Let us define a few well-known and widely used measures:

The most commonly used empirical measure; accuracy

is computed by using the below equation (1),

$$ACC = \frac{TP + TN}{TP + FN + FP + FN} \qquad \text{---------- (1)}$$

Another measure for performance evaluation is AUC. A quantitative representation of a ROC curve is the area under it, which is known as AUC. When only one run is available from a classifier, the AUC can be computed as the arithmetic mean (macro-average) of TP rate and TN rate.

The Area under Curve (AUC) measure is computed by equation (2),

$$AUC = \frac{1 + TP_{RATE} - FP_{RATE}}{2} \qquad \text{---------- (2)}$$

TABLE I. Summary of benchmark datasets used in Machine Learning

S.no	Dataset	Instances	Missing Values	Numeric Attrib.	Nominal Attrib.	Classes
1.	Anneal	898	no	6	32	5
2.	Anneal.ORIG	898	yes	6	32	5
3.	Arrhythmia	452	yes	206	73	13
4.	Audiology	226	yes	0	69	24
5.	Autos	205	yes	15	10	6
6.	Balance-scale	625	no	4	0	3
7.	Breast-cancer	286	yes	0	9	2
8.	Breast-w	699	yes	9	0	2
9.	Colic-h	368	yes	7	15	2
10.	Colic-h.ORIG	368	yes	7	15	2
11.	Credit-a	690	yes	6	9	2
12.	Credit-g	1,000	no	7	13	2
13.	Pima diabetes	768	no	8	0	2
14.	Ecoli	336	no	7	0	8
15.	Glass	214	no	9	0	6
16.	Heart-c	303	yes	6	7	2
17.	Heart-h	294	yes	6	7	2
18.	Heart-statlog	270	no	13	0	2
19.	Hepatitis	155	yes	6	13	12
20.	Hypothyroid	3,772	yes	7	22	4
21.	Ionosphere	351	no	34	0	2
22.	Iris	150	no	4	0	3
23.	Kr-versus-kp	3,196	no	0	36	2
24.	Labour	57	yes	8	8	2
25.	Letter	20,000	no	16	0	26
26.	Lympho	148	no	3	15	4
27.	Mushroom	8,124	yes	0	22	2
28.	Optdigits	5,620	no	64	0	10
29.	Pendigits	10,992	no	16	0	10
30.	Primary-tumour	339	yes	0	17	21
31.	Segment	2,310	no	19	0	7
32.	Sick	3,772	yes	7	22	2
33.	Sonar	208	no	60	0	2
34.	Soybean	683	yes	0	35	19
35.	Splice	3,190	no	0	61	3
36.	Vehicle	846	no	18	0	4
37.	Vote	435	yes	0	16	2
38.	Vowel	990	no	10	3	11
39.	Waveform	5,000	no	41	0	3
40.	Zoo	101	no	1	16	7

In the machine learning experiments, the size of the tree is calculated by the depth of the tree using number of nodes and leaves. Testing errors is computed as the number of errors produced when separate training and testing set is used for training and testing.

IV. Recent Advances in Machine Learning Strategies

Serkan celik *et al.* [4] have examine vocabulary-learning strategies adopted by Turkish EFL students, specifically the frequencies and helpfulness ratings of strategy use, strategy patterns, as well as their change for students across different language levels. The study involved 95 tertiary level English as a foreign language learners.

Data were analyzed statistically and the results indicated that the participants' general use of vocabulary learning strategies was somewhat inadequate and there was a gap between their use of strategies and related perceptions of strategy usefulness. Zhou GuoDong *et al.* [5] have proposed a novel hierarchical learning strategy to deal with the data sparseness problem in semantic relation extraction by modeling the commonality among related classes. For each class in the hierarchy either manually predefined or automatically clustered, a discriminative function is determined in a top-down way. As the upper-level class normally has much more positive training examples than the lower-level class, the corresponding discriminative function can be determined more reliably and guide the discriminative function learning in the lower-level one more effectively, which otherwise might suffer from limited training data. Authors proposed, two classifier learning approaches, i.e. the simple perceptron algorithm and the state-of-the-art Support Vector Machines, are applied using the hierarchical learning strategy.

Edwin Lughofer [6] has proposed a novel active learning strategy for data-driven classifiers, which is based on unsupervised criterion during off-line training phase, followed by a supervised certainty-based criterion during incremental on-line training. In this sense, they call the new strategy hybrid active learning. Sample selection in the first phase is conducted from scratch (i.e.no initial labels/learners are needed) based on purely unsupervised criteria obtained from clusters: samples lying near cluster centers and near the borders of clusters are expected to represent the most informative ones regarding the distribution characteristics of the classes. In the second phase, the task is to update already trained classifiers during on-line mode with the most important samples in order to dynamically guide the classifier to more predictive power.

Both strategies are essential for reducing the annotation and supervision effort of operators in off-line and on-line classification systems, as operators only have to label an exquisite subset of the off-line training data representation give feedback only on specific occasions during on-line phase.

Kevin Duh *et al.* [7] have proposed a flexible transfer learning strategy based on sample selection. Source domain training samples are selected if the functional relationship between features and labels do not deviate much from that of the target domain. This is achieved through a novel application of recent advances from density ratio estimation. The approach is flexible, scalable, and modular. It allows many existing supervised rankers to be adapted to the transfer learning setting. Xiaodong Yu *et al.* [8] have proposed a novel updating algorithm based on iterative learning strategy for delayed coking unit (DCU), which contains both continuous and discrete characteristics. Daily DCU operations under different conditions are modeled by a belief rule-base (BRB), which is then, updated using iterative learning methodology, based on a novel statistical utility for every belief rule. Compared with the other learning algorithms, their methodology can lead to a more optimal compact final BRB. With the help of this expert system, a feed forward compensation strategy is introduced to eliminate the disturbance caused by the drum-switching operations.

R.J. Gil *et al.* [9] have proposed a novel model of an Ontology-Learning Knowledge Support System (OLeKSS) is proposed to keep these KSSs updated. The proposal applies concepts and methodologies of system modeling as well as a wide selection of OL processes from heterogeneous knowledge sources (ontologies, texts, and databases), in order to improve KSS's semantic product through a process of periodic knowledge updating. An application of a Systemic Methodology for OL (SMOL) in an academic Case Study illustrates the enhancement of the associated ontologies through process of population and enrichment.

Md Nasir *et al.* [10] have proposed a variant of single-objective PSO called Dynamic Neighborhood Learning Particle Swarm Optimizer (DNLPSO), which uses learning strategy whereby all other particles' historical best information is used to update a particle's velocity as in Comprehensive Learning Particle Swarm Optimizer (CLPSO). But in contrast to CLPSO, in DNLPSO, the exemplar particle is selected from a neighborhood. This strategy enables the learner particle to learn from the historical information of its neighborhood or sometimes from that of its own.

Moreover, the neighborhoods are made dynamic in nature i.e. they are reformed after certain intervals. This helps the diversity of the swarm to be preserved in order to discourage premature convergence. Biao Niu *et al.* [11] have proposed a novel batch mode active learning scheme for informative sample selection. Inspired by the method of graph propagation, we not only take the correlation between labeled samples and unlabeled samples, but the correlation among unlabeled samples taken into account as well. Especially, considering the unbalanced distribution of samples and the personalized feedback of human we propose an asymmetric propagation scheme to unify the various criteria including uncertainty, diversity and density into batch mode active learning in relevance feedback.

Ching-Hung Lee *et al.* [12] have proposed a hybrid of algorithms for electromagnetism-like mechanisms (EM) and particle swarm optimization (PSO), called HEMPSO, for use in designing a functional-link-based Petri recurrent fuzzy neural system (FLPRFNS) for nonlinear system control. The FLPRFNS has a functional link-based orthogonal basis function fuzzy consequent and a Petri layer to eliminate the redundant fuzzy rule for each input calculation. In addition, the FLPRFNS is trained by the proposed hybrid algorithm. The main innovation is that the random-neighbourhood local search is replaced by a PSO algorithm with an instant-update strategy for particle information. Each particle updates its information instantaneously and in this way receives the best current information. Thus, HEMPSO combines the advantages of multiple-agent-based searching, global optimization, and rapid convergence. Gwénolé Quellec *et al.* [13] have proposed a novel multiple-instance learning framework, for automated image classification. Given reference images marked by clinicians as relevant or irrelevant, the image classifier is trained to detect patterns, of arbitrary size, that only appear in relevant images. After training, similar patterns are sought in

new images in order to classify them as either relevant or irrelevant images. Therefore, no manual segmentations are required. As a consequence, large image datasets are available for training.

TABLE II. RECENT ADVANCES IN LEARNING STRATEGY

ALGORITHM	DESCRIPTION	REFERENECE
Hi-SVM Hi-PA	Hierarchical learning Strategy On SVM and Perceptron Algorithm.	[5]
IL-RIMMER	Iterative learning-RIMMER Algorithm.	[8]
OLeKSS	Ontology-Learning Knowledge Support System	[9]
DNLPSO	Dynamic Neighborhood Learning Particle Swarm Optimizer	[10]
APAL	Asymmetric Propagation based Active Learning algorithm	[11]
HEMPSO	Hybridization of ElectroMagnetism like and Particle Swarm Optimization Algorithm	[12]
MIL	Multiple Instance Learning Framework	[13]
MGDT	Maximum Gain Decision Tree for OR-Decision Tables	[14]
S2D	Simple-to-Complex Human Learning Strategy	[16]
GCSDT	Genetically optimized Cluster Oriented Soft Decision Trees	[17]

Costantino Grana *et al.* [14] have proposed a novel algorithm to synthesize an optimal decision tree from OR-decision tables, an extension of standard decision tables, complete with the formal proof of optimality and computational cost analysis. As many problems which require recognizing particular patterns can be modeled

with this formalism, They select two common binary image processing algorithms, namely connected components labeling and thinning, to show how these can be represented with decision tables, and the benefits of their implementation as optimal decision trees in terms of reduced memory accesses.

Joel E. Denny *et al.* [15] have demonstrate that a well-known algorithm described by David Pager and implemented in Menhir, the most robust minimal LR(1) implementation they have discovered that, it does not always achieve the full power of canonical LR(1) when the given grammar is non-LR(1) coupled with a specification for resolving conflicts. They also detail an original minimal LR(1) algorithm, IELR(1) (Inadequacy Elimination LR(1)), which they have implemented as an extension of GNU Bison and which does not exhibit this deficiency.

Eileen A. Ni*et al.* [16] have proposed a novel, simple and effective machine learning paradigm that explicitly exploits this important simple-to-complex (S2C) human learning strategy, and implement it based on C4.5 efficiently. Sanjay Kumar Shukla *et al.* [17] have developed a novel methodology, genetically optimized cluster oriented soft decision trees (GCSDT), to glean vital information imbedded in the large databases. In contrast to the standard C-fuzzy decision trees, where granules are developed through fuzzy (soft) clustering, in the proposed architecture granules are developed by means of genetically optimized soft clustering. In the GCSDT architecture, GA ameliorates the difficulty of choosing an initialization for the fuzzy clustering algorithm and always avoids degenerate partitions. This provides an effective means for the optimization of clustering criterion, where an objective function can be illustrated in terms of cluster's center. Growth of the GCSDT is realized by expanding nodes of the tree, characterized by the highest inconsistency index of the information granules.

Sanjay Jain *et al.* [18] have a present study aims at insights into the nature of incremental learning in the context of Gold's model of identification in the limit. With a focus on natural requirements such as consistency and conservativeness, incremental learning is analyzed both for learning from positive examples and for learning from positive and negative examples. In [19] authors introduced a novel form of decision tables, namely OR-Decision Tables, which allow including the representation of equivalent actions for a single rule. An heuristic to derive a decision tree for such decision tables was given, without guarantees on how good the derived tree was. In [20], authors presented a preliminary version of a bottom-up dynamic programming proposed by Schumacher et al. [21] which guarantees to find the optimal decision tree given an expanded limited entry (binary) decision table, in which each row contains only one non zero value.

V. CONCLUSION

Traditional classification techniques build the model for the datasets by following traditional and old strategy. New and novel learning strategies which mimic human learning can of great use to improve the process of model building for the datasets. In this paper we first investigate the state of the art methodologies for machine learning. This issue hinders the performance of standard classifier learning algorithms that assume relatively balanced class distributions, and classic ensemble learning algorithms are not an exception.

In recent years, several methodologies integrating solutions to enhance the induced classifiers in the presence of learning strategies by the usage of evolutionary techniques have been presented. However, there was a lack of framework where each one of them could be classified; for this reason, a taxonomy where they can be placed has been taken as our future work. Finally, we have concluded that intelligence based algorithms are the need of the hour for improving the results that are obtained by the usage of data preprocessing techniques and training a single classifier.

In our future work, we will apply our proposed method for learning wide range of tasks, especially for high dimensional feature learning tasks.

REFERENCES

[1] David Hand, Heikki Mannila, and Padhraic Smyth. Principles of Data Mining. MIT Press, August 2001.

[2] Jiawei Han and Micheline Kamber. Data Mining: Concepts and Techniques. Morgan Kaufmann, April 2000.

[3] A. Asuncion D. Newman. (2007). *UCI Repository of Machine Learning Database* (School of Information and Computer Science), Irvine, CA: Univ. of California [Online]. Available: http://www.ics.uci.edu/ ~mlearn/MLRepository.htm

[4] Serkan ÇELİK, Veli TOPTAŞ. Vocabulary learning strategy use of Turkish EFL learners, Procedia Social and Behavioral Sciences 3 (2010) 62–71.

[5] Zhou GuoDong, Zhang Min, Ji DongHong, Zhu QiaoMing. Hierarchical learning strategy in semantic relation extraction, Information Processing and Management 44 (2008) 1008–1021.

[6] Edwin Lughofer. Hybrid active learning for reducing the annotation effort of operators in classification systems, Pattern Recognition 45 (2012) 884–896.

[7] Kevin Duh, Akinori Fujino. Flexible sample selection strategies for transfer learning in ranking, Information Processing and Management 48 (2012) 502–512.

[8] Xiaodong Yu , DexianHuang, YonghengJiang, YihuiJin. Iterative learning belief rule-base inference methodology using evidential reasoning for delayed coking unit, Control Engineering Practice 20 (2012) 1005–1015.

[9] R.J. Gil, M.J. Martin-Bautista. A novel integrated knowledge support system based on ontology learning: Model specification and a case study, Knowledge-Based Systems 36 (2012) 340–352.

[10] Md Nasir, Swagatam Das, Dipankar Maity, Soumyadip Sengupta, Udit Halder, P.N. Suganthan. A dynamic neighborhood learning based particle swarm optimizer for global numerical optimization, Information Sciences 209 (2012) 16–36.

[11] Biao Niu, JianCheng, XiaoBai, HanqingLu . Asymmetric propagation based batch mode active learning for image retrieval, Signal Processing , Article in Press.

[12] Ching-Hung Lee, Yu-Chia Lee. Nonlinear systems design by a novel fuzzy neural system via hybridization of electromagnetism-like mechanism and particle swarm optimisation algorithms, Information Sciences 186 (2012) 59–72.

[13] Gwénolé Quellec, Mathieu Lamard, Michael D. Abràmoff, Etienne Decencière, Bruno Lay, Ali Erginay, Béatrice Cochener, Guy Cazuguel. A multiple-instance learning framework for diabetic retinopathy screening, Medical Image Analysis 16 (2012) 1228–1240.

[14] Grana, C., Montangero, M., Borghesani, D., Optimal Decision Trees for Local Image Processing Algorithms, Pattern Recognition Letters (2012), doi: http://dx.doi.org/10.1016/j.patrec.2012.08.015.

[15] Joel E. Denny, Brian A. Malloy, "The IELR(1) algorithm for generating minimal LR(1) parser tables for non-LR(1) grammars with conflict resolution", Science of Computer Programming 75 (2010) 943_979.

[16] Eileen A. Ni and Charles X. Ling, "Supervised Learning with Minimal Effort", M.J. Zaki et al. (Eds.): PAKDD 2010, Part II, LNAI 6119, pp. 476–487, 2010.

[17] Sanjay Kumar Shukla a, M.K. Tiwari," Soft decision trees: A genetically optimized cluster oriented approach", Expert Systems with Applications 36 (2009) 551–563.

[18] Sanjay Jain a,1, Steffen Lange b, Sandra Zilles, "Some natural conditions on incremental learning", Information and Computation 205 (2007) 1671–1684.

[19] C. Grana, D. Borghesani, R. Cucchiara, Optimized Block-based Connected Components Labeling with Decision Trees, IEEE T Image Process 19 (2010) 1596–1609.

[20] C. Grana, M. Montangero, D. Borghesani, R. Cucchiara, Optimal decision trees generation from or-decision tables, in: Image Analysis and Processing - ICIAP 2011, volume 6978, Ravenna, Italy, pp. 443–452.

[21] H. Schumacher, K. C. Sevcik, The Synthetic Approach to Decision TableConversion, Commun ACM 19 (1976) 343–351.

Design of Semi-Adaptive 190-200 KHz Digital Band Pass Filters for SAR Applications

P Yadav
Dept of Electronics and communication
SIST, Bhopal, India- 462031

A Khare
Dept of Electronics and communication
SIST, Bhopal, India- 462031

K Parandham Gowd
Aisect University, Bhopal-Chiklod Road
Raisen, Bhopal, India

Abstract–Technologies have advanced rapidly in the field of digital signal processing due to advances made in high speed, low cost digital integrated chips. These technologies have further stimulated ever increasing use of signal representation in digital form for purposes of transmission, measurement, control and storage. Design of digital filters especially adaptive or semi adaptive is the necessity of the hour for SAR applications. The aim of this research work is to design and performance evaluation of 380-400 KHz Bartlett, Blackman and Chebyshev digital semi adaptive filters. For this work XILINX and MATLAB softwares were used for the design. As part of practical research work these designs were translated using FPGA hardware SPARTAN-3E kit. These were optimized, analyzed, compared and evaluated keeping the sampling frequency at 5 MHz for 64 orders. Both these filters designed using software and hardware were tested by passing a sinusoidal test signal of 381 KHz along with noise and the filtered output signals are presented.

Keywords–Digital filter; XILINX and MATLAB softwares; Field Programmable Gate Arrays (FPGA); SPARTAN-3E; DSP Chips.

I. INTRODUCTION

The extraordinary development in the field of high speed, low cost microelectronic digital IC's over the past few decades has stimulated an ever increasing use of signal representation in digital form for such purposes as transmission, measurement, storage and control. The conversion of a continuous signal to digital form makes possible the numerical manipulation of the data by IC's which is known as digital signal processing which is utmost necessary in the field of synthetic aperture radar applications(SAR). For remote sensing and detection applications digital signal processing concerns the techniques of processing the data to remove, for example, unwanted noise components, before the signal is reconstructed into analogue form, known as digital filtering, which is of interest in this research paper.

SAR data is required to be processed in real time, hence these filters are required to operate in real time. For real time operation, the complexity of the digital signal processing algorithm is limited by the condition that the numerical manipulation to determine each output sample must be performed in less than the sample period. Thus the design of a real-time filter generally involves a compromise between the complex requirements for a complex algorithm and a high sampling frequency.

The possibility of low-cost, real-time digital filtering first emerged in the 1970s when general purpose microcomputers were introduced. The early digital filters, however, had limited speed and precision, which restricted their use to low-frequency applications and simple algorithms. In the 1980s, higher cost special purpose known as DSP chips were introduced, which contained much faster arithmetic units and on-chip memory for storing filter coefficients and data. In some cases, on chip A/D and D/A converters were included and subsequently rapid improvements in speed and complexity were made possible by ICs, thus resulting in design of digital filters of today. FPGA series of kits availability clearly helps researchers for taking up practical designs of semi adaptive band pass filters from lower to higher frequencies.

II. PROPOSED DESIGN METHODOLOGY

A. *SOFTWARES BASED DESIGN.*

The simulated design methodology is as shown in fig.1. The design process involved the following steps:

1) MATLAB software tool is used to generate the coefficients required for the operation of the filter.
2) Xilinx software tool was used to design the filter.
3) Using this research methodology three types of filters namely, Bartlett, Blackman and Chebyshev Finite Interval Response (FIR) semi adaptive digital band pass filters for 190-200 KHz were designed.
4) Filter response was derived for the sampling frequency of 5 MHz of order 64.
5) MATLAB software program was applied for calculating and plotting of SNR

The (FDA) Filter Design and Analysis tool in MATLAB provides the option to design the digital filter to offer the respective response and coefficients to be implemented within the design using VHDL. Filter design can be carried out often selecting various options available in FDA tool for generation of required coefficients for the respective filter from the target menu using the C header option of the FDA tool. The generated coefficients in the C header files are then used in the

VHDL file for the digital filter designing which is to be convoluted with the sampled data of SAR.

B. HARDWARE BASED DESIGN

The software based design methodology described above was translated on FPGA kit using SPARTA-3E for the practical experimental work. The inputs and outputs were taken on digital storage oscilloscope. In this research work the following practical circuit design steps was carried out as per methodology shown in Fig.2. The circuit designed using the SPARTAN Logic IC X-C3S, a seven segment display, DIP switches is as shown in Fig.3.

1) Using this FPGA kit three types of filters namely, Bartlett, Blackman and Chebyshev Finite Interval Response (FIR) semi adaptive digital band pass filters for 380-400 KHz were practically designed.

2) The SPARTAN Logic IC contains 4X10-6 logic gates and has 208 pins.

3) 8 DIP switches were incorporated for selecting various combinations such as frequency of the filter, sampling rates and input signal.

4) 16 bit A/D and D/A converters are used for conversion and reconstruction of samples.

5) This filter was integrated into the circuit testing system as shown in fig.4.

6) Here a low power test signal (-5dB) of 195 KHz was mixed with AWGN noise and this mixed signal was passed through designed band filters namely Bartlett, Blackman and Chebyshev for the frequency 190-200 KHz.

In the hardware set up out of 8 DIP switches two are used for input/output, two are for selecting sampling rate and four switches for selecting filter coefficients. These four switches with 16 bit data it is possible to generate 64 sets of filter coefficients.

This technique of using Field Programmable Gate Array with DIP switches as shown in Fig.4 for selecting sampling rate for noise, test signal and various filter coefficients can be termed as a concept of semi-adaptive filter design. With this semi-adaptive technique depending on the test signal and noise condition particular set can be recalled there by increasing the signal to noise ratio for SAR to enable better detection. Here simulated and generated SAR signals accompanied with random noise is sampled at a frequency of 5 MHz.

Here SPARTAN-3E was used, configured in designing the 3 types of digital filters in this paper. The achieved filter circuit is as shown in figure.3.

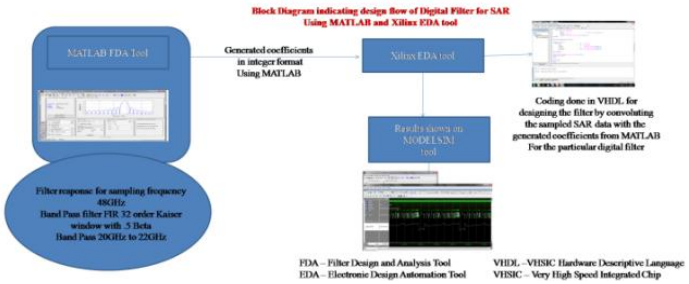

Fig.1. Block diagram of the Design using software methodology

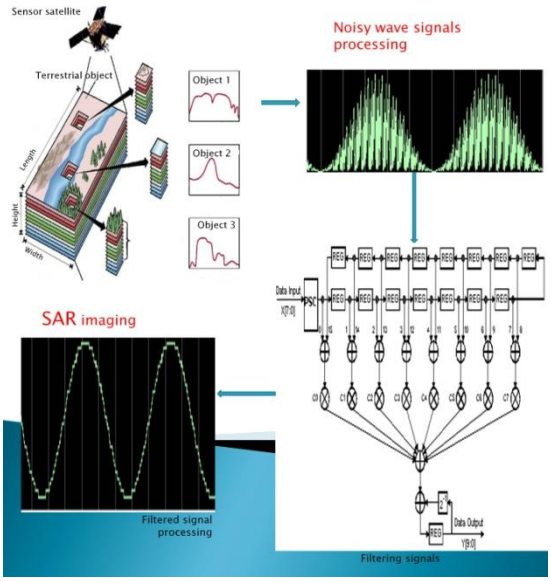

Fig.2. Block Diagram of the Design using Hardware methodology.

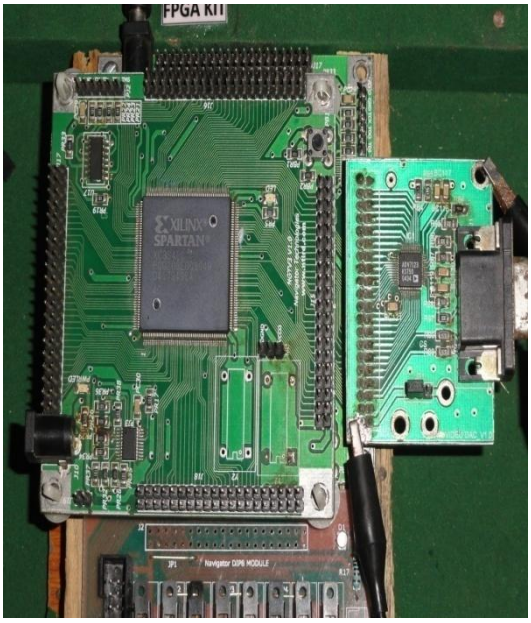

Fig.3. Designed circuit using FPGA kit.

III. RESULTS AND DISCUSSION

Block diagrams used in these designs by software and hardware are as shown in figures 1 and 2 respectively. The

designed circuit and integrated experimental setup utilized for this research work are depicted in fig. 3 and 4 respectively.

The frequency responses of Bartlett, Blackman and Chebyshev FIR band pass filters of order 64 for a sampling frequency of 5 MHz are as shown in figures 5, 6 and 7 respectively. The original sinusoidal test signal of 195 KHz was passed through this 190 to 200 KHz digital band pass FIR filters of Bartlett, Blackman and Chebyshev of order 64 which was designed using XILINX and MATLAB soft wares are as shown in Figures 8, 9 and 10.respectively. The figures 8, 9 and also show the SNR improvement versus iteration number calculated and plotted for Bartlett, Blackman and Chebyshev types of filters. Figure 11 shows the test signal,test signal with noise and filterd signals obtained from practical experimental set up using FPGA kit (SPARTAN-3E kit) observed in a two channel digital oscilloscope.

It is clearly observed from figure 8 that Bartlett type of digital FIR band pass filter clearly suppresses the noise and the output signals passed with and without noise are exactly comparable. The observations from figures 9 the Blackman filter and 10 the Chebyshev filter indicate that noise is not suppressed completely and output is seen with some noise components and far inferior to Bartlett type of filter of the same design.

From this figures 8 and 11, both are of Bartlett types designed using software and hardware respectively, it is clearly seen that noise is suppressed and the test signal has been passed. The figure 11 shows the input test signal and filtered output signal which was passed through the same filter which was designed using SPARTA 3 E kit with logic gates observed in a two channel digital storage oscilloscope. The simulated filter and the practically designed filter have rejected the noise and are comparable with hardly any differences as per expected lines.

It is seen from the figures 9, the Blackman and 10, the Chebyshev types of filters of software based design, that the original signal is completely mixed with noise indicating inferiority of these filters when compared with Bartlett filter of same design.

It is seen the fig. 3 and 4 that the band pass filter design using SPARTA 3E Kit was clearly translated and achieved practically using the methodology proposed in this paper. It is seen from the figures.8 and 10 that the simulated SAR signal clearly passing through the 190 to 200 KHz window in software based and practically designed band pass filters, by suppressing the noise levels, presenting the reflected echo of the SAR signal.

From figures 8, 9 and 10 which also shows the SNR improvement factor versus iteration number, it is clearly observed that SNR improvement factors achieved for Bartlett type of filter is 7.78 dB, for Blackman type of filter is 7.692dB and for Chebyshev type of filter is 7.42dB. Dominance of Bartlett type filter is very clear from the same design achieved for SNR improvement.

IV. Conclusion

In this research work the XILINX and MATLAB softwares based Bartlett, Blackman and Chebyshev FIR digital 190-200 KHz semi adaptive band pass filters design methodology was successfully translated in to practical one using SPARTAN-3E kit along with A/D, D/A converters and DIP switches and seven segment display for 64 orders for a sampling frequency of 5 MHz.

Fig.4. Designed circuit of the proposed methodology.

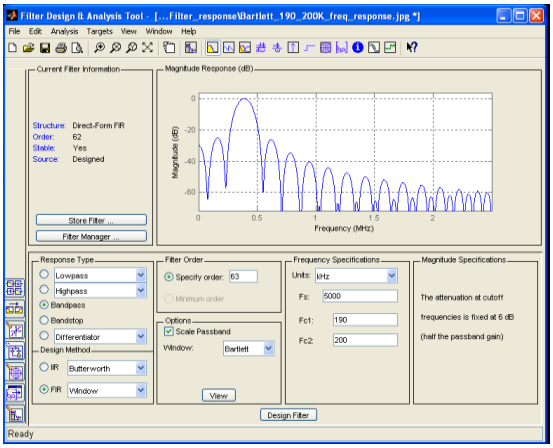

Fig.5. Frequency Response (Bartlett)

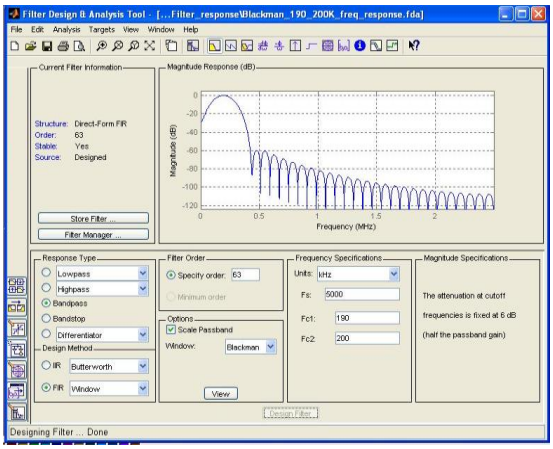

Fig.6. Frequency Response (Blackman)

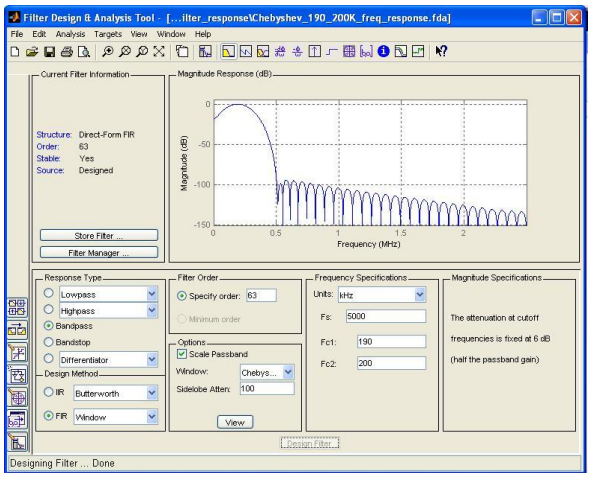

Fig.7. Frequency Response (Chebyshev)

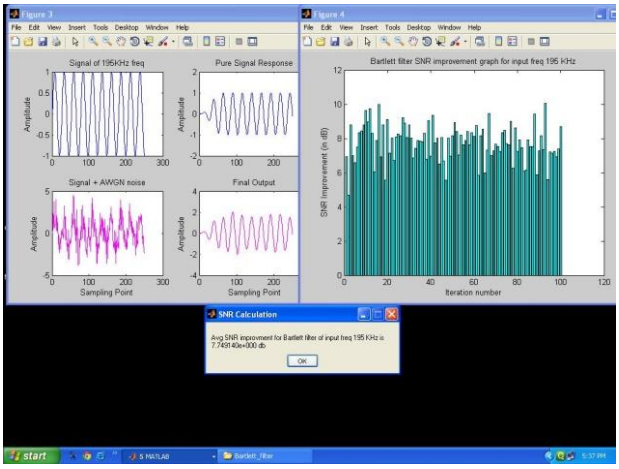

Fig.8. Input signal, signal+ noise, outcomes and SNR improvement (Bartlett)

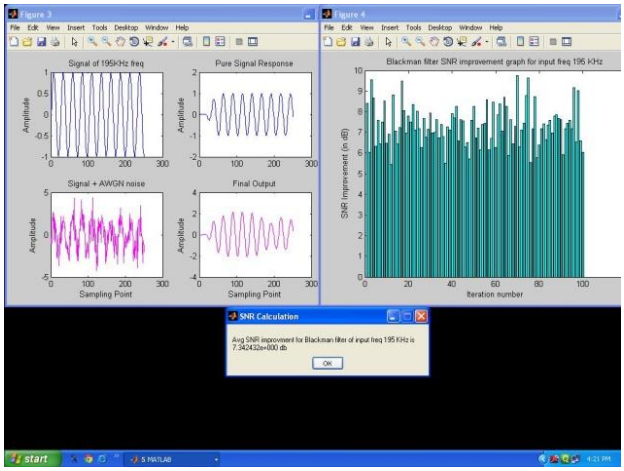

Fig.9. . Input signal, signal+ noise, outcomes and SNR improvement (Blackman)

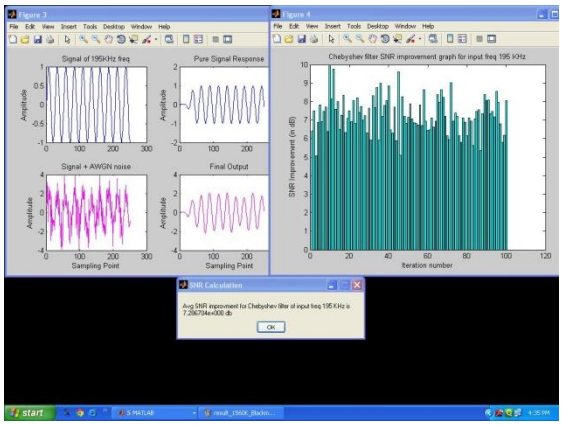

Fig.10. Input signal, signal+ noise, outcomes and SNR improvement (Chebyshev)

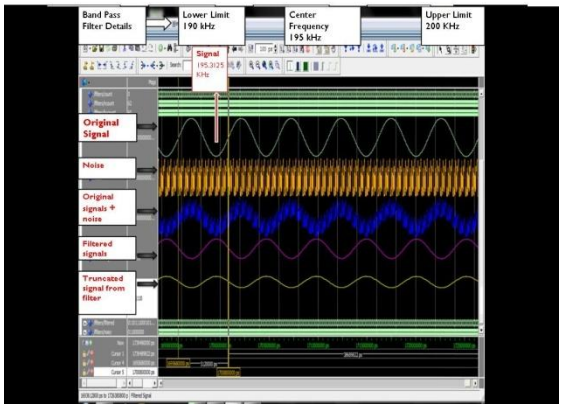

Fig.11. Figure 11. Original signal, noise + signal and filtered signals

The response was successfully obtained for the designed frequency of 195 KHz from both the filters theoretical and practical. The superiority performance of Bartlett type of filter is clearly observed from both types of design using software tools and FPGA kit practically over Blackman and Chebyshev type of filters from the same designs.

SNR improvement factor of 7.78 dB achieved for Bartlett is higher than Chebyshev 0f 7.42 dB and Blackman of 7.692 dB conforming that better quality low frequency FIR semi adaptive digital band pass filters can be achieved through Bartlett type. These filters are suitable for low frequency SAR applications to mitigate random noise levels and give the desired target response so that resolution and identification of desired objects are achieved.

The SPARTAN-3E digital signal processing chip was successfully configured, designed and achieved for semi-adaptive digital FIR filters and test signal was passed with noise and output clearly obtained as shown in figure 11 especially for Bartlett type.

Filters designed in this paper analyzed and evaluated which are comparable and matching well in their responses of filtering out unwanted noise and passing the original signal in the designed frequency band.

In this paper a concept of low frequency digital filters for synthetic aperture radar applications for the purpose of deep detection on earth surfaces and deep sea bed are suitably demonstrated. High frequency SAR images are deteriorated by speckle noise, so in this paper an attempt is made to design a practical digital filter using SPARTA 3E kit for low frequency SAR applications. It is well known that lower frequencies have longer wave length and hence can penetrate deeper in to earth and sea bed for detection applications of SAR.

V. Future Scope

This experiment on practical circuit design of semi-adaptive digital filters using SPARTAN-3E and software based design using XILINX and Mat Lab softwares for SAR applications shows the possibility to formulate fully adaptive digital filters for Remote Sensing applications such as for Disaster management, mining, Forest management and military applications. These filters will play a crucial role in practical implementation in future SAR noise reduction.

REFERENCES

[1] Tomlinson G, H, "Electrical Networks and Filters (Theory and Design)", Prantice Hall Internationalo (UK) Ltd, 1991.

[2] Rhodes, J.D, "Theory of Electrical Filters", London, John Wiley,1976.

[3] Van Valkenberg, M,E, "Analog Filter Design", London, Holt Rinehart and Winston, 1987.

[4] D.M Pozar and D.H Schaubert "The Analysis and Design Of Microstrip Antenna Array".

[5] K. Ragopal, J. Dinesh Babus, Venkataraman, Generalized adaptive IFIR Filter Bank structures, Science Direct Signal Processing, pp 1-20, 2007.

[6] Skolnik, M. I., Radar Handbook, McGraw-Hill, New York, 1970.

[7] Curlander, J. C. and R. N. McDounough, Synthetic Aperture Radar, Systems and Signal Processing, John Wiley & Sons, New York, 1991.

[8] Ulaby, F. T., R. K. Moore, and A. K. Fung, Microwave Remote Sensing: Active and Passive, Vol. I, Artech House, Norwood, 1981.

[9] Drinkwater, M. K., R. Kwok, and E. Rignot, "Synthetic aperture radar polarimetry of sea ice," Proceeding of the 1990 International Geoscience and Remote Sensing Symposium, Vol. 2, 1525–1528, 1990.

[10] Lynne, G. L. and G. R. Taylor, "Geological assessment of SIRB imagery of the amadeus basin," IEEE Trans on Geosc. And Remote Sensing, Vol. 24, No. 4, 575–581, 1986.

[11] Hovland, H. A., J. A. Johannessen, and G. Digranes, "Slick detection in SAR images," Proceeding of the 1994 International Geoscience and Remote Sensing Symposium, 2038–2040, 1994.

[12] Walker, B., G. Sander, M. Thompson, B. Burns, R. Fellerhoff, and D. Dubbert, "A high-resolution, four-band SAR Testbed with real-time image formation," Proceeding of the 1986 International Geoscience and Remote Sensing Symposium, 1881–1885, 1996.

[13] Storvold, R., E. Malnes, Y. Larsen, K. A. Hogda, S.-E. Hamran, K. Mueller, and K. Langley, "SAR remote sensing of snow parameters in norwegian areas — Current status and future perspective," Journal of Electromagnetic Waves and Applications, Vol. 20, No. 13, 1751–1759, 2006.

[14] Kong, J. A., S. H. Yueh, H. H. Lim, R. T. Shin, and J. J. van Zyl, "Classification of earth terrain using polarimetric synthetic aperture radar images," Progress In Electromagnetics Research, PIER 03, 327–370, 1990.

[15] Thompson, T. W., A User's Guide for the NASA/JPL Synthetic Aperture Radar and the NASA/JPL L- and C-band Scatterometers, 83–38, JPL Publication, 1986.

Author's Information

Prof. P Yadav is a post graduate from IIT- Kanpur (India) and a research scholar in Electronics Engg. He has served in Indian Air Force as commissioned officer for 25 yrs, and nine yrs, as a technocrat academician in reputed Engg. Institutes. He is an entrepreneur who has many project patents under his name. He is a fellow of IETE.

Dr Anubhuti Khare received her BE in Electronics and Communication from Government Engineering College, Bhopal in 1994. She obtained her M.Tech and Ph D in Electronics and Communication from MANIT, Bhopal. Presently she is working as Associate Professor in E & C Department, UIT, RGPV, Bhopal. She has more than 50 publications to her credit.

K Prandham Gowd obtained his B.Tech in Electronics and Communication Engineering with distinction from S.V. University, Tirupati (India) and ME (Microwaves and Radar) from IIT Roorkee. In 1994 he has conducted RCS Reduction experiments on coated (by pasting of absorber sheets) and uncoated scaled models of aircraft which is first time in India at IIT Roorkee. He has 41 research publications and 05 Technical reports to his credit most of them on RCS/RCS Reduction/Stealth Technology. He has one copyright to his credit on Dynamic RCS Range Validation Procedure from Govt of India. He is a Life Member of All India Management Association (AIMA), AeSI and Fellow of IETE. He had authored a book on Stealth Aircraft Technology.

Collaborative Learning Skills in Multi-touch Tables for UML Software Design

Mohammed Basheri
Faculty of Computing and IT
King Abdulaziz University
Jeddah, Saudi Arabia

Malcolm Munro
School of Engineering and Computing Sciences
Durham University
Durham, United Kingdom

Liz Burd
School of Engineering and Computing Sciences
Durham University
Durham, United Kingdom

Nilufar Baghaei
Department of Computing
Unitec Institute of Technology
Auckland, New Zealand

***Abstract*— The use of Multi-touch interfaces for collaborative learning has received significant attention. Their ability to synchronously accommodate multiple users is an advantage in co-located collaborative design tasks. This paper explores the Multi-touch interface's potential in collaborative Unified Modeling Language diagramming by comparing it to a PC-based tool, looking at the Collaborative Learning Skills and amount of physical interactions in both conditions. The results show that even though participants talked more in the PC-based condition, the use of the Multi-touch table increased the amount of physical interactions, and encouraged the "Creative Conflict" skills amongst the team members.**

Keywords—Collaborative Design; Multi-touch Table; PC-based; Collaborative Learning Skills

I. INTRODUCTION

The use of Multi-touch interfaces for collaborative learning has received significant attention. They can accommodate more than one user at a time. This is particularly useful for learning through large, shared display systems like tabletops [2]. Another interesting aspect of the Multi-touch environment is that it provides new opportunities for interaction between humans and computers. This area has been investigated by researchers from different educational backgrounds who have found Multi-touch environments to be useful as interaction through touch is both intuitive and natural [3, 4].

Many studies have shown the benefits of using Multi-touch environments to enhance collaborative work. Using such systems encourages students to collaborate and create an environment wherein they can discuss their findings and integrate their ideas seamlessly with no technological hindrances. In addition, such systems can enhance students' interaction skills and promote teamwork. For instance, [5] built a system called Futura which is a game based learning system for learning about sustainable development. In this study, players use Multi-touch surfaces to build healthy environment by supporting population growth in an urban environment. Multi-touch surfaces have also been used for collaborative information gathering. A tool called WebSurface was used to facilitate users' browsing of the Web collaboratively in order to collect information from different websites. With the use of Multi-touch surfaces users were able to seek information, browse multiple pages simultaneously, and easily gather the information they found [6]. Multi-touch surfaces also have the potential to allow co-located collaboration activities, thus permitting small groups to work together collaboratively [7] and offering equal opportunities for such group work [8].

To the best of our knowledge, there has been little research to determine the potential of using Multi-touch tables to enhance co-located collaboration in software design using Unified Modeling Language (UML). Object-oriented analysis and design can be a very complex task, as it requires knowledge of requirements analysis, design and UML. The problem statement is often vague and incomplete and students need a lot of experience to be successful in analysis. UML is a complex modelling language and students have many problems to become skilled at it. Furthermore, UML modelling like other design tasks is not a well-defined process. There is no single best solution for a problem, and often there are several alternative solutions for the same requirements. The level of collaboration in Futura [5] and WebSurface [6] is limited and restricted to simple actions performed by users, such as putting words in the right context, arranging items over tables, and simple click and drag actions. However, UML design involves advanced design issues that raise new collaboration needs, such as linking nodes and annotation. In this paper the potential of using Multi-touch technology for software design using UML is explored by comparing it with PC-based collaborative software design and examining the collaboration learning skills and physical interactions in both conditions.

II. RELATED WORK

A great deal of interesting work has recently been done on Multi-touch tables, much of it investigating the role of Multi-touch in enhancing collaborative activities. Morris et al. [9] investigated the success of using Multi-touch tabletops to improve cooperation during group functions and tasks. They reported that Multi-touch tabletops improved team member awareness considerably, indicating that Multi-touch tabletops

improve information sharing between group members. Harris et al. [10] compared the differences between single and Multi-touch tabletops in group task performance and found that Multi-touch tabletops improved task performance, whereas single-touch tabletops did not. In another research study [11] the effectiveness of Multi-touch tabletops was examined, by comparing multi-mouse and Multi-touch tabletops. Multi-mice were seen to be utilized more than Multi-touch tabletops for the following reasons: (1) users were better able to interact with any part of the display using multi-mice than using Multi-touch; (2) users were more familiar with multi-mouse tabletops; (3) variability in the usage of Multi-touch tables. On the other hand it was noted that users of Multi-touch displayed fewer grammatical errors than those of multi-mouse. A study by [12] shows that Multi-touch tabletops increase the awareness and common ground of group members working collaboratively to achieve a specific outcome, as well as increasing the effectiveness of group tasks and obligations [13]. From the aforementioned research studies, it can be concluded that Multi-touch tabletops enhance group interaction and therefore enhance the realization of group goals.

Much research has been conducted with the aim of improving collaboration among users in software design using UML. This includes studies such as COLLECT-UML [14], CoLeMo [15], CAMEL [16], and AUTO-COLLEAGUE [17]. AUTO-COLLEAGUE does not support collaborative drawing for UML diagrams, as COLLECT-UML and CoLeMo do; it does, however, offer a chat system as its main collaboration tool. These systems are not designed to support a face-to-face collaboration style, but rather for distributed collaborative work. Very little research other than the Software Design Board [18], which is a shared whiteboard application, supports collaborative software design.

III. Comparative Study

Using Multi-touch table for collaborative UML diagramming has not been widely researched. To the best of our knowledge, there is no Multi-touch table based editor for UML diagramming available. We have developed a Multi-touch collaborative UML editor named "MT-CollabUML" [19] to encourage face-to-face collaborative software design. In order to keep a same variable in both Multi-touch table and PC-based conditions, MT-CollabUML tool was used in both settings.

IV. Participants

For the purposes of the research sixteen master program students who were studying "Software Engineering for the Internet" were selected. The participants were all familiar with collaboratively designing software using UML and had completed the course. The participants formed eight groups, each consisted of two people.

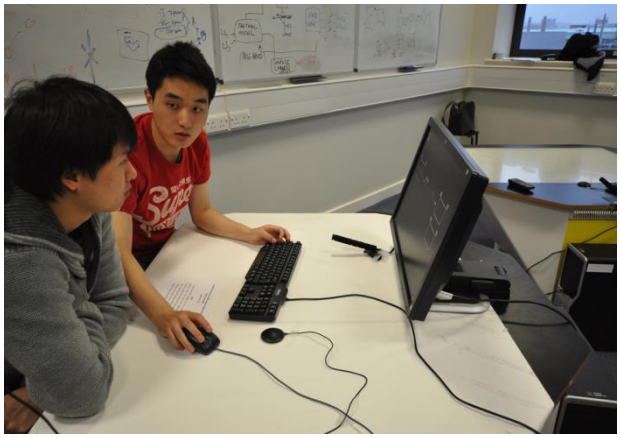

Fig.1. PC-based condition

V. Experiment Design

A within-subject experiment was conducted to compare how the participants used PC with how they used Multi-touch table in terms of collaborative design.

Similarities and differences were studied in terms of qualitative behavior in the eight groups of two students, who worked on creating UML-State diagrams. The goal was to identify differences in the level of collaborative design process across experimental conditions. To ensure the validity of our investigation, we decided to compare the use of MT-CollabUML tool in both PC-based and Multi-touch table conditions. In both conditions, we provided two similar design tasks with the same level of difficulty and complexity.

Two separate tasks were implemented, each of which involved the creation of UML-State diagrams through a process of planning, discussion, decision making, drawing and reflection. In order to ensure that the tasks were of the same complexity and required the same level of skills, the course tutor was consulted.

Counterbalanced measures design was conducted in this experiment to help keep the variability low. For every pair of groups, we gave one group a UML design task and asked them to complete it using the MT-CollabUML tool in PC-based "Fig.1" The other group was asked to complete the same task using the MT-CollabUML tool on Multi-touch table based "Fig. 2". Then the groups switched and were asked to complete the second task using PC and Multi-touch conditions.

Before the experiment began, all the students underwent basic training in the use of the MT-CollabUML tool in the Multi-touch table and PC-based. The experiment took place in Durham University's SynergyNet lab "Fig. 3", and a within-subject study design was used for both the PC-based and the Multi-touch surface. The groups were given as much time as they needed to complete the tasks. All collaborative UML diagramming activities were video recorded for analysis. For the Multi-touch and the PC-based conditions, two cameras were focused on the tables from two directions to ensure all group members captured. Qualitative analysis was followed to analyze the collaborative design process. Timeline (in minutes) for all design activities along with discussion timeline per subject was generated using Microsoft Visio. Design activities

included adding or deleting node, adding or correcting text, linking or unlinking node and moving node.

Furthermore, the quantitative analysis was considered by calculating the physical interactions (design activities) per minute for each subject in Multi-touch and PC-based conditions following Harris el al. work [20].

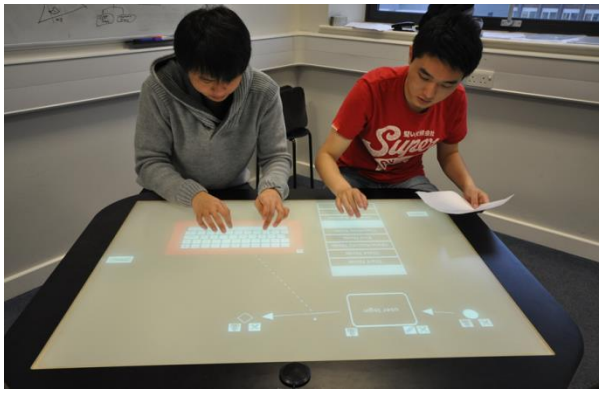

Fig.2. Multi-touch table condition

Fig.3. SynergyNet lab

Group member's learning experience and success are influenced by the quality of communication in team discussion [21]. Collaborative learning Skills includes Active Learning, Creative Conflict and Conversation [21, 22]. According to Soller [23] using Collaborative learning Skills promotes effective collaboration learning. Therefore, the verbal communication among each pair in both conditions were recorded and analyzed to find out if there were differences between conditions in term of type of verbal contribution. Baghaei [1] and Soller [23]'s verbal communication categories were used in this study. Communication Categories includes ten types; *"Request, Inform, Maintain, Acknowledge, Motivate, Argue, Introduce & Plan, Disagree, Task and Off-Task"*. TABLE I describes the communication categories used in the Multi-touch table and PC-based conditions.

VI. Study Findings & Discussion

The aim of this study was to explore the benefits of using a Multi-touch table as a tool to encourage students' collaboration and to enhance the quality of communication amongst team members. We looked at the amount of talking, the amount of physical interaction, collaboration logs and the use of communication categories in both conditions.

TABLE I. Description of Communication Category [1]

Communication Category	Description
Introduce & Plan	Introduce yourself to your team-mates and plan the session in advance before start collaborating.
Inform	Direct or advance the conversation by providing information.
Request	Ask for help in solving the problem, or in understanding a team-mates comment.
Maintain	Support group cohesion and peer involvement.
Acknowledge	Agreement upon team-mate's comment
Argue	Reason about suggestions made by team-mates.
Motivate	Provide positive feedback.
Disagree	Disagree with the comments or suggestions made by team members.
Task	Shift the current focus of the group to a new subtask.
Off-Task	Off-Task discussion.

The results showed that participants talked more in the PC based condition (M= 5.61, SD=2.18) than they did in the Multi-touch table based (M=4.29, SD=1.71). The difference between the conditions was statistically significant (p=0.004). The qualitative analysis for the collaboration logs (design process) explained the reason behind this difference: the PC-based condition did not support parallelism design activities on the face-to-face collaboration, and it only allowed for sequential-participative design to be carried out. Therefore, subjects had to stop designing activities to engage in discussion to decide the next step. However, the Multi-touch table condition supported the parallel-participative design, in which subjects were able to carry out multiple designing activities and discussion at the same time. Also, the PC-based condition increased single-subject domination, in which one subject performed most of the designing activities. A study by Paul Marshall et al. [24] showed that dominant subjects talk more, and the results supported Marshall's findings, showed that the subject who interacted more physically (dominated more) talked the most.

A. Use of Communication Categories

TABLE II shows that "*Inform*" sub-skill used in PC-based condition (35.72%) more than in the Multi-touch based condition (31.53%). In PC and Multi-touch settings subjects tend to "*Request*" help, used "*Acknowledge*", "*Motivate*", "*Maintain*", "*Disagree*" as well as discussed about the next step "*Task* " almost at the same level. However, the subjects discussed about what are they going to do "*Introduce & Plan*" in the Multi-touch condition (2.13%) more than in the PC-based condition (1.49%). Furthermore, Multi-touch setting encouraged "*Argue*" more (21.31%) than the PC setting (19.60%). However, subjects used "*Off-Task*" discussion in the Multi-touch (3.64%) more than in the PC (1.79%). Both conditions promoted the effective collaborative learning. The Multi-touch condition encouraged the "Creative Conflict" skills more than the PC-based condition as shown in TABLE II. The PC-based condition encouraged "Active Learning" skills more

than the Multi-touch condition. It can be seen that the subjects in both conditions engaged in "Conversation" skills almost at the same level.

TABLE II. COLLABORATIVE LEARNING SKILLS IN MULTI-TOUCH AND PC-BASED CONDITIONS

Collaborative Learning Skills	Sub-Skills	Multi-touch		PC-based	
Creative Conflict	Argue	21.31%	23.18 %	19.60%	21.00 %
	Disagree	1.87%		1.39%	
Active Learning	Motivate	1.51%	41.39 %	2.09%	45.97 %
	Inform	31.53%		35.72%	
	Request	6.22%		6.67%	
	Introduce & Plan	2.13%		1.49%	
Conversation	Acknowledge	25.04%	31.79 %	24.48 %	31.24 %
	Maintain	1.15%		1.49%	
	Task	5.60%		5.27%	

Collaborative problem-solving has some benefits such as encouraging students to verbalise their thinking; encouraging students to work together, ask questions, explain and justify their opinions; increasing students' responsibility for their own learning; and encouraging them to elaborate and reflect upon their knowledge [23, 25, 26]. Verbal communication is one of the most important components of any collaboration [27]. In this study, Collaborative Learning Conversation Skills Taxonomy has been applied. Collaborative Learning Conversation Skills Taxonomy is the understanding and knowledge of how to communicate effectively, aimed at enhancing the learning process in a group discussion [23]. Most of the previous studies applied the Collaborative Learning Conversation Skills Taxonomy to structured non-verbal communication in distributed collaboration settings [1, 28, 29]. This taxonomy has been applied in this present study in order to explore which skills might be adopted by subjects in face-to-face collaboration in both experiment conditions without forcing them to use a structured communication. The result shows that there is some difference between the Multi-touch table condition and PC-based conditions in terms of the collaborative learning communication skills that were adopted. TABLE II shows that in the Multi-touch table condition, subjects tended to use the 'Creative Conflict' skills more than when they were in the PC-based condition. Using 'Creative Conflict' skills, which are 'Argue' and 'Disagree', can be useful in producing creative interactions; it leads to productive discussion when it is directed at ideas rather than people [30]. In both conditions, subjects used the 'Conversation' skills almost an equal amount of the time. However, in the PC-based condition, 'Active Learning' skills were used the most, particularly using the 'Inform' skill, which was highest in the PC-based condition. The reason for the frequent use of 'Inform' skills in the PC-based condition is related to single-subject domination, in which the dominant subject used 'Inform'. For example, Subject 2 in Group 1 was the dominant subject in the PC-based condition, and was using leading phrases such as: 'I think it is better to have a circle here and an end button here', and: 'Actually, I think you do not have to make capital letter, write specify amount'. The total number of 'Inform' phrases used by this subject was 58, while in the Multi-touch table condition it was 44.

B. Collaboration Log

The mouse in the PC-based condition played an important role in the use of the MT-CollabUML tool, where it is used for adding, deleting, linking, unlinking, and moving nodes. Therefore, the subject who controls the mouse dominates the physical design activities in the PC-based condition as shown in TABLE III. The collaboration log shows that Subject 2 "Fig. 5" was controlling the mouse in the PC-based condition all the time and he/she was dominating the design activities as well. In contrast, because of using hand gestures instead of the mouse in the Multi-touch condition, the single subject domination decreased as shown in "Fig.4". The Multi-touch table encourages parallel-participative design and equity of physical interaction. These findings are supported by our previous study showing that Multi-touch table increases the equity of participation [31].

TABLE III. DOMINATING IN BOTH CONDITIONS

	Subjects	Control Mouse (PC-based)	Dominating in PC-based	Dominating in Multi-touch
Group 1 PC→Multi-touch	1			✓
	2	✓	✓	✓
Group 2 Multi-touch →PC	3	✓	✓	✓
	4			✓
Group 3 PC→Multi-touch	5	✓	✓	✓
	6			✓
Group 4 Multi-touch →PC	7			
	8	✓	✓	✓
Group 6 Multi-touch →PC	9	✓	✓	✓
	10		✓	✓
Group 7 PC→Multi-touch	11	✓		✓
	12	✓	✓	✓
Group 8 Multi-touch →PC	13	✓	✓	✓
	14			✓
Group 9 PC→Multi-touch	15	✓	✓	✓
	16			✓
Total		10/16	9/16	15/16

The analysis of the collaboration log also shows that the Multi-touch table enabled pairs to engage in more physical design activities than the PC-based condition as shown in TABLE IV and TABLE V. For example, Subject 1 in the PC setting "Fig. 5" was able to interact physically only in some design activities such as "Adding Text" or "Correcting Text". On the other hand, when the same subject (Subject 1) worked in the Multi-touch condition "Fig. 4", it was an opportunity to be engaged in all design activities such as "Adding Node", "Moving Node", "Linking Node", and "Deleting Node".

TABLE IV. DESIGN ACTIVITIES IN PC-BASED CONDITION

Subjects	Add Nodes	Link Node	Add Text	Delete Node	Unlink Node	Correct Text	Move Node
1			✓			✓	
2	✓	✓			✓	✓	✓
3	✓	✓	✓			✓	✓
4	✓		✓	✓		✓	✓
5	✓	✓	✓	✓		✓	✓
6	✓	✓				✓	✓
7			✓			✓	
8	✓	✓		✓			✓
9	✓	✓	✓		✓	✓	✓
10	✓	✓					✓
11	✓	✓	✓		✓	✓	✓
12	✓	✓		✓	✓	✓	✓
13	✓	✓	✓				✓
14	✓	✓	✓		✓	✓	✓
15	✓	✓	✓	✓	✓	✓	✓
16	✓	✓		✓	✓		✓
Total	14/16	13/16	10/16	6/16	7/16	12/16	14/16

TABLE V. DESIGN ACTIVITIES IN MULTI-TOUCH CONDITION

Subjects	Add Nodes	Link Node	Add Text	Delete Node	Unlink Node	Correct Text	Move Node
1	✓	✓	✓	✓	✓	✓	✓
2	✓	✓	✓	✓	✓	✓	✓
3	✓	✓	✓	✓	✓	✓	✓
4	✓	✓	✓		✓		✓
5	✓	✓	✓		✓	✓	✓
6	✓	✓	✓	✓		✓	✓
7	✓	✓	✓				✓
8	✓	✓	✓	✓	✓	✓	✓
9	✓	✓	✓				✓
10	✓	✓	✓		✓		✓
11	✓	✓	✓	✓		✓	✓
12	✓	✓	✓			✓	✓
13	✓	✓	✓	✓	✓		✓
14	✓	✓	✓	✓		✓	✓
15	✓	✓	✓		✓	✓	✓
16	✓	✓	✓	✓	✓		✓
Total	16/16	16/16	16/16	9/16	10/16	10/16	16/16

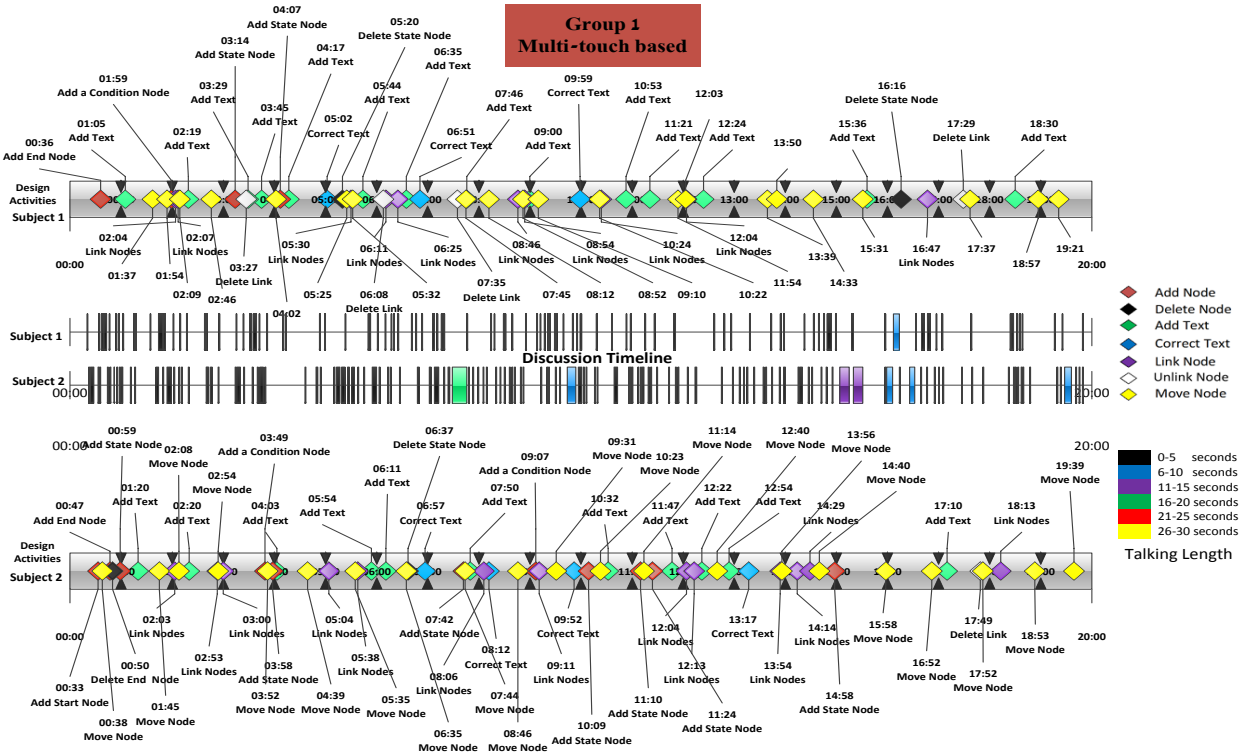

Fig.4. Collaboration log for Multi-touch table collaborative design

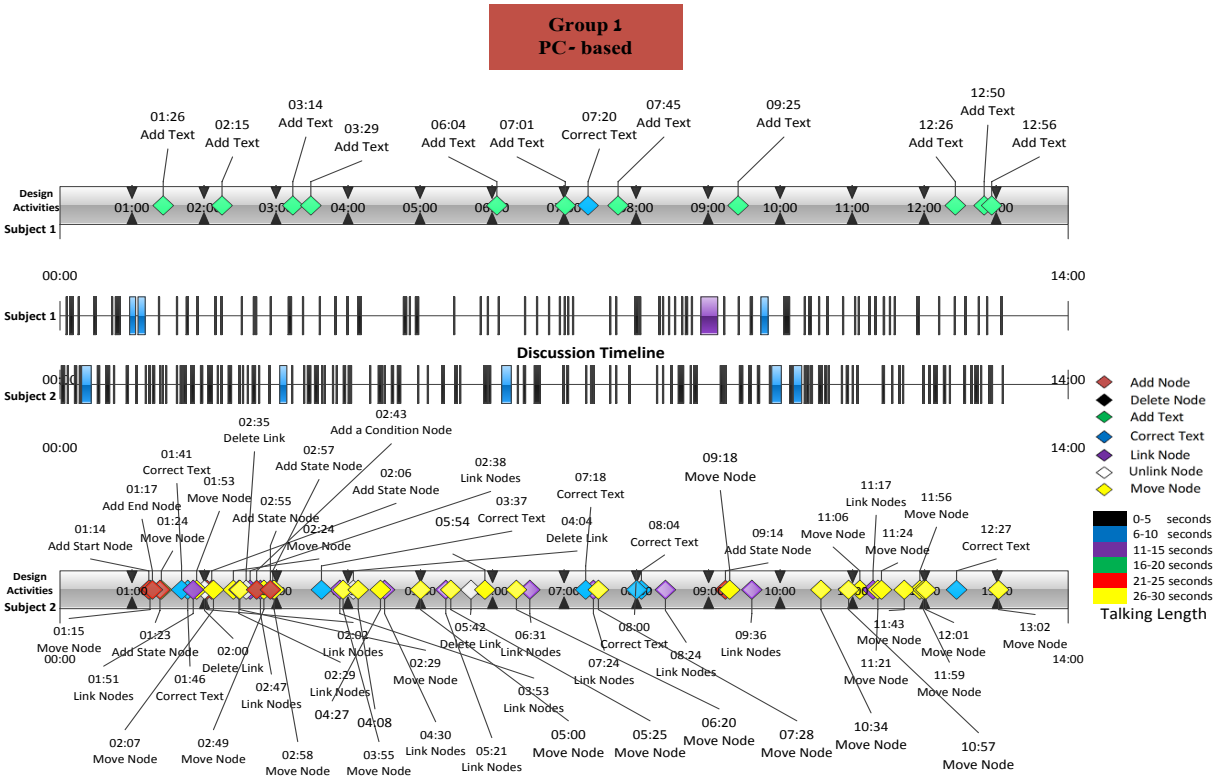

Fig.5. Collaboration log for PC-based collaborative design

VII. CONCLUSION

In this paper, the differences in collaborative software design amongst groups of students working in PC-based vs. Multi-touch conditions were investigated. We hypothesized that the Multi-touch table would increase the effectiveness of the collaborative process by enhancing collaboration learning skills and increasing physical interactions amongst team members.

The results indicate the benefit of using the Multi-touch MT-CollabUML tool as opposed to the PC-based version in enhancing collaborative software design. The Multi-touch environment increases the amount of physical interactions and subjects' engagements in the design activities. MT-CollabUML tool in the Multi-touch setting encouraged subjects to be engaged in a discursive conversation using "Creative Conflict" skills. More research needs be done in this area to fully explore the advantages and disadvantages of using Multi-touch tables in professional software design.

ACKNOWLEDGMENT

The authors acknowledge that the hardware for this research has been provided by the Engineering and Physics Research Council (EPSRC) under grand research number RES-139-25-0400.

REFERENCES

[1] N. Baghaei, A. Mitrovic, and W. Irwin, "Supporting collaborative learning and problem-solving in a constraint-based CSCL environment for UML class diagrams," *International Journal of Computer-Supported Collaborative Learning*, vol. 2, pp. 159-190, 2007.

[2] J. Han, "Low-cost multi-touch sensing through frustrated total internal reflection," in *Proceedings of the 18th Annual ACM Symposium on User Interface Software and Technology*, Seattle, WA, USA 2005, pp. 115-118.

[3] G. Ciocca, P. Olivo, and R. Schettini, "Browsing museum image collections on a multi-touch table," *Information Systems*, vol. 37, pp. 169-182, 2012.

[4] J. Kolb, B. Rudner, M. Reichert, M. Bajec, J. Eder, W. Aalst, J. Mylopoulos, M. Rosemann, M. J. Shaw, and C. Szyperski, "Towards Gesture-Based Process Modeling on Multi-touch Devices " in *Advanced Information Systems Engineering Workshops*. vol. 112, W. Aalst, J. Mylopoulos, M. Rosemann, M. J. Shaw, and C. Szyperski, Eds.: Springer Berlin Heidelberg, 2012, pp. 280-293.

[5] A. N. Antle, A. Bevans, J. Tanenbaum, K. Seaborn, and S. Wang, "Futura: design for collaborative learning and game play on a multi-touch digital tabletop," in *Proceedings of the fifth international conference on Tangible, embedded, and embodied interaction* Funchal, Portugal: ACM, 2010.

[6] P. Tuddenham, I. Davies, and P. Robinson, "WebSurface: an Interface for Co-located Collaborative Information Gathering," in *Proceedings of the ACM International Conference on Interactive Tabletops and Surfaces* Banff, Alberta, Canada: ACM, 2009, pp. 181-188

[7] J. Rick, A. Harris, P. Marshall, R. Fleck, N. Yuill, and Y. Rogers, "Children designing together on a multi-touch tabletop: an analysis of spatial orientation and user interactions," in *Proceedings of the 8th International Conference on Interaction Design and Children* Como, Italy: ACM, 2009.

[8] Y. Rogers, Y. Lim, W. R. Hazlewood, and P. Marshall, "Equal Opportunities: Do Shareable Interfaces Promote More Group

Participation Than Single User Displays?," *Human Computer Interaction*, vol. 24, pp. 79-116, 2009.

[9] M. R. Morris, J. Lombardo, and D. Wigdor, "WeSearch: supporting collaborative search and sensemaking on a tabletop display," in *Proceedings of the 2010 ACM conference on Computer supported cooperative work* Savannah, Georgia, USA: ACM, 2010, pp. 401-410.

[10] A. Harris, J. Rick, V. Bonnett, N. Yuill, R. Fleck, P. Marshall, and Y. Rogers, "Around the table: are multiple-touch surfaces better than single-touch for children's collaborative interactions?," in *Proceedings of the 9th international conference on Computer supported collaborative learning*. vol. 1 Rhodes, Greece: International Society of the Learning Sciences, 2009, pp. 335-344.

[11] T. E. Hansen and J. P. Hourcade, "Comparing multi-touch tabletops and multi-mouse single-display groupware setups," in *Proceedings of the 3rd Mexican Workshop on Human Computer Interaction* Mexico: Universidad Politécnica, 2010, pp. 36-43.

[12] P. Isenberg and D. Fisher, "Collaborative Brushing and Linking for Co-located Visual Analytics of Document Collections," *Computer Graphics Forum*, vol. 28, pp. 1031-1038, 2009.

[13] K. C. Dohse, T. Dohse, J. D. Still, and D. J. Parkhurst, "Enhancing Multi-user Interaction with Multi-touch Tabletop Displays Using Hand Tracking," in *Advances in Computer-Human Interaction, 2008 First International Conference on*, 2008, pp. 297-302.

[14] N. Baghaei and A. Mitrovic, "A constraint-based collaborative environment for learning UML class diagrams," in *Lecture Notes in Computer Science*. vol. 4053/2006, M. Ikeda, K. D. Ashley, and T.-W. Chan, Eds.: Springer Berlin / Heidelberg, 2006, pp. 176-186.

[15] W. Chen, R. H. Pedersen, and Ã. y. Pettersen, "CoLeMo: A collaborative learning environment for UML modelling," *Interactive Learning Environments*, vol. 14, pp. 233 - 249, 2006.

[16] M. Cataldo, C. Shelton, C. Yongjoon, H. Yun-Yin, V. Ramesh, D. Saini, and W. Liang-Yun, "CAMEL: A Tool for Collaborative Distributed Software Design," in *Fourth IEEE International Conference on Global Software Engineering, ICGSE 2009.* , 2009, pp. 83-92.

[17] K. Tourtoglou, M. Virvou, G. Tsihrintzis, R. Howlett, and L. Jain, "User Stereotypes Concerning Cognitive, Personality and Performance Issues in a Collaborative Learning Environment for UML," in *Studies in Computational Intelligence*. vol. 142/2008, G. A. Tsihrintzis, M. Virvou, R. J. Howlett, and L. C. Jain, Eds.: Springer Berlin / Heidelberg, 2008, pp. 385-394.

[18] J. Wu, T. Graham, R. Bastide, P. Palanque, and J. Roth, "The Software Design Board: A Tool Supporting Workstyle Transitions in Collaborative Software," in *Engineering Human Computer Interaction and Interactive Systems*. vol. 3425, R. Bastide, Ed.: Springer Berlin / Heidelberg, 2005, pp. 143-147.

[19] M. Basheri and L. Burd, "Exploring the Significance of Multi-touch Tables in Enhancing Collaborative Software Design using UML," in *Frontiers in Education Conference*, Seattle, Washington, USA (in press), 2012.

[20] A. Harris, J. Rick, V. Bonnett, N. Yuill, R. Fleck, P. Marshall, and Y. Rogers, "Around the table: Are multiple-touch surfaces better than single-touch for children's collaborative interactions?," 2009, pp. 335-344.

[21] S. Jarboe, "Procedures for enhancing group decision making," *Communication and Group Decision Making*, pp. 345-383, 1996.

[22] M. McManus and R. Aiken, "Monitoring computer-based problem solving," *Journal of Artificial Intelligence in Education*, vol. 6, pp. 307-336, 1995.

[23] A. Soller, "Supporting social interaction in an intelligent collaborative learning system," *International Journal of Artificial Intelligence in Education (IJAIED)*, vol. 12, pp. 40-62, 2001.

[24] P. Marshall, E. Hornecker, R. Morris, N. Sheep Dalton, and Y. Rogers, "When the fingers do the talking: A study of group participation with varying constraints to a tabletop interface," in *3rd IEEE International Workshop on Horizontal Interactive Human Computer Systems, 2008.*, 2008, pp. 33-40.

[25] N. Webb, J. Troper, and R. Fall, "Constructive activity and learning in collaborative small groups," *Journal of Educational Psychology*, vol. 87, pp. 406-406, 1995.

[26] N. Rummel and H. Spada, "Learning to Collaborate: An Instructional Approach to Promoting Collaborative Problem Solving in Computer-Mediated Settings," *Journal of the Learning Sciences*, vol. 14, pp. 201-241, 2013/01/24 2005.

[27] D. L. Craig and C. Zimring, "Support for collaborative design reasoning in shared virtual spaces," *Automation in Construction*, vol. 11, pp. 249-259, 2002.

[28] S. I. Ng, C. K. Tan, L. M. Yeo, and K. W. Lee, "Digitally Engendering Soft Skills Through Stixy - A Web-based Bulletin," *3L; Language, Linguistics and Literature, The Southeast Asian Journal of English Language Studies.*, vol. 18, pp. 73-89, 2012.

[29] L. Song and S. W. McNary, "Understanding studentsâ€™ online interaction: Analysis of discussion board postings," *Journal of Interactive Online Learning*, vol. 10, pp. 1-14, 2011.

[30] J. Robertson, J. Good, and H. Pain, "BetterBlether: The design and evaluation of a discussion tool for education," *International Journal of Artificial Intelligence in Education*, vol. 9, pp. 219-236, 1998.

[31] M. Basheri, L. Burd, and N. Baghaei, "A Multi-touch Interface for Enhancing Collaborative UML Diagramming," in *ACM Annual Conference of the Australian Computer-Human Interaction Special Interest Group (OZCHI)* Melbourne, Australia, 2012.

Vicarious Calibration Based Cross Calibration of Solar Reflective Channels of Radiometers Onboard Remote Sensing Satellite and Evaluation of Cross Calibration Accuracy through Band-to-Band Data Comparisons

Kohei Arai
Graduate School of Science and Engineering
Saga University
Saga City, Japan

***Abstract*—Accuracy evaluation of cross calibration through band-to-band data comparison for visible and near infrared radiometers which onboard earth observation satellites is conducted. The conventional cross calibration for visible to near infrared radiometers onboard earth observation satellites is conducted through comparisons of band-to-band data of which spectral response functions are overlapped mostly. There are the following major error sources due to observation time difference, spectral response function difference in conjunction of surface reflectance and atmospheric optical depth, observation area difference. These error sources are assessed with dataset acquired through ground measurements of surface reflectance and optical depth. Then the accuracy of the conventional cross calibration is evaluated with vicarious calibration data. The results show that cross calibration accuracy can be done more precisely if the influences due to the aforementioned three major error sources are taken into account.**

Keywords*—vicarious calibration; cross calibration; visible to near infrared radiometer; earth observation satellite; remote sensing; radiative transfer equation;

I. Introduction

Calibration of solar reflective wavelength coverage of mission instruments onboard remote sensing satellites is research subject for many years [1]-[17]. It is obvious that onboard calibration sources are degraded for time being as Dinguirard and Slater (1999) argued. It cannot be monitored even if onboard monitoring system is used for it because monitoring systems are degraded. Therefore, other calibrations, vicarious and cross calibrations are required. Reflectance based vicarious calibration is not accurate enough for monitoring the degradation. That is same thing for cross calibration.

Usually, the conventional cross calibration can be done through comparisons of band-to-band data of which spectral response functions are overlapped mostly. There are the following major error sources due to observation time difference, spectral response function difference in conjunction of spectral surface reflectance and spectral atmospheric optical depth, observation area difference. These error sources are assessed with dataset acquired through ground measurements of spectral surface reflectance and spectral optical depth. Then the accuracy of the conventional cross calibration is evaluated with vicarious calibration data.

Several researchers investigated cross calibration. Teillet, Fedosejevs, Thome, and Barker (2007) investigated impact of spectral response difference effect between sensors as quantitative indication using simulated data of observation [19]. The effect is called SBDE (Spectral Band Difference Effect) in this research. Twenty sensors were considered in the simulation together with some ground types, various combinations of atmospheric states and illumination geometries. They argued, overall, if spectral band difference effects (SBDEs) are not taken into account, the Railroad Valley Playa site is a 'good 'ground target for cross calibration between most but not all satellite sensors in most but not all spectral regions investigated. 'Good 'is denoted as SBDEs within 3%.

Liu, Li, Qiao, Liu, and Zhang (2004) developed a new method for cross calibration, and then applied the method to sensors Multi-channel Visible Infrared Scanning radiometers (MVIRS) and Moderate Resolution Imaging Spectro-radiometer (MODIS) [18]. They argued,"'An error analysis indicates that the calibration is accurate to within 5%, which is comparable to, or better than, the vicarious calibration method.

The method considers surface bidirectional reflectance distribution function (BRDF) mainly. BRDF indicates distribution of angle of reflection depend on an angle of incidence of illumination on the surface. In these researches, differences of SRF do not be considered. If the impact of its difference can be considered on cross calibration, differences between observed data can be explained more exactly and we can implement cross calibration by higher reliability.

ASTER/VNIR is onboard Terra satellite and is calibrated

with onboard calibration sources [20], vicarious calibration data as well as cross calibration. MODIS is onboard same platform and is calibrated with the aforementioned several types of data [21]. This situation is same thing for MISR [22] and ETM+ onboard the different platform, Landsat-7 [23].

The method proposed here is to check a reliability of the calibration sources through vicarious and cross calibrations for validations of these calibration accuracies. Namely, vicarious calibration requires spectral surface reflectance measurements and spectral optical thickness measurements. By using these ground based acquired data, cross calibration is conducted to improve a reliability of the calibration sources through comparison of vicarious calibration data. The results show that cross calibration accuracy can be done much more precisely if the influences due to the aforementioned three major error sources are taken into account.

The following section describes the proposed cross calibration method together with research background followed by some experiments. Then conclusion is described together with some discussions.

II. Proposed Cross Calibration Method

A. Research Background

The proposed cross calibration method is based on improvement of reliability of calibration accuracy through cross comparison to the vicarious calibration. The conventional cross calibration can be done with cross comparison between two visible to near infrared radiometer data. Therefore, cross calibration coefficients are essentially relative value. Cross calibration may be affected by the difference of wavelength coverage of the different visible to near infrared radiometers in conjunction with spectral surface reflectance and spectral optical depth, the difference between Instantaneous Field of View: IFOV, and the registration error between two visible to near infrared radiometer pixels and is not so good in terms calibration accuracy.

B. Example of Cross Calibration

The mission instrument in concern is VNIR: Visible to Near Infrared Radiometer of ASTER: Advanced Spectrometer for Thermal Emission and Reflectance onboard Terra satellite. Other instruments of which wavelength coverage are overlapped are onboard the same Terra satellite. Namely, the wavelength coverage of MODIS and MISR are overlapped with ASTER/VNIR. The wavelength coverage of these mission instruments are shown in Table 1 together with IFOV: Instantaneous Field of View. Other than these, the wavelength coverage of ETM+ onboard Landsat-5 is also overlapped with that of ASTER/VNIR. Therefore, cross calibration can be done between ASTER/VNIR and MODIS, MISR, ETM+. In MISR, these wavelengths are center wavelength of band. MISR bandwidth in Green, Red, and NIR are 0.028, 0.022, 0.039 *micrometer*, respectively.

Spectral response functions of these instruments are shown in Figure 1. Figure 1 (a) shows spectral responses for Green bands of the three mission instruments in concern while Figure (b) shows those for Red bands.

Furthermore, Figure 1 (c) shows those for Near Infrared bands. Band width and center wavelength are different each other.

Wavelength Coverage of Visible to Near Infrared Radiometers for Cross Calibration in Unit of Micrometer Therefore, influence due to the difference of spectral response functions have to be taken into account. These data are available from the urls listed in Table 2.

Although the data acquisition time of ASTER/VNIR is totally equal to these of MISR, and MODIS because these instruments are onboard the same satellite, Terra, ETM+ onboard Landsat-5 differs from the ASTER/VNIR for about 30 minutes.

TABLE I. Major Specification of Four Radiometers in Concern for Cross Calibration Between ASTER/VNIR and the other threee Radiometrs

	ASTER (15m/px)	MISR (275m/px)	MODIS (250m/px)	ETM+ (30m/px)
Green	0.52 - 0.60 (band1)	0.558	none	0.52 - 0.60 (band2)
Red	0.63 - 0.69 (band2)	0.672	0.62 - 0.67 (band1)	0.63 - 0.69 (band3)
NIR	0.76 - 0.86 (band3N)	0.867	0.84 - 0.87 (band2)	0.75 - 0.90 (band4)

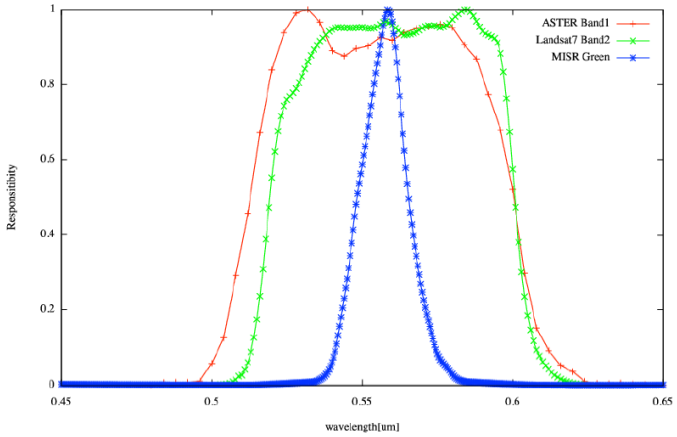

(a)Green bands

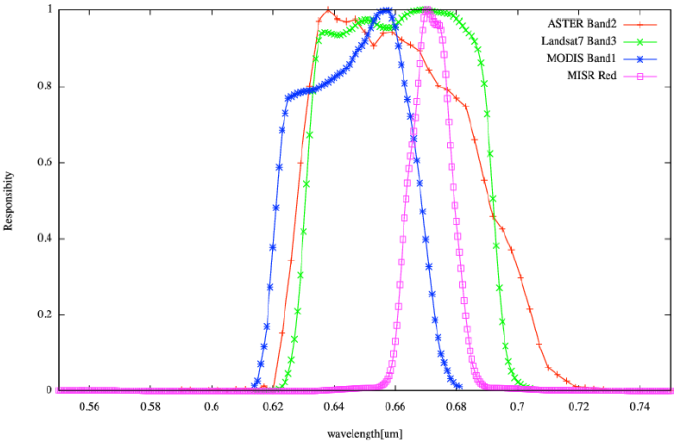

(b)Red bands

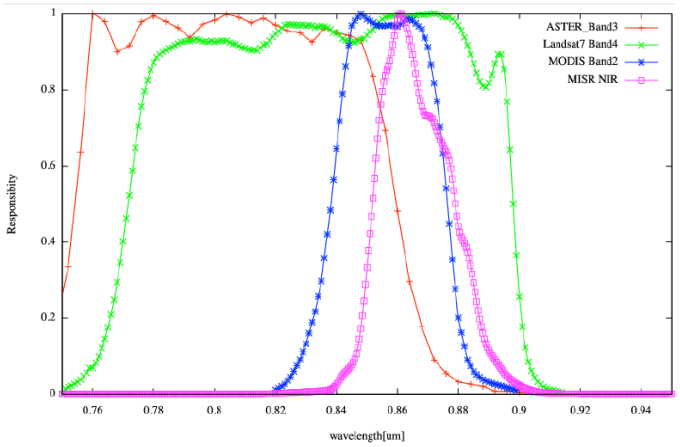

(c)Near Infrared bands

Fig.1. Comparison among the spectral response functions of ASTER/VNIR, MODIS, MISR, and ETM+

TABLE II. URLS OF WHICH VISIBLE TO NEAR INFRARED RADIOMETER DATA CAN BE DOWNLOAD

Sensor	Product name	URL
Terra/ASTER	Level 1B	http://earthexplorer.usgs.gov/
Terra/MODIS	MOD02QKM	http://ladsweb.nascom.nasa.gov/data/search.html
Terra/MISR	MI1B2T	http://l0dup05.larc.nasa.gov/MISR/cgi-bin/MISR/main.cgi
Landsat7/ETM+	Level 1T	http://earthexplorer.usgs.gov/

Other than these, registration error has to be taken into account in cross calibration. Figure 2 shows the illustrative view of the registration error between the pixels of ASTER/VNIR and the other instruments.

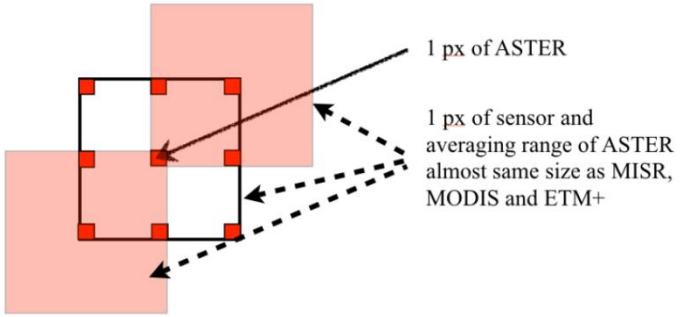

Fig.2. Registration error

Registration of the pixel of ASTER/VNIR in concern does not match perfectly to a corresponding pixel of the other mission instruments. Also, IFOV of ASTER/VNIR differs from those of the other mission instruments.

C. Coventional Cross Calibration

In the conventional cross calibration, the corresponding pixels of ASTER/VNIR are compared to those of the other instruments in unit of radiance. The difference of radiance between ASTER/VNIR and the other instruments is cross calibration coefficients for each band.

It is difficult to take into account the difference of spectral response functions, the difference of acquisition time difference. Influence due to the difference of IFOV and registration error can be taken into account. Therefore, cross calibration coefficients are essentially relative values.

D. Vicarious Calibration

Vicarious calibration coefficients, on the other hand, is defined as the difference between ASTER/VNIR pixel value derived radiance and the estimated radiance derived from the radiative transfer equation with the input parameters of surface reflectance measured on the ground, refractive index and size distribution estimated with atmospheric optical depths measured on the ground at the several wavelengths for aerosol scattering and absorption, and Rayleigh scattering derived from measured atmospheric pressure. Therefore, vicarious calibration coefficients are essentially absolute values.

E. Proposed Cross Calibration

The cross calibration method proposed here provides absolute calibration coefficients with measured reflectance and optical depth which are used for vicarious calibration. Top of the atmosphere: TOA radiance is estimated with radiative transfer equation with the measured surface reflectance and optical depth through convolution with the spectral response functions of the visible to near infrared radiometers in concern. Then cross comparison is made between the estimated TOA radiance of the visible to near infrared radiometers in concern.

Vicarious calibration, on the other hand, uses measured spectral reflectance and spectral optical depth. Therefore, vicarious calibration coefficients are essentially absolute value and are comparatively good in terms calibration accuracy. The difference between the proposed cross calibration and vicarious calibration methods is comparison processes. After the vicarious calibration for different visible to near infrared radiometers, vicarious calibration coefficients of visible to near infrared radiometer are compared each other in the proposed cross calibration.

III. EXPERIMENTS

A. Experiments Conducted

Field campaigns are conducted at the following there test sites,

IV: Ivanpah Playa (35:34N, 115:24W,790m), California
AL: Alkali Lake (37:51N, 117:25W, 1463m), Nevada
RV: Railroad Valley Playa (38:30N, 115:41N, 1440m) Nevada

Table 3 shows the dates of the field campaigns. Target pixel can be identified through visual perception of blue tarp on the test sites. Thus the test site locations are precisely identified with good registration accuracy.

B. Surface Reflectance

The surface reflectance is measured at the test sites for 60 m by 60 m with 10m interval. Figure 6 shows examples of the measured spectral surface reflectance at three test sites, Ivanpah Playa on September 22 2011, Alkali Lake on September 27 2011 and Railroad Valley Playa on September 29 2011.

TABLE III. THE DATES OF THE FIELD CAMPAIGNS

IV	AL	RV
0905 06/10/2002	2159 12/16/2005	2415 07/30/2006
2184 12/11/2005	2829 09/17/2007	3199 09/21/2008
2424 08/08/2006	3197 09/19/2008	3551 09/08/2009
2536 11/28/2006	3549 09/06/2009	3935 09/27/2010
2824 09/12/2007	3935 09/25/2010	4272 08/29/2011
3192 09/14/2008	4270 08/27/2011	4656 09/16/2012
3727 12/03/2008		
3544 09/01/2009		
3928 09/20/2010		
4265 08/22/2011		
4649 09/09/2012		

The first column shows the days after launch

C. ASTER/VNIR Images

Figure 3 shows examples of the ASTER/VNIR NIR band images of three test sites. Red square shows the test site locations.

D. Atmospheric Optical Depth

The atmospheric optical depth is measured at the test sites. Figure 7 shows examples of the measured atmospheric optical depth. In the atmosphere, there are absorption due to water vapor, ozone and aerosols together with scattering due to the atmospheric molecules, aerosols. Atmospheric Optical Depth: AOD (optical thickness) in total, Optical Depth: OD due to water vapor (H_2O), ozone (O_3), molecules (MOL), aerosols (AER), and real observed OD (OBS) are plotted in Figure 7.

(a)Ivanpah Playa

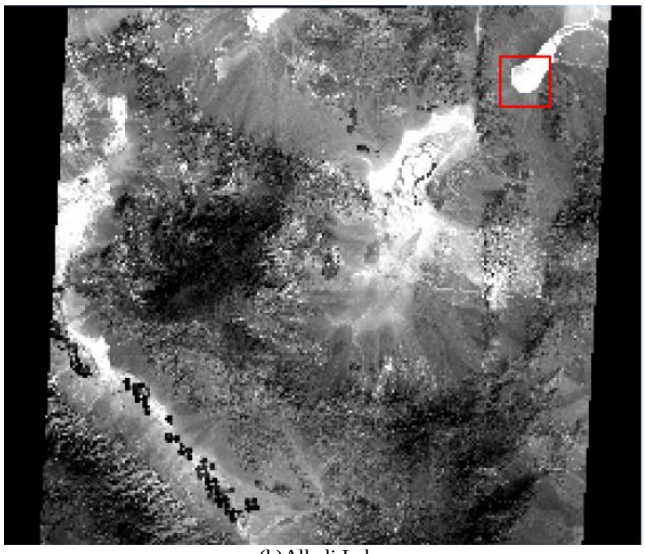

(b)Alkali Lake

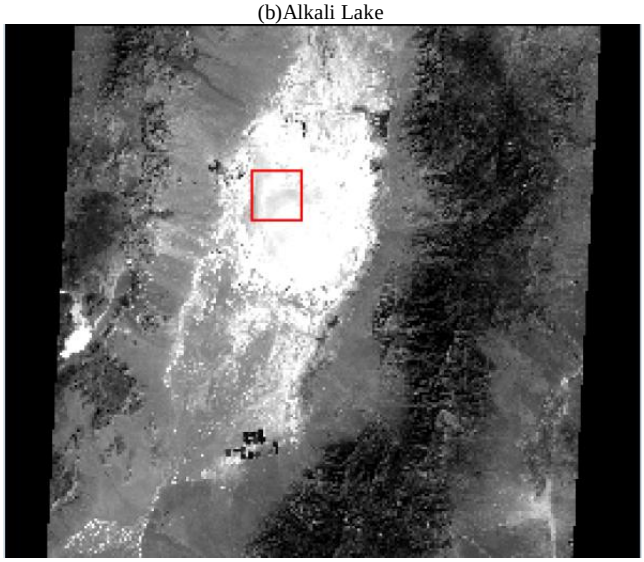

(c)Railroad Valley Playa

Figure 5 Examples of the ASTER/VNIR NIR band images of three test site

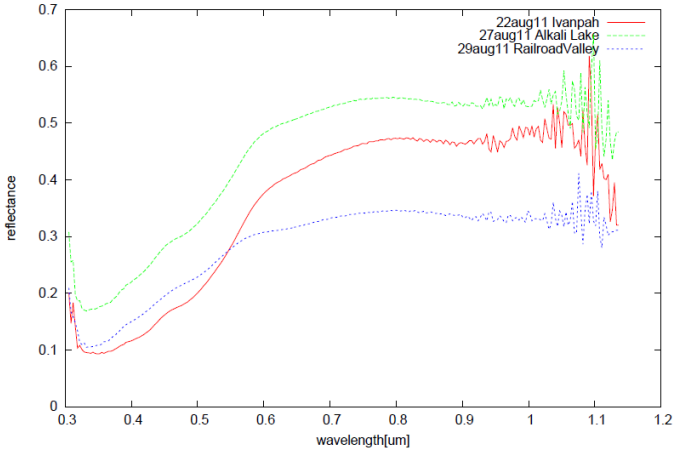

Figure 6 Examples of the measured spectral surface reflectance.

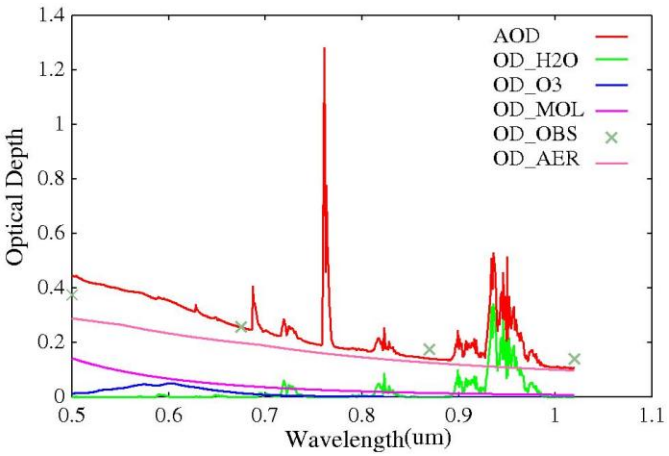

Figure 7 Example of observed atmospheric optical depth in total and the best fit curves of optical depth due to water vapor, ozone, molecules, and aerosols calculated with MODTRAN of atmospheric radiative transfer software code..

E. Vicarious Calibration

Vicarious calibration coefficients are obtained based on radiative transfer software code of MODTRAN with the field campaign data of surface reflectance, total column ozone and water vapor, as well as atmospheric pressure together with aerosol parameters; refractive index and size distribution derived from sky radiometer data and atmospheric optical depth. TOA radiance is estimated through the aforementioned procedure and then is compared to the ASTER/VNIR derived radiance results in calculation of vicarious calibration coefficients. Table 4 shows the calculated vicarious calibration data.

TABLE IV. THE VICARIOSU CALIBRATION COEFFICIENTS

(a)Ivanpah Playa

	Day	DAL	RCC_vc
Band Green	2000/06/04	169	0.89570
	2001/06/07	537	0.79536
	2002/01/17	757	0.76413
	2005/12/11	2148	0.66320
	2006/08/08	2424	0.84946
	2006/11/28	2536	0.84655
	2007/09/12	2824	0.77642
	2008/09/14	3192	0.73081
	2008/11/03	3242	0.64953
	2009/09/01	3544	0.76699
	2010/09/20	3928	0.80678
	2011/08/22	4265	0.83696
	Day	DAL	RCC_vs
Band Red	2000/06/04	169	0.93470
	2001/06/07	537	0.81293
	2002/01/17	757	0.80310
	2005/12/11	2148	0.69795
	2006/08/08	2424	0.85075
	2006/11/28	2536	0.85321
	2007/09/12	2824	0.76921
	2008/09/14	3192	0.75591
	2008/11/03	3242	0.69026
	2009/09/01	3544	0.78700
	2010/09/20	3928	0.79278
	2011/08/22	4265	0.94690
	Day	DAL	RCC_vs
Band NIR	2000/06/04	169	1.00010
	2001/06/07	537	0.87390
	2002/01/17	757	0.90067
	2005/12/11	2148	0.78288
	2006/08/08	2424	0.93711
	2006/11/28	2536	0.95591
	2007/09/12	2824	0.74768
	2008/09/14	3192	0.79275
	2008/11/03	3242	0.73340
	2009/09/01	3544	0.81375
	2010/09/20	3928	0.89448
	2011/08/22	4265	1.00322

(b)Alkali Lake

	Day	DAL	RCC_vc
Band Green	2005/12/16	2159	0.69600471
	2007/09/17	2829	0.66371092
	2008/09/19	3197	0.84800178
	2009/09/06	3549	0.774319
	2010/09/25	3933	0.67612548
	2011/08/27	4270	0.60813229
	Day	DAL	RCC_vs
Band Red	2005/12/16	2159	0.69859583
	2007/09/17	2829	0.77056662
	2008/09/19	3197	0.7507701
	2009/09/06	3549	0.79646567
	2010/09/25	3933	0.70989962
	2011/08/27	4270	0.69222309
	Day	DAL	RCC_vs
Band NIR	2005/12/16	2159	0.80871349
	2007/09/17	2829	0.81529287
	2008/09/19	3197	0.79725186
	2009/09/06	3549	0.90928185
	2010/09/25	3933	0.85319343
	2011/08/27	4270	0.85718958

(c)Railroad Valley Playa

	Day	DAL	RCC_vc
Band Green	2000/06/11	173	0.88235
	2001/06/14	541	0.80184
	2006/07/30	2415	0.94137
	2008/09/21	3199	0.76877
	2010/09/27	3935	0.74499
	2011/08/29	4272	0.70407
	Day	DAL	RCC_vs
Band Red	2000/06/11	173	0.89655
	2001/06/14	541	0.84616
	2006/07/30	2415	0.89336
	2008/09/21	3199	0.80563

	2010/09/27	3935	0.73990
	2011/08/29	4272	0.72334
Band NIR	Day	DAL	RCC_vs
	2000/06/11	173	0.97452
	2001/06/14	541	0.94041
	2006/07/30	2415	0.97833
	2008/09/21	3199	0.81471
	2010/09/27	3935	0.82571
	2011/08/29	4272	0.78299

DAL denotes the days after launch.

In accordance with the days after launch, Radiometric Calibration Coefficient: RCC is decreased as exponential function. Namely, sensitivity of ASTER/VNIR is degraded for time being. There is test site dependency and wavelength dependency. The most degraded band is band 1 followed by band 2 and band 3 depending on the corresponding wavelength. Namely, sensitivity degradation is negatively proportional to the wavelength (degradation of shorter wavelength is much greater than that of longer wavelength).

Sensitivity degradation foe the Alkali test site, on the other hand, is much significant in comparison to the other two test sites, sensitivity degradation for the other two sites indicate almost same though. One of the biggest reasons for this is sensor saturations. Due to the fact that the surface reflectance at Alkali test site is highest comparing to the others, ASTER/VNIR, in particular, band 1 and 2 are saturated. Sensitivity degradation should be same for all the test sites. Therefore, vicarious calibration coefficients for in particular band 1 and 2 derived from the Alkali test site would be better to forget.

F. Cross Calibration Coefficients

Figure 8 (a), (c), (e) shows the Radiometric Calibration Coefficient: RCC of the conventional cross calibration while Figure 8 (b), (d), (f) shows those for the proposed cross calibration. Red solid line in the figure shows RCC derived from Onboard Calibration: OBC data. OBC data derived RCC differs from both the conventional and the proposed cross calibration RCC. These cross calibration coefficients are summarized with their averaged RCC and Standard Deviation: SD together with their Confidence Interval: CI at 95% of confidence level as shown in Table 5. Also Root Mean Square Difference: RMSD between vicarious RCC and the conventional cross calibration RCC as well as the proposed cross calibration RCC is shown in Table 6.

As shown in Table 6, RMSD between the vicarious RCC and the proposed cross calibration RCC is less than that between the vicarious RCC and the conventional cross calibration RCC. Therefore, it is said that the proposed cross calibration method is superior to the conventional cross calibration method obviously. Percent difference of RMSD between the conventional and the proposed cross calibration is shown in Table 7.

It may said that the proposed cross calibration method shows 6 to 89% better cross calibration accuracy in comparison to the conventional cross calibration.

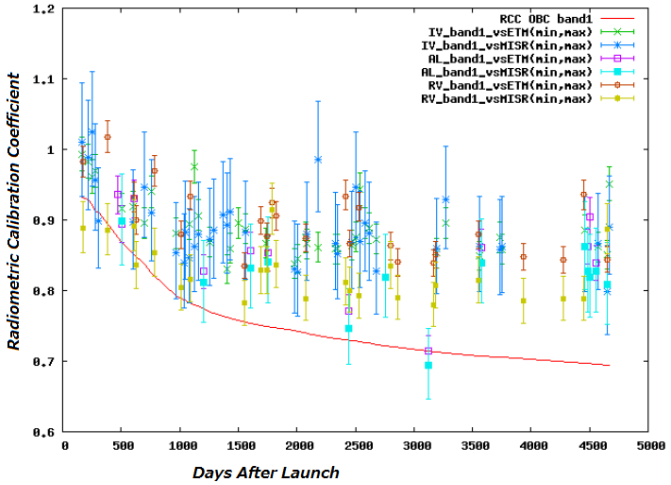

(a)Conventional Band 1

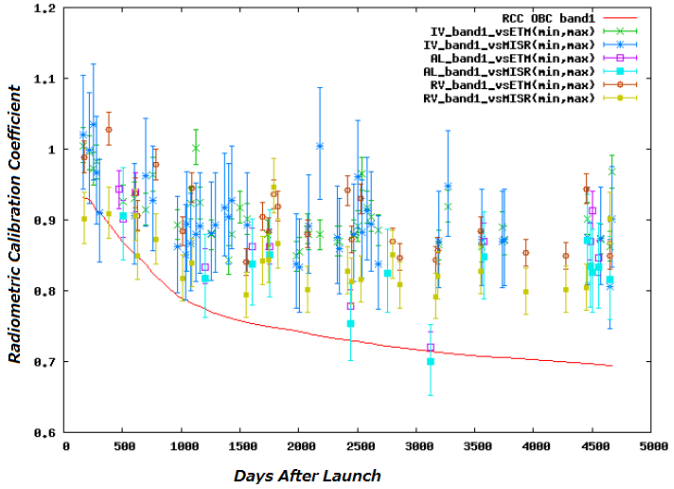

(b)Proposed Band1

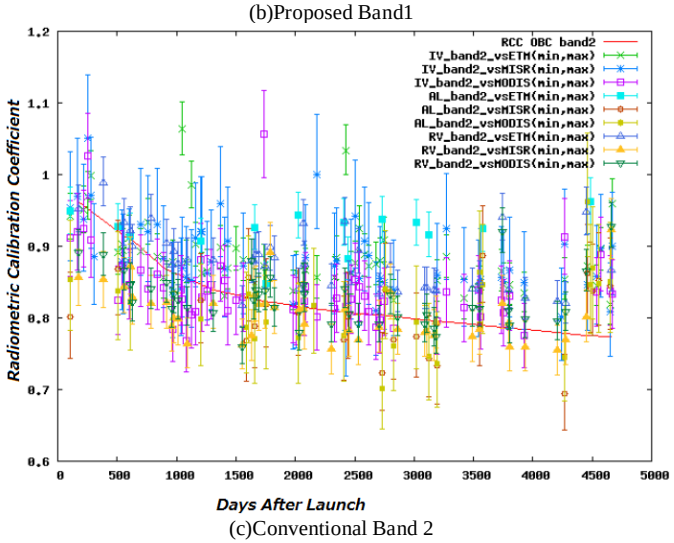

(c)Conventional Band 2

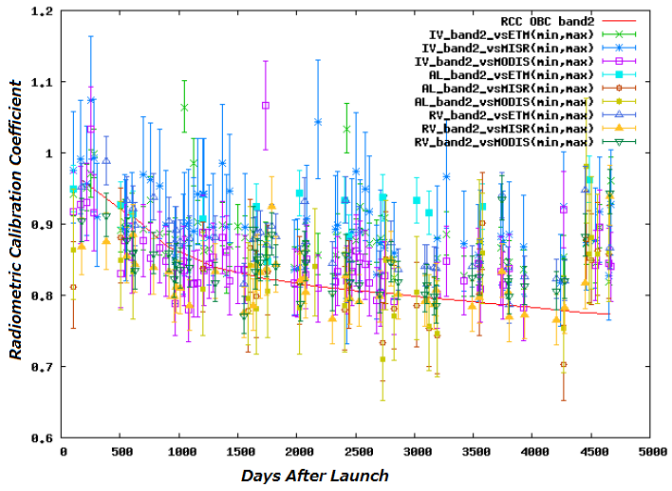

(d)Proposed Band 2

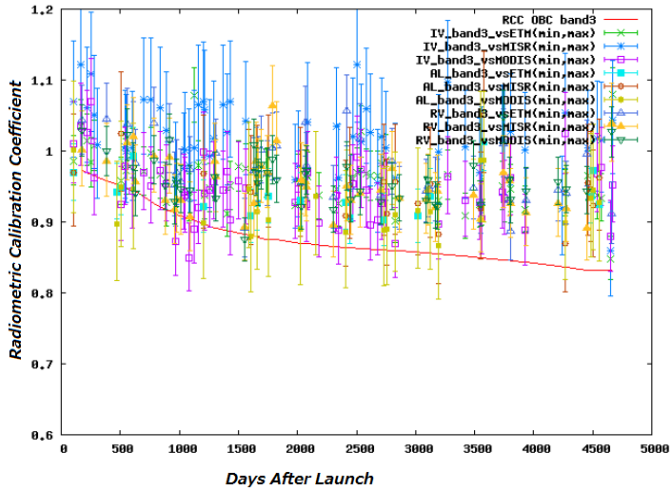

(e)Conventional Band 3

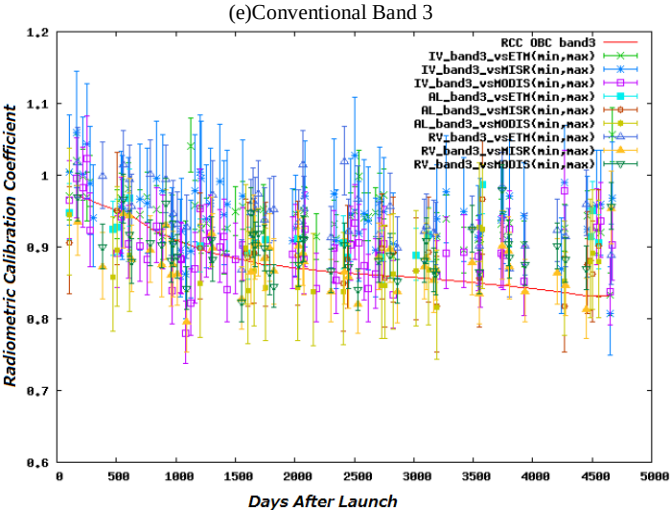

(f)Proposed Band 3

Figure 8 Comparison of cross calibration RCC between the conventional and the proposed cross calibration methods

TABLE V. SUUMARY OF CROSS CALIBRATION COEFFICIENTS

(a)Cross RCC for Green and Red bands

		Green		Red		
		vsETM	vsMISR	vsETM	vsMISR	vsMODIS
IV	average (SD)	1.80 (0.54)	1.38 (0.45)	0.03 (0.15)	3.33 (0.90)	1.15 (1.33)
	95% CI	[1.38, 2.24]	[1.02, 1.74]	[-0.09, 0.15]	[2.61, 4.04]	[0.09, 2.21]
AL	average (SD)	1.41 (0.69)	1.46 (0.58)	-0.05 (0.16)	2.47 (1.02)	2.26 (0.72)
	95% CI	[0.52, 2.31]	[0.72, 2.21]	[-0.26, 0.15]	[1.16, 3.79]	[1.33, 3.19]
RV	average (SD)	0.88 (0.11)	2.34 (0.20)	-0.08 (0.12)	2.23 (0.28)	2.12 (0.29)
	95% CI	[0.74, 1.02]	[2.09, 2.60]	[-0.23, 0.07]	[1.87, 2.59]	[1.75, 2.50]

(b)Cross RCC for NIR band

		NIR		
		vsETM	vsMISR	vsMODIS
IV (N=11)	average (SD)	-1.81 (1.14)	-6.71 (1.83)	-5.09 (1.76)
	95% CI	[-2.72, -0.90]	[-8.17, -5.25]	[-6.49, -3.69]
AL (N=6)	average (SD)	-2.80 (0.97)	-8.94 (1.62)	-7.37 (1.41)
	95% CI	[-4.06, -1.55]	[-11.04, -6.85]	[-9.19, -5.54]
RV (N=6)	average (SD)	-2.67 (0.33)	-7.96 (1.37)	-6.65 (1.14)
	95% CI	[-3.10, -2.24]	[-9.72, -6.19]	[-8.12, -5.18]

TABLE VI. AVERAGED ROOT MEAN SQUARE DIFFERENCE BETWEEN VICARIOUS CALIBRATION RCC AND CROSS CALIBRATION RCC

	Conventional			Proposed		
Site	ETM+	MISR	MODIS	ETM+	MISR	MODIS
Ivanpah	0.0733	0.0798	0.0338	0.0690	0.0645	0.0169
Alkali	0.0280	0.0625	-	0.00312	0.0387	-
Railroad	0.0889	0.0194	0.0619	0.0807	0.0031	0.0346

TABLE VII. PERCENT DIFFERENCE OF RMSD BETWEEN CONVENTIONAL AND PROPOSED CROSS RCC

	% Difference between Conventional and Proposed Cross RCC		
Site	ETM+	MISR	MODIS
Ivanpah	5.866	19.173	50.000
Alkali	88.857	38.080	-
Railroad	9.224	84.021	44.103

IV. CONCLUSION

Accuracy evaluation of cross calibration through band-to-band data comparison for visible and near infrared radiometers which onboard earth observation satellites is conducted. The conventional cross calibration for visible to near infrared radiometers onboard earth observation satellites is conducted through comparisons of band-to-band data of which spectral response functions are overlapped mostly. There are the following major error sources due to observation time difference, spectral response function difference in conjunction of surface reflectance and atmospheric optical depth, observation area difference. These error sources are assessed with dataset acquired through ground measurements of surface reflectance and optical depth. Then the accuracy of the conventional cross calibration is evaluated with vicarious calibration data.

The results show that cross calibration accuracy can be done more precisely if the influences due to the aforementioned three major error sources are taken into account.

ACKNOWLEDGMENT

The author would like to thank Dr. Satoshi Tsuchida and his colleague of The National Institute of Advanced Industrial Science and Technology (AIST), and Dr. Fumihiro Sakuma and his colleague of The Japan Space Systems: JSS people for their support to this research works. The author also would like to thank Mr. Yuichi Sarusawa of Graduate School of Saga University for his efforts to conduct cross calibration experiments.

REFERENCES

[1] Arai,K., Calibration /intercalibration of multi-sensor for satellites, Advances in Space Research, Vol.16, No.10, pp.125-128, A31-002, July 1994.

[2] P.Slater, K.Thome, A.Ono, F.Sakuma, Kohei Arai, F.Palluconi, H.Fujisada, Y.Yamaguchi and H.Kieffer, Radiometric Calibration of ASTER Data, Journal of Remote Sensing Society of Japan, Vol.15, No.2, pp.16-23, Jun.1994.

[3] A.Ono, F.Sakuma, Kohei Arai, Y.Yamaguchi, H.Fujisada, P.Slater, K.Thome, F.Palluconi and H.Kieffer, Pre-filight and In-flight Calibration Plan for ASTER, Journal of Atmospheric and Oceanic Technology, Vol.13, No.2, pp.321-335, Apr.1995.

[4] Kohei Arai, Inflight Test Site Cross Calibration Between Mission Instruments Onboard Same Platform, Advances in Space Research, Vol.19, No.9, pp.1317-1324, Jul.1997.

[5] K.Thome, K.Arai et al., ASTER Preflight and Inflight Calibration and Validation of Level 2 Products, IEEE Trans.on Geoscience and Remote Sensing, Vol.36, No.4, 1161-1172, Sep.1998.

[6] K.Thome, S.Schiller, J.Conel, K.Arai and S.Tasuchida, Results of the 1996 EOS vicarious calibration joint campaign at Lunar Lake Playa, Nevada(USA), Metrologia, Vol.35, pp.631-638, Jan.1999.

[7] K.Arai, Error budget analysis of cross calibration method between ADEOS/AVNIR and OCTS, Advances in Space Research, Vol.23, No.8, pp.1385-1388, June 1999.

[8] K.Arai, Preliminary vicarious calibration for EOS-AM1/ASTER with field campaign, Advances in Space Research, Vol.23, No.8, pp.1449-1457, June 1999.

[9] Kohei Arai and H.Tonooka, Radiometric performance evaluation of ASTER/VNIR, SWIR and TIR, IEEE Trans. on GeoScience and Remote Sensing, 43,12,2725-2732, 2005.

[10] Kohei Arai, Vicarious calibration for solar reflection channels of radiometers onboard satellites with deserted area of data, Advances in Space Research, 39, 1, 13-19, 2007.

[11] Kurtis Thome, Kohei Arai, Satoshi Tsuchida and Stuart Biggar, Vicarious calibration of ASTER via the reflectance based approach, IEEE transaction of GeoScience and Remote Sensing, 46, 10, 3285-3295, 2008.

[12] Chrysoulakis,Abrams, Feidas and Kohei Arai, Comparison of Atmospheric correction methods using ASTER data for the area of Crete, Greece, International Journal of Remote Sensing, 31,24,6347-6385,2010.

[13] Ramachandran, Justice, Abrams(Edt.),Kohei Arai et al., Land Remote Sensing and Global Environmental Changes, Part-II, Sec.5: ASTER VNIR and SWIR Radiometric Calibration and Atmospheric Correction, 83-116, Springer 2010.

[14] Arai, K., & Terayama, Y. (2000). An Experimental Study on Cross Calibration of ADEOS / AVNIR and the Visible Channels of OCTS. *Journal of Remote Sensing Society of Japan*, *20* (2), 60{68.

[15] Cachorro, V. E., Frutos, A. M. D. E., Aplicada, D. D. F., Gonzalez, M. J., & Electrica, D. D. I. (1993). Analysis of the relationships between Junge size distribution and angstrom _ turbidity parameters from spectral measurements of atmospheric aerosol extinction. *Atmospheric Environment*, *27A*(10), 1585{1591.

[16] Chandrasekhar, S. (1960). *Radiative transfer* (1st ed.). New York, US: Dover Publications, Inc.

[17] Dinguirard, M., & Slater, P. (1999). Calibration of space-multispectral imaging sensors: A review. *Remote Sensing of Environment*, *4257* (98), 194{205. Earth Remote Sensing Data Analysis Center. (2005). *ASTER User's Guid Part I General* (Ver.4.0 ed.).

[18] Liu, J.-J., Li, Z., Qiao, Y.-L., Liu, Y.-J., & Zhang, Y.-X. (2004, December). A new method for cross-calibration of two satellite sensors. *International Journal of Remote Sensing*, *25* (23), 5267{5281. Retrieved from http://www.tandfonline.com/doi/abs/10.1080/01431160412331269779 doi: 10.1080/01431160412331269779

[19] Teillet, P. M., Fedosejevs, G., Thome, K., & Barker, J. L. (2007, October). Impacts of spectral band difference effects on radiometric cross-calibration between satellite sensors in the solar-reflective spectral domain. *Remote Sensing of Environment*, *110* (3), 393{409. doi: 10.1016/j.rse.2007.03.003

[20] Tsuchida, S., Sakuma, H., & Iwasaki, A. (2004). *Equations for ASTER radiometric calibration ver.0.20.* Retrieved 2013/01/24, from http://staff.aist.go.jp/s.tsuchida/aster/cal/info/equation/index.html

[21] Xiong, X., Che, N., & Barnes, W. L. (2006). Terra MODIS On-Orbit Spectral Characterization and Performance. *IEEE transactions on Geoscience and Remote Sensing*, *44* (8), 2198{2206.

[22] C.J. Brueggc and D.J. Diner, "Instrument verification tests on the Multi-angle imaging Spectro-Radiometer (MISR)," in *Earth Observing Systems II*, SPIE 3117, San Diego, CA, 28-29 July 1997.

[23] P.M. Teillet, J.L. Barker, B.L. Markham, R.R Irish, G. Fedosejevs, J.C. Storey, Radiometric cross-calibration of the Landsat-7 ETM+ and Landsat-5 TM sensors based on tandem data sets, Remote Sensing of Environment 78 (2001) 39– 54

AUTHORS PROFILE

Kohei Aarai He received BS, MS and PhD degrees in 1972, 1974 and 1982, respectively. He was with The Institute for Industrial Science and Technology of the University of Tokyo from April 1974 to December 1978 and also was with National Space Development Agency of Japan from January, 1979 to March, 1990. During from 1985 to 1987, he was with Canada Centre for Remote Sensing as a Post Doctoral Fellow of National Science and Engineering Research Council of Canada. He moved to Saga University as a Professor in Department of Information Science on April 1990. He was a councilor for the Aeronautics and Space related to the Technology Committee of the Ministry of Science and Technology during from 1998 to 2000. He was a councilor of Saga University for 2002 and 2003. He also was an executive councilor for the Remote Sensing Society of Japan for 2003 to 2005. He is an Adjunct Professor of University of Arizona, USA since 1998. He also is Vice Chairman of the Commission-A of ICSU/COSPAR since 2008. He wrote 30 books and published 332 journal papers.

Interference Aware Channel Assignment Scheme in Multichannel Wireless Mesh Networks

Sunmyeng Kim
Department of Computer Software Engineering
Kumoh National Institute of Technology
Gumi, South Korea

***Abstract*—Wireless mesh networks (WMNs) are gaining significant attention to provide wireless broadband service. Nodes in a wireless mesh network can communicate with each other directly or through one or more intermediate nodes. Because of multi-hop transmissions with multiple contending and competing channels, performance of wireless mesh networks decreases. Supporting high performance is an important challenge in multi-hop mesh networks. Nassiri et al. proposed a Molecular MAC protocol for autonomic assignment and use of multiple channels to improve network performance. In the Molecular MAC protocol, nodes are either nuclei or electrons in an atom. Neighboring atoms use orthogonal channels to operate in parallel data transmissions. Each nucleus selects an idle channel that is not currently being occupied by its neighboring atoms with the assistance from electrons in the same atom. However, this protocol has the following drawback; since a nucleus allocates a channel with help from the electrons in its own transmission range, it is not able to recognize the existence of those atoms in the interference range. Therefore, allocating the same channel to neighboring atoms results in the deterioration of network performance. In order to resolve this problem, we propose a channel allocation scheme with the interference issue taken into account. Based on various simulation results, the proposed scheme was verified that different channels could be allocated to those neighboring atoms in the interference range.**

Keywords—interference; channel assignment; multichannel; mesh network

I. INTRODUCTION

A wireless mesh network (WMN) is a cost-effective access network architecture. It is a promising wireless technology for numerous applications. It is gaining significant attention as a possible way for Internet service providers (ISPs) and carriers in order to provide wireless broadband service. In WMNs, nodes are consisted of mesh routers and mesh clients [1]. Mesh routers have minimal mobility and form the backbone of WMNs. When a node is within the transmission range of another node, they are considered as neighbors, and there is a wireless link between them. Some nodes, called gateways, are connected to the wired network, which connects the WMNs to rest of the Internet.

The packets sent by end users travel through wireless mesh networks over multiple hops. And gateway nodes relay traffic to and from the wired Internet. The performance of multi-hop communication quickly reduces as the number of hops becomes larger due to intra-flow and inter-flow interferences [2-4]. This is because a wireless link is shared among neighboring nodes.

The intra-flow interference occurs because nodes are in each other's interference range along the path of the same flow. Nodes experience different amount of channel contention as shown in Fig. 1. Inter-flow interference occurs since multiple flows on the same channels between different routing paths operate and compete for the medium as shown in Fig. 2.

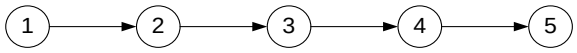

Fig. 1. Intra-flow interference

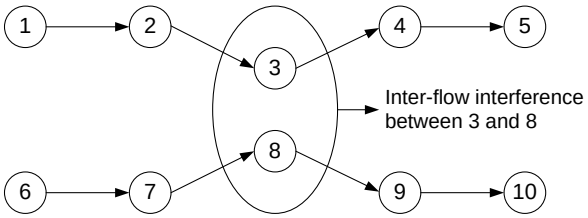

Fig. 2. Inter-flow interference

With a single channel, nodes operate on the same channel. Therefore, network performance decreases. Nodes can be equipped with multiple radios and channels. This means there is a unique frequency used for each wireless hop, and thus enables separation of wireless collision domain and reduces the interference and contention. This can significantly improve network performance without bandwidth degradation.

The design of the MAC protocol is the most likely challenge in WMNs. An interesting problem in WMNs is how to efficiently utilize multiple channels. Several MAC protocols for handling multiple channels have been proposed in the literature [5-17].

The algorithms proposed in [5] select channels for the mesh radios to minimize interference within the mesh network and between the mesh network and co-located wireless networks. A new method for the interference estimation is suggested. All available channels are periodically monitored by each mesh node and measured information of internal channel usage and external interference is shared with mesh nodes within

This research was supported by Basic Science Research Program through the National Research Foundation of Korea (NRF) funded by the Ministry of Education, Science and Technology (2010-0025495).

interference range. Duarte et al. use game theory to design a systematic approach to utilize partially overlapped channels in WMNs while minimizing the adverse effect of adjacent channel interference [6]. In [7], both centralized and distributed algorithms are presented, which aim to minimize the number of pairs of links that are interfering. Molecular MAC protocol was proposed to organize the mesh network according to the molecular analogy [8-12]. It divides the network into atoms with nucleus nodes operating on fixed channels and electrons that dynamically switch channels between neighbor nuclei. Electrons can be shared by numerous atoms.

When a nucleus selects a channel, it receives help from the electrons in its own transmission range. Then, electrons deliver the information about those channels used by their parent atoms to the nucleus. Because an atom cannot be aware of the existence of other neighboring atoms if there are no electrons shared among them, the nucleus may allocate the same channel to such atoms. Although the proposed scheme naturally adopts a fundamental operation principle of the Molecular MAC protocol, it modifies a channel allocation method. The proposed scheme is somewhat similar to the Molecular MAC protocol method in that a channel is selected by the assistance of electrons. Then, a collision probability is applied to allocate a new channel in order to recognize any interference and avoid any overlapped channel allocation.

The paper is organized as follows. We give a brief introduction of the Molecular MAC protocol and its channel assignment problem in Section II. In Section III, the proposed scheme is presented in detail. In Section IV, performance studies are carried out through simulation results. Finally, we draw a conclusion in Section V.

II. Related Work

This Section is designed to briefly specify the Molecular MAC protocol and then touch on certain problem relating to the channel allocation.

A. Molecular MAC Protocol

The IEEE 802.11 wireless network functions well in the infrastructure mode. In addition, it can provide a fair bandwidth to all users by slightly modifying a channel access method. Nevertheless, the IEEE 802.11 network may incur numerous problems on a multi-hop network. The Molecular MAC protocol expands the IEEE 802.11 network in order to transmit data packets on the multi-hop network effectively.

Since the IEEE 802.11 access method works well on a single-hop network, the Molecular MAC protocol divides a wireless mesh network into different spatially distributed atoms. Each atom uses a channel not used by other neighboring atoms. An atom is composed of one nucleus and several electrons, and a nucleus selects a channel to be used by its own atom. Any node within an atom's boundary plays a role as an electron and belongs to a neighboring atom. An electron directly communicates with its nuclei; however, since there is no direct link between electrons, a direct communication among them cannot be implemented. In addition, due to no direct link among nuclei, direct communications among them are also not possible. Therefore, the communication among neighboring electrons can be handled by nuclei while the communication among nuclei can be executed by neighboring electrons.

In the Molecular MAC protocol, each node is assigned with the role as a nucleus or an electron while each nucleus selects a channel to be used by its own atom. Accordingly, each node forms a shortest path-spanning tree to a gateway node linked to a wired Internet. After a tree is formed, the nodes with an even-numbered depth and an odd-numbered depth are assigned with the roles of a nucleus and an electron, respectively. After such roles are assigned, each nucleus requests its own electrons for channel information. Channel information includes a list of active channels and their activities. A list of active channels includes the numbers of active channels in the corresponding electrons' parent atoms. A channel activity is a parameter that is designed to indicate how many data packets are transmitted on each channel in the active channel list, which is expressed in the number of packets transmitted. Requested by a nucleus, each electron makes up a list of active channels, measures each channel's activities, and accordingly responds to the nuclei. Then, a nucleus receives certain responses from all neighboring electrons and accordingly selects a channel according to a subsequent rule. 1) After a list of active channels is received from all neighboring electrons, a channel is randomly chosen out of those non-active channels. 2) If every channel is currently occupied, a channel with the least activity is selected. Once a nucleus allocates a channel, its neighboring electrons use the channel. The corresponding electrons use all channels allocated by their atoms' nuclei.

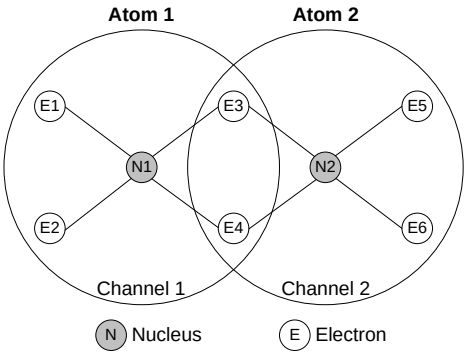

Fig. 3. Basic architecture of Molecular MAC protocol

Fig. 3 illustrates a fundamental structure of the Molecular MAC protocol. As shown in the figure, there are 2 atoms, 2 nuclei and 6 electrons. The atom 1 includes the nucleus N1 and the electrons (E1, E2, E3 and E4), and uses the channel 1. The atom 2 includes the nucleus N2 and the electrons (E3, E4, E5 and E6), and uses the channel 2. The electrons E3 and E4, shared by the two atoms, use both channel 1 and channel 2. If a neighboring atom's nucleus requests information for the allocation of a channel, the corresponding electrons transmit their channel activity information. Furthermore, the electrons E1/E2, E3/E4 and E5/E6 also transmit the active channel lists including the channel 1, the channels 1 & 2 and the channel 2, respectively, to the nucleus. Once all channels are allocated, communications are processed as follows: As shown in the figure, when certain data are to be transmitted from E1 to E6,

E1 transmits the data to N1 using the channel 1 while N1 transmits the date back to E3 or E4. Then, E3 or E4 transmits the data to N2 using the channel 2 while N2 transmits the data back to E6. The neighboring electrons, E1 and E2, do not directly communicate with each other but communicate via the nucleus N1.

B. Channel Assignment Problem in the Molecular MAC Protocol

There is a problem associated with a channel allocation scheme of the Molecular MAC protocol. The active channel list and channel activity information used by a nucleus for allocating a channel are not sufficient. If there are no electrons shared by neighboring atoms and if such atoms exist in the same interference range, the other atom's channel information cannot be identified. Therefore, an identical channel is allocated so that network performance can be deteriorated due to the interference. In addition, since each electron is located out of the other electron's transmission range, the number of packets transmitted cannot be properly measured, hence making the channel activity information inaccurate. As shown in the Fig. 3, because the atoms 1 and 2 share the electrons E3 and E4, one atom can identify the other atom's active channel when the nuclei N1 and N2 allocate a channel. In this way, an overlapped channel allocation can be avoided. That is, the nucleus N1 selects the channel 1 since it is aware that the channel 2 is currently occupied by the atom 2. Similarly, the nucleus N2 is aware of the current occupation of the channel 1 by the atom 1 and thereby selects the channel 2. However, as shown in the Fig. 4, because there is no electron directly linked between the atom 1 and the atom 2, actives channels occupied by the atoms cannot be identified. Therefore, the nuclei N1 and N2 may allocate the same channel. In the figure, the two atoms use the channel 1.

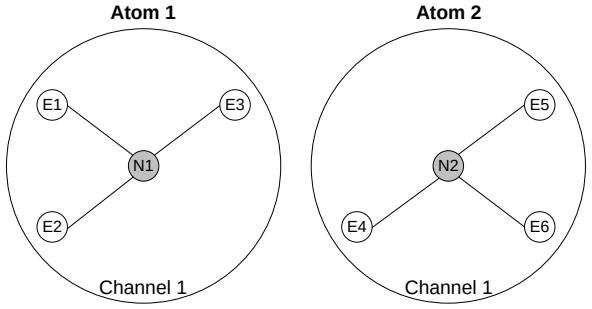

Fig. 4. Channel assignment problem

III. Interference Aware Channel Assignment (IACA) Scheme

In this paper, a new method to resolve such issues involved with the allocation of a channel in the Molecular MAC protocol is proposed. Although the proposed scheme naturally adopts a fundamental operation principle of the Molecular MAC protocol, it modifies a channel allocation method.

Based on the scheme proposed in this paper and with the corresponding interference taken into account, a list of active channels is formed while their activities are measured. Based on this information, a nucleus allocates a channel. In the Molecular MAC protocol, the activity information, expressed in the number of packets transmitted, is applied. However, the proposed scheme utilizes the collision probability information. Although the utilization of a channel is clearly a possible alternative, it is not used since it differs as per an access method (basic or RTS/CTS) or size of data packets. Because a collision probability is independent of an access methods or size of data packets, it is more efficient to apply the probability values. Collision probability is used as a simple and effective estimate of the channel contention level.

When a channel is to be allocated in the Molecular MAC protocol, a nucleus receives a list of active channels from all neighboring electrons and then randomly selects a channel out of those non-active channels. If every channel is currently occupied, a channel with the least activity is selected. However, the proposed scheme uses the active channel list & collision probability information, identifies all non-active channels and then randomly selects a channel from those non-active channels. In addition, if every channel is currently occupied, a channel is chosen based on the collision probability information.

Similar to the Molecular MAC protocol, the proposed scheme first selects a non-active channel using a list of active channels. Then, it uses the collision probability information in order to identify any overlapped channel used by another atom and accordingly allocates a new channel.

In order to measure the collision probability, both a nucleus and an electron manages the number of packets ($Packet_{sent}$) sent and the number of packets ($Packet_{collided}$) collided. The nucleus manages these values for each electron. $Packet_{sent(i,j)}$ and $Packet_{collided(i,j)}$ imply the number of packets sent and collided, respectively, for the node i and the node j. In the variable (i, j), one represents a nucleus and the other denotes an electron. Based on these values, a collision probability ($P_{coll(i,j)}$) can be computed as follows.

$$P_{coll(i,j)} = \frac{Packet_{collided(i,j)}}{Packet_{sent(i,j)}} \quad (1)$$

Note that $P_{coll(i,j)}$ is always in the range of [0, 1] and estimating the value is simple without any additional overheads or costs. If a station does not receive an ACK for the basic method or a CTS for the RTS/CTS method, the station assumes the packet is collided. The station does not count at all any packets from other stations.

Collision probability has to be maintained and updated by each node (nucleus and electrons in an atom). We assume collision probability is updated per each update period (*UpdateTime*) expressed in time. Each node counts the number of packets sent ($sent_n$) and collided ($coll_n$) during the nth update period and then calculates instantaneous collision probability ($P_{coll}^{current}$) using (1). From this value, average

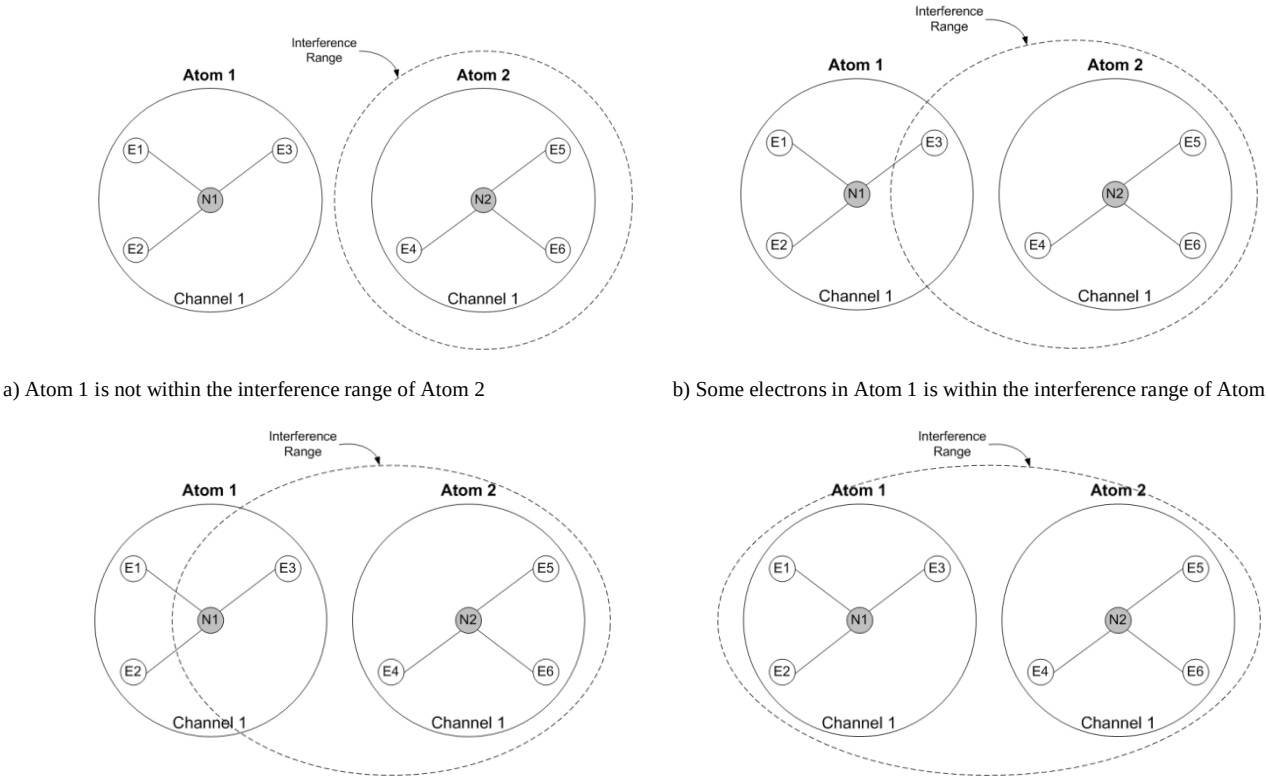

a) Atom 1 is not within the interference range of Atom 2

b) Some electrons in Atom 1 is within the interference range of Atom 2

c) Nucleus and some electrons in Atom 1 is within the interference range of Atom 2

d) Nucleus and all electrons in Atom 1 is within the interference range

Fig. 5. Four cases according to the interference range of atom

collision probability (P_{coll}^{n}) is approximated by exploiting a moving averaging window:

$$P_{coll}^{n} = \alpha \cdot P_{coll}^{n-1} + (1-\alpha) \cdot P_{coll}^{current} \quad (2)$$

where P_{coll}^{n-1} is the average collision probability at the end of the (*n*-1)*th* period and α is a smoothing factor.

An electron calculates a collision probability and periodically transmits it to a nucleus.

As illustrated in the four cases of Fig. 5, the nucleus uses the collision probability and allocates a new channel in order to avoid an overlapped channel allocation.

Firstly, if the atom 1 is not covered by the interference range of the atom 2, the atom 1 is not affected by the atom 2; therefore, the performance of the atom 1 is not deteriorated, and it is okay to continue to utilize the current active channel. That is, there is no need to consider a collision probability.

Secondly, if part of the electrons included in the atom 1 is covered by the interference range of the atom 2, a collision probability measured by the electrons is greater than that measured by the nucleus. Hence, if the two collision probabilities differ by more than a threshold value, it implies that the current active channel is also occupied by other neighboring atoms; therefore, a new channel is allocated. However, if the difference is negligible, the effect of the interference is minimal, therefore making the utilization of the current channel feasible.

Thirdly, if a nucleus and some electrons of the atom 1 are covered by the interference range of the atom 2, a collision probability measured by the nucleus is similar to that measured by the electrons.

Therefore, similar to the second case, a new channel cannot be allocated. However, this issue can be cleared by using an electron of the atom 1 not covered by the interference range of the atom 2 and factoring in a collision probability measured by the electron. A collision probability measured by the non-interfered electron is less than that measured by the nucleus. That is, if there is any difference between the two collision probabilities, it implies that one atom is affected by another atom's interference; therefore, a new channel is allocated.

For the second and the third cases, if the collision probability measured by the nucleus differs from that measured by the electron by more than a threshold value, a new channel is allocated. That is, a new channel can be allocated if the following formula is satisfied. In the variable (*i*, *j*), one represents a nucleus and the other denotes an electron.

$$P_{coll(i,j)} > P_{coll(j,i)} + \beta \quad (3)$$

where, β is a threshold value for changing channel.

Finally, if a nucleus and all electrons of the atom 1 are covered by the interference range of the atom 2, those collision probabilities measured by the nucleus and the electrons is similar; therefore, a new channel cannot be allocated because the (3) cannot be satisfied. Still, the network performance is deteriorated due to the impact by the atom 2. In this case, the nucleus factors in a total collision probability (P_{total_coll}).

$$P_{total\_coll} = \frac{\sum_{j} Packet_{collided(i,j)}}{\sum_{j} Packet_{sent(i,j)}} \quad (4)$$

where, *i* represents a nucleus while *j* denotes an electron.

In order to show the effect of the number of nodes on collision probability, we simulated an IEEE 802.11a network with transmission rates of 54 Mbps for data packets and of 6 Mbps for control packets such as RTS, CTS and ACK, respectively. We assume that each node always has packets to transmit, and all packets are of the same size. This environment is extreme case. In Fig. 4, collision probability for the IEEE 802.11 DCF gets higher as the number of stations becomes larger. This is from the fact that all nodes always try to access the channel and make collisions with one another.

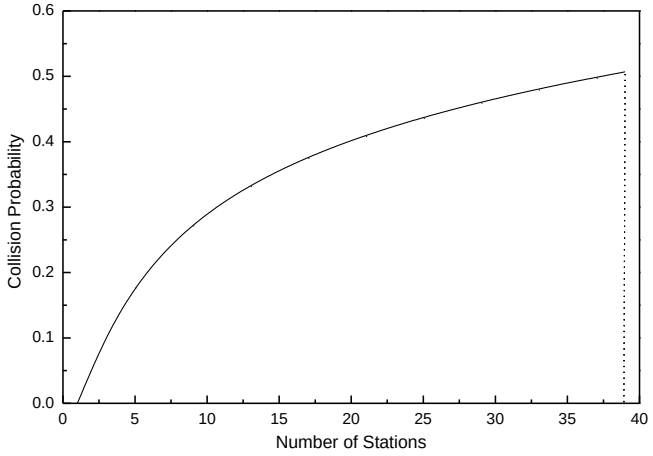

Fig. 6. Collision probability according to the number of nodes

Fig. 6 shows such collision probabilities resulted from the worst-case scenario. That is, any normal environment other than that of Fig. 6 generates better results. Therefore, a specific value based on such results provides an upper bound for a collision probability.

A nucleus determines whether to allocate a new channel using this value. For such determination, the nucleus manages the corresponding collision probabilities on a table-form basis. The nucleus is well aware of the number of electrons included in its own atom. Then, the nucleus compares the total collision probability computed in (4) with the value resulted from Fig. 6 and then determines whether to allocate a new channel. If the total collision probability is greater than that in the collision probability table by more than a threshold value, a new channel is allocated.

$$P_{total\_coll} > P_{coll,n} + \gamma \quad (5)$$

where, $P_{coll,n}$ is the collision probability for n electrons in the table and γ is a threshold value for changing channel.

If there is any non-active channel, a nucleus selects a channel based on the procedures mentioned above. However, if every channel is currently occupied, the nucleus selects a channel with the lowest collision probability.

IV. Simulation Results

In this section, we discuss the simulation results of the proposed IACA scheme. To study the performance of the IACA scheme, we have implemented it. We compare them to the results of the Molecular MAC protocol. We simulated an IEEE 802.11a network with transmission rates of 54 Mbps for data packets and of 6 Mbps for control packets such as RTS, CTS and ACK, respectively. Nodes use a network interface with the transmission range of 10 units and the interference range of 22 units.

The spanning tree construction proceeds as follows. First, the network elects a gateway node, which is connected to the wired Internet. Then, the other nodes construct a spanning tree rooted at the gateway node. We place the gateway node on the top-left corner and randomly the other nodes in a simulation topology.

Main performance metrics of interest are the number of atoms, the number of assigned channels and the number of neighboring atoms. The number of atoms indicates the number of total atoms produced in a spanning tree of the simulation topology. In addition, the number of assigned channels is the number of such channels allocated to nuclei in the simulation topology. That is, it is the minimum number of channels required to serve every node in the simulation topology. The number of neighboring atoms represents the number of those neighboring atoms when an atom's nucleus selects a channel. Because each atom occupies one channel, the number of neighboring atoms means the number of active channels in other neighboring atoms. All simulation results are averaged over ten simulations.

Table I shows the simulation results (number of neighboring atoms, number of assigned channels) when there are 50 nodes. For the Molecular MAC protocol, since each nucleus factors in 3 neighboring atoms on average and accordingly allocates a channel, approximately 4.1 channels are required to serve every node in the simulation topology. However, because the proposed IACA scheme takes 8.1 neighboring atoms into account, roughly 8.7 channels are needed. The Molecular MAC protocol identifies the number of neighboring atoms with help from those electrons in the transmission range of a nucleus and accordingly allocates a channel. However, the proposed scheme expands the scope up to the interference range; therefore, it can identify more neighboring atoms and accordingly allocate a channel. Because the proposed scheme considers 2.7-times more neighboring atoms than the Molecular MAC protocol and accordingly allocate a channel, about 2.1-times more channels can be allocated. Furthermore, in the Molecular MAC protocol, some

neighboring atoms still allocates the same channel, hence deteriorating the performance of a network. On the other hand, the proposed scheme prevents the allocation of the same channel by those neighboring atoms in the interference range and thereby enhances network performance.

TABLE I. SIMULATION RESULTS FOR 50 NODES

	Molecular MAC protocol	IACA scheme
Number of neighboring atoms	3.0	8.1
Number of assigned channels	4.1	8.7

Figs. 7, 8 and 9 show how network performance is changed as the number of nodes increases. In particular, Fig. 7 indicates how the number of those atoms produced in the simulation topology linearly increases in proportion to the number of nodes. If the number of nodes equals to 30, about 27% of total nodes become nuclei. As the number of nodes increase, such percentage declines. For example, if the number of nodes is 70, approximate 18% of total nodes become nuclei. Fig. 8 depicts the number of those neighboring atoms to be considered when each nucleus allocates a channel. In the Molecular MAC protocol, because the information about neighboring atoms is collected from those electrons in the transmission range of a nucleus, the corresponding result value is quite low. On the other hand, the proposed scheme further considers the interference range and accordingly collects the information about neighboring atoms; therefore, the corresponding result value is relatively higher. As the number of nodes increases, the number of neighboring atoms for each nucleus accordingly increases. Fig. 9 shows the number of those channels allocated to serve every node in the simulation topology. This result is similar to that of Fig. 8. As the number of neighboring atoms increases, the number of channels allocated accordingly increases since other channels are allocated to avoid any overlapping. Compared to the Molecular MAC protocol, the IACA scheme requires 1.9-times more and 2.1-times more channels if the number of nodes is 30 and 70, respectively. Based on such results, an identical channel is not allocated to neighboring atoms, therefore enhancing the performance of a network.

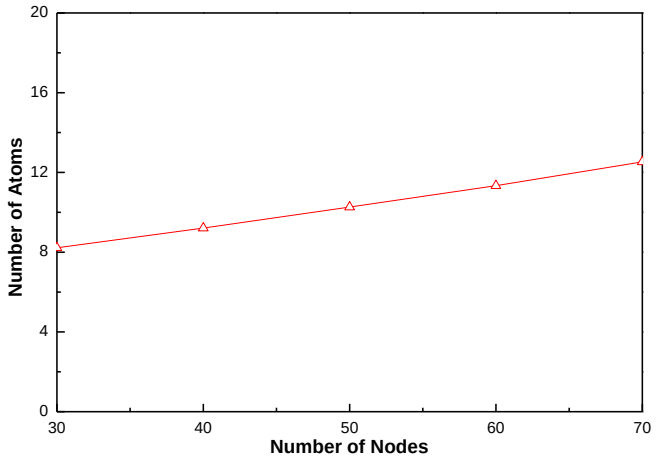

Fig. 7. Number of atoms according to the number of nodes

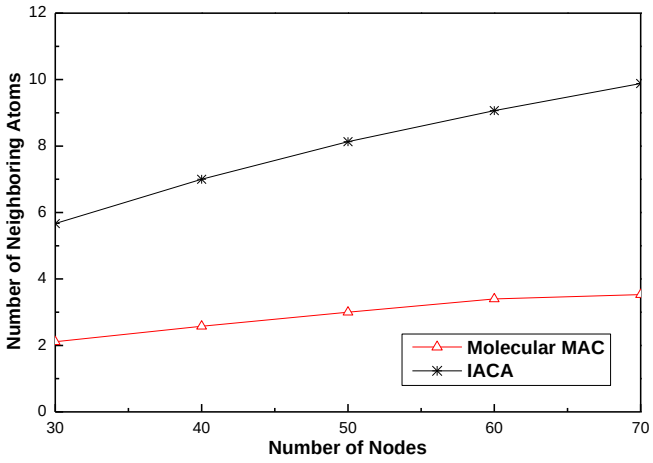

Fig. 8. Number of neighboring atoms according to the number of nodes

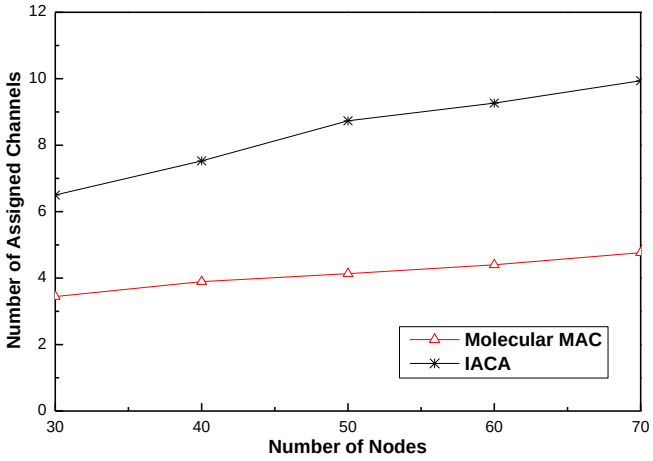

Fig. 9. Number of assigned channels according to the number of nodes

V. CONCLUSION

A wireless mesh network is a promising wireless technology for numerous applications. In mesh networks with a single channel, the functionalities of nodes are performed on the same channel. Therefore, network performance decreases. In order to increase the performance, several MAC protocols have been proposed based on multiple channels. Molecular MAC protocol was proposed by adopting a molecular analogy. In this protocol, a nucleus assigns a channel for its atom with the assistance from electrons in the same atom. It is not able to recognize the existence of those atoms in the interference range. Therefore, allocating the same channel to neighboring atoms results in the deterioration of network performance. In order to resolve this problem, we propose a novel distributed interference aware channel assignment scheme. The proposed scheme is somewhat similar to the Molecular MAC protocol method in that a channel is selected by the assistance of electrons. Then, a collision probability is applied to allocate a new channel in order to recognize any interference and avoid any overlapped channel allocation. Simulation results show that the proposed scheme was verified that different channels could be allocated to those neighboring atoms in the interference range.

REFERENCES

[1] I.F. Akyildiza, X. Wang, and W. Wang, "Wireless mesh networks: a survey," Elsevier Computer Networks, vol. 47, no. 4, pp. 445-487, 2005.

[2] A. Iyer and C. Rosenberg, "Understanding the key performance issues with MAC protocols for multi-hop wireless networks," Wireless Communications and Mobile Computing, vol. 6, no. 6, pp. 745-760, 2006.

[3] H. Zhai, X. Chen, and Y. Fang, "Alleviating intra-flow and inter-flow contentions for reliable service in mobile ad hoc networks," in Proceedings of IEEE MILCOM, vol. 3, pp. 1640-1646, Nov. 2004.

[4] M. Karaliopoulos, T. Spyropoulos, and B. Plattner, "Interference-aware routing in wireless multihop networks," IEEE Transactions on Mobile Computing, vol. 10, no. 5, pp. 716-733, May 2011.

[5] Y. Kim, D. Jung, Y. Kim, S. Choi, and J. Ma, "Efficient interference-aware channel allocation in multi-radio wireless mesh setworks," in Proceedings of International Conference on Advanced Communication Technology (ICACT 2012), pp. 920-925, 2012.

[6] P.B.F. Duarte, Z.M. Fadlullah, A.V. Vasilakos, and N. Kato, "On the partially overlapped channel assignment on wireless mesh network backbone: a game theoretic approach," IEEE Journal on Selected Areas in Communications, vol. 30, no. 1, pp. 119-127, Jan. 2012.

[7] A. Subramanian, H. Gupta, S. R. Das, and J. Cao, "Minimum interference channel assignment in multi-radio wireless mesh networks," IEEE Transactions on Mobile Computing, vol. 7, no. 12, pp. 1459-1473, Dec. 2008.

[8] F. Theoleyre, B. Darties, and A. Duda, "Assignment of roles and channels for a multichannel MAC in wireless mesh networks," in Proceedings of 18th International Conference on Computer Communications and Networks (ICCCN 2009), pp. 1-6, Aug. 2009.

[9] B. Darties, F. Theoleyre, and A. Duda, "A Divide-and-conquer scheme for assigning roles in multi-channel wireless mesh networks," in Proceedings of IEEE 34th Conference on Local Computer Networks (LCN 2009), pp. 277-280, Zurich, Switzerland, Oct. 2009.

[10] D. Abdelali, F. Theoleyre, A. Bachir, and A. Duda, "Neighbor discovery with activity monitoring in multichannel wireless mesh networks," in Proceedings of IEEE Wireless Communications and Networking Conference (WCNC 2010), pp. 1-6, Apr. 2010.

[11] M. Nassiri, F. Theoleyre, M. Heusse, and A. Duda, "Molecular architecture for autonomic wireless mesh networks," In Proceedings of the ACM student workshop - CoNEXT 2007, Dec. 2007.

[12] F. Theoleyre, M. Heusse, and A. Duda, "Molecular MAC for multichannel wireless mesh networks," in Proceedings of IEEE 6th International Conference on Mobile Adhoc and Sensor Systems (MASS 2009), pp. 110-119, Oct. 2009.

[13] S. Pollak, V. Wieser, and A. Tkac, "A channel assignment algorithm for wireless mesh networks with interference minimization," in Proceedings of Wireless and Mobile Networking Conference (WMNC 2012), pp. 17-21, 2012.

[14] K.N. Ramachandran, E.M. Belding, K.C. Almeroth, and M.M. Buddhikot, "Interference-aware channel assignment in multi-radio wireless mesh networks," in Proceedings of IEEE INFOCOM, pp. 1-12, Apr. 2006.

[15] K. Xing, X. Cheng, L. Ma, and Q. Liang, "Superimposed code based channel assignment in multi-radio multi-channel wireless mesh networks," in Proceedings of ACM MobiCom, pp. 15-26, 2007.

[16] H. Skalli, S. Ghosh, S. Das, L. Lenzini, and M. Conti, "Channel assignment strategies for multiradio wireless mesh networks: issues and solutions," IEEE Communications Magazine, vol. 45, no. 11, pp. 86-95, Nov. 2007.

[17] S. Avallone, G. Stasi, and A. Kassler, "A Traffic-aware channel and rate re-assignment algorithm for wireless mesh networks," IEEE Transactions on Mobile Computing, in press, 2013.

Robust Facial Expression Recognition via Sparse Representation and Multiple Gabor filters

Rania Salah El-Sayed
Dept. of Computer science
Faculty of Science,
Al-Azhar University
Cairo. Egypt

Prof.Dr. Ahmed El Kholy
Dept. of Mathematics
Faculty of Science
Al-Azhar University
Cairo. Egypt

Prof.Dr. Mohamed Youssri El-Nahas
Dept. of Systems
Engineering & Computers
Faculty of Engineering
Al-Azhar University, Cairo Egypt.

***Abstract*—Facial expressions recognition plays important role in human communication. It has become one of the most challenging tasks in the pattern recognition field. It has many applications such as: human computer interaction, video surveillance, forensic applications, criminal investigations, and in many other fields. In this paper we propose a method for facial expression recognition (FER). This method provides new insights into two issues in FER: feature extraction and robustness. For feature extraction we are using sparse representation approach after applying multiple Gabor filter and then using support vector machine (SVM) as classifier. We conduct extensive experiments on standard facial expressions database to verify the performance of proposed method. And we compare the result with other approach.**

Keywords—Facial expression recognition (FER); L1-minimization; sparse representation; Gabor filters; support vector machine (SVM).

I. INTRODUCTION

Facial expressions are the changes of facial appearance in response to a person's internal emotional states, intentions, or social communications. And facial expression is one of the most powerful, natural, non-verbal, and immediate means for human beings to communicate their emotions and express their intentions [1]. By recognizing facial expressions from facial images, a number of applications in the field of human computer interaction can be facilitated. We can use facial expressions not only in human computer interaction and data-driven animation but also we can use in video cameras which have recently become an integral part of many consumer devices and can be used for capturing facial images for recognition of people and their emotions.

Last two decades, the developments, as well as the prospects in the field of multimedia signal processing have attracted the attention of many computer vision researchers to concentrate in the problems of the facial expression recognition.

The task of automatically recognizing different facial expressions in human-computer environment is significant and challenging. A variety of systems have been developed to perform facial expression recognition and each system consists of three stages: first, face acquisition; second, facial feature extraction then facial expression classification [16].

Face acquisition is a preprocessing stage to detect face regions in the input images or sequences. One of the most widely used face detector is the real-time face detection algorithm developed by Viola and Jones [14].Once a face is detected in the images, the corresponding face regions are usually normalized.

The automatic facial expression recognition literature can be divided into three approaches: geometric features-based systems, appearance features-based systems and both geometric and appearance feature-based systems [6].

In the geometric features-based systems, the shape and locations of major facial components such as mouth, nose, eyes, and brows, are detected in the images. The approaches used in such system are Active Appearance Model (AAM) [5], manually locating a number of facial points. And recently, Piecewise Bezier Volume Deformation tracker (PBVD) was proposed [6].

In the appearance features-based systems, the appearance changes with changes in facial expressions including skin texture changes, wrinkles, bulges, and furrows, are presented. And in this case image filter can be applied to either the whole-face or specific face regions to extract the facial appearance changes. The existing algorithms are Principal Component Analysis (PCA), Independent Component Analysis (ICA) [20], Linear Discriminant Analysis (LDA) [15], Gabor wavelet analysis, Local Binary Patterns (LBP) [19], Local Phase Quantization (LPQ) [15], The Local Directional Pattern (LDP) [11],Fisher Discriminant Analysis (FDA)[21], Local Feature Analysis (LFA), Circular Local Binary Pattern (CLBP) [8], Speeded Up Robust Features (SURF), and Neural Network Architecture-based 2-D Log Polar Gabor Transform.

In geometric and appearance feature-based methods Yang et al use local Gabor Binary Pattern (LGBP) [14]. Histograms with shape and texture parameters of an Active Appearance Model (AAM)are presented in[9].

The last step of an automatic facial expression recognition system is facial expression classification. A classifier is employed to identify different expressions based on the extracted facial features, such as Nearest Neighbor (NN), K-Nearest Neighbor (KNN)[18],Support Vector Machine (SVM)

[17], and Hidden Markov Model (HMM).Facial expression recognition system can be presented as figure1.

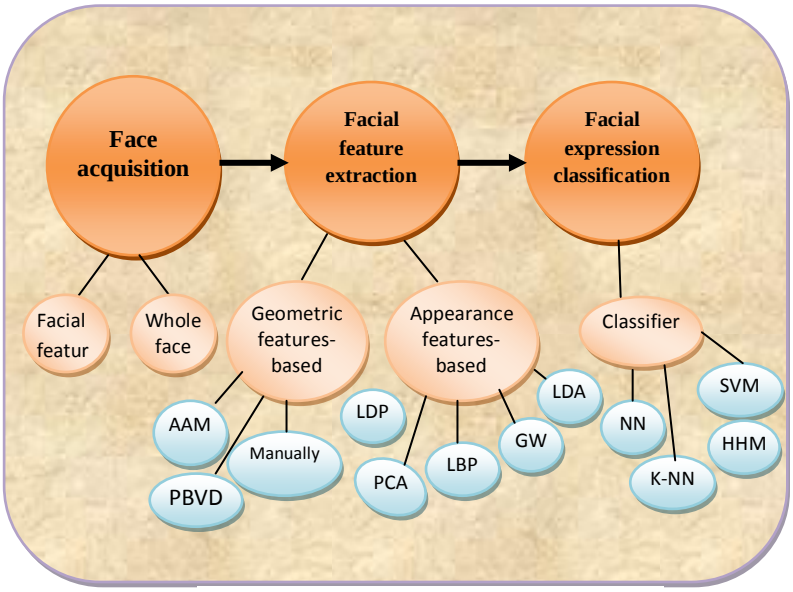

Fig.1. facial expression recognition with associate methods

Sparse representation, also known as compressed sensing [2], has been applied recently to image based facial expression recognition. With sparse representation we can represent each expression by a set of features, which sufficiently characterize each individual expression. With the prior knowledge that expressions of the same individual are similar to each other, a test expression can be considered as being well approximated by linearly combining the number of expressions that have same individual in the training set.

With all the promising advantages, the use of sparse representation for facial expression recognition does not exterminate obstacles posed by several practical issues such as lighting, pose, and robustness to facial expression .In this research we propose a framework which can achieve robustness to facial expressions variations, by using sparse representation of multiple Gabor wavelet filters and SVM as classifier.

This paper is organized as follows. Section 1 is this introduction. Section 2 discusses relevant related works from the literature. Then we introduce Gabor filter's principle, property, and the feature characterization in details in Section 3.In section 4, discussion of sparse representation for facial expression matching is provided. In section 5, details of proposed algorithm are presented. Section 6, provides the details of the conducted experiments along with results .The paper concludes with a brief summary of results and proposal of future research directions in section 7.

II. Related Work

Most facial expression recognition systems use the six principle emotions of Ekman [10]. Ekman considers six basic emotions: happiness, surprise, fear, anger, disgust, sadness; and categorizes facial expressions with these six basic emotions.

A variety of systems have been developed to perform facial expression recognition. Some systems concentrate in two stages: feature extraction and expression classification. Luiz S. Oliveira, Alessandro L. Koerich, and Marcelo Mansano [8] applied feature selection method on the feature matrix extracted by the 2DPCA method, then using KNN and SVM as classifier.

Little wort et al. [22] select the best set of Gabor filters using Gentle Boost and train support vector machines (SVMs) to classify Action Unit (AU) activation.

Tingfan Wu et al. [4], facial expression recognition systems are modeled asa serial pipeline. The first layer detects and normalizes (registers) face images. Second layer applies Gabor energy filters (GEFs) and local Binary Patterns (LBPs) respectively. The final layer consists of a SVM classifier.

Hansung Lee et al. [11], introduce expression recognition systems consist of firstly; Gabor-LBP histogram for face image representation. Secondly, Sparse Representation Classification (SRC) for the face image retrieval.

Praseeda lekshmi.V et al.[12], present a method to analyze facial expression from images by applying Gabor wavelet filter banks on face images. Then theyuse the support vector machine(SVM) for classification.

Zhen Wang et al. [8], expression systems consist of firstly using Gabor filters with different angles, then 2DPCA was used to extract face features and finally Nearest Neighbor (NN) classifier.

In this paper we introduce new hybrid system based on sparse representation, Gabor wavelet filter for feature extraction and support vector machine as classifier. Experimental results show how these techniques reduce error rate of facial expression recognition.

III. Gabor Filters

In recent years, Gabor filters have been successfully used in many applications, because they possess the optimal localization properties in both spatial and frequency domain. And it is obtained by modulating a sinusoid with a Gaussian[12].

The Gabor wavelet representation of images allows description of spatial frequency structure in the image while preserving information about spatial relations.

Let r(x,y) be the original image f(x,y) convolved with a 2D Gabor function g(x,y)[14]

r(x,y) = f(x,y) * g (x,y)

Where * denotes the convolution operator and with g(x,y) being a 2D Gabor filter defined as [16]

$$\boldsymbol{g_{\lambda,\theta,\varphi,\sigma,\gamma}(x,y) = \exp\left(-\frac{x'^2+\gamma^2 y'^2}{2\sigma^2}\right)\cos\left(2\pi\frac{x'}{\lambda}+\varphi\right)} \quad (1)$$

$$x' = x\cos\theta + y\sin\theta$$

$$y' = -x \sin\theta + y \cos\theta$$

The parameters used in Eq.(1)are defined as follows. Wavelength (λ); this is the wavelength of the cosine factor of the Gabor filter kernel, Orientation(s) (θ); it specifies the orientation of the normal to the parallel stripes of a Gabor function. Its value is specified in degrees. Valid values are real numbers between 0 and 360.The Phase offset(s) (φ) in the argument of the cosine factor of the Gabor function is specified in degrees. Valid values are real numbers between -180 and 180.The Aspect ratio (γ) called more precisely the spatial aspect ratio, specifies the ellipticity of the support of the Gabor function, and we can calculate wavelength of Gabor filter using Bandwidth (b) in eq. 2.

$$\frac{\sigma}{\lambda} = \frac{1}{\pi}\sqrt{\frac{ln2}{2}}\cdot\frac{2^b+1}{2^b-1} \quad , \quad b = log_2 \frac{\frac{\sigma}{\lambda}\pi + \sqrt{\frac{ln2}{2}}}{\frac{\sigma}{\lambda}\pi - \sqrt{\frac{ln2}{2}}} \qquad (2)$$

Figure 1, show Gabor filter kernels with values of the orientation parameter of 0, 45 and 90degrees, from left to right, respectively. The values of the other parameters are as follows: wavelength 10, phase offset 0, aspect ratio 0.5, and bandwidth 1.

Fig.2. Gabor filter with three orientations in the spatial and frequency domain

IV. Sparse Representation

Sparse representation aims at describing a high-dimensional signal as a linear combination of a few generating elements.. Specifically, a feature vector in a given class of dimension M should be represented by a small subset of a collection of all elements N. when M=N, the elements are independent, the collection is termed a basis and the representation is unique [13].

Let the training samples be denoted as $A = [A_1\ A_2\ ...\ A_r]$, where each column A_i denotes a facial image and r the total number of training samples.

For a test sample $\mathbf{y} \in R$, it can be approximated by linear combination of selected training samples. The test sample can be expressed as [3]

$$\mathbf{y} = x_1A_1 + x_2A_2 + \ldots + x_rA_r = A\mathbf{x} \qquad (3)$$

Where $\mathbf{x} = [x_1, x_2, \ldots, x_r]$ is coefficient vector whose entries are zero except some important training samples. The problem of sparse representation is to find the sparse solution **x**. This sparse solution **x** explains how to combine all training samples to obtain a global representation of test sample. This is an L1 optimization problem formally defined as

$$\mathbf{x}_1 = \min \|\mathbf{x}\|_1 \text{ subject to } \mathbf{y} = A\mathbf{x} \qquad (4)$$

V. Sparse Representation Classifier

Sparse representation classifier (SRC) chooses the training samples which can best represent each test sample. For i th class, let δ_i be the function that selects the sparse coefficients associated with the i the class. In $\delta_i(x)$, only the elements that are associated with ith class are nonzero [11]. That is

$\mathbf{x} = [0,\ldots, 0, \ldots, x_{i,1}, \ldots, x_{i,ni}, \ldots, 0, \ldots, 0]^T$. The test sample **y** can be approximated by training samples from each class as $\hat{\mathbf{y}}_i = A\,\delta_i(\hat{\boldsymbol{x}})$. Define the residual between test sample y and approximation $\hat{\mathbf{y}}_i$ from each class sample as $r_i = \|y - \hat{y}\|_2$. The test facial expression are assigned to the class that minimizes the residual between **y** and $\hat{y}$

$$\text{identity}(\mathbf{y}) = \arg\min r_i(\mathbf{y}) \qquad (5)$$

$r_i(y)$ represent the classification result of the i th component of test sample. The final result is determined by voting methods. Let the output of the SRC classifier be defined as [7]

$r = [r_1, r_2, \ldots, r_r]$, $r_i \in \{c_1, c_2, \ldots, c_r\}$

Then we define the binary classification function as

$$f(c_r) = \begin{cases} 1 & if\ r = c \\ 0 & if\ r \neq c \end{cases} \qquad (6)$$

The test sample is assigned to the class label which is most observed at the classifier outputs.

For reference we include the algorithm1 given in [23] as follows:

A. Algorithm 1

- **Input:** n training samples divided into r classes, A_1, A_2,...,A_r and a test image y.
- Set $A = [A_1A_2 \ldots A_r]$.
- Normalize columns of matrix A
- Solve the L1 minimization problem : min $\|x\|_1$ subject to $y = Ax$
- **For** each subject i , Compute the residuals: $r_i = \|\mathbf{y} - A\mathbf{x}_i\|_2$ where $\boldsymbol{x}_i$ is obtained by setting the coefficients in $\boldsymbol{x}$, corresponding to training samples not in class *i*, to zero.
- **End**
- **Output**: the class with the smallest residual identity(**y**) = arg min r_i(**y**).

The system architecture for facial expression recognition using sparse representation is presented as shown in Figure 2

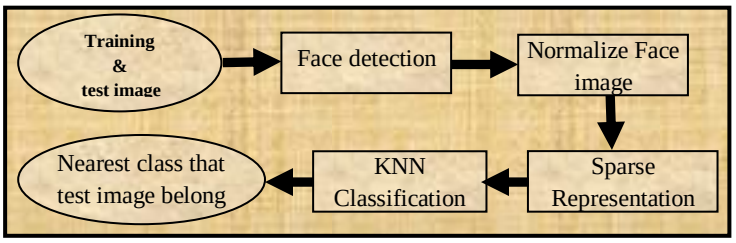

Fig.3. diagram of sparse representation approach

VI. PROPOSED FRAMEWORK

In this paper we propose a new and robust framework for facial expressions recognition. Robustness to variations in illumination conditions and pose variations is achieved by using both Multiple Gabor filters and sparse representation. Then using a SVM for classification should increase system robustness due to generalization property of SVM. The system architecture is shown in Figure3. Face detection is implemented by Viola-Jones method. We focus in this paper on the procedures for feature extraction, sparse representation and SVM classification.

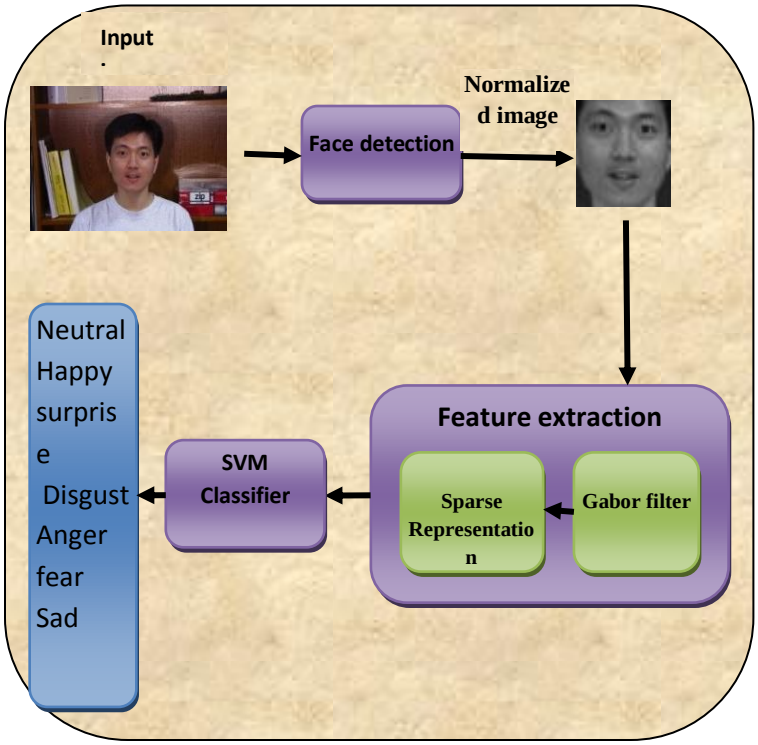

Fig.4. System architecture for proposed facial expressions recognition

A. The Proposed Procedure

- **Input**: *n* training samples partitioned into *r* classes, $S_1, S_2,...,S_r$ and a test sample *z*.
- **For** each subject i ,
  Apply Gabor filter for N times; and
  generate A_i
- **End**
- Apply Gabor filter on test sample *z* for N times; and generate **y**.
  - Set matrix A based on Gabor filter of images
    $\boldsymbol{A} = [A_1 A_2 \ldots A_r]$.
- Normalize columns of matrix A
- Solve the L1 minimization problem
  $\min \|\boldsymbol{x}\|_1$ subject to $\mathbf{y} = A\boldsymbol{x}$
- **Compute** yEstimated = $A\boldsymbol{x}_i$,
  where $\boldsymbol{x}_i$ is obtained by setting the coefficients in $\boldsymbol{x}$, corresponding to training samples not in class *i*, to zero
- **Classify** yEstimated with **SVM** classifier
- **Output:** class to which yEstimated belongs.

Figure 4schematize show SVM classifies the facial expressions.

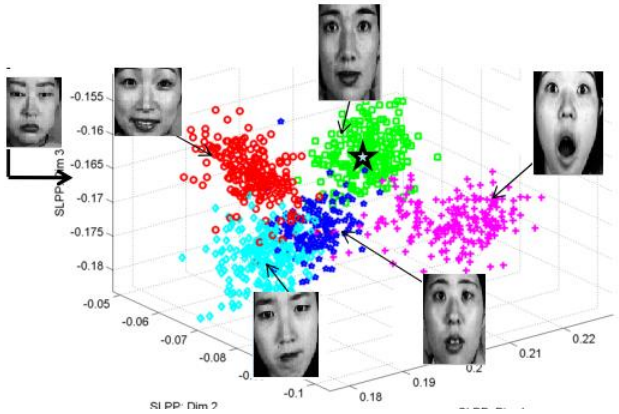

Fig.5. Concept of SVM classifier for facial expressions.

VII. EXPERIMENTS

In this section, we quantitatively verify the performance of different facial expression recognition systems. Such as algorithm 1 with SVM classifier, proposed algorithm, proposed algorithm with K-NN classifier, and Gabor filter with SVM classifier. Using public facial expression databases namely, JAFFE Database which contains 213 images of female facial expressions. Each image has a resolution of 256×256 pixels. The number of images corresponding to each of the seven categories of expressions (anger, joy, sadness, neutral, surprise, disgust and fear) is the same. Figure 5 shows example of facial expression images from JAFFE Database [2].

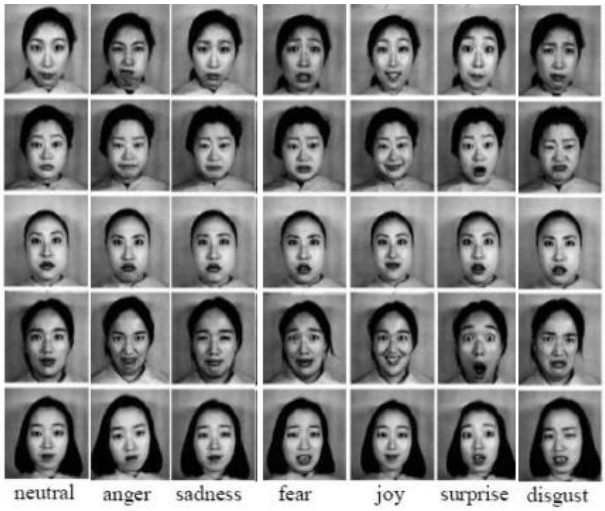

Fig.6. example facial expression images from JAFFE database

In this experimental work, we evaluate five approaches for facial expression recognition and compare the recognition rate of the previously published work with recognition rate of the

proposed approach. First approach [1] used sparse representation to extract features and support vector machine (SVM) for classification, the second applies multiple Gabor filter and uses NN as classifier [25][26], the third approach as done in [2] uses sparse representation classifier after application of Gabor filter. Fourth approach is similar to third one but this time SVM is used as classifier [24], the last is our proposed approach which uses multiple Gabor filters and sparse representation to extract features and then apply SVM as classifier.

The recognition rate for facial expressions for the five approaches is summarized as show in Table 1.

TABLE I. CONFUSION MATRIX FOR 7-CLASSES OF FACIAL EXPRESSIONS

methods	happy	sadness	fear	disgust	surprise	anger	natural	average
SR+SVM	75%	80%	75%	90%	95%	90%	95%	85.71%
Gabor filter NN [26][25]	85%	75%	75%	90%	95%	90%	95%	86.42%
Gabor filter SRC[2]	85%	85%	75%	90%	95%	90%	95%	87.85%
Gabor filter SVM[24]	90%	75%	75%	90%	85%	90%	90%	85%
Proposed (Multiple Gabor filter SR+SVM)	90%	80%	80%	95%	100%	90%	90%	89.28%

TABLE II.
CONFUSION MATRIX WITH PROPOSED ALGORITHM ON THE JAFFE DATABASE

Expression	Anger %	Disgust%	Joy %	Fear%	Sad %	Surprise%	Neutral%
Anger	90	0	0	5	5	0	0
Disgust	0	95	0	5	0	0	0
oy	2	0	90	2	0	1	5
Fear	0	12.5	0	80	7.5	0	0
Sad	0	0	5	5	80	0	10
Surprise	0	0	0	0	0	100	0
Neutral	0	0	0	0	5	5	90

Table 1, shows that the proposed approach achieves the highest performance in facial expression recognition (89.28%) because we used the properties of Gabor filter and sparse representation in the stage of extract feature and then using the properties of support vector machine (SVM) in classification. Compared with the previously reported work [1,2,24,25,26] in which the experimental settings are similar to ours, In [24], on 7-class facial expression recognition tasks they used Gabor filter to extract features, SVM for classification and reported an accuracy of (85%). Additionally, they also make the same test [25] but using NN classifier and reported an accuracy of (86.42%).

In [2], they used Gabor filter to extract features and sparse representation classification and reported an accuracy of (87.85%).

Table 2, shows the confusion matrix of 7-class expressions when using multiple Gabor multiple filters and sparse representation for feature extraction and SVM as classifier. From Table 2, it can be seen that 5-class facial expressions are identified very well with an accuracy of over 90%.

VIII. CONCLUSION

We have presented a hybrid framework for facial expressions recognition based on sparse representation and multiple Gabor filter. Designing a good filter and classifier is a crucial step for any successful facial expression recognition system. An average recognition rate of (89.28%) is achieved under facial expressions variations. This means that our approach achieves a high recognition rate compared to other approaches in published literature. Using multiple Gabor filters rendered the method robust to facial expression variations because each filter has specific property to extract. In addition using generalization property of SVM classifier increased the recognition rate in presence of facial class variations.

We believe that facial expressions recognition under varying conditions is still an interesting area of research, and we anticipate that there will be many further advances in this area.

REFERENCES

[1] Xia H. “Robust Facial Expression Recognition via Sparse Representation Over Overcomplete Dictionaries”. *Journal Of Computational Information Systems*. 2012;1(January):425-433.
[2] Zhang S, Zhao X, Lei B. “Facial Expression Recognition Using Sparse Representation”. *Wseas Transactions On Systems*. 2012;11(8):440-452.
[3] Zhang S, Zhao X, Lei B. “Robust Facial Expression Recognition via Compressive Sensing”. *Sensors (Peterborough, NH)*. 2012:3747-3761.
[4] Wu T, Butko NJ, Ruvolo P, et al. Multilayer Architectures for Facial Action Unit Recognition. 2012;42(4):1027-1038.
[5] Senechal T, Rapp V, Salam H, et al. “Facial Action Recognition Combining Heterogeneous Features via Multikernel Learning”. IEEE. 2012;42(4):993-1005.
[6] Valstar MF, Mehu M, Jiang B, Pantic M, Scherer K. “Meta-Analysis of the First Facial Expression Recognition Challenge”. *IEEE*. 2012;42(4):966-979.
[7] Zhi R, Ruan Q. “Facial expression recognition with facial parts based sparse representation classifier”. *Pattern Recognition*. 2009;7496:1-7.
[8] Yang J, Oliveira LS, Koerich AL, Mansano M. “2D Principal Component Analysis for Face and Facial-Expression Recognition”. *Technology*. 2011:9-13.
[9] Valstar MF, Mehu M, Jiang B, Pantic M, Scherer K. “Meta-Analysis of the First Facial Expression Recognition Challenge”. *Emotion*. 2012;42(4):966-979.
[10] [Donato, G.; Bartlett, M.; Hager, J.; Ekman, P.; Sejnowski, T. “Classifying facial actions”. IEEE Trans. Pattern Anal. Mach. Intell. 1999, 21, 974–989.
[11] Lee H, Chung Y, Kim J, Park D. “Face Image Retrieval Using Sparse Representation Classifier with Gabor-LBP Histogram “. 2011:273-280.
[12] Paper P. “Analysis of Facial Expression using Gabor and SVM”. *International Journal*. 2009;1(2).

[13] Shin Y-suk. “Facial Expression Recognition Based on Dimension Model of Emotion with Autonomously Extracted Sparse Representations”. *Emotion*.2004; (Dlm):81-87.

[14] Yang M, Zhang L. “Gabor Feature based Sparse Representation for Face Recognition with Gabor OcclusionDictionary”. Springer-Verlag Berlin Heidelberg 2010:pp. 448–461.

[15] Zhao X, Zhang S. “Facial expression recognition using local binary patterns and discriminant kernel locally linear embedding”. *EURASIP Journal on Advances in Signal Processing*. 2012(1):20.

[16] Bashyal S, Ã GKV. “Recognition of facial expressions using Gabor wavelets and learning vector quantization”. Engineering Applications of Artificial Intelligence. 2008.

[17] I Kotsia, and I Pitas, “Facial expression recognition in image sequences using geometric deformation features and support vector machines”, IEEE Transactions on Image Processing, Vol. 16, No. 1, 2007, pp. 172-187.

[18] Yousefi, S.; Nguyen, M.P.; Kehtarnavaz, N.; Cao, Y. Facial expression recognition based on diffeomorphic matching. In Proceedings of 17th IEEE International Conference on Image Processing (ICIP), Hong Kong, China, 26–29 September 2010; pp. 4549–4552.

[19] S. Moore and R. Bowden, “Local binary patterns for multi-view facial expression recognition,” Compute. Vis. Image Understand., vol. 115, no. 4, pp. 541–558, Apr. 2011.

[20] M. S. Bartlett, J. R. Moverllan, T. J. Sejnowski, "Face recognition by independent component analysis," IEEE Transactions on Neural Network, 13 (6), 1450--1464 (2002).

[21] Simona E. Grigorescu, Nicolai Petkov, and Peter Kruizing, “Comparison of Texture Features Based on Gabor Filters”. IEEE, VOL. 11, NO. 10, october2002

[22] G. Littlewort, J. Whitehill, T. Wu, I. Fasel, M. Frank, J. Movellan, and M. Bartlett, “The computer expression recognition toolbox (cert),” in Proc. IEEE Int. Conf. Autom. Face Gesture Recog., 2011, pp. 298–305.

[23] Wright J, Member S, Yang AY, et al. Robust Face Recognition via Sparse Representation. IEEE. 2009;31(2):210-227

[24] R. Ramanathan, K.P. Soman, Arun. S. Nair, V. VidhyaSagar, and N. Sriram. A support vector machines approach for efficient facial expression recognition. Advances in Recent Technologies in Communication and Computing, International Conference on, 0:850{854, 2009.

[25]] Jia-Jun Wong and Siu-Yeung Cho. “ Facial emotion recognition by adaptive processing of tree structures “. In SAC '06: Proceedings of the 2006 ACM symposium on Appliedcomputing, pages 23{30, New York, NY, USA, 2006. ACM.8

[26] curryguinn, thomasjanicki,” active appearance models for affect recognition using facial expressions”.2010

New Technique for Suppression Four-Wave Mixing Effects in SAC-OCDMA Networks

Ibrahim Fadhil Radhi, S. A. Aljunid, Hilal A. Fadhil, and Thanaa Hussein Abd
School of Computer and Communication Engineering, University Malaysia Perlis (UniMAP)
Perlis, MALAYSIA

***Abstract*—A new technique invented for suppressing the FWM in SAC-OCDMA systems based on adding idle code at the sideband of the code construction to generate the virtual FWM power at the sideband of the signal, and then by subtracting these virtual FWM power from the original FWM power in the system and filtering the data part at the channel. This technique is applied for both SAC codes, Random Diagonal Code (RD) and Multi Diagonal Code (MD). Moreover, in terms of cost, the reported technique is considered a cost-effective as the LED light source is used to generate the sideband codes. The results showed that the FWM reduced approximately 25 dBm after using the technique. For example, in the RD code the FWM power at 40km fiber length and input power is 15 dBm using the SMF fiber type is approximately -55 dBm before using the technique, after using the technique at the same values of parameters the FWM power is approximately -90dBm. In other words, at the MD code the FWM power before using the technique is approximately -61 dBm, the same parameters values, however after using our technique the value of the FWM power is approximately -81dBm. However, These results gave impact on the Bit Error Rate (BER) also, for example the value of BER in the RD code at the input power -10dBm and 35km fiber length before using the technique is 1.6×10-23 and after using the technique the value of BER will become 4.05×10-28. In addition at the MD code the BER value before using the technique is 9.4×10-22 and after using the technique the value of BER is 7.4×10-31.**

Keywords*—Optical code division multiple access (OCDMA); Spectral amplitude coding (SAC); Multi diagonal (MD); Random Diagonal (RD); Four-Wave Mixing (FWM); Light Emitting Diode (LED).)

I. INTRODUCTION

OCDMA is a technique in which user uses a specific unique code rather a specific wavelength or a time slot. The OCDMA uses the spread spectrum technique of CDMA combined with the optical link for transmission of data [1]. The OCDMA provides the large communication bandwidth along with the capability of secure data transmission. The key advantage of OCDMA is the multiple access technique which allows many users to share the same optical link simultaneously.

This is done by giving each user a specific code which can be decoded only by the required user. OCDMA has many unique features that make it favorable data transmissions. Its characteristics make it suitable to increase the capacity and number of users in bursty networks [2]. The OCDMA can accommodate a large no. of channels on a single carrier frequency. It can utilize the bandwidth effectively through coding system. The OCDMA systems provide high degree of scalability and security. It provides high noise tolerance [3].Fiber nonlinearities represent the fundamental limiting on the amount of data that can be transmitted on optical fiber. Nonlinearities of optical fiber can be divided into two categories. The first category encompasses the nonlinear inelastic scattering processes. These are Stimulated Brillouim Scattering (SBS) and Stimulated Raman Scattering (SRS) [4]. The second category of nonlinear effects arises from intensity-dependent variations in the refractive index in optical fiber. This produces effects such as Self- Phase Modulation (SPM), Cross Phase Modulation (XPM) and Four Wave Mixing (FWM) [5].When a high-power optical signal is launched into a fiber, the linearity of the optical response is lost. One such nonlinear effect, which is due to the third-order electric susceptibility, is called the optical nonlinear effect.

The FWM occurs when light of two or more different wavelengths is launched into a fiber. Generally speaking FWM occurs when light of three different wavelengths is launched into a fiber, giving rise to a new wave (known as an idler), the wavelength of which does not coincide with any of the others.FWM is a kind of optical parametric oscillation [6].In other words, the FWM has been widely studied with various kinds of optical fibers. In particular, FWM has been investigated as a technique of realizing wavelength tunable light sources, and as a means of measuring fiber properties, such as the third order nonlinearity in a fiber [7]. In this paper, we proposed the new technique to suppress the FWM in SAC-OCDMA systems using the RD and the MD codes. This technique based on adding idle code at the sideband of the code construction to generate the virtual FWM power at the sideband of the signal, and then by subtracting these virtual FWM power from the original FWM power in the system and filtering out the data part at the channel.

II. FOUR WAVE MIXING

The origin of FWM process lies in the nonlinear response of bound electrons of a material to an applied optical field. In fact, the polarization induced in the medium contains not only linear terms but also the nonlinear terms. The magnitude of these terms is governed by the nonlinear susceptibilities of different orders.

The FWM process originates from third order nonlinear susceptibility ($\chi 3$). If three optical fields with carrier frequencies f1, f2 and f3, propagate inside the fiber simultaneously, ($\chi 3$) generates a fourth field with frequency f4, which is related to other frequencies by a relation, f4 = f1 ± f2±

f3. In quantum-mechanical context, FWM occurs when photons from one or more waves are annihilated and new photons are created at different frequencies such that net energy and momentum are conserved during the interaction. The effect of FWM on optical transmission is signal-to-noise degradation and cross-talk. As the signal input power of f1, f2, and f3 increases, or as the channel spacing decreases, the FWM mixing output increases [8, 9]. Figure (1), (2), and (3), explain the FWM power in different, input power, channel spacing, and fiber length respectively.

These results show that when power per channel is increased the spurious power increase, too. The power of the FWM produced is found to be inversely proportional to the square of the channel spacing, when all channels have the same input power. Furthermore, the FWM effects increase exponentially as the level of the optical power from the signal sources is increased, as shown in the figure (1). Based on results presented, it is clear that when the channel spacing is smaller, then the FWM effect becomes more significant due to the phase matching, as shown in Figure (2). In addition, the if the fiber length increases the FWM power decrease as shown in the figure (3). The equations below explain the FWM power works [10]:

$$\Delta k = \left(\frac{2\pi\lambda^2}{c}\right) \times \Delta f^2 \left[Dc + \frac{\lambda^2}{2c} \times 2\Delta f \times SD\right] \quad (1)$$

Phase mismatches equation

Where SD → Slope Dispersion

Dc → Chromatic Dispersion

Δf → Channel Spacing

λ → Wavelength

$$\eta = \frac{\alpha^2}{\alpha^2 + \Delta k^2}\left\{1 + \frac{4\exp(-\alpha L)\sin^2\left(\frac{\Delta k L}{2}\right)}{[1-\exp(-\alpha L)]^2}\right\} \quad (2)$$

FWM efficiency equation

α → Attenuation

L→ Fiber Length

$$P_{FWM} = \frac{1024\pi^6}{n^4\lambda^2c^2}\left(\frac{d \times x_{1111} \times Leff}{Aeff}\right)^2 P_{in} \times \exp(-\alpha L) \times \eta \quad (3)$$

n → refractive index

Leff → effective Length

Aeff → effective Area

X_{1111} → third order susceptibility.

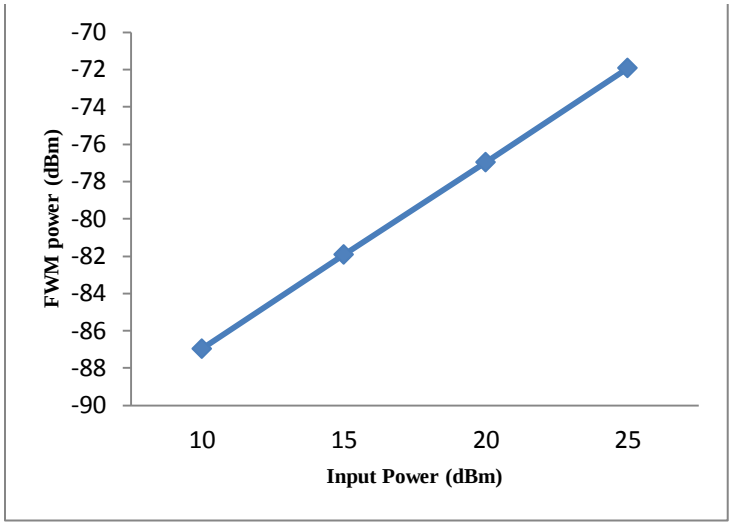

Fig.1. the FWM power versus Input Power

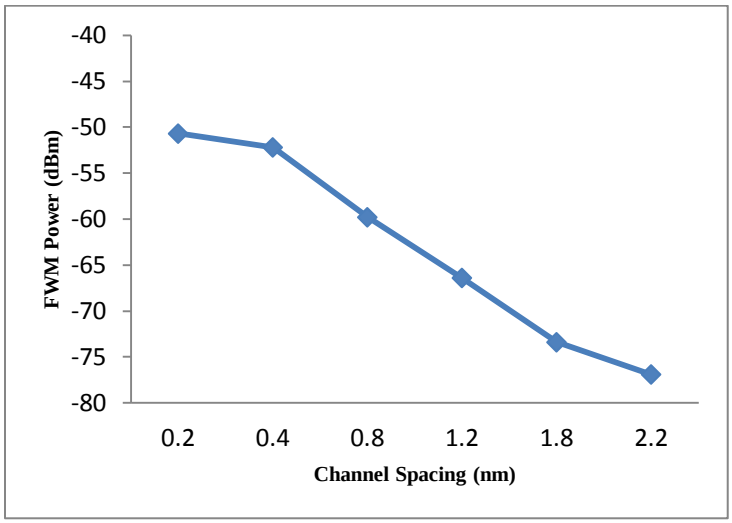

Fig.2. the FWM power versus Channel Spacing

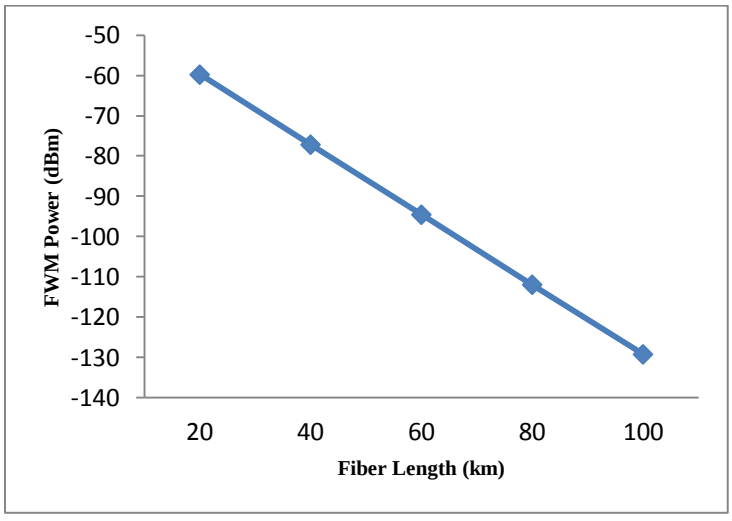

Fig.3. the FWM power versus Fiber Length

III. THE NEW TECHNIQUE FOR SUPPRESSION THE FWM

The FWM occurs when two or more frequencies of light propagate through an optical fiber together. Providing a condition known as phase matching is satisfied, light is generated at new frequencies using optical power from the original signals. Generation of light through four-wave mixing has serious implications for the rapidly expanding telecommunications field [9]. The generation of new frequencies from two or three input signals is shown in figure (4) below.

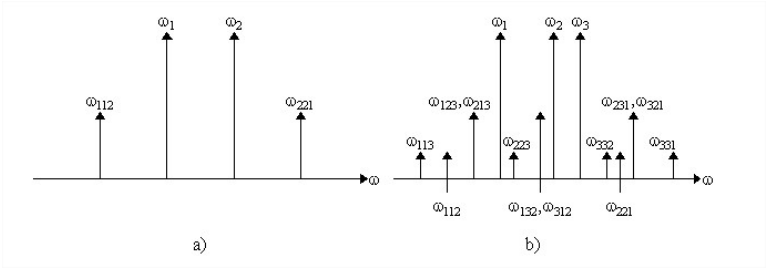

Fig.4. the additional frequencies generated through in the partial degenerated (a) and non degenerated (b), the equation will be *wijk=wi+wj-wk* [11].

Consequently, in the SAC-OCDMA we generate the virtual FWM power at the sideband of the system design using the idle code (it will be explain in the next sections), and then subtracting the virtual FWM from the original FWM power in the system and filtered the data part in the channel using filters. This technique applied for SAC-OCDMA codes, the RD code and the MD code. Moreover, in terms of cost, the reported technique is considered a cost-effective as the LED light source is used to generate the sideband codes.

IV. SAC-OCDMA CODES

A. The RD Codes before and after Using the Technique

The RD code is one of the important codes in the SAC OCDMA system. We will explain in this code according to the properties and the code construction that we used it in our simulation design. We suppress the FWM power in this code approximately 30dBm after using our technique. We denote a code by (N, W, λ), where N is the code length, W is the code weight, and λ is in-phase cross correlation. When $\lambda = 1$, it is considered that the code possess ideal in phase cross correlation. The design of this new code can be performed by dividing the code sequence into two groups, which are code segment and data segment.

- Data segment: let the elements in this group contain only one "1" to keep cross correlation zero at data level ($\lambda = 0$). This property is represented by the matrix ($K \times K$) where K will represent number of users. These matrices have binary coefficientand a basic Zero cross code ($W=1$) is defined as [Y1]. For example, three users ($K=3$), $y(K \times K)$ can be expressed as:

$$[Y1]=\begin{vmatrix} 0\,0\,1 \\ 0\,1\,0 \\ 1\,0\,0 \end{vmatrix}$$

Where [Y1] consists of $(K \times K)$ identity matrices. Notice, for the above expression the cross correlation between any two rows is always zero. code segment: the representation of this matrix can be expressed as follows for $W=4$:

$$[Y2]=\begin{vmatrix} 1\,1\,0 & 1\,0 \\ 0\,1\,1 & 0\,1 \\ 1\,0\,1 & 1\,0 \end{vmatrix}$$

Where [Y2] consists of two parts -weight matrix part and basics matrix part. Basic part [B] can be expressed as:

$$[B]=\begin{vmatrix} 1\,1\,0 \\ 0\,1\,1 \\ 1\,0\,1 \end{vmatrix}$$

And weight part called M matrix can be expressed as:

$$[M]=\begin{vmatrix} 1\,0 \\ 0\,1 \\ 1\,0 \end{vmatrix}$$

Which is responsible for increasing number of weights. Let $i = (W-3)$ and [Mi]:

$$[Mi]=\begin{vmatrix} 1\,0 \\ 0\,1 \\ 1\,0 \end{vmatrix}$$

Where i represent number of Mi matrix on matrix [M], given by:

$$M=< M1 \mid M2 \mid M3 \ldots\ldots Mi > \qquad (4)$$

For example, if W=5, from Equation (4),

i=2, so that M =< M1 | M2 >

$$[M]=\begin{vmatrix} 1\,0\,1\,0 \\ 0\,1\,0\,1 \\ 1\,0\,1\,0 \end{vmatrix}$$

Notice that to increase the number of users simultaneously with the increase of code word length we can just repeat each row on both Matrixes [M] and [B]. For Kth user matrix [M] and [B] can be expressed as:

$$[M](j)=\begin{vmatrix} 0\,1 \\ 1\,0 \\ 0\,1 \\ 1\,0 \\ .\,. \\ a_{j1}\ a_{j2} \end{vmatrix} \qquad [B](j)=\begin{vmatrix} 0\,1\,1 \\ 1\,1\,0 \\ 1\,0\,1 \\ 0\,1\,1 \\ .\,.\,. \\ a_{j1}\ a_{j2}\ a_{j3} \end{vmatrix}$$

Where j represents the value for *Kth* user (*j=1,2…K*), and the value of aj is either zero or one. The weights for code part for both matrix [M], [B] are equal to *W-1*, so the total combination of code is represented as (*K*×*N*) where *K=3*, *N=8*, as given by [Z], [Z] = [Y1|Y2]. Notice that we will use [M] and [B] in other code as the code part to stimulate the FWM power

$$[Z]=\left\{\begin{array}{c|c} 0\,0\,1 & 1\,1\,0\,1\,0 \\ 0\,1\,0 & 0\,1\,1\,0\,1 \\ 1\,0\,0 & 1\,0\,1\,1\,0 \end{array}\right\}$$

From the above basic matrix *Z*, determine the number of users (*K*) and the code length (*N*), as given by (*K*×*N*) matrix. Notice that the code weight of each row is equal to 4, and the relation between N and K for this case (*W=4*) can be expressed as:

$$N=K+5 \qquad (5)$$

As a result we can find that for W=5, 6, and 7 code, word length N can be expressed as K+7, K+9 and K+11 respectively. As a result the general equation describing number of users K, code length N and code weight W is given as [12]:

$$N=K+2W-3 \qquad (6)$$

And finally, after using the technique there is no change at this equations comparing with other codes (as will see in the MD code because the RD code is already using the code part as his construction. However, The RD code construction will change after using the technique as shown below:

[RDx]=[M] | [Y1] | [B]

$$[RDx]=\left\{\begin{array}{c|c|c} 1\,0\,0 & 0\,1 & 0\,1\,1 \\ 0\,1\,0 & 1\,0 & 1\,1\,0 \\ 1\,0\,1 & 0\,0 & 1\,0\,1 \end{array}\right\}$$

B. The MD Code before and after Using the Technique

This section will be divided into two parts. Firstly, explaining the code construction of the MD code before using the technique. Secondly, explaining the code construction after using the technique. This code is also following by parameters (N,W, λc) that explained at the RD code in the previous section. This code has zero cross correlation, in linear algebra, the identity matrix or unit matrix of size N is the N-by-N square matrix with ones on the main diagonal and zeros elsewhere. It is denoted by IN, or simply by I if the size is immaterial or can be trivially determined by the context. From the MD matrix design in [13] the rows determine the number of users (*K*). Notice that the association between code weight (*W*), code length (*N*) and number of subscribers (*K*) can be expressed as:

$$N=K\times W \qquad (7)$$

The total MD code sequence where *K=3, W=2, and N=6* will be:

$$MD=\begin{vmatrix} 1\,0\,0\,1\,0\,0 \\ 0\,1\,0\,0\,1\,0 \\ 0\,0\,1\,0\,0\,1 \end{vmatrix}$$

The MD code design depicts that changing matrices element in the same diagonal part will result in a constant property of zero cross correlation, and it is constructed with zero cross correlation properties. The MD code presents more flexibility in choosing the W, K parameters and with a simple design to supply a large number of users [13]. After using the technique, the code construction of the MD will be change as we will explain below:

In this part, the matrix [M] will use at the sidebands. Consequently, the MD code construction after using the MD code will be:

$$[M1]=\begin{vmatrix} 1\,0 \\ 0\,1 \\ 1\,0 \end{vmatrix}$$

[MDx]=[M1] | [MDx] | [M1]

$$[MDx]=\left|\begin{array}{c|c|c} 1\,0 & 1\,0\,0\,1\,0\,0 & 1\,0 \\ 0\,1 & 0\,1\,0\,0\,1\,0 & 0\,1 \\ 1\,0 & 0\,0\,1\,0\,0\,1 & 1\,0 \end{array}\right|$$

From the above basic matrices, the rows determine the number of users (*K*). Notice that the association between code weight (*W*), code length (*N*) and number of subscribers (*K*) can be expressed as:

$$N=K\times W+4 \qquad (8)$$

V. Results And Discussion

A. The FWM effects in the RD Code before and after using the technique

Figure 5 illustrate the FWM effects in the RD code before and after using the technique, the figure shows the FWM power versus the fiber length, the FWM power decreased after using the technique approximately 30 dBm. In addition, both figures (6 a, and b), show the spectrum signal of the system before and after using the technique respectively and the FWM power signal shown at the sideband. It clearly shows that the FWM power suppress after using the technique. For example, at 40 km fiber length the FWM power values before and after using the technique is approximately -55 dBm and -90 dBm respectively.

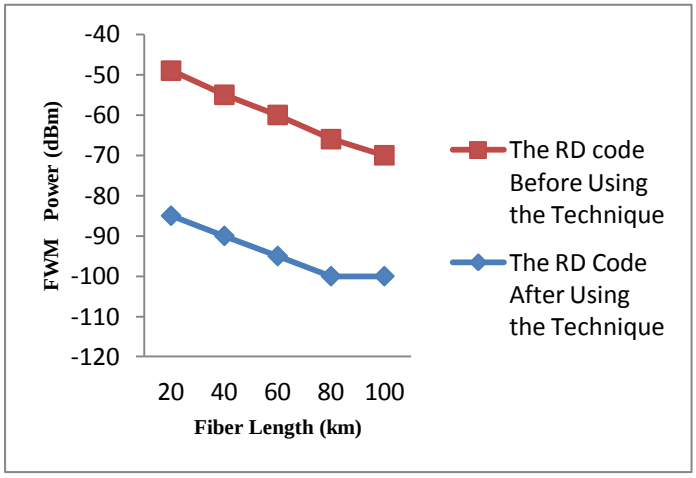

Fig.5. The FWM Power vs Fiber Length

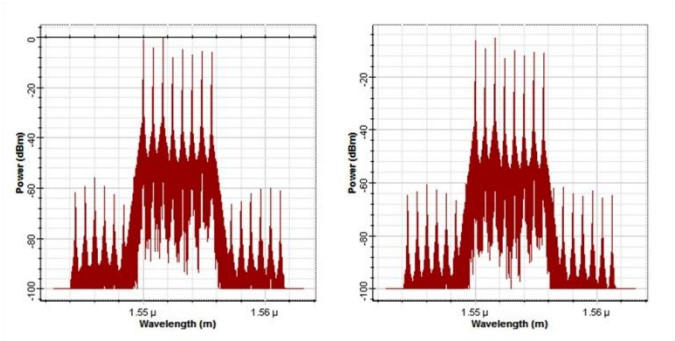

Fig.6. a) Spectrum of the FWM power at 40 km and 60 km respectively before using the technique

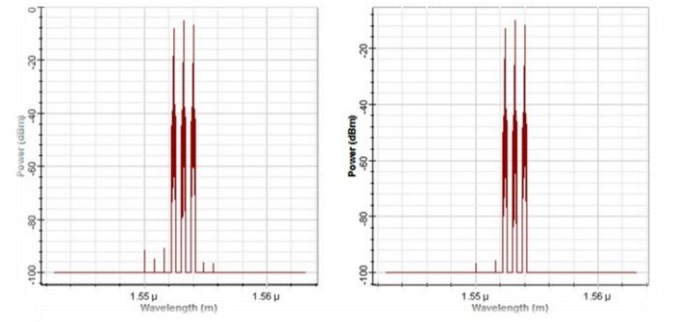

Fig.6. b) Spectrum of the FWM power at 40 km and 60 km respectively after using the technique

B. *The BER performance of the RD code before and after Using the Technique*

Figure (7) shows the BER versus fiber length before and after using the technique, the BER performance get better after using the technique. The data rate value of this system is 622 Mbps at input power -10 dBm.

A longer length of fiber has a higher insertion loss, thus a smaller output power. In fact, when the fiber length decreases, the data rate should increase to recover a similar degradation of the signal form. Thus, in order to design and optimize link parameters, the maximum fiber length should be defined as short as possible, to obtain a high data rate and to achieve a desired system performance. In this system, the technique gives good performance when the fiber length is short as shown in figure (7). The performance of the system was characterized by referring to the BER and eye pattern.

The eye pattern for the RD code system is shown in figures 8 (a, and b), before and after using the technique at 35 km fiber length. The eye diagram gives a quick examination of the quality of the optical signal; it's clearly depicted that after using the technique, the code system gives a better performance, having a large eye opening. The vertical distance between the top of the eye opening and the maximum signal level gives the degree of distortion.

The more the eye closes, the more difficult it is to distinguish between 1s and 0s in the signal. Hence in our results in the data rate 622 Mbps the BER at for the code before and after using the technique will be equal to 4.18×10^{-23}, and 1.6×10^{-13} at 35 km and 40 km fiber length respectively before using the technique, after using the technique the BER values is 3.69×10^{-28}, 4.05×10^{-19} at 35 km and 40 km respectively.

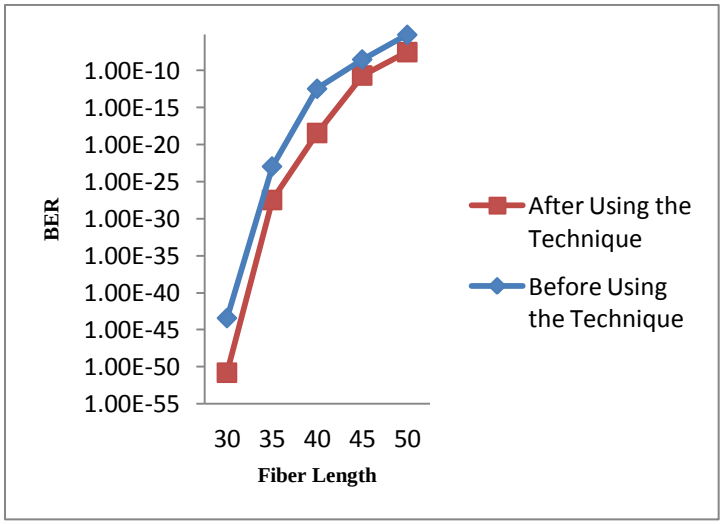

Fig.7. Variation of BER as a Function of fiber length

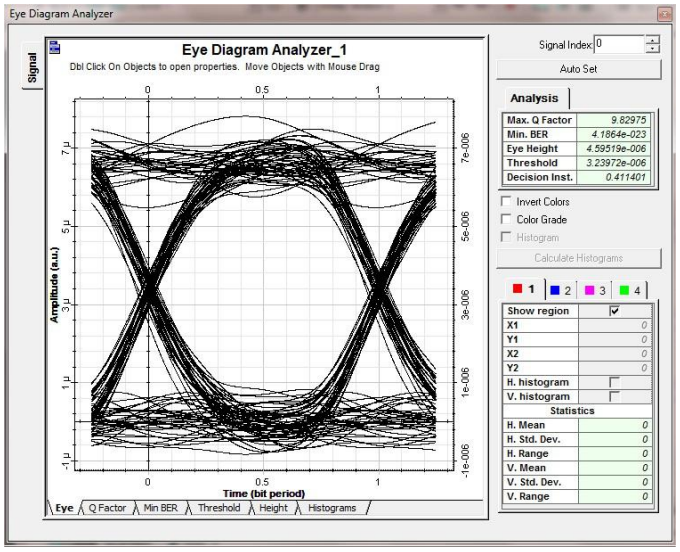

Fig.8. a) Eye diagram of the RD code at 35 km fiber length before using the technique

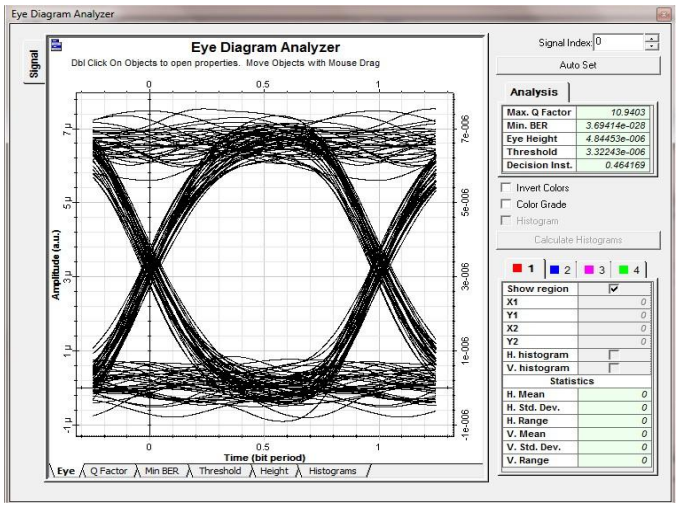

Fig.8. b) Eye diagram of the RD code at 35 km fiber length after using the technique

C. The FWM effects in the RD Code before and after using the technique

In the following process, the fiber length was varied from 20 km to 80 km, it is clear that if the fiber length is lower effect of the FWM becomes very severe. From the results in figures (9), and (10 a, and b), the FWM power suppress after using the technique approximately 20 dBm. For example, at 40 km the FWM power before using the technique is approximately -60 dBm and after using the technique the FWM power value became -80 dBm. Figures 10 a and b show the spectrum of the MD code before and after using technique at 40km and 60km fiber length respectively.

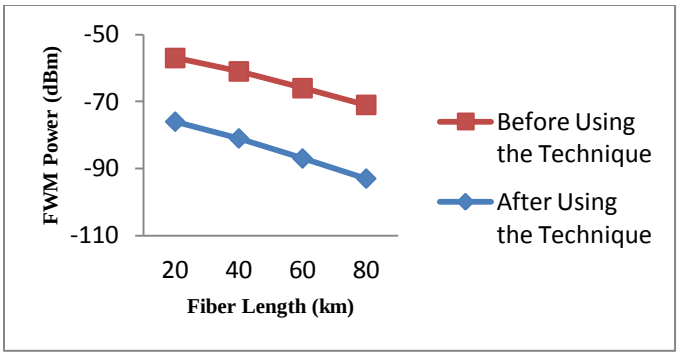

Fig.9. The FWM power vs fiber length

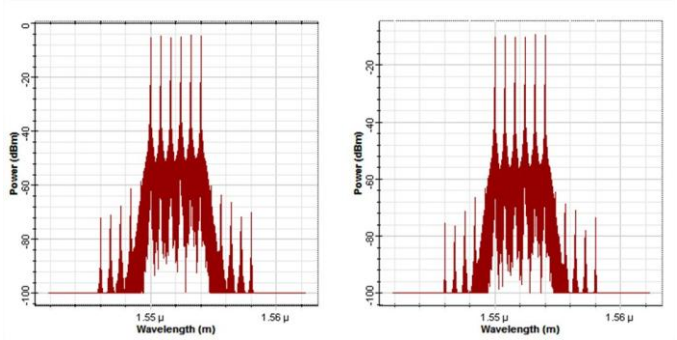

Fig.10. a) Spectrum of the FWM power at 40 km and 60 km respectively before using the technique

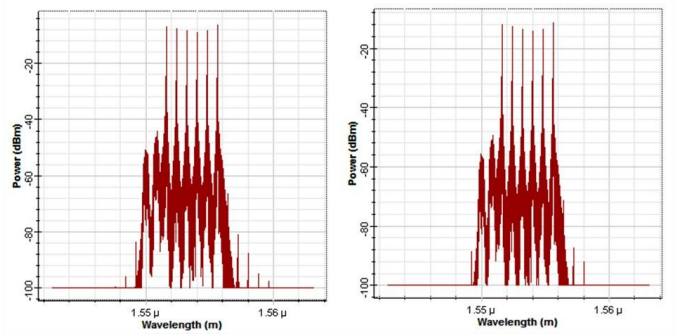

Fig.10. b) Spectrum of the FWM power at 40 km and 60 km respectively after using the technique

A. The BER performance of the MD code before and after Using the Technique

Figure 11 shows the relation between the BER and the fiber length based on the MD code before and after using the technique. It clearly shows that after using the technique the performance of the BER get better comparing with the system before using the technique. For example at 35 km the BER values before and after using the technique is 1.20×10^{-23} and 3.6×10^{-28} respectively. Figures 12 a, and b, illustrate the eye diagram of the MD code before and after using the technique.

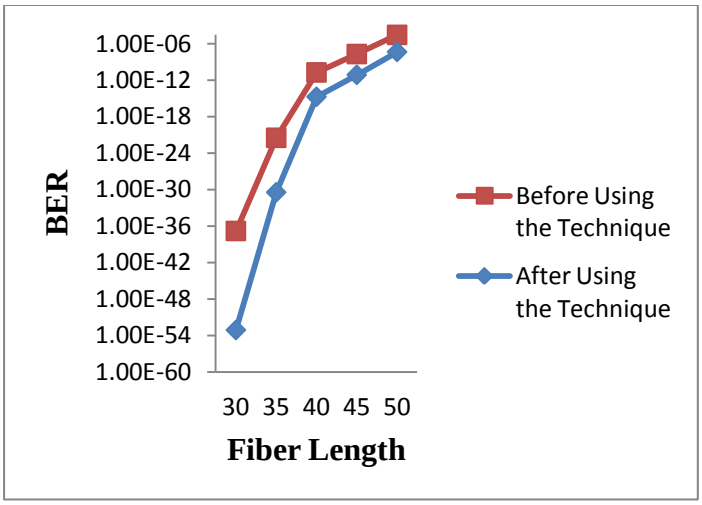

Fig.11. Variation of BER as a Function of fiber length

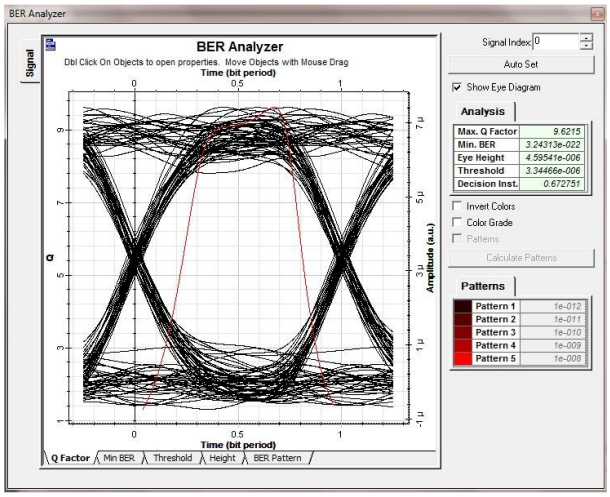

Fig.12. a) Eye diagram of the MD code at 35 km fiber length before using the technique

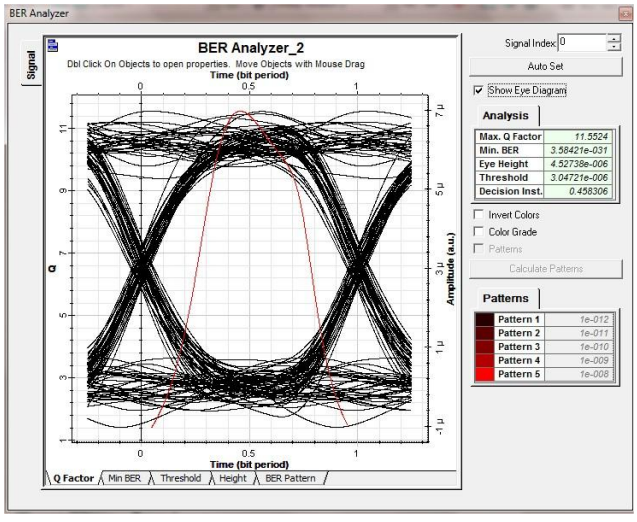

Fig.12. b) Eye diagram of the MD code at 35 km fiber length after using the technique

VI. CONCLUSION

We have illustrated a new technique based on adding idle code at the sideband of the code construction to generate the virtual FWM power at the sideband of the signal, and then by subtracting these virtual FWM power from the original FWM power in the system and filtering the data part at the channel. This technique is applied for both SAC codes, the RD and the MD codes. The systems give better performance in BER after using the technique comparing with the systems before using the techniqe. In addition, the FWM power reducing in the MD code more than 20 dBm and in the RD code more than 30 dBm. For example, in the RD code the FWM power at 40km fiber length and input power is 15 dBm is approximately -55 dBm before using the technique, after using the technique the FWM power is approximately -90dBm. In other words, at the MD code the FWM power before using the technique is approximately -61 dBm, the same parameters values, however after using our technique the value of the FWM power is approximately -81dBm. In adittion, for example at the BER values, the BER in the RD code at the input power -10dBm and 35km fiber length before using the technique is 1.6×10^{-23} and after using the technique the value of BER will become 4.05×10^{-28}. In addition at the MD code the BER value before using the technique is 9.4×10^{-22} and after using the technique the value of BER is 7.4×10^{-31}.

REFERENCES

[1] Abtin Keshavarzian, J. A. S. "Optical Orthogonal Code Acquisition in Fiber-Optic CDMA Systems via the Simple Serial-Search Method." IEEE Transactions on Communication **Vol. 50, No. 3** (2002).

[2] Indu Bala, V. R. "Performance analysis of SAC based non-coherent optical CDMA system for OOC with variable data rates under noisy environment." Indian Journal of Science and Technology **Vol.2 No. 8**: 49-52 (2009)

[3] Harmandeep Singh, Dr. YADUVIR SINGH. "Performance Analysis of Optical CDMA using Fuzzy Logic Generator". Department of Electrical and Instrumentation Engineering, THAPAR UNIVERSITY (2008).

[4] [4]. Fuad A. Hatim, F. N. H., Sahbudin Shaari. "Effects of Nonlinear Stimulated Brillouin Scattering on Performance Analysis of an Optical CDMA Transmission System." Journal of Optical Communications **30**: 104-108(2009).

[5] Boyd, R. W, "Nonlinear Optics (2nd ed.)". USA: Elsevier Science (2003).

[6] Osamu Aso, M. T., Shu Namiki. "Four-Wave Mixing in Optical Fibers and Its Applications." Furukawa Review **19**: 63-68 (2000)

[7] K.P. Lor, K. S. C.. "Theory of nondegenerate four-wave mixing in a birefringent optical fibre." Optics Communications **152**: 26-30 (1998)

[8] Banerjee, P. ," Nonlinear Optics: Theory, Numerical Modeling, and applications". New York: Marcel Dekker, Inc. (2004).

[9] Singh, A., Sharma, A. K., & Kamal, T. S, "Four-wave mixing analysis in WDM optical communication systems with higher-order dispersion". Optik - International Journal for Light and Electron Optics, 119(16), 788-792. (2008).

[10] S. P. Singh, N. S.. "Nonlinear Effects In Optical Fibers: Origin, Managment And Applications." Progress In Electromagnetics Research, PIER **Vol. 73**: 249–275 (2007).

[11] Billington, R. "A report on four-wave mixing in optical fibre and its metrological applications". R – Report. United Kingdom (1999). http://www.opengrey.eu/item/display/10068/697218

[12] Fadhil, H. A., Aljunid, S. A., & Ahmad, R. B, "Performance of random diagonal code for OCDMA systems using new spectral direct detection technique". Optical Fiber Technology, 15(3), 283-289. (2009).

[13] Abd, T. H., S. A. Aljunid, et al. "Development of a new code family based on SAC-OCDMA system with large cardinality for OCDMA network." Optical Fiber Technology **17**(4): 273-280. (2011).

Selection of Eigenvectors for Face Recognition

Manisha Satone
Sinhgad College of Engineering
Pune,India

G.K.Kharate
University of Pune
Pune, India

***Abstract*—Face recognition has advantages over other biometric methods. Principal Component Analysis (PCA) has been widely used for the face recognition algorithm. PCA has limitations such as poor discriminatory power and large computational load. Due to these limitations of the existing PCA based approach, we used a method of applying PCA on wavelet subband of the face image and two methods are proposed to select best of the eigenvectors for recognition. The proposed methods select important eigenvectors using genetic algorithm and entropy of eigenvectors. Results show that compared to traditional method of selecting top eigenvectors, proposed method gives better results with less number of eigenvectors.**

Keywords—face recognition; PCA; wavelet transform; genetic algorithm

I. INTRODUCTION

Many recent events, exposed defects in most sophisticated security systems. Therefore, it is necessary to improve security systems based on the body or behavioral characteristics, called biometrics. With the interest in the development of human and computer interface and biometric identification, human face recognition has become an active research area. Face recognition offers several advantages over other biometric methods. Nowadays, Principal Component Analysis (PCA) has been widely adopted for the face recognition algorithm. Yet still, PCA has limitations such as poor discriminatory power and large computational load [1].

In view of the limitations of the existing PCA-based approach, here we used a method of applying PCA on wavelet subband of the face image and two methods are proposed to select a best eigenvectors for recognition. In the proposed method, face image is decomposed into a number of subbands with different frequency components using the wavelet transform (WT). Out of the different frequency subbands, a mid-range frequency subband image is selected. The resolution of the selected subband is 16x16. The proposed method works on lower resolution, instead of 128 x 128 resolution of the original image. Working on lower resolution images, reduces the computational complexity. Experimental results show that applying PCA on WT sub-image with mid-range frequency components gives better recognition accuracy and discriminatory power than applying PCA on the entire original image [2][3]. In PCA, all the eigenvectors are not equally informative. This paper proposes two methods of eigenvector selection. In comparison with the traditional use of PCA, the proposed methods select the eigenvectors based on genetic algorithm and entropy of eigenvectors.

Paper is organized as follows: Section II reviews the wavelet. Section III reviews the background of PCA and eigenfaces. Section IV is about the eigenvector selection. Experiments and results are discussed in Sections V and conclusion in section VI.

II. WAVELET TRANSFORM

Multiresolution methods are powerful tools, which are widely used in feature extraction, image compression and denoising applications. Wavelet decomposition is a widely used multiresolution technique in image processing. Wavelet analysis has generated a great interest in both theoretical and applied mathematics, and the wavelet transform has proven to be an effective tool for data analysis, numerical analysis, and image processing. Wavelets are functions which give different frequency components of data. They have advantages over fourier methods in analyzing physical situations where the signal contains discontinuities and sharp spikes. The advantages of WT are good time and frequency localizations [4].

WT is chosen to be used in image frequency analysis and image decomposition because of the following reasons:

• The resolutions of the images can be reduced by decomposing an image using WT. Working on a lower resolution image reduces computational complexity.

• Wavelet transform provides local information in both space domain and frequency domain.

Wavelet transform can be performed for every scale and translation, resulting in Continuous Wavelet Transform (CWT), or only in multiples of scale and translation intervals, resulting in Discrete Wavelet Transform (DWT). CWT provides redundant information and requires a lot of computations, DWT is generally preferred. A two-dimensional wavelet transform is derived from two one-dimensional wavelet transform by taking tensor products. The implementation of WT is carried out by applying a one-dimensional transform to the rows of the original image data and the columns of the row transform data respectively.

Using wavelet transform, an image is decomposed into four subbands. The band *LL* is a coarser approximation to the original image. The band gives the edges along horizontal directions, whereas band *HL* record the edges along the vertical directions. The *HH* band records the diagonal edges present in the image. This is the first level decomposition. Further decomposition can be conducted on the *LL* subband. After applying a 3-level wavelet transform, an image is decomposed into subbands of different frequency components. Figure 1 shows 1-level and 3- level wavelet decomposition. In this paper, Daubechies wavelet D4 is adopted for image decomposition. G.C. Feng, P.C. Yuen and D.Q. Dai [5] has

shown that Daubechies wavelet D4 is better than other wavelets. Therefore, Daubechies wavelet D4 is adopted for image decomposition in our system.

Nastar et al. [2][3] have found the relationship between variations in facial appearance and their deformation spectrum. They found that facial expressions and small occlusion affect the intensity manifold locally. Under the frequency-based representation, only the high frequency spectrum was affected, whereas changes in illumination affected the intensity manifold globally, in which only the low frequency spectrum was affected. When there was a change in human face, all frequency components were affected. Based on Nastar et al.'s findings, we used subbands containing mid-range frequencies. Among subbands 1 to 4, subbands 2 to 4 were the mid-range frequency subbands. Further experimental results in [5] showed that applying PCA on subband 4 gave better recognition accuracy and class separability compared with applying PCA on the whole image, or applying PCA on subbands 1, 2 or 3. Hence we have chosen subband 4.

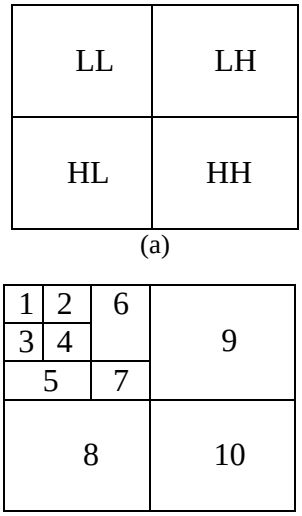

(a)

(b)

Fig.1. (a) 1-level wavelet decomposition and (b) 3-level wavelet decomposition

III. Principal Component Analysis

To linearly project an image in a low-dimensional space, PCA [6] is used where images are represented in eigenpace. This space is spanned by eigenvectors corresponding to the largest eigenvalues of the training images. After an image has been projected in the eigenspace, a feature vector containing the coefficients of the projection is used to represent the image. These features can be called as eigenfeatures [6].

Representing each image $I(x, y)$ as a NxN vector Γi , first, the average face $\boldsymbol{\psi}$ is computed:

$$\psi = \frac{1}{R}\sum_{i=1}^{R} I_i \qquad (1)$$

Where R is the number of faces in the training set.

Next, the difference Ø of each face from the average face is computed:

$$\phi_i = I_i - \psi \ . \qquad (2)$$

Then the covariance matrix is estimated by:

$$C = \frac{1}{R}\sum_{i=1}^{R} \phi_i \phi_i^T = AA^T \qquad (3)$$

Where, $A=[Ø_1 \quad Ø_2 \quad Ø_3 \quad Ø4\,]$

The eigenspace can then be defined by computing the eigenvectors μ_i of C.

Since C is very large (N^2 X N^2) , computing its eigenvectors will be very expensive. Instead, we can compute v_i, the eigenvectors of $A^T A$, an R X R matrix.

Then, μ_i can be computed from v_i as follows:

$$\mu_i = \sum_{j=1}^{R} v_{ij}\phi_{j,}\ j = 1.....R \qquad (4)$$

Given a new image, I, we subtract the mean ($Ø=I-\boldsymbol{\psi}$) and compute the projection:

$$\phi = \sum_{i=1}^{R_k} w_i u_i \qquad (5)$$

Where $w_i = u_i^T \phi$ are the coefficients of the projection.

Using projection coefficients images can be represented as linear combinations of the eigenvectors. The projection coefficients define a compact image representation. The eigenspace representation of images is very powerful and it has been used in various applications.

IV. The Importance of Eigenvector Selection

Feature selection is the first and one of the most important steps in pattern recognition. The aim of feature selection is driving an optimal subset of features from a given space leading to high classification performance.

In the eigenspace, all the eigenvectors are not equally informative. It has been found in several studies that different eigenvectors encode different kind of information [7][8].

Generally, in most of techniques the order of the eigenvalues determines the importance of eigenvectors, but as it is discussed in researches such as [9][10] ,this order is not always suitable to describe the data. For example, the first few eigenvectors seem to encode lighting while other eigenvectors seem to encode features such as glasses or moustaches [7]. Although many of the eigen-features are very important for face recognition, they might actually confuse the classifier in other applications. In this study, we consider GA and entropy of eigenvectors to select a good subset of eigen-features in order to improve face recognition performance. It reduces computation and increases recognition rate also.

A. Eigenvector Selection using GA

Selecting a set of eigenvectors for best classification performance is an optimization problem which can be solved by using the genetic algorithm (GA). GAs are inspired by the mechanisms of natural selection [11]. GAs operates iteratively on a population of structures, each of which represents a candidate solution to the problem, encoded as a string of symbols called chromosome. A randomly generated set of chromosomes forms the initial population from which the GA starts its search.

Each image is represented as a vector of eigen-features which are the coefficients of the linear expansion of the image in the eigenspace. In our encoding scheme, the chromosome is a bit string whose length is determined by the number of eigenvectors. Each eigenvector, computed using PCA, is associated with one bit in the string. If the i^{th} bit is 1, then the i^{th} eigenvector is selected, otherwise, that component is ignored. The goal of feature subset selection is to use less features to achieve the same or better performance. If we select only two eigenvectors then in chromosome only two bits are 1, all others are 0. Each chromosome thus represents a different eigen-feature subset.

The initial population is generated randomly. We will end up with a population where each individual contains for example two number of 1's only. The 1's are randomly scattered in the chromosome. Each chromosome is tested to see how good it is at solving the problem at hand and assign a *fitness score* accordingly.

The fitness score is a measure of how good that chromosome is at solving the problem at hand. The fitness of chromosome is measured in terms of recognition accuracy. Individuals with higher accuracy will outweigh individuals with lower accuracy. Mutation is the chance that a bit within a chromosome will be flipped. In proposed method only predefined numbers of bits are flipped. Chromosome with best fitness function is selected for face recognition.

Following are the steps to carryout genetic algorithm.

- Initialized the first population randomly (Only predefined number of bits are 1, all others are 0).
- Begin the evolution loop until the stoppings criteria (maximum number of trials) are reached.Here maximum numbers of trials are 200.
- For each chromosome in the population multiply the chromosome gene values to Eigenfaces.
- For each chromosome compute the fitness function.
- Apply the selection operator and select the fitted chromosomes population to generate the intermediate population.
- Apply mutation operators to form the next generation.

B. Feature Selection Using Entropy of Eigenvectors

Entropy is a statistical measure of randomness that can be used to characterize the texture of the input image. Entropy is defined as

$$E = \sum_{i=1}^{n} P_i \log_2 P_i \qquad (6)$$

Where P_i is probability of occurrence of pixel value *i*.

In this paper method based on entropy ranking is used. To evaluate the importance and obtain the ranking list of eigenvectors each eigenvector is removed in turn and the corresponding entropy of the rest of the eigenvectors set is computed. If the removal of an eigenvector causes more disorder in the system than another, it shows more importance and higher rank of this eigenvector. For recognition only top ranking eigenvectors are selected.

V. Experiments And Results

The experiment is performed on ORL, GTAV and YALE databases. Face database from AT&T (Olivetti) Research Laboratories, Cambridge (ORL database) [12] contains 40 individuals with each person having ten frontal images. So there are total 400 images in database. There are variations in facial expressions such as open or closed eyes, smiling or no smiling, and glasses or no glasses. All images are 8-bit grayscale of resolution 112 X 92 pixels. For testing of proposed methods we used 340 images (6 images per person) for training and 160 images (4 images per person) for testing. Image features are extracted using D4 wavelet transform. Four level decomposition is carried out on images and LL subband A3 of each level is used for further processing.

For genetic algorithm base eigenvector selection, experiment is performed in two steps. First A4 subbands of randomly selected 20 images from 160 images are used for testing. Using genetic algorithm best eigenvectors are selected. In second step best eigenvectors selected in first step are used for recognition of all 160 test images. For eigenvector selection using entropy, calculations are done by considering all eigenvectors and then by removing each eigenvector in turn. Top eigenvectors which are causing more difference in entropy after removing are used for reducing dimensionality in PCA.

Same experiment is performed on GTAV [13] and YALE [14] database. In GTAV, 92 images are used as test images and 138 images are used for training. In YALE database 1900 images are used as test images and 570 images are used for training. Similarity measurement between the test image and the training images in the library was performed to determine whether the input test image was matched with any of the images in the library. Here Euclidean distance is used for similarity measurement. Given the test image representation *X* and the training image representation *Y*, the similarity measurement *d(X,Y)* between the two images *X* and *Y* is defined by,

$$d(X,Y) = L_{P=2}(X,Y) = \|X - Y\| \qquad (7)$$

Table 1. shows the recognition rate for different number of eigenvectors for ORL database.Table 2 and Table 3 shows recognition rate for GTAV and YALE databases respectively.

TABLE I. % RECOGNITION RATE FOR ORL DATABASE

No. of Eigenvectors	% Recognition Rate		
	Top Eigenvectors	*Genetic Algorithm*	*Entropy of Eigenvectors*
2	47.5	52.5	37.5
4	79.375	81.25	81.25
6	83.125	90.625	85.00
8	81.875	93.75	90.00
10	81.875	95.00	88.125
12	81.875	96.875	90.00
20	85.625	96.875	90.00

TABLE II. % RECOGNITION RATE FOR GTAV DATABASE

No. of Eigenvectors	% Recognition Rate		
	Top Eigenvectors	*Genetic Algorithm*	*Entropy of Eigenvectors*
2	80.43	81.52	76.08
4	89.13	91.30	82.60
6	86.95	90.625	89.13
8	84.78	93.75	90.21
10	93.4	95.00	94.56
12	94.56	97.82	94.56
20	96.73	98.91	97.82

TABLE III. % RECOGNITION RATE FOR YALE DATABASE

No. of Eigenvectors	% Recognition Rate		
	Top Eigenvectors	*Genetic Algorithm*	*Entropy of Eigenvectors*
2	37.00	49.00	35.00
4	76.00	79.00	79.00
6	78.00	81.50	80.00
8	78.42	81.50	80.00
10	79.00	85.00	82.00
12	80	86.00	83.00
20	80	86.00	83.00

VI. CONCLUSION

Generally, in most of techniques in PCA the order of the eigenvalues determines the importance of eigenvectors, but this order is not always suitable to describe the data. In this paper two methods using genetic algorithm and entropy of eigenvectors are proposed to select best eigenvectors.

With less number of eigenvectors, proposed methods increase the recognition rate. Methods are implemented on A4 subband of wavelet transform which reduces computation.

REFERENCES

[1] B. Moghaddam, W Wahid and A pentland, Beyond eigenfaces: Probabilistic matching for face recognition, *Proceeding of face and gesture recognition*, pp. 30 –35, 1998.

[2] C. Nastar, "The image shape spectrum for image retrieval", *Technical report*, No. 3206, INRIA, June 1997.

[3] C. Nastar, B Moghaddam and A Pentland, "Flexible images: matching and recognition using learned deformations", *Computer Vision and Image Understanding*, Vol. 65, No. 2, pp. 179-191, 1997.

[4] I. Daubechies, "Ten Lectures on Wavelets", *CBMS-NSF series in Applied Mathematics*, Vol.61,SIAM Press, Philadelphia, 1992.

[5] G. C. Feng , P C Yuen and D Q Dai, "Human Face Recognition Using PCA on Wavelet Subband", *J. Electron. Imaging* 9, 226, 2000.

[6] M. Turk and A. Pentland. "Eigenfaces for recognition", *Journal of cognitive neuroscience*. vol 3, no.1 pp. 71-86, 1991.

[7] W. Yambor, B. Draper, and R. Beveridge, "Analyzing PCA-based Face Recognition algorithms: Eigenvector Selection and Distance Measures", *2nd Workshop on Empirical Evaluation in Computer Vision*,2000.

[8] D. Valentin et al, "Principal Component and Neural Network Analyses of Face Images: What can be Generalized in Gender Classification?", *Journal of Mathematical Psychology*, vol. 41, pp. 398-413, 1997.

[9] T. Xiang and S. Gong, "Spectral clustering with eigenvector selection," Pattern Recognition, vol. 41, pp. 1012-1029, 2008.

[10] F. Zhao, et al., "Spectral clustering with eigenvector selection based on entropy ranking," Neurocomputing, vol. 73, pp. 1704-1717, 2010.

[11] D. Goldberg, Genetic Algorithms in Search, Optimization, and Machine Learning, Addison Wesley, 1989.

[12] ORL database http://www.cl.cam.ac.uk/research/dtg/attarchive/facedatabase.html.

[13] F.Tarrés, A. Rama, *GTAV Face Database*. "http://gps-tsc.upc.es/GTAV/ResearchAreas/UPCFaceDatabase/GTAVFaceDatabase.htm"

[14] [Yale University Face Database, 2002. "http://cvc.yale.edu/projects/yale faces /yalefaces.html"

Sentiment Analyzer for Arabic Comments System

Alaa El-Dine Ali Hamouda
Faculty of Engineering
Al-Azhar University

Fatma El-zahraa El-taher
Faculty of Engineering,
Al-Azhar University

***Abstract*—Today, the number of users of social network is increasing. Millions of users share opinions on different aspects of life every day. Therefore social network are rich sources of data for opinion mining and sentiment analysis. Also users have become more interested in following news pages on Facebook. Several posts; political for example, have thousands of users' comments that agree/disagree with the post content. Such comments can be a good indicator for the community opinion about the post content. For politicians, marketers, decision makers …, it is required to make sentiment analysis to know the percentage of users agree, disagree and neutral respect to a post. This raised the need to analyze theusers' comments in Facebook. We focused on Arabic Facebook news pages for the task of sentiment analysis. We developed a corpus for sentiment analysis and opinion mining purposes. Then, we used different machine learning algorithms – decision tree, support vector machines, and naive bayes - to develop sentiment analyzer. The performance of the system using each technique was evaluated and compared with others.**

Keywords*—Analysis for Arabic comments; machine learning algorithms; sentiment analysis; opinion mining

I. INTRODUCTION

Recently the rate of users comments and reviews increased dramatically as a medium of expressing ideas across the WWW specially in Facebook (Active users of Facebook increased from just a million in 2004 to over 750 million in 2011[1]). The fast growth of such content has not been fully harnessed yet. Information left by the users is not analysis yet.

Users are interested in knowing the percentage of users agree, disagree and neutral respect to a post in news pages on Facebook. For example, a lot of posts in the Arabic news pages like رصد، سلفيو كوستا، 6أبريل كلنا خالد سعيد، الصفحه الرسميه لرئاسة مجلس الوزراء، (Rassd, Silvio Costa, 6 April, We are all Khaled Said, official page for the presidency of the Council of Ministers) get thousands of comments on each post. The posts can express politician declarations, government decision, products announcement… The politician analysts, marketers, and decision makers, newspapers and news channels need to measure the community opinions about a certain topic expressed by a post. This is the motive for us to design and develop an analyzer system for Arabic comments.

An important part of our information-gathering behavior has always been to find out what other people think. With the growing availability and popularity of opinion-rich resources such as online review sites and personal blogs, new opportunities and challenges arise as people now can, and do, actively use information technologies to seek out and understand the opinions of others. The sudden eruption of activity in the area of opinion mining and sentiment analysis, which deals with the computational treatment of opinion, sentiment, and subjectivity in text, has thus occurred at least in part as a direct response to the surge of interest in new systems that deal directly with opinions as a first-class object [2].

Existing supervised learning methods can be readily applied to sentiment classification, e.g., naïve Bayesian, and support vector machines (SVM), etc. Pang et al. [3] took this approach to classify movie reviews into two classes, positive and negative. It was shown that using unigrams (a bag of individual words) as features in classification performed well with either naïve Bayesian or SVM.

Some researchers have been performed for creating automatic analysis of Twitter posts during recent years. Some of these researchers investigate the utility of linguistic features for detecting the sentiment of Twitter messages [4].Other researchers use text messages from Twitter, a popular microblogging platform, for building a dataset of emotional texts. Using the built dataset, the system classifies the meaning of adjectives into positive or negative sentiment polarity according to the given context. The approach is fully automatic. It does not require any additional hand-built language resources and it is language independent [5].

In [6], the authors use web-blogs to construct a corpus for sentiment analysis and use emotion icons assigned to blog posts as indicators of users' mood. The authors applied SVM and CRF learners to classify sentiments at the sentence level and then investigated several strategies to determine the overall sentiment of the document. Emoticon; a textual representation of an author's emotion was used in Internet blogs and textual chats. The winning strategy was defined by considering the sentiment of the last sentence of the document as the sentiment at the document level [6].

Although there is some work for twitter analysis, there is no real work –to the best of our knowledge- to investigate and develop such analyzer for Facebook comments.

Our proposed system uses classification methods to analyze users' comments and detect the comments that agree, disagree or is neutral with respect to a post .The system structure is presented in section 2 including features, classifiers and corpus details. Then, implementation and system evaluation are discussed in sections 3 and 4 respectively. Finally, conclusion comes in section 5.

II. PROPOSED SENTIMENT ANALYZER SYSTEM

Proposed system uses classification techniques to get better results using specified set of features. To train the classifiers, labeled (annotated) training and testing corpus are prepared .The system components include preprocessing,

features selection, and classification methods to make the sentiment analysis for comments. The system components are described in details in the following sections.

A. Preprocessing

Preprocessing phase includes stop words removal and very long comments removal. Stop words are common words that carry less important meaning than keywords. Removing stop words from the comments return the most important words. By sampling 6000 comments in Egyptians pages in most important pages about 80% of very long comments in most cases are advertise for pages on Facebook.

B. The Proposed Features

The input comments are segmented into words, spaces, commas, parenthesis and new line for identifying words .Our approach is to use different machine learning classifiers and feature extractors. We use two groups of features and evaluate them. These features are explained in the following sections.

1) Common Words between Post and Comments Features

The first group of features includes the number of words in post only, comment only, both post and comment. They are normalized by them by the length of comment and post. The idea behind these features is that the intersection between important words (not stop words) in post and comment may express if the comment agrees or disagrees with the post or not. The used equations for each feature are as follows.

Feature 1: Number of Words in Post Only Number of words in post only feature is (after stop words removal) computed using equation 1.

$$\frac{\text{Num Of words in Post Only}}{(\text{length of comment} + \text{length of post})} \quad (1)$$

Feature 2: Number of Words in Comment Only Number of words in comment only feature is (After stop word removal) computed using equation 2.

$$\frac{2 * \text{Num Of words inComment only}}{(\text{length of comment} + \text{length of post})} \quad (2)$$

The numerator is multiply by 2 for normalization .If the comment and post are similar will give one

Feature 3: Number of Words Common between Post and Comment:

Number of words common between post and comment feature is (After stop word removal) computed using equation 3.

$$\frac{\text{Number of Words common between post and comment}}{(\text{length of comment} + \text{length of post})} \quad (3)$$

2) *All Words in Posts and Comments Features*

The second group of features is the union of all words in the posts and comments. Each word (feature) takes one of the four values:

- "C "if the word is not in the post or the comment
- "M" if the word is in the post only
- "N" if the word is in the comment only
- "H" if the word is in both of the post and the comment

By that, we have number of features equal to the union of the words in both posts and comments.

Example:

Pots: الشرطة العسكرية تمارس «الضبطية القضائية»

"Military Police applied 'judicial officers'"

Comment1: واضح اننا هنشوف ايام سوداء من الشرطة العسكرية

"It is clear that we will see bad days"

Comment 2: بجد لا تعليق

"No comment"

	الشرطه	العسكريه	تمارس	الضبطيه	القضائيه	واضح	هنشوف	ايام	سوداء	بجد	تعليق
Comment 1	H	H	M	M	M	N	N	N	N	C	C
Comment 2	H	H	H	H	H	C	C	C	C	N	N

3) *Negation and Relevance Features*

The negation and similarity features are added to the features in group one and group two to improve the results. The negation words like (لن ، لا ، لم ، ما ، ليس) (no, not) .these features are:

Feature 1: Number of Negation Words in Post: Number of Negation words in post feature are (after stop words removal) computed using equation 4.

$$\frac{\text{Number of negative words in post}}{\text{length of post}} \quad (4)$$

Feature 2: Number of Negation Words in Comment: Number of negative words in comment feature are (after stop words removal) computed using equation 5.

$$\frac{\text{Number of negative words in comment}}{\text{length of comment}} \quad (5)$$

Feature 3: Relevance with Post

Relevance with post feature measures the relation between comments and post. The term frequency; Tf for each word in the post and comments (after stop words removal) are computed using equation 6.

$$Tf = F \quad (6)$$

F is the term frequency for a word in the comment. The vectors for the post and comments are formed.

Then, the relevance is computed using Cosine Similarity [7] method.

C. Classifiers

Using machine learning, several classifiers are developed to predict the type of each comment; agree, disagree or neutral to the post. Different machine learning techniques are used as follows.

1) Naive Bayes

Naive Bayes is a simple model which works well on text categorization [8]. We use a multinomial Naive Bayes model. Class c* is assigned to comment d, where

$$C^* = argmac_c P_{NB}(c|d)$$

$$P_{NB}(c|d) = \frac{P(c)\sum_{i=1}^{m} P(f|c)^{n_{i(d)}}}{P(d)} \qquad (7)$$

In this formula, f represents a feature and ni (d) represents the count of feature fi found in comment d. There are a total of m features. Parameters P(c) and P (f|c) are obtained through maximum likelihood estimates, and add-1 smoothing is utilized for unseen features

2) Decision Tree

The task of inducing a decision tree is typically handled by a recursive partitioning algorithm which, at each non-terminal node in the tree, branches on that attribute which discriminates best between the cases filtered down to that node [9].

3) Support Vector Machines

Standard support vector machines (SVMs), which are powerful tools for data classification, classify 2-category points by assigning them to one of two disjoint half spaces in either the original input space of the problem for linear classifiers, or in a higher dimensional feature space for nonlinear classifiers [10].

III. Implementation

To apply the proposed system, we developed the following components as follows.

A. Preprocessing

In this phase, the data is prepared before feeding to the classifiers .We used stop words listed in [11] and added additional stop words for the Colloquial Arabic. Stop words for the Colloquial Arabic are like (..... ,اللى ,ده دى) (Da, de, Elly, ...)

The similarity feature is used to detect the redundant comments. If two comments have similarity value equal to or more than a threshold (0.4), the shortest one will be removed. For long comments, they are not included in the summary. We ignore comments with number of words -after stop words removal- more than 150 words. The preprocessing also includes removing special characters like #, @, !, % and others. In addition, the redundant letters like منقووووول (Menkowoowol) are removed to get single written way for the same word.

B. The Proposed Features

The value of each feature is normalized to be between zero and one. The features explained in section 2 are used.

C. Data Corpus

To train the classifiers, a corpus is collected from the news pages in the Facebook. Recent "Egypt" and "Arabic Region" news were selected. We used the news pages of

رصد، سلفيو كوستا، 6أبريل ، كلنا خالد سعيد، الصفحه الرسميه لرئاسة مجلس الوزراء، شبكه اخبار مصر، اخر اخبار ميدان التحرير، المصرى اليوم.

(Rassd, Silvio Costa, 6 April, We are all Khaled Said, official page for the presidency of the Council of Ministers, Egypt News Network, Tahrir Square News, Egyptian today).

The total corpus size is 2400 comments collected from 220 posts; 800 neutral comments, 800 supportive comments, and 800 attacking comments. Each comment is represented into a single record, and then grouped manually into 3 groups; group one with the value "y" corresponding to supportive comments, group two with the value "n" corresponding to attacking comments and group three with the value "u" corresponding to neutral comments.

D. The Classifiers

The training data is used to learn all classifiers including Naive Bayes, decision tree and support vector machines.

IV. System Evaluations and Results

Classification approach is to classify comments to neutral comments, supportive comments, and attacking comments. After training the classifier, it will able to classify new comment to one of the three classes. Comparing these labeled of comments with those labeled that given manually by a human expert, we calculate the precision and recall.

For system evaluation, we tried different groups of features with different classifiers; support vector machines, naive bayes, and decision trees to find the features that give the best performance. The classifiers classify the comments to three categories; supportive comments 'y', attacking comments 'n', and neutral comments 'u'. Adding negation words and similarity features for all words in posts and comments features give the best performance. Naive Bayes gives 59.9%. With the decision tree, the precision and recall improved with 10%. Finally, SVM gives the best results 73.4% for precision and recall.

TABLE I. Using Common Words between Post and Comments Features

	SVM		Naive Bayes		Decision Trees	
	Precision	Recall	Precision	Recall	Precision	Recall
Attacking	34.1%	10.8 %	40.8%	27.3 %	25%	1%
Neutral	28.6%	20.7 %	34.1%	11.7 %	51.1%	18.4 %

Supporting	33.9%	66.8%	34.1%	66.8%	35.4%	92%
Average	32.3%	32.7%	36.5%	36.5%	36.6%	37%

TABLE II. Adding Negation Words and Similarity Features for Common Words between Post and Comments Features

	SVM		Naive Bayes		Decision Trees	
	Precision	Recall	Precision	Recall	Precision	Recall
Attacking	40.3%	30.4%	42.8%	22.7%	34.6%	6.3%
Neutral	46.5%	23%	49.3%	28.9%	69.9%	281%
Supporting	35.5%	61.3%	35.8%	67.2%	37.4%	90.1%
Average	40.3%	30.4%	42.5%	39.6%	46.6%	41.3%

TABLE III. Using All Words in Posts and Comments Features

	SVM		Naive Bayes		Decision Trees	
	Precision	Recall	Precision	Recall	Precision	Recall
Attacking	66.7%	67.6%	59.2%	51.6%	63.8%	66.5%
Neutral	75%	62.2%	61.2%	53.7%	75.8%	58.1%
Supporting	77.3%	82.9%	61.1%	76.4%	71.7%	85.2%
Average	73%	72.7%	60.5%	60.5%	70.4%	70%

TABLE IV. Adding Negation Words and Similarity Features for All Words in Posts and Comments Features

	SVM		Naive Bayes		Decision Trees	
	Precision	Recall	Precision	Recall	Precision	Recall
Attacking	67%	68.7%	58.9%	49.5%	64.1%	68.7%
Neutral	75.8%	62.6%	61.3%	53.3%	71.1%	59.3%
Supporting	77.5%	88.9	59.7%	77.1	73.3%	80.1
Average	73.4%	73.4%	59.9%	59.9%	69.5%	69.4%

TABLE V. Show Precision/ Recall for two human experts that show the difference between people in detect the class of comment

	Precision	Recall
Attacking	87.4%	31%
Neutral	79.8%	25.8%
Supporting	72.4%	33.8%
Average	79.8%	30.2%

V. Conclusions

In this paper, we used Facebook to collect training data to perform a sentiment analysis. We constructed corpora for supportive comments, attacking comments, and neutral comment with regard to different posts. We tried different groups of features. We improved them by adding similarity and sentiment words features. We use different classifiers; support vector machines, naive bayes, and decision tree. The best result was obtained by the support vector machine classifier. We could reach up to 73.4% of accuracy on their test set.

References

[1] Shu-Chuan Chu," VIRAL ADVERTISING IN SOCIAL MEDIA: PARTICIPATION IN FACEBOOK GROUPS AND RESPONSES AMONG COLLEGE-AGED USERS", Journal of Interactive Advertising, 2011

[2] Bo Pang , Lillian Lee, "Opinion Mining and Sentiment Analysis, Foundations and Trends in Information Retrieval", v.2 n.1-2, p.1-135, January 2008

[3] B. Pang, L. Lee, and S. Vaithyanathan, "Thumbs up? Sentiment classification using machine learning techniques," Proceedings of the Conference on Empirical Methods in Natural Language Processing (EMNLP), pp. 79–86, 2002

[4] EfthymiosKouloumpis,TheresaWilson,JohannaMoore,"Twitter Sentiment Analysis:The Good the Bad and the OMG!", Proceedings of the Fifth International AAAI Conference on Weblogs and Social Media,2011.

[5] Alexander Pak, Patrick Paroubek "Twitter Based System: Using Twitter for Disambiguating Sentiment Ambiguous Adjectives," Proceedings of the 5th International Workshop on Semantic Evaluation, ACL 2010, pages 436–439.

[6] Changhua Yang, Kevin Hsin-Yih Lin, and Hsin-Hsi Chen. 2007. Emotion classification usingweb blog corpora. In WI '07: Proceedings of the IEEE/WIC/ACM International Conference on Web Intelligence, pages 275–278, Washington, DC, USA. IEEE Computer Society.

[7] Anna Huang, Similarity Measures for Text Document Clustering, New Zealand, Computer Science Research Student Conference 2008, April 2008.

[8] C. D. Manning and H. Schutze. Foundations of statistical natural language processing.MIT Press, 1999.

[9] [White and Liu, 1994] A.P. White and W.Z. Liu. Bias in Information-based measures in decision tree induction. Machine Learning, 15:321-329, 1994.

[10] GLENN M. FUNG, O. L. MANGASARIAN, Multicategory Proximal Support Vector Machine Classifiers, 2005 Springer Science + Business Media, Inc. Manufactured in The Netherlands.

[11] Ibrahim Abu El-Khair, Effects of stop words elimination for Arabic information retrieval a comparative study, study, International Journal of Computing and Information Sciences, Decembers 2006.

[12] Cyril Goutte and Eric Gaussier, A Probabilistic Interpretation of Precision, Recall and F-score, with Implication for Evaluation, The final version of this paper will appear in:D.E. Losada and J.M. Fernaandez-Luna (eds) Proceedings of the European Colloquium on IR Resarch (ECIR'05), LLNCS 3408 (Springer), pp. 345-359

Routing Discovery Algorithm Using Parallel Chase Packet

Muneer Bani Yassein
Dept. Computer Science
Jordan University of Science and Technology
Irbid, Jordan

Yaser M. Khamayseh
Dept. Computer Science
Jordan University of Science
and Technology
Irbid, Jordan

Amera Al-Ameri
Dept. Computer Science
Jordan University of Science and Technology
Irbid, Jordan

Wail E. Mardini
Dept. Computer Science
Jordan University of Science
and Technology
Irbid, Jordan

***Abstract*—On demand routing protocols for ad hoc networks such as Ad Hoc On Demand Distance Vector (AODV) initiate a route discovery process when a route is needed by flooding the network with a route request packet. The route discovery process in such protocols depends on a simple flooding as a broadcast technique due to its simplicity. Simple flooding results in packet congestion, route request overhead and excessive collisions, namely broadcast storm problem. A number of routing techniques have been proposed to control the simple flooding technique. Ideally, the broadcast of route request or the route discovery process must be stopped as soon as the destination node is found. This will free the network from many redundant packets that may cause network collision and contention.**

In this paper, chasing packet technique is used with standard AODV routing protocol to end the fulfilled route requests. The chase packet is initiated by the source node and is broadcasted in parallel with route request packet. As soon as the destination is found the chase packet starts its work by trying to catch and discard the route request in early stages before it broadcasts further in the network.

Performance evaluation is conducted using simulation to investigate the performance of the proposed scheme against the existing approach that uses chase packet technique such as Traffic Locality Route Discovery Algorithm with Chase (TLRDA-C). Results reveal that the proposed scheme minimizes end-to-end packet delays and achieves low routing request overhead.

***Keywords*—MANET; Chase Packets; AODV; Broadcast Storm Problem.**

I. INTRODUCTION

A computer network is a collection of independent devices interconnected together with the aid of some communication facilities. Wired networks were useful but not suitable for mobile environments. The production and popularity of mobile devices (such as laptops, and mobile phones) increased the interest in wireless networks, and increased the need to adopt changes in the communication ways [2,12,13].

IEEE 802.11 standard defines two different modes for wireless network: infrastructure and infrastructure-less. The later is commonly known as Mobile Ad Hoc Network (MANET)? Infrastructure mode consists of a control unit called base station or access point and a number of mobile and/or fixed stations (nodes) [12]. The base station is responsible for managing and controlling the communication between the mobile stations as well as providing the connections to wired stations. MANET consists of a collection of distributed nodes that communicate with each other over a wireless medium using multi-hop communication techniques without the need of the base station [2].

The process of transmitting data from a source to a destination node in the network is called routing. During this process, one or more intermediate nodes cooperate to transfer the data. Routing involves two main tasks: first, determining the best path from the source to the destination node. Second task is transmitting data packets between the nodes [3]. Flooding is the simplest broadcast technique used to transmit the packet to the destination. It means that every node in the network receives the packet and rebroadcasts it to all its neighbors. Flooding consumes network resources and leads to low network delivery ratio [4].

According to the literature, there are many proposed schemes to alleviate the effects of conventional flooding, control the broadcast technique to cover part of the network and improve network performance in terms of overhead and congestion levels. They have been classified to the following four categories: Time-To-live (TTL), chase packets, location, and neighbor's information [5, 6, 7, 8].

In this paper we propose a scheme that uses chasing packet with standard AODV routing protocol to stop the fulfilled route request. The chase packet is initiated by the source node and broadcasted in parallel with route request packet. As soon as the destination is found the chase packet starts its work by trying to catch and discard the route request in early stages before it broadcasts further in the network. The rest of this paper is organized as follows. Section 2 provides some algorithms that are related to our work. Section 3 describes and illustrates the idea of the proposed scheme.

Simulations results are analyzed and evaluated against existing routing protocol are provided in section 4. Finally, we conclude the paper in section 5.

II. Related Work

Chase packet based schemes broadcast control packets (called chase packet) to stop the continuous propagation of route requests once a path is discovered [2]. Limited Broadcasting algorithm (L-B) [6] uses the chase packet strategy to control the broadcast process. In this scheme, the source nodes commence a route request procedure using traditional broadcast mechanism. Once the path is found and an acknowledgement is received by the source, it commences an intercepting process to stop the search. L-B divides the network into two channels which means that the time slots will be divided into periods.

The time slots are divided among the two channels to match their given speeds. For example, if the given speed for channel 1 is 1/4, and the given speed for channel 2 is 3/4, then one fourth of the time slots in each period are assigned to channel 1, and the rest of the time slots are assigned to channel 2. Typically, the route requests use channel one which means that it will use only ¼ of the channel time. This wills slowdown the route request propagation while the rest of the channel time is used to transmit route replies and broadcast chase packets. Therefore, the chase packets are three times faster than route requests. This will give the chase packets a chance to catch the fulfilled route requests [2, 11]. The main deficiency of the L-B algorithm is favoring the chase packets and route replies over the route requests from the beginning. Route requests are delayed from the beginning before discovering the needed route which would delay all route discoveries.

Limited-Hop Broadcast Algorithm (LHBA) proposed in [9] overcomes the shortcoming in L-B algorithm by allowing any node that discovers the route to initiate the chase packet. The finder will broadcast the chase packet to *K* hop neighbors to stop the further broadcast of the route requests. This algorithm allows any route finder or the destination itself to initiate the chase packet. Therefore, many chase packets will be initiated for the same route request [2].

Blocking- Expanding Ring Search (B-ERS) is an improvement of the Expanding Ring Search (ERS) proposed in [5] where each new ring starts from the previous ring instead of starting from the source node as in ERS. B-ERS introduces a delay equals 2* hop count at each node within the ring. Two stop signals can be used to control the flooding of route request RREQ. One is the reply packet RREP which can be sent by any route node and the other is the chase packet which is called *stop_instruction*, it is sent by the source node only [5].

The RREP message informs that the destination is found. After the 2* hop count units of time delay, the intermediate nodes in the current ring may receive a chase packet from the source node.

Stop instruction packet broadcasts to cover the current ring only where the finder of the route is located. Once the chase packet is received, the intermediate node will discard both chase and request packets. If no chase packet is received within the 2* hop count units of time, this means that there is no node in this ring having any route information then a new ring will be initiated.

The Traffic Locality Oriented Route Discovery Algorithm with Chase Packet (TLRDA-C) proposed in [2] divides the network into two regions: First, neighborhood region which includes the most likely destination for the source node. Second, beyond-neighborhood region. Each node in neighborhood region will broadcast the RREQ packet without adding any extra delays. This will improve the route request discovery process. However, in beyond-neighborhood region, the route request is further broadcasted with a deliberate additional delay.

Once the source node receives the reply packet (RREP), it broadcasts chase packet to terminate the route request. The chase packet is broadcast without adding any delay in an effort to terminate the propagation of the fulfilled route request as soon as possible. The catching occurs in the beyond-neighborhood region as the chase packet travels faster than its associated route request within this region; the route request is subject to a slight delay while propagating in this region [2]. The route discovery process may be delayed when the destination is located out of neighborhood region. TLRDA-C assumes that the route finder, F, is not located near the boundaries of the network [1]. In the case of source node mobility, it needs to re- initiate its neighborhood region [2, 13].

III. Ad Hoc On Demand Distance Vector with Parallel Chase Packet (AODV-PC)

This paper presents a modified scheme that utilizes the AODV routing protocol with chase packet concept. Instead of delay the route request when it reaches the beyond-neighborhood region, the modified scheme broadcasts the route request using the same speed in any network region. It broadcast the chase packet parallel with the route request packet. The default state of the chase packet is an inactive state. When the destination is found, it will change the chase packet state into an active state and broadcast it to inform the other intermediate nodes that the route request should be stopped [11].

The chance to catch and discard the route request before covering a large area is high. The chase packet is very close to the route request when the destination is found. The chase packet is broadcasted without adding any delays similar to the route request to terminate the propagation of the fulfilled route request as soon as possible. Figure 1 shows the chase packet format used in the proposed scheme. Packet size should be chosen carefully because the transmitting and receiving operations consume bandwidth and power in wireless networks [1].

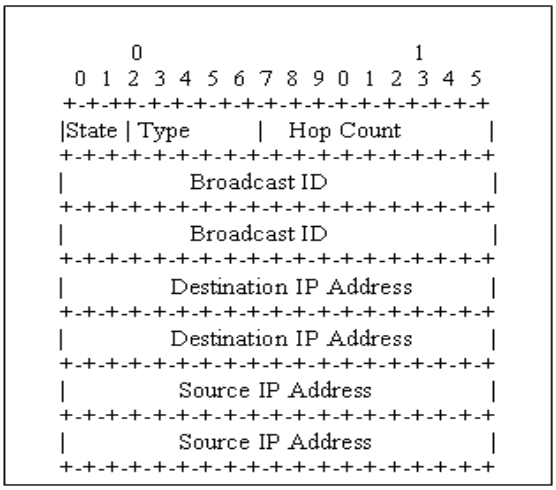

Fig.1. Chase packet format

In MANETs, the packets cross multiple nodes. Using small packets is more efficient in order to minimize resources consumption. So, chase packets in the proposed scheme are kept small in size, 14 bytes, compared to a route request packet where its sizes in TLRDA-C [2] and AODV [10] are 25 and 24 bytes respectively.

Figure 2 indicates the steps that are performed by each node when receiving the route request packet. The first step is to discard any duplicated route requests (line 2).

If the route request received for the first time (line 3), the node searches for the stored information in order to match chase packet. If it is found (line 4), the route request will be discarded after storing the needed information (lines 5-6). If no matching chase packet is received, the route request is processed according to the AODV routing protocol (line 8) [1].

Steps preformed by each node upon receiving the chase packet in AODV-PC
1: If the chase is a duplicate
2: Discard it
3: Else
4: If the current node is the destination
5: change the chase packet state to active
6: broadcast the chase packet
7: Else
8: If chase state is active then
9: insert into list
10 broadcast the chase packet
11: Else
12: broadcast the chase packet
13: End IF
14: End IF
15: End IF

Fig.2. Processing of route requests at a node in AODV-PC

Once the chase packet is received, the steps in Figure 3 are executed at each node. The request is discarded by the node if the chase packet is a duplicate, (line 2). Otherwise, if the receiving node is the destination node, it changes the state of the chase packet to be active (line 5). Active state means that the chase packet starts its work and tries to discard the associated route request packet. If the receiving node is a normal intermediate node and the state of the chase packet is active then the node inserts the chase packet to the active chase packet list (line 9). This guarantees that if the chase packet is received before the request packet, it will do its work and discard the incoming route request packet [1].

In AODV-PC, the source node is always the initiator of the chase packets. This enables AODV-PC to avoid initiating many chase packets for the same route request.

Steps preformed by each node upon receiving a route request in AODV-PC
1: If route request is a duplicate
2: Discard the route request
3: Else
4: If active chase packet has been received then
5: Store route request information
6: Discard the route request
7: Else
8: Continue according to standard AODV protocol
9: End IF
10: End IF

Fig.3. Processing chase packet at node in AODV-PC

IV. Simulation Results And Analysis

In order to compare our results to other related works we used a simulation model that is similar to ones used in the literature. The simulation model consists of the following main components: Mobile nodes with specific transmission range in specific area. The typical values are transmission range up to 250m in a square area of 600mx600m.

The number of nodes will be varied for different simulation experiments. The simulation time used is 600 seconds. The IEEE 802.11 is used as the underlying MAC layer communication model. Packet generation rate is 4packet/second. Table 1 summarizes the main simulation parameters used.

The following performance metrics has been used in order to evaluate the performance of our technique [12]:

- **Packet loss:** Which is defined as the total number of dropped packets in the whole network. The main factors affecting and causing packet loss are congestion and mobility.
- **Route request overhead**: This is defined as the total number of route requests received in all nodes in the network. Some request might not be satisfied and those sending new request will cause this metric to increase indicating network low performance.
- **End-to-end delay**: This metric includes all times from the time the packet was ready to be sent at the source node and the time it reaches the destination node. It includes all time delays due to route discovery, queuing, and propagation delay.
- **Route request latency**: This is usually defined as the average delays per hop among all route requests in a single simulation scenario. Latency of one route request is the average delay experienced by the route request per hop from the time it was sent by a source node until the time it was discarded by the chase packet which is usually called the Rout Request Life time RRL [2].

In the following subsections we study the effect of the network density and the mobility on the network performance using the above metrics.

A. The Effect of Network Density

Figs. 4 to 7 display the performance results for TLRDA-C versus AODV-PC using networks with different densities. The number of nodes increased from 20 to 100 in multiples on 20. The nodes speed is varying from a minimum of 1 m/s and a maximum speed of 15m/s. The number of the traffic load is four. The end-to-end delay increases with the network density for both algorithms because the hop count of transmission path increases which in turn increases the delay including the discovery time for the route.

TABLE I. PARAMETERS USED IN SIMULATION

Parameters	Value
Simulator	NS2.33
Transmission Range	250m
Network Size	600m x600m
Simulation time	900s
Packet Size	512 byte
Packet Rate	4pkt/s
Traffic Type	Constant Bit Rate (CBR)
Routing Protocol	AODV
Number of Nodes	20,40,60,80,100
Number of runs per point	20
MAC protocol	IEEE 802.11
Minimum speed	1m/s
Maximum speed	2,5,7,10,13 m/s
Pause time	50s
Mobility model	Random WayPoint model (RWP)

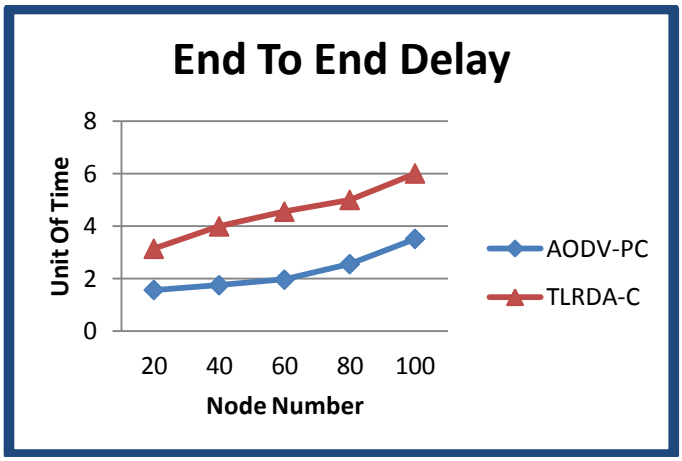

Fig.4. End-to-End delay versus network density

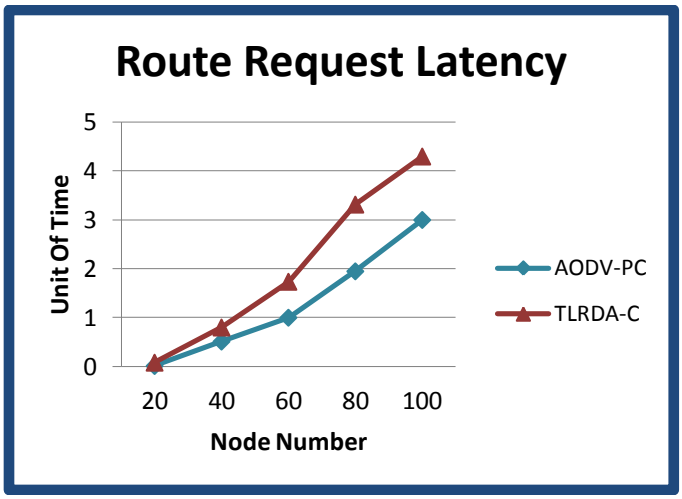

Fig.5. Average route request latency versus network density

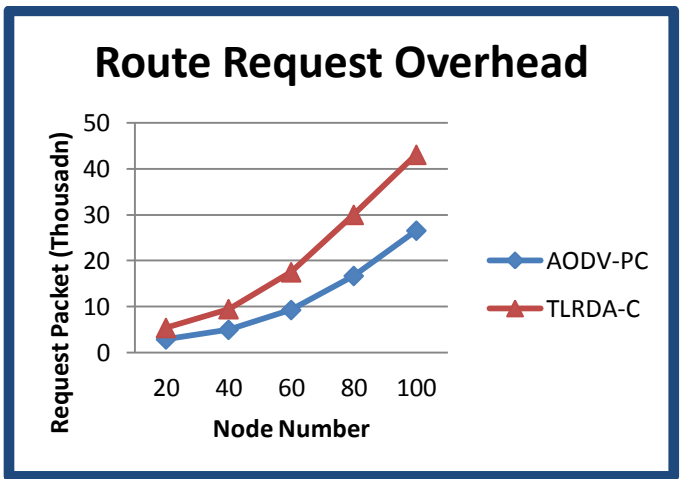

Fig.6. Average route request latency versus network density

AODV-PC improves the end to end delay. TLRDA-C algorithm performs well when the destination or the route finder locates at the neighborhood region. Otherwise, route request will be delayed to give the chase packet a chance to catch it. This will delay the route discovery process and increases the end to end delay.

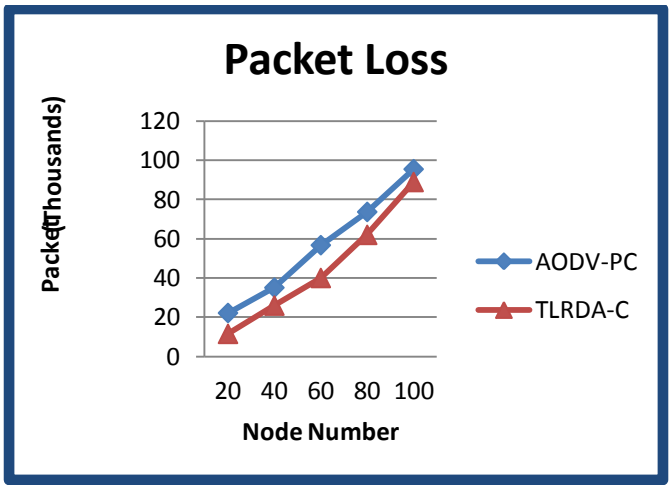

Fig.7. Packet loss versus network density

AODV-PC improves the average of route request latency in high density network. When the network density is 20 nodes the value of latency is approximately equal. This is due to the chosen scenario at that point; it means that the destination node may be in the neighborhood region. Therefore, the TLRDA-C algorithm performs well and catches the route request in early stages which is in turn reduces the latency.

The route request may reach more nodes each time it propagates further in the network and catching process may be difficult. The success of the catching process by the chase packet frees the network from more fulfilled route requests which improves the overhead. The main factors that have a high impact on the packet loss are mobility and congestion. Although our proposed scheme is less congests in general, but the TLRAD-C algorithm has less number of control packet such as chase packet, too many small chase packet in AODV-PC algorithm may cause a high congestion in the area that is located between the source and destination where the data packet will be transmitted.

B. The Effect of Mobility

Figs. 8 to 11 display the effect of mobility on our metrics. The results are extracted from simulating both algorithms using networks of size 60 nodes. We use six different maximum speeds where the actual speed is randomly selected from [1, max speed]. The six maximum speeds take the following values: 2, 5, 7, 10, and 13 m/s respectively. The traffic load was fixed to be 4.

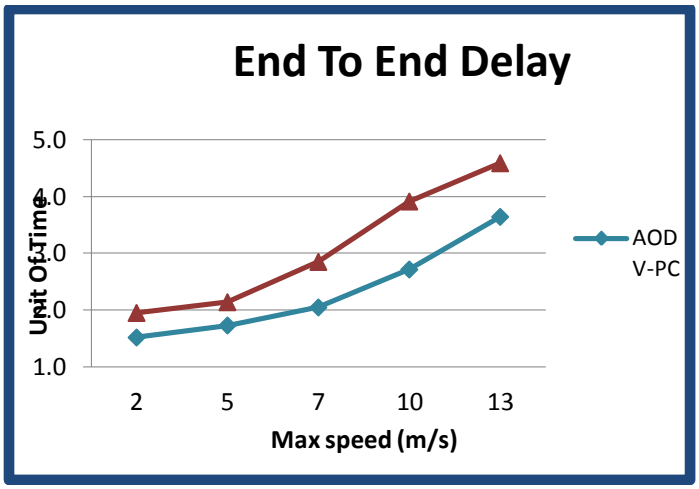

Fig.8. End-to-end delay versus maximum speed

AODV–PC offers better end-to-end delay as shown in Fig.8. This improvement is due to less congested environment provided by AODV-PC algorithm and quick broadcasting within the network regardless of the region.

The route request latency increases with the increment of speed due to the link breakage regardless of used algorithm as shown in Fig.9. AODV-PC reduces the route request latency this is due to the quick broadcasting within the network regardless of the region and due to better success rate (The ability to discard route request in early stages) achieved by proposed algorithm. TLRDA-C algorithm is very depends on the used scenario which specifies the destination location.

Fig.10 demonstrates the route request overhead. As we mentioned before many route request will be reinitiated because of high network link breakage the network success rate has a high impact on the route request overhead. Lower number of redundant hop count (number of hops that the route request passes before it is discarded by the chase packet) means that better catching for the route request in early stages. This will free the network from many route requests and reduce its overhead.

Fig.11 explores the effect of node speed on the packet loss. We can easily notice that the value of packet loss on both algorithms is approximately equal in highly mobile network. This is due to high congestion in the area located in between source and destination caused by the chase packet. High mobility increases the probability of link breakage which increases the packet loss.

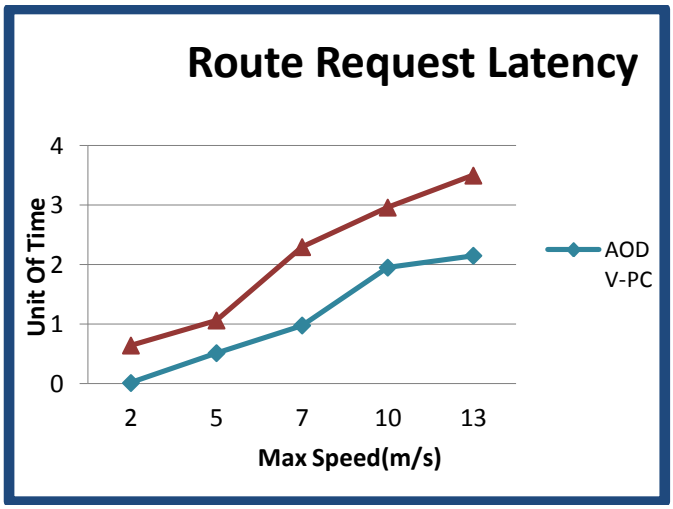

Fig.9. Route request latency versus maximum speed

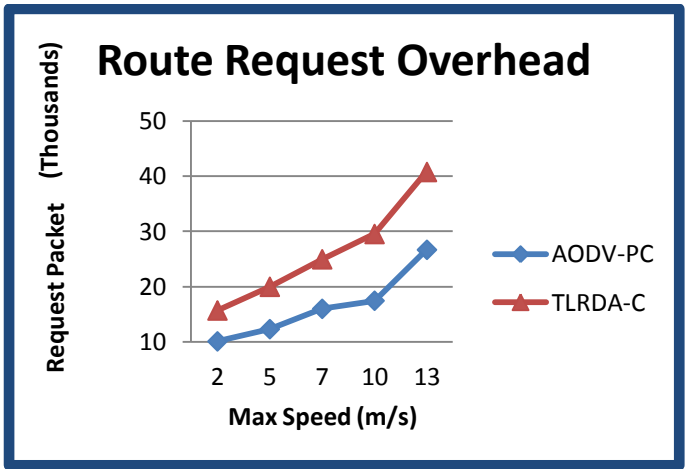

Fig.10. Route request overhead versus maximum speed

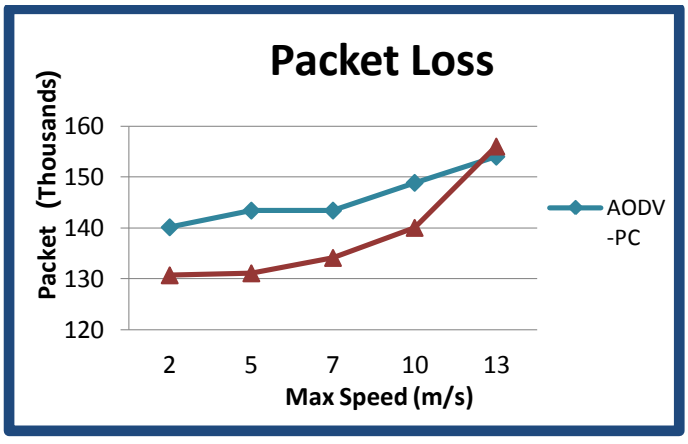

Fig.11. Packet loss versus maximum speed

CONCLUSION

This paper suggests new chasing packet technique used with standard On Demand Distance Vector protocol (AODV). A simulation and analysis for the proposed scheme are presented.

Some simulation experiments have been carried out to study AODV-PC and compare its performance with TLRDA-C algorithm that uses chase packet concept. The simulation environments have considered different network scenarios with different parameters e.g. network density, and maximum speed under RWP model.

Simulation performance results show that that AODV-PC outperforms TLRDA-C in terms of the success rate of the catching process, end-to-end delay, route request latency. Due to avoiding the delay added to the route request when it reach to beyond-neighborhood region AODV-PC achieves better end-to-end delay when varying network density.

Furthermore, the route request latency improvement was up to 30%. Despite the both algorithms have approximately equal results in term of packet loss; AODV-PC is less congests due to the reduction in the overhead caused by broadcasting the route request after the route is found.

REFERENCES

[1] Amera H. Al-Amery. Anew Routing Discovery Algorithm Using Parallel Chase Packets [dissertation]. Jordan University Of Science and Technology; 2010.

[2] Mznah A. Al-Rodhaan. Traffic Locality Oriented Route Discovery Algorithms for Mobile Ad Hoc Networks [dissertation]. University of Glasgow; 2009.

[3] Krishna G. Routing Protocols in Mobile Ad Hoc Networks [dissertation]. Sweden, Umea University; 2006 June.

[4] Peter L. Analysis of Routing Algorithms for Mobile Ad Hoc Networks [dissertation]. Chalmers University of Technology, Department of Computer Engineering, Gothenburg; 2002

[5] M. Aminu, M. Ould-Khaoua, L. M. Mackenzie and J. Abdulai. Performance Evaluation of an Efficient Counter-Based Scheme for Mobile Ad Hoc Networks based on Realistic Mobility Model. Proceedings of IEEE International Conference on Signal Processing and Communications; 2009.

[6] Incheon Park, Jinguk Kim, Ida Pu. Blocking Expanding Ring Search Algorithm for Efficient Energy Consumption in Mobile Ad Hoc Networks. Third Annual Conference on Wireless On-demand Network Systems and Services .2006. 191-195.

[7] Young-Bae Ko and Nitin H. Vaidya. Location-Aided Routing (LAR) in Mobile Ad Hoc Networks. Proceedings of the 4th Annual ACM/IEEE International Conference on Mobile Computing and Networking (Mobicom_98), November 1998; 66-75. Dallas.

[8] Ming-Yee Iu. Selective Flooding in Ad Hoc Networks [dissertation]. University of Waterloo, Waterloo, Ontario, Canada, 2002.

[9] I. Eltahir. The Impact of Different Radio Propagation Models for Mobile Ad Hoc Networks (MANET). Proceedings of the 2nd International Conference on Wireless Broadband and Ultra Wideband . 2007. 30-32.

[10] Royer. E .Perkins. Ad Hoc On Demand Distance Vector Routing. Proceedings of 2nd IEEE Workshop on Mobile Computing Systems and Applications; 1999.

[11] Najla Al-Nabhan, Bowu Zhang, Mznah Al-Rodhaan, Abdullah Al-Dhelaan: Two Connected Dominating Set Algorithms for Wireless Sensor Networks. WASA 2012: 705-713.

[12] Muneer Bani Yassein, B. Abed Al-Hameed, Constandinos X. Mavromoustakis: Adaptive counter-based broadcasting scheme in mobile ad hoc networks. HP-MOSys 2012:47-52.

[13] Marios C. Charalambous, Constandinos X. Mavromoustakis, Muneer Bani Yassein: A Resource Intensive Traffic-Aware Scheme for Cluster-based Energy Conservation in Wireless Devices. HPCC-ICESS 2012:879-884.

Simulation of a WiMAX network to evaluate the performance of MAC IEEE 802.16 during the IR phase of Network Entry and Initialization

Namratha M
Mtech in Software Engineering,
Department of Information Science,
PESIT Bangalore, India

Pradeep
Mtech in Software Engineering,
Department of Information Science,
PESIT Bangalore, India

Manu G V
BE, MBA, Mtech in Computer Science, SJCIT, Chikkabalapur
Technical Lead-Testing, Calsoft Labs, Bangalore, India

***ABSTRACT*—Pervasive Computing is also called as Ubiquitous Computing, which means "being present everywhere at once" or "constantly encountered". The main idea behind making these pervasive computing systems is that these systems improve living by performing computations on their own, without having to be monitored by anyone. These systems are targeted to become invisible to the user i.e., they perform their tasks without the user's knowledge.**

To achieve this environment, the underlying requirement is a Network. One of the biggest constraints in achieving this environment is the "Last Mile" problem. It refers to the last leg of delivering connectivity from a communications provider to a customer. In recent years there has been increasing interest shown in wireless technologies for subscriber access, as an alternative to traditional twisted-pair local loop.

WiMAX, Worldwide Interoperability for Microwave Access, is a Telecommunications technology that provides wireless transmission of data and is based on the IEEE 802.16 standard (also called Broadband Wireless Access). 802.16 uses paired radio channels Up Link Channel (UL) and Down Link Channel (DL) for establishing a communication between Base Station (BS) and Subscriber Station (SS). When a SS wants to establish connectivity with a BS it goes through the Network Entry and Initialization procedure of which Initial Ranging (IR) is a very important part. IR is the process of acquiring the correct timing offset and power adjustments such that the SS's transmissions are aligned to maintain the UL connection with the BS. All the SS's of a BS will compete for the contention slots for their network entry. Whenever the SS has to transmit the request packets it performs the Truncated Binary Exponential Backoff procedure. This method is the contention resolution procedure used in IEEE 802.16 networks.

Our focus here was to simulate a WiMAX network so as to evaluate the performance of MAC IEEE 802.16 during the IR phase of Network Entry and Initialization. We have used Network Simulator-2 (NS-2) for our simulation purposes. We are using WiMAX "patch" which simulates the PHY and the MAC features of a WiMAX network. We have evaluated the performance of MAC IEEE 802.16 for various topologies.

Keywords—Backoff delay; Circular topology; Linear topology; Markov Model; Pervasive computing; Ubiquitous computing; WiMAX

I. INTRODUCTION

Ubiquitous computing is roughly the opposite of virtual reality. Where virtual reality puts people inside a computer-generated world, ubiquitous computing forces the computer to live out here in the world with people.

Pervasive computing has many potential applications, from health and home care to environmental monitoring and intelligent transport systems. Pervasive computing systems[1] and services may lead to a greater degree of user knowledge of, or control over, the surrounding environment, whether at home, or in an office or car. They may also show a form of 'intelligence' that will make life easier. A few examples are worth mentioning here. A refrigerator can automatically signal the grocery shop once the milk or juice comes below a certain level, thus alleviating the owner from the task of notifying the grocery shop or going and buying. Various home appliances can become pervasive computing systems with similar 'intelligence', like a television that automatically switches on and tunes itself to a particular channel at a pre-defined time or an air conditioner that switches on automatically and brings the room to a specified temperature. A phone call can be made or answered only by gestures.

The main idea behind making these pervasive computing systems are, that these systems improve the living of the humans by performing the computation on their own, without having to be monitored by anyone. These systems are targeted to become invisible to the user i.e., they perform their tasks without the user's knowledge.

II. MATHEMATICAL ANALYSIS OF THE DELAY FOR THE IR SCHEME

In this section we analyze the IR scheme and evaluate mathematically the delay involved in the procedure. First we structure the IR mechanism as a set of distinct states with transitions among these states. Then this information is used to model IR as a Markov process [1]. In a Markov process, the probability of the system making a transition to a particular state depends only on the state the system is currently in.

Also, in this Markov process, we calculate the delays associated with the transitions between the states. Finally, by making use of the delays and probabilities associated with each of the transitions, we derive a mathematical equation describing the total IR delay. The Markov process is derived for IR in case of OFDMA PHY, since it covers all the steps in the OFDM based procedure as well. In case of the OFDMA PHY, Code Division Multiple Access (CDMA) codes are used instead of the RNG-REQ messages in the first part of the IR procedure.

A. *Modeling IR as a Markov Process*

Markov processes[2] provide very flexible, powerful, and efficient means for the description and analysis of dynamic (computer) system properties. Performance and dependability measures can be easily derived. Moreover, Markov processes constitute the fundamental theory underlying the concept of queuing systems. In fact, the notation of queuing systems has been viewed sometimes as a high-level specification technique for (a sub-class of) Markov processes. A stochastic process is defined as a family of random T, which is usually called the time parameter if T is a subset of the set of positive real numbers. The set of all possible values of X_t (for each $t \in T$) is known as the state space S of the stochastic process. A large number of stochastic processes belong to the important class of Markov processes. A stochastic process is a Markov process when the future state of the process depends only the current state and not on the history of the system. A Markov process is a memory-less stochastic process.

After analyzing the Initial Ranging procedure [3], we enumerate the following states as well as transitions needed for modeling the procedure.

State 1: Waiting for UL-MAP. This is also the start state.

State 2: SS is performing Backoff procedure.

State 3: Waiting for an RNG-RSP message from BS.

State 4: Continue

State 5: Success State – Wait for CDMA Allocation IE.

State 6: Abort – Start network entry procedure at a different DL channel

State 7: Waits for RNG-RSP again.

State 8: Proceed to next phase of network entry

State 9: Commence Periodic Ranging

The transitions among the states are as follows. In State 1, the SS waits for a UL-MAP. After receiving this message it makes a transition to State 2. Transmission of CDMA code occurs at end of State 2. Also a timer is set for waiting for RNG-RSP message. This transition leaves the system in State 3. When in State 3, if the timer for RNG-RSP expires then SS increments the power level and goes back to State 1. When in State 3, if RNG – RSP is obtained with Ranging code as well as the Ranging slot, then it makes a transition to State 4. Here the necessary adjustments specified in RNG-RSP are made and system moves to State 1.

When in State 3, if RNG-RSP is obtained with success status, then the system transits to State 5. Here it waits for CDMA Allocation IE. After reception it sends RNG-REQ message on the allocated bandwidth and moves to State 7. When in State 7, on reception of RNG-RSP with success status it moves to State 8. On reception of RNG-RSP with continue status it moves to State 9. Else on reception of RNG-RSP with abort status, it goes to State 6 and SS starts the network entry procedure again. When in State 3, if RNG-RSP is obtained with abort status then the system goes to State 6 and SS starts the network entry procedure again. The following matrix diagram shows the transition probability matrix for IR. Using these probabilities we design the Markov process representation of IR. The states 6, 8 and 9 lead out of IR and are the absorbing states. For these states, transition occurs back to the same state with a probability one. In states 3 and 7, the outgoing probabilities are marked with algebraic symbols a1 to a4 and b1 to b3. This is because the probabilities of the transitions originating from these states are non-deterministic in nature. The sum of probabilities of all transitions originating from states 3 and 6 are still equal to 1. Next, the transition matrix is used to obtain the overall delay formula.

The details of the delays [4] involved along with the associated probabilities are given in the table 2.

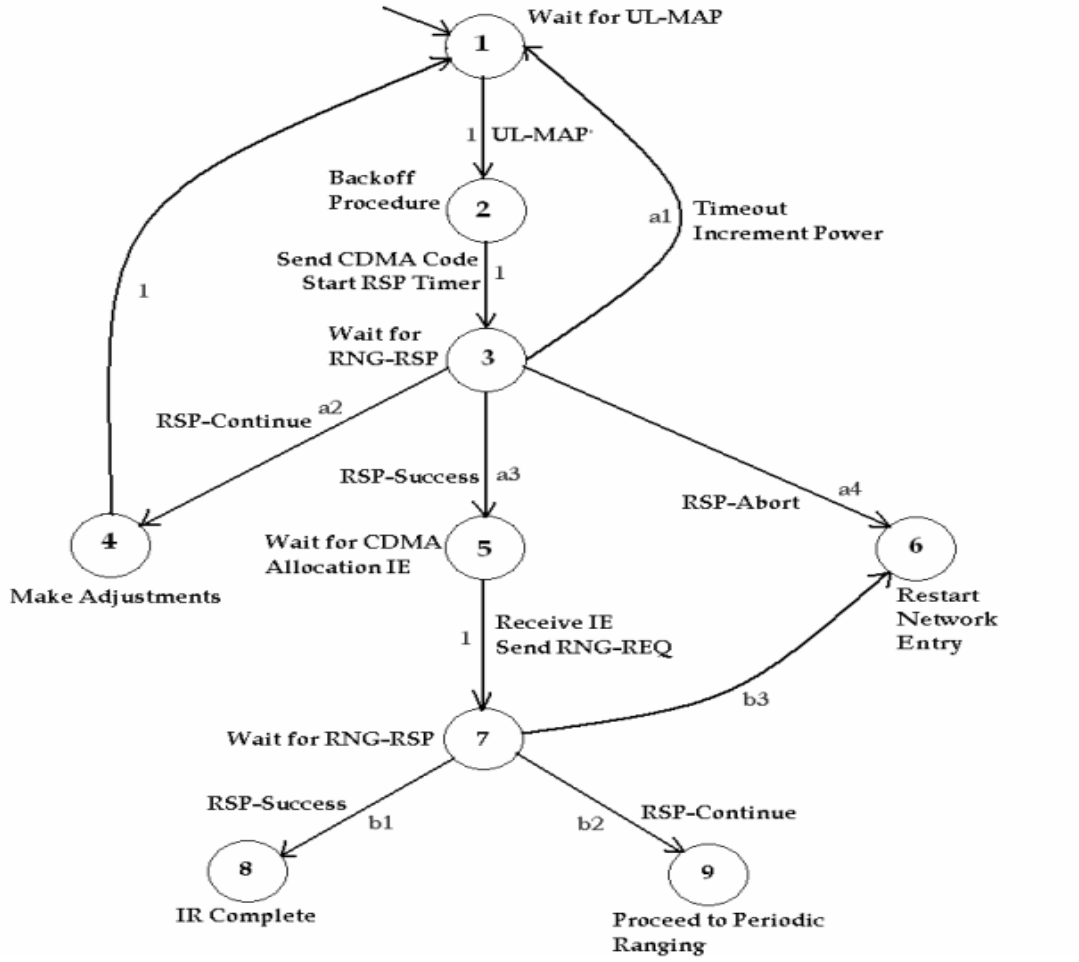

Fig.1. IR Procedure as a Markov Process

Table 2-Delay components in IR

Delay Involved	Probabilities
UL-MAP Reception (1 to 2)	1
Backoff Delay + Sending CDMA (2 to 3)	1
RNG-RSP Timeout (3 to 1)	a1
RNG-RSP Reception + Processing (3 to 4, 5 or 6)	a2,a3,a4
IE Allocation Delay + Sending RNG-REQ (5 to 7)	1
RNG-RSP Reception + Processing (7 to 8, 9 or 6)	b1,b2,b3

B. Mathematical Derivation of the Backoff Delay

Consider the first time an SS enters Backoff procedure [5]. Let the Initial Contention window be w. The random number will be picked in the range [0, w-1]. Let this random number be called k. The SS has to defer a total of k contention slots (CSs). Let the number of CSs in a frame be n. The number of frames that have to be deferred is k / n.00cscs. The delay involved here will be (k / ncs) * frame length. After k / ncs frames have passed the SS defers a further k modulo ncs CSs. The delay involved here is equal to (k % n cs) * Tcs, where Tcs is the length of one CS and % denotes the modulo operation. Therefore the total delay incurred so far is (k / n_{CS}) * frame length + (k % n_{CS}) * T_{CS}. Here the value of k can vary from 0 to w_0-1. Thus, we take an average of the delay over the random number.

AD_0 = (1/w_0) *Sum of [(k/n_{CS})*frame length + (k % n_{CS})*T_{CS}] as k varies from 0 to w_0-1.

Next we make an assumption that the probability of a successful transmission in a CS is ‘p’. Thus, probability of failure will be ‘1-p’. In case of a failure the contention window is doubled in size. Let the new window be equal to [0, w_1-1]. Similar to previous derivation the delay involved will be

AD_1 = (1/w_1) *Sum of [(k/n_{CS})*frame length + (k% n_{CS})*T_{CS}] as k varies from 0 to w_1-1.

Here w_1 = 2 * w_0.

Again there could be success or failure. So, it will enter the third Backoff window phase [0, w_2-1]. Continuing in this fashion, we get the following delays for the next three phases.

AD_2 = (1/w_2) *Sum of [(k/ n_{CS})*frame length + (k% n_{CS})* T_{CS}] as k varies from 0 to w_2-1.

AD_3 = (1/w_3) *Sum of [(k/ n_{CS})*frame length + (k% n_{CS})* T_{CS}] as k varies from 0 to w_3-1.

AD_4 = (1/w_4) *Sum of [(k/ n_{CS})*frame length + (k% n_{CS})* T_{CS}] as k varies from 0 to w_4-1.

Here w_2 = 2 * w_1, w_3 = 2 * w_2 and w_4 = 2 * w_3.

We make another assumption at this point. The SS is assumed to complete successful transmission of its CDMA code, in a maximum of 5 Backoff phases. Thus, the worst case of transmission will be four failures followed be a success. The final formula for the delay will be as follows.

$$\text{Backoff Delay (BD)} = p*\{AD_0 + t/2\}$$
$$+ ((1-p))*p*\{[AD_0 + t] + [AD_1 + t/2]\}$$
$$+ ((1-p)^2)*p*\{[AD0 + AD_1 + 2t] + [AD_2 + t/2]\}$$
$$+ ((1-p)^3)*p*\{[AD0 + AD_1 + AD_2 + 3t] + [AD_3 + t/2]\}$$
$$+ ((1-p)^4)*p*\{[AD0 + AD_1 + AD_2 + AD_3 + 4t]$$
$$+ [AD_4 + t/2]\}$$

Here t is the time-out after which failure is assumed. So, we take half that value for success i.e. t/2.

C. Mathematical Derivation of the Overall IR delay

By traversing the transition diagram[6] and multiplying the probabilities with the corresponding delays, the total delay can be calculated. The first part of the delay is in the loops 1-2-3-1 and 1-2-3-4-1. We call this D_{loop}. Then either success or abort occurs which is added to this part to get the final formula.

D_{loop} = 1*UL-MAP + 1*(BD + CDMA sending) + a_1 * (Timeout T3 + D-loop) + a_2 * (RSP + D-loop) Simplifying we get,

Now, the total delay involved can be represented

$$D_{loop} = \frac{1- (a_1+a_2)UL + BD + CDMA\ sending + a_1*T3 + a_2*RSP}{1- (a_1+a_2) + a_3* (RSP + CDMA\_IE + RNG\text{-}REQ + RSP) + a_4 * RSP}$$

Now, the total delay involved can be represented using the formula given below.

D_{total} = D_{loop} + a_3 * (RSP + CDMA_IE + RNG-REQ + (b_1+ b_2 + b_3)*RSP) + a_4 * RSP

(here b_1 + b_2 +b_3 = 1)

Substituting the expression for the delay in the loop into the formula for overall delay in IR, we get the following final formula.

$$D_{loop} = \frac{UL + BD + CDMA\ sending + a_1*T3 + a_2*RSP}{1- (a_1+a_2) + a_3* (RSP + CDMA\_IE + RNG\text{-}REQ + RSP) + a_4 * RSP}$$

III. Working Of The Code

A. TCL script

The Tcl file [8],[9] contains the codes to run the simulation for 1 base station and variable number of mobile station. The file accepts the following arguments

i. The number of mobile nodes/stations
ii. The seed value (for random number generation)

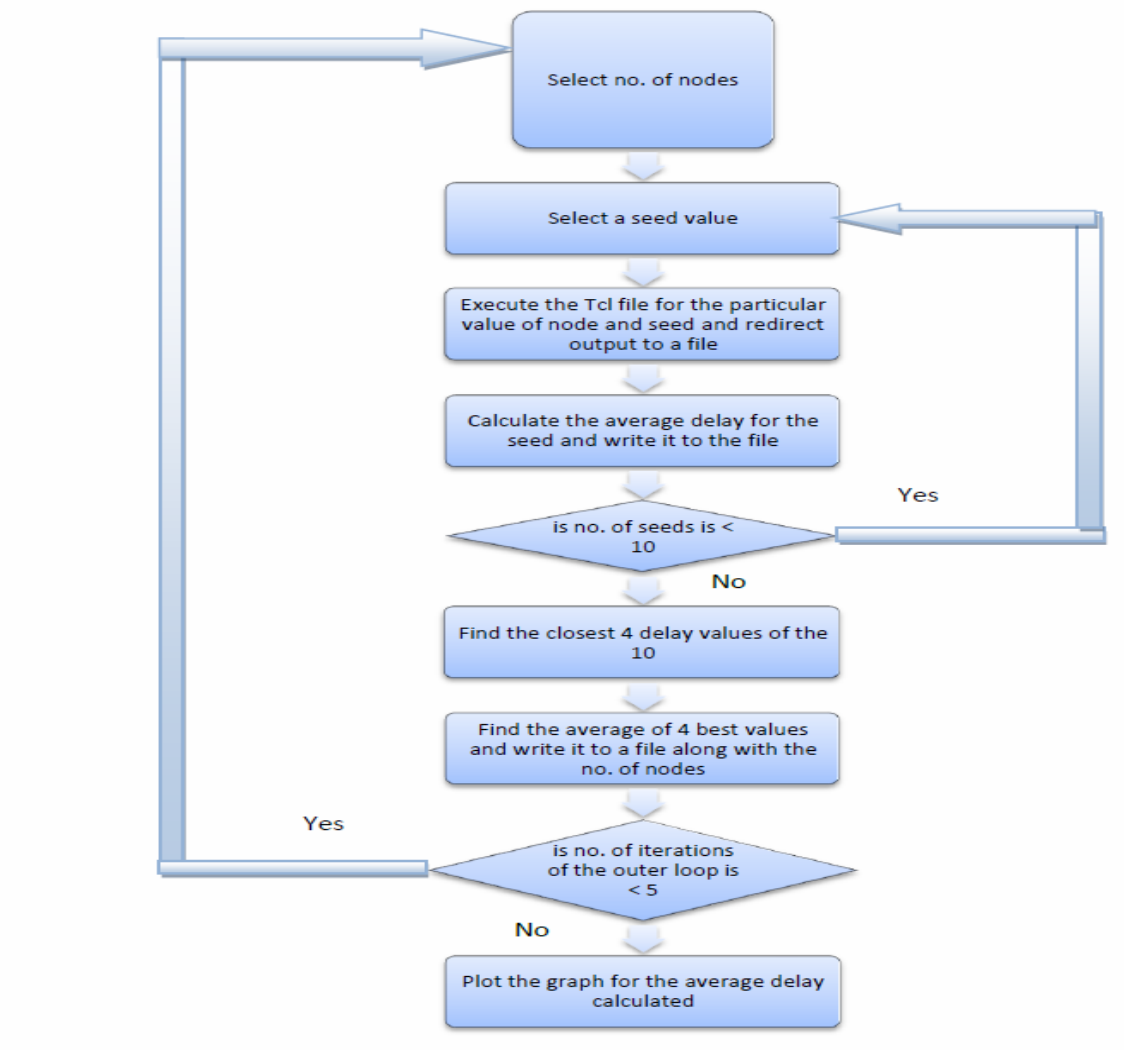

Fig.2. Process Flow

```
set nb_mn [lindex $argv 0]
set enteredSeed [lindex $argv 1]                    ;# max number of mobile node
set packet_size          1500                       ;# packet size in bytes at CBR
Applications
set output_dir .
set gap_size 1 ;#compute gap size between packets
puts "gap size=$gap_size"
set traffic_start 5 set traffic_stop    20          set
simulation_stop 30
set diuc 7 ;#modulation for MNs
Mac/802_16 set debug_ 0
Mac/802_16 set rtg_ 20
Mac/802_16 set ttg_ 20
Mac/802_16 set client_timeout_ 50                   ;#to avoid BS disconnecting the
SS
Phy/WirelessPhy/OFDM set g_ 0.25
#define debug values
Mac/802_16 set debug_ 1
Mac/802_16 set print_stats_ 1
Mac/802_16 set t21_timeout_ 20
```

```
#Fix: instead of using the send-scan manually, use a link going down trigger
Mac/802_16 set lgd_factor_ 1.8                    ;#note: the higher the value the earlier the trigger
Mac/802_16 set client_timeout_ 60 ;#to avoid BS disconnecting the SS
Agent/WimaxCtrl set adv_interval_ 1.0
Agent/WimaxCtrl set default_association_level_ 0
Agent/WimaxCtrl set synch_frame_delay_ 0.5
Agent/WimaxCtrl set debug_ 1

#define coverage area for base station: 20m coverage
Phy/WirelessPhy set Pt_ 0.025
Phy/WirelessPhy set RXThresh_ 2.025e-12 ;#500m radius
Phy/WirelessPhy set CSThresh_ [expr 0.9*[Phy/WirelessPhy set RXThresh_]]
# Parameter for wireless nodes
set opt(chan)                   Channel/WirelessChannel          ;# channel type
set opt(prop)                   Propagation/TwoRayGround         ;# radio-propagation
model
set opt(netif)                  Phy/WirelessPhy/OFDM             ;# network interface type
set   opt(mac)                  Mac/802_16/BS                    ;#   MAC type
set   opt(ifq)                  Queue/DropTail/PriQueue          ;#   interface queue type
set   opt(ll)                   LL                               ;#   link layer type
set   opt(ant)                  Antenna/OmniAntenna              ;#   antenna model
set   opt(ifqlen)               50                    ;#   max packet in      ifq
set   opt(adhocRouting)         DSDV                             ;# routing      protocol
set opt(namtr)                  newrng-irmsa.nam                 ;# for the nam trace file
set   opt(tr)           newrng-irmsa.tr                          ;# for the trace file
set   opt(x)            1100                          ;#   X  dimension of the topography
set   opt(y)            1100                          ;#   Y  dimens
```

The above are used to setup the WiMAX environment [10],[11] by assigning appropriate values to the various parameters.

```
set ns [new Simulator]
$ns use-newtrace
#create the topography
set topo [new Topography]
$topo load_flatgrid $opt(x) $opt(y)
#puts "Topology created"
#nam
set nf [open newrng-irmsa.nam w]
$ns namtrace-all-wireless $nf $opt(x) $opt(y)
#open file for trace
set tf [open newrng-irmsa.tr w]
$ns trace-all $tf
puts "Output file configured"

global defaultRNG
$defaultRNG seed $enteredSeed
# set up for hierarchical routing (needed for routing over a basestation)
#puts "start hierarchical addressing"
$ns node-config -addressType hierarchical
AddrParams set domain_num_ 2                              ;# domain number lappend cluster_num 1 1
                                                  ;# cluster number for each domain
AddrParams set cluster_num_ $cluster_num
lappend eilastlevel 1 [expr ($nb_mn+1)]           ;# number of nodes for
each cluster (1 for sink and one for mobile nodes + base station
AddrParams set nodes_num_ $eilastlevel
puts "Configuration of hierarchical addressing done"
```

```
# Create God
Create-god [expr ($nb_mn + 2)]                    ;# nb_mn + 2 (base station and sink node)
#puts "God node created"
```

The above lines are used to setup the simulation environment [12], which includes-

i. Creating a new instance of the ns2 simulator
ii. Creating a new topology
iii. Configuring the nam and trace files
iv. Specifying that the entered value of the seed should be used by the default Random Number Generator
v. Creating an address hierarchy, and configuring it *
vi. Creating a 'God object'. The number of mobile nodes is passed as argument which is used by God to create a matrix to store connectivity information of the topology

```
set sinkNode [$ns node 0.0.0]
#provide some co-ord (fixed) to base station node
$sinkNode set X_ 600.0
$sinkNode set Y_ 500.0
$sinkNode set Z_ 0.0
#puts "sink node created"
#creates the Access Point (Base station)
$ns node-config -adhocRouting $opt(adhocRouting) \
                -llType $opt(ll) \
                -macType Mac/802_16/BS \
                -ifqType $opt(ifq) \
                -ifqLen $opt(ifqlen) \
                -antType $opt(ant) \
                -propType $opt(prop)          \
                -phyType $opt(netif) \
                -channel [new $opt(chan)] \
                -topoInstance $topo \
                -wiredRouting ON \
                -agentTrace ON \
                -routerTrace ON \
                -macTrace ON        \
                -movementTrace OFF
puts "Configuration of base station"

set bstation [$ns node 1.0.0]
$bstation random-motion 0
#puts "Base-Station node created"
#provide some co-ord (fixed) to base station node
$bstation set X_ 550.0
$bstation set Y_ 550.0
$bstation set Z_ 0.0
[$bstation set mac_(0)] set-channel 0
```

The above lines are used to-

i. Create a sink node. The sink node acts as a dropped target (any packets dropped at the base station are sent to the sink node.)
ii. Change the node configuration and create a base station

```
$ns node-config -macType Mac/802_16/SS \
                -wiredRouting ON \
                -macTrace ON                    ;# Mobile nodes cannot do
                                                Routing.
```

The following lines are used for configuring the mobile node-

```
set wl_node [$ns node 1.0.[expr $i + 1]] ;# create the node with particular        #address
$wl_node random-motion 0
$wl_node base-station [AddrParams addr2id [$bstation node-addr]]
$wl_node set X_ [expr 340.0+$i*10]
```

```
$wl_node set Y_ [expr 550.0-$i*10]
$wl_node set Z_ 0.0
$ns at 0 "$wl_node setdest 1060.0 550.0 1.0" puts "wireless node $i created ..."
[$wl_node set mac_(0)] set-channel 0 [$wl_node set mac_(0)] set-diuc
$diuc
```

The above lines are used for the following

i. Creating the mobile node and setting the location of the node in the topology created
ii. Disabling the random motion of the nodE
iii. Establishing the connection with Base Station(BS)
iv. Setting the motion for the mobile node
v. Setting the channel and Downlink Interval Usage Code(DIUC)

```
set udp [new Agent/UDP]
$udp set packetSize_ 100
$ns attach-agent $wl_node $udp
```

These lines set up the UDP agent for each of the mobile node

```
set cbr [new Application/Traffic/CBR]
$cbr set packetSize_ 100
$cbr set rate_ 0.2Mb
$cbr attach-agent $udp
```

The above lines help in setting up a Constant Bit Rate (CBR) traffic source ,which is then attached to a UDP agent ('udp' in this case). The mobile nodes cannot exchange data on their own. They must have agents attached to them for this purpose. In simple words, traffic sources create traffic (packets), and agents exchange them.

```
# Create the Null agent to sink traffic set null [new Agent/Null]
$ns attach-agent $sinkNode $null
# Attach the 2 agents
$ns connect $udp $null
```

The above lines set up a Null agent[13] (whose default behavior is to receive packets). Then the UDP agent and the Null agent are connected to establish a link between two nodes.

The above 4 code snippets are placed inside a for loop, which iterates 'n' number of times , where n is the number of mobile stations i.e. the for loop creates n mobile stations.

```
$ns at $traffic_start "$cbr start"
$ns at $traffic_stop "$cbr stop"
```

The above lines initiates and terminates the traffic source which will be in a for loop whose termination condition will be number of nodes at the time specified in the variables traffic_start and traffic_stop.

```
proc finish {} {
        global ns tf out.txt nb_mn nf
        $ns flush-trace
        close $tf close $nf
        exec nam newrng-irmsa.nam &
}
```

This procedure is used to flush the trace of NAM output and close all the open file descriptor which was used for trace file and nam trace file. It also executes the nam file.

The above indicates to the simulator to stop the simulation at the time specified in variable simulation_stop.

```
$ns at $simulation_stop "finish"
```

```
$ns run
```

The above line marks the starting point for the simulation.

B. Shell Script[14],[15]

1. for nodes in 4 8 16 32 40

This line initializes an array which contains the number of nodes for which we are going to be running the simulation(s).

2. for seed in 1973272912 1822174485 1998078925 678622600 999157082 934100682 558746720 2081634991 144443207 513791680

This line initializes an array which contains the seed values for which we are going to be running the simulation(s).

3. ns newrng-irmsa.tcl $nodes $seed > out.txt

This line runs the ns command for the file newrng-irmsa.tcl, passing $node and $seed as parameters. The output is redirected into the file out.txt.

4. grep "found ranging opportunity" out.txt | cut -d " " -f 2 > startTime.txt

This line searches the file out.txt for lines containing "found ranging opportunity", which indicates that a ranging opportunity has been found at the specific times. The lines thus selected are passed to the cut function, where we select the 2nd column (field). The values in this column are stored in startTimes.txt, which thus contains the times at which the nodes start the initial ranging procedure.

5. grep "Ranging response" out.txt | cut -d " " -f 2 > endTime.txt

This line searches the file out.txt for lines containing "Ranging Response", which indicates that a ranging response has been found at the specific times. The lines thus selected are passed to the cut function, where we select the 2nd column (field). The values in this column are stored in endTimes.txt, which thus contains the times at which the nodes finish the initial ranging procedure.

6. nl -n ln endTime.txt | tr -d '\t' | tr -s ' '> ourNewEndTimes.txt nl -n ln startTime.txt | tr -d '\t' | tr -s ' '>
ourNewStartTimes.txt

These two lines add lines numbers, deleted tabs and compress spaces in the files startTimes.txt and endTimes.txt, and store the results in ourNewStartTimes.txt and ourNewEndTimes.txt respectively. The adding of lines, deletion of tabs and compression of spaces is needed for further steps.

```
8. lineVar=0
   total_delay=0
   while [ $lineVar -lt $nodes ]
   do
         #echo "$total_delay + ${delay[$li
         total_delay=`echo "$total_delay +
         lineVar=`expr $lineVar + 1`
   done
```

These lines calculate the total delay, for a particular value of nodes and seed. The total delay is simply the sum of delays for individual nodes.

9. avg=`echo "scale=10; $total_delay / $nodes" | bc`

This line calculates the average delay for a particular value of nodes and seed. The average delay is the total delay, divided by the number of need.

7.newCounter=1

```
while [ $newCounter -le $nodes ]
do
endt=`grep ^"$newCounter " ourNewEndTimes.txt | cut -d " " -f 2` startt=`grep ^"$newCounter " ourNewStartTimes.txt | cut -d " " -f 2` delay[`expr $newCounter - 1`]=`echo $endt - $startt | bc` newCounter=`expr $newCounter + 1`
done
```

These lines calculate the delays for all nodes. The start times are obtained from ourNewStartTimes.txt and the end times are obtained from ourNewEndTimes.txt. The delay for a node is the difference between the end time and start time for that particular node. We find the delay for all nodes by using a while loop, which iterates n number of times, where n is the number of nodes for this particular simulation. The delays are stored in an array called delay.

10. Echo "$nodes $seed $avg" >> finalAvg$nodes.txt

This line send the number of nodes, seed value and average delay for a particular simulation into a file called finalAvg$nodes.txt. The average delay for 4 nodes, and different seeds, will be stored in a file called finalAvg4.txt, and the average delay for 8 nodes, and different seeds, will be stored in a file called finalAvg8.txt, and so on.

11. Steps 3 to 10 are performed for all seed values in the array called seed (10 values), using the variable seed.

12. Steps 3 to 11 are performed for all node values in the array called node (5 values), using the variable nodes.

IV. Simulation Results

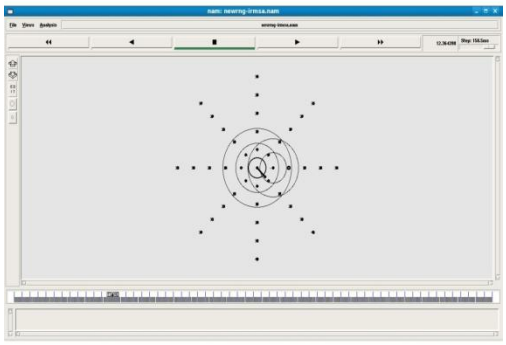

Fig.3. Circular Topology with No Motion

No. of nodes	Average Delay
4	0.107043
8	0.2336790937
16	0.3319343906
32	0.5845947968

Table 3- Average Delay for Circular topology with no motion

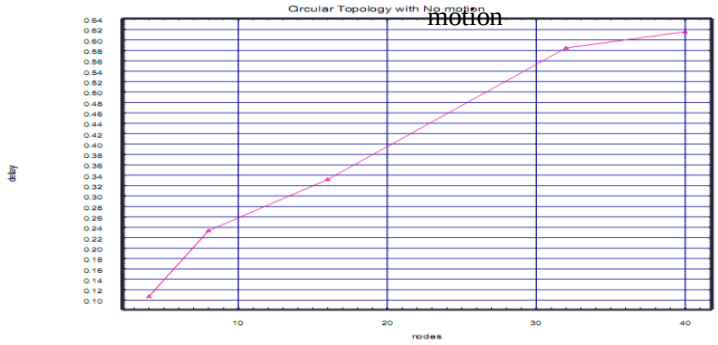

Fig.4. Delay Graph for Circular Topology with No Motion

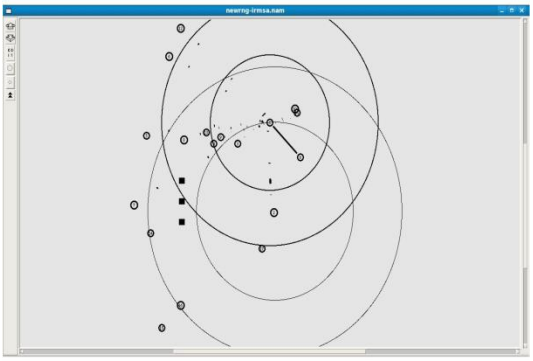

Fig.5. Circular Topology with Random Motion

No of nodes	Average Delay
4	0.1060478750
8	0.1580645937
16	0.4885501400
32	0.6211589296
40	0.63626995621

Table 4-Average Delay for Circular topology with random motion

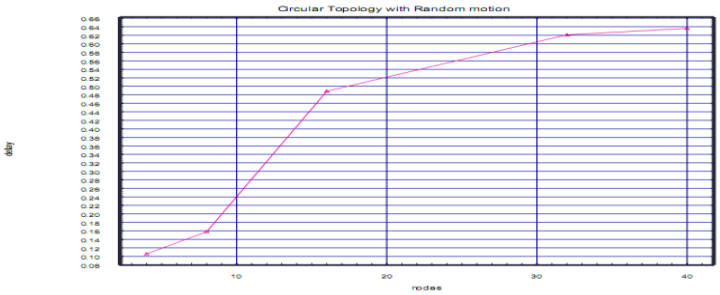

Fig.6. Delay Graph for Circular Topology with Random Motion

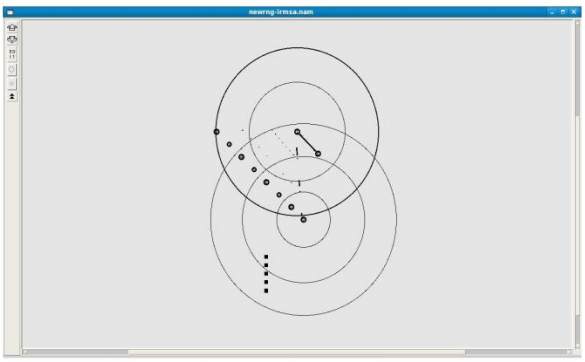

Fig.7. Linear Topology with Linear Motion

No of nodes	Average Delay
4	0.1070430000
8	0.2033068437
16	0.4859907031
32	0.6827474921
40	0.6965447375

Table 6-Average Delay for Linear topology with linear motion

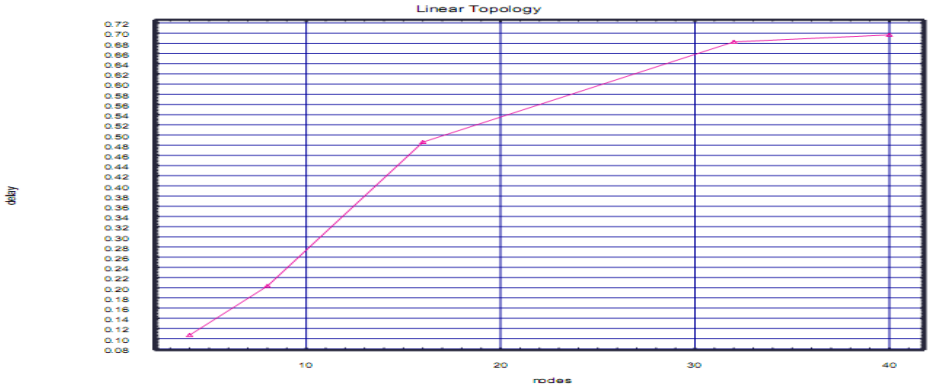

Fig.8. Delay Graph for Linear Topology with Linear Motion

REFERENCES

[1] Fundamentals of WiMAX by Jeffrey G. Andrews, Arunabha Ghosh, Rias Muhamed
[2] IEEE Standard for Local and metropolitan area networks Part 16: Air Interface for Fixed Broadband Wireless Access Systems by LAN/MAN Standards Committee of the IEEE Computer Society and the IEEE Microwave Theory and Techniques Society
[3] The Design and Implementation of WiMAX Module for ns-2 Simulator by Jenhui Chen,Chih-Chieh Wang,Frank Chee-Da Tsai,Chiang-Wei Chang,Syao-Syuan Liu,Jhenjhong Guo, Wei-Jen Lien, Jui-Hsiang Sum, and Chih-Hsin Hung
[4] The ns Manual by the VINT project
[5] Evaluation and Enhancement of the Initial Ranging Mechanism for MAC 802.16 inWiMAX Networks by R. Bhakthavathsalam and Aniruddha Niranjan
[6] The Network Simulator NS-2 NIST add-on IEEE 802.16 model (MAC+PHY)
[7] Tutorial for the Network Simulator "ns" by Marc Greiss
[8] cl/Tk: A Developer's Guide by Clif Flynt
[9] On Shortcomings of the ns-2 Random Number Generator by Bernhard Hechenleitner and Karl Entacher
[10] Experiences with the ns-2 Network Simulator - Explicitly Setting Seeds Considered Harmful by Martina Umlauft and Peter Reichl
[11] Deploying Mobile WiMAX By Max Riegel, Aik Chindapol, Dirk Kroeselberg
[12] Introduction to Network Simulator NS2 by Teerawat Issariyakul and Ekram Hossain
[13] NS Simulator for beginners by Eitan Altman and Tania Jimenez
[14] WiMAX Networks: Techno-Economic Vision and Challenges by Ramjee Prasad, Fernando J. Velez
[15] http://ieeexplore.ieee.org/xpl/login.jsp?tp=&arnumber=4446432&url=http%3A%2F%2Fieeexplore.ieee.org%2Fxpls%2Fabs_all.jsp%3Farnumber%3D4446432

Joint Operation in Public Key Cryptography

Dragan Vidakovic[1], Olivera Nikolic, Jelena Kaljevic[1]
Faculty of Business Valjevo, Singidunum
University Belgrade, Serbia

Dusko Parezanovic[2]
Club of young math. and computer scientists
Infomat Ivanjica, Serbi

***Abstract*—We believe that there is no real data protection without our own tools. Therefore, our permanent aim is to have more of our own codes. In order to achieve that, it is necessary that a lot of young researchers become interested in cryptography. We believe that the encoding of cryptographic algorithms is an important step in that direction, and it is the main reason why in this paper we present a software implementation of finding the inverse element, the operation which is essentially related to both ECC (Elliptic Curve Cryptography) and the RSA schemes of digital signature.**

Keywords—Public-key cryptography; RSA & ECC Digital Signature; Inverse element; Code

I. INTRODUCTION

It has already been mentioned that we believe the best protection is achieved by developing our own software. However, this process requires a lot of knowledge, skills, patience and great responsibilities [7], provided that the undisputed cryptic of cryptography itself was previously overcome and that there are courage and willingness to enter more deeply into the matter.

In this paper we want to show that it is possible to implement the inverse element without any software-hardware facilities (in the arithmetic of large numbers), which is a very important operation in the process of realization of both leading schemes of a public key – ECC and RSA [1] [4] [6].

II. TASK AND AIM

In the arguments for and against in a trial of strength of ECC and RSA, the simple fact that they are performed by the same tools made for operations with large numbers, is usually overlooked. Mathematical bases of RSA and ECC are completely different [1] [5], but they need the same operations: addition, subtraction, multiplication, division, finding the remainder, calculating d from the equation $e*d \equiv 1 \pmod p$ for fixed values of e and p, and more joint auxiliary operations needed for the realization of a digital signature.

When it comes to joint operations, we have opted for finding the inverse element. Therefore, we will present a brief review of the RSA and ECC and point out those steps in algorithms in which it is necessary to calculate the inverse element.

A. Algorithm Key Generation for the RSA Signature Scheme

As we can see, for the given public key e and the number ϕ, d should be calculated from the equation in order to get e private key – the most important element of the RSA digital signature scheme, or, in other words, we should find the inverse element of the element e.

Sumary: each entity creates an RSA public key and a corresponding private key. Each entity A should do the following [1]:

1) Generate two large distinct random primes p and q, each roughly the same size (see x11.3.2).
2) Compute n = pq and $\phi = (p - 1)(q - 1)$.
3) Select a random integer e, $1 < e < \phi$ such that gcd(e, ϕ) = 1.
4) Use the extended Euclidean algorithm ([2]) to compute the unique integer
d, $1 < d < \phi$, such that $ed \equiv 1 \pmod \phi$)
5) A's public key is (n; e); A's private key is d

As we can see for a given public key e and modulo ϕ, we have to find inverse element d- secret key- for RSA digital signature. So, finding the inverse element is very important stage the RSA signature scheme.

B. The shortest of the ECC

Efficient and secure public-key cryptosystems are essential in today's age of rapidly growing Internet communications. Elliptic curve scalar multiplication in particular, which refers to the operation of multiplying a large integer by a point on an elliptic curve, is crucial for both data encryption technology as well as testing the security of cryptographic systems.[5]

In reality it's very hard to find k (large number) that k*P=Q where P and Q are given points on an Eliptic curve.(P, Q are public keys, and k is private or secret key)

Practicaly we have to solve *P+P and P+Q to* get thrid point R=P+P or R=P+Q.

To put it simply, in the field, say F_p , where p is prime, for two points $P(x_p,y_p)$, $Q(x_q,y_q)$ on an elliptic curve, using chord-tangent-rule, to give the third elipting curve point $R(x_r,y_r)$.

Coordinates of the third point are calculated by the following formulas:

$x_r = ((y_q - y_p)/ (x_q - x_p))^2 - x_p - x_q$,
$y_r = ((y_q - y_p)/ (x_q - x_p))(x_p - x_r) - y_p$
It is obvious that it is very important to find $(x_q - x_p)^{-1}$

III. CODE FOR FINDING THE INVERSE ELEMENT

In the previous paragraph, we pointed out the place and significance of finding the inverse element of a fixed element in the field Fp, where p is a prime. Since our goals are to avoid the general story and to develop the software that can operate in real conditions (with large numbers), in this paragraph we will present the code by which we can solve the equation ed ≡

1 (mod ϕ) for (arbitrarily) large fixed number ϕ and the fixed e.

A. *The Code for Calculating the Inverse Element – Delphi 7 Console Application*

In order to calculate the inverse element, it is necessary to encode Binary extended gcd algorithm. For the fixed inputs e and ϕ, wwe will get the output d, and this will be the solution of the modular equation above.

```
Program for_inverse;
{$APPTYPE CONSOLE}
uses SysUtils, Unit22;
label 1,2;
var a,b,c,g,u,v,a1,b1,d:array[0..nn1] of integer;
gcd,w:array[0..nn] of integer;
i,s1,s2,i1,p1,c1:integer;
ff:file of integer;
 x,y,k:array[0..nn] of integer;
k1:longint;
begin
s1:=0; s2:=0;
writeln('calculating the inverse element');
 assign(ff,'brojfi.dat'); rewrite(ff);
   {Example module (10111)-binary, (23)-decimal}
    x[0]:=1;x[1]:=1;x[2]:=1;x[3]:=0;x[4]:=1;
write(ff,x[0]);write(ff,x[1]);write(ff,x[2]);write(ff,x[3]);write(f
f,x[4]);
reset(ff); i:=0;
while not eof(ff) do
begin
read(ff,x[i]); i:=i+1;
end;
assign(ff,'javni.dat'); rewrite(ff);
{Example elements (100)-binary, 4 decimal}
y[0]:=0;y[1]:=0;y[2]:=1;y[3]:=0;
write(ff,y[0]);write(ff,y[1]);write(ff,y[2]);write(ff,y[3]);
reset(ff); i:=0;
while not eof(ff) do
begin
read(ff,y[i]); i:=i+1;
end;
s1:=0; s1:=0;s2:=0;
  for i:=0 to nn do
 begin
 g[i]:=0;u[i]:=0;v[i]:=0;a[i]:=0;b[i]:=0;c[i]:=0;d[i]:=0;w[i]:=0;
  end;
    g[0]:=1;p1:=0;
   while ((x[0]=0) and (y[0]=0)) do
   begin
    for i:=1 to nn do  begin
    x[i-1]:=x[i]; y[i-1]:=y[i];end;
     for i:=nn-1 downto 0 do g[i+1]:=g[i];
  g[p1]:=0;p1:=p1+1; end;
     for i:=0 to nn do begin
   u[i]:=x[i]; v[i]:=y[i];end;
     a[0]:=1;b[0]:=0;c[0]:=0;d[0]:=1;
     1:   while u[0]=0 do
     begin
        for i:=1 to nn do u[i-1]:=u[i];
            if ((a[0]=0) and (b[0]=0)) then begin
               for i:=1 to nn do a[i-1]:=a[i];
                for i:=1 to nn do b[i-1]:=b[i];  end
                           else  begin
                          saberi(a,y,w);
                  for i:=1 to nn do w[i-1]:=w[i];
                  for i:=0 to nn do a[i]:=w[i];
                 oduzmi(b,x,w);
                  for i:=1 to nn do w[i-1]:=w[i];
                  for i:=0 to nn do b[i]:=w[i]; end;end;
    while v[0]=0 do begin
        for i:=1 to nn do v[i-1]:=v[i];
         if ((c[0]=0) and (d[0]=0)) then begin
            for i:=1 to nn do c[i-1]:=c[i];
             for i:=1 to nn do d[i-1]:=d[i]; end
                    else  begin
                   saberi(c,y,w);
                for i:=1 to nn do w[i-1]:=w[i];
                for i:=0 to nn do c[i]:=w[i];
                oduzmi(d,x,w);
                for i:=1 to nn do w[i-1]:=w[i];
                for i:=0 to nn do d[i]:=w[i]; end; veci1(v,s1);
end;
   i:=nn;veci1(u,s1);
   while u[i]=v[i] do i:=i-1;
   if i<0 then i:=i+1;
   if u[i]>=v[i] then  begin
     oduzmi(u,v,w);
    for i1:=0 to nn do u[i1]:=w[i1];
    oduzmi(a,c,w);
    for i1:=0 to nn do a[i1]:=w[i1];
    oduzmi(b,d,w);
    for i1:=0 to nn do b[i1]:=w[i1]; end
          else begin
            oduzmi(v,u,w);
    for i1:=0 to nn do v[i1]:=w[i1];
            oduzmi(c,a,w);
            for i1:=0 to nn do c[i1]:=w[i1];
      oduzmi(d,b,w);
    for i1:=0 to nn do d[i1]:=w[i1]; end;
         s1:=0;veci1(u,s1);
      if s1<>0 then goto 1;
       for i1:=0 to nn do a1[i1]:=c[i1];
            for i1:=0 to nn do k[i1]:=d[i1];
  s1:=0;   veci1(g,s1);   s2:=0;   veci1(v,s2);
if ((s1=1) and (g[0]=1) and (s2=1) and (v[0]=1)) then
begin
  s1:=0;
   veci1(k,s1);
  if s1<0 then begin
  for i:=0 to nn do
    k[i]:=abs(k[i]);
       oduzmi(x,k,k);
      end;
  dokle(y,s2);
```

```
 dokle(k,s2);
 assign(ff,'tajni.dat');
 rewrite(ff);
for i:=0 to s2 do
  write(ff,k[i]);
  reset(ff);    i:=0;
  while not eof(ff) do
  begin
    read(ff,k[i]);       i:=i+1;
    end;
    dokle(k,s2);
    for i:=s2 downto 0 do
    write(k[i]);   writeln;
 writeln('found a secret key for RSA-The inverse element for
ECC');
 readln;
   end
 else
 writeln('no inverse element, gcd(module,elements)<>1');
 readln;
  end.
```

B. The unit that serves the program above (III.A)

The program above, together with the unit Unit22, can be run as a Delphi 7 console application in order to do the testing and present the result of the two examples on both schemes of a public key.

Besides the basic operations in arithmetic of large numbers, the unit also contains some auxiliary functions.

```
unit Unit22;
 interface
{  for larger numbers set larger nn, nn1 }
const nn=100;
const nn1=100;
procedure saberi(x,y:array of integer;var w:array of integer);
procedure oduzmi(x,y:array of integer;var w:array of integer);
procedure veci1(var x:array of integer;var s:integer);
procedure  dokle(var a:array of integer;var s1:integer);
implementation
procedure saberi(x,y:array of integer;var w:array of integer);
var c1,i1,s1,s2:integer;
begin
s1:=0;s2:=0;veci1(x,s1);veci1(y,s2);
if ((s1>=0) and (s2>=0)) then begin
c1:=0;
for i1:=0 to nn1 do begin
  w[i1]:=(x[i1]+y[i1]+c1) mod 2;
  if (x[i1]+y[i1]+c1)<2 then c1:=0
              else c1:=1;end;
  w[nn1]:=c1; end
    else
  if ((s1>=0) and (s2<0)) then begin
  for i1:=0 to nn1 do y[i1]:=abs(y[i1]);
    oduzmi(x,y,w);end
       else
      if ((s1<0) and (s2>=0)) then begin
       for i1:=0 to nn1 do x[i1]:=abs(x[i1]);
          oduzmi(y,x,w);end
            else if ((s1<0) and (s2<0)) then begin
           for i1:=0 to nn1 do x[i1]:=abs(x[i1]);
             for i1:=0 to nn1 do y[i1]:=abs(y[i1]);
             saberi(x,y,w);
             for i1:=0 to nn1 do w[i1]:=-w[i1]; end; end;
  procedure oduzmi(x,y:array of integer;var w:array of
integer);
  label 1;
 var i1,c1,k,s1,s2:integer;
 begin
 s1:=0;s2:=0;veci1(x,s1);veci1(y,s2);
  if ((s1>=0) and (s2>=0)) then begin
  k:=0;
1: c1:=0;
 for i1:=0 to nn1 do begin
  w[i1]:=abs(x[i1]-y[i1]+c1) mod 2;
 if (x[i1]-y[i1]+c1 )>=0 then c1:=0
           else c1:=-1; end;
    if k=1 then
   c1:=0;
   if c1=-1 then begin
    for i1:=0 to nn do x[i1]:=0;
    for i1:=0 to nn do y[i1]:=w[i1];
     c1:=0;k:=1;goto 1;end;
    if k=1 then
    for i1:=0 to nn do w[i1]:=-w[i1];end
    else if ((s1>=0) and (s2<0)) then begin
       for i1:=0 to nn do y[i1]:=abs(y[i1]); saberi(x,y,w);
         end
       else if ((s1<0) and (s2>=0)) then begin
          for i1:=0 to nn1 do x[i1]:=abs(x[i1]);saberi(x,y,w);
          for i1:=0 to nn1 do w[i1]:=-w[i1];end
            else if ((s1<0) and (s2<0)) then begin
              for i1:=0 to nn1 do x[i1]:=abs(x[i1]);
                for i1:=0 to nn1 do y[i1]:=abs(y[i1]);
                oduzmi(y,x,w); end; end;
  procedure veci1(var x:array of integer;var s:integer);
       var i1:integer;
       begin
       s:=0;
       for i1:=0 to nn do s:=s+x[i1]; end;
procedure  dokle(var a:array of integer;var s1:integer);
begin
s1:=nn;
while a[s1]=0 do s1:=s1-1;
end;
 procedure koji(var u,v:array of integer;var l:integer);
 var i:integer;
 begin
 l:=0; i:=nn;
  while u[i]=v[i] do i:=i-1;
   if i<0 then l:=0
   else
   if u[i]>v[i] then l:=1
   else l:=-1;
   end;
```

end.

IV. EXAMPLES

Here, we will give two examples to illustrate the use of inverse element in RSA and ECC.

A. RSA example

In [2] we can find solutions of the equation ed ≡1 (mod ϕ) for fixed values e, and ϕ. More precisely, for the public key e, and a module ϕ we can calculate the secret key d, element required for RSA scheme.

If ϕ-module:

10000000000000000000000000000000000000000000000000000000000
000000000000000000000000000000000000000000000000000000000000000
000000000000000000000000000000000000000000000000000000000000000
000000000000000000000000000000000000000000000000000000000000000
000000010000000000000000000000000000000000000000000000000000000
000000000000000000000000000000000000000000000000000000000000000
000000000100000000000000000000000000100000000000000000000000000
000000000000000000000000100000000000000000000000000000000000000
110100011110100000000000000000000000000000000000000000000000000
000000000000000000000000000000000000000000000000000000000000000
000000000000010000000000000000000000000001000000000000000000000
000000000000000000000000000010000000000000000000000000000000000
000011010001111010000000000000000000000000100000000000000000000
000000010000000000000000000000100000000000000000000000000100000
000000110100011110000000000000000011010001111000000000000000000
000000000000000000000111100000010000000000000000000000000000101
0100001110100111000.

e-public key: 111

Then d-RSA secret key:

10010010010010010010010010010010010010010010010010010010010
010010010010010010010010010010010010010010010010010010010010010
010010010010010010010010010010010010010010010010010010010010010
010010010010010010010010010010010010010010010010010010010010010
010010100100100100100100100100100100100100100100100100100100100
100100100100100100100100100100100100100100100100100100100100100
100100101001001001001001001001001001101101101101101101101101101
10110110110110110110111001001001001001001001001001001001001001 1
001110010000100100100100100100100100100100100100100100100100100
100100100100100100100100100100100100100100100100100100100100100
100100100100110110110110110110110110111001001001001001001001001
001001001001001001001001001001011011011011011011011011011011011
011111001011010100100100100100100100100100101001001001001001001
001001011011011011011011011100000000000000000000000000000100100
100101100000100010010010010010011001110010000000000000000000000
000000000000000000001000100101001001001001001001001001001001111
0010100010111111.

B. ECC example

Let p=23. Consider an elliptic curve $y^2 = x^3 +x+4$ defined over F_{23} ($E(F_{23})$) [4]. Using code in III. A we can find coordinates of the point R=P+Q.

If P(4,7) and Q(13,11), based on the relation of II. B. we can calculate the x coordinate of the point R.

$x_r =((11-7)/(13-4))^2 -4-13$ (mod 23)

Using code (III. A.) we can calculate $(13-4)^{-1} =9^{-1}$.

Output on the screen:

calculating the inverse element

10010

found a secret key for RSA-The inverse element for ECC.

We can see that 10010 (base 2) is 18 (base 10). Indeed: 9*18=162, 162 mod 23=1, so 9^{-1} =18 is the inverse element. For further computation, the other necessary operations are located in Unit22 (subtraction and addition-In Serbian language *saberi, oduzmi)* and in [2], *mnozi, ostatatk (* multiplication, and the remainder in English) and many auxiliary functions, which we will show in the forthcoming paper.

V. CONCLUSION

We believe that each country must stimulate young people's interest in cryptography, because we doubt that our secret data can be protected using someone else's software [3].

Of course, it is very difficult to develop our own protection mechanisms, but we think it is far better to protect data using our own mechanisms first, and then, thus modified, leave them to someone else's software, than to allow the original data be protected by somebody else's mechanisms, which is a logical nonsense.

That is the reason why we always insist on more our own softwares and a greater interest in cryptography, which seems itself (in case it wasn't brought closer to a reader) pretty cryptic and bouncing. So, this work is primarily addressed to young researches as an incentive to try to develop their own tools for data protection. Those tools do not have to be flawless, they may be far below the level of the tools found on the market. However, they should be good enough for the beginning of a hard work that would lead researches to some great commercial solutions.

REFERENCES

[1] A. Menezes, P.C. van Oorschot, S. Vanstone, "Handbook of Applied Cryptography", CRC Press, New York, 1997.
[2] D. Vidaković, "Analysis and implementation of asymmetric algorithms for data secrecy and integrity protection", Master Thesis (mentor Jovan Golic), Faculty of Electrical Engineering, Belgrade,Serbia, 1999.
[3] D. Vidakovic, D. Simic, "A Novel Approach To Building Secure Systems", ARES 2007, Vienna, Austria, pp 1074-1084.
[4] Don Johnson, Alfred Menezes and Scott Vanstone, "The Elliptic Curve Digital Signature Algorithm (ECDSA)", Certicom Research, Canada, Dept. of Combinatorics & Optimization, University of Waterloo, Canada
[5] N. Koblitz, "Elliptic Curve Cryptosystems", Mathematics of Computations, 48, pp. 203-209, 1987.
[6] A. Menezes, "Elliptic curve public key cryptosystems", Kluwer Academic Publishers, 1993.
[7] D.Vidakovic, O. Nikolic, D. Parezanovic, "Acceleration Detection of Large (Probably) Prime Numbers", International Journal of UbiComp (IJU), Vol.4, No.1, January 2013

Diagnosing Learning Disabilities in a Special Education by an Intelligent Agent Based System

Khaled Nasser elSayed
Computer Sciences Department,
College of Computer and Information Systems, Umm-AlQura University
Makkah AlMokaramah, Saudi Arabia Kingdom

***Abstract*—The presented paper provides an intelligent agent based classification system for diagnosing and evaluation of learning disabilities with special education students. It provides pedagogy psychology profiles for those students and offer solution strategies with the best educational activities. It provides tools that allow class teachers to discuss psycho functions and basic skills for learning skills, then, performs psycho pedagogy evaluation by comprising a series of strategies in a semantic network knowledge base. The system's agent performs its classification of student's disabilities based on its past experience that it got from the exemplars that were classified by expert and acquired in its knowledge base.**

Keywords—Intelligent Agent; Learning Disabilities; Special Education; Semantic Network; Psych Pedagogy Evaluation; Exemplar Based Classification

I. INTRODUCTION

Educational software programs in science education have become increasingly complex in both concept and design. Thus, there is a paradigm shift in the role of computer from solely a transmitter of knowledge to a tool that aids in the construction of knowledge. This is due to the fact the science concepts are abstracts, as in [1].

Students in a special mental education have disabilities in their learning, especially in the basic education. They need psycho pedagogy evaluation as a strategy for analyzing problems that children may have in the teaching-learning process. This evaluation can be done manually by specialists and professionals in the special education, who are sometimes not enough in the special education schools.

Class teachers, who are always, keeping track of students whose learning is not as expected. This student should be evaluated by a specialist, who diagnose the case and specifies reasons of that problem. If possible, the specialist also determines strategies that should be applied on that case to help in decreasing his LDs.

In the time being, Artificial Intelligence algorithms, techniques, and applications have wide use in education and tutoring systems. One of the AI techniques is the intelligent agent, which can be used in education.

An intelligent agent is an autonomous calculated entity. In the dynamic changes information environment without prior modeling, it can independently plan complex operation steps to solve practical problems, can independently discover and obtain the available resources the learners needed and then provide the corresponding services under the circumstance that the learners do not take part in [13].

Currently, the state of intelligent is focused on one-to-one learning instruction. Some examples include ACT systems [1], DEBUGGY [2], and PIXIE [11] and. specifically, the kind of learning modality used is centered on learning by being told [3]. The agent has to collect users' personal interests and give fast response according to the pre-specified demands of users. The personal agent can discover users' personal interests voluntarily without bothering the users. It is very suitable for personalized e-learning by voluntarily recommending learning materials [7].

An agent is something that perceives and acts in an environment. The agent function for an agent specifies the action taken by the agent in response to any percept sequence as in [10]. Intelligent agents are task-oriented software components that have the ability to act intelligently. They may contain more knowledge about the needs, preferences and pattern of the behaviors of a person or a process as in [8].

Intelligent agents should have the ability of adaptive reasoning. They must have the capability to access information from other sources or agents and perform actions leading to the completion of some task. Also, they must control over their internal state and behavior and work together to perform useful and complex tasks. Thus, they should be able to examine the external environment and the success of previous actions taken under similar conditions and adapt their actions as in [9].

According to the observation and implementation of unstructured interviews with specialist in the special basic education institute (in a primary school in Makkah AlMokaramah area, Saudi Kingdom), it was evident that most institutes have a few specialist staff in LDs, not providing an efficient care to all students who have special educational needs.

The presented paper proposes a framework design for an Intelligent Agent Based classification System. It provides a methodology for the design and development of an intelligent agent-based system for diagnosing of learning and disabilities with children in special education.

Regarding that those students spend most of their times with their classroom teacher, it is desirable that he can diagnose

certain disabilities and carry out some activities with the student for better care of their problems. So, it is necessary that that the classroom teacher is guided by a specialist in LDs.

The proposed system performs structuring a knowledge base with strategies for psycho pedagogy evaluation, for helping the classroom teacher in diagnosing and in selecting, applying appropriate strategies in the care of children with LDs.

II. Disabilities in Teaching-Learning Process

LDs do not include, "...learning problems that are primarily the result of visual, hearing, or motor disabilities, of mental retardation, of emotional disturbance, or of environmental, cultural, or economic disadvantage." In the last few years an increasing number of children who have difficulties in learning their school work have been referred to child psychiatrists and child psychoanalysts. This increase in problems of learning may be real or it may be an apparent one.

Some of those problems, particularly reading problems, may be inherent in the difficulties in learning to read, write and spell the English language. This means that many children, who are really not capable of higher learning, have to try and their failures may increase the relative high percentage of these difficulties. In recent years psychologists and educators tend to regard the majority, if not all, of the children who seem [4].

A. What is LD

It is a general term that describes specific kinds of learning problems. A LD can cause a person to have trouble learning and using certain skills. The skills most often affected are: reading, writing, listening, speaking, reasoning and doing math [17].

LDs vary from person to person. One person with LDs may not have the same kind of learning problems as another person with LDs. One person may have trouble with reading and writing. Another person with LDs may have problems with understanding math. Still another person may have trouble in each of these areas, as well as with understanding what people are saying (National Dissemination Center for Children and Youth with Disabilities [17].

Researchers think that LDs are caused by differences in how a person's brain works and how it processes information. Children with LDs are not "dumb" or "lazy." In fact, they usually have average or above average intelligence. Their brains just process information differently [17].

The definition of "learning disability" just below comes from the Individuals with Disabilities Education Act (IDEA). The IDEA is the federal law that guides how schools provide special education and related services to children with disabilities [17].

Our nation's special education law, the Individuals with Disabilities Education Act, defines a specific learning disability as “a disorder in one or more of the basic psychological processes involved in understanding or in using language, spoken or written, that may manifest itself in an imperfect ability to listen, think, speak, read, write, spell, or do mathematical calculations, including conditions such as perceptual disabilities, brain injury, minimal brain dysfunction, dyslexia, and developmental aphasia."

There are some common red flags for learning disorders. Children who don’t have LDs may still experience some of these difficulties at various times. The time for concern is when there is a consistent unevenness in child’s ability to master certain skills. Grades 5-8 signs and symptoms of LDs include : Difficulty with reading comprehension or math skills, Trouble with open-ended test questions and word problems, Dislikes reading and writing; avoids reading aloud, Spells the same word differently in a single document, Poor organizational skills (bedroom, homework, desk is messy and disorganized), Trouble following classroom discussions and expressing thoughts aloud, Poor handwriting [5].

B. Problems with reading, writing, and math

LDs are often grouped by school-area skill set. If a child is in school, the types of learning disorders that are most conspicuous usually revolve around reading, writing, or math. Children with difficulties in mathematics-only seem to be superior to children with difficulties in mathematics and reading in areas that may be mediated by language but not in ones that rely on numerical magnitudes, visuospatial processing, and automaticity. Both groups performed worse than normally achieving groups in most areas of mathematical cognition. The two groups did not differ in approximate arithmetic and understanding of place value and written computation [6].

a) LDs in reading (dyslexia): There are two types of LDs in reading. Basic reading problems occur when there is difficulty understanding the relationship between sounds, letters and words. Reading comprehension problems occur when there is an inability to grasp the meaning of words, phrases, and paragraphs.

Signs of reading difficulty include problems with: letter and word recognition, understanding words and ideas, reading speed and fluency, and general vocabulary skills.

b) LDs in math (dyscalculia): LDs in math vary greatly depending on the child’s other strengths and weaknesses. A child’s ability to do math will be affected differently by a language learning disability, or a visual disorder or a difficulty with sequencing, memory or organization.

A child with a math–based learning disorder may struggle with memorization and organization of numbers, operation signs, and number “facts” (like 5+5=10 or 5x5=25). Children with math learning disorders might also have trouble with counting principles (such as counting by 2s or counting by 5s) or have difficulty telling time.

c) LDs in writing (dysgraphia) : LDs in writing can involve the physical act of writing or the mental activity of comprehending and synthesizing information. Basic writing disorder refers to physical difficulty forming words and letters. Expressive writing disability indicates a struggle to organize thoughts on paper. Symptoms of a written language learning disability revolve around the act of writing. They include problems with: neatness and consistency of writing, accurately

copying letters and words, spelling consistency, and writing organization and coherence

C. Other types of LDs and disorders

Reading, writing, and math aren't the only skills impacted by learning disorders. Other types of LDs involve difficulties with motor skills (movement and coordination), understanding spoken language, distinguishing between sounds, and interpreting visual information.

a) LDs in motor skills (dyspraxia):

Motor difficulty refers to problems with movement and coordination whether it is with fine motor skills (cutting, writing) or gross motor skills (running, jumping). A motor disability is sometimes referred to as an "output" activity meaning that it relates to the output of information from the brain. In order to run, jump, write or cut something, the brain must be able to communicate with the necessary limbs to complete the action.

Signs that your child might have a motor coordination disability include problems with physical abilities that require hand-eye coordination, like holding a pencil or buttoning a shirt.

b) LDs in language (aphasia/dysphasia):

Language and communication LDs involve the ability to understand or produce spoken language. Language is also considered an output activity because it requires organizing thoughts in the brain and calling upon the right words to verbally explain something or communicate with someone else.

Signs of a language-based learning disorder involve problems with verbal language skills, such as the ability to retell a story and the fluency of speech, as well as the ability to understand the meaning of words, parts of speech, directions, etc.

D. Treatments of LDs

The most common treatment for LDs is special education. Specially trained educators may perform a diagnostic educational evaluation assessing the child's academic and intellectual potential and level of academic performance. Once the evaluation is complete, the basic approach is to teach learning skills by building on the child's abilities and strengths while correcting and compensating for disabilities and weaknesses. Other professionals such as speech and language therapists also may be involved. Some medications may be effective in helping the child learn by enhancing attention and concentration. Psychological therapies may also be used [16].

There is no "cure" for LDs. They are life-long conditions. However, children with LDs can be high achievers and can be taught ways to get around the learning disability. With the right help, children with LDs can and do learn successfully. In some people, several overlapping LDs may be apparent. Other people may have a single learning problem that has little impact on their lives [15].

III. The Main Parts of the System

The proposed system has the following main parts:

- **User Interface**; which is a menu-driven dialogs to help the user to interact with the tool directly in easy manner. The user could present new disable student to the system to be diagnosed.
- **Intelligent Agent**; which manages the process of diagnosing and classification During diagnosing process, the agent acquires disabilities (categories), builds an indexing structure through its semantic network, and acquires the domain knowledge needed for explanation and reasoning processes. Consequently, the agent learns to classify accurately and efficiently and is able to explain its classification.

  The agent uses explanation to aid in its heuristics classification, because great variation possible in disable student descriptions. It uses links which are filled with indices to restrict and guide the agent search for a solution of the presented student.
- **Semantic KB**; which is a semantic network used to represent all knowledge of LDs in its nodes and links (relations between nodes). It holds an indexing structure used by the inference engine to locate questions. Each node or link is represented by an object of a suitable class.

IV. LDs's Semantic Network Knowledge Base

The knowledge manipulated by the proposed system is represented in frames that are allocated in nodes and links of a semantic network, that shown in Fig. 1. Each node may be related (linked), from zero to many times, to other node.

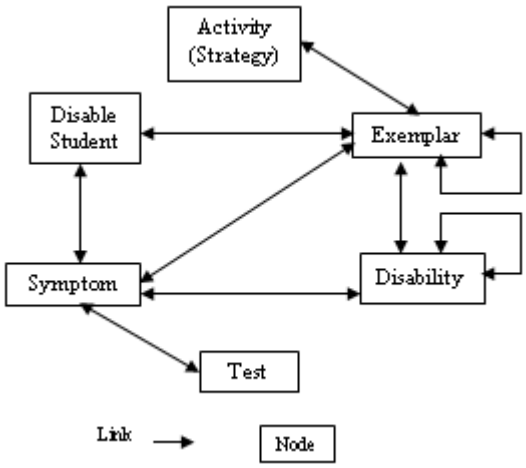

Fig.1. The Semantic Network Knowledge Base.

A. Knowledge Represented in Nodes

The semantic network, shown in Fig. 1, has six types of nodes. Four nodes store some substantive (descriptive) knowledge such as: *disability*, *disable student*, *exemplar* and *symptom*.

The other two nodes store some action knowledge such as: *test* and *activity* (*strategy*). The description of each node is as follows:

- The *disability* node represents a concept or a solution (name of category and classification of a disability for certain disable student).
- The node of *disable student* stores the name of the diagnosed disable student.
- The *exemplar* node represents the acquired, retained and previously classified disable student.
- The *symptom* node represents the feature of disability recognized that describe a disable student.
- The *test* node represents the test to be done on a diagnosed disable student.
- Finally, the *activity* or *strategy* node represents the action to be done as a treatment or skills to be performed.

B. Knowledge Represented in Links

The semantic network, shown in Fig. 1, has nine types of links. Those links are very important to relate the nodes listed above and hold majority of the knowledge acquired and represented in the semantic network. They hold substantial (descriptive), search control and strategic knowledge.

Each link is manipulated as a frame with its more specialized slots. The first seven links hold substantive and search control knowledge, while the last two links mainly hold strategic knowledge beside substantive knowledge. The description of those links is as follows:

- The *Disability-Disability* link relates disability categories to formulate the category tree. It links a category with its family in the network to enable inheritance of properties between categories. (It holds search control knowledge).
- The *Exemplar-Exemplar* link relates two exemplars located in the same category or in different categories. It used to discriminate an exemplar from another. (This link named a difference link).
- The *Symptom-Disability* link stores free text relation-name and qualifier beside the parameters assigned to the linked symptom, which are both combined to explain the relation of a feature with certain category in the network. It is used for describing to what extent the symptom *reminds* or *rejects* certain disability category to be a predicted classification. Only one explanation (one link) is needed over the entire network to explain the relation between certain symptom node, having certain parameters and certain disability node.
- The *Symptom-Exemplar* link relates symptoms to their exemplars. There may be different links between an exemplar and several features. Also, this link holds the importance of a symptom to an exemplar which depends on the strength of the relation between that symptom and the classification (disability) of that exemplar. (It holds substantive knowledge and search control knowledge).
- The *Disability-Exemplar* link relates the retained disable students (exemplars) to their classification (disabilities). It holds the family-resemblance of the exemplar which depends on the strength of relations of the features of that exemplar to its classification. It specifies to what extent an exemplar cover range of the category space. The summation of family-resemblance of all exemplars assigned to certain category is equal to one unit. Each exemplar share part of that cake. So the family-resemblance of an exemplar depends on that of brothers exemplars within the same category.
- The *Symptom-Disable Student* link relates a new presented disable student with its symptoms.
- The *Exemplar-Disable Student* link relates a new presented disable student to the most similar Exemplar (classified disable student). Both of them have the same classification.
- The *Symptom-Test* link holds strategic knowledge. It specifies how to apply certain tests on a newly presented disable student if he has a symptom.
- The *Exemplar-Activity* link holds strategic knowledge. It holds the method of executing certain activity or strategy.

V. Agent Performs Diagnosing

The proposed system performs diagnosing of disable students through heuristic classification of LDs and reasons under uncertainty. Its classification and reasoning performance are always tuned. It uses the presented disable student (problem) and closest-matching exemplar to generate a solution. This solution is validated through feedback and approval from the expert. The system incorporates expert classification with agent classification.

A. The Reasoning Process and Expert Diagnosing

In the first use of the system, an expert presents a disable student data to the system to be diagnosed; it performs reasoning through several steps, as shown in Fig. 2, Most of the steps done in the reasoning process, incorporate knowledge acquisition and learning with heuristic classification of LDs.

B. Agent Diagnosing Procedure

If the reminding list, in Fig. 2, is empty or if it is rejected at all by the expert, the agent will initiate expert-classification procedure, shown in Fig. 3, for acquiring diagnosing from the expert. It also acquires explanation of rejecting the reminded LDs's categories to prevent reoccurring of this failure. Then, it retrieves an exemplar from the knowledge base, and uses it as a model for matching with the new case. If the matching is not correct, it retrieves another exemplar from the same category or from next category in the reminded list.

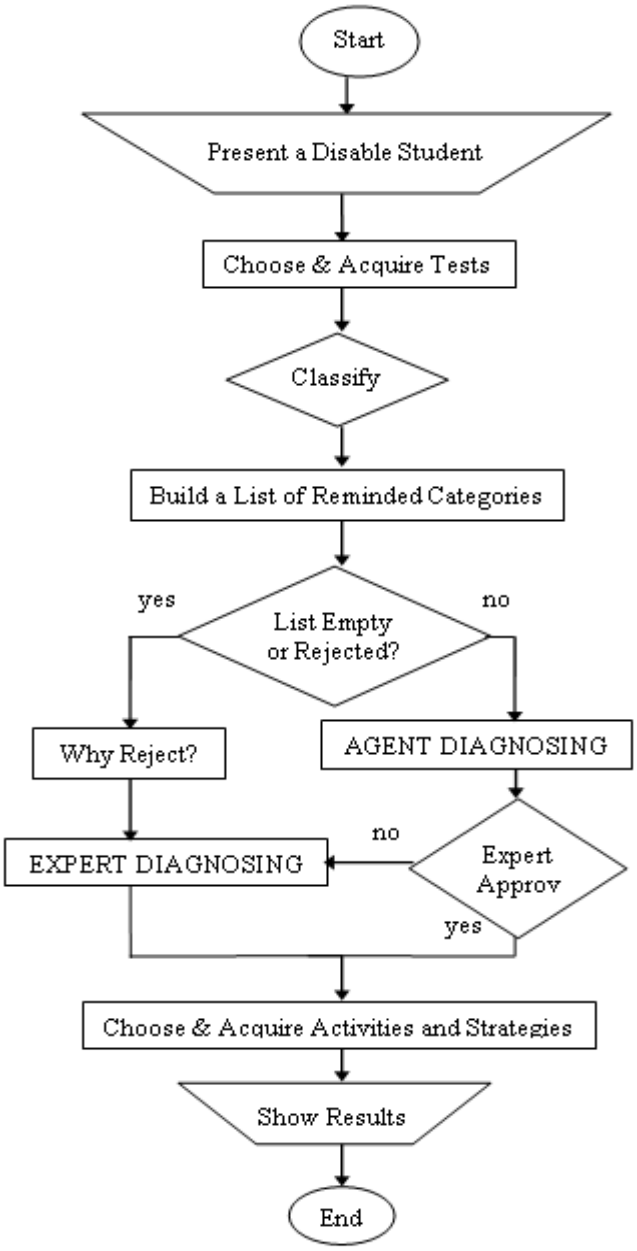

Fig.2. Reasoning Process Algorithm.

Looking for a matched exemplar is done by Knowledge-Based Pattern matching process. This process continues until one similar exemplar is found and approved by the expert or the agent fails to find a similar one. In this situation, the agent invokes Expert-Diagnosing procedure to get diagnosing from the expert.

C Knowledge-Based Pattern Matching

This is the most important module in the diagnosing process. Its function is to compare the symptoms of a new diagnosed disable student with exemplar symptoms, and to compute the matching ratio between the student and the exemplar. The matching ratio is computed by accumulated the importance of all matched symptoms of the retrieved exemplar. This module incorporates learning with reasoning. It performs its process in two different phases; direct matching and indirect matching shown in Fig. 4.

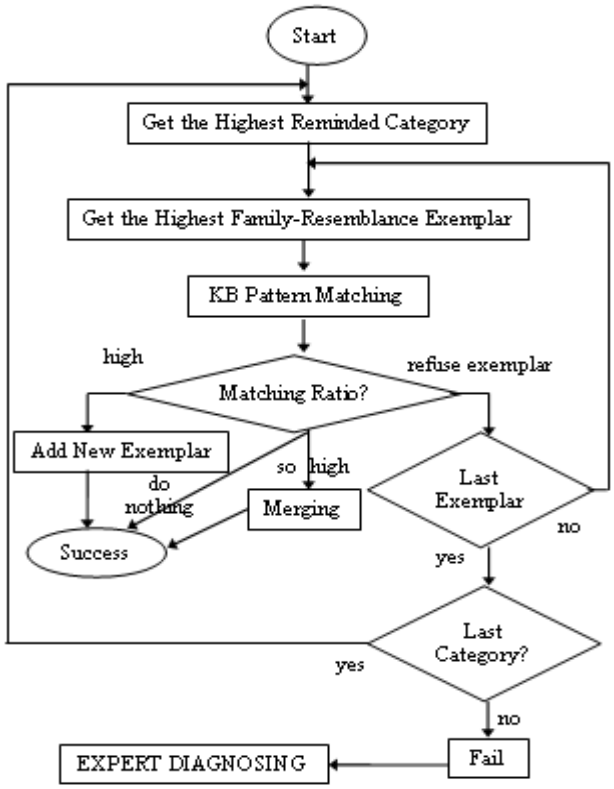

Fig.3. Agent Diagnosing Algorithm.

VI. CONCLUSIONS

The proposed systems is an agent based classification system that provides interactive aid in problem solving and acquires new domain knowledge by generalizing from training examples acquired through the normal course of its use. It performs diagnosing of disable students through heuristic classification under guidance of the domain expert. It demonstrates the viability of engaging the expert in a debugging style dialog, acquiring knowledge in the context of a running application. It performs classification and reasoning as a problem solving method to make use of specific past experiences rather than a corpus of general knowledge.

The system enables classroom teachers to get psycho pedagogical evaluation for student who has LDs. It also, provides teachers with the best educational activities for those students. It cooperates with teachers in a diagnostic evaluation practice. It incorporates the basic guidelines for general evaluation, and provides models of diagnostic tools and educational activities handling several weaknesses in psycho functional areas.

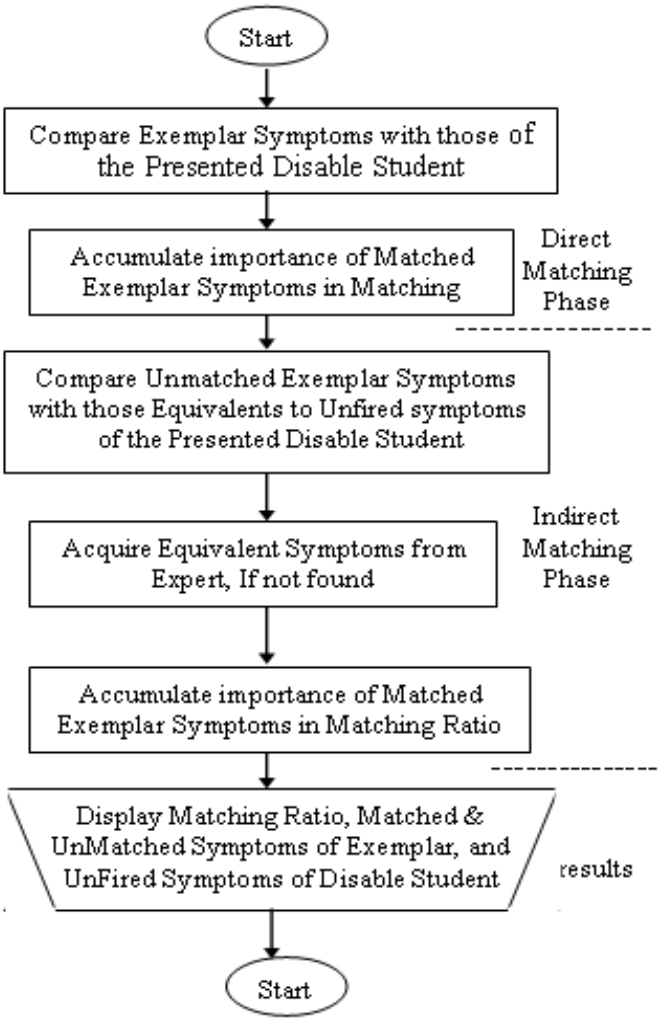

Fig.4. Block Diagram of Pattern Matching Process.

REFERENCES

[1] Anderson, J., F. Boyle, A. Corbett, and M. Lewis, "Cognitive Modeling and Intelligent Tutoring, Advanced Computer Project", Carnegie-Mellon University, Pittsburgh, PA, USA. Artificial Intelligence, 42, pp 7-49, Elsevier Science Publishers, B. V. (North Holland), 1990.

[2] Burton, R., "Diagnosing Bugs in a Simple Procedural Skills", Xerox Palo Alto Research Center, Cognitive and Instructional Sciences Group, Palo, Alto, CA 94304, 1986.

[3] Florea, A. M., "An Agent-Based Collaborative Learning System, Advanced Research in Computers and Communications in Education", G. Cumming et al, IOS Press, International Conference on Computers in Education, 1999, 161-164.

[4] Gerald H.J. & Pearson, M.D., "A Survey of Learning Difficulties in Children, Psychoanalytic Study of the Child", 7:322-386, 1952, Last access 2013. http://www.pep-web.org/document.php?id=psc.007.0322a Gina Kemp, M.A., Melinda Smith, M.A., and Jeanne Segal, "Learning Disability in Children", on HELPGUID.org, Ph.D. Last updated: November 2011. http://www.helpguide.org/mental/learning_disabilities.htm#signs

[5] Hanich, Laurie B.; Jordan, Nancy C.; Kaplan, David; Dick, Jeanine, "Performance across different areas of mathematical cognition in children with learning difficulties", Journal of Educational Psychology, Vol 93(3), Sep 2001, 615-626. doi: 10.1037/0022-0663.93.3.615 http://psycnet.apa.org/journals/edu/93/3/615/

[6] Jin-Ling Lin and Ming-Hung Chen, "An Intelligent Agent for Personalized E-Learning" , IEEE Computer Society, 27-31, 2008.

[7] Mohammed, H. K., "An Intelligent Agent to Teach C-Language", proceedings of ICECS'97, Cairo, Egypt, 483-488, December 15-18, 1997.

[8] Nissen, M., "Intelligent Agents: A Technology and Business Application Analysis", Telecommunications and Distributed Processing, November 1994.

[9] Russell, S. J & Norvig, P., "Artificial Intelligence – A Modern Approach", 3rd edition, Prentice Hall, 2009.

[10] Sleeman, D., "Frameworks for Cooperation in Distributed Problem Solving, Readings in Distributed Artificial Intelligence", Morgan Kaufmann Publishers, Inc. San Mateo, California, 61-69, 1982.

[11] Tsang, H.W.; Hung, L.M.; Ng, S.C. "A multimedia distance learning system on the Internet", proceedings of IEEE International Conference on Systems, Man, and Cybernetics (SMC), Vol. 2, 243 –246, 1999.

[12] Ying-Han Fang1 & Lei Shao2, "Agent-Based E-Learning System Research and Implementation", proceedings of the 7th International Conference on Machine Learning and Cybernetics, Kunming, 12-15 July 2008, 4080-4084.

[13] Zhi Liu & Bo Chen, "Model and Implement an Agent Oriented E-Learning System", Proceedings of the 2005 International Conference on Computational Intelligence for Modelling, Control and Automation, and International Conference Intelligent Agents, Web Technologies and Internet Commerce (CIMCA-IAWTIC'05) 0-7695-2504-0/05 $20.00 © 2005 IEEE.

[14] "LDs (LD) Alternative Treatments", on sharecare.com, last access 2013, http://www.sharecare.com/topic/learning-disabilities-alternative-treatment

[15] "LDs Causes, Symptoms, Diagnosis and Treatments", on MedicenNet.com, last access 2013. http://www.medicinenet.com/learning_disability/article.htm

[16] "National Dissemination Center for Children and Youth with Disabilities", Last access 2013.http://nichcy.org/publications.

A Fresnelet-Based Encryption of Medical Images using Arnold Transform

Muhammad Nazeer[1], Bibi Nargis[2], Yasir Mehmood Malik[3], and Dai-Gyoung Kim[1*]
[1]Department of Applied Mathematics, Hanyang University, Ansan, 426-791, South Korea
[2]School of Computer Science, University of Manchester, Manchester, UK
[3]Department of Neurology, Rashid Hospital, Dubai, UAE

***Abstract*—Medical images are commonly stored in digital media and transmitted via Internet for certain uses. If a medical information image alters, this can lead to a wrong diagnosis which may create a serious health problem. Moreover, medical images in digital form can easily be modified by wiping off or adding small pieces of information intentionally for certain illegal purposes. Hence, the reliability of medical images is an important criterion in a hospital information system. In this paper, the Fresnelet transform is employed along with appropriate handling of the Arnold transform and the discrete cosine transform to provide secure distribution of medical images. This method presents a new data hiding system in which steganography and cryptography are used to prevent unauthorized data access. The experimental results exhibit high imperceptibility for embedded images and significant encryption of information images.**

Keywords—Fresnelet transform; wavelet transform; Arnold transform, data hiding; and image encryption

I. INTRODUCTION

Due to recent expansions of information technology, the circulation of medical images among hospitals has become a common trend. Medical images are often distributed for specific purposes such as for teleconferences and interdisciplinary exchanges among medical personnel [1]. The transmission of medical imaging should be carefully treated to ensure reliability and authenticity verification [2]. Privacy is also a critical issue in medical images especially in case of medical jurisprudence where a small manipulation of brain contusion or hairline bony fractures can alter the situation drastically. For interdisciplinary data exchange clarity of image is mandatory such as in multiple sclerosis, a disease of nervous system [3]. If small demyelinating plaques are missed in this disease, whole the diagnostic picture, treatment plan, and even prognostic outcome would be altered. Similarly in infectious diseases of chest and abdomen or minimal trauma, if any misinterpretation is found because of imaging defect, clinical outcome would be seriously affected. Thus it is essential to ensure the protection of image information for both legislative and diagnostic reasons. A digital data hiding technique can provide this needed protection by embedding medical information data into other data (called the host or cover data) and has been developed for information security that is strongly based on cryptography and steganography [4].

Steganography and cryptography are both used for data confidentiality. Cryptography is employed for scrambling meaningful information into uncorrelated data keeping the contents of a message secret, whereas steganography hides the significant information under some cover data keeping the existence of a message secret [5]. Each technique enhances the security and privacy for protection of information data. Furthermore, combining both schemes into one system is likely to provide even better security and confidentiality [6]. In other words, steganography prevents an unintended recipient from suspecting the existence of data and the security of the steganography system relies on secrecy of the data encoding system [7, 8].

One way of data hiding entails the manipulation of the least significant bit (LSB) plane, from direct replacement of the cover LSB's with message bits to some type of logical or arithmetic combination between the cover image and the amount of information data which needs to be hidden. Several examples of LSB schemes have been presented in [9-11]. Mainly this technique achieves both high capacity and low perceptibility. However, this embedding scheme only overwrites the LSB plane of the cover image with the secret bit stream according to a pseudorandom number generator (PRNG). As a result, some structural asymmetry (never decreasing even pixels and increasing odd pixels when hiding the data) is introduced so that LSB makes the disclosure of hidden message very easy even at a low embedding rate using some reported steganalytic algorithms, such as the Chi-squared attack, regular/singular groups (RS) analysis, sample pair analysis [10], and the general framework for structural steganalysis [12].

Most existing steganographic approaches usually assume that the LSB of natural cover images is insignificant and random enough, and thus those pixels/pixel pairs for data hiding can be selected freely using a PRNG. However, such an assumption is not always true, especially for images with many smooth regions [10]. Based on the stated researches, we found that natural images usually contain some flat regions as small as 5 by 5 blocks which are hard to be noticed. The LSB's in those regions have the values 1 or 0. Therefore, embedding the secret data into these regions will make the LSB of stegano-images more and more random, which may lead to visual and statistical differences between cover and stegano images appearing as a noise-like distribution. The pixel-value differencing (PVD)-based scheme [13] is another kind of edge adaptive scheme which determines the number of embedded bits by the difference between a pixel and its neighbor. This shows the larger the difference is, the larger the

This work was supported by the National Research Foundation of Korea (NRF) grant funded by the Korea government (MEST) (NRF-2011-0026245).

number of secret bits can be embedded. Based on our explorative experiments, however, we found that the existing PVD-based approaches cannot make full use of edge information for data hiding, so that the embedded image data does not have a good perceptibility.

Chang et al. extended Iwata et al.'s idea [14-16] and presented a lossless steganographic scheme for hiding secret data in each block of quantized DCT coefficients in JPEG images [17]. This method uses two successive zero coefficients of the medium-frequency components in each block to hide secret data. They further modified the quantization table to maintain the quality of the stegano-image while concealing a higher payload compared with Iwata et al.'s method. Their scheme achieved reversibility and acceptable image quality of the stegano-image at the same time. However, this scheme can only embed secret bits into the zero coefficients located in the successive *zero* coefficients in the medium area; non-zero coefficients in the medium area cannot be used. Later, Lin et al. embedded the secret values into the middle frequency of the quantized DCT coefficients, and reduced nonzero values of the quantized DCT coefficients which participate in the data hiding procedure. The aim was to design an adaptive and reversible DCT-based data hiding scheme [18]. Lin and Shiu combined Chang et al.'s [17] method and designed a 2-layer data hiding scheme for DCT-based images. This scheme outperforms Chang et al.'s scheme [16] in hiding capacity but the size of the hidden secret data is still less than 70k bits on average because it retains the reversibility function.

A medical image is distributed among a number of clinicians in telediagnosis and teleconsultation which require maximum information exchange over an unsecure network. Disclosing the information about an important patient's medical condition to general public can be a confidentiality risk. Access to medical information especially image data during transmission which should not be granted to an unauthorized party, demands an important confidentiality measurement. The integrity, on the other hand, demands that images should not be modified in the processes of transmission [19]. However, emerging technologies in field of medical imaging lead to the high demand of protection and confidentiality of the medical information, which must follow strict ethics and legislatives rules. Once the medical images are stolen or abused, the rights of the patients will suffer violation. Tso, H.-K, et al [20] proposes a secret sharing scheme to protect the security of the medical images based on the firstly secret sharing technique proposed by Shamir [21]. According to this technique, no one can obtain any information from one of the shared images unless acquiring the hidden information from all the authorized users. Furthermore, this technique is not efficient for embedding the complete information of secret data in one cover image [22]. Conventionally, information sharing and data hiding are two irrelevant concerns in the field of secure distribution of the information data. In our proposed method, however, a complete information data (e.g., medical image) can be embedded in single cover image (such as patient identity image or face image), rather than distributing in several cover images.

In this study, we proposed a novel technique for data hiding based upon the Fresnelet transform [23] along with applications of discrete cosine transform (DCT) and the Arnold transform [24]. The method based on the Fresnelet transform was initially designed for reconstruction of high resolution digital holography. Irrespective of traditional optical holography, the digital holography has a significant advantage of fast reconstruction process for target object data [25]. Therefore, the Fresnelet transform can be applied to protecting copyrights of digital multimedia contents and data hiding [26]. Besides it is recommended to make use of the Fresnelet transform to complex encryption procedures for providing more security and reliability to information data. Using the Fresnelet transform, an extracted information image data from embedded (cover) image can be obtained with high resolution [27]. In this regard, our proposed method will be useful for data hiding of medical data in the rapid digital communication of medical imaging system. Preserving the high resolution of medical image data at embedding stage and retrieving the precise resolution at extraction stage are the keys to more precise understanding of the anatomy. The precise retrieve of medical data can support early detection of abnormalities and increase the accuracy in the assessment of the size and morphology of the organs, effectively [28].

In this paper, we propose a data hiding algorithm to improve security and privacy by integrating both steganography and cryptography with an efficient embedding and extracting process of large size information data. Note that in the proposed method, the Fresnelet transform is employed in order to build a more flexible data hiding system than one using only the Fresnel transform [29] or the wavelet transform [30]. One of the main features of the proposed method is a multi-scale distribution of information on the Fresnelet transform domain yielding robust key parameters for security and privacy. In our presented method, it is not possible to attain the hidden information data without the precise key parameters, even if an attacker perceives the embedding algorithm of the method.

This paper is organized as follows. In Section II, the Fresnelet transform and Arnold transform are reviewed as the basic transforms in the proposed algorithm. The embedding and extraction schemes based on these basic transforms are presented in Section III. Numerical simulations and analysis are conducted to evaluate the proposed method in Section IV. In Section V, conclusions are discussed.

II. BASIC TRANSFORMS

A. Fresnelet transform

A new class of multiresolution bases can be obtained by applying the Fresnel transform to a wavelet basis. The Fresnelet transform has been used for image reconstructions from digital holograms with various parameters related to wavelength, resolution scale, and distance between object and image plane. A review of the Fresnel transform follows from [23].

The Fresnel transform is used to approximately model diffraction phenomena through the propagation of complex

waves [29]. The one-dimensional Fresnel transform is defined on a function $f \in L_2(\mathbb{R})$ as the convolution integral:

$$\tilde{f}_\tau(x) = (f * k_\tau)(x) \text{ with } k_\tau(x) = \frac{1}{\tau} exp\left(i\pi \frac{x^2}{\tau^2}\right) \quad (1)$$

where $\tau > 0$ is the parameter related to wavelength and the distance at a diffracted wave. The two-dimensional Fresnel transform is obtained by convolving with the tensor product of the one-dimensional kernel $k_\tau(x)$. That is, for $f \in L_2(\mathbb{R}^2)$,

$$\tilde{f}_\tau(x,y) = (f * K_\tau)(x,y) \text{ with } K_\tau(x,y) = k_\tau(x)k_\tau(y) \quad (2)$$

Notice that the kernel $K_\tau(x,y)$ is separable, so that the useful properties of one-dimensional Fresnel transform are readily extended to two-dimensions. The Fresnel transform has many useful properties. One is the unitary property: processing via the Fresnel transform provides a perfect reconstruction of given data.

The two-dimensional wavelet is obtained from a one-dimensional wavelet by separable extension. The wavelet transform is also defined on $L_2(\mathbb{R})$ as convolution integrals with a two parameter family $\{\psi_{j,l}\}_{j,l\in\mathbb{Z}}$, which forms a Riesz basis for $L_2(\mathbb{R})$, where

$$\{\psi_{j,l}(x) = 2^{j/2}\psi(2^j x - l)\}_{j,l\in\mathbb{Z}}. \quad (3)$$

The simplest example of a wavelet is the Haar wavelet that generates an orthonormal basis for $L_2(\mathbb{R})$. Processing via the wavelet transform provides a perfect reconstruction and a multiresolution decomposition of the data, as well. The properties of wavelet transforms are given in [14]. By applying the Fresnel transform to the wavelet basis, the Fresnelet basis is defined as follows:

$$\left\{\left(\psi_{j,l}\right)_\tau^{\sim}\right\}_{j,l\in\mathbb{Z}} \text{ with } \left(\psi_{j,l}\right)_\tau^{\sim}(x) = 2^{j/2}\tilde{\psi}_{2^j\tau}(2^j x - l) \quad (4)$$

With an orthogonal wavelet basis $\{\psi_{j,l}\}_{j,l\in\mathbb{Z}}$, we can have an orthonormal Fresnelet basis. For fixed τ, by letting $\theta_{j,l}(x) = \left(\psi_{j,l}\right)_\tau^{\sim}(x)$, we have a Fresnelet decomposition:

$$f = \sum_{j,l} c_{j,l}\, \theta_{j,l} \text{ with } c_{j,l} = \langle f, \theta_{j,l}\rangle. \quad (5)$$

Here, the coefficients $c_{j,l}$ are called the Fresnelet coefficients. From the separable nature of the Fresnelet, we may extend the one-dimensional Fresnelet transform to two-dimensional space. In this case, four combinations of tensor products are obtainable:

$$\Theta_{LL} = \left(\phi_{j,l}\right)_\tau^{\sim}(x)\left(\phi_{j,l}\right)_\tau^{\sim}(y)$$

$$\Theta_{LH} = \left(\phi_{j,l}\right)_\tau^{\sim}(x)\left(\psi_{j,l}\right)_\tau^{\sim}(y)$$

$$\Theta_{HL} = \left(\psi_{j,l}\right)_\tau^{\sim}(x)\left(\phi_{j,l}\right)_\tau^{\sim}(y)$$

$$\Theta_{HH} = \left(\psi_{j,l}\right)_\tau^{\sim}(x)\left(\psi_{j,l}\right)_\tau^{\sim}(y)$$

where ϕ and ψ are the scaling function and wavelet function, respectively, generating low-pass and high-pass filters, respectively. Applying the basis function above to data f, we obtain the four types of Fresnelet coefficients:

$$C_{LL} = \langle f, \Theta_{LL}\rangle, \quad C_{LH} = \langle f, \Theta_{LH}\rangle,$$

$$C_{HL} = \langle f, \Theta_{HL}\rangle, \; C_{HH} = \langle f, \Theta_{HL}\rangle. \quad (6)$$

The coefficient C_{LL} is the low-passed data and the others are the high-passed data. Fig. 2 shows the Fresnelet coefficients of (6) applied to the medical information data shown in Fig. 1. In Fig. 2, note that the information image data is encrypted by the Fresnelet transform.

Fig.1. Medical image for data hiding.

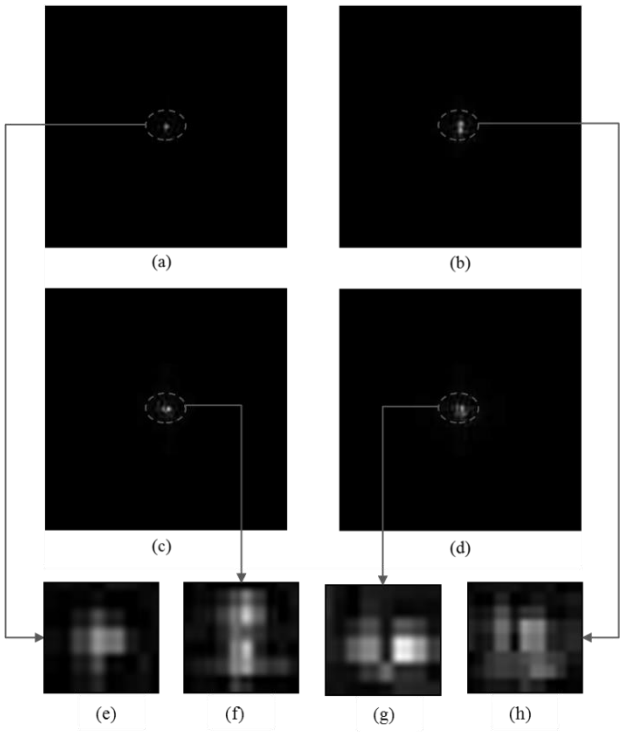

Fig.2. The magnitude of complex data sets of the Fresnelet coefficients applied to the medical information data shown in Fig. 1: (a) approximate data, (b) horizontal detail data, (c) vertical detail data, (d) diagonal detail data. Moreover, the (e) , (f), (g), and (h) are the zooming parts of marked portion of (a), (b), (c), and (d).

Thanks to the unitary property of the Fresnel transform and wavelet transform, data reconstruction is readily performed by applying the transpose of the forward processing as the inverse Fresnelet transform. Fig. 3 shows the inverse transformed data from Fig. 2, and Fig. 4 shows the result of the reconstruction of the medical information data from the data in Fig. 3. Note here that the proposed transform algorithm depends on the distance and the wavelength key parameters, which are very important for exact reconstruction of the information data. Furthermore, the nature of the reconstruction image is a complex field due to the propagation of complex waves. The complex image is beneficial for medical analysis based on multiresolution wavelet bases, just as for applications to digital holography [23, 25-27].

For the Fresnelet transform application to the data shown in Fig. 2, the encrypted information data may be covered to protect against a high degree of scrutiny. Also, in the reconstruction phase, the complete information may be acquired by using the exact keys as shown in Fig. 4..

B. Arnold transform

It is known that the Arnold transform works well in applications for encrypting images [5]. For an $N \times N$ image, the Arnold transform, for example, is given as

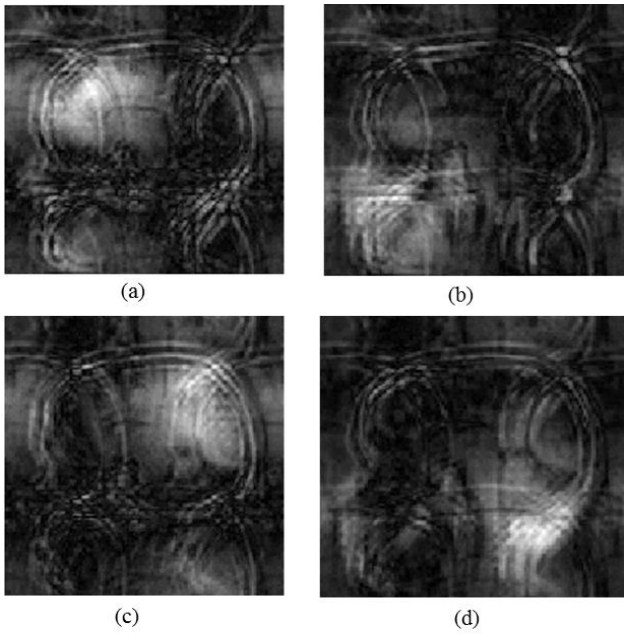

Fig.3. The magnitude of the inverse Fresnelet transformed data from the four sub-bands of complex data shown in Fig. 2: (a) from approximate data, (b) from horizontal detail data, (c) from vertical detail data, (d) from diagonal detail data.

Fig.4. The reconstruction of the medical information data by combining with the magnitude of four sub-bands of complex data shown in Fig. 3.

$$\begin{bmatrix} x \\ y \end{bmatrix} = \begin{bmatrix} 1 & 1 \\ 1 & 2 \end{bmatrix} \begin{bmatrix} a \\ b \end{bmatrix} \pmod{N} \tag{7}$$

where (a, b) and (x, y) express the pixel co-ordinates of the original and encrypted images, respectively, as shown in Fig. 5. With the periodic boundary treatment, the image encryption using n iterations of the Arnold transform may be written as

$$I(x, y)^{(k)} = ID(a, b)^{(k-1)} \pmod{N} \tag{8}$$

where $k = 1, 2, \cdots, n$, and $I(x, y)^{(0)} = I(a, b)$. The Arnold transform matrix is given as D in (7) and I is an $N \times N$ image field.

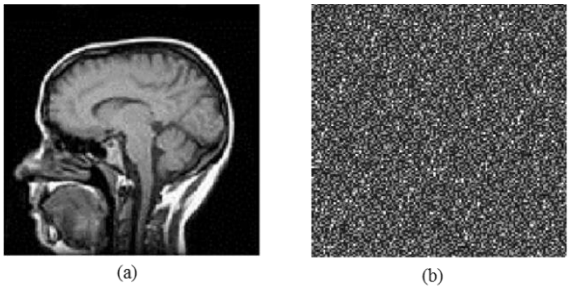

Fig.5. The 5 iterations of the Arnold transforms of a medical information image: (a) Medical information image. (b) Information image scrambled by the Arnold transforms.

The encrypted image may be inverted by applying the inverse of the Arnold matrix D n times as follows:

$$I(a, b)^{(k)} = ID^{-1}(x, y)^{(k-1)} \pmod{N} \tag{9}$$

where $(x, y)^{(0)}$ is the pixel of the encrypted image. An original image may reappear after T iterations, depending on the size of the given image.

The periodicity T depends on the size of the images, as shown in Table 1.

TABLE 1. PERIODICITY OF ARNOLD TRANSFORMS

N	128	256	480	512
T	96	192	240	384

III. DATA HIDING METHOD

A. The embedding process

The embedding process consists of two phases. First, the Arnold transform is applied on the host image following the wavelet transform. Second, to encrypt the information data, the Fresnelet transform is performed with a single FFT (fast Fourier transform) approach up to the first level by specifying the sampling interval and distance as key parameters. In this case, the sub-bands of information data are of complex data. In the immediate phase, we separate the complex data into real and imaginary parts, respectively.

In this way, we obtain the two sets of four sub-band images (approximation details, horizontal details, vertical details, and diagonal details). Applying the IDWT (inverse discrete wavelet transforms) on each set separately, we obtain two coded images. These two images of real and imaginary parts are embedded into the same size as the sub-bands of the host image after performing the DCT on each sub-band. Real part which contains important detail of information data is embedded into approximation and horizontal sub-bands of host image, whereas imaginary part is embedded into vertical and diagonal detail of host image. To obtain information embedded data, the IDCT is performed on the each embedded sub-bands of cover image. It is used for distributing the amplitude values of Fresnelet coefficients of information data image of the processed data as shown in Fig. 6.

In this process, the approximate and horizontal detailed parts are modified with real part data, which leads to enhance the strength of the information data, and the vertical and diagonal detailed parts are modified with imaginary part data to balance the transparency of the host image. The intensity of the transformed pattern is embedded into the host image with a strength factor. After embedding, the IDWT is performed to write out the image file as an embedded image for digital media handling or internet transmission.

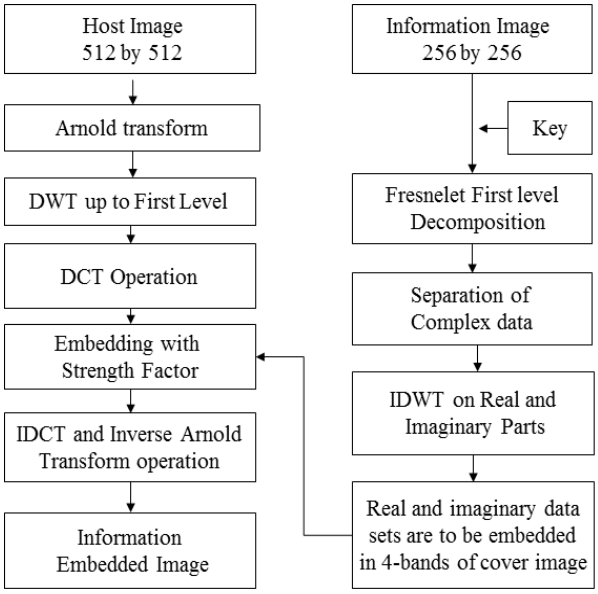

Fig.6. The schematic diagram of the embedding process.

B. The extraction process

In order to extract the embedded information data, the Arnold transform followed by DWT (discrete wavelet transform) is performed on the embedded data to obtain the sub-bands of the approximate data (E_a), horizontal data (E_h), vertical data (E_v), and diagonal data (E_d). The Arnold transform followed by DWT up to the first level is also performed on the original host image, and then each sub-band of the host date is subtracted from the sub-band data E_a, E_h, E_v, and E_d, respectively.

Applying DCT on the difference data is performed to extract the information coded data. After DWT is applied, the real and imaginary parts are separated to reconstruct the complex sub-band images for performing the inverse Fresnelet transform. As a result, the extraction information image is obtained in the form of complex. The whole process of the extraction is shown in Fig. 7.

IV. NUMERICAL SIMULATION AND EVALUATION

A. Simulation and measurement of quality

In this simulation, the size of all the cover images is 512×512 and the size of the information images is 256×256. To analyze the algorithm, MATLAB simulations are performed separately for embedding and extraction of the information data image.

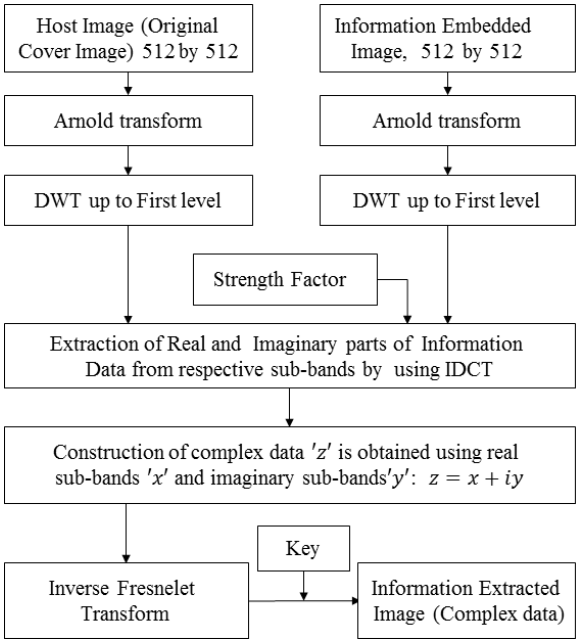

Fig.7. The schematic diagram of the extraction process.

The distance z and the wavelength λ are key parameters of the Fresnelet transform that improve the security level of the embedded images. In the proposed method, we considered a wavelength; $\lambda = 632.8$ nm , sampling interval; $\Delta = 10$ nm, and the distance; $d = 200$ cm. The Arnold transform iteration may also be considered as an additional key parameter. The correlation coefficient (CC) is used to measure the quality of the extracted information data with respect to the original information data before embedding [31]. Specially, ultrasonic detection in medical images is based on amplitude for non-destructive evaluation [32].

In the correlation approach, each signal is correlated with its nearest neighbors for application of matched filtering. A confidence level specifies the relative degree of confidence between two images, with lower to higher values of 0 to 1. The correlation coefficient is given by

$$CC = \frac{\sum_i \sum_j (I_{emb}(i,j) - \bar{I}_{emb})(I_{ext}(i,j) - \bar{I}_{ext})}{\sqrt{\sum_i \sum_j (I_{emb}(i,j) - \bar{I}_{emb})^2} \sqrt{\sum_i \sum_j (I_{ext}(i,j) - \bar{I}_{ext})^2}} \quad (10)$$

where $\bar{I}_{emb}$ and $\bar{I}_{ext}$ are the averages of embedded and extracted information data images, respectively. In addition, the *PSNR* (peak signal noise ratio) is a common estimate of the quality of the embedded image data [33].

Higher values of *PSNR* indicate better imperceptibility of the embedded information data with respect to the cover data:

$$PSNR = 10 \log\left(\frac{255^2}{MSE}\right) \quad (11)$$

with

$$MSE = \frac{1}{mn} \sum_{i=0}^{m-1} \sum_{j=0}^{n-1} [I_O(i,j) - I_E(i,j)]^2 \quad (12)$$

where *MSE* is the mean square error between original image I_O and embedded image I_E. The difference $I_O - I_E$ is an encrypted information data that considered as a noisy like image as shown in Fig. 9-c and Fig. 9-f. Moreover, in order to evaluate the perception quality of human visual system, the structural similarity index measure (SSIM) is used to measure the distortion difference two images. The SSIM metric is designed by modeling any image distortion as a combination of three factors: loss of correlation, luminance and contrast distortions. The SSIM comparison for measuring the perceptual quality between two images is defined as

$$SSIM(a,b) = l(a,b)c(a,b)s(a,b) \quad (13)$$

$$l(a,b) = \frac{2\mu_a\mu_b + C_1}{\mu_a^2 + \mu_b^2 + C_1} \quad (14)$$

$$c(a,b) = \frac{2\sigma_a\sigma_b + C_2}{\sigma_a^2 + \sigma_b^2 + C_2} \quad (15)$$

$$s(a,b) = \frac{2\sigma_{ab} + C_3}{\sigma_{ab} + C_3} \quad (16)$$

where $l(a,b)$ is the function of luminance comparison to measure the images closeness on the base of mean luminance μ_a and μ_b of 2D images a and b. Maximum value of $l(a,b)$ is equal to 1, if and only if $\mu_a = \mu_b$. The second term $c(a,b)$ in (13) is used to measure the contrast on the base of standard deviation σ_a and σ_b.

The maximal value of contrast term as given in (15) is achieved when $\sigma_a = \sigma_b$ .The third term $s(a,b)$ in (13) measures the structure comparison between the two images. In (16), σ_{ab} is the covariance that is useful to analyze the correlation between two images. In the equations (14)-(16) above, the positive constants C_1, C_2, and C_3 are used to avoid the null denominator. The quality value of SSIM is varied in [0, 1]. The value of 1 shows that two images are having the same quality and the value of 0 shows no correlation between the two image.

B. Evaluation criteria

In this algorithm, the information image data is embedded in a cover image to increase the security level and improve the imperceptibility of the cover media. For evaluation of the proposed method, the PSNR and SSIM of cover image after embedding of information data are evaluated as shown in Table. 2. Also the CC factor and SSIM of the information image after extraction are analyzed as shown in Table. 3. The numeric results show the superior performance of the proposed algorithm.

A slight effect may be presented due to auto focus nature of the Fresnelet transform, where the Fresnelet sparsity criterion is employed for extraction of information data in the form of complex values, as shown in Fig. 8 through 11. The corresponding *PSNR* and *SSIM* are shown in Tables 2 for signature image 1 (the brain image in Fig. 8-a), signature image 2 (the backbone image in Fig. 8-b), and signature image 3 (the USAF target image in Fig. 8-c). Note that the signature images are high resolution information image data.

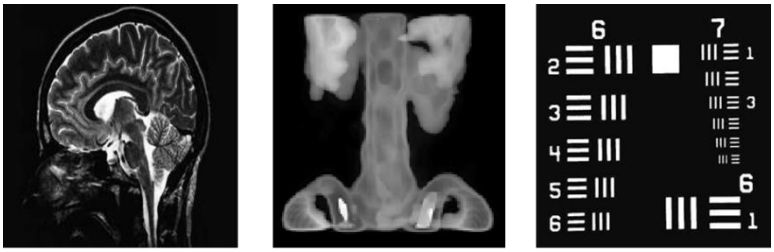

Fig.8. High resolution signature image data with size 256×256: (a) the brain medical image, (b) the backbone medical image, and (c) the USAF test image.

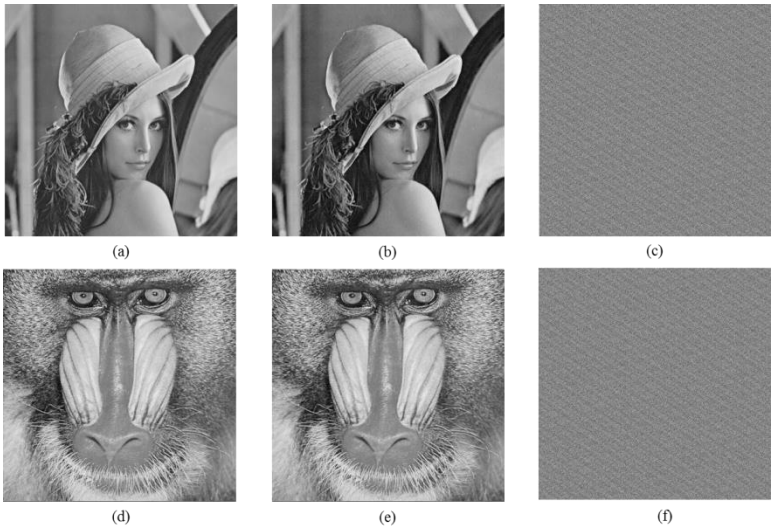

Fig.9. The cover images embedded with signature image 1 as shown in Fig. 8-a: (a) the original cover Lena image, (b) the cover Lena image embedded with signature image 1 (c) the difference between the original cover Lena image and the embedded Lena image with signature image 1 where MSE is 4.3273, (d) the original cover Mandrill image, (e) the embedded Mandrill image with signature image 1, and (f) the difference between the original cover Mandrill image and embedded Mandrill image with signature image 1 where MSE is 4.3268.

Table 2. PSNR and SSIM of the embedded images: Lena and Mandrill

Test data	**Extraction from embedded Lena image**		**Extraction from embedded Mandrill image**	
	PSNR	***SSIM***	***PSNR***	***SSIM***
Signature image 1	38.8483	0.9982	40.8311	0.9985
Signature image 2	36.0625	0.9966	36.0638	0.9956
Signature image 3	36.7419	0.9971	38.7388	0.9976

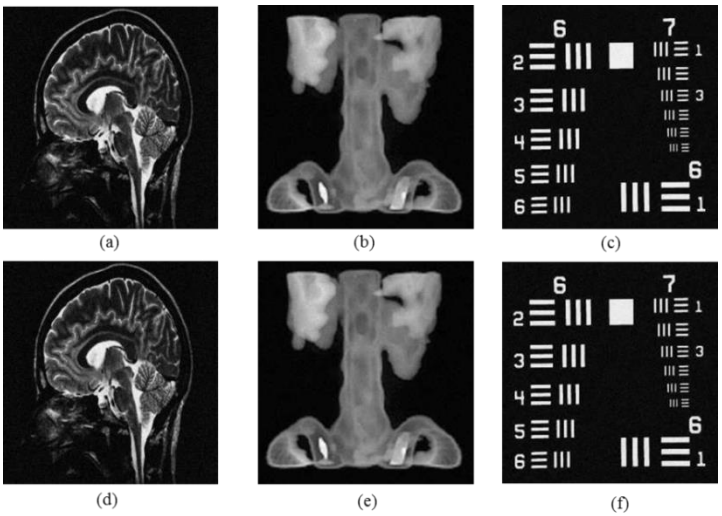

Fig.10. Extraction of signature images from embedded images of Lena and Mandrill: (a) the signature image 1 extracted from embedded Lena image, (b) the signature image 2 extracted from embedded Lena image, (c) the signature image 3 extracted from embedded Lena image, (d) the signature image 1 extracted from embedded Mandrill image, (e) the signature image 2 extracted from embedded Mandrill image, and (f) the signature image 3 extracted from embedded Mandrill image.

Table 3. CC factor and SSIM of signature data extracted from embedded images: Lena and Mandrill

Test data	**Extraction from embedded Lena image**		**Extraction from embedded Mandrill image**	
	CC factor	***SSIM***	***CC factor***	***SSIM***
Signature Image 1	0.9965	1.0000	0.9947	1.0000
Signature Image 2	0.9978	1.0000	0.9977	1.0000
Signature Image 3	0.9981	1.0000	0.9972	1.0000

Table 4. The comparison of image quality using PSNR (dB) and embedding capacity (bits)

Cover Images	**Lena (512×512)**		**Baboon (512×512)**	
Measurements	***Capacity (bits)***	***PSNR (dB)***	***Capacity (bits)***	***PSNR (dB)***
Celik et al.'s [18]	74600	38.00	15176	38.00
Xuan et al.'s [19]	85507	36.60	14916	32.80
Tian et al.'s [20]	233067	29.97	95852	29.41
Alattar et al.'s [21]	173655	36.60	86264	36.60
Wu-Tsai's al.'s [26]	51219	38.94	57146	33.43
Kamstra et al.'s [22]	135547	35.20	103653	30.12
Chin-C. C et al.'s [32]	36850	30.34	35402	26.46
Luo, W et al.'s [27]	66064	38.80	68007	33.33
Mandal et al.'s [24]	216000	**40.92**	216000	**40.97**
Proposed Method	**263222**	38.65	**263222**	38.65

The SSIM and CC factor evaluations of Table. 4 show the competency of proposed method. However, it is not appropriate to compare the extraction results of information data with those of other existing methods due to complex values extraction results of proposed method (usually, existing methods do not extract the secret image in the form of complex values). To further prove our scheme's performance on hiding capacity, we compare our proposed scheme with other existing schemes. That is, in order to compare the quality of the embedded images and view the degradation caused by embedding a hidden data, it is necessary to look at embedded cover images with a special payload size [34]. Usually, the resulting perceived quality or PSNR and payload or bits per pixel (bpp) are the two most commonly used criteria for evaluating the performance of reversible data hiding techniques [35].

Table. 4 shows the comparison of our results with Celik et al.'s [36] technique based on compressing the quantization residuals of pixels instead of compressing LSB planes to obtain more extra space for embedding secret data. The compressed residuals and secret data are concatenated and embedded into the cover image. Xuan et al.'s [37] proposed a scheme based on integer wavelet transform (IWT) and created more space in high frequency sub-bands. Tian et al.'s [38] proposed a high capacity reversible data embedding technique that is called difference-expansion (DE) embedding. Alattar et al.'s [39] extended Tian's scheme by introducing the differences expansion of a vector to obtain more extra space for embedding secret data. Afterwards, many techniques, such as Kamstra et al.'s algorithm [40], Chin-C et al.'s [41], Luo et al.'s [42], and Mandal et al.'s [43] have been proposed to increase the embedding capacity and keep the distortion low. But all such methods do not maintained the high resolution images (e.g., medical images etc.) in their extraction phase. However, it is found that hiding capacity of Mandal et al.'s method is higher than other such prevailing techniques, but its hiding capacity is less than our proposed method with cover image size 512×512 and payload size 256×256. Moreover, overall performance of our proposed method shows significant improvement compared with other existing schemes under typical circumstances as demonstrated in Table. 4. Besides this, our proposed method is highly capable to preserve the high resolution of information data images at their extraction stage. Additionally, multi-key establishment for extraction phase provides the high end confidentiality to concealed information data, whereas appropriate encryption develops the great imperceptibility for embedded image. The experimental results presented in Table 4 for comparison of image quality using PSNR (dB) and embedding capacity (bits) are referred to their original experimental results in their papers. The size of payload data (bits) in a cover image can be modified without deteriorating the integrity of the cover image [35]. However, it is not possible to simultaneously maximize robustness, imperceptiveness, and capacity. Therefore, the acceptable balance of these items must be dictated by the application. For example, an information-hiding scheme may forgo robustness in favor of capacity and low perceptibility, whereas a watermarking scheme, which may not require large capacity or low perceptibility, would certainly support increased robustness [6].

V. CONCLUSION

The present paper proposes a novel data hiding scheme to increase the security and privacy of medical information image data by integrating both steganography and cryptography, based on the Fresnelet transform. The main feature of the proposed method is a multi-scale distribution of information on the Fresnelet transform domain with robust key parameters for security, so that the very small distortion in the cover image provides sufficient privacy for the embedded information.

In particular, the Fresnelet decomposition provides robustness to leakage of the energy of information data during the embedding process. For greater security, a combination of the Arnold transform and DCT has been employed in the embedding process. Numerical simulation results have been analyzed with PSNR, SSIM, MSE, and CC factors. Higher values of PSNR, SSIM, and CC factors and smaller value of MSE show the effectiveness of the proposed novel algorithm to achieve great imperceptibility of embedded information image data with required security.

REFERENCES

[1] Munchh, H., Engelmann , U., Schroeter, A., and Meinzer, H.: 'Web-based distribution of radiological images from PACS to EPR', International Congress Series., 2003, 1256, pp. 873-879.

[2] Boucherkha. S and Benmohamed . M.: 'A Lossless Watermarking Based Authentication System For Medical Images'. Proc. of International Conf on Computational Intelligence, Istanbul, Turkey, 2004, pp. 240-243.

[3] Pitt, , et al.: 'Imaging cortical lesions in multiple sclerosis with ultra-high-field magnetic resonance imaging',Archives of Neurology, 67(7), 2010, pp. 812-818.

[4] Al-Frajat A. K. and Jalab H..: 'On the differences between hiding information and cryptography techniques: An overview', Journal of Applied Sciences, 2010, vol. 10, (15), pp. 1650-1655.

[5] Dickman, S. D.: 'An Overview of Steganography', JMU-INFOSEC-TR-2007-002, http://citeseerx.ist.psu.edu/viewdoc/summary?doi=10.1.1.137.5129.

[6] Li, J. He, J. Huang and Y. Q. Shi.: 'A Survey on Image Steganography and Steganalysis', Journal of Information Hiding and Multimedia Signal Processing, 2(2), 2011, pp. 142-172.

[7] Wu, H.-C et al.: 'Image steganographic scheme based on pixel-value differencing and LSB replacement methods'. Vision, Image and Signal Processing, IEE Proceedings, 152(5), 2005, pp. 611-615.

[8] Luo, W et al.: 'Edge Adaptive Image Steganography Based on LSB Matching Revisited' IEEE Transactions on Information Forensics and Security, 5(2), 2010, pp. 201-214.

[9] Fridrich, J., Goljan, M., Du, and R .: 'Detecting LSB steganography in color, and gray-scale images', IEEE Multimedia, 8(4), 2001, pp. 22–28.

[10] Dumitrescu, S., Wu,X. and Wang, Z.: 'Detection of LSB steganography via sample pair analysis," IEEE Trans. Signal Process., 51(7), 2003, pp. 1995–2007.

[11] Yang, H., et al.: 'A High-Capacity Image Data Hiding Scheme Using Adaptive LSB Substitution', Journal of Radioengineering,18(4), 2009, pp. 509-516

[12] Ker, A. D.: 'A fusion of maximum likelihood and structural steganalysis', in Proc. 9th Int. Workshop on Information Hiding, 2007, vol. 4567, pp. 204–219.

[13] Zeng, X.-T et al.: 'A Reversible Data Hiding Scheme using Center Pixel Difference', Journal of Multimedia. 5(4), 2010, pp. 377-384

[14] Chang, C.-C., Lin, C.-C., Tseng, C.-S., & Tai, W.-L.:' Reversible hiding in DCT-based compressed images', Information Sciences, 177(13), 2007, 2768-2786.

[15] Iwata, M., Miyake, K., and Shiozaki, A.: 'Digital Steganography Utilizing Features of JPEG Images, IEICE Trans. Fundamentals, E87-A(4), 2004, pp. 929–936.

[16] Lin , C. Y., Chang, C. C., and Wang, Y. Z.: 'Reversible Steganographic Method with High Payload for JPEG Images', IEICE Trans. Information and Systems, 91-D(3), 2008, pp. 836–845.

[17] Lin, C. C. and Shiu, P. F.: 'DCT-based reversible data hiding scheme, in Proc. of the 3rd International Conference on Ubiquitous Information Management and Communication (ICUIMC'09), 2009, pp. 327–335.

[18] Conway, M.: 'Code Wars: Steganography, Signals Intelligence, and Terrorism', Knowledge Technology & Policy, Springer, 16(2), 2003, pp. 45-62.

[19] Song, Set al .: 'A Novel Secure Communication Protocol Combining Steganography and Cryptography', Elsevier Inc, Advanced in Control Engineering and Information Science, 15, 2011, pp. 2767 – 2772.

[20] Tso, H.-K. and Lou, D.-C.: 'Medical image protection using secret sharing scheme', in Proc. of International Conference on Ubiquitous Information Management and Communication, 2012, pp. 93-93.

[21] Shamir, A.: 'How to share a secret', Communication of the ACM, 22(11), 1979, pp. 612-613.

[22] Fallahpour, M., Megias, D., & Ghanbari, M. .: 'Reversible and high-capacity data hiding in medical images', IET Image Processing, 5(2), 2011, pp. 190–197.

[23] Liebling, M., Blu,T., and Unser , M.: 'Fresnelets: New Multiresolution Wavelet Bases for Digital Holography', IEEE Transactions on Image Processing, 2003, vol. 12,(1), pp. 29-43.

[24] Yang, J.: 'Algorithm of image information hiding based on new anti-Arnold transform and Blending in DCT domain'. Proc. of IEEE Conf on Communication Technology, Nanjing, China, 2010, pp. 312 – 315.

[25] Sun, M. and Zhu, Z.: 'Digital Image Hiding Technology Based on Three-Dimension Object Digital Holography Encoded by Double-Random Phase," 2010. '. Proc. of Photonics and Optoelectronic, 2010, pp. 1-4.

[26] Nazeer, M., and Kim, D. G.: 'A novel Fresnlet based robust data hiding algorithm for medical images'. Proc.of IEEE Conf on Imaging Systems and Techniques, Manchester, U.K, 2012, pp. 213-216.

[27] Liebling, M., & Unser, M.: 'Autofocus for Digital Fresnel Holograms by Use of a Fresnelet-Sparsity Criterion', Journal of the Optical Society of America, 21(12), 2004, pp. 2424-2430.

[28] Greenspan, H et al.:'Super-Resolution in Medical Imaging' , The Computer Journal, 52(1), 2009, pp. 43-63.

[29] Kang , S., and Aoki, Y.: 'A multiple data embedding technique for DRM using Fresnel transform'. Proc.of IEEE Conf on Electrical and Computer Engineering, Saskatoon, Canada , 2005, pp. 2174 – 2177.

[30] Dandapat, S., Xu, J., Chutatape, O., and Krishnan, S.: 'Wavelet transform domain data embedding in a medical image'. Proc. of IEEE Conf on Engineering in Medicine and Biology Society, San Francisco, CA, 2004, pp. 1541 – 1544.

[31] Unfeng, Li and Wenzhan, Dai.: 'Image quality assessment based on the correlation coefficient and the 2-D discrete wavelet transform'. Proc. of IEEE Conf on Automation and Logistics, 2009, pp. 789 -793.

[32] Cepel, R et al.: 'Spatial Correlation Coefficient Images for Ultrasonic Detection' IEEE Transactions on Ultrasonics, Ferroelectrics and Frequency Control, 54(9), 2007, pp. 1841-1850.

[33] Wang, Z et al.: 'Image quality assessment: from error visibility to structural similarity',IEEE Transactions on Image Processing, 13(4), 2004, pp. 600-612.

[34] Chen, W.-J et al.: 'High payload steganography mechanism using hybrid edge detector', Expert Systems with Applications. 37(4), 2010, pp. 3292-3301.

[35] Mare, S. F et al.: 'High capacity steganographic algorithm based on payload adaptation and optimization'. Proc. of IEEE Conf on Applied Computational Intelligence and Informatics, 2012, pp. 87-92.

[36] Celik, M.U, et al. : 'Lossless watermarking for image authentication: A new framework and an implementation," IEEE Transactions on Image Processing, 15,(4), 2006, pp.1042-1049.

[37] Xuan, G et al.: 'Algorithm of image information hiding based on new anti-Arnold transform and Blending in DCT domain', IEE Electron. Lett., vol. 38, (25), 2002, pp.1646–1648.

[38] Tian, J.: 'Reversible data embedding using a difference expansion', IEEE Trans. Circuits and Systems for VideoTechnology, 13(8), 2003, pp.890-896.

[39] Alattar, A.M.: 'Reversible watermark using the difference expansion of a generalized integer transform', IEEE Trans. Image Processing. 13(8), 2004, pp.1147-1156.

[40] Kamstra, L., and Heijmans, H.: 'Reversible data embedding into images using wavelet techniques and sorting', Image Processing, IEEE Transactions on, 14(12), 2005, 2082-2090.

[41] Chen, W.-J et al.: 'High payload steganography mechanism using hybrid edge detector', Expert Systems with Applications. 37(4), 2010, pp. 3292-3301.

[42] Luo, W et al.: 'Edge Adaptive Image Steganography Based on LSB Matching Revisited' IEEE Transactions on Information Forensics and Security, 5(2), 2010, pp. 201-214.

[43] Mandal, J. K, et al.: 'A Novel Genetic Algorithm Based Data Embedding Technique in Frequency Domain Using Z Transform', Proc. of Advances in Intelligent S.

AUTHORS PROFILES

The first author of this paper, Mr. Nazeer Muhammad is currently pursuing the Ph.D. degree in the department of Applied Mathematics, Hanyang University, South Korea. In 2010, he received the prestigious Pakistan Government higher education commission (HEC) scholarship award. His interests are digital signal watermarking, data hiding, digital image denoising, digital holography, OFDM, and information theory.

Ms. Nargis Bibi is a postgraduate research student in the School of Computer Science, University of Manchester. She received her M.Sc from Fatima Jinnah Women University (FJWU), Pakistan. She is currently employed in FJWU as lecturer. Her interests are digital signal processing, OFDM, coding theory and information theory.

Mr. Yasir Mehmood Malik is a Specialist registrar at Rashid Hospital, Dubai in Department of Neourology. He received his Bachelor of Medicine and Bachelor of Surgery (MBBS) from King Edward Medical College, Lahore, Pakistan. He has completed his course for Fellow of College of Physicians and Surgeons (FCPS), Pakistan in 2011. His area of interest is interventional Neurology.

The corresponding author of this paper, Kim, Dai-Gyoung* is a professor of the Department of Applied Mathematics, Hanyang University. He received a B.S. (1983) and M.S (1986) in Mathematics from Hanyang University, and a Ph.D. (1994) in Applied Mathematics from Purdue University. Before joining the Hanyang University faculty in 1995, Professor Kim had been on the IMA of University of Minnesota as a postdoctoral fellow. Also, he was a visiting scholar of IMAGERS UCLA Image Processing Research Group during 2003~2004.

Professor Kim has been teaching various courses of applied mathematics such as linear algebra, numerical analysis, mathematical modeling, real analysis, functional analysis, numerical PDE, wavelet theory and applications. His research mainly focuses on the numerical PDE applied to signal/image processing, wavelet theory and its applications, and 3D holography as well as scientific computations in physics and chemistry.

Readers can contact the author at dgkim@hanyang.ac.kr.

A New Type Method for the Structured Variational Inequalities Problem

Chengjiang Yin
Linyi University at Feixian
Feixian, Shandong, P.R.China

***Abstract*—In this paper, we present an algorithm for solving the structured variational inequality problem, and prove the global convergence of the new method without carrying out any line search technique, and the global R-convergence rate are also given under the suitable conditions.**

Keywords—structured variational inequality problem; algorithm; globally convergent; R-linear convergent

I. INTRODUCTION

Leting mappings $f: X \to R^n, g: Y \to R^m$, the structured variational inequality problem with linear constraint is to find vector $u^* \in \Omega$ such that

$$(u-u^*)^T T(u^*) \geq 0, u \in \Omega \qquad (1.1)$$

where $u = \begin{pmatrix} x \\ y \end{pmatrix}, T(u) = \begin{pmatrix} f(x) \\ g(y) \end{pmatrix}$, $\Omega = \{(x,y) \mid x \in X, y \in Y, Ax + By = b\}$, $X \subseteq R^n, Y \subseteq R^m$ are given nonempty closed convex sets, f, g are given continuous monotone operators, $A \in R^{r \times n}, B \in R^{r \times m}, b \in R^r$. We denote the solution set of the VI by Ω^*, and assume that it is nonempty throughout this paper.

By attaching a Lagrange multiplier vector $\lambda \in R^r$ to the linear constraints $Ax + By = b$,(1.1)can be equivalently transformed into the following compact form, denoted by VI: Find $w^* \in W$ such that

$$(w-w^*)^T Q(w^*) \geq 0, w \in W \qquad (1.2)$$

where $w = \begin{pmatrix} x \\ y \\ z \end{pmatrix}, Q(w) = \begin{pmatrix} f(x) + A^T\lambda \\ g(y) + B^T\lambda \\ Ax + by - b \end{pmatrix}$, $W = X \times Y \times R^r$, and the solution set of (1.2) is denoted by W^* which is always assumed to be nonempty.

This problem has important applications in many fields, such as network economics, traffic assignment, game theoretic problems, etc. For example, Nagurney et al. ([1]) developed a variational inequality based supply chain network equilibrium model consisting of three tiers of decision-makers in the network. They established some governing equilibrium conditions based on the optimality conditions of the decision-makers along with the market equilibrium conditions. In recent years, many methods have been proposed to solve the VI ([2-8]). The alternating direction method (ADM) is a powerful method for solving the structured problem (1.2), since it decompose the original problems into a series subproblesm with lower scale, which was originally proposed by Gabay and Mercier ([5]) and Gabay（[6]）. Ye and Yuan [7] proposed a new descent method for VI by adding an additional projection step to the above ADM. Han ([8]) proposed a modified alternating direction method for variational inequalities with linear constraints. At each iteration, the method only makes an orthogonal projection to simple set and some function evaluations. Motivated by [7, 8], we present a new algorithm for the structured variational inequality problem, and prove the global convergence of the new method without carrying out any line search technique. Furthermore, we also show that this method is global R – linear convergent under the suitable conditions.

Some notations used in this paper are in order. The vectors considered in this paper are all taken in Euclidean space equipped with the standard inner product, which is denoted by R^n. We let $\|\cdot\|$ and $\|\cdot\|_1$ respectively denote the usual Euclidean 2-norm and 1-norm of vectors in R^n. The transpose of matrix M (vector x) be denoted by M^T (x^T).

II. PRELIMINARIES

In this section, we first give the following definition of projection operator and some relate properties ([9]). For nonempty closed convex set $\Omega \subset R^n$ and any vector $x \in R^n$, the orthogonal projection of x onto Ω is denoted by $P_\Omega(x)$.

Lemma 2.1 For any $u \in R^n, v \in \Omega$, then $\langle P_\Omega(u) - u, v - P_\Omega(u)\rangle \geq 0$.

For (1.2), $\beta > 0$ is constant,

$$e(w,\beta) = w - P_W[w - \beta Q(w)]$$

$$= \begin{pmatrix} e_1(w,\beta) \\ e_2(w,\beta) \\ e_3(w,\beta) \end{pmatrix} = \begin{pmatrix} x - P_X[x - \beta(f(x) + A^T\lambda)] \\ y - P_Y[y - \beta(g(y) + B^T\lambda)] \\ \beta(Ax + By - b) \end{pmatrix}$$

is called projection-type residual function, and let $r(\omega) := \|e(\omega)\|$. The following conclusion provides the

relationship between the solution set of (1.2) and that of projection-type residual function ([10]).

Lemma 2.2 ω is a solution of (1.2) if and only if $r(\omega)=0.$

To establish theoretical analysis of the following algorithm, we also need the following definition.

Definition 2.1 The mapping $f:R^n\to R^m$ is said to be co-coercive with modulus $\mu>0$ is

$$\langle f(x)-f(y),x-y\rangle\geq\mu\| f(x)-f(y)\|^2,\quad \forall x,y\in R^n.$$

Definition 2.2 The mapping $f:R^n\to R^m$ is said to be strongly monotone if there is constant $\mu>0$ such that

$$\langle f(x)-f(y),x-y\rangle\geq\mu\| x-y\|^2,\quad \forall x,y\in R^n.$$

Obviously, suppose that f is strongly monotone with positive constant μ, and is Lipschitz continuous with positive constant $L>0$. Then the f is co-coercive, i.e., for any $x,y\in R^n$, we have

$$\begin{aligned}\langle f(x)-f(y),x-y\rangle&\geq\mu\| x-y\|^2=\frac{\mu}{L^2}(L\| x-y\|)^2\\&\geq\frac{\mu}{L^2}\| f(x)-f(y)\|^2.\end{aligned}\tag{2.1}$$

III. Algorithm and Convergence

In this following, we formally state our algorithm.

Algorithm 3.1

Step1. Take $\varepsilon>0,\ 0<\beta<2\min\left\{\frac{\sqrt{\mu_1}}{\sqrt{n}},\frac{\sqrt{\mu_2}}{\sqrt{m}},\frac{\sqrt{\mu_3}}{\sqrt{r}}\right\}$, where the positive constants μ_1, μ_2, μ_3 are defined in the following Theorem 3.1, and take initial point $x^0\in R^n$. Set $k=0$;

Step2. Compute

$$\omega^{k+1}=P_W[\omega^k-\beta Q(\omega^k)]=\begin{pmatrix}P_X[x^k-\beta(f(x^k)+A^T\lambda^k)]\\P_Y[y^k-\beta(g(y^k)+B^T\lambda^k)]\\\lambda^k-\beta(Ax^k+By^k-b)\end{pmatrix};\tag{3.1}$$

Step3. If $\| \omega^{k+1}-\omega^k\|\leq\varepsilon$ stop, otherwise, go to Step 2 with $k:=k+1.$

Remark The algorithm is based on problem (1.2). Obviously, if $\omega^{k+1}=\omega^k$, combining Lemma 2.2, then ω^k is a solution of (1.2), and so is also (1.1). In the following theoretical analysis, we assume that Algorithm 3.1 generates an infinite sequence.

Lemma 3.1 Suppose that the matrix $\bar{M}$ is positive semi-definite, and $\mu_{max}\neq 0$ is a maximum eigenvalue of $\bar{M}$, we have

$$y^T\bar{M}y\geq(1/\mu_{max})\| \bar{M}y\|^2(\forall y\in R^l),\ \text{where}\ \bar{M}=\begin{pmatrix}0&0&A^T\\0&0&B^T\\A&B&0\end{pmatrix}.$$

Proof: Since the matrix $\bar{M}$ is positive semi-definite, then there exists an orthogonal matrix P such that $P\bar{M}P^*=\mathrm{diag}(\sigma_1,\sigma_2,\cdots,\sigma_s,0,\cdots,0),$ where $\sigma_1\geq\sigma_2\geq\cdots\geq\sigma_s>0.$ Set $\xi=Py$, then

$$\begin{aligned}y^*\bar{M}y&=y^*P^*\,\mathrm{diag}(\sigma_1,\sigma_2,\cdots,\sigma_s,0\cdots,0)Py\\&\geq(1/\mu_{max})(\sigma_1^2\xi_1^2+\sigma_2^2\xi_2^2+\cdots+\sigma_s^2\xi_s^2)\\&=(1/\mu_{max})y^*P^*\,\mathrm{diag}(\sigma_1^2,\sigma_2^2,\cdots,\sigma_s^2,0\cdots,0)Py\\&=(1/\mu_{max})\| \bar{M}y\|^2.\end{aligned}$$

Theorem 3.1 Suppose that f,g are co-coercive with positive constants μ_1,μ_2, respectively, and the matrix $\bar{M}$ is positive semi-definite.

Then the sequence $\{\omega^k\}$ converges globally to a solution of (1.1).

Proof: By Lemma 2.1, we have

$$\langle\beta Q(\omega^k)+[\omega^{k+1}-\omega^k],\omega-\omega^{k+1}\rangle\geq 0,\forall\omega\in W.\tag{3.2}$$

We take $\omega^*\in W^*$, then

$$\langle\beta Q(\omega^*),\omega-\omega^*\rangle\geq 0,\forall\omega\in W.\tag{3.3}$$

Let $\omega=\omega^*$ in (3.2), take $\omega=\omega^{k+1}$ in (3.3), adding these two inequalities yields

$$\begin{aligned}&0\leq\langle\beta[Q(\omega^k)-Q(\omega^*)]+\omega^{k+1}-\omega^k,\omega^*-\omega^{k+1}\rangle\\&=\langle\beta[Q(\omega^k)-Q(\omega^*)],\omega^*-\omega^{k+1}\rangle+\langle\omega^{k+1}-\omega^k,\omega^*-\omega^{k+1}\rangle\\&=\langle-\beta[Q(\omega^k)-Q(\omega^*)],\omega^k-\omega^*+\omega^{k+1}-\omega^k\rangle+\\&\quad\langle\omega^{k+1}-\omega^k,\omega^*-\omega^{k+1}\rangle\\&=\langle-\beta[Q(\omega^k)-Q(\omega^*)],\omega^k-\omega^*\rangle-\langle\beta[Q(\omega^k)-Q(\omega^*)],\omega^{k+1}-\omega^k\rangle\\&\quad+\langle\omega^{k+1}-\omega^k,\omega^*-\omega^{k+1}\rangle\\&=-\beta\begin{pmatrix}(f(x^k)-f(x^*))+A^T(\lambda^k-\lambda^*)\\(g(y^k)-g(y^*))+B^T(\lambda^k-\lambda^*)\\A(x^k-x^*)+B(y^k-y^*)\end{pmatrix}^T\begin{pmatrix}x^k-x^*\\y^k-y^*\\\lambda^k-\lambda^*\end{pmatrix}\\&\quad-\langle\beta[Q(\omega^k)-Q(\omega^*)],\omega^{k+1}-\omega^k\rangle+\langle\omega^{k+1}-\omega^k,\omega^*-\omega^{k+1}\rangle\\&=-\beta[(f(x^k)-f(x^*))^T(x^k-x^*)+(g(y^k)-g(y^*))^T(y^k-y^*)]\\&\quad-\beta[(\lambda^k-\lambda^*)^TA(x^k-x^*)+(x^k-x^*)^TA^T(\lambda^k-\lambda^*)+(\lambda^k-\lambda^*)^TB(y^k-y^*)\\&\quad+(y^k-y^*)^TB^T(\lambda^k-\lambda^*)]\\&\quad-\langle\beta[Q(\omega^k)-Q(\omega^*)],\omega^{k+1}-\omega^k\rangle+\langle\omega^{k+1}-\omega^k,\omega^*-\omega^{k+1}\rangle\\&\leq-\beta[\mu_1\| f(x^k)-f(x^*)\|^2+\mu_2\| g(y^k)-g(y^*)\|^2+\mu_3\left\|\begin{pmatrix}A^T(\lambda^k-\lambda^*)\\B^T(\lambda^k-\lambda^*)\\A(x^k-x^*)+B(y^k-y^*)\end{pmatrix}\right\|^2]\\&\quad-\langle\beta[Q(\omega^k)-Q(\omega^*)],\omega^{k+1}-\omega^k\rangle+\langle\omega^{k+1}-\omega^k,\omega^*-\omega^{k+1}\rangle\end{aligned}$$

$$
\begin{aligned}
&\le -\beta[\mu_1\| f(x^k)-f(x^*)\|^2+\mu_2\| g(y^k)-g(y^*)\|^2+\mu_3\left\|A(x^k-x^*)+B(y^k-y^*)\right\|^2]\\
&\quad -\langle\beta[Q(\omega^k)-Q(\omega^*)],\omega^{k+1}-\omega^k\rangle+\langle\omega^{k+1}-\omega^k,\omega^*-\omega^{k+1}\rangle\\
&\le -\beta\left[\sqrt{\mu_1}\| f(x^k)-f(x^*)\|+\sqrt{\mu_2}\| g(y^k)-g(y^*)\|+\sqrt{\mu_3}\| A(x^k-x^*)+B(y^k-y^*)\|\right]^2\\
&\quad -\langle\beta[Q(\omega^k)-Q(\omega^*)],\omega^{k+1}-\omega^k\rangle+\langle\omega^{k+1}-\omega^k,\omega^*-\omega^{k+1}\rangle\\
&\le -\beta\left[\frac{\sqrt{\mu_1}}{\sqrt{n}}\| f(x^k)-f(x^*)\|_1+\frac{\sqrt{\mu_2}}{\sqrt{m}}\| g(y^k)-g(y^*)\|_1+\frac{\sqrt{\mu_3}}{\sqrt{r}}\| A(x^k-x^*)+B(y^k-y^*)\|_1\right]^2\\
&\quad -\langle\beta[Q(\omega^k)-Q(\omega^*)],\omega^{k+1}-\omega^k\rangle+\langle\omega^{k+1}-\omega^k,\omega^*-\omega^{k+1}\rangle\\
&\le -\beta\mu\left[\left\|\begin{pmatrix} f(x^k)-f(x^*)\\ g(y^k)-g(y^*)\\ (Ax^k+By^k-b)-(Ax^*+By^*-b)\end{pmatrix}\right\|_1\right]^2-\langle\beta[Q(\omega^k)-Q(\omega^*)],\omega^{k+1}-\omega^k\rangle\\
&\quad +\langle\omega^{k+1}-\omega^k,\omega^*-\omega^{k+1}\rangle\\
&\le -\beta\mu\left[\left\|\begin{pmatrix} f(x^k)-f(x^*)\\ g(y^k)-g(y^*)\\ (Ax^k+By^k-b)-(Ax^*+By^*-b)\end{pmatrix}\right\|\right]^2-\langle\beta[Q(\omega^k)-Q(\omega^*)],\omega^{k+1}-\omega^k\rangle\\
&\quad +\langle\omega^{k+1}-\omega^k,\omega^*-\omega^{k+1}\rangle\\
&\le -\beta\mu\left[\left\|\left(Q(\omega^k)-Q(\omega^*)\right)\right\|\right]^2+\langle\beta[Q(\omega^k)-Q(\omega^*)],\omega^k-\omega^{k+1}\rangle\\
&\quad +\langle\omega^{k+1}-\omega^k,\omega^*-\omega^{k+1}\rangle\\
&\le -\beta\mu\left[\left\|Q(\omega^k)-Q(\omega^*)\right\|\right]^2+\beta\| Q(\omega^k)-Q(\omega^*)\|\ \|\omega^{k+1}-\omega^k\|\\
&\quad +\langle\omega^{k+1}-\omega^k,\omega^*-\omega^{k+1}\rangle\\
&\le -\beta\mu\left\|Q(\omega^k)-Q(\omega^*)\right\|^2+\beta\mu\left\|Q(\omega^k)-Q(\omega^*)\right\|^2+\frac{\beta}{4\mu}\|\omega^{k+1}-\omega^k\|^2\\
&\quad +\langle\omega^{k+1}-\omega^k,\omega^*-\omega^{k+1}\rangle\\
&=\frac{\beta}{4\mu}\|\omega^{k+1}-\omega^k\|^2-\frac{1}{2}\|\omega^*-\omega^{k+1}\|^2+\frac{1}{2}\|\omega^*-\omega^k\|^2-\frac{1}{2}\|\omega^{k+1}-\omega^k\|^2\\
&=\frac{1}{2}(\frac{\beta}{2\mu}-1)\|\omega^{k+1}-\omega^k\|^2-\frac{1}{2}\|\omega^*-\omega^{k+1}\|^2+\frac{1}{2}\|\omega^*-\omega^k\|^2,
\end{aligned}
$$

where the second inequality follows from the fact that f,g are co-coercive with positive constants μ_1,μ_2 and Lemma 3.1; the fourth inequality is obtained by

$$a^2+b^2+c^2\le(a+b+c)^2\qquad(a\ge0,b\ge0,c\ge0),$$

the fifth inequality and the seventh inequality follow from the fact that

$$\|x\|\le\|x\|_1\le\sqrt{n}\|x\|,\forall x\in R^n,$$

and the sixth inequality is true by letting $\mu=\min\left\{\frac{\sqrt{\mu_1}}{\sqrt{n}},\frac{\sqrt{\mu_2}}{\sqrt{m}},\frac{\sqrt{\mu_3}}{\sqrt{r}}\right\}$, the ninth inequality follows from the Cauchy-Schwarz inequality. Thus, we have

$$(\frac{\beta}{2\mu}-1)\|\omega^{k+1}-\omega^k\|^2-\|\omega^*-\omega^{k+1}\|^2+\|\omega^*-\omega^k\|^2\ge0.$$

Combining this with $0<\beta<2u$, we have

$$\|\omega^{k+1}-\omega^k\|^2\le\frac{2u-\beta}{2u}\|\omega^*-\omega^k\|^2-\frac{2u-\beta}{2u}\|\omega^*-\omega^{k+1}\|^2 \tag{3.4}$$

i.e.,

$$r(\omega^k)^2\le\frac{2u-\beta}{2u}\|\omega^*-\omega^k\|^2-\frac{2u-\beta}{2u}\|\omega^*-\omega^{k+1}\|^2. \tag{3.5}$$

by (3.4), we conclude that the nonnegative sequence $\{\|\omega^k-\omega^*\|\}$ is strictly decreasing and convergent. Thus, we have $r(x^k)$ converges to 0 by (3.5). We also obtain that the sequence $\{\|\omega^k-\omega^*\|\}$ is bounded since it is convergent, and so is $\{\omega^k\}$. Let $\{\omega^{k_j}\}$ be a subsequence of $\{\omega^k\}$ and converges to $\bar{\omega}$, since $r(\omega)$ is continuous, we have $r(\bar{\omega})=0$, i.e., $\bar{\omega}$ is a solution of (1.1).

On the other hand, we suppose that ω is also a accumulation point of $\{\omega^k\}$, and let $\{\omega^{k_j}\}$ be a subsequence of $\{\omega^k\}$ and converges to ω. For any k_j, there exists i such that $k_i<k_j$, by (3.4), we obtain that $\|\omega^{k_j}-\hat{\omega}\|^2\le\|\omega^{k_i}-\hat{\omega}\|^2\to0$ as $k_i\to\infty$. Using (3.4) again, we can also obtain $\|\omega^{k_j}-\omega^{k_i}\|\to0$. Thus, we have

$$\|\hat{\omega}-\bar{\omega}\|\le\|\omega^{k_i}-\bar{\omega}\|+\|\omega^{k_j}-\hat{\omega}\|+\|\omega^{k_j}-\omega^{k_i}\|\to0\ \text{ as }\ k_i\to\infty,$$

i.e., $\hat{\omega}=\bar{\omega}$. Thus, the sequence $\{\omega^k\}$ converges globally to a solution of (1.1).

To establish the $R-$ linear convergence rate of Algorithm3.1, we also need the following conclusion which is crucial to convergence rate of algorithm.

Lemma 3.2 Suppose that f,g are strongly monotone with positive constants μ_1,μ_2, and are Lipschitz continuous with positive constants $L_1>0,L_2>0$, respectively, the matrix $\begin{pmatrix}A^T\\B^T\end{pmatrix}$ has full-column rank. Then for any $\omega\in R^{n+m+r}$, there exists a solution ω^* of (1.1) such that

$$\|\omega-\omega^*\|\le\max\{u_1^{-1},u_2^{-1},v_3^{-1}\}\frac{1}{\beta}\{1+\beta L\}r(\omega). \tag{3.6}$$

Proof: Since $\omega-e(\omega)=P_W[\omega-\beta Q(\omega)]\in W$, by (1.1),

$$\beta(\omega-e(\omega)-\omega^*)^TQ(\omega^*)\ge0. \tag{3.7}$$

Combining $\omega^*\in W^*$ with Lemma 2.1, we have

$$\langle\omega^*-P_W[\omega-\beta Q(\omega)],P_W[\omega-\beta Q(\omega)]-[\omega-\beta Q(\omega)]\rangle\ge0. \tag{3.8}$$

Substituting $P_W[\omega-\beta Q(\omega)]$ in (3.8) by $\omega-e(\omega)$ yields

$$(\omega-\omega^*-e(\omega))^T[e(\omega)-\beta Q(\omega)]\ge0. \tag{3.9}$$

Adding (3.7) and (3.9), one has

$$[(\omega-\omega^*)-e(\omega)]^T[e(\omega)+\beta(Q(\omega^*)-Q(\omega))]\ge0,$$

i.e.,

$$(\omega-\omega^*)^T\beta[Q(\omega^*)-Q(\omega)]+e(\omega)^T[(\omega-\omega^*)-\beta(Q(\omega^*)-Q(\omega))]$$
$$-e(\omega)^T e(\omega)\geq 0.$$

Combining this with Definition 2.2, a direct computation yields

$$\begin{aligned}
&\| \omega-\omega^*\|^2=\|x-x^*\|^2+\|y-y^*\|^2+\|\lambda-\lambda^*\|^2\\
&\leq \max\{u_1^{-1},u_2^{-1},v_3^{-1}\}[(f(x)-f(x^*))^T(x-x^*)+(g(y)-g(y^*))^T(y-y^*)\\
&+(\omega-\omega^*)^T\overline{M}(\omega-\omega^*)]\\
&=\max\{u_1^{-1},u_2^{-1},v_3^{-1}\}\begin{pmatrix}(f(x)-f(x^*))+A^T(\lambda-\lambda^*)\\(g(y)-g(y^*))+B^T(\lambda-\lambda^*)\\A(x-x^*)+B(y-y^*)\end{pmatrix}^T\begin{pmatrix}x-x^*\\y-y^*\\\lambda-\lambda^*\end{pmatrix}\\
&=\max\{u_1^{-1},u_2^{-1},v_3^{-1}\}\begin{pmatrix}(f(x)+A^T\lambda)-(f(x^*)+A^T\lambda^*)\\(g(y)+B^T\lambda)-(g(y^*)+B^T\lambda^*)\\(Ax+By-b)-(Ax^*+By^*-b)\end{pmatrix}^T\begin{pmatrix}x-x^*\\y-y^*\\\lambda-\lambda^*\end{pmatrix}\\
&=\max\{u_1^{-1},u_2^{-1},v_3^{-1}\}[(\omega-\omega^*)^{\cdot}(Q(\omega)-Q(\omega^*))]\\
&\leq \max\{u_1^{-1},u_2^{-1},v_3^{-1}\}\frac{1}{\beta}\{e(x)^T[(\omega-\omega^*)+\beta(Q(\omega^*)-Q(\omega))]-e(\omega)^T e(\omega)\}\\
&\leq \max\{u_1^{-1},u_2^{-1},v_3^{-1}\}\frac{1}{\beta}\{\|e(\omega)\|(\|\omega-\omega^*\|+\beta\|(Q(\omega^*)-Q(\omega))\|)\}\\
&\leq \max\{u_1^{-1},u_2^{-1},v_3^{-1}\}\frac{1}{\beta}r(\omega)\{\|\omega-\omega^*\|+\beta L\|\omega-\omega^*\|\},
\end{aligned}$$

where $v_3^{-1}=\left\|\left((A,B)\begin{pmatrix}A^T\\B^T\end{pmatrix}\right)^{-1}(A,B)\right\|^2$. Thus, we can conclude that (3.6) holds.

Theorem 3.2 Suppose that the hypotheses of Lemma 3.2 holds, and β satisfies the condition

$$1>\frac{2u-\beta}{2u}-\frac{\beta^2}{\max\{u_1^{-1},u_2^{-1},v_3^{-1}\}^2\{1+\beta L\}^2}>0,$$

then the sequence $\{\omega^k\}$ converges to a solution of (1.1) $R-$linearly.

Proof: Combining (3.5) with (3.6), one has

$$\begin{aligned}
&\frac{\beta^2}{\max\{u_1^{-1},u_2^{-1},v_3^{-1}\}^2\{1+\beta L\}^2}\|\omega^k-\omega^*\|^2\\
&\leq r(\omega^k)^2\leq\frac{2u-\beta}{2u}\|\omega^k-\omega^*\|^2-\frac{2u-\beta}{2u}\|\omega^*-\omega^{k+1}\|^2.
\end{aligned}$$

i.e.,

$$\|\omega^*-\omega^{k+1}\|^2\leq\left(\frac{2u-\beta}{2u}-\frac{\beta^2}{\max\{u_1^{-1},u_2^{-1},v_3^{-1}\}^2\{1+\beta L\}^2}\right)\|\omega^k-\omega^*\|^2$$

By $1>\frac{2u-\beta}{2u}-\frac{\beta^2}{\max\{u_1^{-1},u_2^{-1},v_3^{-1}\}^2\{1+\beta L\}^2}>0$, then the desired result follows.

IV. Conclusions

In this paper, we proposed a new iterative method for solving the structured variational inequality problem (VI), and have proved its global convergence without carrying out any line search technique. Furthermore, the error bound estimation for VI is also established under the suitable conditions, based on this, we prove that the method has global R-linear convergence rate. Surely, under milder conditions, we may established global error bounds for VI, and may use the error bound estimation to establish quick convergence rate of the method for solving the VI. This is a topic for future research.

Acknowledgment

The author wish to give their sincere thanks to the editor and the anonymous referees for their valuable suggestions and helpful comments which improved the presentation of the paper.

References

[1] Stadtler H. and Kilger C., Supply chain management and advanced planning. Berlin, Germany: Springer-Verlag, 2002.

[2] Facchinei F.and Pang J.S.,Finite-dimensional Variational Inequality and Complementarity Problems. New York:Springer, 2003.

[3] Wang Y.J., Xiu N.H. and Zhang J.Z.,"Modified extragradient methods for varitional inequalities and verification of solution existence,"J. Optim. Theroy Appl,vol.119,pp. 167-183,2003.

[4] Wang Y.J.," A new projection and contraction method for varitional inequalities," Pure Math. and Appl,vol.13,no.4, pp.483-493,2002.

[5] Gabay D.,"Applications of the method of multipliers to variational inequalities."In:M.Fortin and R.Glowinski(Eds) Augmented Lagrange Methods. Applications to the Solution of Boundary valued Problems(Amsterdam: North Holland), pp.299-331,1983.

[6] Gabay D. and Mercier B.,"A dual algorithm for the solution of nonlinear variational problem svia finite-element approximations,"Computers and Mathematics with Applications ,vol.2, pp.17-40,1976.

[7] Ye C. H. and Yuan X. M.," A descent method for structured monotone variational inequalities," Optimization Methods and Software,vol. 22,no.2, pp.329-338,2007.

[8] Han D.R.,"A modified alternating direction method for variational inequality problems," Applied Mathematics and Optimization,vol. 45, pp.63-74,2002.

[9] Wang Y. J., Xiu N.H., Theory and algorithms for nonlinear programming. Xian: Shanxi science and technology press, pp.171, 2008. (In Chinese)

[10] Noor M.A., "General variational inequalities", Appl. Math. Lett., 1(2), pp. 119-121,1988.

A Posteriori Error Estimator for Mixed Approximation of the Navier-Stokes Equations with the $C_{a,b,c}$ Boundary Condition

J. EL Mekkaoui, M A. Bennani, A.Elkhalfi
Mechanical engineering laboratory
Faculty of sciences and techniques-B.P. 2202 Route Imouzzer
Fes

A. Elakkad
Department of mathematics
Regional Centre for Professions of Education and Training,
Fes, B.P: 243 Sefrou Morocco

***Abstract*—In this paper, we introduce the Navier-Stokes equations with a new boundary condition. In this context, we show the existence and uniqueness of the solution of the weak formulation associated with the proposed problem. To solve this latter, we use the discretization by mixed finite element method. In addition, two types of a posteriori error indicator are introduced and are shown to give global error estimates that are equivalent to the true error. In order to evaluate the performance of the method, the numerical results are compared with some previously published works and with others coming from commercial code like ADINA system.**

Keywords—Navier-Stokes Equations; $C_{a,b,c}$ ***boundary condition; Mixed Finite element method; Residual Error Estimator;***

I. INTRODUCTION

This paper describes a numerical solutions of Navier-stoks equations with a new boundary condition generalizes the will known basis conditions, especially the Dirichlet and the Neumann conditions. So, we prove that the weak formulation of the proposed modelling has an unique solution. To calculate this latter, we use the discretization by mixed finite element method. Moreover, we propose two types of a posteriori error indicator which are shown to give global error estimates that are equivalent to the true error. To compare our solution with the some previously ones, as ADINA system, some numerical results are shown. This method is structured as a standalone package for studying discretization algorithms for PDEs and for exploring and developing algorithms in numerical linear and nonlinear algebra for solving the associated discrete systems. It can also be used as a pedagogical tool for studying these issues, or more elementary ones such as the properties of Krylov subspace iterative methods [15].

The latter two PDEs constitute the basis for computational modeling of the flow of an incompressible Newtonian fluid. For the equations, we offer a choice of two-dimensional domains on which the problem can be posed, along with boundary conditions and other aspects of the problem, and a choice of finite element discretizations on a quadrilateral element mesh.

Whereas the discrete Navier-Stokes equations require a method such as the generalized minimum residual method (GMRES), which is designed for non symmetric systems [15]. The key for fast solution lies in the choice of effective preconditioning strategies. The package offers a range of options, including algebraic methods such as incomplete LU factorizations, as well as more sophisticated and state-of-the-art multigrid methods designed to take advantage of the structure of the discrete linearized Navier-Stokes equations. In addition, there is a choice of iterative strategies, Picard iteration or Newton's method, for solving the nonlinear algebraic systems arising from the latter problem.

A posteriori error analysis in problems related to fluid dynamics is a subject that has received a lot of attention during the last decades. In the conforming case there are several ways to define error estimators by using the residual equation. in particular, for the Stokes problem, M. Ainsworth, J. Oden [10], C.Carstensen, S.A. Funken [12], D.Kay, D.Silvester [13] and R.Verfurth [14], introduced several error estimators and provided that that they are equivalent to the energy norm of the errors. Other works for the stationary Navier-Stokes problem have been introduced in [5, 8, 15, 16].

The plan of the paper is as follows. Section II presents the model problem used in this paper. The weak formulation is presented in section III. In section IV, we show the existence and uniqueness of the solution.

The discretization by mixed finite elements is described in section V. Section VI introduced two types of a posteriori error bounds of the computed solution. Numerical experiments carried out within the framework of this publication and their comparisons with other results are shown in Section VII.

II. GOVERNING EQUATIONS

We will consider the model of viscous incompressible flow in an idealized, bounded, connected domain in IR^2.

$$-\nu\nabla^2\vec{u}+\vec{u}.\nabla\vec{u}+\nabla p=\vec{f} \text{ in } \Omega, \quad (1)$$

$$\nabla.\vec{u}=0 \text{ in } \Omega, \quad (2)$$

$$\vec{n}^T\left(pI-\nu\nabla\vec{u}\right)=\vec{u}^T A-\vec{g} \text{ on } \Gamma. \quad (3)$$

We also assume that Ω has a polygonal boundary $\Gamma := \partial\Omega$, so $\vec{n}$ that is the usual outward-pointing normal.

The vector field $\vec{u}$ is the velocity of the flow and the scalar variable *p* represents the pressure.

Our mathematical model is the Navier-stoks system with a new boundary condition (3) noted $C_{a,b,c}$. where $\nu \succ 0$ a given constant is called the kinematic viscosity, ∇ is the gradient, $\nabla.$ is the divergence and ∇^2 is the Laplacien operator, $\vec{f} \in L^2(\Omega)$, $\vec{g} \in L^2(\Gamma)$ and *A* is a real matrix defined as

- $A(x,y) = \begin{bmatrix} a(x,y) & c(x,y) \\ c(x,y) & b(x,y) \end{bmatrix}$ *for all* $(x,y) \in \Gamma$ (4)

- There are two strictly positive constants α_1 and β_1, such that:

$$\alpha_1 \le X^T A(x,y) X \le \beta_1 \quad (5)$$

for all $(x,y) \in \Gamma$ and $X \in S = \{ X \in IR^2 / \|X\|_2 = 1 \}$. Where a, b and c are the function continuous defined on Γ.

III. The Weak Formulation

We define the following spaces:

$$h^1(\Omega) = \left\{ u : \Omega \to IR / u; \frac{\partial u}{\partial x}; \frac{\partial u}{\partial y} \in L^2(\Omega) \right\} \quad (6)$$

$$H^1(\Omega) = \left[h^1(\Omega) \right]^2 \quad (7)$$

$$L_0^2(\Omega) = \left\{ q \in L^2(\Omega) / \int_\Omega q = 0 \right\}, \quad (8)$$

$$H_{n,0}^1(\Omega) = \left\{ \vec{v} \in H^1(\Omega) / \vec{v}.\vec{n} = 0 \; in \; \Gamma \right\}, \quad (9)$$

$$V_{n,0}^1(\Omega) = \left\{ \vec{v} \in H_{n,0}^1(\Omega) / \nabla.\vec{v}. = 0 \text{ in } \Omega \right\}. \quad (10)$$

The standard weak formulation of the Navier-Stokes flow problem (1) - (2)-(3) is the following:

Find $\vec{u} \in H^1(\Omega)$ and $p \in L^2(\Omega)$ such that

$$\begin{cases} \bullet \int_\Omega \nu \nabla\vec{u} : \nabla\vec{v} + \int_\Omega (\vec{u}\nabla\vec{u})\vec{v} + \int_\Gamma \vec{u}^T A\vec{v} - \int_\Omega p\nabla.\vec{v} \\ \qquad = \int_\Omega \vec{f}\vec{v} + \int_\Gamma \vec{g}\vec{v}, \\ \bullet -\int_\Omega q\nabla.\vec{u} ds = 0, \end{cases} \quad (11)$$

for all $(\vec{v}, q) \in H_{n,0}^1(\Omega) \times L_0^2(\Omega)$.

Let the bilinear forms

$A : H_{n,0}^1(\Omega) \times H_{n,0}^1(\Omega) \to IR$; $B : H_{n,0}^1(\Omega) \times L_0^2(\Omega) \to IR$

$d : L_0^2(\Omega) \times L_0^2(\Omega) \to IR$.

$$A(\vec{u},\vec{v}) = \nu \int_\Omega \nabla\vec{u} : \nabla\vec{v} + \int_\Gamma \vec{u}^T A\vec{v} \quad (12)$$

$$B(\vec{u}, q) = -\int_\Omega q\nabla.\vec{u} \quad (13)$$

$$d(p,q) = \int_\Omega p.q \quad (14)$$

And the tri-linear forms

$C : H_{n,0}^1 \times H_{n,0}^1 \times H_{n,0}^1 \to IR$; $D : H_{n,0}^1 \times H_{n,0}^1 \times H_{n,0}^1 \to IR$

$$C(\vec{u},\vec{v},\vec{z}) = \int_\Omega (\vec{u}\nabla\vec{v})\vec{z} \quad (15)$$

$$D(\vec{u},\vec{v},\vec{z}) = A(\vec{u},\vec{v}) + C(\vec{u},\vec{v},\vec{z}) \quad (16)$$

Given the functional $L : L_0^2(\Omega) \to IR$

$$L(\vec{v}) = \int_\Gamma \vec{g}.\vec{v} + \int_\Omega \vec{f}.\vec{v} \quad (17)$$

The underlying weak formulation (11) may be restated as:

find $(\vec{u}, p) \in H_{n,0}^1(\Omega) \times L_0^2(\Omega)$ such that

$$\begin{cases} A(\vec{u},\vec{v}) + C(\vec{u},\vec{u},\vec{v}) + B(\vec{v}, q) = L(\vec{v}) \\ B(\vec{u}, q) = 0 \end{cases} \quad (18)$$

for all $(\vec{v}, q) \in H_{n,0}^1(\Omega) \times L_0^2(\Omega)$.

In the sequel we can assume that $\vec{g} = \vec{0}$.

IV. The Existence and Uniqueness of the Solution

In this section we will study the existence and uniqueness of the solution of problem (18), for that we need the following results.

Theorem 4.1. There are two strictly positive constants c_1 and c_2 such that:

$$c_1 \|\vec{v}\|_{1,\Omega} \le \|\vec{v}\|_{J,\Omega} \le c_2 \|\vec{v}\|_{1,\Omega} \quad \textit{for all } \vec{v} \in H_{n,0}^1(\Omega) \quad (19)$$

with

$$\|\vec{v}\|_{J,\Omega} = \left(\nu \int_\Omega \nabla\vec{v} : \nabla\vec{v} + \int_\Gamma \vec{v}^T A\vec{v} \right)^{\frac{1}{2}} \quad (20)$$

$$\|\vec{v}\|_{1,\Omega} = \left(|\vec{v}|_{1,\Omega}^2 + \|\vec{v}\|_{0,\Omega}^2 \right)^{\frac{1}{2}} \quad (21)$$

Proof. **1**) The mapping $\gamma_0 : H^1(\Omega) \to L^2(\Gamma)$ is continuous

(See [6] theorem 1, 2), then there exists $c \succ 0$ such that: $\|\vec{v}\|_{0,\Gamma} \le c\|\vec{v}\|_{1,\Omega}$ for all $\vec{v} \in H^1(\Omega)$. Using (5) gives,

$$\alpha_1 \|\vec{v}\|_{0,\Gamma}^2 \le \int_\Gamma \vec{v}^T A\vec{v} \le \beta_1 \|\vec{v}\|_{0,\Gamma}^2, \quad (22)$$

then $\|\vec{v}\|_{J,\Omega} \le c_2 \|\vec{v}\|_{1,\Omega}$ for all $\vec{v} \in H^1(\Omega)$,

with $c_2 = \left(\beta_1 c^2 + \nu \right)^{\frac{1}{2}}$.

On the other hand. According to 5.55 in [1], there exists a constant $\rho \succ 0$ such that $\|\vec{v}\|_{0,\Omega}^2 \le \rho(\|\nabla\vec{v}\|_{0,\Omega}^2 + \|\vec{v}\|_{0,\Gamma}^2)$.

Using (22), gives

$$c_1 \|\vec{v}\|_{1,\Omega} \le \|\vec{v}\|_{J,\Omega} \text{ for all } \vec{v} \in H^1(\Omega),$$

with $c_1 = \left(\frac{\rho C}{\nu\alpha_1} + \frac{1}{\nu} \right)^{-\frac{1}{2}}$ and $C = \max\{\alpha_1; \nu\}$.

Finally, $c_1 \|\vec{v}\|_{1,\Omega} \le \|\vec{v}\|_{J,\Omega} \le c_2 \|\vec{v}\|_{1,\Omega}$ for all $\vec{v} \in H^1(\Omega)$.

This result allows us to prove that $(H^1_{n,0}(\Omega), \|.\|_{J,\Omega})$ is a Hilbert space which is obliged condition for to obtain the existence and uniqueness of the solution.

Theorem 4.2. $(H^1_{n,0}(\Omega), \|.\|_{J,\Omega})$ is a real Hilbert space.

Proof. $(H^1(\Omega), \|.\|_{1,\Omega})$ is a real space and $H^1_{n,0}(\Omega)$ is closed in $H^1(\Omega)$ and $\|.\|_{1,\Omega}$ and $\|.\|_{J,\Omega}$ are equivalent norms, then $(H^1_{n,0}(\Omega), \|.\|_{J,\Omega})$ is a real Hilbert space for two norms.

Theorem 4.3

1) $$A(\vec{u},\vec{v}) \le \|\vec{u}\|_{J,\Omega}\|\vec{v}\|_{J,\Omega} \quad (23)$$

for all $(\vec{u},\vec{v}) \in H^1_{n,0}(\Omega)\times H^1_{n,0}(\Omega)$

2) A is $H^1_{n,0}(\Omega)$ - elliptic for the norm $\|.\|_{J,\Omega}$ and

$$A(\vec{v},\vec{v}) = \|\vec{v}\|^2_{J,\Omega} \quad (24)$$

for all $\vec{v} \in H^1_{n,0}(\Omega)$.

Proof: it is easy.

Theorem 4.4

1) $$B(\vec{v},q) \le \sqrt{\frac{2}{\nu}}\|q\|_{0,\Omega}\|\vec{v}\|_{J,\Omega}, \quad (25)$$

for all $(\vec{v},q) \in H^1_{n,0}(\Omega)\times L^2_0(\Omega)$

2) The bilinear form b is satisfies the inf-sup: There exists a constant $\beta \succ 0$ such that

$$\sup_{\vec{v}\in H^1_{n,0}(\Omega)} \frac{B(\vec{v},q)}{\|\vec{v}\|_{J,\Omega}} \ge \beta\|q\|_{0,\Omega} \quad for\ all \quad q \in L^2_0(\Omega) \quad (26)$$

Proof.

1) Let $(\vec{v},q) \in H^1_{n,0}(\Omega)\times L^2_0(\Omega)$, we have

$$B(\vec{v},q) \le \|q\|_{0,\Omega}\|\nabla.\vec{v}\|_{0,\Omega}$$
$$\le \sqrt{2}\|q\|_{0,\Omega}\|\nabla\vec{v}\|_{0,\Omega}$$
$$\le \sqrt{\frac{2}{\nu}}\|q\|_{0,\Omega}\|\vec{v}\|_{J,\Omega}.$$

2) Let $q \in L^2_0(\Omega)$, we have

$$\sup_{\vec{v}\in H^1_0(\Omega)} \frac{B(\vec{v},q)}{|\vec{v}|_{1,\Omega}} \ge \beta'\|q\|_{0,\Omega} \ (\text{see [6]}),$$

since

$$H^1_0(\Omega) = \{\vec{v} \in H^1(\Omega) / \vec{v} = \vec{0}\ in\ \Gamma\} \subset H^1_{n,0}(\Omega)$$

and $|\vec{v}|_{1,\Omega} = \|\vec{v}\|_{1,\Omega}$ for all $\vec{v} \in H^1_0(\Omega)$

$$\sup_{\vec{v}\in H^1_{n,0}(\Omega)} \frac{B(\vec{v},q)}{\|\vec{v}\|_{1,\Omega}} \ge \sup_{\vec{v}\in H^1_0(\Omega)} \frac{B(\vec{v},q)}{\|\vec{v}\|_{1,\Omega}}$$
$$= \sup_{\vec{v}\in H^1_0(\Omega)} \frac{B(\vec{v},q)}{|\vec{v}|_{1,\Omega}}$$
$$\ge \beta'\|q\|_{0,\Omega}.$$

Using (19) gives

$$\sup_{\vec{v}\in H^1_{n,0}(\Omega)} \frac{B(\vec{v},q)}{\|\vec{v}\|_{J,\Omega}} \ge \beta\|q\|_{0,\Omega}, \text{ with } \beta = \frac{\beta'}{c_2}.$$

Theorem 4.5

1) There exists a constant $m \succ 0$ such that

$$C(\vec{u},\vec{v},\vec{z}) \le m\|\vec{u}\|_{J,\Omega}\|\vec{v}\|_{J,\Omega}\|\vec{z}\|_{J,\Omega} \quad (27)$$

for all $(\vec{u},\vec{v},\vec{z}) \in H^1_{n,0}\times H^1_{n,0}\times H^1_{n,0}$.

2) $$C(\vec{u},\vec{v},\vec{z}) = -C(\vec{u},\vec{z},\vec{v}) \quad (28)$$

for all $(\vec{u},\vec{v},\vec{z}) \in V^1_{n,0}\times V^1_{n,0}\times V^1_{n,0}$.

3) $$C(\vec{v},\vec{u},\vec{u}) = 0 \quad (29)$$

for all $(\vec{u},\vec{v}) \in V^1_{n,0}\times V^1_{n,0}$.

4) $$D(\vec{w},\vec{v},\vec{v}) = A(\vec{v},\vec{v}) = \|\vec{v}\|^2_{J,\Omega} \quad (30)$$

5) $\vec{u}_m \to \vec{u}$ weakly in $V_{n,0}(\Omega)$ (as $m \to \infty$) imply that $D(\vec{u}_m,\vec{u}_m,\vec{v}) \to D(\vec{u},\vec{u},\vec{v})$ (31)

Proof

1) Let $\vec{z},\vec{u},\vec{v} \in H^1_{n,0}(\Omega)$, we have

$$C(\vec{u},\vec{v},\vec{z}) \le m'\|\vec{u}\|_{1,\Omega}|\vec{v}|_{1,\Omega}\|\vec{z}\|_{1,\Omega} \ (\text{see in [6]})$$
$$\le \frac{m'}{c_1^3}\|\vec{u}\|_{J,\Omega}\|\vec{v}\|_{J,\Omega}\|\vec{z}\|_{J,\Omega}$$

2) Let $\vec{z},\vec{u},\vec{v} \in V^1_{n,0}(\Omega)$, we have

$$C(\vec{z},\vec{u},\vec{v}) + C(\vec{z},\vec{v},\vec{u}) = \int_\Omega \vec{z}.(\nabla\vec{u}.\vec{v} + \nabla\vec{v}.\vec{u})$$
$$= \int_\Omega \vec{z}.\nabla(\vec{u}.\vec{v})$$

By Green formula, we have

$$C(\vec{z},\vec{u},\vec{v}) + C(\vec{z},\vec{v},\vec{u}) = \int_{\partial\Omega}(\vec{z}.\vec{n})(\vec{u}.\vec{v}) - \int_\Omega div\ \vec{z}.(\vec{u}.\vec{v})$$

Since $\vec{z} \in V_{n,0}(\Omega)$ then $\vec{z}.\vec{n} = 0$ and $div\ \vec{z} = 0$,

finally $C(\vec{z},\vec{u},\vec{v}) = -C(\vec{z},\vec{v},\vec{u})$.

3) It's easy, just take $\vec{v} = \vec{u}$ in (28).

4) It' suffices to apply (29).

5) The same proof of V.Girault and P.A. Raviart in [6] page 115.

According the theorems 1.2 and 1.4, chapter IV in [6], the results (18)-(30) ensure the existence at least one pair $(\vec{u},p) \in H^1_{n,0}(\Omega)\times L^2_0(\Omega)$ satisfies (18).

We define

$$N = \sup_{\vec{u},\vec{v},\vec{z}\in H^1_{n,0}} \frac{C(\vec{u},\vec{v},\vec{z})}{\|\vec{u}\|_{J,\Omega}\|\vec{v}\|_{J,\Omega}\|\vec{z}\|_{J,\Omega}} \quad (32)$$

$$\|\vec{f}\|_* = \sup_{\vec{v}\in V_{n,0}} \frac{\int_\Omega \vec{f}.\vec{v}}{\|\vec{v}\|_{J,\Omega}} \quad (33)$$

Then a well-know (sufficient) condition for uniqueness is that forcing function is small in the sense that $\|\vec{f}\|_* \le \frac{1}{N}$ (it suffices to apply theorems 1.3 and 1.4 chapter IV in [6]).

Theorem 4.6. Assume that ν and $\vec{f} \in L^2(\Omega)$ satisfy the following condition

$$\left|\int_\Omega \vec{f}.\vec{v}\right| \le \frac{\delta}{N}\|\vec{v}\|_{J,\Omega} \text{ for all } \vec{v} \in H^1_{n,0}(\Omega) \qquad (34)$$

For some fixed number $\delta \in [0,1[$.

Then there exists an unique $(\vec{u}, p) \in H^1_{n,0}(\Omega) \times L^2_0(\Omega)$ satisfies (18), and holds

$$\|\vec{u}\|_{J,\Omega} \le \frac{\delta}{N}. \qquad (35)$$

Proof. The some proof of theorem 2.4 chapter IV in [6].

V. Mixed Finite Element Approximation

In this section we assume that $\vec{f}, a, b$ and c are the polynomials.

Let $T_h ; h \succ 0,$ be a family of rectangulations of Ω. For any $T \in T_h$, ω_T is of rectangles sharing at least one edge with element T, $\tilde{\omega}_T$ is the set of rectangles sharing at least one vertex with T. Also, for an element edge E, ω_E denotes the union of rectangles sharing E, while $\tilde{\omega}_E$ is the set of rectangles sharing at least one vertex whit E.

Next, ∂T is the set of the four edges of T we denote by $\varepsilon(T)$ and N_T the set of its edges and vertices, respectively.

We let $\varepsilon_h = \cup_{T \in T_h} \varepsilon(T)$ denotes the set of all edges split into interior and boundary edges.

$$\varepsilon_h = \varepsilon_{h,\Omega} \cup \varepsilon_{h,\Gamma}$$

Where $\varepsilon_{h,\Omega} = \{E \in \varepsilon_h : E \subset \Omega\}$

$$\varepsilon_{h,\Gamma} = \{E \in \varepsilon_h : E \subset \partial\Omega\}$$

We denote by h_T the diameter of a simplex, by h_T the diameter of a face E of T, and we set $h = \max_{T \in T_h}\{h_T\}$.

A discrete weak formulation is defined using finite dimensional spaces $X^1_h \subset H^1_{n,0}(\Omega)$ and $M^h \subset L^2_0(\Omega)$

The discrete version of (15) is:

$$\begin{cases} find\ \vec{u}_h \in X^1_h \text{ and } p_h \in M^h \text{ such that:} \\ A(\vec{u}_h, \vec{v}_h) + C(\vec{u}_h, \vec{u}_h, \vec{v}_h) + B(\vec{v}_h, p_h) = L(\vec{v}_h) \\ B(\vec{v}_h, p_h) = 0 \end{cases} \qquad (36)$$

For all $\vec{u}_h \in X^1_h$ and $q_h \in M^h$.

We define the appropriate bases for the finite element spaces, leading to non linear system of algebraic equations. Linearization of this system using Newton iteration gives the finite dimensional System:

$find\ \delta\vec{u}_h \in X^1_h$ and $\delta p_h \in M^h$ such that:

$$\begin{cases} \nu\int_\Omega \nabla\delta\vec{u}_h : \nabla\vec{v}_h + \int_{\partial\Omega}\delta\vec{u}_h^T A\vec{v}_h + C(\delta\vec{u}_h, \vec{u}_h, \vec{v}_h) \\ \quad + C(\vec{u}_h, \delta\vec{u}_h, \vec{v}_h) + B(\vec{v}_h, \delta p_h) = R_k(\vec{v}_h) \\ \quad B(\delta\vec{u}_h, q_h) = r_k(q_h) \end{cases} \qquad (37)$$

For all $\vec{u}_h \in X^1_h$ and $q_h \in M^h$.

Here, $R_k(\vec{v}_h)$ and $r_k(q_h)$ are the non linear residuals associated with the discrete formulations (36). To define the corresponding linear algebra problem, we use a set of vector-valued basis functions $\{\vec{\varphi}_i\}_{i=1,\dots n_u}$ So that

$$\vec{u}_h = \sum_{j=1}^{n_u} u_j\vec{\varphi}_j;\ \delta\vec{u}_h = \sum_{j=1}^{n_u}\Delta u_j\vec{\varphi}_j. \qquad (38)$$

We introduce a set of pressure basis functions $\{\psi_k\}_{k=1,\dots n_p}$ and set

$$p_h = \sum_{k=1}^{n_p} p_k\psi_k;\ \delta p_h = \sum_{k=1}^{n_p}\Delta p_k\psi_k. \qquad (39)$$

Where n_u and n_p are the numbers of velocity and pressure basis functions, respectively.

We find that the discrete formulation (37) can be expressed as a system of linear equations

$$\begin{pmatrix} A_0 + N + W & B_0^T \\ B_0 & 0 \end{pmatrix}\begin{pmatrix} \Delta U \\ \Delta P \end{pmatrix} = \begin{pmatrix} f \\ 0 \end{pmatrix}. \qquad (40)$$

The system is referred to as the discrete Newton problem.

The matrix A_0 is the vector Laplacian matrix and B_0 is the divergence matrix

$$A_0 = [a_{i,j}];\ a_{i,j} = \nu\int_\Omega \nabla\vec{\varphi}_i : \nabla\vec{\varphi}_j + \int_\Gamma \vec{\varphi}_i^T A\vec{\varphi} \qquad (41)$$

$$B_0 = [b_{k,j}];\ b_{k,j} = -\int_\Omega \psi_k \nabla.\vec{\varphi}_j \qquad (42)$$

The vector-convection matrix N and the Newton derivative matrix W are given by

$$N = [n_{i,j}];\ n_{i,j} = \int_\Omega (\vec{u}_h.\nabla\vec{\varphi}_i)\vec{\varphi}_j \qquad (43)$$

$$W = [w_{i,j}];\ w_{i,j} = \int_\Omega (\vec{\varphi}_i.\nabla\vec{u}_h)\vec{\varphi}_j \qquad (44)$$

For $i; j = 1,\dots, n_u$ and $k = 1,\dots, n_p$.

The right-hand side vectors in (40) are

$$f = [f_i];\ f_i = \int_\Omega \vec{f}.\vec{\varphi}_i + \int_\Gamma \vec{g}\vec{\varphi}_i, \qquad (45)$$

for $i = 1,\dots, n_u$,

For Picard iteration, we give the discrete problem

$$\begin{pmatrix} A_0 + N & B_0^T \\ B_0 & 0 \end{pmatrix}\begin{pmatrix} \Delta U \\ \Delta P \end{pmatrix} = \begin{pmatrix} f \\ 0 \end{pmatrix}. \qquad (46)$$

VI. A Posteriori Error Estimator

In this section we propose two types of a posteriori error indicator, a residual error estimator and local Poisson problem

estimator, which are shown to give global error estimates that are equivalent to the true error.

A. A Residual Error Estimator

The bubble functions on the reference element $\tilde{T} = (0,1)\times(0,1)$ are defined as follows:

$$b_{\tilde{T}} = 2^4 x(1-x)y(1-y)$$
$$b_{\tilde{E}_1,\tilde{T}} = 2^2 x(1-x)(1-y)$$
$$b_{\tilde{E}_2,\tilde{T}} = 2^2 y(1-y)x$$
$$b_{\tilde{E}_3,\tilde{T}} = 2^2 y(1-x)x$$
$$b_{\tilde{E}_4,\tilde{T}} = 2^2 y(1-y)(1-x)$$

Here $b_{\tilde{T}}$ is the reference element bubble function, and $b_{\tilde{E}_i,\tilde{T}}, i = 1:4$ are reference edge bubble functions. For any $T \in T_h$, the element bubble functions is $b_T = b_{\tilde{T}} \circ F_T$ and the element edge bubble function is $b_{E_i,T} = b_{\tilde{E}_i,\tilde{T}} \circ F_T$, where F_T the affine map form $\tilde{T}$ to T.

For an interior edge $E \in \varepsilon_{h,\Omega}$, b_E is defined piecewise, so that $b_{E/T_i} = b_{E,T_i}, i = 1:2$ where $\mathrm{E} = \overline{\mathrm{T}_1} \cap \overline{\mathrm{T}_2}$.

For a boundary edge $\mathrm{E} \in \varepsilon_{h,\Gamma}$, $b_E = b_{E,T}$, where T is the rectangle such that $\mathrm{E} \in \partial T$.

With these bubble functions, ceruse et al ([3], lemma 4.1] established the following lemma.

Lemma 6.1. Let T be an arbitrary rectangle in T_h and
For any $\vec{v}_T \in P_{k_0}(T)$ and $\vec{v}_E \in P_{k_0}(E)$, the following inequalities hold.

$$c_k \|\vec{v}_T\|_{0,T} \le \left\| \vec{v}_T b_T^{\frac{1}{2}} \right\|_{0,T} \le C_k \|\vec{v}_T\|_{0,T} \quad (47)$$

$$|\vec{v}_T b_T|_{1,T} \le C_k h_T^{-1} \|\vec{v}_T\|_{0,T} \quad (48)$$

$$c_k \|\vec{v}_E\|_{0,E} \le \left\| \vec{v}_E b_E^{\frac{1}{2}} \right\|_{0,E} \le C_k \|\vec{v}_E\|_{0,E} \quad (49)$$

$$\|\vec{v}_E b_E\|_{0,T} \le C_k h_E^{\frac{1}{2}} \|\vec{v}_E\|_{0,E} \quad (50)$$

$$|\vec{v}_E b_E|_{1,T} \le C_k h_E^{-\frac{1}{2}} \|\vec{v}_E\|_{0,E} \quad (51)$$

Where c_k and C_k are tow constants which only depend on the element aspect ratio and the polynomial degrees k_0 and k_1.

Here, k_0 and k_1 are fixed and c_k and C_k can be associated with generic constants c and *C* In addition, $\vec{v}_E$ which is only defined on the edge E also denotes its natural extension to the element T.

From the inequalities (50) and (51), we established the following lemma:

Lemma 6.2. Let T be a rectangle and $E \in \partial T \cap \varepsilon_{h,\Gamma}$. For any $\vec{v}_E \in P_{k_0}(E)$, the following inequalities hold.

$$\|\vec{v}_E b_E\|_{J,T} \le C_k h_E^{-\frac{1}{2}} \|\vec{v}_E\|_{0,E} \quad (52)$$

Proof. Since $\vec{v}_E b_E = \vec{0}$ in the other three edges of rectangle T, it can be extended to the whole of Ω by setting $\vec{v}_E b_E = \vec{0}$ in $\Omega - \overline{T}$, then
$\|\vec{v}_E b_E\|_{1,T} = \|\vec{v}_E b_E\|_{1,\Omega}$ and $\|\vec{v}_E b_E\|_{J,T} = \|\vec{v}_E b_E\|_{J,\Omega}$
Using the inequalities (19), (50) and (51) gives

$$\begin{aligned}
\|\vec{v}_E b_E\|_{J,T} &= \|\vec{v}_E b_E\|_{J,\Omega} \\
&\le c_2 \|\vec{v}_E b_E\|_{1,\Omega} \\
&= c_2 \|\vec{v}_E b_E\|_{1,T} \\
&= c_2 \left(\|\vec{v}_E b_E\|_{0,T}^2 + |\vec{v}_E b_E|_{1,T}^2 \right)^{\frac{1}{2}} \\
&\le c_2 C_k \left(h_E + h_E^{-1} \right)^{\frac{1}{2}} \|\vec{v}_E\|_{0,E} \\
&\le c_2 C_k \left(D^2 + 1 \right)^{\frac{1}{2}} h_E^{-\frac{1}{2}} \|\vec{v}_E\|_{0,E} \\
&\le C h_E^{-\frac{1}{2}} \|\vec{v}_E\|_{0,E}
\end{aligned}$$

With D is the diameter of Ω and $C = c_2 C_k \left(D^2 + 1 \right)^{\frac{1}{2}}$.

We recall some quasi-interpolation estimates in the following lemma.

Lemma 6.3. Clement interpolation estimate: Given $\vec{\mathrm{v}} \in H^1(\Omega)$, let $\vec{v}_h \in \mathrm{X}_{\mathrm{h}}^1$ be the quasi-interpolant of $\vec{v}$ defined by averaging as in [4]. For any $T \in T_h$,

$$\|\vec{v} - \vec{v}_h\|_{0,T} \le C h_T |\vec{v}|_{1,\tilde{\omega}_T}, \quad (53)$$

and for all $E \in \partial T$,

$$\|\vec{v} - \vec{v}_h\|_{0,E} \le C h_E^{\frac{1}{2}} |\vec{v}|_{1,\tilde{\omega}_E} \quad (54)$$

We let $(\vec{u}, p)$ denote the solution of (18) and let denote $(\vec{u}_h, p_h)$ the solution of (36) with an approximation on a rectangular subdivision T_h.

Our aim is to estimate the velocity and the pressure errors
$\vec{e} = \vec{u} - \vec{u}_h \in H_{n,0}^1(\Omega)$ and $\varepsilon = p - p_h \in L_0^2(\Omega)$.
The element contribution $\eta_{R,T}$, of the residual error estimator η_R is given by

$$\eta_{R,T}^2 = h_T^2 \left\| \vec{R}_T \right\|_{0,T}^2 + \|R_T\|_{0,T}^2 + \sum_{E \in \partial T} h_E \left\| \vec{R}_E \right\|_{0,E}^2 \quad (55)$$

and the components in (55) are given by

$$\vec{R}_T = \left\{ \vec{f} + \nu \nabla^2 \vec{u}_h - \vec{u}_h \nabla \vec{u}_h - \nabla p_h \right\} / T$$

$$R_T = \{\nabla.\vec{u}_h\}/T$$

$$\vec{R}_E = \begin{cases} \frac{1}{2}[\![\nu\nabla\vec{u}_h - p_h I]\!]; E \in \varepsilon_{h,\Omega} \\ \vec{g} - \left(\vec{u}_h^T A + (\nu\nabla\vec{u}_h - p_h I)\vec{n}_{E,T}\right); E \in \varepsilon_{h,\Gamma} \end{cases}$$

With the key contribution coming from the stress jump associated with an edge E adjoining elements T and S:

$$[\![\nu\nabla\vec{u}_h - p_h I]\!] = (\nu\nabla\vec{u}_h - p_h I)/T - (\nu\nabla\vec{u}_h - p_h I)/S$$

The global residual error estimator is given by:

$$\eta_R = \sqrt{\sum_{T\in T_h} \eta_{R,T}^2}$$

Our aim is bound $\|\vec{u} - \vec{u}_h\|_X$ and $\|p - p_h\|$ with respect to the norm $\|.\|_J$ for velocity $\|\vec{v}\|_X = \|\vec{v}\|_{J,\Omega}$ and the quotient norm for the pressure $\|p\|_M = \|p\|_{0,\Omega}$.

For any $T \in T_h$, and $E \in \partial T$, we define the following two functions:

$$\vec{w}_T = \vec{R}_T b_T \; ; \; \vec{w}_E = \vec{R}_E b_E \; ,$$

- $\vec{w}_T = \vec{0}$ on ∂T,
- if $E \in \partial T \cap \varepsilon_{h,\Omega}$ then $\vec{w}_E = \vec{0}$ on $\partial\omega_E$.
- if $E \in \partial T \cap \varepsilon_{h,\Gamma}$ then $\vec{w}_E = \vec{0}$ in the other edges of rectangle T.
- $\vec{w}_E$ and $\vec{w}_T$ can be extended to whole of Ω by setting:

$\vec{w}_T = \vec{0}$ in Ω - $\overline{\text{T}}$

$\vec{w}_E = \vec{0}$ in $\Omega - \overline{\omega_E}$ if $E \in \partial T \cap \varepsilon_{h,\Omega}$.

$\vec{w}_E = \vec{0}$ in Ω - T if $E \in \partial T \cap \varepsilon_{h,\Gamma}$.

With these two functions we have the following lemmas:

Lemma 6.4. For any $T \in T_h$ we have:

$$\int_T \vec{f}.\vec{w}_T = \int_T (\nu\nabla\vec{u} - pI) : \nabla\vec{w}_T + \int_T (\vec{u}.\nabla\vec{u}).\vec{w}_T \qquad (56)$$

Proof

Using (1) gives

$$\int_T \vec{f}.\vec{w}_T = \int_T -\left(\nu\nabla^2\vec{u} + \vec{u}.\nabla\vec{u} + \nabla p\right).\vec{w}_T$$

By applying the Green formula and $\vec{w}_T = \vec{0}$ on ∂T, we obtain

$$\begin{aligned}\int_T \vec{f}.\vec{w}_T &= -\int_{\partial T} (\nu\nabla\vec{u} - pI)\vec{n}.\vec{w}_T \\ &+ \int_T (\nu\nabla\vec{u} - pI) : \nabla\vec{w}_T + \int_T (\vec{u}.\nabla\vec{u}).\vec{w}_T \\ &= \int_T (\nu\nabla\vec{u} - pI) : \nabla\vec{w}_T + \int_T (\vec{u}.\nabla\vec{u}).\vec{w}_T .\end{aligned}$$

Lemma 6.5

i) if $E \in \partial T \cap \varepsilon_{h,\Omega}$ we have:

$$\int_{\omega_E} \vec{f}.\vec{w}_E = \int_{\omega_E} (\nu\nabla\vec{u} - pI) : \nabla\vec{w}_E + \int_{\omega_E} (\vec{u}.\nabla\vec{u}).\vec{w}_E \qquad (57)$$

ii) if $E \in \partial T \cap \varepsilon_{h,\Gamma}$, We have:

$$\begin{aligned}\int_T \vec{f}.\vec{w}_E &= \int_T (\nu\nabla\vec{u} - pI) : \nabla\vec{w}_E \\ &+ \int_{\partial T} \left(\vec{u}^T A - \vec{g}\right)\vec{w}_E + \int_T (\vec{u}.\nabla\vec{u}).\vec{w}_T\end{aligned} \qquad (58)$$

Proof.

i) The same proof of (56).

ii) If $E \in \partial T \cap \varepsilon_{h,\Gamma}$, We have:

$$\begin{aligned}\int_T \vec{f}.\vec{w}_T &= \int_T -(\nu\nabla^2\vec{u} + \vec{u}.\nabla\vec{u} + \nabla p).\vec{w}_T \\ &= \int_T (\nu\nabla\vec{u} - pI) : \nabla\vec{w}_E - \int_{\partial T} (\nu\nabla\vec{u} - pI)\vec{n}.\vec{w}_E \\ &+ \int_T (\vec{u}.\nabla\vec{u}).\vec{w}_T\end{aligned}$$

We have

$$\vec{n}^T(pI - \nu\nabla\vec{u}) = \vec{u}^T A - \vec{g} \quad on \; E \subset \Gamma \text{ and } \vec{w}_E = \vec{0}$$

in the other tree edges of rectangle T, then

$$\begin{aligned}\int_T \vec{f}.\vec{w}_E &= \int_T (\nu\nabla\vec{u} - pI) : \nabla\vec{w}_E \\ &+ \int_{\partial T} \left(\vec{u}^T A - \vec{g}\right)\vec{w}_E + \int_T (\vec{u}.\nabla\vec{u}).\vec{w}_T .\end{aligned}$$

We define the bilinear form

$$G((\vec{u},\vec{p});(\vec{v},q)) = A(\vec{u},\vec{v}) + B(\vec{u},q) + B(\vec{v},p)$$

We define also the following functional

$$\theta(K,\vec{x},\vec{y},\vec{v}) = \int_K (\vec{x}.\nabla x).\vec{v} - \int_K (\vec{y}.\nabla\vec{y}).\vec{v}$$

for all $K \subset \Omega$ and $\vec{x},\vec{y},\vec{v} \in H^1_{n,0}(\Omega)$.

Lemma 6.6. There exists $C \succ 0$ and $h_0 \succ 0$ such that

$$\theta(K,\vec{u},\vec{u}_h,\vec{v}) \le C\|\vec{e}\|_{J,K}\|\vec{v}\|_{J,K}, \qquad (59)$$

for all $h \le h_0$, $\vec{v} \in H^1_{n,0}(\Omega)$ and $K \subset \Omega$.

Proof. Using (27), (32) and (35), we have that for $\vec{v} \in H^1_{n,0}(\Omega)$

$$\begin{aligned}\theta(K,\vec{u},\vec{u}_h,\vec{v}) &= \int_K (\vec{u}.\nabla\vec{u}).\vec{v} - \int_K (\vec{u}_h.\nabla\vec{u}_h).\vec{v} \\ &= \int_K (\vec{u}.\nabla\vec{e}).\vec{v} + \int_K (\vec{e}.\nabla\vec{u}_h).\vec{v} \\ &\le N(\|\vec{u}\|_{J,K}\|\vec{e}\|_{J,K}\|\vec{v}\|_{J,K} + \|\vec{e}\|_{J,K}\|\vec{u}_h\|_{J,K}.\|\vec{v}\|_{J,K}) \\ &\le N(2\|\vec{u}\|_{J,K}\|\vec{e}\|_{J,K}\|\vec{v}\|_{J,K} + \|\vec{e}\|^2_{J,K}.\|\vec{v}\|_{J,K}) \\ &\le (2\delta + N\|\vec{e}\|_{J,K})\|\vec{e}\|_{J,K}\|\vec{v}\|_{J,K}\end{aligned} \qquad (60)$$

We have

$\lim_{h\to 0}\vec{u}_h = \vec{u}$ in $H^1_{n,0}(\Omega)$, then there exists $h_0 \succ 0$ such that

$$\|\vec{e}\|_{J,K} = \|\vec{u} - \vec{u}_h\|_{J,K} \le 1 \text{ for all } h \le h_0.$$

Using this result and (60), we obtain

$$\theta(K,\vec{u},\vec{u}_h,\vec{v}) \le C\|\vec{e}\|_{J,K}\|\vec{v}\|_{J,K}$$

for all $h \le h_0$ and $\vec{v} \in H^1_{n,0}(\Omega)$, with $C = 2\delta\nu + N$.

We have

$$\begin{aligned} G((\vec{e},\varepsilon);(\vec{v},q)) &= A(\vec{u}-\vec{u}_h,\vec{v}) + B(\vec{u}-\vec{u}_h,q) + B(\vec{v},p-p_h) \\ &= G((\vec{u},p);(\vec{v},q)) - G((\vec{u}_h,p_h);(\vec{v},q)) \\ &= L(\vec{v}) - C(\vec{u},\vec{u},\vec{v}) - G((\vec{u}_h,p_h);(\vec{v},q)) \\ &= L(\vec{v}) - C(\vec{u},\vec{u},\vec{v}) - A(\vec{u}_h,\vec{v}) - B(\vec{v},p_h) \\ &\quad - B(\vec{u}_h,q). \end{aligned}$$

Then

$$\begin{aligned} G((\vec{e},\varepsilon);(\vec{v},q)) + \theta(\Omega,\vec{u},\vec{u}_h,\vec{v}) &= -C(\vec{u}_h,\vec{u}_h,\vec{v}) + L(\vec{v}) \\ &\quad - A(\vec{u}_h,\vec{v}) - B(\vec{v},p_h) - B(\vec{u}_h,q) \end{aligned} \tag{61}$$

for all $(\vec{v},q) \in H^1_{n,0}(\Omega)\times L^2_0(\Omega)$.

We find that theerrors $\vec{e} \in H^1_{n,0}(\Omega)$ and $\varepsilon \in L^2_0(\Omega)$ Satisfy the non-linear equation

$$\begin{aligned} &G((\vec{e},\varepsilon);(\vec{v},q)) + \theta(\Omega,\vec{u},\vec{u}_h,\vec{v}) \\ &= \sum_{T\in T_h}\left\{ (\vec{R}_T,\vec{v})_T - \sum_{E\subset\partial T}(\vec{R}_E,\vec{v})_E + (R_T,q)_T \right\} \end{aligned} \tag{62}$$

for all $(\vec{v},q) \in H^1_{n,0}(\Omega)\times L^2_0(\Omega)$.

We define a pair $(\vec{\varphi},\psi) \in H^1_{n,0}(\Omega)\times L^2_0(\Omega)$ to be the Ritz projection of the modified residuals

$$\begin{aligned} A(\vec{\varphi},\vec{v}) + d(\psi,q) &= A(\vec{e},\vec{v}) + B(\vec{e},q) + B(\vec{v},\varepsilon) + \theta(\Omega,\vec{u},\vec{u}_h,\vec{v}) \\ &= G((\vec{e},\varepsilon);(\vec{v},q)) + \theta(\Omega,\vec{u},\vec{u}_h,\vec{v}) \end{aligned} \tag{63}$$

for all $(\vec{v},q) \in H^1_{n,0}(\Omega)\times L^2_0(\Omega)$.

Lemma 6.7

$$A(\vec{\varphi},\vec{v}_h) = 0 \text{ for all } \vec{v}_h \in X^1_h \tag{64}$$

Proof: we set $q = 0$ and $\vec{v} = \vec{v}_h$ in (62), we obtain

$$\begin{aligned} A(\vec{\varphi},\vec{v}_h) &= A(\vec{e},\vec{v}_h) + B(\vec{v}_h,\varepsilon) + \theta(\Omega,\vec{u},\vec{u}_h,\vec{v}_h) \\ &= A(\vec{u},\vec{v}_h) - A(\vec{u}_h,\vec{v}_h) + B(\vec{v}_h,p) - B(\vec{v}_h,p_h) \\ &\quad + C(\vec{u},\vec{u},\vec{v}_h) - C(\vec{u}_h,\vec{u}_h,\vec{v}_h) \\ &= L(\vec{v}_h) - L(\vec{v}_h) = 0. \end{aligned}$$

Next, we establish the equivalence between the norms of $(\vec{e},\varepsilon) \in H^1_{n,0}(\Omega)\times L^2_0(\Omega)$ and the norms of the solution $(\vec{\varphi},\psi) \in H^1_{n,0}(\Omega)\times L^2_0(\Omega)$ of (63).

Theorem 6.8. Let the conditions of theorem 4.6 hold. There exist two positive constants k_1 and k_2, independent of h, such that

$$k_1\left\{\|\vec{\varphi}\|^2_{J,\Omega} + \|\psi\|^2_{0,\Omega}\right\} \le \left\{\|\vec{e}\|^2_{J,\Omega} + \|\varepsilon\|^2_{0,\Omega}\right\} \le k_2\left\{\|\vec{\varphi}\|^2_{J,\Omega} + \|\psi\|^2_{0,\Omega}\right\}$$

Proof. The same proof of theorem 3 in [9].

Theorem 6.9.

For all $(\vec{w},s) \in H^1_{n,0}(\Omega)\times L^2_0(\Omega)$, we have

$$\sup_{(\vec{v},q)\in H^1_{n,0}\times L^2_0} \frac{A(\vec{w},\vec{v}) + d(s,q)}{\|\vec{v}\|_{J,\Omega} + \|q\|_{0,\Omega}} \ge \frac{1}{2}(\|\vec{w}\|_{J,\Omega} + \|s\|_{0,\Omega}). \tag{65}$$

Proof. Let $(\vec{w},s) \in H^1_{n,0}(\Omega)\times L^2_0(\Omega)$, we have

$$\begin{aligned} \sup_{(\vec{v},q)\in H^1_{n,0}\times L^2_0} \frac{A(\vec{w},\vec{v}) + d(s,q)}{\|\vec{v}\|_{J,\Omega} + \|q\|_{0,\Omega}} &\ge \frac{A(\vec{w},\vec{w}) + d(s,0)}{\|\vec{v}\|_{J,\Omega} + \|0\|_{0,\Omega}} \\ &= \frac{A(\vec{w},\vec{w})}{\|\vec{w}\|_{J,\Omega}} = \|\vec{w}\|_{J,\Omega} \end{aligned} \tag{66}$$

We also have

$$\begin{aligned} \sup_{(\vec{v},q)\in H^1_{n,0}\times L^2_0} \frac{A(\vec{w},\vec{v}) + d(s,q)}{\|\vec{v}\|_{J,\Omega} + \|q\|_{0,\Omega}} &\ge \frac{A(\vec{w},0) + d(s,s)}{\|0\|_{J,\Omega} + \|s\|_{0,\Omega}} \\ &= \frac{d(s,s)}{\|s\|_{0,\Omega}} = \|s\|_{0,\Omega}. \end{aligned} \tag{67}$$

We gather (66) and (67) to get

$$\sup_{(\vec{v},q)\in H^1_{n,0}\times L^2_0} \frac{A(\vec{w},\vec{v}) + d(s,q)}{\|\vec{v}\|_{J,\Omega} + \|q\|_{0,\Omega}} \ge \frac{1}{2}(\|\vec{w}\|_{J,\Omega} + \|s\|_{0,\Omega}).$$

Theorem 6.10. For any mixed finite element approximation (not necessarily inf-sup stable) defined on rectangular grids T_h, the residual estimator η_R satisfies:

$$\|\vec{e}\|_{J,\Omega} + \|\varepsilon\|_{0,\Omega} \le C\eta_R,$$

and $\eta_{R,T} \le C\left(\sum_{T'\in\omega_T}\left\{\|\vec{e}\|^2_{J,T'} + \|\varepsilon\|^2_{0,T'}\right\}\right)^{\frac{1}{2}}$.

Note that the constant C in the local lower bound is independent of the domain, and

$$\|\vec{e}\|^2_{J,T} = \nu\int_T \nabla\vec{e} : \nabla\vec{e} + \int_{\partial T}\vec{e}^{\,T} A.\vec{e}.$$

Proof. To establish the upper bound we let $(\vec{v},q) \in H^1_{n,0}(\Omega)\times L^2_0(\Omega)$ and $\vec{v}_h \in X^1_h$ be the clement interpolation of $\vec{v}$. Using (63), (61) and (62), give

$$A(\vec{\varphi},\vec{v})+d(\psi,q)=A(\vec{\varphi},\ \vec{v}-\vec{v}_h)+d(\psi,q)$$
$$=\sum_{T\in T_h}\left\{(\vec{R}_T,\vec{v}-\vec{v}_h)_T-\sum_{E\subset\partial T}(\vec{R}_E,\ \vec{v}-\vec{v}_h)_E+(R_T,q)_T\right\}$$
$$\le\sum_{T\in T_h}\left\{\left\|\vec{R}_T\right\|_{0,T}\left\|\vec{v}-\vec{v}_h\right\|_{0,T}+\sum_{T\in\partial T}\left\|\vec{R}_E\right\|_{0,T}\left\|\vec{v}-\vec{v}_h\right\|_{0,E}+\|q\|_{0,T}\|R_T\|_{0,E}\right\}$$
$$\le\left(\sum_{T\in T_h}h_T^2\left\|\vec{R}_T\right\|_{0,T}^2\right)^{\frac{1}{2}}\left(\sum_{T\in T_h}\frac{1}{h_T^2}\left\|\vec{v}-\vec{v}_h\right\|_{0,T}^2\right)^{\frac{1}{2}}+\left(\sum_{T\in T_h}\sum_{E\in\partial T}h_E\left\|\vec{R}_E\right\|_{0,T}^2\right)^{\frac{1}{2}}\left(\sum_{T\in T_h}\sum_{E\in\partial T}\frac{1}{h_E}\left\|\vec{v}-\vec{v}_h\right\|_{0,E}^2\right)^{\frac{1}{2}}$$

Using (52) and (53), then gives

$$A(\vec{\varphi},\vec{v})+d(\psi,q)\le C\left(\sum_{T\in T_h}\left\{\|\vec{v}\|_{J,T}^2+\|q\|_{0,T}^2\right\}\right)^{\frac{1}{2}}$$
$$\times\left(\sum_{T\in T_h}\left\{h_T^2\left\|\vec{R}_T\right\|_{0,T}^2+\|R_T\|_{0,T}^2+\sum\nolimits_{E\in\partial T}h_E\left\|\vec{R}_E\right\|_{0,E}^2\right\}\right)^{\frac{1}{2}}.$$

Finally, using (65) gives:

$$\|\vec{\varphi}\|_{J,T}+\|\psi\|_{0,T}\le C\sum_{T\in T_h}\left\{h_T^2\left\|\vec{R}_T\right\|_{0,T}^2+\|R_T\|_{0,T}^2+\sum\nolimits_{E\in\partial T}h_E\left\|\vec{R}_E\right\|_{0,E}^2\right\}$$

According to theorem 6.8, we have

$$\|\vec{e}\|_{J,T}+\|\varepsilon\|_{0,T}\le C_\Omega\sum_{T\in T_h}\left\{h_T^2\left\|\vec{R}_T\right\|_{0,T}^2+\|R_T\|_{0,T}^2+\sum\nolimits_{E\in\partial T}h_E\left\|\vec{R}_E\right\|_{0,E}^2\right\}$$

This establishes the upper bound.

Turning to the local lower bound. First, for the element residual part, we have:

$$\int_T\vec{R}_T.\vec{w}_T=\int_T(\vec{f}+\nu\nabla^2\vec{u}_h-\vec{u}_h.\nabla\vec{u}_h-\nabla p_h).\vec{w}_T$$
$$=\int_T\vec{f}.\vec{w}_T-\int_T(\nu\nabla\vec{u}_h-p_hI):\nabla\vec{w}_T+\int_{\partial T}(\nu\nabla\vec{u}_h-p_hI)\vec{n}.\vec{w}_T-\int_T(\vec{u}_h\nabla\vec{u}_h).\vec{w}_T$$

See that $\vec{w}_T=\vec{0}$ in ∂T , using (56) and (57) gives:

$$\int_T\vec{R}_T.\vec{w}_T=\int_T(\nu\nabla\vec{e}-\varepsilon I):\nabla\vec{w}_T+\theta(T,\vec{u},\vec{u}_h,\vec{w}_T)$$
$$\le C'(|\vec{e}|_{1,T}+\|\varepsilon\|_{0,T})|\vec{w}_T|_{1,T}+C''\|\vec{e}\|_{J,T}\|\vec{w}\|_{J,T}$$

Since $\vec{w}_T=\vec{0}$ in ∂T, then $\|\vec{w}\|_{J,T}=\sqrt{\nu}|\vec{w}_T|_{1,T}$,

Using (48), gives

$$\int_T\vec{R}_T.\vec{w}_T\le C(\|\vec{e}\|_{J,T}^2+\|\varepsilon\|_{0,T}^2)^{\frac{1}{2}}h_T^{-1}\left\|\vec{R}_T\right\|_{0,T}$$

In addition, from the inverse inequality (47)

$$\int_T\vec{R}_T.\vec{w}_T=\left\|\vec{R}_Tb_T^{\frac{1}{2}}\right\|_{0,T}^2\ge c_k\left\|\vec{R}_T\right\|_{0,T}^2,$$

Thus, $$h_T^2\left\|\vec{R}_T\right\|_{0,T}^2\le C(\|\vec{e}\|_{J,T}^2+\|\varepsilon\|_{0,T}^2)\qquad(68)$$

Next comes the divergence part,

$$\|R_T\|_{0,T}=\|\nabla.\vec{u}_h\|_{0,T}=\|\nabla.(\vec{u}-\vec{u}_h)\|_{0,T}\le\sqrt{2}|\vec{u}-\vec{u}_h|_{1,T}\le\sqrt{\frac{2}{\nu}}\|\vec{u}-\vec{u}_h\|_{J,T}=\sqrt{\frac{2}{\nu}}\|\vec{e}\|_{J,T}\qquad(69)$$

Finally, we need to estimate the jump term. For an edge if $E\in\partial T\cap\varepsilon_{h,\Omega}$, We have

$$2\int_E\vec{R}_E.\vec{w}_E=\sum_{i=1:2}\int_{\partial T_i}(\nu\nabla\vec{u}_h-p_hI)\vec{n}.\vec{w}_E=\int_{\omega_E}(\nu\nabla\vec{u}_h-p_hI):\nabla\vec{w}_E+\sum_{i=1:2}\int_{T_i}(\nu\nabla^2\vec{u}_h-\nabla p_h).\vec{w}_E.$$

Using (57) and $\vec{w}_E=\vec{0}$ in $\partial\omega_E$, gives :

$$2\int_E\vec{R}_E.\vec{w}_E=-\int_{\omega_E}(\nu\nabla\vec{e}-\varepsilon I):\nabla\vec{w}_E+\sum_{i=1:2}\int_{T_i}\vec{R}_{T_i}\vec{w}_E-\theta(\omega_E,\vec{u},\vec{u}_h,\vec{w}_E)$$
$$\le(\nu|\vec{e}|_{1,\omega_E}+\|\varepsilon\|_{0,\omega_E})|\vec{w}_E|_{1,\omega_E}+\sum_{i=1:2}\left\|\vec{R}_{T_i}\right\|_{0,T_i}\|\vec{w}_E\|_{0,T_i}+C\|\vec{e}\|_{J,\omega_E}\|\vec{w}_E\|_{J,\omega_E}$$

Since $\vec{w}_E=\vec{0}$ in $\partial\omega_E$, then $\|\vec{w}\|_{J,\omega_E}=\sqrt{\nu}|\vec{w}_T|_{1,\omega_E}$

Using (50) and (51), to get

$$2\int_E\vec{R}_E.\vec{w}_E\le C'(|\vec{e}|_{1,\omega_E}^2+\|\varepsilon\|_{0,\omega_E}^2)^{\frac{1}{2}}h_E^{-\frac{1}{2}}\left\|\vec{R}_E\right\|_{0,E}+\sum_{i=1:2}\left\|\vec{R}_{T_i}\right\|_{0,T_i}h_E^{\frac{1}{2}}\left\|\vec{R}_E\right\|_{0,E}$$

Using (68), gives

$$2\int_E\vec{R}_E.\vec{w}_E\le C(\|\vec{e}\|_{J,\omega_E}^2+\|\varepsilon\|_{0,\omega_E}^2)^{\frac{1}{2}}h_E^{-\frac{1}{2}}\left\|\vec{R}_E\right\|_{0,E}\qquad(70)$$

Using the inverse inequality (49) and thus using (70) gives

$$h_E\left\|\vec{R}_E\right\|_{0,E}^2\le C(\|\vec{e}\|_{J,\omega_E}^2+\|\varepsilon\|_{0,\omega_E}^2)\qquad(71)$$

Also need to show that (70) holds for boundary edges.

For an $E\in\partial T\cap\varepsilon_{h,\Gamma}$, We have

$$\int_E\vec{R}_E.\vec{w}_E=\int_{\partial T}\left[\vec{u}_h^TA+(\nu\nabla\vec{u}_h-p_hI)\vec{n}-\vec{g}\right]\vec{w}_E$$
$$=\int_{\partial T}\left(\vec{u}_h^TA-\vec{g}\right)\vec{w}_E+\int_{\partial T}((\nu\nabla\vec{u}_h-p_hI)\vec{n}).\vec{w}_E$$
$$=\int_{\partial T}\left(\vec{u}_h^TA-\vec{g}\right)\vec{w}_E+\int_T((\nu\nabla\vec{u}_h-p_hI)):\nabla\vec{w}_E+\int_T\left((\nu\nabla^2\vec{u}_h-\nabla p_h)\right).\vec{w}_E$$

Using (58), (59) and (4), gives

$$\begin{aligned}\int_E \vec{R}_E.\vec{w}_E &= -\int_T ((\nu\nabla\vec{e}-\varepsilon I)):\nabla\vec{w}_E - \int_{\partial T}\vec{e}^{\,T}A.\vec{w}_E \\ &\quad + \int_T \vec{R}_T.\vec{w}_E - \theta(T,\vec{u},\vec{u}_h,\vec{w}_E) \\ &\le (\nu|\vec{e}|_{1,T} + \|\varepsilon\|_{0,T})|\vec{w}_E|_{1,T} + \beta_1\|\vec{e}\|_{0,\partial T}\|\vec{w}_E\|_{0,\partial T} \\ &\quad + C'\|\vec{e}\|_{J,T}\|\vec{w}_E\|_{J,T} + \|\vec{R}_T\|_{0,T}\|\vec{w}_E\|_{0,T} \\ &\le C(\|\vec{e}\|_{J,T} + \|\varepsilon\|_{0,T})\|\vec{w}_E\|_{J,T} + \|\vec{R}_T\|_{0,T}\|\vec{w}_E\|_{0,T}\end{aligned}$$

Using (50) and (52) gives

$$\int_E \vec{R}_E.\vec{w}_E \le C_1(\|\vec{e}\|_{J,T}^2 + \|\varepsilon\|_{0,T}^2)^{\frac{1}{2}} h_E^{-\frac{1}{2}}\|\vec{R}_E\|_{0,E} + \|\vec{R}_T\|_{0,T} h_E^{\frac{1}{2}}\|\vec{R}_E\|_{0,E}$$

Using (69) gives

$$\int_E \vec{R}_E.\vec{w}_E \le C(\|\vec{e}\|_{J,T}^2 + \|\varepsilon\|_{0,T}^2)^{\frac{1}{2}} h_E^{-\frac{1}{2}}\|\vec{R}_E\|_{0,E} \quad (72)$$

Using (49), then

$$\int_E \vec{R}_E.\vec{w}_E = \left\|\vec{R}_E b_E^{\frac{1}{2}}\right\|_{0,E}^2 \ge c\|\vec{R}_E\|_{0,E}^2,$$

and using (71), gives

$$h_E\|\vec{R}_E\|_{0,E}^2 \le C(\|\vec{e}\|_{J,T}^2 + \|\varepsilon\|_{0,T}^2) \quad (73)$$

Finally, combining (68), (69), (71) and (73) establishes the local lower bound.

B. The Local Poisson Problem Estimator.

The local Poisson problem estimator defined as:

$$\eta_P = \sqrt{\sum_{T\in T_h}\eta_{P,T}^2}$$

$$\eta_{P,T}^2 = \|\vec{e}_{P,T}\|_{J,T}^2 + \|\varepsilon_{P,T}\|_{0,T}^2 \quad (74)$$

Let

- $V_T = \{\vec{v}\in H^1(T):\vec{v}.\vec{n}=0 \text{ on } \partial T\cap\partial\Omega\}$
- $A_T(\vec{e}_{P,T},\vec{v}) = \nu\int_T \nabla\vec{e}_{P,T}:\nabla\vec{v} + \int_{\partial T}\vec{e}_{P,T}^{\,T}A\vec{v}.$

$\vec{e}_{P,T}\in V_T$ Satisfies the uncoupled Poisson problems

$$A_T(\vec{e}_{P,T},\vec{v}) = (\vec{R}_T,\vec{v})_T - \sum_{E\in\varepsilon(T)}(\vec{R}_E,\vec{v})_E \quad (75)$$

for any $\vec{v}\in V_T$.

$$\text{And} \quad \varepsilon_{P,T} = \nabla.\vec{u}_h - \overline{T}. \quad (76)$$

Theorem 6.11. $\eta_{P,T}$ is equivalent to $\eta_{R,T}$ estimator:

$$c\eta_{P,T} \le \eta_{R,T} \le C\eta_{P,T}.$$

Proof. For the upper bound, we first let $\vec{w}_T = \vec{R}_T b_T$ (b_T is an element interior bubble).

From (75),

$$\begin{aligned}(\vec{R}_T,\vec{w}_T)_T &= \nu(\nabla\vec{e}_{P,T},\nabla\vec{w}_T)_T \\ &\le \nu|\vec{e}_{P,T}|_{1,T}|\vec{w}_T|_{1,T}\end{aligned}$$

Using (48) we get

$$(\vec{R}_T,\vec{w}_T)_T \le Ch_T^{-1}\|\vec{R}_T\|_{0,T}\left(\|\vec{e}_{P,T}\|_{J,T}^2 + \|\varepsilon_{P,T}\|_{0,T}^2\right)^{\frac{1}{2}} \quad (77)$$

In addition, from the inverse inequalities (47),

$\|\vec{R}_T\|_{0,T}^2 \le C.(\vec{R}_T,\vec{w}_T)_T$ And using (77), to get

$$h_T^2\|\vec{R}_T\|_{0,T}^2 \le C\left(\|\vec{e}_{P,T}\|_{J,T}^2 + \|\varepsilon_{P,T}\|_{0,T}^2\right) \quad (78)$$

Next, we let $\vec{w}_E = \vec{R}_E b_E$ (b_E is an edge bubble function).

If $E\in\partial T\cap\varepsilon_{h,\Gamma}$, using (75), (78), (50) and (51) give

$$\begin{aligned}(\vec{R}_E,\vec{w}_E)_E &= -A_T(\vec{e}_{P,T},\vec{w}_E)_T + (\vec{R}_T,\vec{w}_E)_T \\ &\le \|\vec{e}_{P,T}\|_{J,T}\|\vec{w}_E\|_{J,T} + \|\vec{R}_T\|_{0,T}\|\vec{w}_E\|_{0,T} \\ &\le Ch_E^{-\frac{1}{2}}\|\vec{R}_E\|_{0,E}\left(\|\vec{e}_{P,T}\|_{J,T}^2 + \|\varepsilon_{P,T}\|_{0,T}^2\right)^{\frac{1}{2}}\end{aligned}$$

if $E\in\partial T\cap\varepsilon_{h,\Omega}$,

See that the matrix *A* defined just in Γ, then we can posed $A=0$ in $\Omega-\Gamma$.

Using (75), (50), (51) and (78) give

$$\begin{aligned}(\vec{R}_E,\vec{w}_E)_E &= -\nu(\nabla\vec{e}_{P,T},\nabla\vec{w}_E)_T + (\vec{R}_T,\vec{w}_E)_T \\ &\le \nu|\vec{e}_{P,T}|_{1,T}|\vec{w}_E|_{1,T} + \|\vec{R}_T\|_{0,T}\|\vec{w}_E\|_{0,T} \\ &\le Ch_E^{-\frac{1}{2}}\|\vec{R}_E\|_{0,E}\left(\|\vec{e}_{P,T}\|_{J,T}^2 + \|\varepsilon_{P,T}\|_{0,T}^2\right)^{\frac{1}{2}}\end{aligned}$$

Finally, for any $T\in T_h$ and any $E\in\partial T$, we have

$$(\vec{R}_E,\vec{w}_E)_E \le Ch_E^{-\frac{1}{2}}\|\vec{R}_E\|_{0,E}\left(\|\vec{e}_{P,T}\|_{J,T}^2 + \|\varepsilon_{P,T}\|_{0,T}^2\right)^{\frac{1}{2}}$$

From this result and the inverse inequalities (49), give

$$h_E\|\vec{R}_T\|_{0,T}^2 \le C\left(\|\vec{e}_{P,T}\|_{J,T}^2 + \|\varepsilon_{P,T}\|_{0,T}^2\right). \quad (79)$$

We have also $\|R_T\|_{0,T} = \|\nabla.\vec{u}_h\|_{0,T} == \|\varepsilon_{P,T}\|_{0,T}$,

then

$$\|R_T\|_{0,T}^2 \le \left(\|\vec{e}_{P,T}\|_{J,T}^2 + \|\varepsilon_{P,T}\|_{0,T}^2\right). \quad (80)$$

Combining (78), (79) and (80), establishes the upper bound in the equivalence relation.

For the lower, we need to use (65):

$$\eta_{P,T} = \left(\left\| \vec{e}_{P,T} \right\|_{J,T}^2 + \left\| \varepsilon_{P,T} \right\|_{0,T}^2 \right)^{\frac{1}{2}}$$
$$\leq \left(\left\| \vec{e}_{P,T} \right\|_{J,T} + \left\| \varepsilon_{P,T} \right\|_{0,T} \right)$$
$$\leq 2 \sup_{(\vec{v},q) \in V_T \times L_0^2(T)} \frac{A_T(\vec{e}_{P,T}, \vec{v}) + d(\varepsilon_{P,T}, q)}{\left\| \vec{v} \right\|_{J,T} + \left\| q \right\|_{0,T}}$$

Using (75) and (76) give

$$\eta_{P,T} \leq 2 \sup_{(\vec{v},q) \in V_T \times L_0^2(T)} \frac{(\vec{R}_T, \vec{v})_T - \sum_{E \subset \partial T} (\vec{R}_E, \vec{v})_E + (R_T, q)_T}{\left\| \vec{v} \right\|_{J,T} + \left\| q \right\|_{0,T}},$$

then

$$\eta_{P,T} \leq 2 \sup_{(\vec{v},q) \in V_T \times L_0^2(T)} \frac{\left\| \vec{R}_T \right\|_{0,T} \left\| \vec{v} \right\|_{0,T} + \sum_{E \subset \partial T} \left\| \vec{R}_E \right\|_{0,E} \left\| \vec{v} \right\|_{0,E} + \left\| R_T \right\|_{0,T} \left\| q \right\|_{0,T}}{\left\| \vec{v} \right\|_{J,T} + \left\| q \right\|_{0,T}} \quad (82)$$

Now, since $\vec{v}$ is zero at the four vertices of T, a scaling argument and the usual trace theorem, see e.g. [15, Lemma 1.5], shows that $\vec{v}$ satisfies

$$\left\| \vec{v} \right\|_{0,E} \leq C h_E^{\frac{1}{2}} \left| \vec{v} \right|_{1,T} \quad (83)$$

$$\left\| \vec{v} \right\|_{0,T} \leq C h_T \left| \vec{v} \right|_{1,T} \quad (84)$$

Combining these two inequalities with (82) immediately gives the lower bound in the equivalence relation.

Consequence 6.12. For any mixed finite element approximation (not necessarily inf-sup stable) defined on rectangular grids T_h, the residual estimator η_P satisfies:

$$\left\| \vec{e} \right\|_{J,\Omega} + \left\| \varepsilon \right\|_{0,\Omega} \leq C \eta_P$$

Note that the constant C in the local lower bound independent of the domain.

VII. Numerical Simulation

In this section some numerical results of calculations with mixed finite element Method and ADINA system will be presented. Using our solver, we run the flow over an obstacle [15] with a number of different model parameters.

Example: Flow over an obstacle. This is another classical problem. The domain is Ω and is associated with modelling flow in a rectangular channel with a square cylindrical obstruction. A Poiseuille profile is imposed on the Inflow boundary $(x = 0;\ -1 \leq y \leq 1)$, and noflow (zero velocity) condition is imposed on the obstruction and the top and bottom walls. A Neumann condition is applied at the outflow boundary which automatically sets the mean outflow pressure to zero. Ω a disconnected rectangular region $(0, 8) \times (-1, 1)$ generated by deleting the square $(7/4, 9/4) \times (-1/4, 1/4)$.

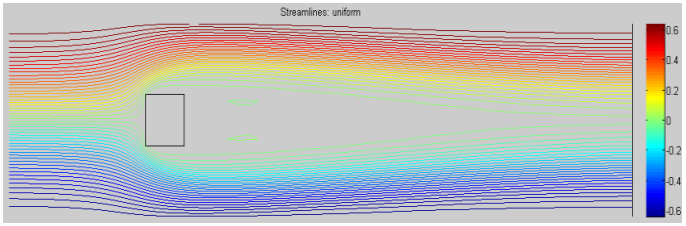

Fig.1. Equally distributed streamline plot associated with a 32×80 square grid $Q_1 - P_0$ approximation and $\nu = 1/500$.

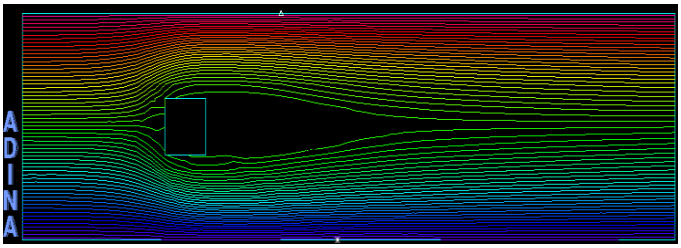

Fig.2. uniform streamline plot computed with ADINA System, associated with a 32 × 80 square grid and $\nu = 1/500$.

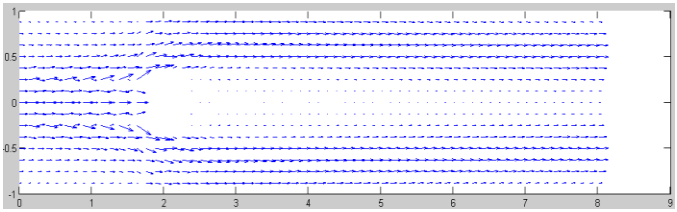

Fig.3. Velocity vectors solution by MFE with a 32 × 80 square grid and $\nu = 1/500$.

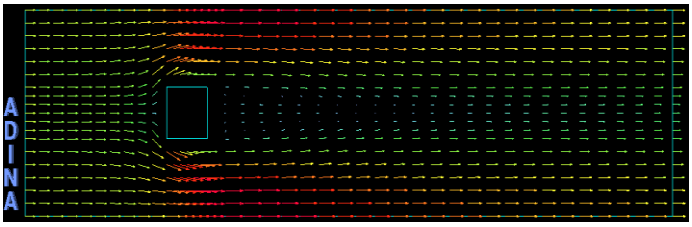

Fig.4. The solution computed with ADINA system. The plots show the velocity vectors solution with a 32 × 80 square grid and $\nu = 1/500$.

The two solutions are therefore essentially identical. This is very good indication that my solver is implemented correctly.

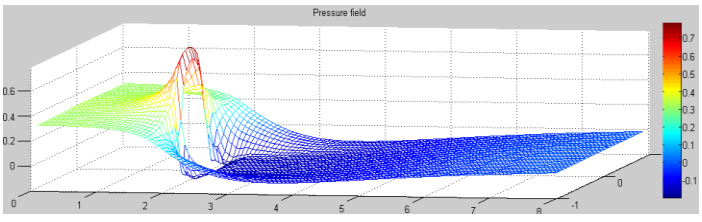

Fig.5. Pressure plot for the flow with a 32 × 80 square grid.

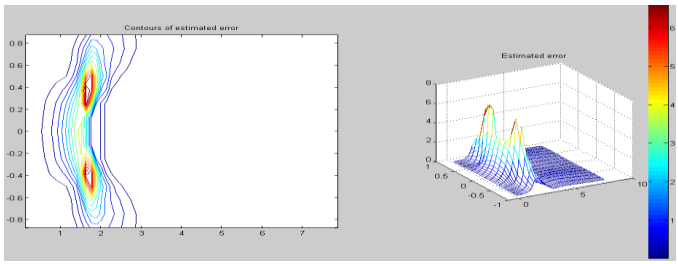

Fig.6. Estimated error $\eta_{R,T}$ associated with 32 × 80 square grid and $Q_1 - P_0$ approximation

TABLE I. TABLE1. The local Poisson problem error estimator Flow over an obstacle with Reynolds number Re = 1000.

$\left\|\nabla.\vec{u}_h\right\|_\Omega$ estimated velocity divergence error.

Grid	$\left\|\nabla.\vec{u}_h\right\|_{0,\Omega}$	η_P
8 × 20	5.892389e-001	3.210243e+001
16 × 40	1.101191e-001	6.039434e+000
32 × 80	3.707139e-002	2.802914e+000
64 ×160	1.160002e-002	1.484983e+000

TABLE II. A residual error estimator for Flow over an obstacle with Reynolds number Re = 1000.

Grid	η_R
8 × 20	9 ,309704e+00
16 × 40	1,727278e+000
32 × 80	8,156479e -001
64 × 160	4.261901e-001

VIII. CONCLUSION

We were interested in this work in the numeric solution for two dimensional partial differential equations modelling (or arising from) model steady incompressible fluid flow. It includes algorithms for discretization by mixed finite element methods and a posteriori error estimation of the computed solutions. Our results agree with Adina system.

Numerical results are presented to see the performance of the method, and seem to be interesting by comparing them with other recent results.

ACKNOWLEDGMENT

The authors would like to express their sincere thanks for the referee for his/her helpful suggestions.

References

[1] Alexandre Ern, Aide-mémoire Eléments Finis, Dunod, Paris, 2005.
[2] P.A. Raviart, J. Thomas, Introduction l'analyse numérique des équations aux dérivées partielles, Masson, Paris, 1983.
[3] E. Creuse, G. Kunert, S. Nicaise, A posteriori error estimation for the Stokes problem: Anisotropic and isotropic discretizations, M3AS, Vol.14, 2004, pp. 1297-1341.
[4] P. Clement, Approximation by finite element functions using local regularization, RAIRO. Anal. Numer, Vol.2, 1975, pp. 77-84.
[5] T. J. Oden,W.Wu, and M. Ainsworth. An a posteriori error estimate for finite element approximations of the Navier-Stokes equations, Comput. Methods Appl. Mech. Engrg, Vol.111, 1994, pp. 185-202.
[6] V. Girault and P.A. Raviart, Finite Element Approximation of the Navier-Stokes Equations, Springer-Verlag, Berlin Heiderlberg New York, 1981.
[7] A. Elakkad, A. Elkhalfi, N. Guessous. A mixed finite element method for Navier-Stokes equations. J. Appl. Math. & Informatics, Vol.28, No.5-6, 2010, pp. 1331-1345.
[8] R. Verfurth, A Review of A Posteriori Error Estimation and Adaptive Mesh-Refinement Techniques, Wiley-Teubner, Chichester, 1996.
[9] M. Ainsworth and J. Oden. A Posteriori Error Estimation in Finite Element Analysis. Wiley, New York, [264, 266, 330, 334, 335], 2000.
[10] M. Ainsworth, J. Oden, A posteriori error estimates for Stokes' and Oseen's equations, SIAM J. Numer. Anal, Vol. 34, 1997, pp. 228–245.
[11] R. E. Bank, B. Welfert, A posteriori error estimates for the Stokes problem, SIAM J. Numer. Anal, Vol.28, 1991, pp. 591–623.
[12] C. Carstensen,S.A. Funken. A posteriori error control in low-order finite element discretizations of incompressible stationary flow problems. Math. Comp., Vol.70, 2001, pp. 1353-1381.
[13] D. Kay, D. Silvester, A posteriori error estimation for stabilized mixed approximations of the Stokes equations, SIAM J. Sci. Comput, Vol.21, 1999, pp. 1321–1336.
[14] R. Verfurth, A posteriori error estimators for the Stokes equations, Numer. Math, Vol.55, 1989, pp. 309–325.
[15] H. Elman, D. Silvester, A. Wathen, Finite Elements and Fast Iterative Solvers: with Applications in Incompressible Fluid Dynamics, Oxford University Press, Oxford, 2005
[16] V. John. Residual a posteriori error estimates for two-level finite element methods for the Navier-Stokes equations, App. Numer. Math., Vol.37, 2001, PP. 503-518.
[17] D. Acheson, Elementary Fluid Dynamics, Oxford University Press, Oxford, 1990.

Mitigating Cyber Identity Fraud using Advanced Multi Anti-Phishing Technique

Yusuf Simon Enoch
Department of Mathematics and Computer Science
Federal University, Kashere
Gombe, Nigeria

Adebayo Kolawole John
Department of Computer Science
Oduduwa University, Ipetumodu
Ile-Ife, Nigeria

Adetula Emmanuel Olumuyiwa
Department of Computer Science
University of Ibadan, Ibadan
Nigeria

***Abstract*—Developing Countries are gradually transiting from cash to an electronic based economy by virtue of cashless policy implementation. With this development, cyber criminals and hackers who hitherto attacked businesses and individuals across the Atlantic now see this development as a new venture for their criminal acts and are thus re-directing their energies towards exploiting possible loopholes in the electronic payment system in order to perpetuate fraud. In this paper, we proposed an enhanced approach to detecting phishing attempts and preventing unauthorized online banking withdrawal and transfer. We employed the use of Semantics Content Analysis, Earth Mover Distance and Biometric Authentication with finger print to construct a model. We demonstrated the efficacy of the implemented model with the experiments conducted, a good and considerable result was achieved.**

***Keywords*—Security; authentication; attack; Cybercrime; Identify theft**

I. INTRODUCTION

The ubiquitous nature and fast pace of the internet growth has aided the number of criminal exploits on the cyberspace. Criminals targeting user information are able to profit from the increased adoption of online services for many day-to-day activities, including banking, shopping, and leisure activities. Today, the Internet is used for espionage and as a medium to commit terrorism and global crimes.

Cybercrime refer to misconducts in the cyber space as well as wrongful use of the internet for criminal purposes. Various categories of these crimes include cyber stalking, phishing (identity theft), virus attacks, malware attack, the use of anonymous proxies to masquerade and sniff information and the popular electronic spam mail problem [16].

The days of dramatic bank heists have been over for years, ambitious criminals are globally embracing cybercrime and other fraudulent cyber activities; this is partly due to the wide availability of automated software tools, mostly intelligently driven being employed by these cyber-criminals. This makes them almost deceptive to detection and poses a hard problem combating crime on the cyber space. As a matter of fact, the newest cyber grenades have fully automated capabilities that eliminate the need for hackers to manually transfer funds from one account to another.

This allows the criminals to stay much more hidden than in the past. Hackers also now use entire servers that are customized to target individual banks and other victims; unfortunately, most users being attacked don't even suspect that their account has been compromised until long after their money has disappeared [13].

Several approaches exist to deceiving unsuspecting users. These include the offer to fill out a survey for an online banking site with a monetary reward if the user includes account information, and email messages claiming to be from a reward clubs, asking users to verify credit card information that a customer may store on the legitimate site for reservation purposes.

Often included in the message is a URL for the victim to use, which then directs the user to a site to enter their personal information. This site is crafted to closely mimic the look and feel of the legitimate site. The information is then collected and used by the criminals. Over time, these fake emails and web sites have evolved to become more technically deceiving to casual investigation.

II. CONSEQUENCES AND TREND OF CYBERCRIME

According to Internet Crime Complaint Centre Report, cybercrime cost a total loss of $485,253,871 in the year 2011. On the other hand, the Economic and Financial Crimes Commission Report [7][8] ranks Nigeria as third among the top ten sources of cyber-crime in the world. It is estimated that after the United States with 65 per cent of cyber-criminal activities and the United Kingdom with 9.9 per cent, Nigeria is the next hub of cyber criminals in the world with 8 percent.

The growth of online banking further presents enhanced opportunities for perpetrators of cyber-crime. Funds can be embezzled using wire transfer or account takeover. Criminals may submit fraudulent online applications for bank loans; disrupt e-commerce by engaging in denial of service attacks, and by compromising online banking payment systems [2][27].

Identity takeover can also affect online banking, as new accounts can be taken over by identity thieves, thus raising concerns regarding the safety and soundness of financial institutions [27].

TABLE I. TOP 10 COUNTRIES - PERPETRATOR OF CYBERCRIME

Year 2008		Year 2009		Year 2010		Year 2011	
United States	66.1 %	United States	65.4 %	United States	65.9 %	United States	90.99 %
United Kingdom	10.5 %	United Kingdom	9.9%	United Kingdom	10.4 %	Canada	1.44 %
Nigeria	7.5%	Nigeria	8.0%	Nigeria	5.8%	United Kingdom	0.97 %
Canada	3.1%	Canada	2.6%	China	3.1%	Australia	0.66 %
China	1.6%	Malaysia	0.7%	Canada	2.4%	India	0.50 %
South Africa	0.7%	Ghana	0.7%	Malaysia	0.8%	Puerto Rico	0.22 %
Ghana	0.6%	South Africa	0.7%	Spain	0.8%	South Africa	0.22 %
Spain	0.6%	Spain	0.7%	Ghana	0.7%	France	0.19 %
Italy	0.5%	Cameroon	0.6%	Cameroon	0.6%	Germany	0.19 %
Romania	0.5%	Australia	0.5%	Australia	0.5%	Russian Federation	0.17 %

Source: Internet Crime Complaint Centre Report [29].

In the USA, online fraud has overtaken viruses as the greatest source of financial loss [26]. Among on-line fraud threats, phishing represents a major threat for financial institutions and according to the Anti-Phishing group organization, 93.8% of all phishing attacks in 2007 are targeted at financial institutions. Also a recent study indicates that phishing attacks in the USA alone soared in 2007 to 3.6 Million victims for a total reported customer loss of USD 3.2 Billion. During 2011, FBI-related scams were the most reported offense with 35, 764 complain with claim of dollars losses, followed by identity theft with 28, 915 then advance fee fraud with 27, 892 [29].

III. RELATED WORK

A wide range of phishing detection techniques have been proposed and deployed. One of the most used techniques seems to be blacklisting. Most of the anti-phishing applications available, including those built into mainstream web browsers, use blacklists for detecting phishing sites.

Some other widely available phishing detection techniques include whitelisting [4] and heuristics [6][12]. The disadvantage of the blacklisting approach is that non blacklisted phishing sites are not recognized. The approaches are only effective as the quality of the lists.

In contrast, whitelists manage a list of known-good websites. Whitelists are generally divided into global lists updated by central servers and personalized lists managed by the end users as needed. Due to its inherent usability issues, whitelists are currently used only in the preprocessing step, i.e. before the heuristics are checked, to reduce false positives. Kirda and Krugel [14] have developed a browser extension called AntiPhish to maintain trusted websites' domain names and credentials.

Some of the well-known Anti-phishing tools are PWDHASH [3] and SpoofGuard [20]. PWDHASH create domain specific passwords that are been rendered useless if submitted to another domain [5] .SpoofGuard in contrast looks for phishing obfuscated URLs symptoms in web pages and raise alerts**.**

A. Social Engineering

Social engineering is the act of tricking computer users into performing actions or revealing private and confidential information e.g. passwords, email addresses etc, by exploiting the natural tendency of a person to trust and/or by exploiting a person's emotional response. Phishing, Scamming, Spamming are some techniques used for social Engineering.

Social engineering schemes use spoofed e-mails purporting to be from legitimate businesses and agencies, designed to lead consumers to counterfeit websites that trick recipients into divulging financial data such as usernames and passwords. Technical subterfuge schemes plant crime-ware in form of robots or malware agents onto PCs to steal credentials directly, often using systems to intercept consumers online account user names and passwords and to corrupt local navigational infrastructures to misdirect consumers to counterfeit websites (or authentic websites through phisher controlled proxies used to monitor and intercept consumers' keystrokes) [22] .

B. Phishing

The word "phishing" is used to describe hackers and cyber-criminals "fishing" the Internet for personal information such as credit card numbers, bank account information and passwords.

Phishing is a criminal mechanism employing both social engineering and technical subterfuge to steal consumers' personal identity data and financial account credentials [22]. The idea behind the term is that if they send out enough fake emails, some receivers will surely "take the bait."

The Anti-Phishing Working Group estimates that the volume of phishing e-mail is growing at a rate of over 30%, month after month [30]. Furthermore, the attacks are becoming more sophisticated as attackers leverage vulnerabilities in client software (mail user agents and web browsers) as well as design vulnerabilities in targeted website applications [30].

In February 2010, some attackers craftily cloned the (Central Bank of Nigeria) CBN site, they periodically send email to bank customers requesting them to update their records with the CBN for a new exercise being carried out to create a database of all the commercial banks' customers in Nigeria, the victims allegedly, were to submit their various account numbers and ATM pins before a deadline date. Victims who clicked on the link in the email were taken to a clone of the CBN's site, thereby posing as the legal CBN site [21].

Most phishing occurs on hacked or compromised Web servers. The United States continued to be the top country hosting phishing sites during the first quarter of 2012.

TABLE II. TOP 10 COUNTRIES – HOSTING PHISHING SITE.

January		February		March	
USA	68.92%	USA	70.86%	USA	66.20%
Canada	11.20%	Romania	3.25%	Germany	3.04%
Egypt	4.32%	Germany	2.66%	B. Virgin II	2.63%
Germany	1.85%	UK	2.62%	Brazil	2.54%
France	1.35%	Russia	1.78%	Egypt	1.98%
Israel	1.29%	France	1.73%	UK	1.91%
Netherlands	1.19%	Canada	1.66%	Netherlands	1.84%
Russia	0.68%	Netherlands	1.51%	Canada	1.83%
UK	0.68%	Brazil	1.35%	Turkey	1.54%
Turkey	0.63%	Australia	1.01%	France	1.51%

Source: Phishing Activity Trend Report [22].

The number of unique phishing sites detected in February, 2012 was 56, 859 by Anti-Phishing Work Group, which was an all-time high. The February figure eclipsed the previous highest record which was in August, 2009 by 1 percent [22].

Source: Phishing Activity Trend Report [22].

C. Spoofing Attacks

Spoofing is a broad term used to describe website, email or even caller ID entry made to trick a victim into thinking it is something other than what it really is. It is a method of attacking a network in order to gain unauthorized access. In a spoofing attack, the intruder sends a message to a computer indicating the message has come from a trusted system. To be successful, the intruder first determine the IP address of a trusted system and then modify the packet headers so that it appears that the packets are coming from the trusted system.

In essence, the attacker is fooling (spoofing) the distant computer into believing that they are legitimate members of the network. The goal of the attack is to establish a connection that will allow the attacker to gain root access to the host, allowing the creation of a backdoor entry path into the target system [10]. There are mainly four types of spoofing attacks. They are: IP Address spoofing, ARP poisoning, WEB spoofing, DNS spoofing.

D. Spoofing in Phishing

Hackers using phishing tactics to acquire victims' personal information often use spoofing in an effort to convince such victims to give up their sensitive information. For instance, to get peoples' bank account information, they send you email seemingly originating from their bank, include the banks logos and a spoofed "From" line to reflect a false sender. The email often contains a link to a spoof of such banks' website. The phishers aim is to use it to give the victims a false sense of security and not to give viruses or other harmful files. By tricking their victims into thinking they are on their bank's website, they can easily give up more information. The mail below shows a crafted mail of a particular bank, requesting customers to click on the link and providing vital information pertaining to their account information.

All customers who entered their details on the fraudulent pop-up were compromised. One must note that the targeted unsolicited email was directed to random email users who may not be Internet registered users. Hence there is a potential risk to non-Internet Banking users, who inevitably entered their ATM card (Master card / Verve card) and pin number, as instructed by the attacker.

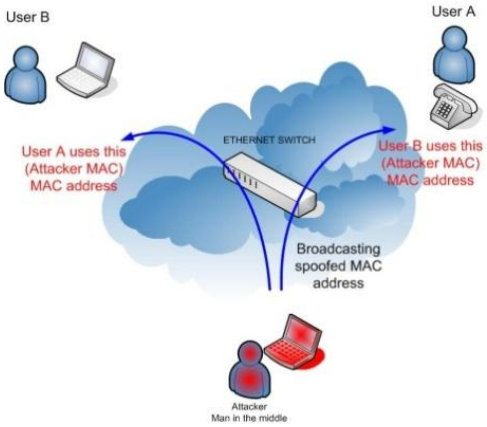

Fig.1. Spoofing Attack

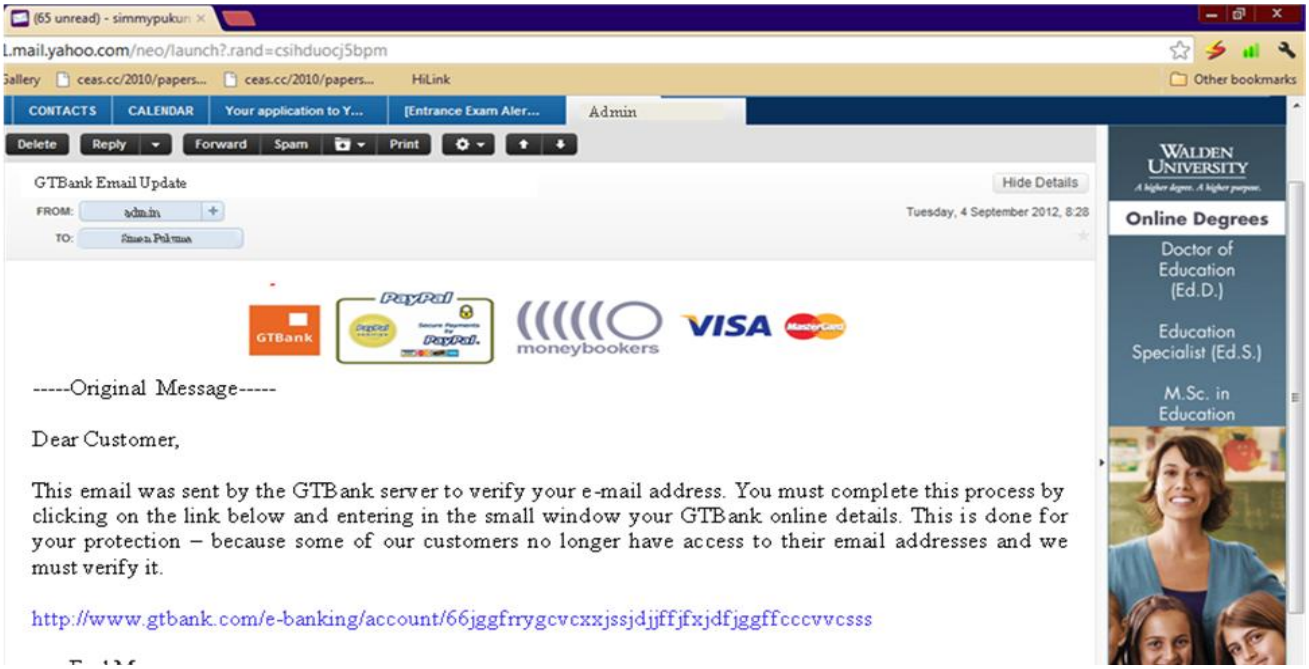

Fig.2. Screenshot of e-mail allegedly to be from GTBank adminstrator

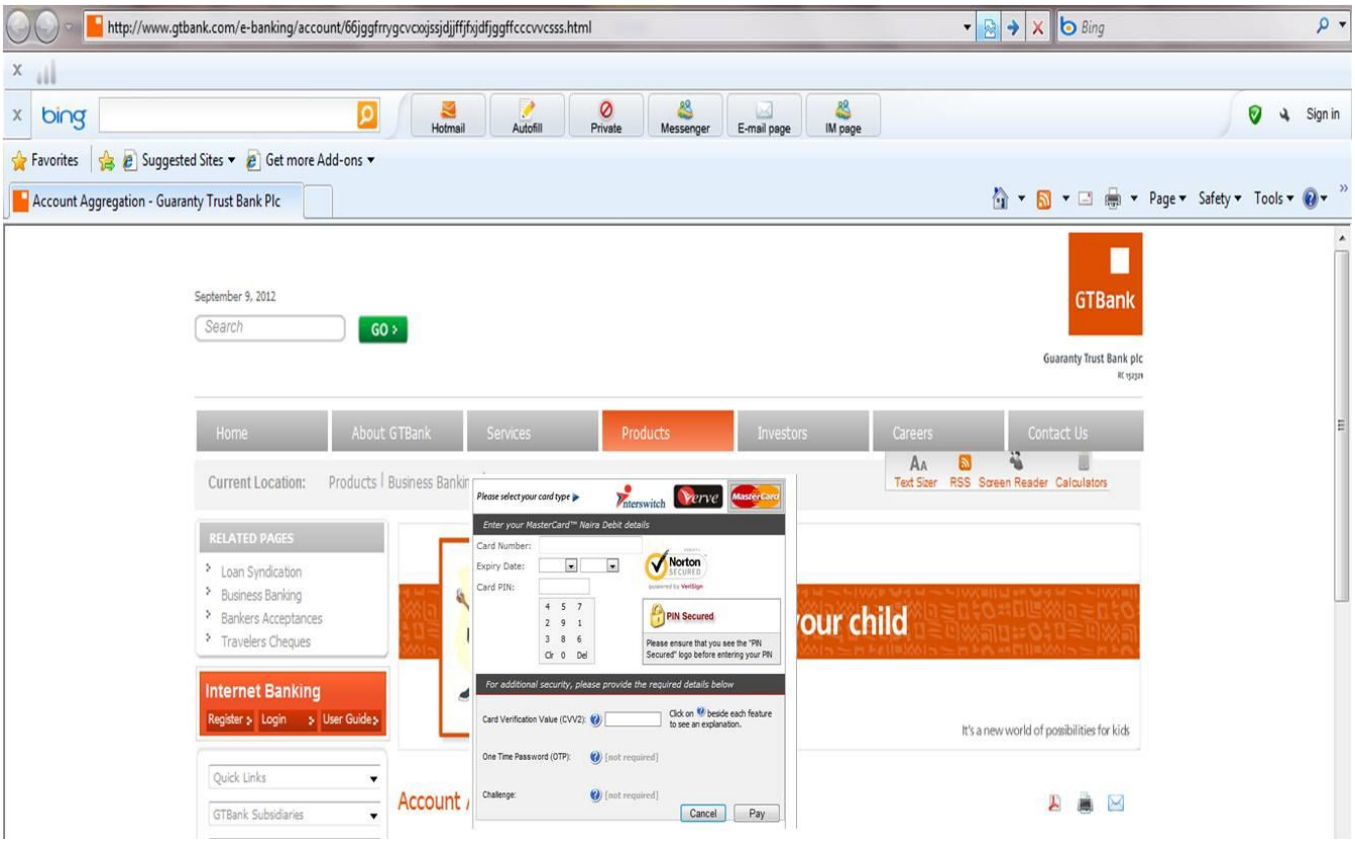

Fig.3. Screenshot of Scam pop up purportedly to be from GTBank website

E. Strategies employed by Phishers

Web Page Obfuscation: To prevent detection from HTML based phishing detector, Phishers employ the use of visual – based content such as images and flash in web site. They also use downloaded web page from real web site to make the phishing web page appear and react exactly the same as the real one.

Web link Obfuscation: This can be carried out in three ways. The first is by using an actual link different from the visible link. Secondly, by using cousin domain names (e.g. replacing certain characters in the target URL with similar characters) [9], thirdly, by adding a suffix to a domain name and redirecting the link to the phishing web pages[1].

F. Challenges with exisitng System

1) Phishers duplicate the content of the target site by using automated tools to download web pages and then use the downloaded web page to achieve main attack on their victim.

2) System that use password authentication fail the requirement for strong authentication, as password can be captured and replayed. Yingjie [28] demonstrated how PWDHASH can be faked.

3) Blacklisting approaches [25], only provide a partial solution with partial list of global phishing websites, and are not completely effective against new phishing websites.

To make the matters worse, the majority of the phishing websites are short-lived (e.g. lasting hours) and hundreds of new ones appear every day[19], making it difficult to update and check against the central databases [12].

IV. METHODOLOGY

This paper employs both primary and secondary research technique of data collection and analysis. This involves the distribution of questionnaire, interview, collection and review of relevant documentation on the evolution of Cybercrime. Data exploited includes; published reports; conference papers; newspaper articles and other media coverage; information accessed through the internet and official records from government agencies.

We proposed a model where by online financial transaction can be secured using a multi-agent system involving biometrics application and an anti-phishing model. We then proceed to present our findings, impediments, and discuss the measures that can be employed by banks to combat Phishing.

In essence, this paper proposes an enhanced approach to detecting phishing web pages and preventing unauthorized online banking withdrawal and transfer. We employed the use of semantics content analysis, earth Mover distance [11] and Biometric authentication[32].

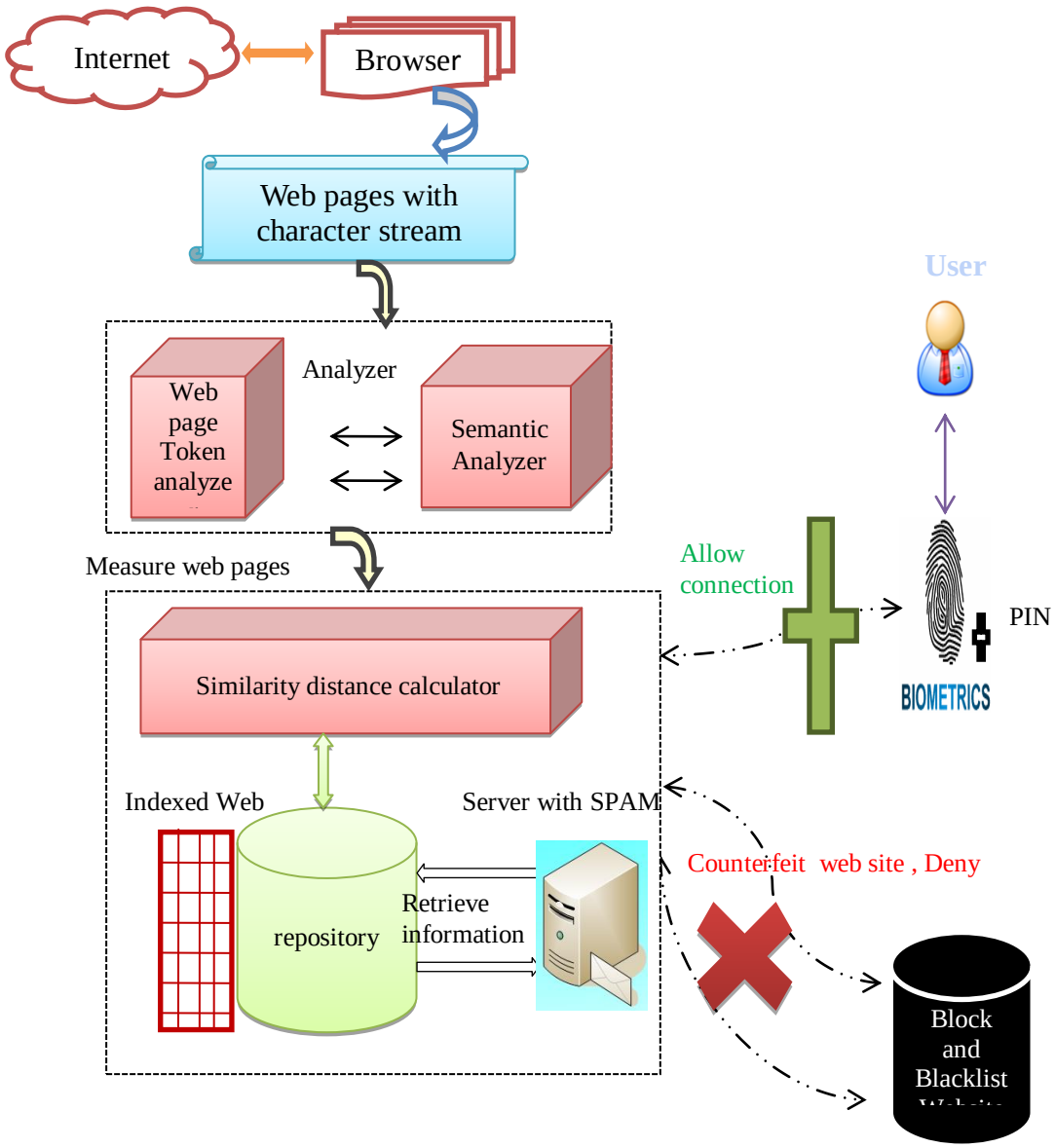

Fig.4. Design Architecture

1) Semantic Content Analysis: Here, sentences from web pages are broken down into small pieces called Token, a finite state automata was used to recognize each regular expression. The semantic analyzer converts all token to upper case letter, which are indexed according to web page and stored in a word repository. The token storage and retrieval scheme can be represented with a 4-tuple as follows:

$<W_p , C_r , q_e , q_f>$

Where,

W_p = set of all words in web pages

C_r = a classifier that Index words in repository

q_e = query matching evaluation function

q_f = feedback function

2) Biometric Authentication: Most popular anti-phishing methods include authentication, which includes email authentication, web page authentication, email filtering and web page filtering, all this listed authentication methods can be intruded by illegitimate professional programmers. We propose the use of finger print authentication [33][34][35][36] mechanism on web pages carrying sensitive information such as credit card information and Personal Information Number-PIN, etc; this is to replace single password verification and impersonation on internet transaction. Online transaction entries are accepted if both the PIN and the fingerprint of the user match with the Account holder. These basic information's are encrypted as they are captured. We adopted the use of biometrics characteristics because they contains physiological characteristics of individuals, are distinctive, cannot be forgotten or lost, and the person to be authenticated needs to be physically present at the point of the identification.

*3) Earth Mover Distance (EMD):*Internet user fall victim of phishing because phishing site has high similarities with original web pages. We adopted [1], EMD Visual Similarity Assessment. The Earth Mover distance was used to assess and calculate the distance between set of features and their respective weight with a bare minimum total price tag. The assessment was carried out on the graphic point of a computer screen. Web pages were converted to images and the coordinate feature and color of the image was used to represent the signature distances. The suspected web page and original web page retrieved from its respective URL will be converted to image and compared.

The EMD is represented as:

$$EMD(P,C,D) = \frac{\sum_{i=1}^{m}\sum_{j=1}^{n}(f_{ij}.d_{ij})}{\sum_{i=1}^{m}\sum_{j=1}^{n}f_{ij}}$$

Where:

P = Producer

C = Customer

w = respective weight

F = flow matrix, indicating the amount of product to be moved from one producer to consumer. F = $[f_{ij}]$ where $1 \leq i \leq m$ and $I \leq j \leq n$.

n and m= number of customers and producers respectively

D= distance of each pair in distance matrix (Producer and Consumer). D = $[d_{ij}]$ where $1 \leq i \leq m$ and $I \leq j \leq n$.

V. EXPERIMENTAL SETUP AND RESULT

The study sample consisted of some commercial banks in Nigeria. Data was collected to know the level of phishing and other online financial fraud each of the bank experience. Statistical Package for Social Sciences (SPSS) was used as the statistical analysis tool while descriptive statistics were computed and used in the interpretation of findings. A total of fifty (50) questionnaires were randomly administered to IT personnel from different bank. Thirty-nine (39) were returned, which represents 78.00% of the total respondents or participants.

We randomized and attached some set of scores to each of the question raised in the questionnaire distributed in order to rank and determine the susceptibility of each bank, their level of awareness and steps already being put in place to stop the problems encountered. We observed that based on the returned questionnaire, attacks based on internet/online banking (42%)fraud takes the lead, followed by email scam (34%) and finally identity fraud (13%) also leading to online banking fraud while the other salient questions such as illegal ATM withdraw etc. takes the remaining space. We were actually concerned about the three most ranked attacks which are ostentatiously being perpetrated online.

The proposed model works like this, when the browser which have the system installed as a plugin was used to open the web pages, it triggers off the semantic analyzer which parsed the contents of the pages, if the semantic analyzer detects any broken link as a form of spoofed link based on some coded rules, it notifies the similarity distance calculator. The similarity distance calculator have access to the web pages that were used to train the system, it measures, ranks and index each pages based on rules allotted to it. The similarity calculator then index and rank the webpage supplied by the semantic analyzer earlier and compares it to the ranks of web pages in the database and which were used to train the similarity calculator. If a match exists in a region based on a particular threshold which is a set of allowable distance between the web pages being compared, the system index the page as genuine and triggers the authentication module which accepts the biometrics feature of the user and allows any financial transaction else if the distance exceeds the region of the thresholds, the similarity calculator indexed this page as a fake webpage and the authentication module remains calm.

We implemented our model as a system to monitor and safeguard online financial transaction. To test the efficacy of the system, we collected twenty-three sensitive web pages over the course of 8 months, these web pages were used in testing the efficacy of the model presented. The system developed was integrated into the browser as a plugin. Demo web pages mimicking each of the collected web pages and containing a spoofed link to a compromised site were also developed. We also had a demo database which contains some stored customers' details such as their fingerprint, personal ID and some other data. We made an attempt of redirecting the user from the mimic or the fake website to a site totally in our control and where acting as attackers, we could actually siphon information from unsuspecting users.

For the experiment as explained earlier, 23 sample web pages majorly dealing with online financial transactions were collected over the course of 8 months, our system was trained by these sample web pages. We designed some 17 web pages that are identical to the collected web pages albeit with spoofed links to another compromised site. The goal is to re-direct the user to a compromised website which should be in control of the attacker. It should be noted that also acting as the user, we used a browser which contains the system we developed as plugin. For the experiment conducted,20 web pages containing 17 fake pages and 3 original web pages included in the training pages were used to test the system while the whole of the initially collected 23 sample pages were used to train the system. Of the 20 test pages, 16 of the test web pages were suspected to have contained spoofed links when analyzed by the semantic analyzer and the similarity distance calculator. This represents a total of 80.00% accuracy. These pages were totally blacklisted by the system and when re-enrolled the user was automatically denied access through the page. We conducted another experiment in order to discover why one of the fake web pages was left undetected, for this experiment, we included another 7 sample web pages from the similarity calculator's database i.e. pages among those earlier used to

train the system and included the one that our system was not able to identify earlier, the total test pages thus used was 8 web pages. We used the earlier sample web pages used to train the system again. The result returned was however surprising, 1 of the web pages was returned by the system to contain a spoofed link, even though the webpage is genuine and actually part of the pages used in the system training. This shows a roughly 12.5% false positive rate. If we deduct this false positive from the initial true positive accuracy obtained earlier, we get 67.5% which we can use as a baseline accuracy rate for now. This anomalous behavior though unacceptable is still unclear to us i.e. we don't know why the system was not able to detect one fake page and why it detected one genuine page as compromised. We believe this should prompt another research in constructing a more robust system and will form the baseline of our future works where the rules employed by the semantic analyzer and the similarity calculator will be significantly altered.

The biometric authentication aspects come in when pages are certified to be okay by the system, we believe it will ensure trustworthiness and security since users will be authenticated by features unique to them and not what they possess like passwords which are still the de-facto approach. This we believe will definitely strengthen financial transactions on the internet.

The table below shows the results obtained.

TABLE III.

Web pages	True Positive %	True Negative %
With our model	80	20
Without our model	8	92

CONCLUSION

Unfortunately, all the existing solutions proposed to mitigate phishing attacks have their weakness. The increasing rate of novel security challenges in an online banking transaction calls for an unvarying fresh technique that mitigates such challenges. In this paper, we presented a novel technique that replaces the single password verification, web page obfuscation, web link obfuscation using biometric authentication, semantic content analysis and Earth mover distance which was incorporated into browsers as plug-in. The performance of our model shows a considerable improvement to existing systems and clearly opens up a new frontier of research space to be explored in the future. Presently, the proposed system achieved 80% accuracy which is commendable. The experimental result shows that the system effectively strengthens the numerous phishing (identity theft) security challenges on the World Wide Web.

REFERENCES

[1] Anthony Y. F., Wenyin L., and Xiaotie D.(2006). Detecting Phishing Web Pages with Visual Similarity Assessment Based on Earth Mover's Distance (EMD) IEEE Transactions on Dependable and Secure Computing, vol. 3, no. 4, October-December 2006.

[2] Atherton, M. (2010) Criminals switch attention from cheques and plastic to internet transactions. The Sunday Times of March 10, 2010.

[3] Blake R., Collin J., Nicholas M., Dan B., and John C. M. (2005). Stronger Password Authentication Using Browser Extensions. In 14th Usenix Security Symposium, 2005.

[4] Cao, Y., Han, W., Le, Y. (2008). Anti-phishing based on automated individual whitelist. In: DIM 2008: Proceedings of the 4th ACM Workshop on Digital Identity Management, pp. 51–60. ACM, New York (2008).

[5] Christian L., Sean M., Engin K., Christopher K. (2008). On the Effectiveness of Techniques to Detect Phishing Sites. Secure Systems Lab, Technical University Vienna.2008

[6] Chou, N., Ledesma, R., Teraguchi, Y., Mitchell, J.C.(2004). Client-Side Defense Against Web-Based Identity Theft. In: NDSS 2004: Proceedings of the Network and Distributed System Security Symposium (2004).

[7] EFCC/ NBS/ (2009) Business Survey on Crime & Corruption and Awareness of EFCC in Nigeria, Summary Report.

[8] EFCC/ NBS/ (2010) Business Survey on Crime & Corruption and Awareness of EFCC in Nigeria, Summary Report.

[9] Fu, A. Y. , Deng X. , and Liu, W., (2005). "A Potential IRI Based Phishing Strategy," Proc. Sixth Int'l Conf. Web Information Systems Eng. (WISE '05), pp. 618-619, Nov. 2005.

[10] Hamanta, R. B. (2010). A Protol for Network Security Assessment and Methodology. Unpublished Master's thesis, Anglia Ruskin University Chelmsford united kingdom.

[11] Hitchcock F.L. (1941). "The Distribution of a Product from Several Sources to Numerous Localities," J. Math. Physics, vol. 20, pp. 224-230, 1941.

[12] Huh, J. H. and Kim, H. (2010). Phishing Detection with Popular Search Engines: Simple and Effective. www.cl.cam.ac.uk/~hk331/Publications/PhishingDetectionSearchEngine.pdf

[13] Kellerman, T. (2012) Systems Technology Consultants Ltd. Available at http://www.sytech-consultants.com/blog/tag/tom-kellermann accessed date 24th July, 2012.

[14] Kirda, E., Kruegel, C.: Protecting Users Against Phishing Attacks with AntiPhish.(2005). In: COMPSAC 2005: Proceedings of the 29th Annual International Computer Software and Applications Conference, pp. 517–524. IEEE Computer Society, Washington, DC, USA (2005)

[15] Liu W., Guanglin H., Liu X., Zhang M., and Xiaotie D.(2005). Detection of phishing webpages based on visual similarity. In 14th International Conference on World Wide Web (WWW): Special Interest Tracks and Posters, 2005.

[16] Longe, O. B., Mbarika, V., Kourouma, M., Wada, F. &Isabalija, R, (2009).Seeing Beyond the Surface: Understanding and Tracking Fraudulent Cyber Activities.International Journal of Computer Science and Information Security, Vol. 6, No. 3, 2009

[17] Mello, J. P. (2011) "SpyEye Trojan Targets Online Banking Security Systems" Avaialable at http://www.pcworld.com/article/241263/spyeye_trojan_targets_online_banking_security_systems.html#tk.mod_stln

[18] MilletaryJ.(2006).www.cert.org/archive/pdf/Phishing_trends.pdf

[19] Moore, T., Clayton, R.(2007). Examining the impact of website take-down on phishing. In: eCrime 2007: Proceedings of the Anti-Phishing Working Groups 2nd Annual eCrime Researchers Summit, pp. 1–13. ACM, New York (2007)

[20] Neil C., Robert L., Yuka T., Dan B., and John M. (2005). Client-side defense against web-based identity theft. In 11th Annual Network and Distributed System Security Symposium (NDSS '04), San Diego, 2005.

[21] Onifade, O.F.W. and Adebayo, K. J.(2011).Phishing and Identity Thefts on the Internet.Journal of Information Technology Impact Vol. 11, No. 2, pp. 133-144, 2011

[22] Phishing Activity Trend Report, Quarter 2012 January – March 2012 Published July 2012. http://www.antiphishing.org/reports/apwg_trends_report_q1_2012.pdf

[23] Sarah Jacobsson. Purewals Sunday Times Hackers Steal $6.7 Million in Cyber Bank Robbery Available at

http://www.pcworld.com/article/248340/hackers_steal_67_million_in_cyber_bank_robbery.html#tk.mod_stln

[24] Schneider F., Provos, N., Moll, R., Chew, M., and Rakowski, B.(2007). Phishing Protection Design Documentation. http://wiki.mozilla.org/Phishing_Protection:_Design_Documentation , 2007.

[25] Sheng, S., Wardman, B., Warner, G., Cranor, L.F., Hong, J., Zhang, C.: An empirical analysis of phishing blacklists. In: CEAS 2009: Proceedings of the 6th Conference on Email and Anti-Spam (2009).

[26] Symantec threat report http://www.symantec.com/business/theme.jsp?themeid=threatreport Gartner study: http://www.gartner.com/it/page.jsp?id=565125

[27] Wada, F. & Odulaja, G.O. (2012). Assessing Cyber Crime and its Impact on E-Banking in Nigeria Using Social Theories.Afr J. of Comp & ICTs.Vol 5.No. 1. pp 69-82.

[28] Yingjie , A. F. (2006) Web Identity Security: Advanced Phishing Attacks and Counter Measures. Doctor of Philosophy Thesis. City Univerdity of Hong Kong September 2006

[29] USIC3 (2012)- Internet Crime Complaint Centre Report (2007-2010). www.ic3.gov/media/annualreports.aspx

[30] www.antiphishing.org/Evolution%20of%20Phishing%20Attacks.pdf

[31] Adebayo Kolawole John, Onifade Olufade and Dada Adeniyi: "Vdetector- A model for combating phishing and identity theft on the internet". In Proc of Intl conference on ICT for Africa, Vol. 2, pg. 72-83, March 2011. *Available online at www.ictforafrica.org*

[32] Onifade, F.W. Olufade and Adebayo, J. Kolawole: "Biometric authentication with face recognition using principal component analysis and a feature-based technique", In International Journal of Computer Applications USA. (0975 – 8887) pg 13 – 20, Volume 41– No.1, March 2012. *Available online at www.ijca.org*

[33] Wahab A, S.H. Chin and Tan E.C: "Novel approach to automated fingerprint recognition" In IEEE proceedining of visual image signal process vol145, No 3, June 1998

[34] Nanili Ratha, Kale Karu, Shaoyun Chen and Anil Chain: "A realtime matching system for large fingerprint database" in IEEE transaction on pattern analysis and machine intelligence. Vol 18, no8, junme 1996

[35] Anil K. Jain, Salil Prabhakar, Lin Hong, and Sharath Pankanti: "Filterbank-Based Fingerprint Matching" In Ieee Transactions On Image Processing, Vol. 9, No. 5, May 2000

[36] Anil Jain, Lin Hong, and Ruud Bolle: "On-Line Fingerprint Verification" In Ieee Transactions On Pattern Analysis And Machine Intelligence, Vol. 19, No. 4, April 1997

A New Viewpoint for Mining Frequent Patterns

Thanh-Trung Nguyen
Department of Computer Science
University of Information Technology,
Vietnam National University HCM City
Ho Chi Minh City, Vietnam

Phi-Khu Nguyen
Department of Computer Science
University of Information Technology,
Vietnam National University HCM City
Ho Chi Minh City, Vietnam

***Abstract*—According to the traditional viewpoint of Data mining, transactions are accumulated over a long period of time (in years) in order to find out the frequent patterns associated with a given threshold of support, and then they are applied to practice of business as important experience for the next business processes. From the point of view, many algorithms have been proposed to exploit frequent patterns. However, the huge number of transactions accumulated for a long time and having to handle all the transactions at once are still challenges for the existing algorithms. In addition, today, new characteristics of the business market and the regular changes of business database with too large frequency of added-deleted-altered operations are demanding a new algorithm mining frequent patterns to meet the above challenges. This article proposes a new perspective in the field of mining frequent patterns: accumulating frequent patterns along with a mathematical model and algorithms to solve existing challenges.**

Keywords*—accumulating frequent patterns; data mining; frequent pattern; horizontal parallelization; representative set; vertical parallelization

I. INTRODUCTION

Frequent pattern mining is a basic problem in data mining and knowledge discovery. Frequent patterns are set of items which occur in dataset more than user specified number of times. Identifying frequent patterns will play an essential role in mining associations, correlations, and many other interesting relationships among data (Prakash et. al. 2011). Recently, frequent pattern has been studied and applied into many areas such as: text categorization (Yuan et. al. 2013), text mining (Kim et. al. 2012), social network (Nancy and Ramani 2012), frequent subgraph (Wang and Ramon 2012) … Various techniques have been proposed to improve the performance of frequent pattern mining algorithms. In general, methods of finding frequent patterns may fall into 3 main categories: Candidate Generation Methods, Without Candidate Generation Methods and Parallel Methods.

The common rule of Candidate Generation Methods is probing dataset many times to generate good candidates which can be used as frequent patterns of dataset. Apriori algorithm, proposed by Agrawal and Srikant in 1995 (Prasad and Ramakrishna 2011), is a typical technique in this approach. Recently, many researches focus on Apriori and improve this algorithm to reduce the complexity and increase the efficiency of finding frequent patterns. Partitioning technique (Prasad and Ramakrishna 2011), pattern based algorithms and incremental Apriori based algorithms (Sharma and Garg 2011) can be viewed as the Candidate Generation Methods. Many improvements of Apriori were presented. An efficient improved Apriori algorithm for mining association rules using Logical Table based approach was proposed (Malpani and Pal 2012). Another group focuses on map/reduce design and implementation of Apriori algorithm for structured data analysis (Koundinya et. al. 2012) while some researchers proposed an improved algorithm for mining frequent patterns in large datasets using transposition of the database with minor modification of the Apriori-like algorithm (Gunaseelan and Uma 2012). The custom-built Apriori algorithm (Rawat and Rajamani 2010), and the modified Apriori algorithm (Raghunathan and Murugesan 2010) were introduced but the time consuming has been still a big obstacle. Reduced Candidate Set (RCS) is an algorithm which is more efficiency than original Apriori algorithm (Bahel and Dule 2010). Record Filter Approach is a method which takes less time than Apriori (Goswami et. al. 2010). In addition, Sumathi et. al. 2012 also proposed the algorithm taking vertical tidset representation of the database and removes all the non-maximal frequent item-sets to get exact set of Maximal Frequent Itemset directly. Besides, a method was introduced by Utmal et. al. 2012. This method firstly finds frequent 1_itemset and then uses the heap tree to sort frequent patterns generated, and so repeatedly. Although Apriori and its developments are proved the effectiveness, many scientists still focus on the other heuristic algorithms and try to find better algorithms. Genetic algorithms (Prakash et. al. 2011), Dynamic Function (Joshi et. al. 2010) and depth-first search were studied and applied successfully in reality. Besides, a study presented a new technique using a classifier which can predict the fastest ARM (Association Rule Mining) algorithm with a high degree of accuracy (Sadat et. al. 2011). Another approach was also based on Apriori algorithm but provides better reduction in time because of the prior separation in the data (Khare and Gupta 2012).

Apriori and Apriori-like algorithms sometimes create large number of candidate sets. It is hard to pass the database and compare the candidates. Without Candidate Generation is another approach which determines complete set of frequent item sets without candidate generation, based on divide and conquer technique. Interesting patterns, Constraint-based mining are typical methods which were all introduced recently (Prasad and Ramakrishna 2011). FP-Tree, FP-Growth and their developments (Aggarwal et. al. 2009) – (Kiran and Reddy 2011) – (Deypir and Sadreddini 2011) – (Xiaoyun et. al. 2009) – (Duraiswamy and Jayanthi 2011) introduced a prefix tree structure which can be used to find out frequent patterns in

datasets. In other hand, researchers studied a transaction reduction technique with FP-tree based bottom up approach for mining cross-level pattern (Jayanthi and Duraiswamy 2012), and construction of FP-tree using Huffman Coding (Patro et. al. 2012). H-mine is a pattern mining algorithm which is used to discover features of products from reviews (Prasad and Ramakrishna 2011) – (Ghorashi et. al. 2012). Besides that, a novel tree structure called FPU-tree was proposed which is efficient than available trees for storing data streams (Baskar et. al. 2012). Another study tried to find improved association to show that which item set is most acceptable association with others (Saxena and Satsangi 2012). Q-FP tree was introduced as a way to mine data streams for association rule mining (Sharma and Jain 2012).

Applying parallel technique to solve high complexity problems is an interesting field. In recent years, several parallel, distributed extensions of serial algorithms for frequent pattern discovery have been proposed. A study presented a distributed, parallel algorithm, which makes feasible the application of SPADA to large data sets (Appice et. al. 2011) while another group introduced HPFP-Miner algorithm, based on FP-Tree algorithm, to integrate parallelism into finding the frequent patterns (Xiaoyun et. al. 2009).

A method for finding the frequent occurrence patterns and the frequent occurrence time-series change patterns from the observational data of the weather-monitor satellite applied successfully parallel method to solve the problem of calculation cost (Niimi et. al. 2010). PFunc, a novel task parallel library whose customizable task scheduling and task priorities facilitated the implementation of clustered scheduling policy, was presented and proved its efficiency (Kambadur et. al. 2012). Another method is partitioning for finding frequent pattern from huge database. It is based on key based division for finding the local frequent pattern (LFP). After finding the partition frequent pattern from the subdivided local database, it then find the global frequent pattern from the local database and perform the pruning from the whole database (Gupta and Satsangi 2012).

Fuzzy frequent pattern mining has been also a new approach recently (Picado-Muiño et. al. 2012).

Although there are significant improvement in finding frequent patterns recently, working with the varying database is still a big challenge. Especially, it need not scan again the whole database whenever having need of adding a new element or deleting/modifying an element. Besides, a number of algorithms are effective, but their basis of mathematics and way of installation are complex. In addition, it is the limit of computer memory. Hence, combining how to store the data mining context most effectively with costing the memory least and how to store frequent patterns is also not a small challenge. Finally, ability of dividing data into several parts for parallel processing is also concerned.

Furthermore, characteristics of the medium and small market also produce challenges need to be solved:

- Most enterprises have medium and small scale, such as: interior decoration, catering business, computer training, foreign language traning, motor business, and so on. The number of categories of goods which they trade in is about 200 to 1000. Cases up to 1000 items, it is usually the supermarkets with diverse categories such as food, appliances, makeup, homemaker, …
- The purchasing invoices have the same general principle is that the number of categories sold is about 20 (the invoice form is in accordance with the government)
- The fact that the laws indicating a shopping tendency of the market in the best way are drawn from the number of invoices having accumulated time from 6 months to 1 year before. Because the current market needs and design, utility, function of goods change rapidly and continuously, so it can not use the laws of the previous years to apply to the current time.
- Market trends in different areas are different.
- Businesses need to regularly change the minimum support threshold in order to find acceptable laws based on the number of buyers.
- Due to the specific management of enterprises, the operations such as adding, deleting, editing frequently impact on database.
- The need of accumulating the results immediately after each operation on the invoice to be able to refer to the laws at any time.

In this article, a mathematical space will be introduced with some new related concepts and propositions to design new algorithms which are expected to solve remain issues in finding frequent patterns.

II. MATHEMATICAL MODEL

Definition 1: Given 2 bit chains with the same length: $a = a_1a_2\ldots a_m$, $b = b_1b_2\ldots b_m$. a is said to cover b or b is covered by a – denoted $a \hookrightarrow b$ – if $pos(b) \subseteq pos(a)$ where $pos(s) = \{i \mid s_i = 1\}$

Definition 2:

+ Let u be a bit chain, k is a non-negative integer, we say $[u; k]$ is a *pattern*.

+ Let S be the set of size-m bit chains (chains with the length of m), u is a size-m bit chain. If there are k chains in S cover u, we say: u is a *form* of S with frequency k; and $[u; k]$ is a pattern of S – denoted $[u; k]_{\to S}$

For instance: S = {1110, 0111, 0110, 0010, 0101} and u = 0110. We say u is a form with frequency 2 in S, so $[0110; 2]_{\to S}$

+ A pattern $[u; k]$ of S is called *maximal pattern* – denoted $[u; k]_{\max\to S}$ – if and only if it doesn't exist k' such that $[u; k']_{\max\to S}$ and $k' > k$. With the above instance, $[0110; 3]_{\max\to S}$

Definition 3: P is *representative set* of S when $P = \{[u; p]_{\max\to S} \mid \nexists [v; q]_{\max\to S} : (v \hookrightarrow u \text{ and } q > p)\}$. Each element in P is called a *representative pattern* of S

Proposition 1: Let S be a set of size-m bit chains with representative set P, then two arbitrary elements in P do not coincide with each other.

Maximal Rectangle: If we present the set *S* in the form of matrix with each row being an element in *S*, intuitively, we can see that each element [*u*; *k*] of the representative set *P* forms a *maximal rectangle* with *maximal height* of *k*.

For instance, given *S* = {1110, 0111, 1110, 0111, 0011}, the representative set of *S*: *P* = {[1110; 2], [0110; 4], [0010; 5], [0111; 2], [0011; 3]}.

A 5x4 matrix:				*and*	[0110; 4]:			
1	1	1	0		1	**1**	**1**	0
0	1	1	1		0	**1**	**1**	1
1	1	1	0		1	**1**	**1**	0
0	1	1	1		0	**1**	**1**	1
0	0	1	1		0	0	1	1

Fig.1. A 5x4 matrix for [0110; 4].

Figure 1 shows a maximal rectangle with boldface 1s and a maximal height of 4 corresponding to the pattern [0110; 4]. Other maximal rectangles formed by elements of *P* are:

[1110; 2]:				[0010; 5]:				[0111; 2]:				[0011; 3]:			
1	**1**	**1**	0	1	1	**1**	0	1	1	1	0	1	1	1	0
0	1	1	1	0	1	**1**	1	0	**1**	**1**	**1**	0	1	**1**	**1**
1	**1**	**1**	0	1	1	**1**	0	1	1	1	0	1	1	1	0
0	1	1	1	0	1	**1**	1	0	**1**	**1**	**1**	0	1	**1**	**1**
0	0	1	1	0	0	**1**	1	0	0	1	1	0	0	**1**	**1**

Fig.2. Matrices for [1110; 2], [0010; 5], [1110; 2] and [0011; 3].

Definition 4 (Binary relations):

+ Two size-*m* bit chains *a* and *b* is said to be equal – denoted $a = b$ – if and only if $a_i = b_i \ \forall i \in \{1, \dots, m\}$, otherwise $a \neq b$

+ Given 2 patterns $[u_1; p_1]$ and $[u_2; p_2]$. $[u_1; p_1]$ is said to be contained in $[u_2; p_2]$ – denoted $[u_1; p_1] \subseteq [u_2; p_2]$ – if and only if $u_1 = u_2$ and $p_1 \leq p_2$, otherwise $[u_1; p_1] \not\subset [u_2; p_2]$

+ Given 2 size-*m* bit chains *a* and *b*. A size-*m* bit chain *z* is called *minimum chain* of *a* and *b* – denoted $z = a \wedge b$ – if and only if $z_k = \min(a_k, b_k) \ \forall k \in \{1, \dots, m\}$

+ *Minimum pattern* of 2 patterns $[u_1; p_1]$ and $[u_2; p_2]$ is a pattern $[u'; p']$ – denoted $[u'; p'] = [u_1; p_1] \text{ o } [u_2; p_2]$ – where $u' = u_1 \wedge u_2$ and $p' = p_1 + p_2$

III. Practical Issue

A. Presenting the Problem

We have a set of transactions and the goal is to produce the frequent patterns according to a specific bias called *min support*.

We can present the set of transactions as a set *S* of bit chains. For a chain in *S*, the i^{th} bit is set to 1 when the i^{th} item is chosen and otherwise. The representative set *P* of *S* is the set of all patterns in *S* with maximal occurrence time.

We can calculate the frequent patterns easily according to *P*.

So, the problem is transferred to rebuilding the representative set *P* whenever *S* is modified (add, delete or alter elements).

B. Adding a New Transaction

We just simply use the above algorithm to rebuild the representative set *P* when a new transaction is added.

Algorithm for rebuilding the representative set when adding a new element to *S*: Let *S* be a set of *n* size-*m* bit chains with representative set *P*. In this section, we consider the algorithm for rebuilding the representative set when a new chain is added to *S*.

```
ALGORITHM NewRepresentative (P, z)
// Finding new representative set for S when one chain is
   added to S.
// Input: P is the representative set of S,
          z is a chain added to S.
// Output: The new representative set P of S ∪ {z}.
1.  M = ∅ // M: set of new elements of P
2.  flag1 = 0
3.  flag2 = 0
4.  for each x ∈ P do
5.    q = x o [z; 1]
6.    if q ≠ 0 // q is not a chain with all bits 0
7.      if x ⊆ q then P = P \ {x}
8.      if [z; 1] ⊆ q then flag1 = 1
9.      for each y ∈ M do
10.       if y ⊆ q then
11.         M = M \ {y}
12.         break for
13.       endif
14.       if q ⊆ y then
15.         flag2 = 1
16.         break for
17.       endif
18.     endfor
19.   else
20.     flag2 = 1
21.   endif
22.   if flag2 = 0 then M = M ∪ {q}
23.   flag2 = 0
24. endfor
25. if flag1 = 0 then P = P ∪ {[z; 1]}
26. P = P ∪ M
27. return P
```

The complexity of the algorithm:

The complexity of *NewRepresentative* algorithm is $nm2^{2m}$, where *n* is the number of transactions and *m* is the number of items. (Of course, if we are more careful, we may get a better estimate, however the above estimate is linear in *n*, and this is the most important thing).

Proof: Let P be the representative set before adding z, and let Q the new representative set after adding z. Let $|P|$ be the cardinal of P (i.e. the number of elements of P).

The key observation is that $|P| \leq 2^m$. This is because we can not have two elements $[z; p]$ and $[z'; p']$ in P such that $z = z'$ and $p \neq p'$. Therefore, the number of elements of P will always less than or equal to the number of chains of m bits, the latter is 2^m.

Fixed an x in P.

In line 5, the complexity will be m.

In line 7, the complexity will be m again.

In line 8, the complexity is m again.

In lines 9-13, the cardinal $|M|$ is at most $|P|$, since from the definition of M on line 22 the worst case is when we add every thing of the form $q = x \circ [z; 1]$ into M, here x runs all over P, and in this case $|M| = |P|$. Hence the complexity of these lines 9-13 is less than or equal to $|P|$.

Lines 18-24 the complexity is at most m.

Hence when we let x vary in P (but fix a transaction z), we see that the total complexity for lines 5-24 is about $m|P|^2 \leq m2^{2m}$.

If we vary the transactions z (whose number is n), we see that the complexity for the whole algorithm is $nm2^{2m}$.

Theorem 1:

Let S be a set of size-m bit chains and P be representative set of S. For $[u; p], [v; q] \in P$ and $z \notin S$, let $[u; p] \circ [z; 1] = [t; p+1]$, $[v; q] \circ [z; 1] = [d; q+1]$. Only one of the following cases must be satisfied:

i. $[u; p] \subseteq [t; p+1]$ and $[u; p] \subseteq [d; q+1]$, $t = d$

ii. $[u; p] \subseteq [t; p+1]$ and $[u; p] \not\subset [d; q+1]$, $t \neq d$

iii. $[u; p] \not\subset [t; p+1]$ and $[u; p] \not\subset [d; q+1]$.

Proof: From *Proposition 1*, obviously $u \neq v$. The theorem is proved if the following claim is true: Let

(a): $u = t$, $u = d$, and $t = d$;

(b): $u = t$, $u \neq d$, and $t \neq d$;

(c): $u \neq t$ and $u \neq d$,

only one of the above statements is correct.

By the method of induction on the number m of entries of chain, in the first step, we show that the claim is correct if u and v differ at only one k^{th} entry.

Without loss of generality, we assume that $u_k = 0$ and $v_k = 1$. The following cases must be true:

- Case 1: $z_k = 0$; Then $\min(u_k, z_k) = \min(v_k, z_k) = 0$, hence

$t = u \wedge z = (u_1, u_2, \ldots, 0, \ldots, u_m) \wedge (z_1, z_2, \ldots, 0, \ldots, z_m) = (x_1, x_2, \ldots, 0, \ldots, x_m)$, $x_i = \min(u_i, z_i)$, for $i = 1, \ldots, m$, $i \neq k$;

$d = v \wedge z = (v_1, v_2, \ldots, 1, \ldots, v_m) \wedge (z_1, z_2, \ldots, 0, \ldots, z_m) = (y_1, y_2, \ldots, 0, \ldots, y_m)$, $y_i = \min(v_i, z_i)$, for $i = 1, \ldots, m$, $i \neq k$.

From the assumption $u_i = v_i$ when $i \neq k$ thus $x_i = y_i$, so $t = d$. Hence, if $u = t$ then $u = d$ and (a) is correct. On the other hand, if $u \neq t$ then $u \neq d$, therefore (c) is correct.

- Case 2: $z_k = 1$; We have $\min(u_k, z_k) = 0$, $\min(v_k, z_k) = 1$ and $t = u \wedge z = (u_1, u_2, \ldots, 0, \ldots, u_m) \wedge (z_1, z_2, \ldots, 1, \ldots, z_m) = (x_1, x_2, \ldots, 0, \ldots, x_m)$, $x_i = \min(u_i, z_i)$, for $i = 1, \ldots, m$, $i \neq k$;

$d = v \wedge z = (v_1, v_2, \ldots, 1, \ldots, v_m) \wedge (z_1, z_2, \ldots, 1, \ldots, z_m) = (y_1, y_2, \ldots, 1, \ldots, y_m)$, $y_i = \min(v_i, z_i)$, for $i = 1, \ldots, m$, $i \neq k$.

So, $t \neq d$. If $u = t$ then $u \neq d$, thus the statement (b) is correct.

In summary, the above claim is true for any u and v of S that differ only at one entry.

By induction in the second step, it is assumed that the claim is true if u and v differ at r entries, and only one of the three statements (a), (b) or (c) is true.

Without loss of generality, we assume that the first r entries of u and v are different, and they differ at $(r + 1)$-*th* entries. Applying the same method in the first step where $r = 1$ to this instance, it is obtained

True statements when $u \neq v$, and their first r entries are different:	True statements when $u \neq v$, and their first $r + 1$ entries are different:	True statements when combining the two possibilities:
(a)	(a)	(a)
(a)	(b)	(b)
(a)	(c)	(c)
(b)	(a)	(b)
(b)	(b)	(b)
(b)	(c)	(c)
(c)	(a)	(c)
(c)	(b)	(c)
(c)	(c)	(c)

Fig.3. Cases in comparison.

Therefore, if u and v are different at $r + 1$ entries, only one of the (a), (b), (c) statements is correct. The above claim is true, and *Theorem 1* is proved.

Theorem 2:

Let S be a set of n size-m bit chains. The representative set of S is determined by applying *NewRepresentative* algorithm to each of n elements of S in turn.

Proof: We prove the theorem by induction on the number n of elements of S.

Firstly, when applying the above algorithm to the set S of only one element, this element is added into P and then P with that only element is the representative set of S. Thus, theorem 2 is proved in the case of $n = 1$.

Next, assume that whenever S has n elements, the above algorithm can be applied to S to obtain a representative set P_0.

Now we prove that when S has $n + 1$ elements then the above algorithm can be applied to yield a representative P for S. We assume that S is the union of a set S_0 of n elements and an element z, and that we already had a representative set P_0 for S_0. Each element of P_0 allows forming a maximal rectangle from S_0, and we call p the number of elements of P_0.

The fifth statement in the *NewRepresentative* algorithm shows that the operator ○ can be applied to z and p elements of P_0 to produce p new elements belonging to P. This means z "scans" all elements in the set P_0 to find out new rectangle forms when adding z into S_0. Consequently, three groups of $2p + 1$ elements in total are created from the sets P_0, P, and z.

To remove redundant rectangles, we have to check whether each element of P_0 is contained by elements of P or not, whether elements of P contain other one another, and whether z is contained by an element in P.

Let x be an element of P_0 and consider the form x ○ $[z; 1]$. There are two cases: if the form of z covers the one of x then x is a new form; or if the form of x covers the one of z then z is a new form. In either case, the frequency of the new form is always one unit greater than frequency of the original.

According to *Theorem 1*, with $x \in P_0$, if some pattern w contains x then w must be a new element which belongs to P, and that new element is $q = x$ ○ $[z; 1]$. To check whether x is contained by elements belonging to P, we need only to check that whether x is contained by q or not. If x is contained by q, it must be removed from the representative set (line 7).

In summary, first, the algorithm checks whether elements belonging to P_0 is contained by elements belonging to P. Then, the algorithm checks whether elements of P contain one another (from line 9 to line 18), and whether $[z; 1]$ is contained by elements belonging to P or not (line 8).

Finally, the above *NewRepresentative* algorithm can be used to find new representative set when adding new elements to S.

C. Deleting a Transaction

Definition 5: Let S be a set of bit chains and P received by applying the algorithm *NewRepresentative* to S be the representative set of S. Given $[p; k] \in P$, and $s_1, s_2, \ldots, s_r \in S$ are r ($r \le k$) chains participating in taking shape p, i.e., these chains participate in creating a rectangle with the form p in S, denoted p_crd: $s_1, s_2, \ldots, s_r$, otherwise, p_crd: $!s_1, !s_2, \ldots, !s_r$

For example, with *Figure 1*, the chains 1110 and 0111 are 2 in 4 chains participating in creating [0110; 4]. Let $s_1 = 1110$, $s_2 = 0111$ and $p = 0110$, we have p_crd = s_1, s_2. Besides, the chain $s_3 = 0011$ does not participate in creating [0110; 4], so p_crd = $!s_3$

Theorem 3:

Let S be a set of bit chains and P received by applying the algorithm *NewRepresentative* to S be the representative set of S. With an arbitrary $s \in S$, we have:

$\forall [p; k] \in P \mid p$_crd: $s, s \hookrightarrow p$ and $\forall [p'; k'] \in P \mid p'$_crd: $!s, s \not\hookrightarrow p'$

Proof: Suppose to the contradiction that *Theorem 3* is wrong. It has 2 cases:

(1) $\exists [p; k] \in P \mid p$_crd: $s, s \not\hookrightarrow p$ or

(2) $\exists [p'; k'] \in P \mid p'$_crd: $!s, s \hookrightarrow p'$

With (1), we have $s \not\hookrightarrow p$. According to the algorithm *NewRepresentative*, s can not participate in creating p, p_crd: $!s$, hence (1) is wrong.

With (2), we have $s \hookrightarrow p'$. According to the algorithm *NewRepresentative*, s have to participate in creating p', p'_crd: s, hence (2) is wrong.

To sum up, *Theorem 3* is right.

When having *Theorem 3*, modifying the representative set after a transaction was deleted is rather simple. We just use the chain/transaction deleted to scan all elements of the representative set and reduce their frequency by 1 unit if they are covered by this chain. The example for this situation will be showed in the section III.*E* Now the algorithm *NewRepresentative_Delete* are generated:

```
ALGORITHM NewRepresentative_Delete (P,
z)
// Finding new representative for S when one chain is
removed from S.
// Input: P is the representative set of S,
          z is a chain removed from S.
// Output: The new representative set P of S \ {z}
1. For each x ∈ P do
2.   if z ↪ x.Form then
3.     x.Frequency ← x.Frequency – 1
4.     if x.Frequency = 0 then P ← P \
{x}
5.   endif
6. endfor
```

D. Altering a Transaction

The operation of altering a transaction is equivalent to deleting that transaction and adding new transaction with the changed content.

E. Example

Give the set S of transactions $\{o_1, o_2, o_3, o_4, o_5\}$ and the set I of items $\{i_1, i_2, i_3, i_4\}$. *Figure 4* describes elements in S.

	i_1	i_2	i_3	i_4
o_1	1	1	1	0
o_2	0	1	1	1
o_3	0	1	1	1
o_4	1	1	1	0
o_5	0	0	1	1

Fig.4. Bit chains of S.

- Step 1: Consider line 1: [1110; 1] (l_1)

Since P now is empty means should we put (l_1) in P, we have:

$P = \{ [1110; 1] \}$ (1)

- Step 2: Consider line 2: [0111; 1] (l_2)

Let (l_2) perform the o operation with the elements existing in *P* in order to get the new elements

(l_2) o (1): [0111; 1] o [1110; 1] = [0110; 2] (n_1)

Considering excluded:

- Considering whether or not the old elements in *P* is contained in the new elements: We remain: (1)

- Considering whether or not the new elements contain each other (note: (l_2) is also a new element): We remain: (l_2) and (n_1)

After considering excluded, we put the elements into *P*:

P = { [1110; 1] (1);

[0110; 2] (2);

[0111; 1] (3) }

- Step 3: Consider line 3: [0111; 1] (l_3)

Let (l_3) perform the o operation with the elements existing in *P* in order to get the new elements

(l_3) o (1): [0111; 1] o [1110; 1] = [0110; 2] (n_1)

(l_3) o (2): [0111; 1] o [0110; 2] = [0110; 3] (n_2)

(l_3) o (3): [0111; 1] o [0111; 1] = [0111; 2] (n_3)

Considering excluded:

- Considering whether or not the old elements in *P* is contained in the new elements: We remove: (2) because of being contained in (n_1), and (3) because of being contained in (n_3); we remain: (1)

- Considering whether or not the new elements contain each other (note: (l_3) is also a new element): We remove: (n_1) because of being contained in (n_2), and (l_3) because of being contained in (n_3); we remain: (n_2) and (n_3)

After considering excluded, we put the elements into *P*:

P = { [1110; 1] (1);

[0110; 3] (2);

[0111; 2] (3) }

- Step 4: Consider line 4: [1110; 1] (l_4)

Let (l_4) perform the o operation with the elements existing in P in order to get the new elements

(l_4) o (1): [1110; 1] o [1110; 1] = [1110; 2] (n_1)

(l_4) o (2): [1110; 1] o [0110; 3] = [0110; 4] (n_2)

(l_4) o (3): [1110; 1] o [0111; 2] = [0110; 3] (n_3)

Considering excluded:

- Considering whether or not the old elements in *P* is contained in the new elements: We remove: (1) because of being contained in (n_1), and (2) because of being contained in (n_2); we remain: (3)

- Considering whether or not the new elements contain each other (note: (l_4) is also a new element): We remove: (n_3) because of being contained in (n_2), and (l_4) because of being contained in (n_1); we remain: (n_1) and (n_2)

After considering excluded, we put the elements into *P*:

P = { [0111; 2] (1);

[1110; 2] (2);

[0110; 4] (3) }

- Step 5: Consider line 5: [0011; 1] (l_5)

Let (l_5) perform the o operation with the elements existing in P in order to get the new elements

(l_5) o (1): [0011; 1] o [0111; 2] = [0011; 3] (n_1)

(l_5) o (2): [0011; 1] o [1110; 2] = [0010; 3] (n_2)

(l_5) o (3): [0011; 1] o [0110; 4] = [0010; 5] (n_3)

Considering excluded:

- Considering whether or not the old elements in *P* are contained in the new elements: We remain: (1), (2), and (3)

- Considering whether or not the new elements contain each other (note: (l_5) is also a new element): We remove: (l_5) because of being contained in (n_1), and (n_2) because of being contained in (n_3); we remain: (n_1) and (n_3)

After considering excluded, we put the elements into *P*:

P = { [0111; 2] (1);

[1110; 2] (2);

[0110; 4] (3);

[0011; 3] (4);

[0010; 5] (5) }

So, the frequent patterns satisfying *min support* = 40% (2/5) is listed:

{ {i_2, i_3, i_4} (2/5); {i_1, i_2, i_3} (2/5); {i_2, i_3} (4/5); {i_3, i_4} (3/5); {i_5} (5/5) }

In addition, we also can list immediately the frequent patterns satisfying *min support* = 60% (3/5):

{ {i_2, i_3} (4/5); {i_3, i_4} (3/5); {i_3} (5/5) }

When the invoice o_1 = 1110 is deleted, we need only scan through each element of *P* and examine whether their forms are covered by o_1. If they are covered then we reduce their frequency by 1 unit. Specifically, we have:

P = { [0111; 2] (1);

[1110; 1] (2);

[0110; 3] (3);

[0011; 3] (4);

[0010; 4] (5) }

To increase the speed of computation, we can realize intuitively that grouping the chains/transactions in the period of preprocessing data, before running the algorithms is a good idea.

Form	Frequency
1110	2
0111	2
0011	1

Fig.5. The result after grouping the bit chains of *S*.

IV. Experimentation 1

The experiments of *NewRepresentative* algorithm are conducted on a machine with Intel(R) Core(TM) i3-2100 CPU @ 3.10GHz (4 CPUs), ~3.1GHz and 4096MB main memory installed. The operating system is Windows 7 Ultimate 64-bit (6.1, Build 7601) Service Pack 1. Programming language is C#.NET.

The proposed algorithm is tested on two datasets: the Retail data taken from a small and medium enterprise in reality and the T10I4D100K data taken from *http://fimi.ua.ac.be/data/* website. First 10,000 transactions of T10I4D100K is run and compared with 12,189 transactions of Retail data.

Datasets	**No. of transactions**	**The maximum number of items which customer can purchase**	**The maximum number of items in the dataset**	**Running time (second)**	**No. of frequent patterns**
Retail	12,189	8	38	0.9000515	44
T10I4D100K	10,000	26	1,000	702.13816	139,491

Fig.6. The experimental results when running proposed algorithm on 2 datasets.

Figure 6 shows the experimental results. The running time and the number of frequent patterns of T10I4D100K are absolutely larger than Retail. The result shows that the number of frequent patterns in reality of a store or an enterprise is often small. T10I4D100K is generated using the generator from the IBM Almaden Quest research group so that the transactions fluctuate much and the number of frequent patterns increases sharply when adding a new transaction.

The fast increase of number of frequent patterns leads to a big issue in computation: overflow. Although the large and the fast growth of frequent patterns, it is easy to prove that the maximum number of frequent pattern cannot be larger than a specified value. For example, if *M* is the maximum number of items in a store and *N* is the maximum number of items which a customer can purchase. The number of frequent patterns in the store is always not larger than $C_M^1 + C_M^2 + ... + C_M^N$. It means the number of frequent patterns may increase fast but it is not big enough to make the system to be crashed.

To reduce the running time of the algorithm, parallelization is one of good ways. Parallelization was applied to find frequent patterns from huge database in the past (Gupta and Satsangi 2012). The large amount of frequent patterns is a reason makes us apply parallelization method to the *NewRepresentative* algorithm.

One of the big issues when developing an algorithm in parallel systems is the complexity of algorithms. Some algorithms can not divide into small part to run simultaneously in separate sites or machines. Fortunately, the *NewRepresentative* algorithm can be expanded for parallel systems easily. The following section introduces two ways to parallelize the algorithm: Horizontal Parallelization and Vertical Parallelization. The parallelization methods share the resource of machines and reduce the running time. It's one of the efficient ways to increase the speed of algorithms having high executing complexity.

V. The Principles of Parallel Computing

Parallel computing is a form of computation in which many calculations are carried out simultaneously operating on the principle that large problems can often be divided into smaller ones, which are then solved concurrently.

The parallel system of the *NewRepresentative* algorithm has the following structure:

At first, the fragmentation will be implemented. The whole data will be divided into small and equal fragments. In Horizontal Parallelization, the transactions in data will be divided while the items are the information which will be divided in Vertical Parallelization. After the data is fragmented properly, all fragments must be allocated in various sites of network. A master site has responsibility for fragmenting data, allocating fragments to sites and merging the results from site into the final result. Sites will run the *NewRepresentative* algorithm with the fragments which are assigned to them simultaneously and finally, send the results into the master site for merging.

VI. Horizontal Parallelization

Consider a set of *n* transactions *S*. If there are *k* machine located in *k* separate sites. Horizontal Parallelization (*HP*) will divide the set *S* into *k* equal fragments and allocate those fragments to *k* sites. The *NewRepresentative* algorithm is applied on *n*/*k* transactions in each site. After running algorithm, every site has its own representative set. All representative sets are sent back to master site for merging.

Merging representative sets from sites in mater site is similar to find representative set when adding new transactions into dataset.

```
ALGORITHM HorizontalMerge(PM, PS)
//Input: PM: representative set of master site.
        PS: the set of representative sets from other sites.
//Output: The new representative set of horizontal
parallelization.
1.  for each P ∈ PS do
```

```
2.    for each z ∈ P do
3.      PM = NewRepresentative(PM, z);
4.    end for;
5.  end for;
6.  return PM;
```

Theorem 4:

Horizontal Parallelization method returns the representative set.

Proof: We prove by induction on *k*.

If $k = 1$, then the *HP* method is the *NewRepresentative* method, hence returns the representative set.

If $k = 2$, then let the two sites be S_1 and S_2, and let $(u_1, p_1), \dots, (u_m, p_m)$ be the representative set for S_1, and let $(v_1, q_1), \dots, (v_n, q_n)$ be the representative set for S_2. We need to show that the *HP* algorithm will give us the representative for the union of S_1 and S_2 ($S_1 \cup S_2$). Let (w, r) be a representative element for $S_1 \cup S_2$. We denote by (w_1, r_1) the restriction of (w, r) to S_1, that is $w_1 = w$ and $r_1 =$ the number of when w appears in S_1. Similarly we define (w_2, r_2). Then by definition we must have $r_1 + r_2 = r$. Also, there must be one of the representative elements in S_1, called (u_1, p_1), so that $u_1 \hookrightarrow w$ and $p_1 = r_1$. In fact, by definition of representative elements, there must be such a (u_1, p_1) for which $u_1 \hookrightarrow w$ and $p_1 \geq r_1$. We also have a (v_1, q_1) in S_2 with $v_1 \hookrightarrow w$ and $q_1 \geq r_2$. Now we must have $p_1 = r_1$ and $q_1 = r_2$ because otherwise w will appear $p_1 + q_1 > r_1 + r_2 = r$ times in $S_1 \cup S_2$. Now when we apply the *HP* algorithm then we will see at least one element (w', r) where $w' = u_1 \wedge v_1$, and in particular w' must cover w. Then w' must be in fact w, otherwise, we have an element (w', r) with $w' \hookrightarrow w$ but the frequency of w' is strictly larger than of w, and hence (w, r) cannot be a representative element. Then we see that (w, r) is produced when using the *HP* algorithm as wanted.

Assume that we proved the correctness of the *HP* algorithm for k sites. We now prove the correctness of the *HP* algorithm for $k + 1$ sites. We denote these sites by $S_1, S_2, \dots, S_k, S_{k+1}$. By the induction assumption, we can find the representative set for k sites $S_1, S_2, \dots, S_k$ using the *HP* algorithm. Denote by $S = \bigcup_{i=1}^{k} S_i$. Now apply the case of two sites which we proved above to the two sites S and S_{k+1}, we have that the *HP* algorithm produces the representative set for $S \cup S_{k+1}$, that is we have the representative set for the union of the $k + 1$ sites $S_1, \dots, S_k, S_{k+1}$. Therefore we completed the proof of *Theorem 4*.

VII. Vertical Parallelization

Vertical Parallelization is more complex than Horizontal Parallelization. While Horizontal Parallelization focuses on transactions, Vertical Parallelization focuses on items. Vertical Parallelization (*VP*) divides the dataset into fragments based on items. Each fragment contains a subset of items. Fragments are allocated into separate sites. In each sites, they run *NewRepresentative* algorithm to find out representative sets. The representative sets will be sent back to the master site and will be merged to find the final representative set.

Vertical merging is based on *merged-bit operation* and *vertical merging operation*.

***Definition 6* (*merged-bit operation* $\cup$)**: *merged-bit operation* is a dyadic operation in bit-chain space $(a_1a_2 \dots a_n) \cup (b_1b_2 \dots b_m) = (a_1a_2 \dots a_nb_1b_2 \dots b_m)$.

***Definition 7* (*vertical merging operation* $\nleftrightarrow$)**: *Vertical merging operation* is a dyadic operation between two representative patterns from two different vertical fragments:

$[(a_1a_2 \dots a_n), p, \{o_1, o_2, \dots, o_p\}] \nleftrightarrow [(b_1b_2 \dots b_m), q, \{o_1, o_2, \dots, o_q\}] = [vmChain, vmFreq, vmObject]$;

$vmChain = (a_1a_2 \dots a_n) \cup (b_1b_2 \dots b_m) = (a_1a_2 \dots a_nb_1b_2 \dots b_m)$

$vmObject = \{o_1, o_2, \dots, o_p\} \cap \{o_1, o_2, \dots, o_q\} = \{o_1, o_2, \dots, o_k\}$

$vmFreq = k$

At the master site, representative sets of other sites will be merged into representative set of master site. The below algorithm is run to find out the final representative set.

```
ALGORITHM VerticalMerge(PM, PS)
//Input: PM: representative set of master site.
       PS: the set of representative sets from other sites.
//Output: The new representative set of vertical
parallelization.
1.  for each P ∈ PS do
2.    for each m ∈ PM do
3.      flag = 0;
4.      M = ∅ // M: set of used elements in P
5.      for each z ∈ P do
6.        q = m ↮ z;
7.        if frequency of q ≠ 0 then
8.          flag = 1; // mark m as used element
9.          M = M ∪ {q}; // mark q as used
                                        element
10.         PM = PM ∪ {q};
11.       end if;
12.     end for;
13.     if flag = 1 then
14.       PM = PM ∪ {m}
15.     end if;
16.     PM = PM ∪ (P \ M);
17.   end for;
18. end for;
19. return PM;
```

Theorem 5:

Vertical Parallelization method returns the representative set.

Proof: We prove by induction on *k*.

If $k = 1$, this is the *NewRepresentative* algorithm, hence gives the representative set.

If $k = 2$, we let S_1 and S_2 be the two sites, and let S be the union. Let $R = (\{i_1, \dots, i_n\}, k, \{o_1, \dots, o_k\}) = (I, k, O)$ be a

representative element for S. Let R_1 be the restriction of R to S_1, that is $R_1 = (I_1, p_1, O_1)$, where I_1 is the intersection of $\{i_1, \dots, i_n\}$ with the set of items in S_1, O_1 is the set of transactions in R_1 containing all items in I_1. We define similarly $R_2 = (I_2, p_2, O_2)$ the restriction of R to S_2. Note that if $I_1 = \varnothing$ then $p_1 = 0$, otherwise p_1 must be positive ($p_1 > 0$). Similarly, if $I_2 = \varnothing$ then $p_2 = 0$, otherwise p_2 must be positive ($p_1 > 0$). We use the convention that if $I_1 = \varnothing$ then $O_1 = O$, and if $I_2 = \varnothing$ then $O_2 = O$. Remark that at least one of I_1 or I_2 is non-empty. Now by definition, there must be a representative element $Q_1 = (I_1', p_1', O_1')$ in S_1 with $I_1 \subseteq I_1'$, $O_1 \subseteq O_1'$, and $p_1' >= p_1$. Similarly, we have a representative element $Q_2 = (I_2', p_2', O_2')$ in S_2 with $I_2 \subseteq I_2'$, $O_2 \subseteq O_2'$, and $p_2' >= p_2$. When we do the vertical merging operation of Q_1 and Q_2, then we must obtain I. Otherwise, we obtain an element $R' = (I', k', O')$ where $I \subseteq I'$, $O \subseteq O'$, and $k' >= k$, and at least one of these is strict. This is a contradiction to the assumption that R is a representative element of S. Now that we proved the correctness of the algorithm for $k = 1$ and $k = 2$. Then, assume that we proved the correctness of the *VP* algorithm for k sites. We now prove the correctness of the *VP* algorithm for $k + 1$ sites. We denote these sites by $S_1, S_2, \dots, S_k, S_{k+1}$. By the induction assumption, we can find the representative set for k sites $S_1, S_2, \dots, S_k$ using the *VP* algorithm. Denote by $S = \bigcup_{i=1}^{k} S_i$. Now apply the case of two sites which we proved above to the two sites S and S_{k+1}, we have that the *VP* algorithm produces the representative set for $S \cup S_{k+1}$, that is we have the representative set for the union of the $k + 1$ sites $S_1, \dots, S_k, S_{k+1}$. Therefore we completed the proof of *Theorem 5*.

Example: Give the set S of transactions $\{o_1, o_2, o_3, o_4, o_5, o_6, o_7\}$ and the set I of items $\{i_1, i_2, i_3\}$.

	i_1	i_2	i_3
o_1	0	0	1
o_2	0	1	0
o_3	0	1	1
o_4	1	0	0
o_5	1	0	1
o_6	1	1	0
o_7	1	1	1

Fig.7. Bit-chains of *S*.

Divide the items into two segments: $\{i_1\}$ and $\{i_2, i_3\}$.

	i_1
o_1	0
o_2	0
o_3	0
o_4	1
o_5	1
o_6	1
o_7	1

Fig.8. The first segment.

	i_2	i_3
o_1	0	1
o_2	1	0
o_3	1	1
o_4	0	0
o_5	0	1
o_6	1	0
o_7	1	1

Fig.9. The second segment.

Allocate two segments in two separate sites and run *NewRepresentative* algorithm on those fragments simultaneously.

It is easy to get the representative sets from two sites:

The site has $\{i_1\}$ fragment: $P_{\{i_1\}} = \{[(1); 4; \{o_4, o_5, o_6, o_7\}]\}$

The site has $\{i_2, i_3\}$ fragment: $P_{\{i_2, i_3\}} = \{[(01); 4; \{o_1, o_3, o_5, o_7\}], [(10); 4; \{o_2, o_3, o_6, o_7\}], [(11); 2; \{o_3, o_7\}]\}$

Merge both of them:

$[(1); 4; \{o_4, o_5, o_6, o_7\}] \nleftrightarrow [(01); 4; \{o_1, o_3, o_5, o_7\}] = [(101); 2; \{o_5, o_7\}]$

$[(1); 4; \{o_4, o_5, o_6, o_7\}] \nleftrightarrow [(10); 4; \{o_2, o_3, o_6, o_7\}] = [(110); 2; \{o_6, o_7\}]$

$[(1); 4; \{o_4, o_5, o_6, o_7\}] \nleftrightarrow [(11); 2; \{o_3, o_7\}] = [(111); 1; \{o_7\}]$

The full representative set P is:

$P = \{[(100); 4; \{o_4, o_5, o_6, o_7\}],$
$[(001); 4; \{o_1, o_3, o_5, o_7\}],$
$[(010); 4; \{o_2, o_3, o_6, o_7\}],$
$[(011); 2; \{o_3, o_7\}],$
$[(101); 2; \{o_5, o_7\}],$
$[(110); 2; \{o_6, o_7\}],$
$[(111); 1; \{o_7\}]\}$

VIII. EXPERIMENTATION 2

The experiments of Vertical Parallelization Method are conducted on machines which has similar configuration: Intel(R) Core(TM) i3-2100 CPU @ 3.10GHz (4 CPUs), ~3.1GHz and 4096MB main memory installed. The operating system is Windows 7 Ultimate 64-bit (6.1, Build 7601) Service Pack 1. Programming language is C#.NET.

The proposed methods are tested on *T10I4D100K* dataset taken from *http://fimi.ua.ac.be/data/* website. First 10,000 transactions of *T10I4D100K* are run and compared with the result when running without parallelization.

Dataset	No. of transactions	The maximum No. of items which customer can purchase	The maximum No. of items in the dataset	Running time (second)	No. of frequent patterns
T10I4D100K	10,000	26	1,000	702.13816	139,491

Fig.10. The result when running the algorithm in single machine.

Vertical Parallelization model is applied in 17 machines with the same configuration. Each machine is located in a separate site. 1,000 items is digitized into 1,000-tuple bit-chain. The master site will divide the bit-chain into 17 fragments (16 60-tuple bit-chains and a 40-tuple bit-chain).

Fragments	Length of bit-chain	Running Time	Number of frequent patterns
1	60	18.0870345s	899
2	60	10.5576038s	535
3	60	14.9048526s	684
4	60	12.2947032s	548
5	60	8.0554607s	432
6	60	10.3075896s	560
7	60	17.7480151s	656
8	60	10.8686217s	526
9	60	21.3392205s	856
10	60	13.3007607s	682
11	60	9.6135499s	617
12	60	16.1179219s	736
13	60	15.4338827s	587
14	60	21.4922293s	928
15	60	18.2790455s	834
16	60	17.011973s	701
17	40	4.4142525s	223

Fig.11. The result of running the algorithm in sites.

After running the algorithm in sites, the representative sets are sent back to master site for merging. The merging time is 27.5275745s and the number of final frequent patterns is 139,491. So, the total time of Parallelization is:

max(Running Times) + Merging Time = 21.4922293s + 27.5275745s = 49.0198038s

It is easy to see the efficiency and accuracy of Vertical Parallelization method.

IX. Conclusion

Proposed algorithms (*NewRepresentative* and *NewRepresentative_Delete*) solved cases of adding, deleting, and altering in the context of mining data without scanning the database.

Users can regularly change the minimum support threshold in order to find acceptable laws based on the number of buyers without rerunning the algorithms.

With accumulating frequent patterns, users can refer to the laws at any time.

The algorithm is easy for implement with low complexity ($nm2^m$, where n is number of transactions and m is number of items).

Practically, it is easy to prove that the maximum number of frequent patterns cannot be larger than a specified value. Because the invoice form is in accordance with the government (the number of categories sold is a constant called r), the number of frequent patterns in the store is always not larger than $C_m^1 + C_m^2 + ... + C_m^{r-1} + C_m^r$

The set P obtained represents the context of the problem. In addition, the algorithm allows segmenting the context to solve partially.

This approach is simple for expanding for parallel systems. By applying parallel strategy to this algorithm to reduce time consuming, the article presented two methods: Vertical Parallelization and Horizontal Parallelization methods.

References

[1] C. C. Aggarwal, Y. Li, Jianyong Wang, and Jing Wang, "Frequent pattern mining with uncertain data," Proceeding KDD '09 Proceedings of the 15th ACM SIGKDD International Conference on Knowledge Discovery and Data Mining, June 28 – July 1, 2009, Paris, France.

[2] A. Appice, M. Ceci, and A. T. D. Malerba, "A parallel, distributed algorithm for relational frequent pattern discovery from very large datasets," Intelligent Data Analysis 15 (2011) pp. 69–88.

[3] M. Bahel and C. Dule, "Analysis of frequent itemset generation process in apriori and rcs (reduced candidate set) algorithm," International Journal of Advanced Networking and Applications, Volume: 02, Issue: 02, Pages: 539–543 (2010).

[4] M. S. S. X. Baskar, F. R. Dhanaseelan, and C. S. Christopher, "FPU-Tree: frequent pattern updating tree," International Journal of Advanced and Innovative Research, Vol.1, Issue 1, June 2012.

[5] M. Deypir and M. H. Sadreddini, "An efficient algorithm for mining frequent itemsets within large windows over data streams," International Journal of Data Engineering (IJDE), Vol.2, Issue 3, 2011.

[6] K. Duraiswamy and B. Jayanthi, "A new approach to discover periodic frequent patterns," International Journal of Computer and Information Science, Vol. 4, No. 2, March 2011.

[7] S. H. Ghorashi, R. Ibrahim, S. Noekhah, and N. S. Dastjerdi, "A frequent pattern mining algorithm for feature extraction of customer reviews," IJCSI International Journal of Computer Science Issues, Vol. 9, Issue 4, No.1, July 2012.

[8] D. N. Goswami, A. Chaturvedi, and C. S. Raghuvanshi, "Frequent pattern mining using record filter approach," IJCSI International Journal of Computer Science Issues, Vol.7, Issue 4, No.7, July 2010.

[9] D. Gunaseelan and P. Uma, "An improved frequent pattern algorithm for mining association rules," International Journal of Information and Communication Technology Research, Vol.2, No.5, May 2012.

[10] R. Gupta and C. S. Satsangi, "An efficient range partitioning method for finding frequent patterns from huge database," International Journal of Advanced Computer Research (ISSN (print): 2249–7277 ISSN (online): 2277–7970) Vol.2, No.2, June 2012.

[11] B. Jayanthi and K. Duraiswamy, "A novel algorithm for cross level frequent pattern mining in multidatasets," International Journal of Computer Applications (0975 – 8887) Vol.37, No.6, January 2012.

[12] S. Joshi, R. S. Jadon, and R. C. Jain, "An implementation of frequent pattern mining algorithm using dynamic function," International Journal of Computer Applications (0975 – 8887), Vol.9, No.9, November 2010.

[13] P. Kambadur, A. Ghoting, A. Gupta, and A. Lumsdaine, "Extending task parallelism for frequent pattern mining," CoRR abs/1211.1658 (2012).

[14] P. Khare and H. Gupta, "Finding frequent pattern with transaction and occurrences based on density minimum support distribution," International Journal of Advanced Computer Research (ISSN (print):

2249–7277 ISSN (online): 2277–7970) Vol.2, No.3, Issue 5, September 2012.

[15] H. D. Kim, D. H. Park, and Y. L. C. X. Zhai, "Enriching text representation with frequent pattern mining for probabilistic topic modeling," ASIST 2012, October 26–31, 2012, Baltimore, MD, USA.

[16] R. U. Kiran and P. K. Reddy, "Novel techniques to reduce search space in multiple minimum supports-based frequent pattern mining algorithms," Proceeding EDBT/ICDT '11 Proceedings of the 14th International Conference on Extending Database Technology, March 22–24, 2011, Uppsala, Sweden.

[17] A. K. Koundinya, N. K. Srinath, K. A. K. Sharma, K. Kumar, M. N. Madhu, and K. U. Shanbag, "Map/Reduce design and implementation of apriori algorithm for handling voluminous data-sets," Advanced Computing: An International Journal (ACIJ), Vol.3, No.6, November 2012.

[18] K. Malpani and P. R. Pal, "An efficient algorithms for generating frequent pattern using logical table with AND, OR operation," International Journal of Engineering Research & Technology (IJERT) Vol.1, Issue 5, July – 2012.

[19] P. Nancy and R. G. Ramani, "Frequent pattern mining in social network data (facebook application data)," European Journal of Scientific Research, ISSN 1450–216X Vol.79 No.4 (2012), pp.531–540, © EuroJournals Publishing, Inc. 2012.

[20] A. Niimi, T. Yamaguchi, and O. Konishi, "Parallel computing method of extraction of frequent occurrence pattern of sea surface temperature from satellite data," The Fifteenth International Symposium on Artificial Life Robotics 2010 (AROB 15th '10). B-Con Plaza, Beppu, Oita, Japan, February 4–6, 2010.

[21] S. N. Patro, S. Mishra, P. Khuntia, and C. Bhagabati, "Construction of FP tree using huffman coding," IJCSI International Journal of Computer Science Issues, Vol.9, Issue 3, No.2, May 2012.

[22] D. Picado-Muiño, I. C. León, and C. Borgelt, "Fuzzy frequent pattern mining in spike trains," IDA 2012: 289–300.

[23] R. V. Prakash, Govardhan, and S. S. V. N. Sarma, "Mining frequent itemsets from large data sets using genetic algorithms," IJCA Special Issue on "Artificial Intelligence Techniques – Novel Approaches & Practical Applications" AIT, 2011.

[24] K. S. N. Prasad and S. Ramakrishna, "Frequent pattern mining and current state of the art," International Journal of Computer Applications (0975 – 8887), Vol. 26, No.7, July 2011.

[25] A. Raghunathan and K. Murugesan, "Optimized frequent pattern mining for classified data sets," ©2010 International Journal of Computer Applications (0975 – 8887), Vol.1, No.27.

[26] S. S. Rawat and L. Rajamani, "Discovering potential user browsing behaviors using custom-built apriori algorithm," International Journal of Computer Science & Information Technology (IJCSIT) Vol.2, No.4, August 2010.

[27] M. H. Sadat, H. W. Samuel, S. Patel, and O. R. Zaïane, "Fastest association rule mining algorithm predictor (FARM-AP)," Proceeding C3S2E '11 Proceedings of the Fourth International Conference on Computer Science and Software Engineering, 2011.

[28] K. Saxena and C. S. Satsangi, "A non candidate subset-superset dynamic minimum support approach for sequential pattern mining," International Journal of Advanced Computer Research (ISSN (print): 2249–7277 ISSN (online): 2277–7970) Vol.2, No.4, Issue 6, December 2012.

[29] H. Sharma and D. Garg, "Comparative analysis of various approaches used in frequent pattern mining," International Journal of Advanced Computer Science and Applications, Special Issue on Artificial Intelligence IJACSA pp. 141–147 August 2011.

[30] Y. Sharma and R. C. Jain, "Analysis and implementation of FP & Q-FP tree with minimum CPU utilization in association rule mining," International Journal of Computing, Communications and Networking, Vol.1, No.1, July – August 2012.

[31] K. Sumathi, S. Kannan, and K. Nagarajan, "A new MFI mining algorithm with effective pruning mechanisms," International Journal of Computer Applications (0975 – 8887) Vol.41, No.6, March 2012.

[32] M. Utmal, S. Chourasia, and R. Vishwakarma, "A novel approach for finding frequent item sets done by comparison based technique," International Journal of Computer Applications (0975 – 8887) Vol.44, No.9, April 2012.

[33] C. Xiaoyun, H. Yanshan, C. Pengfei, M. Shengfa, S. Weiguo, and Y. Min, "HPFP-Miner: a novel parallel frequent itemset mining algorithm," Natural Computation, 2009. ICNC '09. Fifth International Conference on 14–16 Aug. 2009.

[34] M. Yuan, Y. X. Ouyang, and Z. Xiong, "A text categorization method using extended vector space model by frequent term sets," Journal of Information Science and Engineering 29, 99–114 (2013).

[35] Y. Wang and J. Ramon, "An efficiently computable support measure for frequent subgraph pattern mining," – ECML/PKDD (1) 2012: 362–377.

Pilot Study: The Use of Electroencephalogram to Measure Attentiveness towards Short Training Videos

Paul Alton Nussbaum and Rosalyn Hobson Hargraves
Department of Electrical and Computer Engineering
Virginia Commonwealth University
Richmond, VA USA

***Abstract*—Universities, schools, and training centers are seeking to improve their computer-based [3] and distance learning classes through the addition of short training videos, often referred to as podcasts [4]. As distance learning and computer based training become more popular, it is of great interest to measure if students are attentive to recorded lessons and short training videos.**

The proposed research presents a novel approach to this issue. Signal processing of electroencephalogram (EEG) has proven useful in measuring attentiveness in a variety of applications such as vehicle operation and listening to sonar [5] [6] [7] [8] [9] [10] [11] [12] [13] [14] [15]. Additionally, studies have shown that EEG data can be correlated to the ability of participants to remember television commercials days after they have seen them [16]. Electrical engineering presents a possible solution with recent advances in the use of biometric signal analysis for the detection of affective (emotional) response [17] [18] [19] [20] [21] [22] [23] [24] [25] [26] [27].

Despite the wealth of literature on the use of EEG to determine attentiveness in a variety of applications, the use of EEG for the detection of attentiveness towards short training videos has not been studied, nor is there a great deal of consistency with regard to specific methods that would imply a single method for this new application. Indeed, there is great variety in EEG signal processing and machine learning methods described in the literature cited above and in other literature [28] [29] [30] [31] [32] [33] [34].

This paper presents a novel method which uses EEG as an input to an automated system that measures a participant's attentiveness while watching a short training video. This paper provides the results of a pilot study, including a structured comparison of signal processing and machine learning methods to find optimal solutions which can be extended to other applications.

Keywords*—*Electroencephalogram; EEG; Signal Analysis; Machine Learning; Attentiveness; Training; Videos

I. INTRODUCTION

For the purposes of this experiment, the affective state of the participant watching the short training video is deemed to be attentive when the participant has a high positive affect, including feelings of satisfaction, engagement, interest, and involvement. This definition of short training video attentiveness is not the only possible definition, but it is justified by related research in similar applications.

In [20] the authors propose a brief and easy to administer mood scale called the Positive and Negative Affect Schedule (PANAS), where the orthogonal axis of emotion are "negative affect" and "positive affect" and high positive affect is associated with terms such as high energy, full concentration, and pleasurable engagement.

In [21] affect is explored not from the point of view of the learner having an emotional response, but rather a computerized tutoring system having an avatar that uses facial expressions and body movements to communicate an affective state to the learner. With regard to the range of emotions expressed by the avatar, the researchers explain "…because their role is primarily to facilitate positive learning experiences, only a critical subset of the full range of emotive expression is useful for pedagogical agents.

For example, they should be able to exhibit body language that expresses joy and excitement when learners do well, inquisitiveness for uncertain situations (such as when rhetorical questions are posed), and disappointment when problem-solving progress is less than optimal.

In [22] the authors defines a model of emotions and learning that explains the emotional state of the learner as being in one of four quadrants, depending on the positive or negative value on two axes. The first axis is "learning," and the second axis is "affect." The positive side of the affect axis is associated with terms such as awe, satisfaction, curiosity, and hopefulness.

In [32] the researchers use machine learning to predict a participant's self-assessed emotion when presented with the results of a quiz and personality test. The participant finds out the results, and then expresses their emotions by selecting one of the following words: disappointment, distress, joy, relief, satisfaction or fear-confirmed.

In [26] researchers analyze the affective state of participants while they are performing a learning task with a computerized natural language tutor using both online and offline self-reports by participants as well as peers and trained judges observing facial features. Words that the study used in both self-reports and reports by observers are defined in TABLE I.

It is useful to note that this study found the inter-rater reliability coefficient, Kappa, of trained judges who watch the facial expressions of the participants and code facial actions to provide affective judgments was only 0.36. Although Kappa is a conservative measure of agreement, it still shows that emotions are tough to judge even by those who are trained to do so.

TABLE I. DEFINITION OF AFFECTIVE STATES

Affective state	Definition
Boredom	State of being weary and restless through lack of interest
Confusion	Failure to differentiate similar or related ideas/ noticeable lack of understanding
Flow	State of interest that results from involvement in an activity
Frustration	Making vain or ineffectual efforts however vigorous; a deep chronic sense or state of insecurity and dissatisfaction arising from unresolved problems or unfulfilled needs; dissatisfaction or annoyance
Neutral	No apparent emotion or feeling
Surprise	Wonder or amazement, especially from the unexpected

The Mathematical definition of Kappa is shown in Equation (1) where Pr(a) is the relative observed agreement among raters, and Pr(e) is the hypothetical probability of chance agreement, using the observed data to calculate the probabilities of each observer randomly saying each category.

$$\kappa = \frac{\Pr(a) - \Pr(e)}{1 - \Pr(e)} \quad (1)$$

If the raters are in complete agreement then $\kappa = 1$. If there is no agreement among the raters other than what would be expected by chance, as defined by Pr(e), $\kappa = 0$.

In [23] the researchers attempt to dive deeper into the affective state of the learner by gathering, in their own words, the definition of what they mean by "engagement in courses" and "What makes a course engaging to you?" The learners in this study were male and female freshman and sophomores in engineering, and the researchers were able to group the responses into categories, as well as give specific wording terms that the students used. Some notable popular categories and terms used include: active participation, hands on, faculty enthusiasm and interest, discussion, interaction between faculty and students, as well as other similar terms, and other less popular terms.

So for the purposes of this pilot study, the definition of attentiveness is when the participant has a high positive affect towards a short training video.

II. EXPERIMENTAL SETUP

Recent research has demonstrated the use of a single dry frontal electrode for the capture of EEG in similar applications. For this research experiment, the MindWave Mobile device from NeuroSky was used.

In [28], the same make and model of EEG data collection device, showed a positive correlation between EEG data collected and participant self-reported attention during an experiment where the participant interacts with a computer generated three-dimensional avatar.

Also using the same make and model of EEG data collection equipment is [17], where 78% of the time the brain wave data accurately identified the participant's self-categorization of affective state during an experiment which presented increasingly stressful mental challenges to the participant. [27] also used the same device to predict with accuracy levels significantly better than chance whether or not the participant was reading an easy or a hard sentence. Finally, the presentation related to [36] indicated that the correlation analysis could just as effectively use only the frontal contact.

In [25], the participant's affective state while using an Intelligent Tutoring System (ITS) is measured using a single frontal lobe EEG electrode with earlobe grounds showing an accurate detection (82%) of affective state from the brainwaves. [25] was based on earlier work [31] which also used the same EEG sensor setup and revealed an ability to use brainwaves to accurately predict participant self-assessed emotion according to the Self-Assessment Manikin (SAM) scale. [33] also uses only a frontal electrode (two electrodes are used, however the difference in voltage between the two is used as the only single EEG data stream over time) to achieve an 85.7% accuracy in identifying if the participant is watching an interesting video versus an uninteresting video. In [35], the single electrode is placed at F3 or F4 alternatively in an experiment that also collected facial expressions when watching emotion inducing videos, revealing that noisy correlated EEG-facial expression data could also be correctly recovered to as high in 95.2% cases.

A. Watching Short Training Videos

Participants are fitted for the dry contact EEG, sitting in front of the data collection and video playback laptop as seen in Figure 1. The headset is adjusted until a strong signal is generated without interruption, and blinks can be seen on the EEG graph displayed in real-time.

Fig.1. Participant with single dry contact EEG sensor

Once the setup is operational, the recording is started, and the video playback begins. The video starts with a relaxation segment that begins with a text message as in Figure 2.

Fig.2. Relaxing Intro Sequence

After 2.5 minutes of relaxing empty-beach photos with the sound of waves and seagulls in the background, the short training video plays for an additional 2.5 minutes. The training videos explain a hypothetical technical lesson regarding an imaginary device with components names such as "Alpha Module" and "Beta Module". The participant must learn how to troubleshoot the device and decide whether or not to replace a component. The videos include enhanced podcast (essentially a PowerPoint slide show that is narrated) as well as worked example style training that asks the participant to act along with the still pictures and live video of the trainer. The participant is encouraged to act along with the instructor in the video. That acting may be to hold up their hand, or to grasp their thumb or grasp their index and middle finger. This is done as a memory aid because the fictional device purposely looks like the fingers of a hand. One scene is shown in Figure 3.

Fig.3. Motion Picture Scene of a Worked Example

B. Data Collection

EEG signal is collected at 512 Hz in 1 second frames which can be concatenated to any length. To test some of the procedures and mathematical algorithms prior to the proposed research study, a set of seven participants were asked to participate, and detailed notes were taken during this testing by an observer who also sat in the room. After the videos were done, the participant removed the EEG headset and answers a second questionnaire, including a set of closed ended questions (yes or no) and a multiple choice quiz relating to the lesson provided.

Once the EEG data is collected, the data is segmented into areas where the participant is expected to be inattentive (during the beach pictures) and where the participant is expected to be attentive (during the short training video). The goal is to collect exemplary data of attentive and inattentive epochs gathered from participants observing videos that are purposely designed to induce an inattentive or attentive state. Once the system is trained, it can then be used as an automated detection mechanism for attentiveness, because it has learned by example, what the EEG data contains in these situations. Even if the participants are not perfectly attentive for the entire duration of the training video, they are attentive for the majority of the time, and outlier data points will be in the minority.

For the Pilot study, each participant has 150 seconds of inattentive EEG data (watching the beach photos), and 150 seconds of attentive EEG data (watching the training video), for a total of 300 seconds (5 minutes) of EEG data. Since data collection is in 1-second epochs, a total of 2100 sample epochs are collected across 7 participants.

III. Analysis of EEG Data

Analysis consists of windowing, transformation, data reduction, and machine learning and pattern recognition.

A. Windowing

Non-overlapping 512 sample one-second windows are used. While many possible windowing functions are available this Pilot Study uses the Hanning window shown in Equation (2) which reduces ripple in the frequency power spectrum.

$$x'_n = x_n \frac{(1-cos\frac{2\pi n}{N})}{2} \qquad n = 0, \dots, N-1 \qquad (2)$$

B. Transformation

After windowing is complete, the transformation of the data is required. This is done to extract important features that will be used by machine learning, and also in large part to remove instance by instance timing variations that are not important to the problem at hand.

The Pilot study compares Discrete Fourier Transform (DFT) with Discrete Wavelet Transform (DWT). Both DFT and DWT provide banded spectrum information. Equation (3) shows the transformation of the sampled data xn into the frequency domain Xk using DFT and Equation (4) shows the magnitude of the Fourier transform |Xk| used to remove phase information leaving only the frequency information.

$$X_k = \sum_{n=0}^{N-1} x'_n e^{-i2\pi k\frac{n}{N}} \qquad k = 0, \dots, N-1 \qquad (3)$$

$$|X_k| = \sqrt{X_k X^*_k} \qquad (4)$$

Each element |Xk| now represents the power of that frequency within the original signal, fk ranging from zero Hz (sometimes called DC for electrical signals) all the way up to the Nyquist frequency of the sampled data window of width T seconds, as seen in Equation (5).

$$f_k = \frac{k}{T} \qquad k = 0, \dots, \frac{N}{2} - 1 \qquad (5)$$

Note that the sequence of values |Xk| are symmetrical about N/2 as shown in Equation (6).

$$|X_{N-k}| = |X_k| \quad k = 1, \dots, \frac{N}{2} \tag{6}$$

Also used for comparison in the Pilot study is the DFT as shown in equations (7) and (8) where the original windowed signal x'n is transformed into two signals, each of half the duration (down sampled by a factor of two) called Xappn and Xdetn, the approximation coefficients and the detail coefficients, respectively. The signals hn and gn are a specially matched set of filters, low-pass and high-pass respectively (called Mallat wavelet decomposition), which are generated from the desired wavelet function.

$$Xapp_n = \sum_{k=0}^{N-1} x'_k h_{2n-k} \quad n = 0, \dots, N-1 \tag{7}$$

$$Xdet_n = \sum_{k=0}^{N-1} x'_k g_{2n-k} \quad n = 0, \dots, N-1 \tag{8}$$

DWT can sometimes be a preferred transformation over DFT, because it preserves the sequencing of time varying events, and has greater resolution with regard to the timing of signal events (rather than only phase information). DFT can be made to approximate DWT benefits by using smaller window size with a tradeoff in low frequency resolution, and variations on such Short Time Fourier Transform (STFT) including window overlay and window averaging appear in literature. Similarly, a limitation of DWT is that it provides scale information, but not specifically frequency information. Here too, techniques described in literature show a means to extract frequency info from DWT based on the down sampling nature of the algorithm. For example, the selection of a window size that is a power of 2 (such as 512 samples used in the Pilot study) allows repeated iterations of the wavelet transform to focus on different frequency bands.

DWT decompositions can be repeated again and again, saving the detail coefficients, and then taking the approximation coefficients and passing them through Equations (7) and (8) again. Each such repetition is called a Level of DWT, so the first level is on the original signal using a window size of N. The second iteration is Level 2, using a window size of N/2. The lth iteration is Level l, using a window size of N/2l. Equations (9) and (10) describe how the detail coefficients Xdetn of the Level l DWT decomposition represent a subset of the frequencies contained within the original signal. FNyquist is the Nyquist frequency of the sampled signal, and the range of frequencies in the detail coefficients range from a low of Fdet_L to a high of Fdet_H.

$$Fdet\_H_l = \frac{F_{Nyquist}}{2^{l-1}} \tag{9}$$

$$Fdet\_L_l = \frac{F_{Nyquist}}{2^{l}} \tag{10}$$

In the Pilot study, windows of 512 samples are used, representing one-second of collected data (512 Hz sampling rate). The Nyquist frequency, FNyquist, is therefore half the sampling rate (256 Hz) and represents the highest frequency represented in the sample. Any frequency higher than 256 Hz that appears in the signal prior to sampling (analog to digital conversion) will result in aliasing, and so must be removed prior to sampling (using hardware filters in the EEG data collection device). In the Pilot study, a 6th level DWT decomposition was use employing the Daubechies db1 wavelet (equivalently the Haar wavelet, which is a step function with values 1 and -1 of equal duration). This was repeated six times, and the equivalent frequency ranges for each level are shown in **Error! Reference source not found.**

TABLE II. MAPPING OF DWT DECOMPOSITION LEVELS TO EEG FREQUENCY BANDS

Decomposition transform	Frequencies contained in the transformed data	Common EEG Band Name (literature naming and ranges vary)
Xdet1	128 – 256 Hz	Noise [12]
Xdet2	64 – 128 Hz	Gamma+ [25]
Xdet3	32 – 64 Hz	Gamma
Xdet4	16 – 32 Hz	Beta
Xdet5	8 – 16 Hz	Alpha
Xdet6	4 – 8 Hz	Theta
Xapp6	1 – 4 Hz	Delta

The Pilot study compares both DFT and DWT algorithms.

C. Data Reduction

Data reduction is needed to speed the machine learning algorithms, and to reduce the issues of high dimension data causes machine learning algorithms to over-fit on the training data. This causes them to have reduced ability for generalization (to correctly categorize data that is not part of the training set). This is sometimes called the curse of dimensionality.

Data reduction can take place using transformation-independent algorithms such as Principal Component Analysis or Fischer Discriminant analysis. These algorithms seek to find an optimal linear transformation that reduces the number of dimensions while keeping the data as spread out as possible, thereby keeping the dimensional information most useful to distance metric machine learning algorithms. Data reduction techniques can also be specific to the transformation algorithm, using the knowledge of the algorithm to find an optimal data reduction scheme.

Data reduction of DFT is described in literature by throwing away frequency information, or by banding adjacent frequency power values by averaging them into a single band-power value. The Pilot study compares different data reduction algorithms. For the DFT, frequency data is discarded at the high end in increments of the powers of 2, to compare machine learning accuracy with reduced data sets. So the Pilot study examines presenting the machine learning algorithm with data sets having dimensionality 256, 128, 64, 32, 16, 8, 4, and 2.

Data reduction of DWT is described in literature as grouping the various detail coefficients and the approximation coefficients into one or more descriptive attributes regarding that set of data. For example, literature describes taking a set of detail coefficients and combining them into a set of parameters including Energy, Power, Median, Entropy, Mean, Min, Max,

and Slope. For the Pilot study, the DWT is examined at each of 6 levels of decomposition, where at each level the detail coefficients are used to calculate the aforementioned eight parameters, and at the 6th level of decomposition, the approximation coefficients are also used to calculate these parameters. So the Pilot study uses 7 sets of coefficients each yielding 8 parameters giving the data sets the dimensionality of 8x7 or 56.

D. Machine Learning and Pattern Recognition

The purpose of N-Fold cross validation is to put the problem solution through rigorous quality assurance using the data that is available. Nested N-fold cross validation adds the additional step of changing the EEG signal analysis parameters. So for example, if 10 different possible ways of performing EEG signal analysis are to be compared using 10-fold cross validation, then 100 different tests will be performed.

Figure 4 shows such a nested 10-Fold cross validation comparison showing percentage of incorrect classifications for DFT across a number of dimension reduction options, and a number of machine learning algorithms. Shown in the figure is the DFT with the full 256 spectral power values, as well as a number of reduced dimensions achieved by keeping only the lowest frequency values (keeping only the lowest 2, 4, 8, 16, 32, 64, and 128 power frequency values). Furthermore, a number of machine learning algorithms, some from the literature, and others used for comparison, are compared. They are, in order of listing in the graph key, kNN algorithm with k-1 and k-5, the Random Tree algorithm, the Random Forest algorithm, a Multi-Layer Perceptron with the number of hidden layer neurons = (# attributes + 2)/2, and a Support Vector Machine using a Hinge loss function.

Fig.4. Nested 10-Fold cross validation comparison of Machine Learning methods showing percentage of incorrect classifications with different DFT dimensionality presentation data.

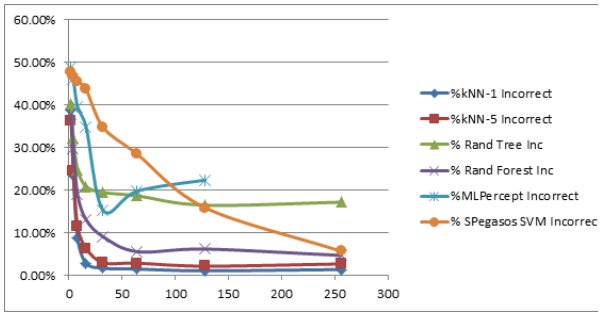

Similarly, Figure 5 - also shows a nested 10-Fold cross validation comparison showing percentage of incorrect classifications, this time for DWT, across a number of dimension reduction options, and a number of machine learning algorithms. Shown in the figure is the DWT with the full 7 Coefficient sets, as well as a number of reduced dimensions achieved by keeping only the lowest frequency coefficient sets (keeping only the lowest 1, 2, 3, 4, 5, and 6 coefficient sets). As noted above, the coefficient sets for a sixth level DWT decomposition include Detail Coefficient Sets 1 through 6, plus the Approximation Coefficient Set for level 6.

Note that in the Pilot study, for each coefficient set, we calculate 8 parameters for each coefficient set. Just as in Figure 4 - the same set of machine learning algorithms are compared.

Fig.5. Nested 10-Fold cross validation comparison of Machine Learning methods showing percentage of incorrect classifications with different DWT dimensionality presentation data.

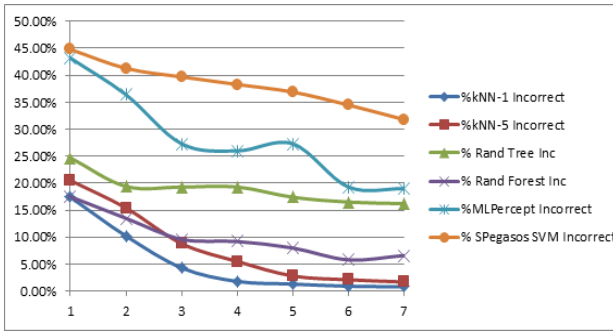

IV. Conclusions and Future Work

The results and review encourage the author to do more investigation in this area. The conclusions reached from the pilot study is that some future work on improvements is needed, which should not be very difficult to accomplish in order to achieve the goal of solving the problem of signal processing of EEG for the detection of attentiveness under the constraints of watching short training videos.

A. Experimental Setup

There were a number of improvements that will be needed on the experimental setup. These improvements were discovered as part of conducting the trial run of the experiments, and by having the educational podcasts (short training videos) reviewed by an expert in the field. The improvements planned include:

- Beach scene may be made to induce further inattentiveness (more boring). May use single candle burning or other simpler video without audio.
- Improve the training video based on feedback from the professional review. Have the videos instruct the participant to complete simple tasks that allow external measurement if the participant is on task or not.
- Ask participants to go to the bathroom first.
- Insist that cellphones have to be turned off.
- Find a more quiet room to do experiment - occasional voices through the walls, and slamming doors outside distracting.
- Rescale the "age" question. Negative reaction to having to check "45+"

The post-experiment questions will be improved to include more data collected. Open-ended questions will be added. This will allow the proposed research, which is basic research and intended to produce an automated system, also collect data for applied research, such as may research that employs the final method and apparatus under direction of an educational

psychologist. Open ended questions may include formations such as "tell me what you were thinking when…?" and "what were you feeling when…?"

Data collection improvements are also needed, with some ideas including:

- Use a fresh AAA battery before every experiment or two, as the wireless EEG headset loses connection after 2 or 3 uses.
- Have a more precise time stamping method for synchronization of video playback and start of EEG collection (because sometimes the PC is slow to start up the video playback). Perhaps a stopwatch with lap timer separate from the experiment laptop, so it is unaffected by CPU usage dependency that might delay the recording of when the operator clicks a button.
- Even though outside distractions will be minimized as per the above, there should still be a time stamping method of recording precisely when observed unplanned events take place (a cough, the time when a participant sighs or lifts their hand, etc.)

B. Signal Processing

There were some improvements needed for the proposed research that were discovered during the Pilot study. These include the application of Principal Component Analysis (PCA) and other methods of data reduction to ensure the maximum amount of useful information is obtained. Also, it may be beneficial to eliminate noise such as muscle and eye movement prior to feature extraction. Based on test results, the most suitable methods will be selected in terms of both performance and speed.

Finally, the Pilot study confirms the need for a structured and orderly comparison using a nested n-fold cross validation in which all such options are tested, compared and optimized.

C. Other Future Work

A few of the references in this paper are older. These are wonderful foundational documents; however additional reference search will look for advances which can be helpful to the research.

Also noted is the need for additional detail on the results obtained in comparison. This reaffirms the need for structured nested n-fold cross validation which not only provides an interpretation of the results, but also definitively reveals the optimal solution for the experimental problem through direct side-by-side comparison.

REFERENCES

[1] R. D. Bakera, S. D'Mellob, M. Rodrigo and A. Graesser, "Better to be frustrated than bored: The incidence, persistence, and impact of learners' cognitive–affective states during interactions with three different computer-based learning environments," Int. J. Human-Computer Studies, vol. 68, p. 223–241, 2010.

[2] R. H. Kay, "Exploring the use of video podcasts in education: A comprehensive review of the literature," Computers in Human Behavior, vol. 28, p. 820–831, 2012.

[3] D. Sandberg, T. Åkerstedt, A. Anund, G. Kecklund and M. Wahde, "Detecting Driver Sleepiness Using Optimized Nonlinear Combinations of," IEEE trans. Intelligent transportations systems, vol. 12, no. 1, pp. 97-108, 2010.

[4] K. HAYASHI, K. ISHIHARA, H. HASHIMOTO and K. OGURI, "Individualized Drowsiness Detection during Driving by Pulse Wave Analysis with Neural," Intelligent Transportation Systems, 2005. Conference Proceedings., pp. 901-906, 2005.

[5] B. J. Wilson and T. D. Bracewell, "Alertness Monitoring Using Neural Networks for EEG Analysis," Neural Networks for Signal Processing X, 2000. Proceedings of the 2000 IEEE Signal Processing Society Workshop, vol. 2, pp. 814-820, 2002.

[6] T. Jung, S. Makeig, M. Stensmo and T. Sejnowski, "Estimating Alertness from the EEG power Spectrum," IEEE Transactions on bio-medical engineering, vol. 44, no. 11, pp. 60-70, 1997.

[7] A. Subasi, M. K. Kiymik, M. Akin and O. Erogul, "Automatic recognition of vigilance state by using a wavelet-based artificial neural networks," Neural Computations and Applications, vol. 14, no. 1, pp. 45-55, 2005.

[8] V. Khare, J. Santhosh, S. Anand and M. Bhatia, "Classification of Five mental Tasks from EEG Data Using Neural Networks Based on Principal Component Analysis," The IUP Journal of Science & Technology, vol. 5, no. 4, pp. 31-38, 2009.

[9] R. Palaniappan, "Utilizing Gamma Band to Improve Mental Task Based Brain- Computer Interface Design," Neural Systems and Rehabilitation Engineering, IEEE Transactions on Neural Systems and Rehabilitation Engineering, vol. 14, no. 3, pp. 299-303, 2006.

[10] A. Chakraborty, P. Bhowmik, S. Das, A. Halder, A. Konar and K. Nagar, "Correlation between Stimulated Emotion Extracted from EEG and its Manifestation on Facial Expression," Proceedings of the 2009 IEEE International Conference on Systems, Man, and Cybernetics, pp. 3132-3137, 2009.

[11] R. Khosrowabadi, M. Heijnen, A. Wahab and H. Chai Quek, "The Dynamic Emotion Recognition System Based on Functional Connectivity of Brain Regions," 2010 IEEE Intelligent Vehicles Symposium, pp. 377-381, 2010.

[12] M. Murugappan, "Human Emotion Classification using Wavelet Transform and KNN," 2011 International Conference on Pattern Analysis and Intelligent Robotic, pp. 148-153, 2011.

[13] S. H. Lee, B. Abibullaev, W.-S. Kang, Y. Shin and J. An, "Analysis of Attention Deficit Hyperactivity Disorder in EEG Using Wavelet Transform and Self Organizing Maps," International Conference on Control, Automation and Systems 2010 in KINTEX, pp. 2439-2442, 2010.

[14] F. De Vico Fallani and e. al, "Structure of the cortical networks during successful memory encoding in TV commercials," Clinical Neurophysiology, vol. 119, pp. 2231-2237, 2008.

[15] K. Crowley, A. Sliney, I. Pitt and D. Murphy, "Evaluating a Brain-Computer Interface to Categorise Human Emotional Response," IEEE International Conference on Advanced Learning Technologies, vol. 10th, pp. 276-278, 2010.

[16] C. Berka, D. Levendowski, M. Cvetinovic, M. Petrovic, G. David, M. Limicao, V. Zivkovic, M. Popovic and R. Olmstead, "Real-Time Analysis of EEG Indexes of Alertness, Cognition, and memory Acquired with a Wireless EEG Headset," International Journal of Human-Computer Interaction, vol. 17 (2), pp. 151-170, 2004.

[17] C. Lisetti and F. Nasoz, "Using Noninvasive Wearable Computers to Recognize Human," EURASIP Journal on Applied Signal Processing, vol. 2004, no. 11, pp. 1672-1687, 2004.

[18] D. Watson, L. A. Clark and A. Tellegen, "Development and Validation of Brief Measures of Positive and Negative Affect: The PANAS Scales," Journal of Personality and Social Psychology, vol. Vol. 54, no. No. 6, pp. 1063-1070, 1988.

[19] J. C. Lester, S. G. Towns and P. J. Fitzgerald, "Achieving Affective Impact: Visual Emotive Communication in Lifelike Pedagogical Agents," International Journal of Artificial Intelligence in Education, vol. (IJAIED) 10, pp. 278-291, 1999.

[20] B. Kort, R. Reilly and R. Picard, "An Affective Model of Interplay Between Emotions and Learning: Reengineering Educational Pedagogy—Building a Learning Companion," Proc. Int. Conf. Advanced Learning Technologies, vol. 2002, p. 43–48, 2002.

[21] R. S. HELLER, C. BEIL, K. DAM and B. HAERUM, "Student and Faculty Perceptions of Engagement in Engineering," Journal of Engineering Education, pp. 253-261, July 2010.

[22] N. Garnefski, V. Kraaij and P. Spinhoven, "Negative life events, cognitive emption regulation and emotional problems," Personality and Individual Differences, vol. 30, no. 2001, pp. 1311-1327, 2001.

[23] C. Frasson and P. Chalfoun, "Managing Learner's Affective States in Intelligent Tutoring Systems," Advances in Intelligent Tutoring Systems, vol. SCI, no. 308, p. 339–358, 2010.

[24] S. K. D'Mello, S. D. Craig and A. C. Graesser, "Multimethod assessment of affective experience and expression during deep learning," Int. J. Learning Technology, vol. Vol. 4, no. Nos. 3/4, pp. 165-187, 2009.

[25] J. Mostow, K.-m. Chang and J. Nelson, "Toward Exploiting EEG Input in a Reading Tutor," Proceedings of the 15th International Conference on Artificial Intelligence in Education, vol. 15th, pp. 230-237, 2011.

[26] G. Rebolledo-Mendez, I. Dunwell, E. A. Martínez-Mirón, M. D. Vargas-Cerdán, S. de Freitas, F. Liarokapis and A. R. García-Gaona, "Assessing NeuroSky's Usability to Detect Attention Levels in an Assessment Exercise," Human-Computer Interaction, vol. Part I, no. HCII 2009, p. 149–158, 2009.

[27] H. Nagashino, T. Kawano, M. Akutagawa, Q. Zhang, Y. Kinouch, F. Shichijo and S. Nagahiro, "Application of Neural Networks to Dynamics Identification by EEG," Seventh International Conference on control, Automation, Robotics And Vision, vol. 1, pp. 554-559, 2002.

[28] S.-i. Ito, Y. Mitsukura, K. Sato, S. Fujisawa and M. Fukumi, "Study on Association between User's Personality and Individual Characteristic of Left Prefrontal Pole EEG Activity," 2010 Sixth International Conference on Natural Computation (ICNC 2010), pp. 2163-2166, 2010.

[29] A. Heraz and C. Frasson, "Predicting the Three Major Dimensions of the Learner's Emotions from Brainwaves," World Academy of Science, Engineering and Technology, vol. 31, pp. 323-329, 2007.

[30] P. Chalfoun, S. Chaffar and C. Frasson, "Predicting the Emotional Reaction of the Learner with a Machine Learning Technique," Workshop on Motivaional and Affective Issues in ITS,, vol. ITS'06, 2006.

[31] A. Belle, R. Hobson Hargraves and K. Najarian, "An Automated Optimal Engagement and Attention Detection System Using Electrocardiogram," Computational and Mathematical Methods in Medicine, vol. 2012, no. Article ID 528781, pp. 1-12, 2012.

[32] S. Selvan and R. Srinivasan, "Removal of Ocular Artifacts from EEG Using an Efficient Neural Network Based Adaptive Filtering Technique," IEEE Signal Processing Letters, vol. 6, no. 12, pp. 330-332, 1999.

[33] T. Green and K. Najarian, "Correlations between emotion regulation, learning performance, and cortical activity," in Proceedings of the 29th Annual Conference of the Cognitice Science Society, Nashville, TN, 2007.

[34] A. Chakraborty, P. Bhowmik, S. Das, A. Halder, A. Konar and A. K. Nagar, "Correlation between Stimulated Emotion Extracted from EEG and its Manifestation on Facial Expression," Proceedings of the 2009 IEEE International Conference on Systems, Man, and Cybernetics, vol. 2009, pp. 3132-3137, 2009.

[35] P. A. Nussbaum, "LITERATURE REVIEW OF SIGNAL PROCESSING OF ELECTROENCEPHELOGRAM FOR THE DETECTION OF ATTENTIVENESS TOWARDS SHORT TRAINING VIDEOS," Advances in Artificial Intelligence, 2013 (Under Review, not yet published).

Camera Mouse Including "Ctrl-Alt-Del" Key Operation Using Gaze, Blink, and Mouth Shape

Kohei Arai [1]
Graduate School of Science and Engineering
Saga University
Saga City, Japan

Ronny Mardiyanto [2]
Department of Electronics Engineering
Institute Technology of Surabaya
Surabaya City, Indonesia

***Abstract*—This paper presents camera mouse system with additional feature: "CTRL - ALT - DEL" key. The previous gaze-based camera mouse systems are only considering how to obtain gaze and making selection. We proposed gaze-based camera mouse with "CTRL - ALT - DEL" key. Infrared camera is put on top of display while user looking ahead. User gaze is estimated based on eye gaze and head pose. Blinking and mouth detections are used to create "CTR - ALT - DEL" key. Pupil knowledge is used to improve robustness of eye gaze estimation against different users. Also, Gabor filter is used to extract face features. Skin color information and face features are used to estimate head pose. The experiments of each method have done and the results show that all methods work perfectly. By implemented this system, troubleshooting of camera mouse can be done by user itself and makes camera mouse be more sophisticated.**

Keywords*—Camera Mouse; User Gaze; Combination keys function

I. INTRODUCTION

Camera mouse that is a pointing device which utilizes only camera have recently been gaining a great deal of attention. Camera mouse likes usual mouse. However, no additional hardware is required except camera only. Recently, camera mouse is become good issues because of its function can be used for handicap person. Typically, mouse is controlled by hand, but the camera mouse can be controlled without touching anything. Only web camera is required for using this system. The function of the camera mouse is also same with typically mouse, but further function also can be used for handicap person who cannot use their movement organ. Mostly all types of mouse are always used as pointing tool. This pointing tool allows people with disability uses computer and also other tools.

Typically, output of mouse can be divided into: (1) pointing value, (2) left click (making decision), (3) right click (showing menus), and (4) scroll. The problem of existing camera mouse methods are still cannot replace all functions of ordinary mouse. Most of them only yield pointing and decision values. Also, because of users cannot use their hand, it is necessary to create "CTRL - ALT - DEL" key in order to end task not responding program. This function allows users do troubleshooting by themselves. Moreover, camera mouse have to robust against various users, head movement, illumination changes, and accuracy. The published camera mouse methods can be broadly classified into following approaches,

1) Motion based approaches [1][2][3][4][6], (method of using selected face image and then follow its motion),

2) Gaze based approaches [5][8], (The pointing value is obtained from user gaze),

3) Hybrid approaches [7][9], (Combination between motion and gaze).

Mouse utilizes web camera have been proposed [1]. Mouse pointer follows face areas which have been selected first. Clicking is done when mouse pointer stops with specific time. Camera mouse that lets users move the cursor around with their head is proposed [2]. Camera mouse for people with severe disabilities is proposed [3]. The system tracks the computer user's movements with a video camera and translates them into the movement of the mouse pointer on screen. Visual tracking algorithm is based on cropping an online template of the tracked feature from current image and finds the new location of this by using template matching method. Mouse pointer controlled by gesture is proposed [4]. This system can be controlled by moving user's hand or face. Camera mouse controlled by user gaze is proposed [5]. This system uses eye tracking to find eye location. Infrared illumination is used to estimate dark pupil location and used to estimate user gaze. Camera mouse driven by 3D model based visual face tracking technique is proposed [6]. The human facial movement is decomposed into rigid movement, e.g. rotation and translation, and non-rigid movement, such as the open/close of mouth, eyes, and facial expressions. Camera mouse based on face and eye blinking tracking are proposed [7]. Face features and detect eye blinking are tracked using combination between optical flow and Harris corner detection. Camera mouse based on eye gaze is proposed [8]. The mean shift algorithm is used to track the detected eyes. Motion based camera mouse is easy to developed. The weakness of this approach requires user movement, it is difficult to use for users who cannot move their organs. Even though gaze approach is more difficult to developed, it has high sensitivity and is convenience.

In this paper we proposed camera mouse based on user gaze with combination key: "CTRL - ALT - DEL". The objective of this research is to overcome troubleshooting when computer not responding by providing "CTRL - ALT - DEL" key. Moreover, we improve robustness against different users, illumination changes, head movement, and accuracy. Our proposed system utilizes single IR camera which put on top of

screen display. The IR camera will improve robustness against illumination changes. User gaze which used to control pointing value is estimated based on eye gaze and head pose. In order to create "CTRL - ALT - DEL" key, we use open-closed mouth detection. When system runs in the first times, Haar-classifier is used to detect eyes location. After eyes location is found, roughly position of mouth estimated based on eye location. The detail position of mouth and eye corners position is estimated by using Gabor filter. After all face features are found, optical flow Lucas-Kanade method is used for tracking them. "CTRL - ALT - DEL" key is created by utilizing open-closed shape of mouth. When mouth is open, it means that SHIFT is selected. When mouth is open and left eye is closed, it means that CTRL, ALT, and DEL are selected. In order to avoid disturbance (noise when user talking), these conditions are selected when it is done within two seconds. Improvement of robustness against various uses is done by using pupil knowledge. Pupil knowledge such as shape, size, and color are used as first knowledge. When first knowledge fails, sequential of pupil location is used as next knowledge. Last, when all steps fail, pupil is estimated based on their motion. Also, improvement against head movement is done by estimating gaze also based on head poses.

The camera mouse system by user gaze is proposed in Chapter 2. Moreover, blink and mouth detection methods which are the important component engineering of proposed system are explained in full detail. Chapter 3 shows the experiment method and a result, and show that a proposed system can work very well. Then, the remarks that finally relate to an experimental result are described.

II. Proposed Method

The problem of the utmost importance of a proposed system camera mouse system is combination keys function. In order to consider that it is free hand touch, it is important to create combination key: "CTRL - ALT - DEL" in order to avoid undesired computer condition. When PC system is halt, all programs will halts. The only way is press CTRL - ALT - DEL to end not responding program. Even though camera mouse program also possible halts, it is possible to setup our program using another memory location and make it always runs. Therefore, the camera mouse system to propose aimed at providing the combination key: "CTRL - ALT - DEL" using eye-mouth combination.

A. System Configuration

The configuration of the proposed system is shown in Figure 1. As shown in the figure, a user looking at the screen while camera put on top of screen display. Only camera which mounted on top of screen display is required. Optiplex 755 dell computer with Core 2 Quad 2.66 GHz CPU and 2G RAM is used. We develop our software under C++ Visual Studio 2005 and OpenCv Image processing Library which can be downloaded as free on their website. The specification of IR camera is shown in Table 1. The pointing value is determined based on head poses and eye gaze

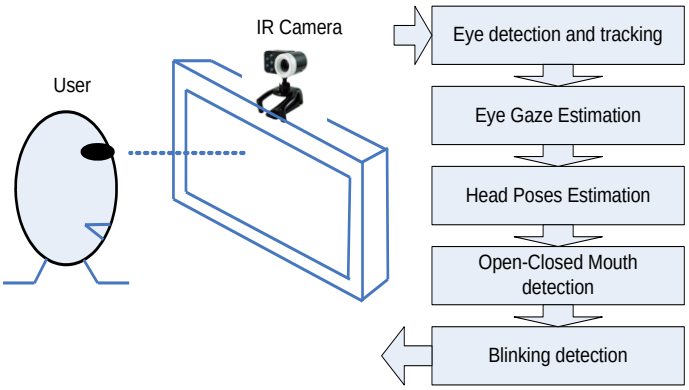

Fig.1. Camera mouse configuration.

TABLE I. Specification of IR Camera

Pixel	1.3 M
Resolution	1280×1024
Frame rate	1280 x 1024 : 7.5fps, 640 x 480 : 30fps
Dimension	52mm (W) × 65mm (D) × 70mm (H)
Weight	85g
Operating condition	0 - 40deg.C
Interface	USB 2.0
IR Illumination	7 IR LED

B. Key Cadidate Selection and Determination

Combination between eye gaze and head poses are used to obtain user gaze. The determination key is done by blink. Generally, we can use all windows programs. In order to typing, combination between Microsoft Word and windows screen keyboard can be used. Because of windows screen keyboard is used for typing, user may look at the desired keys and blinks in order to make selection. In special conditions, combination keys important to be provided. CTRL - ALT - DEL combination keys can be done by using eye and mouth shape. Unfortunately, user also may open their mouth unintentionally.

Fig.2. Windows screen keyboard. This software allows user to type onto MS Word.

For instance, when user become sleepy and open their mouth, when user says something, etc. In order to avoid conflicts with these situations, our mouth shape is created with sequential states.

In our system, "CTR -ALT - DEL" key is done when mouth shape is closed-open-closed during for two seconds and end with left eye blinks.

C. Gaze Estimation

In order to analyze eye gaze, eye should be detected and tracked first. Figure 3 shows flow of eye detection and tracking. The published eye detection approaches can be broadly classified into two categories: the active infrared (IR)-based approaches [10], [11], [19] and the traditional image-based passive approaches [12], [13], [14], [15], [16], [17], [18]. Eye detection based on Hough transform is proposed [12], [13], [14]. Hough transform is used in order to find the pupil. Eye detection based on motion analysis is proposed [10]. Infrared lighting is used to capture the physiological properties of eyes (physical properties of pupils along with their dynamics and appearance to extract regions with eyes). Motion analysis such as Kalman filter and Mean Shift tracking are used. Support vector machine classifier is used for pupil verification. Eye detection using adaptive threshold and Morphologic filter is proposed [15]. Morphologic filter is used to eliminate undesired candidates for an eye. Hybrid eye detection using combination between color, edge and illumination is proposed [18]. Eye detection based on motion analysis [10], [11] will fail when eyes are closed or occluded.

In our system, we cannot use this method. Our pupil detection have to works when eye shape changes. When eyeball moves, eyebrow and pupil will also move and yield two kinds of motion. Because of other eye components move when eye moves, the ambiguity problem to distinguish between eyebrow and pupil will happen. Eye detection based on Hough transform [12], [13], [14] is susceptible against noise influence. Eye detection using morphological filter [15] which eliminate noise and undesired candidate of eye will not robust against user variance. Morphologic method will not work when noises have same shape and size with pupil. Eye detection based on template matching [16], [17], segments of an input image are compared to previously stored images, to evaluate the similarity of the counterpart using correlation values.

The problem with simple template matching is that it cannot deal with eye variations in scale, expression, rotation and illumination. Use of multi scale templates was somewhat helpful in solving the previous problem in template matching. When eye detector only relies on eye appearance [18], this method will fail when eye unseen or closed. This method also will be faced on variance user color skin. Basically, our system detects eye based on deformable template method [20]. This method matches between eye template and source images. We create template by using Gaussian smother onto this image. Deformable template method detects roughly position of eye. Benefit of deformable template method is that it takes less time than classifier methods.

Although this method faster than classifier type, the robustness is still less. In our system, when deformable template fails to detect eye position, viola-Jones classifier will detects eye. It means that Viola-Jones method is used only when deformable template fails to detect eye. The viola-Jones classifier employs adaboost at each node in the cascade to learn a high detection rate the cost of low rejection rate multi-tree classifier at each node of the cascade. To apply the viola-Jones classifier onto system, we use viola-Jones function in OpenCV [21]. Before use the function, we should create XML file. The training samples (face or eye image) must be collected. There are two samples: negative and positive sample. Negative sample corresponds to non-object images. Positive sample corresponds to object image. After acquisition of image, OpenCV will search the face center location followed by searching the eye center location. By using combination between deformable eye template and Viola-Jones method, eye location easier to be detected. Advantages of these methods are fast and robust against circumstances change.

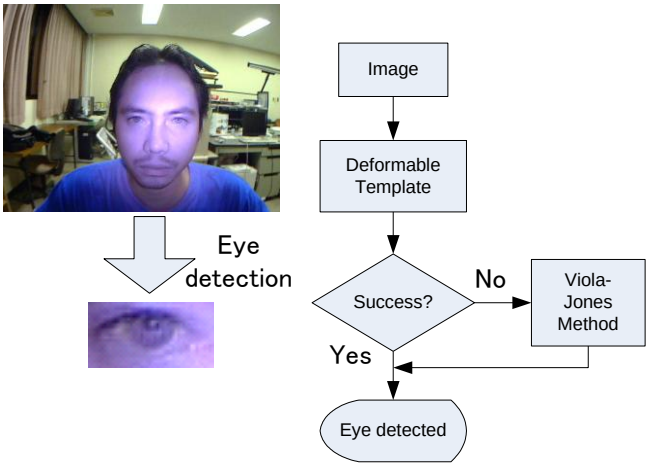

Fig.3. Eye detection flow

After the roughly eye position is found, next position of eye is tracked using Lucas-Kanade optical flow method. It means that we do not repeat the eye detection again. Eye gaze is estimated based on pupil location. Because of this system rely on the pupil location, pupil detection with perfectly accurate and robustness is required. Pupil is detected by using its knowledge. Flow of pupil detection is shown in Figure 4. Three types of knowledge are used. We use pupil size, shape, and color as the first knowledge. First, adaptive threshold method is applied onto eye image. Threshold value T is obtained from average pixel value (mean) of eye image μ. We set threshold value is 27% bellow from mean.

$$\mu = \frac{1}{N}\sum_{i=0}^{N-1} I_i \quad (1)$$

$$T = 0.27\mu \quad (2)$$

Pupil is signed as black pixels on image. In the first case, when the pupil clearly appears on eye image, the result of adaptive threshold itself is able to detect pupil location. Pupil is marked as one black circle on image. By using connected labeling component method, we can easily estimate the pupil location. While noise appears on image, we can distinguish them by estimate its size and shape. Next case, when eye is looking at right or left, the form of eye will change. This condition makes the pupil detection is hard to find. Noise and interference between pupil and eyelid appear. This condition brings through others black pixels which have same size and

shape with pupil. To solve this problem, we utilize the previous pupil location. The reasonable pupil location is always in surrounding previous location. Last case, when all steps above fail to detect pupil location, we estimate pupil location by its motion. This situation happens when the black pixels mixed with other black pixel or no black pixels at all on image. We put this knowledge as last priority to avoid ambiguity motion between pupil and other eye components. We monitor pupil location using its previous location. We adopt Kalman filter [22] to estimate pupil location. A simple eye model is defined on Figure 5. The eyeball is assumed to be a sphere with radius R. Actually, it is not quite a sphere but this discrepancy does not affect our methodology. The pupil is located at the front of eyeball.

The distance from the center gaze to current gaze is r. Gaze is defined as angle θ_{eye} between normal gaze and r. The relation between R, r and θ_{eye} is expressed in equation (3) and (4), respectively.

$$r = R \sin\theta \quad (3)$$

$$\theta_{eye} = \arcsin(\frac{r}{R}) \quad (4)$$

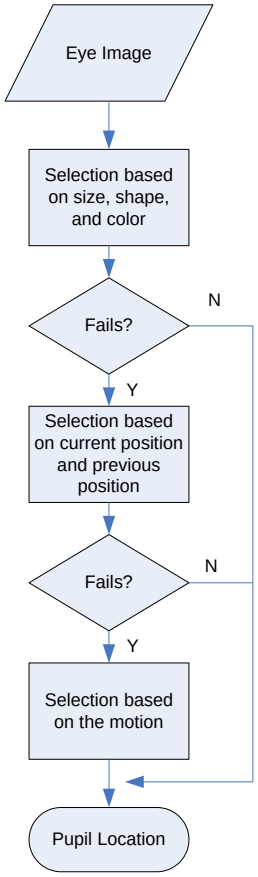

Fig.4. Flow of Pupil detection methods. Pupil detection works using three steps: (1) based on size, shape, and color, (2) based on its sequential position, and (3) based on the motion.

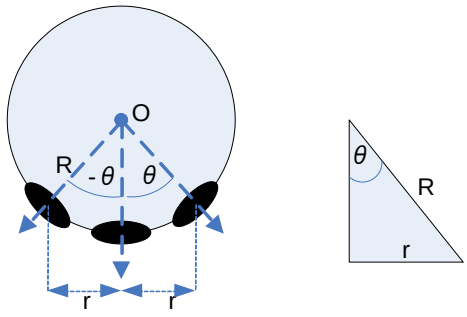

Fig.5. Eye model.

The radius of the eyeball ranges from 12 mm to 13 mm according to the anthropometric data [23]. Hence, we use the anatomical average assumed in [24] into our algorithm. Once r has been found, gaze angle θ_{eye} is calculated easily. In equation 4 is shown that eye gaze calculated based on r value. In order to measure r, the normal gaze should be defined. In our system, when system starts running, the user should looks at the center. At this time we record that this pupil location is normal gaze position. In order to avoid error when acquiring normal gaze, normal gaze position is verified by compare between its value and center of two eye corners.

D. Head Pose Estimation

Head poses estimation is intrinsically linked with visual gaze estimation. Head pose provides a coarse indication of gaze that can be estimated in situation when the eyes of a person are not visible. When the eyes are visible, head pose becomes a requirement to accurately predict gaze direction.

The conceptual approaches that have been used to estimate head pose are categories into[25] (1) Appearance template methods, (2) Detector array methods, (3) Nonlinear regression methods, (4) Manifold embedding methods, (5) Flexible models, (6) Geometric methods, (7) Tracking methods, and (8) Hybrid methods. Our proposed head pose estimation based on Geometric methods. Face features such as eyes location, the end of mouth, and boundary of face are used to estimate head pose. After eyes location are found, mouth location is presume based on eyes location. Two of end of mouth are searched by using Gabor filter. The boundary of face is searched based on skin color information. From eyes and two end of mouth, face center is estimated. Head pose is estimated by difference between face center and face boundary. Head pose estimation flow is shown in Figure 6.

Head pose can be calculated with equation (5) to (8).

$$f_c = \frac{eye_L + eye_R + mth_L + mth_R}{4} \quad (5)$$

$$f_h = \frac{f_{top} + f_{btm} + f_L + f_R}{4} \quad (6)$$

$$r_{ch} = f_c - f_h \quad (7)$$

$$\theta_{head} = \arcsin\left(\frac{r_{ch}}{R_{head}}\right) \quad (8)$$

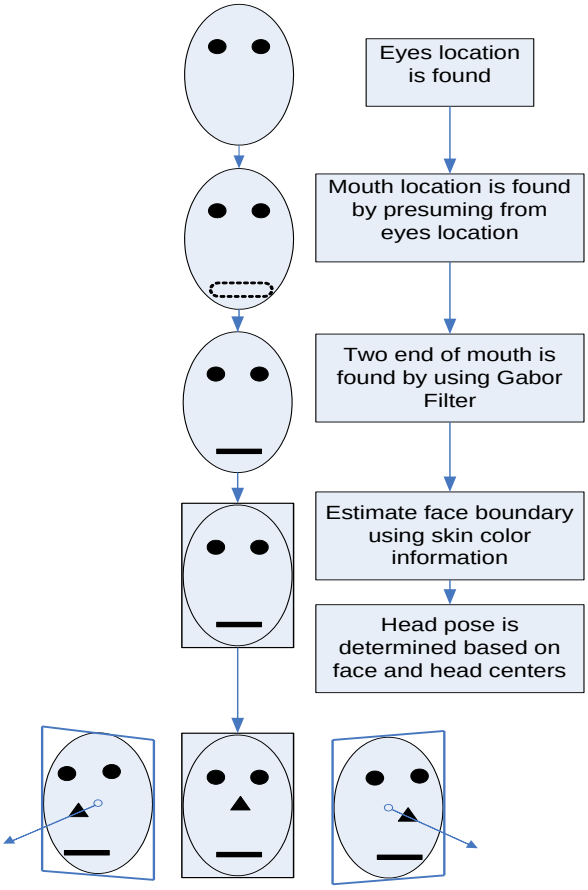

Fig.6. Head pose estimation flow, head pose is determined based on face and head centers.

where f_c is face center, eyeL and eyeR are locations of left and right eyes, mthL and mthR are left and right mouth locations, f_h is head center, f_{top}, f_{btm}, f_L, and f_R are top, bottom, left, and right head boundary locations. r_{ch} is distance between face and head centers. R_{head} is radial of head. θ_{head} is head pose angle.

E. Mouth Detection

Open-closed mouth shape is one of feature that will be used to create "CTRL - ALT - DEL" key. When left eye closed while mouth is open (during for two seconds), system will send "CTRL - ALT - DEL" command. This combination keys is important when computer halt. Our mouth shape detection based on skin color information. Normalized RGB based skin color detection is used to extract mouth [26]. Because of mouth was surrounded by skin, mouth shape will easily to detect by removing skin color.

F. Blink Detection

Considering of the blinking application, the accuracy and success rate become important. Many techniques based on image analysis methods have been explored previously for blinking detection. Blinking detection based on Hough Transform in order to find iris location is proposed [27]. Eye corners and iris center based detector is proposed [28]. Blinking detection system uses spatio-temporal filtering and variance maps to locate the head and find the eye-feature points respectively is proposed [29]. Open eye template based method is proposed [30]. Using a boosted classifier to detect the degree of eye closure is proposed [31]. Lucas-Kanade and Normal Flow based method is proposed [32].

The methods above still did not give perfectly success rate. Also, common problem is difficult to implement in real time system because of their time consumption. Because of these reasons, we propose blinking detection method which able to implement in real time system and has perfectly success rate. Basically, our proposed method is measure percentage of open-closed eye condition by estimating the distance between topside of arc eye and the bottom side. Gabor filter is used to extract arcs of eye. By utilize connected component labeling method, top-bottom arcs are detected and measured. The distance between them can be used to determine the blinking. Blinking detection flow is shown in Figure 7.

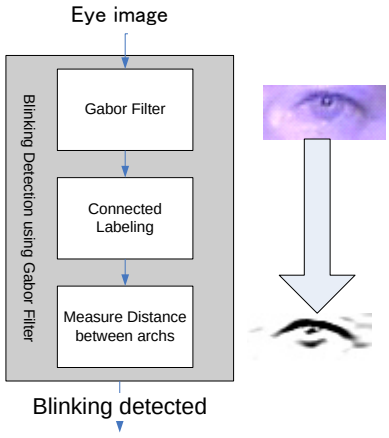

Fig.7. Blink detection flow. Gabor filter is used to extract arcs of eye.

III. Experiments

In order to measure the performance of our proposed system, each block function is tested separately. The experiments involve eye gaze, head pose estimation, blinking detection, and open-closed mouth detection.

A. Gaze Detection

Eye gaze estimation experiments include eye detection success rate against different user, illumination influence, noise influence, and accuracy. The eye detection experiment is carried out with six different users who have different race and nationality: Indonesian, Japanese, Sri Lankan, and Vietnamese. We collect data from each user while making several eye movements. Three of Indonesian eyes who have different race are collected. The collected data contain several eye movement such as look at forward, right, left, down, and up. Two of Indonesian eyes have width eye with clear pupil. Numbers of images are 552 samples and 668 samples. Another Indonesian eye has slanted eyes and the pupil is not so clear. Numbers of images of this user are 882 samples. We also collected data from Sri Lankan people. His skin color is black with thick eyelid. Numbers of images are 828 samples. The

collected data of Japanese is bright with slanted eyes. Numbers of images are 665 samples.

The first experiment investigates the pupil detection accuracy and variance against various users. We count the success samples followed by counting the success rate. Our method is compared with adaptive threshold method and Template matching method. The adaptive threshold method uses combination between adaptive threshold itself and connected labeling method. The template matching method use pupil template as reference and matched with the images. The result data is shown in Table 2.

TABLE II. ROBUSTNESS AGAINST VARIOUS USERS, THIS TABLE SHOWS THAT OUR METHOD ROBUST ENOUGH AGAINST VARIES USER AND ALSO HAS HIGH SUCCESS RATE

User Type	Nationality	Adaptive Threshold (%)	Template Matching (%)	Our Method (%)
1	Indonesian	99.85	63.04	99.99
2	Indonesian	80.24	76.95	96.41
3	Sri Lankan	87.80	52.17	96.01
4	Indonesian	96.26	74.49	99.77
5	Japanese	83.49	89.10	89.25
6	Vietnamese	98.77	64.74	98.95
Average		**91.07**	**70.08**	**96.73**
Variance		**69.75**	**165.38**	**16.27**

The result data show that our method has high success rate than others. Also, our method is robust against the various users (the variance value is 16.27).

The next experiment measures influence of illumination changes against eye detection success rate. This experiment measures the performance when used in different illumination condition. Adjustable light source is given and recorded the degradation of success rate. In order to measure illumination condition, we used Multi-functional environmental detector LM-8000. Experiment data is shown in Figure 8.

Data experiment show that our proposed method allow works with zero illumination condition (dark place). This ability is caused of IR light source which automatically adjust the illumination. Our proposed method will fail when illumination condition is too strong. This condition may happen when sunlight hit directly into camera.

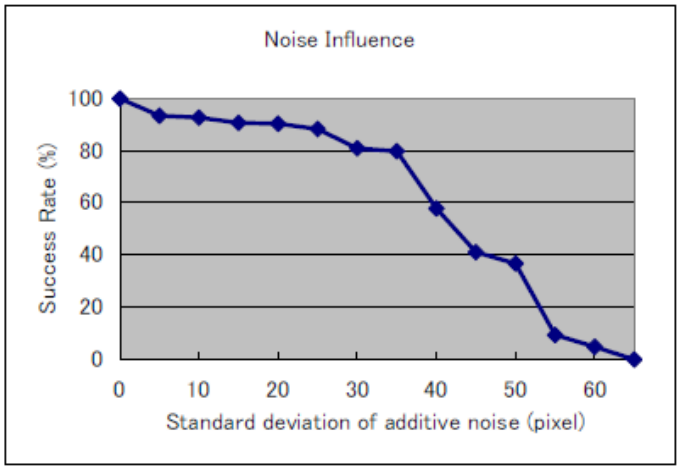

Fig.8. Illumination Influence, this figure shows that our proposed method allow works with minimum illumination.

The next experiment measures noise influence against eye detection success rate. Normal distributed random noise is added into image. We add noise with mean is 0 and standard deviation of normal distributed random noise is changed. Robustness due to noise influence is shown in Figure 9. The experiment data show that our system robust enough due to noise influence.

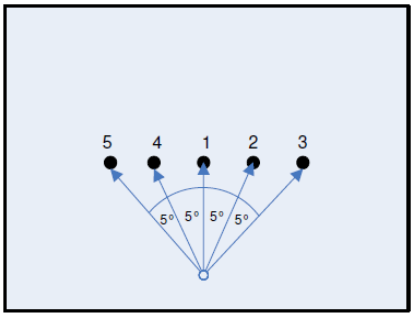

Fig.9. Noise influence against eye detection success rate

The next experiment measures accuracy of eye gaze estimation. Users will look at several points which are shown in Figure 10 and calculate the error. Error is calculated from designated angle and real angle. The errors are shown in Table 3. These experiment data show that our proposed system has accuracy 0.64°.

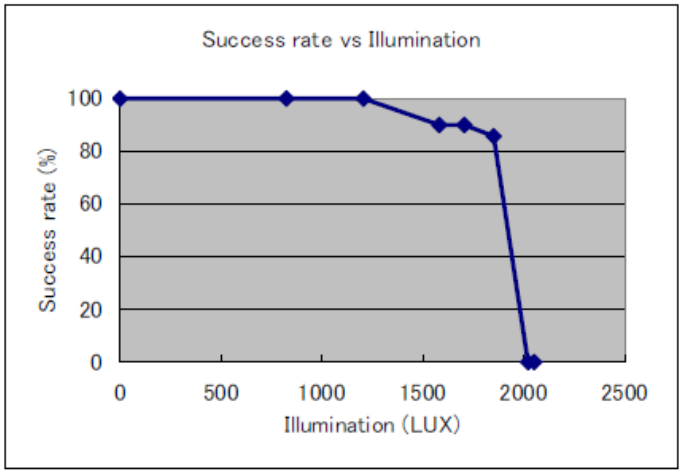

Fig.10. Experiment of eye gaze accuracy. Five points are used to measure the accuracy.

TABLE III. EYE GAZE ESTIMATION ACCURACY

Point	Error (^{0})
1	0
2	0.2
3	0.2
4	0.2
5	3.12
Average	**0.64**

B. *Head Pose Estimation*

This experiment measure accuracy of head poses in yaw and pitch directions. In order to measure head pose, head center is estimated first. Head center is estimated by using skin color information. RGB normalization method is used to detect skin color

Fig.11. Head center estimation using skin color information

Next is estimates face center. Face center is estimated using four face features (two ends of eyes and two ends of mouth). Face features are extracted using Gabor Filter.

Fig.12. Face feature extracted using Gabor filter. Gabor image is shown in left side.

By using head center and average position from four face features, head pose is estimated.

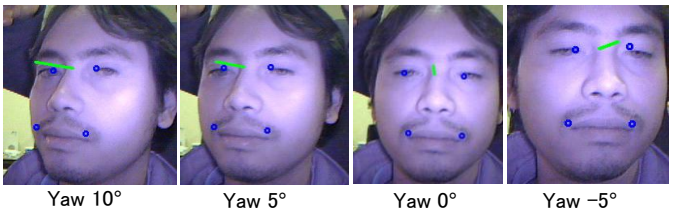

Fig.13. Head pose estimation; head pose is estimated using center of four face features and head center.

The complete experiment of head pose estimation is shown in Table 4. The result show that error will increase when yaw angle rises. This condition is caused by when head move with high angle, ear will visible. Because of ear color same with skin color, it causes result of head center estimation shift and obtains error.

TABLE IV. HEAD POSE ESTIMATION IN YAW DIRECTION

Yaw angle (^{0})	Error (^{0})
15	6.41
10	2.34
5	0.33
0	0
-5	1.12
-10	-2.18
-15	-4.47
Average	**0.51**

TABLE V. HEAD POSE ESTIMATION IN PITCH DIRECTION

Pitch Angle (^{0})	Error (^{0})
-20	13
-10	5
0	0
10	4
20	4
Average	**5.2**

C. Blink Detection

This measurement is conducted by counting the success and fail ones when position of user face is constant, but eye gaze changes. IR camera is put on the top of monitor display and the user face looking forward. Distance between camera and user is 30 cm. This experiment is shown in Figure 14. We recorded the success rate when user face position is constant and eye gaze angle changed. The result is shown in Table 6.

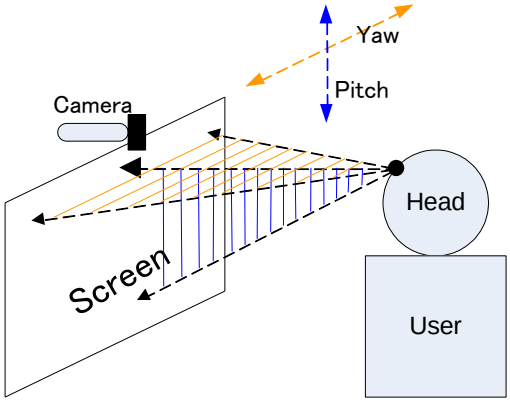

Fig.14. Blink detection experiment.

The results show that our method will give 100% success rate when pitch angle is below than 15° and the maximum of roll angle is 30°. When pitch angle of eye gaze exceed 15°, the success rate become decrease. It happens because method fails to distinguish between open and closed eyes images. Alteration of eye images when eye gaze changes are shown in Figure 15. This figure shows that when pitch angle become greater, eye will look like closed eye. This condition will not benefit for our method.

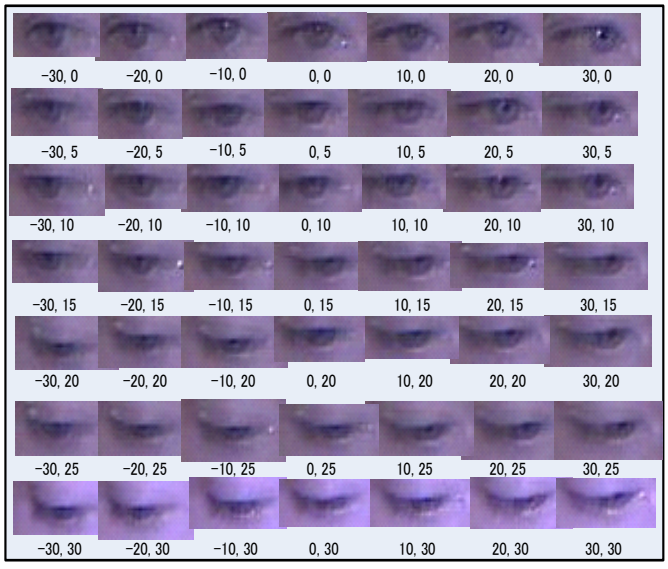

Fig.15. Eye images when eye gaze changes

TABLE VI. BLI9NK DETECTION ACCURACY

Success Rate (%) / Pitch Angle (degree)	Yaw Angle (degree)						
	-30	-20	-10	0	10	20	30
0	100	100	100	100	100	100	100
5	100	100	100	100	100	100	100
10	100	100	100	100	100	100	100
15	100	100	100	100	100	100	100
20	95	99	99	99	85.5	39	25
25	6	15	63	72	36	5	2
30	4	15	26	54	18	3	2

D. Mouth Detection

Performance of mouth shape detection is measured by detecting open-closed mouth shapes. User does 10 times open-closed condition while system analyzed it. Figure 16 shows the open-closed mouth shape. Experimental data show that our mouth states detection works very well.

IV. CONCLUSION

Each block of camera mouse with "CTRL - ALT - DEL" key have been successfully implemented. Estimation of eye gaze method shows good performance is robust to various users, illumination changes, and robust showing success rate greater than 96% and variance is small enough.

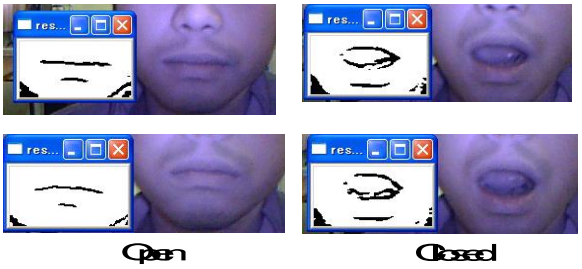

Fig.16. Open-Closed Mouth Shape. Mouth shape is extracted by using Gabor filter. Left side is output of Gabor filter and right side is mouth images.

Also, estimation of head pose is simple. However, it shows good performance when used to estimate in yaw and pitch directions. Furthermore, blinking and mouth shape detections show good performance when detect open-closed eyes and mouth conditions. Moreover, all of our methods do not require any previous calibration. Beside can be used for creating "CTRL - ALT - DEL" key, it also can be used to create other combination keys. By implemented this system, camera mouse will be more sophisticated when it is used by disable person.

REFERENCES

[1] www.cameramouse.org
[2] Open source assistive technology software, www.oatsoft. Org

[3] Betke, M.; Gips, J.; Fleming, P.: The Camera Mouse: visual tracking of body features to provide computer access for people with severe disabilities, IEEE Transactions of Neural Systems and Rehabilitation Engineering, Vol 10, pp 1 -10, (2002)

[4] uMouse, http://larryo.org/work/information/umouse/index. html

[5] EyeTech Digital Systems, http://www.eyetechds.com/

[6] Jilin Tu; Huang, T.; Hai Tao.: Face as mouse through visual face tracking, proceeding of The 2nd Canadian Conference on Computer and Robot Vision, pp 339 – 346, (2005)

[7] Zhu Hao, Qianwei Lei, Vision-Based Interface: Using Face and Eye Blinking Tracking with Camera, iita, vol. 1, pp.306-310, 2008 Second International Symposium on Intelligent Information Technology Application, (2008)

[8] Tao Liu, Changle Pang.: Eye-Gaze Tracking Research Based on Image Processing, cisp, vol. 4, pp.176-180, 2008 Congress on Image and Signal Processing, Vol. 4, (2008)

[9] Tien, G. and Atkins.: Improving hands-free menu selection using eye gaze glances and fixations. In Proceedings of the 2008 Symposium on Eye Tracking Research & Applications, pp 47-50, (2008).

[10] Haro. A, Flickner. M, Essa, I.: Detecting and Tracking Eyes By Using Their Physiological Properties, Dynamics, and Appearance, Proceeding of CVPR 2000, pp 163-168, (2000)

[11] Zhiwei Zhu, Qiang Ji, Fujimura, K., Kuangchih Lee.: Combining Kalman Filtering and mean shift for real time eye tracking under active IR illumination, Proceeding of 16th Pattern Recognition International Conference, vol. 4,pp 318- 321, (2002)

[12] Takegami. T, Gotoh. T, Kagei. S, Minamikawa-Tachino. R.: A Hough Based Eye Direction Detection Algorithm without On-site Calibration, Proceeding of 7th Digital Image Computing: Techniques and Applications, pp 459-468, (2003)

[13] K.M.Lam, H.Yan.: Locating and extracting eye in human face images, Pattern Recognition, 29(5), pp 771-779, (1996)

[14] G.Chow, X.Li.: Towards a system of automatic facial feature detection, Pattern Recognition (26), pp 1739-1755, (1993)

[15] Rajpathaka. T, Kumarb, R, Schwartzb. E.: Eye Detection Using Morphological and Color Image Processing, Proceeding of Florida Conference on Recent Advances in Robotics, (2009)

[16] R.Brunelli, T.Poggio, Face Recognition.: Features versus templates, IEEE Trans. Patt. Anal. Mach. Intell. 15(10), 1042-1052, (1993)

[17] D.J.Beymer.: Face Recognition under varying pose, IEEE Proceedings of Int. Conference on Computer Vision and Pattern Recognition (CVPR'94), Seattle, Washington, USA, pp.756-761, (1994)

[18] Shafi. M, Chung. P. W. H.: A Hybrid Method for Eyes Detection in Facial Images, International Journal of Electrical, Computer, and Systems Engineering, pp 231-236, (2009)

[19] Morimoto, C., Koons, D., Amir, A., Flickner. M.: Pupil detection and tracking using multiple light sources, Image and Vision Computing, vol. 18, no. 4, pp. 331-335, (2000)

[20] A. Yuille, P. Haallinan, D.S. Cohen.: Feature extraction from faces using deformable templates, Proceeding of IEEE Computer Vision and Pattern Recognition, pp 104-109, (1989)

[21] Gary Bradski, Andrian Kaebler.: Learning Computer Vision with the OpenCV Library, O'REILLY, 214-219, (2008)

[22] http://citeseer.ist.psu.edu/443226.html

[23] K.-N. Kim and R. S. Ramakrishna.: Vision-based eye gaze tracking for human computer interface, Proceedings of IEEE International Conference on Systems, Man, and Cybernetics, Vol. 2, pp.324-329, (1999)

[24] R. Newman, Y. Matsumoto, S. Rougeaux and A. Zelinsky.: Real-time stereo tracking for head pose and gaze estimation, Proceedings of Fourth International Conference on Automatic Face and Gesture Recognition, pp. 122-128, (2000)

[25] Murphy-Chutorian, E. Trivedi, M.M.: Head Pose Estimation in Computer Vision: A Survey, IEEE Transactions on Pattern Analysis and Machine Intelligence, Vol 31, pp 607-626, (2009)

[26] Cheol-Hwon Kim, and June-Ho Yi.: An Optimal Chrominance Plane in the RGB Color Space for Skin Color Segmentation, Vol.12, pp 72-81, (2006)

[27] Lei Yunqi, Yuan Meiling, Song Xiaobing, Liu Xiuxia, Ouyang Jiangfan.: Recognition of Eye States in Real Time Video, Proceeding of IEEE International Conference on Computer Engineering and Technology, 554 – 559, (2009)

[28] S. Sirohey, A. Rosenfeld and Z. Duric.: A method of detecting and tracking irises and eyelids in video. Pattern Recognition, vol. 35, num. 6, pp. 1389-1401, (2002)

[29] T. Morris, P. Blenkhorn and F. Zaidi.: Blink detection for real-time eye tracking. Journal of Network and Computer Applications, vol. 25, num. 2, pp. 129-143, (2002)

[30] Michael Chau and Margrit Betke.: Real Time Eye Tracking and Blink Detection with USB Cameras. Boston University Computer Science Technical Report No. 2005-12, (2005)

[31] Gang Pan, Lin Sun, Zhaohui Wu and Shihong Lao.: Eyeblink-based anti-spoofing in face recognition from a generic webcamera. The 11th IEEE International Conference on Computer Vision (ICCV'07), Rio de Janeiro, Brazil, (2007)

[32] Matjaž Divjak, Horst Bischof.: Real-time video-based eye blink analysis for detection of low blink-rate during computer use, Institute for Computer Graphics and Vision Graz University of Technology Austria, (2008)

AUTHORS PROFILE

Kohei Arai, He received BS, MS and PhD degrees in 1972, 1974 and 1982, respectively. He was with The Institute for Industrial Science, and Technology of the University of Tokyo from 1974 to 1978 also was with National Space Development Agency of Japan (current JAXA) from 1979 to 1990. During from 1985 to 1987, he was with Canada Centre for Remote Sensing as a Post Doctoral Fellow of National Science and Engineering Research Council of Canada.

He was appointed professor at Department of Information Science, Saga University in 1990. He was appointed councilor for the Aeronautics and Space related to the Technology Committee of the Ministry of Science and Technology during from 1998 to 2000. He was also appointed councilor of Saga University from 2002 and 2003 followed by an executive councilor of the Remote Sensing Society of Japan for 2003 to 2005. He is an adjunct professor of University of Arizona, USA since 1998. He also was appointed vice chairman of the Commission "A" of ICSU/COSPAR in 2008. He wrote 30 books and published 332 journal papers.

Multi-resolution Analysis of Multi-spectral Palmprints using Hybrid Wavelets for Identification

Dr. H.B. Kekre
Senior Professor, Department of Computer Science,
Mukesh Patel School of Technology Management and Engineering
Mumbai, India

Dr. Tanuja Sarode
Associate Professor, Department of Computer Science, Thadomal Shahani College of Engineering
Mumbai, India

Rekha Vig
Asst. Prof. and Research Scholar, Dept. of Electronics and Telecom.,
Mukesh Patel School of Technology Management and Engineering
Mumbai, India

***Abstract*—Palmprint is a relatively new physiological biometric used in identification systems due to its stable and unique characteristics. The vivid texture information of palmprint present at different resolutions offers abundant prospects in personal recognition. This paper describes a new method to authenticate individuals based on palmprint identification. In order to analyze the texture information at various resolutions, we introduce a new hybrid wavelet, which is generated using two or more component transforms incorporating both their properties. A unique property of this wavelet is its flexibility to vary the number of components at each level of resolution and hence can be made suitable for various applications. Multi-spectral palmprints have been identified using energy compaction of the hybrid wavelet transform coefficients. The scores generated for each set of palmprint images under red, green and blue illuminations are combined using score-level fusion using AND and OR operators. Comparatively low values of equal error rate and high security index have been obtained for all fusion techniques. The experimental results demonstrate the effectiveness and accuracy of the proposed method.**

Keywords—Hand-based biometrics; Hybrid wavelet; Multi-resolution; Energy compaction, fusion;

I. INTRODUCTION

With increasing threat to security there is a grave need for identification in our society. Immense focus is in development of accurate and reliable security systems and to facilitate the development of such systems biometrics is considered as a highly effective automatic mechanism for personal identification. As each human being is unique [1], so are his physical characteristics like fingerprint, palmprint, ear, iris etc. and behavioral characteristics like voice, gait etc. These characteristics are considered as biometrics and can be utilized for such automated personal identification system. Palmprints are becoming more popular over fingerprints as biometrics as they offer more stable and reliable features; even the palm-veins [2] are being analysed as separate biometrics. The main objective behind the automated systems is to extract the unique features of the biometrics and not treat the entire biometric-trait for identification. Feature extraction can be done in many possible ways. For palmprints the various approaches that can be used are: 1) Line-based approach: Palm lines are prominent and unique features of a palm. The extraction of these lines by using edge-based detection methods [3] and morphological operations [4] are quite common. 2) Subspace (appearance)-based approach: Principle component analysis (PCA), independent component analysis (ICA) and linear discriminant analysis (LDA) are used and their coefficients are considered as the features [5], [6]. 3) Texture-based approach: In this approach various filters like Gabor filter [7]-[9] and transforms like Discrete Cosine Transform and wavelets [10], [11] etc. are used to analyze texture based information of palmprints. Attempts have been made to combine the features [12] produced by few or all the techniques mentioned above.

The texture features are supposed to contain more information and hence they have been successfully analysed using Gabor filter earlier. There exist verification/identification systems based on extracted features using various transforms such as Fourier Transform [13] (where Fourier range and angle features have been extracted to identify the palm-print image) and [14] (where cepstum coefficients are matched), Karhunen-Loeve transform [5], Discrete Cosine Transform, Walsh Transform [18] etc. It has been observed that different transforms analyze the palmprint in different ways. Attempt has been done by Kekre et. al. [17] to combine more than one transforms to generate hybrid transform and use it for palmprint identification. Properties of many transforms can be combined in hybrid transform and hence the results are better than those obtained using single transform. This was further extended to bi-resolution hybrid wavelets [18] which analyze palmprints at only global and local levels of resolution and were successfully used for identification purpose. In this paper we present multi-resolution hybrid wavelets, which provide with palmprint image analysis at local, semi-global (at various levels) and global levels of resolution. Since palmprints have principle lines (less texture) which can be viewed at low resolution, minor lines (medium texture) which can be viewed at various resolutions at medium level and ridges and valleys (high texture) which can only be viewed at high resolution, it becomes essential to analyze the palmprint at various resolutions.

The rest of the paper is organized as follows. Section II describes the generation of Hybrid Wavelet using Kronecker product and Hybrid transform. Section III illustrates the algorithm used in the proposed method for palmprint

identification for multi-spectral images. In section IV the fusion scheme used to combine scores for multi-spectral palmprints is explained and section V presents the results obtained using the proposed method. The paper is concluded in section VI.

II. HYBRID WAVELET

A. Generation of Hybrid Wavelet

The hybrid wavelet transform matrix is generated using hybrid transform matrix, which can be produced using Kronecker product of two or more existing orthogonal transforms[15]. For any hybrid transform of size nxn = pqxpq (component transforms A and B of size pxp and qxq respectively), a hybrid wavelet H_W, of size pqxpq can be generated. If r_0, r_1, r_2,….r_{n-1}(except 1 and p itself) are the divisors of p (for example, if p =32 then 2, 4, 8 and 16 will be r_0, r_1, r_2 and r_3 respectively), arranged in ascending order, then the hybrid wavelet is given by,

$$H_W = \begin{bmatrix} A_p \otimes B_{q(0:i_1)} \\ I_{r_0} \otimes \left(Ap_{/r_0} \otimes B_{q(i_1+1:i_2)} \right) \\ I_{r_1} \otimes \left(Ap_{/r_1} \otimes B_{q(i_2+1:i_3)} \right) \\ \vdots \\ I_{r_{n-1}} \otimes \left(Ap_{/r_{n-1}} \otimes B_{q(i_{n-2}+1:i_{n-1})} \right) \\ I_p \otimes \left(B_{q(i_{n-1}:q)} \right) \end{bmatrix} \begin{matrix} \textbf{Resolution} \\ \text{Global} \\ \text{Semi-global}(1^{st}) \\ \text{Semi-global}(2^{nd}) \\ \vdots \\ \text{Semi-global}(n^{th}) \\ \text{Local} \end{matrix} \quad (1)$$

where $B_{q(i:j)}$ represents the rows i to j of B matrix of size q and $A_{p/r}$ represents A matrix of size p/r. Here, the transform matrix A of size p and its lower order matrices of sizes p/r_0, p/r_1, ….p/r_{n-1} are multiplied (using Kronecker product) with certain rows of B transform matrix. Note that the rows of B are not repeated. The scaling operation used in the generation of existing wavelets like Haar, has been replaced by making use of lower order matrices of transform matrix A. The shifting operation is being realized by making use of the identity matrix (I) which is multiplied (using Kronecker product) with the lower order hybrid transform components. The lower the order of the transform matrix A, the higher is the order of I matrix by the same factor.

For example, employing the component transforms Walsh and Kekre transform matrices of sizes p = 4 and q = 3 (Walsh 4X4 and Kekre 3X3), a hybrid wavelet can be generated as in equation (2).

$$H_W = \begin{bmatrix} W_4 \otimes K_{3_{(0)}} \\ I_2 \otimes \left(W_{4_{/2}} \otimes K_{3(1)} \right) \\ I_4 \otimes \left(K_{3(2)} \right) \end{bmatrix} \quad (2)$$

which gives

$$H_W = \begin{bmatrix} 1 & 1 & 1 & 1 & 1 & 1 & 1 & 1 & 1 & 1 & 1 & 1 \\ 1 & 1 & 1 & 1 & 1 & 1 & -1 & -1 & -1 & -1 & -1 & -1 \\ 1 & 1 & 1 & -1 & -1 & -1 & -1 & -1 & -1 & 1 & 1 & 1 \\ 1 & 1 & 1 & -1 & -1 & -1 & 1 & 1 & 1 & -1 & -1 & -1 \\ -2 & 1 & 1 & -2 & 1 & 1 & 0 & 0 & 0 & 0 & 0 & 0 \\ -2 & 1 & 1 & 2 & -1 & -1 & 0 & 0 & 0 & 0 & 0 & 0 \\ 0 & 0 & 0 & 0 & 0 & 0 & -2 & 1 & 1 & -2 & 1 & 1 \\ 0 & 0 & 0 & 0 & 0 & 0 & -2 & 1 & 1 & 2 & -1 & -1 \\ 0 & -1 & 1 & 0 & 0 & 0 & 0 & 0 & 0 & 0 & 0 & 0 \\ 0 & 0 & 0 & 0 & -1 & 1 & 0 & 0 & 0 & 0 & 0 & 0 \\ 0 & 0 & 0 & 0 & 0 & 0 & 0 & -1 & 1 & 0 & 0 & 0 \\ 0 & 0 & 0 & 0 & 0 & 0 & 0 & 0 & 0 & 0 & -1 & 1 \end{bmatrix}$$

Here the first p (=4) rows represent global components, the next p rows represent semi-global and the last p rows represent local components of the hybrid wavelets.

With A and B as component transforms, hybrid wavelet H_W can be formed in the following different ways:

1) p and q can take different values for the same value of n, both being the factors of n.

2) A and B can be interchanged, if the transform matrices of the corresponding sizes exist.

3) The values of i_0 through i_{n-1} can be varied such that size of H_W remains pq x pq.

B. Properties of Hybrid Wavelet

1) Orthogonal: The hybrid wavelet follows the principle of orthogonality i.e.

$$H_W * {H_W}^T = \mu_W \quad (3)$$

$$\mu_w = \begin{bmatrix} \mu_{A_p} \otimes \mu_{B_{q(0:i_1)}} \\ \mu_{A_{p/r_1}} \otimes \mu_{B_{q(i_1+1:i_2)}} \\ \mu_{A_{p/r_2}} \otimes \mu_{B_{q(i_2+1:i_3)}} \\ \vdots \\ \mu_{A_{p/r_{n-1}}} \otimes \mu_{B_{q(i_{n-2}+1:i_{n-1})}} \\ \mu_{B_{q(i_{n-1}:q)}} \end{bmatrix} \quad (4)$$

where μ_W is a diagonal but may not be an identity matrix and μ_A and μ_B are the diagonal matrices given by $\mu_A = AA^T$ and $\mu_B = BB^T$.

2) Hybrid wavelet coefficients: To calculate the hybrid wavelet coefficients F, of a one-dimensional discrete function f, we use,

$$F = H_W * f \quad (5)$$

and to obtain the discrete function from the coefficients F we use

$$f = {H_W}^T * {\mu_W}^{-1} * F \quad (6)$$

The coefficients D of a two-dimensional function d are obtained by

$$D = H_W * d * {H_W}^T \quad (7)$$

And the inverse is obtained by first calculating G matrix whose (i,j)th element is given by,

$$G_{ij} = \frac{H_{W_{ij}}}{\mu_{w_{ij}}} \quad (8)$$

where $\mu_{Wij} = \mu_{Wii} * \mu_{Wjj}$ for all values of i and j.

Then,

$$d = G^T * D * G \quad (9)$$

Energy in each transform coefficient D in frequency domain is given by

$$E_{ij} = \frac{{D_{ij}}^2}{\mu_{wij}} \quad (10)$$

Thus the total energy in the function d is given by

$$E = \sum_{i,j=1}^{n} \frac{{D_{ij}}^2}{\mu_{wij}} = \sum_{i,j=1}^{n} {d_{ij}}^2 = input\ energy \quad (11)$$

III. Algorithm for Palmprint Identification

The hybrid wavelet developed in the previous section has been used with various component transforms for the purpose of multi-spectral palmprint identification. As transforms and wavelets are known to show energy compaction in the lower frequency coefficients and higher frequency coefficients are minusculed, it is possible to discard these low energy (high frequency) coefficients. This is the basis for the reduction in feature vector size. The algorithm used in the process is as shown in the figure 1.

A. Enrollment phase:

Each ROI extracted palmprint image is transformed using the hybrid wavelet transform as generated in section II using equation (1). The hybrid wavelet transform is generated using transforms matrices A and B, which can be any of the existing orthogonal transforms like DCT, Walsh, Kekre, etc. The size of the hybrid wavelet matrix is the same as that of the palmprint image used; here the image is 128X128 (n = 128), the H_W is of the same size and is generated with values of p = 16, and q = 8 (or any other factor combination like p = 32 and q = 4). Various component transforms were tried and the best results were obtained using a hybrid wavelet with Walsh and DCT as component transforms.

Energy in each transform coefficient is its magnitude squared and scaled by the energy matrix coefficient, μ_{Wij} of hybrid wavelet as in equation (10). The coefficient energy matrices of all database images are averaged to generate mean energy matrix. This energy matrix is divided into blocks of 4x4 and mean of each block is calculated, thus reducing the size to 32x32. This is primarily done to reduce the feature vector size. These mean energy values of mean energy matrix are arranged in descending order of individual component energy and those blocks are selected whose cumulative energy is more than threshold energy. The selected blocks form the **Energy Map**. The standard deviation values of the transform coefficients of these blocks are the Feature Vector. Higher the threshold energy larger the feature vector size and better the identification rate. But beyond certain threshold energy value, there is negligible increase in the identification rate, though the feature vector size increases considerably.

B. Identification Phase:

The ROI extracted test palmprint is transformed and its energy matrix is generated. This is also divided into 4x4 blocks and the mean energy of each block is calculated. Those blocks are selected which map to the energy map as generated in enrollment phase. Then the standard deviation values of the transform coefficients of these blocks of the test palmprint are its features.

C. Matching criteria:

Absolute Distance (AD) has been used as a distance measure to compare the FV of test image (FV_t) with that of each image in the database (FV_d). The m_{th} AD between the test image and m_{th} database image is given by equation (12)

$$AD_m = \sum_{i=1}^{s} \left| FV_{ti} - FV_{(dm)_i} \right| \quad (12)$$

where s is the number of enrolled images. A genuine match is defined as a match between the palmprints from the same palm and an imposter match is the match between the palmprints from different palms. If the AD is lower than a given threshold value, a match is obtained. This value of threshold is varied to obtain the genuine acceptance ratio (GAR) and false acceptance ratio (FAR). The performance of the proposed method is obtained by plotting the receiver operating characteristics (ROC) and calculating the equal error rate (EER).

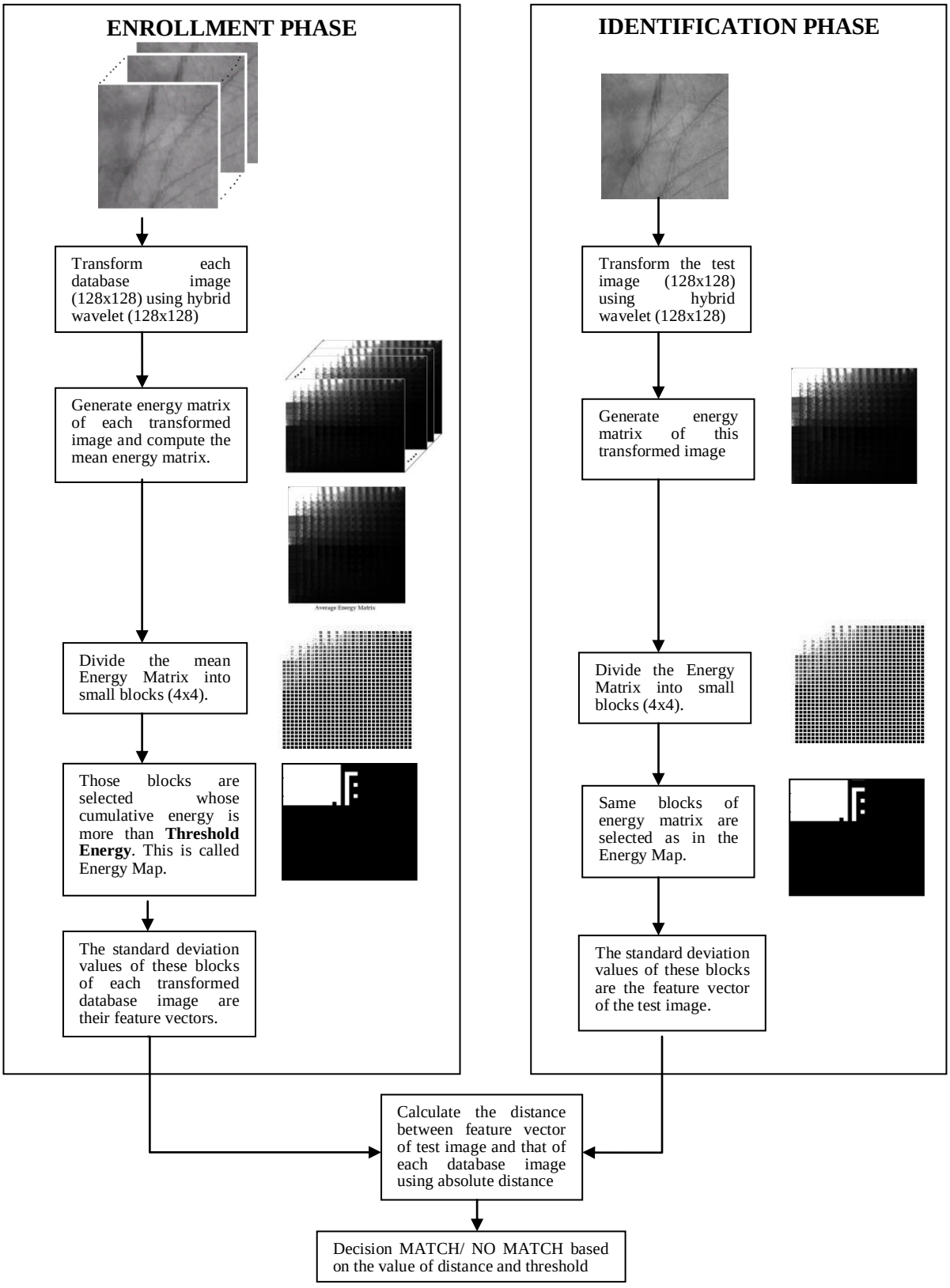

Fig 1. Flow diagram of algorithm for palmprint identification using the proposed method

D. Score Level Fusion Scheme

Fusion of the scores obtained for multi-spectral palmprints under red, green and blue (RGB) illumination is done to combine the characteristics of palmprints under each illumination. The fusion rules aim at improving the performance of a system from that of a single palmprint. Fusion can be done at three general levels: feature level, score level and decision level. The score level fusion of feature sets has been used most commonly and gives significant improvement in performance. In this paper we have used score level fusion for multi-spectral palmprint images to combine the scores produced individually for multispectral palmprint images under red, green and blue illuminations [10] (henceforth referred to as R, G and B images) as shown in Figure 2. Three types of fusions schemes using AND and OR operators are used to combine scores and final matching decision can be taken for either of the three fusion strategies. Considering S_R, S_G and S_B as the scores produced for R, G and B images respectively, they have been combined in the following three ways to obtain the final score S_F:

I. $S_F = S_R$ OR S_G OR S_B
II. $S_F = \{S_R$ AND $S_G\}$ OR $\{S_R$ AND $S_B\}$ OR $\{S_B$ AND $S_G\}$
III. $S_F = S_R$ AND S_G AND S_B

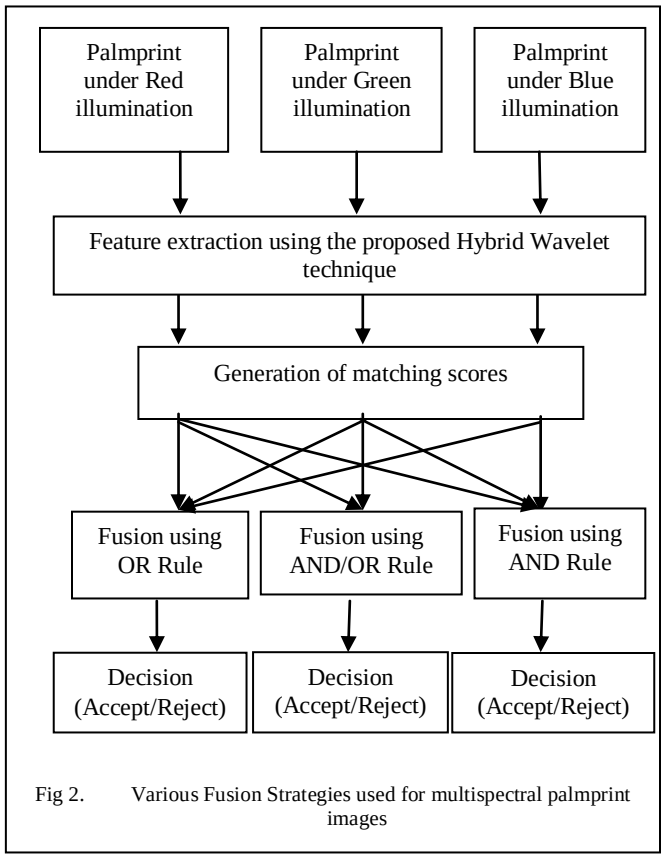

Fig 2. Various Fusion Strategies used for multispectral palmprint images

For different applications requiring different levels of security, various score level fusion strategies can be used. The fusion strategy using AND operator is more stringent, as it gives a match only when all R, G, and B images match and hence is used for applications requiring higher level of security whereas OR operator is more liberal in terms of security but better in accuracy. In between these two extremes is the AND/OR based fusion rule which is a compromise between level of security and accuracy.

IV. Results and Discussion

A. Database

This experiment was performed on the multi-spectral palmprint database of Hongkong Polytechnic University, which consists of multi-spectral palmprint images under R, G and B illuminations. As different features of palmprints are captured at different wavelengths of light, multi-spectral palmprints are more effective in the analysis. Multispectral imaging in any area is supposed to preserve detailed radiance information and has great discriminative power[19].

The database [16] used here comprises of three sets of 6000 (12 samples of 500 persons) ROI extracted palmprint images of size 128 x 128, each under red, green and blue illuminations. For the experiment purpose, each of these sets has been divided into 2 sets: 4800 (12 samples of 400 persons) as enrolled and 1200 (12 samples of 100 persons) as imposters' palmprints. For genuine palmprint identification each of the 4800 palmprints of the enrolled set is individually treated as test image and matched against the remaining 4799 palmprints. For checking imposter identification, each of the imposters' palmprint set is treated as test image and matched against the enrolled set.

B. Results

For multi-resolution analysis of multi-spectral palmprints, many component transform pairs from DCT, Walsh, Kekre, Haar for generating hybrid wavelet have been tried. The best results obtained are using DCT (8x8) and Walsh (16x16 and lower order) as component transform matrices and have been discussed here. The performance of the proposed method has been quantitatively evaluated using False Reject Rate (FRR), False Acceptance Rate (FAR) and Equal Error Rate (EER). For evaluation of FRR, each of the 4800 images of each of the R, G and B set is considered as a test image and identified against the remaining 4799 images. For calculation of FAR, 1200 images of the test set are identified against 4800 images of the training set. Once the matching results are obtained, we get the complete palmprint matching score using rule based score-level fusion. The experimental results show that significant improvement in the performance can be achieved from the combination of scores of multi-spectral palmprint images. Figure 3 shows the plot of GAR vs. FAR for all the three fusion schemes and it can be observed that OR-based fusion scheme gives the best performance for GAR. The ROC plot for the three fusion scheme shown in figure 3, indicate that the EER obtained for OR-based fusion scheme is the least at 1.833%, whereas for AND-based fusion scheme it is 2.604%. The value of threshold (static) at which EER is seen to be lower for OR-based fusion and is 375 and for AND-based fusion technique the same is 810. The higher the value of threshold, more secure the system is. Another parameter called security index has been introduced, which can be used to judge the performance of a system with respect to security and can be defined as

$$S_p = \frac{T_Z}{T_E} \quad (13)$$

where, T_Z is the maximum value of threshold for which FRR is zero and T_E is the value of threshold where EER is obtained. S_P is security index and lies between 0 and 1 and if the value is 1 then it is an ideal system in terms of security at which EER becomes zero. For the proposed system, the values of S_P for AND and AND-OR based fusion systems are 0.875 and 0.887 respectively and for OR based fusion system it is obtained as 0.853, clearly indicating that AND based systems are highly secure.

Hence it can be concluded that the proposed method, when used with AND-based fusion technique can be used for applications where high level of security is demanded and OR-based fusion where higher efficiency is required with slight compromise in security.

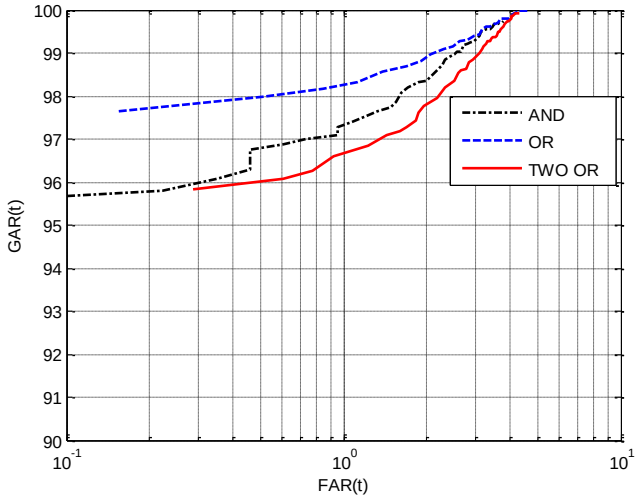

(a)

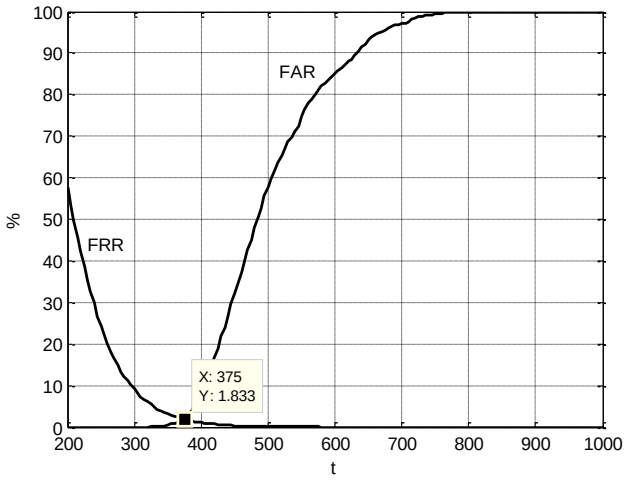

(b)

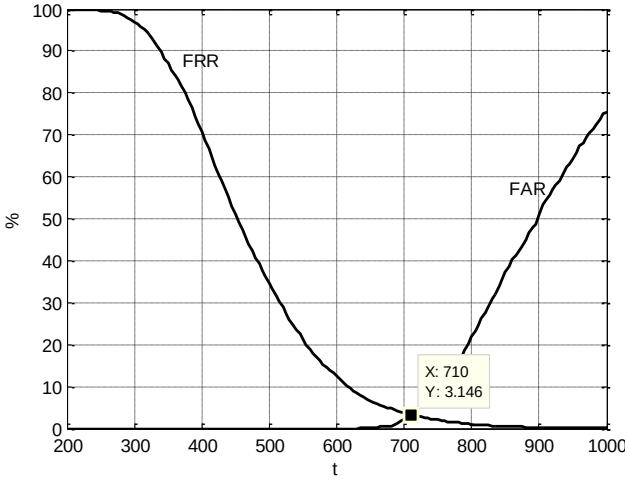

(c)

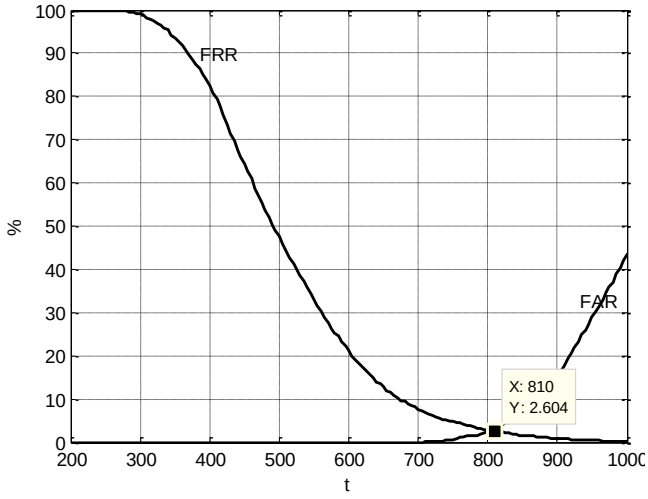

(d)

e at
ısed

c) AND-OR based d) AND based fusion

V. CONCLUSION

In this paper palmprint identification using a new hybrid wavelet employing multi-resolution analysis is proposed. The hybrid wavelet used here is a flexible wavelet which analyzes functions at all levels of resolutions where number of components at each level can be controlled and the wavelet itself can be varied by using different component transforms. The hybrid wavelet used here gives far better performance than the individual component transforms in various applications like image data compression, content-based image retrieval etc. Multi-spectral palmprints are identified using the features generated by energy compaction of the hybrid wavelet coefficients and fusion of the scores of each set of the red, green and blue images using OR and AND based techniques is used to find best system. The performance of the proposed method is analysed by calculating equal error rate and security performance index and the values of EER of 1.833% suggests that system using OR-based fusion scheme

gives better performance efficiency, whereas S_P of 0.887 and 0.875 for AND-OR and AND fusion based system respectively indicate that these are highly secured systems. Future scope where hybrid wavelet with more than two different transforms can be used for palmprint identification. Application of this technique for other biometrics is open for further analysis and research.

REFERENCES

[1] Anil K. Jain, Encyclopedia of Biometrics, Springer Publication, August 27, 2009

[2] Yingbo Zhou and Ajay Kumar. Human Identification Using Palm-Vein Images. IEEE Transactions on Information Forensics and Security, vol. 6(4) 2011, p.1259-1274.

[3] X. Wu, K. Wang and D. Zhang, "Line feature extraction and matching in palmprint", *in* Proceeding of the Second International Conference on Image and Graphics, 2002, p. 583-590.

[4] C.C. Han, H.L. Cheng, C.L. Lin and K.C. Fan, "Personal authentication using palm-print features", *Pattern Recognition*, vol. 36, no. 2, 2003, p. 371-381.

[5] Lu, G., David, Z., Wang, K., "Palmprint recognition using eigenpalms features", Pattern Recognition Letters, 24(9-10), 2003, p 1473-1477.

[6] X.Q. Wu, D. Zhang, K. Q. Wang, "Fisherpalms Based Palmprint Recognition", Pattern Recognition Letters, vol. 24, 2003, pp. 2829-2838,

[7] David Zhang, Zhenhua Guo, Guangming Lu, Lei Zhang, and Wangmeng Zuo. An Online System of Multi-spectral Palmprint Verification. IEEE Transactions on Instrumentation and Measurement, vol. 59(2), 2010, p. 480-490,

[8] Dong Han, Zhenhua Guo, and David Zhang. Multispectral Palmprint Recognition using wavelet-based Image Fusion. International Conference on Signal Processing, 2008, p.2074-2077.

[9] David Zhang, Wai-kin Kong, Jane You and Michael Wong. On-line palmprint identification. IEEE Transactions on Pattern Analysis and Machine Intelligence, vol. 25(9) 2003, p.1041-1050.

[10] L. Zhang, Z. Guo, Z. Wang, and D. Zhang. Palmprint Verification using Complex Wavelet Transform. ICIP (2), 2007, p. 417-420,

[11] G. Lu, K. Wang and D. Zhang "Wavelet based feature extraction for palmprint identification", Second International Conference on Image and Graphics, 2002, p. 780-784.

[12] A. Kumar and D. Zhang, "Personal authentication using multiple palmprint representation", Pattern Recognition, vol. 38, no. 10, 2005, p. 1695-1704,

[13] W. Li, D. Zhang, and Z. Xu. Palmprint Identification by Fourier Transform. Int'l J. Pattern Recognition and Artificial Intelligence, vol. 16(4), 2002, p. 417-432.

[14] Dr. H.B.Kekre, Dr. Tanuja Sarode, Rekha Vig, "Automated Fingerprint Identification System based on Sectorized Complex Walsh Plane", IJCA Proceedings on International Conference on Technology Systems and Management (ICTSM), 2011, p. 6–11.

[15] Dr. H.B.Kekre, Dr. Tanuja Sarode, Rekha Vig. Unified Fast Algorithm for Most Commonly used Transforms using Mixed Radix and Kronecker product. International Journal of Computer Science and Information Security, 2011, p. 271–350.

[16] http://www.comp.polyu.edu.hk/~biometrics/MultispectralPalmprint/MSP.htm

[17] Dr. H.B.Kekre, Dr. Tanuja Sarode, Rekha Vig, Pranay Arya, Aashita Irani, Saurabh Bisani, Palmprint Identification using Kronecker Product of DCT and Walsh Transforms for Multi-spectral Images, International Conference on Hand-Based Biometrics , 2011.

[18] Dr. H.B.Kekre, Dr. Tanuja Sarode, Rekha Vig, Pranay Arya, Aashita Irani, Saurabh Bisani, Identification of Multi-spectral Palmprints using Energy Compaction by Hybrid Wavelet, International Conference on Biometrics, 2011

[19] Zhenhua Guo, David Zhang, Lei Zhang, and Wenhuang Liu. Feature Band Selection for Online Multispectral Palmprint Recognition. IEEE Transactions on Information Forensics and Security, vol. 7(3) 2012, p.1094-1099.

Method for Psychological Status Estimation by Gaze Location Monitoring Using Eye-Based Human-Computer Interaction

Kohei Arai[1]
Graduate School of Science and Engineering
Saga University
Saga City, Japan

Ronny Mardiyanto[2]
Department of Electronics Engineering
Institute Technology of Surabaya
Surabaya City, Indonesia

***Abstract*—Method for psychological status estimation by gaze location monitoring using Eye-Based Human-Computer Interaction: EBHCI is proposed. Through the experiment with English book reading of e-learning content, relation between psychological status and the distance between the correct location of English sentence reading points and the corresponding location derived from EBHCI is clarified. Psych9ological status is estimated from peak alpha frequency derived from eeg signals. It is concluded that psychological status can be estimated with gaze location monitoring.**

Keywords—psychological status; gaze estimation; computer input by human eyes only

I. INTRODUCTION

These experiments are aimed for measuring and monitoring the student attention. The student attention monitoring will be useful for a teacher evaluates the learning process under e-learning system. In the e-learning system, the interaction between teacher and student is limited. The occurred interaction is only under the content in the e-learning system. Hence, the student monitoring is being investigated to obtain the best way to monitor and evaluate the performance of a student.

Computer key-in system by human eyes only (just by sight) is proposed [1],[2]. The system allows key-in when student looks at the desired key (for a while or with blink) in the screen keyboard displayed onto computer screen. Also blink detection accuracy had to be improved [3],[4]. Meanwhile, influence due to students' head pose, different cornea curvature for each student, illumination conditions, background conditions, reflected image (environmental image) on students' eyes, eyelashes affecting to pupil center detection, un-intentional blink, etc. are eliminated for gaze detection accuracy improvement [5],[6]. On the other hands, the system is applied for communication aid, having meal aid, electric wheel chair control, content access aid (e-learning, e-comic, e-book), phoning aid, Internet access aid (including Web search), TV watching aid, radio listening aid, and so on [7]-[17].

The method for key-in accuracy improvement with moving screen keyboard is also proposed [18]. Only thing student has to do is looking at one of the following five directions, center, top, bottom, left and right so that key-in accuracy is remarkably improved (100% perfect) and student can use the system in a relax situation.

The following section describes the proposed method for psychological status estimation by gaze location monitoring using EBHCI followed by some experiments with English book reading of e-learning content. Then conclusion is described together with some discussions.

II. PROPOSED METHOD

A. System Configuration

System configuration of the proposed method is shown in Figure 1. We create a software consisting function as follow: (1) Tracking the eye, (2) Estimating the user sight, (3) Sight trajectory and blinking logger, and (4) EEG signal logger. In Figure 1, it explains the methodology of our investigation. In our methodology, user/student access/use the e-learning content using personal computer. The used e-learning content consist of teacher voice (we recorded it using recorder and storage it as voice data) and the text shown on the screen. These two content are connected each other. The saying voice has same timeline with the text, so student could follow the teacher voice (hearing using ear phone) while he read the text on screen.

The concept of our this experiment is how we could make a relation between the eye behavior to student attention, so we would measure the student attention by synchronizing between hearing voice and the student sight/gaze to text on the screen. We compare between the trajectory sight points on the text with the true one. We make assumption of the relation between student attentions and sight point as if student do not looking at the displayed text while the teacher voice speaking at, we judge it as student do not focus to the content. Otherwise, if student could follow the teacher voice by looking at on the same text, we judge it as student focus to the content. The difference between true trajectory text points and user sight trajectory point will be evaluated to determine whether the student is focus to the content or not. Also, we measure the happened blinking manually through the saved video file saved while experiment is conducted. We count the number of blinking and record it by time frame.

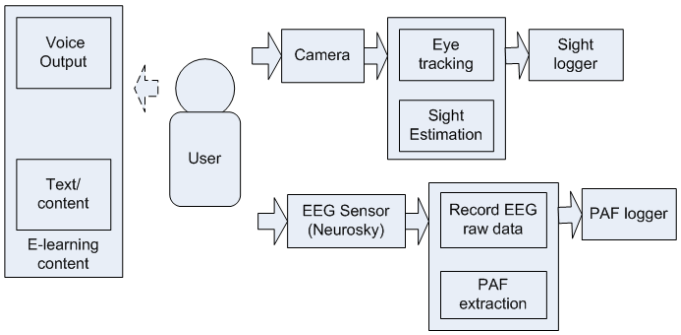

Fig.1. System configuration of the proposed psychological status estimation with EBHCI

We measure the brain activity of student simultaneously. We record the raw EEG data by using Neurosky mindset EEG sensor. This EEG signal will represent the brain condition of student whether student under the stress condition or not. Such stress condition could be measure by using Peak Alpha Frequency of EEG signal.

B. Hardware Configuration

Major specifications of the proposed system including the eeg sensor used are as follows,

1) Measures:

We record the EEG signal by using NeuroSky Mindset EEG sensor and OpenVibe software. By using the openvibe software, we could record the EEG signal and process it to peak alpha frequency.

- Raw-Brainwaves
- EEG power spectrums (Alpha, Beta, etc.)
- eSense meter for Attention and Meditation
- Quality of data being collected (can be used to detect poor contact and whether the device is off the head)

2) Signal and EEG:

- Maximum signal input range: 1mV pk-pk
- Hardware filter range: 3Hz to 100Hz
- MS001: includes 60Hz environmental AC noise filtering
- MS002: includes 50Hz environmental AC noise filtering
- Amplification gain: 2000x
- ADC resolution: 12 bits (-2048 to 2047)
- Sampling rate: 512Hz
- eSense interpretation update rate: 1Hz
- 0% byte loss (ie packet loss)
- 1Hz eSense interpretation rate
- UART Baudrate: 57,600 Baud
- SPP through put: 9600 Baud
- S/N ratio: >70dB
- Class 2 Bluetooth Radio Range: 10 m 6dBm RF max power
- 250kbit/s RF data rate

3) Bluetooth Dongle:

- Bluetooth Standard: V2.0+EDR (backward compatible with V1.1/V1.2)
- Profiles support: Serial Port, Dial Up Networking, Fax, Headset, Printer, PIM Item Transfer, PIM Synchronization,

  File Transfer, LAN Access, Generic Object Exchange, Object Push, HCRP, HID, A2DP, AVRCP
- Frequency Range: 2.402-2.480 GHz / 79 Channel FHSS
- Transfer rates (Max): 3 Mbps(Max)
- Power Class: Class 2 (10M distance)
- Receiving Sensitivity: -80dBm at 0.1% BER
- Antenna: Integrated Antenna
- Current Consumption: Standby mode: 25mA / Transmission mode: 80mA
- Interface: USB A type
- LED indicator: Power on
- OS Support: Windows 2000 / XP / Vista / 7

4) Power/Battery

- USB Jack Rating: DC5V 1A
- USB Jack Insertion Force: 2Kgf max.
- USB Jack Life: 5000 Cycles (INTERNAL ONLY. NOT FOR CONSUMER)
- USB Jack Size: Mini-B Type Jack (7.7×9.9×3.9mm)
- Rate Power: 30mW
- Max Power: 50mW
- Battery Run time: 7 hours
- Battery Capacity: 550mAh

- Battery Charging Time: 4 hours

C. Eye Tracking and Line of Sight Estimation

We use the eye tracking method utilizing adaptive threshold and pupil knowledge which is robust for various users and illumination changes. Our system utilizes IR camera mounted on glass to allow user`s movement. Pupil knowledge such as shape, size, location, and motion are used. This knowledge works based on the knowledge priority. Pupil appearance such as size, color, and shape is used as first priority.

When this step fails, then pupil is estimated based on its location as second priority. If all steps failed, then we estimate pupil based on its motion as last priority. The eye tracking block diagram is shown in Figure 2. We develop our software under C++ Visual Studio 2005 and OpenCv Image processing Library which can be downloaded as free on their website. Our system utilize infrared web camera NetCowBow DC-NCR 131 as real time data input. This camera has benefit when illumination changes. By using 7 IR LED, this camera will adjust the illumination. This will cause the input image has minimum influence against illumination changes. The camera is mounted on the glass.

Outlook of the eeg sensor is shown in Figure 3. Meanwhile, example of the raw eeg signal and its spectral data as well as frequency component is shown in Figure 4

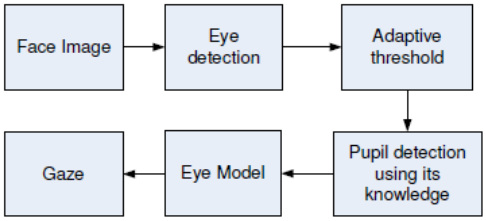

Fig.2. Eye tracking and line of sight estimation

Fig.3. Outlook of the eeg sensor

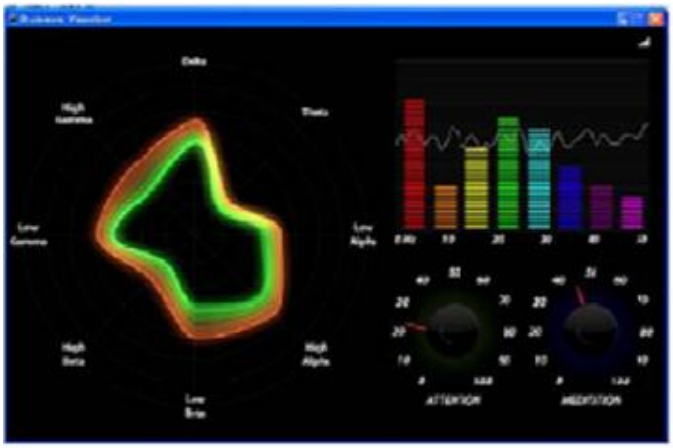

Fig.4. Example of raw eeg signal and its spectral data as well as frequency component

D. Peak Alpha Frequency

Peak Alpha Frequency: PAF is measured using NeuroSky and OpenVibe software. Peak Alpha Frequency: PAF of eeg signals [1] represent how relax do students during learning processes with e-learning contents [19].

In order to connect NeuroSky with OpenVibe, we installed OpenVibe v.7. First, OpenVibe is connected with neurosky by using openvibe acquisition server as depicted in Figure 5. After acquisition server is opened and start the connection, the streamed EEG data were ready for acquiring. We use openvibe designer to create scenario and play it. The used scenario for PAF measurement is depicted in Figure 6 and 7.

[1] http://www.springerlink.com/content/pj62w726373h45x6/ http://www.carelinks.net/books/ch/memory.htm

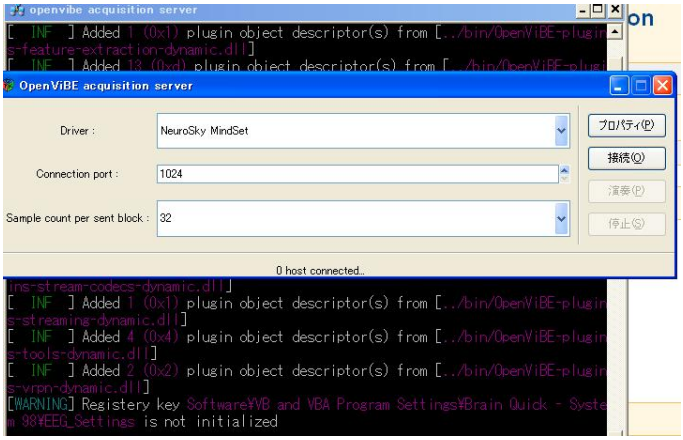

Fig.5. Connect between acquisition server and designer tool

As depicted in Figure 6, we acquire streamed EEG data by using Acquisition client box. This box will take data from openvibe acquisition server. After streamed EEG data were taken, we use signal display box to display the signal as depicted in Figure 7.

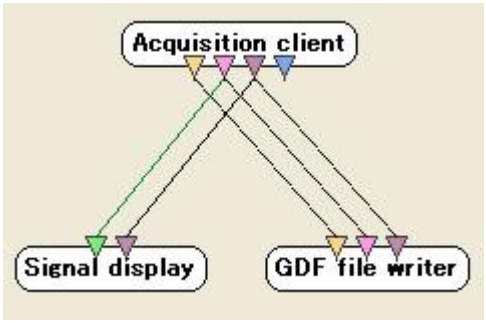

Fig.6. Scenario for recording EEG data

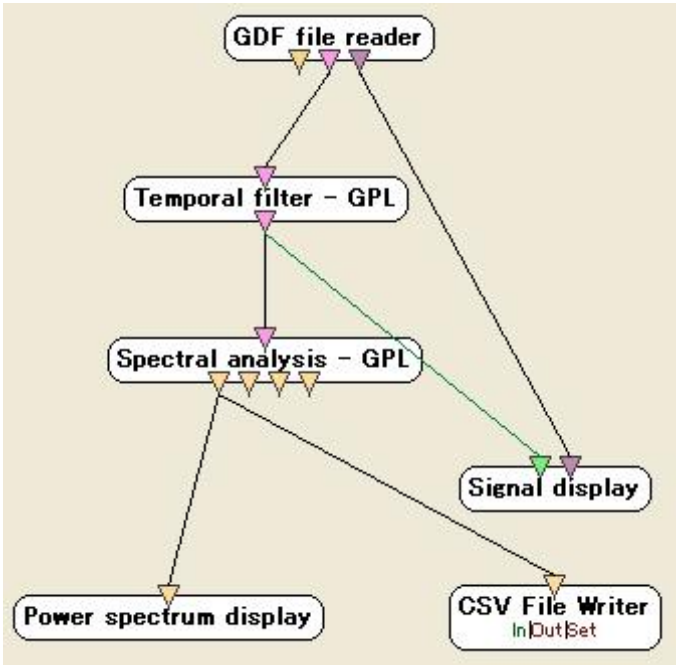

Fig.7. Scenario for converting EEG signal spectrum frequency

Also we use GDF file writer to save the streamed EEG data into file. After we save the streamed EEG data, next is selection of alpha band and show its spectrum frequency. We use temporal filter box (Filter method is set to Butterworth, filter type is set to Band pass, filter order is set to 4, Low cut frequency is set to 6 Hz, High cut frequency is set to 15 Hz, and Pass band ripple is set to 0.5 dB). After selection of alpha range, next is convert to power spectrum. We use spectral analysis (FFT operator) to convert this signal into power spectrum. The output of power spectrum then is saved into CSV file by using CSV File writer box. The power spectrum display is shown in Figure 8 and streamed EEG signal is shown in Figure 9.

After we got alpha spectrum, next is determination of peak alpha. Next calculation was done by using Math Lab. We determine Peak Alpha Frequency by using command line of Math Lab and output will be saved into excel file as follow,

```
clear
fid = fopen('PAFronny1.txt', 'wt');
load ronny1.dat
[n,p] = size(ronny1)
t=0

tmax=0;
for step=0:(n/256-1)
max=0;
for t = 1+(256*step):256+(256*step)
   if (max<ronny1(t,2))
      max=ronny1(t,2);
      tmax=t-(256*step);
   end
end
fprintf(fid, '%f    %f  %f\n', step,max,tmax);
step
max
tmax
end
fclose(fid)
```

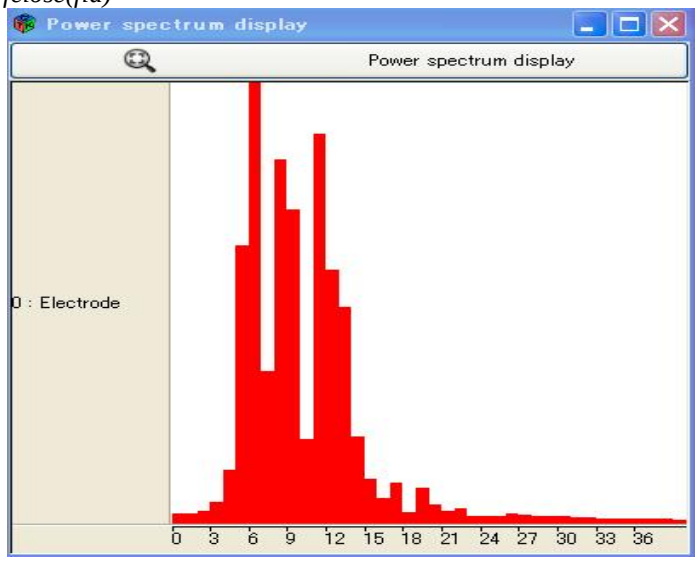

Fig.8. Power spectrum display

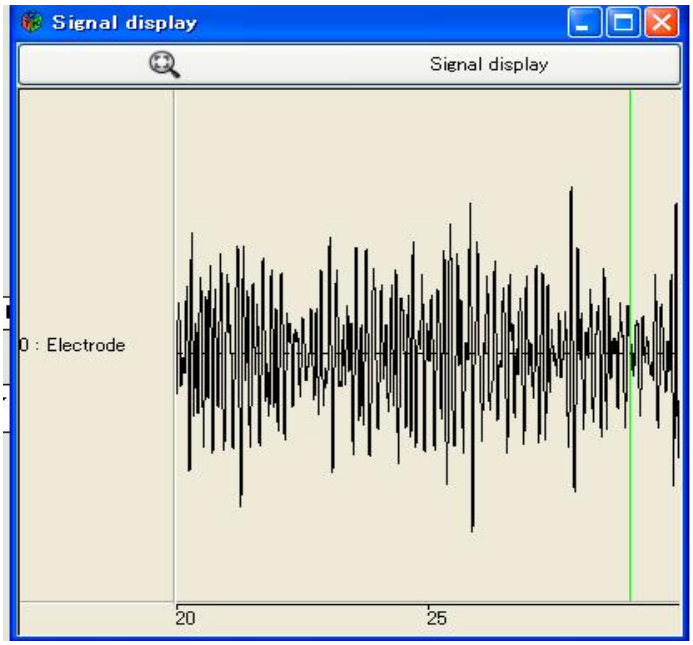

Fig.9. Streamed EEG signal

As example of PAF, we conducted two experiments: (1) Resting condition by using closed his eye and (2) condition when user was reading. The PAF of resting condition is shown in Figure 10 and PAF of reading condition is shown in Figure 11.

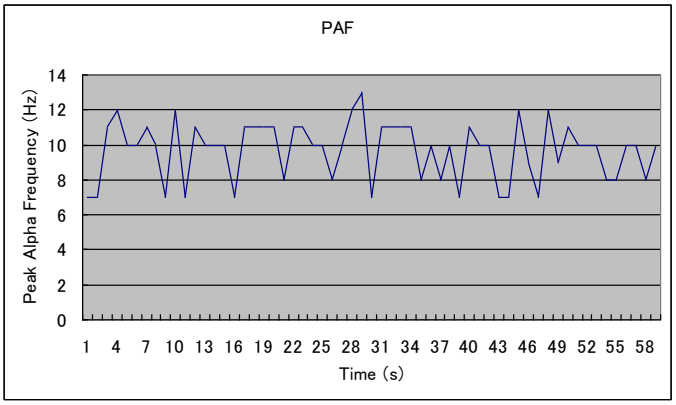

Fig.10. resting condition

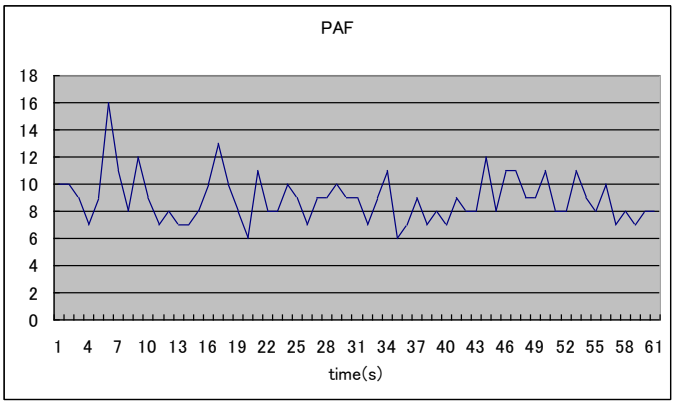

Fig.11. Reading condition

The average of PAF of resting condition is 9.695 Hz and reading condition is 8.902 Hz. It is make sense that according to Klimesch journal that PAF will decrease when the task demand is increase. In the experiment data, PAF decrease about 0.793 Hz.

E. Gaze Location Estimation

In Figure 12, it is shown gaze location distribution. This distribution was taken while user was looking at 6 keys serially. While user looking at these key, we recorded the gaze result and created its distribution. This figure shows that at key 5, the gaze result has more scattered than others. It was caused by the position of eye at this key little bit occluded and it made the gaze result become unstable (the instability become increase).

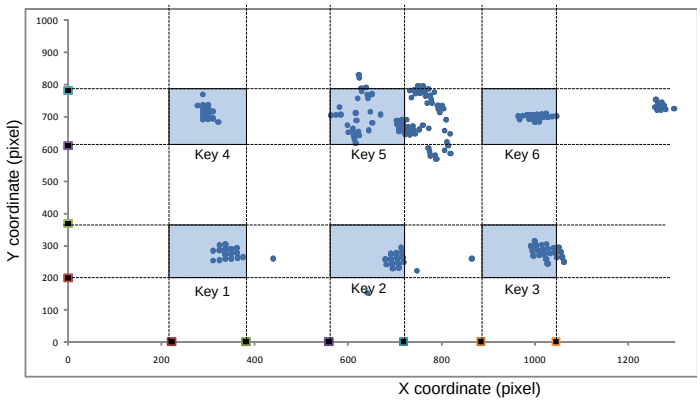

Fig.12. Example of the estimated gaze location plots for six targeted keys

3D distribution of gaze location is illustrated with Matlab. Figure 13 was calculated from distribution of gaze result of all keys. Normalization is required for the points (points coordinate – keys coordinate) of each key and calculate the distribution by using this code (matlab code as follows,):

```
xd = inputx(:,1); %x input
yd = inputy(:,2); %y input
n = 49;
xi = linspace(min(x(:)), max(x(:)), n);
yi = linspace(min(y(:)), max(y(:)), n);
xr = interp1(xi, 0.5:numel(xi)-0.5, x, 'nearest');
yr = interp1(yi, 0.5:numel(yi)-0.5, y, 'nearest');
% [yr xr]: Y then X because the plotting commands take matrices that look
% like Z(y-coord, x-coord)
Z = accumarray([yr xr] + 0.5, 1, [n n]);
figure(1);
surf(xi, yi, Z);
xlabel('x');
ylabel('y');
zlabel('count');
```

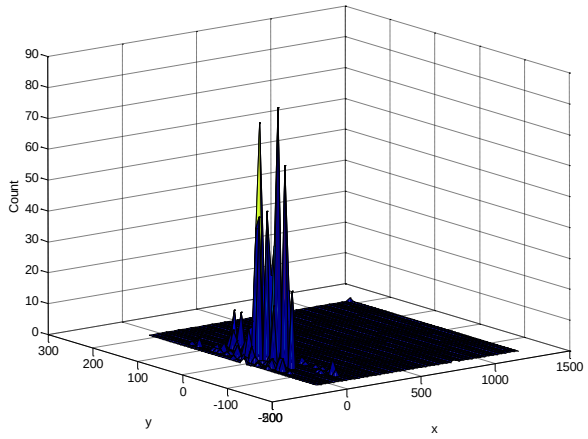

Fig.13. Example of 3D distribution of gaze location estimated for the case of the aforementioned six targeted keys

III. EXPERIMENTS

A. Method of the Experiment

The experiment is conducted by the following steps,

1) User sit on the prepared seat
2) User wears the glasses camera sensor
3) User uses ear phone to hear the sound instruction
4) User wear the Electroencephalograph (EEG, Neurosky mind set)
5) All the sensor above were wear simultaneously
6) Take a calibration of the sight estimation system
7) Our system play the recorded voice representing the text on the screen
8) Student has to read the text in the same time with the hear audio voice from ear phone
9) We record the trajectory of user gaze, blinking, and the EEG signal
10) We analyze the data

Figure 14 shows the English book reading used for the experiment.

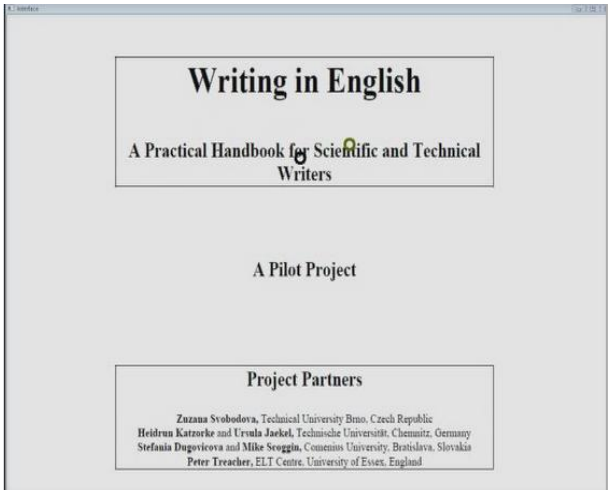

Fig.14. Example of reading types of e-learning contents

Students read the English book by character by character, by word by word, by sentence by sentence, and by page by page. The location at which content creator would like students to look at is indicated with black circle while the location at which students is looking at is also indicated on display with green circle. Therefore, the distance between two locations can be calculated by frame by frame. In the meantime, eeg signal is acquired. Thus relation between psychological status derived from eeg signal and the distance between two locations results in estimation of psychological status with gaze movement.

B. *Modification of eeg Sensor*

The neurosky (eeg sensor) is replaced to the eye glasses as shown in Figure 15. The two positions of electrodes are used in the experiment to measure the difference between two points of head (one point is at center of two eyes and another one is at forehead). The main goal of this experiment is for measuring signal to noise ratio (SNR). Unfortunately, the experiment was done using two computers separately. Due to this, the recorded signals are difficult to compared directly using raw signal. Fortunately, we already know that the glasses will be used for measuring the brain load activity. Therefore, I just made comparison in output of Peak Alpha Frequency (PAF). We could judge whether two points of electrodes have similar or same output through the PAF output. If the two points of electrodes have similar output, we could see it through the shape of PAF signal. Otherwise, if the two points of electrodes are different (noise is too high), we will see the different shape of PAF signal. The output signal of PAF is shown in Figure 16.

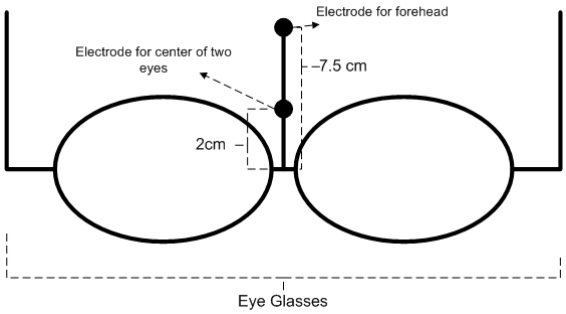

Fig.15. eeg sensor attached to the glass.

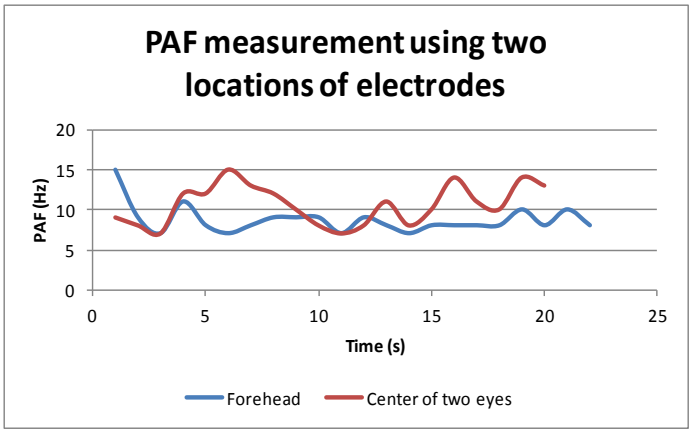

Fig.16. PAF measurement result

The output of PAF signals has different shape. It means that the placement of electrode at center of eyes is different with the placement of electrode at the forehead. So, my conclusion is the modification of neurosky to neuroglasses sensor has to put the sensor in the forehead (same point/location with the original neurosky sensor).

C. *Results from the Experiment*

We record three kind of data: (1) Blinking, (2) Sight trajectory point, and (3) EEG signal. By using these data, we would investigate the relationship/correlation between eye behaviors to user attention level.

Blinking

We count the happened blinking manually (from the saved experiment video). The blinking data by valuating the closed eye as "1" and opened eye as "0" we present the blinking data as shown in Figure 17.

In the data above, it shows that increasing the time (in frame, 4 frame per second), the frequency of blinking occurrence increases. It shows that the blinking has a linear correlation to student attention. Such situation happen caused by student become tired follows the content under long duration and he need take a rest a while through closing the eye. After taking a rest (by closing the eye), student becomes fresh again to follow the content.

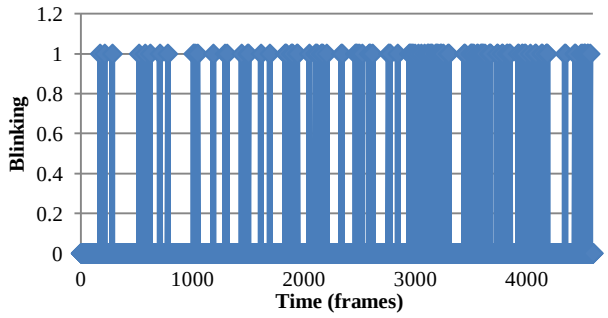

Fig.17. Blink occurence

To analyze student attention using the sight, we calculate the error by measuring the distance between the sight trajectory points and the real point (tracked manually). It is shown in Figure 18.

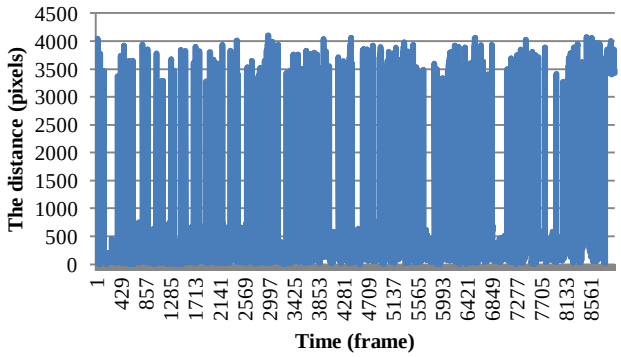

Fig.18. The difference of Sight trajectory points to the true one

The time frame in Figure 18 is 8 frames per seconds. From the figure above, we can see that on the frame above to 2800, the frequency of error increase. It is caused by student was looking at different point with the true one (the true one collected manually and used it as the true reference).

Also, we investigate the correlation between student attentions monitoring to EEG signal. We acquired the EEG signal while student using e-learning system and calculate the peak alpha frequency. The PAF data is shown in Figure 19.

In the figure above, it is not clearly when student focus to content or not. It may happen because a human has ability to recovery his brain performance by doing physiological action such as blinking, taking a rest for a while, etc.

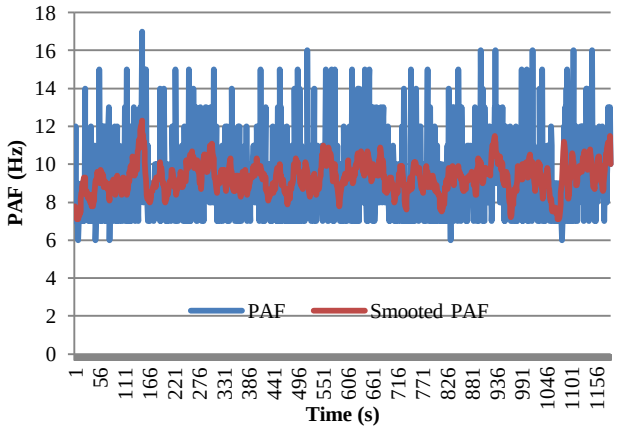

Fig.19. Student attention measurement using EEG

Figure 20 shows the example of the location at which content creator would students like to look at and the location at which students are looking at one page of English reading book.

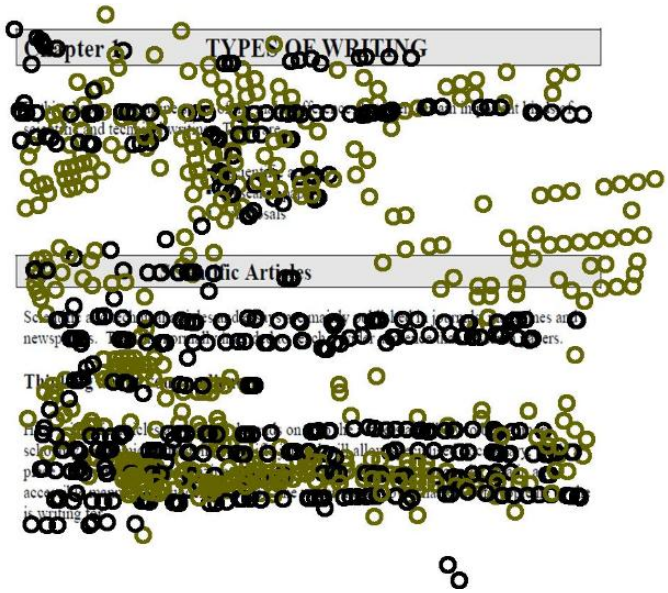

Fig.20. example of the location at which content creator would students like to look at and the location at which students are looking at one page of English reading book

As shown in Figure 20, the distance between two locations is sometime significant when the student take a long time to read and to understand the words. At that time PAF and alpha frequency component derived from eeg signal is decreasing results in student feels frustration.

IV. Conclusion

Method for psychological status estimation by gaze location monitoring using Eye-Based Human-Computer Interaction: EBHCI is proposed. Through the experiment with English book reading of e-learning content, relation between psychological status and the distance between the correct location of English sentence reading points and the corresponding location derived from EBHCI is clarified. Psych9ological status is estimated from peak alpha frequency derived from eeg signals. It is concluded that psychological status can be estimated with gaze location monitoring.

From the investigation data, we can conclude that for monitoring the student attention to e-learning content, the blinking is most dominant parameter that could be used to determine whether a student focus to content or not. The second dominant parameter is sight trajectory point although the high performance of sight estimation method has to be used to avoid the error/noise. The last dominant (less dominant) parameter is peak alpha frequency of EEG signal.

Acknowledgment

The author would like to thank participants to the experiments.

References

[1] Arai K. and H. Uwataki, Computer key-in based on gaze estimation with cornea center determination which allows students' movement, Journal of Electrical Engineering Society of Japan (C), 127、7、1107-1114、2007

[2] Arai K. and H. Uwataki, Computer input system based on viewing vector estimation with iris center detection from face image acquired with web camera allowing students' movement, Electronics and Communication in Japan, 92, 5, 31-40, John Wiley and Sons Inc.,2009.

[3] Arai K., and M. Yamaura, Blink detection accuracy improvements for computer key-in by human eyes only based on molforgic filter, Journal of Image Electronics Engineering Society of Japan, 37、5、601-609、2008.

[4] Arai K. and R. Mardiyanto, Real time blinking detection based on Gabor filter, International Journal of Human Computer Interaction, 1, 3, 33-45, 2010.

[5] Arai K. and R. Mardiyanto, Camera mouse and keyboard for handicap person with trouble shooting capability, recovery and complete mouse events, International Journal of Human Computer Interaction, 1, 3, 46-56, 2010.

[6] Arai K. and M. Yamaura, Computer input with human eyes only use two Purkinje images which work in a real time basis without calibration, International Journal of Human Computer Interaction, 1, 3, 71-82, 2010.

[7] Arai K., and K. Yajima, Communication aid based on computer key-in with human eyes only, Journal of Electric Engineering Society of Japan, (C), 128 -C, 11, 1679-1686, 2008.

[8] Djoko P., R. Mardiyanto and K. Arai, Electric wheel chair control with gaze detection and eye blinking, Artificial Life and Robotics, AROB Journal, 14, 694,397-400, 2009.

[9] Arai K. and K. Yajima, Communication Aid and Computer Input System with Human Eyes Only, Electronics and Communications in Japan, 93, 12, 1-9, John Wiley and Sons, Inc., 2010.

[10] Arai K., R. Mardiyanto, A prototype of electric wheel chair control by eye only for paralyzed student, Journal of Robotics and Mechatronics, 23, 1, 66-75, 2010.

[11] Arai K. and K. Yajima, Robot arm utilized having meal support system based on computer input by human eyes only, International Journal of Human Computer Interaction, 2, 1, 120-128, 2011.

[12] Arai K. and T. Herman, Automatic e-comic content adaptation, International Journal of Ubiquitous Computing, 1,1,1-11,2010

[13] Arai K., T. Herman, "Method for Real Time Text Extraction from Digital Manga Comic", International Journal of Image Processing, 4, 6, 669-676, 2011.

[14] Arai K., T. Herman, Module based content adaptation of composite e-learning content for delivering to mobile devices, International Journal of Computer Theory and Engineering, 3, 3, 381-386, 2011.

[15] Arai K., T. Herman, Method for extracting product information from TV commercial, International Journal of Advanced Computer Science and Applications, 2, 8, 125-131, 2011

[16] Arai K., T. Herman "Module Based Content Adaptation of Composite E-Learning Content for Delivering to Mobile Learners", International Journal of Computer Theory and Engineering (IJCTE), Vol 3, No. 3, pp. 381-386, June 2011

[17] Arai K., T. Herman, Efficiency improvements of e-learning document search engine for mobile browser, International Journal of Research and Reviews on Computer Science, 2, 6, 1287-1291, 2011.

[18] Arai K., R. Mardiyanto, Evaluation of Students' Impact for Using the Proposed Eye Based HCI with Moving and Fixed Keyboard by Using EEG Signals, International Journal of Review and Research on Computer Science(IJRRCS), 2, 6, 1228-1234, 2011

[19] Siew Cheok Ng and P. Raveendran, EEG Peak Alpha Frequency as an Indicator for Physical Fatigue, Proceedings of the 11th Mediterranean Conference on Medical and Biomedical Engineering and Computing 2007 IFMBE Proceedings, 2007, Volume 16, Part 14, 517-520, DOI: 10.1007/978-3-540-73044-6_132

AUTHORS PROFILE

Kohei Arai**,** He received BS, MS and PhD degrees in 1972, 1974 and 1982, respectively. He was with The Institute for Industrial Science, and Technology of the University of Tokyo from 1974 to 1978 also was with National Space Development Agency of Japan (current JAXA) from 1979 to 1990. During from 1985 to 1987, he was with Canada Centre for Remote Sensing as a Post Doctoral Fellow of National Science and Engineering Research Council of Canada. He was appointed professor at Department of Information Science, Saga University in 1990. He was appointed councilor for the Aeronautics and Space related to the Technology Committee of the Ministry of Science and Technology during from 1998 to 2000. He was also appointed councilor of Saga University from 2002 and 2003 followed by an executive councilor of the Remote Sensing Society of Japan for 2003 to 2005. He is an adjunct professor of University of Arizona, USA since 1998. He also was appointed vice chairman of the Commission "A" of ICSU/COSPAR in 2008. He wrote 30 books and published 332 journal papers

A Survey of Environment and Demands Along with a Marketing Communications Plan for WatPutthabucha Market to Promote Agricultural Tourism through Main Media and Online Social Network Media

Kuntida Thamwipat
Department of Educational Communications and Technology
Faculty of Industrial Education and Technology
King Mongkut's University of Technology Thonburi
Bangkok, Thailand

Nakorn Thamwipat
Wat Phothaimanee Buddhism School
Wat Phothaimanee
Phetchaburi, Thailand

***Abstract*—This study was aimed to examine the current environment and the demands and to make a marketing communications plan for WatPuttabucha Market to promote agricultural tourism through main media and online social network media. Moreover, it was aimed to build up working experiences for research with communities near the campus through the integration of course instruction and community service. The data were collected in the second term of academic year 2012 between January and February 2013 in WatPuttabucha Market and nearby communities. There were 2 sampling groups as in King Mongkut's University of Technology Thonburi students (50 persons) and WatPuttabucha Market and nearby community members (50 persons). In total, there were 100 persons for the survey. This collection was based on an accidental basis. According to the data concerning the environment, WatPuttabucha Market had 9 interesting shops for agricultural tourism and 4 major tourist attractions. As for the demands, it was found that 47 students (or 94%) would like WatPuttabucha Market to be open as a site for agricultural tourism mainly on Saturday and Sunday. 47 persons from WatPuttabucha Market and nearby communities (or 94%) also would like it to be open mainly on Saturday and Sunday. As for the communicative plan, it was found that there were 7 kinds of main media. There were 5 kinds of online social network media for check-in special events. The majority of students (mean score of 4.89 and standard deviation of 0.86) agreed with the integration of research in their Marketing Communication course because it allowed them to get more familiar with communities near the campus and recommended continuing this similar project for the next year.**

Keywords*—Environment; Marketing Communications Plan; Demands; Agricultural Tourism; Main Media; Online Social Network Media

I. INTRODUCTION

Department of Educational Communications and Technology, Faculty of Industrial Education and Technology, King Mongkut's University of Technology Thonburi initiated an ETM 358 Marketing Communications course [1] based on theories and practical fieldwork. In this course, students are expected to be able to apply theories and practical knowledge for their research to make a marketing communications plan through the integration of course instruction and community service within the area near the campus. Simultaneously, the representative from WatPuttabucha Market committee Mr SangiamNagasuthi, the host of E-Radio programme on agricultural tourism [2], asked for collaboration from the Department to use new kind of media, i.e. online social network media, along with main traditional existing media to promote agricultural tourism around WatPuttabucha Market. Hence, this research study on the survey of environment and demands as well as a marketing communications plan to promote agricultural tourism for WatPuttabucha Market and nearby communities.

A. Research Objectives

1) To examine the current environment and the demands as well as to make a marketing communications plan to promote agricultural tourism for WatPuttabucha Market and nearby communities through online social network media and traditional media.

2) To build up working experiences for research with communities near the campus through the integration of course instruction and community service.

B. Expected Outcomes

1) There would be data about the current environment and the demands as well as the marketing communications plan for WatPuttabucha Market to promote agricultural tourism through main media and online social network media.

2) Participants in this research would gain working experiences for research with the communities near the campus through the integration of course instruction and community service.

C. Research Scope

The data in this research were collected in the second term of the academic year 2012 between January and February 2013 in WatPuttabucha Market and nearby communities only.

II. Population and Sampling Group

To make a survey of the environment and the demands as well as a marketing communications plan, there were 2 sampling groups as in King Mongkut's University of Technology Thonburi students (50 persons) and WatPuttabucha Market and nearby community members (50 persons). In total, there were 100 persons and the data were collected on an accidental basis.

III. Variables in This Study

Below are the variables in this study:

A. *The current environment of WatPuttabucha Market for agricultural tourism.*

B. *The demands on WatPuttabucha Market for agricultural tourism.*

C. *The marketing communications plan for WatPuttabucha Market for agricultural tourism through main media and online social network media.*

IV. Research Methodology

Below are the tools used in this research:

A. *The data regarding the current environment of WatPuttabucha Market for agricultural tourism were collected through practical fieldwork for 2 months between January and February 2013 from WatPuttabucha Market and nearby communities.*

B. *The demands on WatPuttabucha Market for agricultural tourism were collected through a questionnaire.*

C. *The marketing communications plan for WatPuttabucha Market to promote agricultural tourism through main media and online social network media were collected through practical fieldwork and interviews with community leaders.*

V. Research Results

A. *The current environment of WatPuttabucha Market for agricultural tourism*

1) *Food and Dessert from 9 interesting shops.*

a) Curry noodle: Location At the beginning of SoiPracha-Utit69, Pracha-Utit Road, Chef's dish:Meat curry noodle, Special flavour noodle, delicious curry soup, Price regular 20 Baht / special 30 Baht.

Fig. 1. Curry noodle.

b) Pork Noodle by Sister Sa: Location In front of Lotus Pracha-Utit Department Store, Chef's dish: Pork noodle, Price: regular 15 Baht/Special 20 Baht/Takeaway 25 Baht.

Fig. 2. Pork Noodle.

c) Wooden House Restaurant: Location SoiPuttabucha24 orRama II RoadSoi33, a few blocks from Rung-arun School, Chef's dish -Healthy food such as Mushroom salad, fried rice with gourami, grouper in chilli sauce, fried egg, fried rice with shrimp paste, tofu salad, Price 59-99 Baht.

Fig. 3. Healthy food.

d) Seafood Restaurant (Sister Priaw): Location Pracha-Utit91, Chef's dish:Crab meat fried rice and other kinds of seafood, Price from 40 Baht.

Fig. 4. Seafood Restaurant.

e) Bunnak Vietnamese Restaurant: Location Before PuttabuchaSoi 24, Chef's dish:Vietnamese sausage salad, Prawn in tiles, Vietnamese fried cake, pork rice ball, Price between 30-150 Baht.

f) Elephant's Neck Noodle Shop: Location SoiPuttabucha45, Chef's dish:Duck noodle, duck rice, pork satay, crunchy pork; Desserts include ladcheag, grilled sticky rice, Price regular noodle30 Baht/ special35 Baht/ with thigh 40 Baht.

Fig. 5. Bunnak Vietnamese Restaurant.

Fig. 6. Elephant's Neck Noodle Shop.

g) Duck Jelly Thanan: Location Pracha-Utit Soi54, Chef's dish:Duck jelly with fragrant coconut, Price small box of 14 pieces 30 Baht/ big box of 42 pieces 80 Baht.

Fig. 7. Duck Jelly Thanan.

h) Dessert Shop Auntie Supaporn: Location Bangmod Housewife Community in SoiPuttabucha 36, Chef's dish:Pandan cake (Sukothai royal palace), filled bun, auspicious desserts (for wedding and merit occasions), Price Large tray of pandan cake350 Baht/3 bags of filled bun10 Baht/ Egg threads 250 Baht per kilogramme.

Fig. 8. Dessert Shop Auntie Supaporn.

i) Malabar tamarind Juice: Location Behind WatPuttabucha, near fish food shop at WatPuttabucha quayside, Recommended drink: malabar tamarind juice which could last for 2 months under the research by AjarnWannaphop Klomklieng, King Mongkut's University of Technology Thonburi, Priceone bottle13 Baht/150 Baht per kilogramme.

Fig. 9. Malabar Tamarind Juice.

2) Major tourist attractions.

a) Buddhism-Muslim Religious Centre: There are 3 old mosques: Darunnaeem, Al-Istikomah and Darul-Aeihsan (Sornsomboon).

b) Trail of 4 temples in Bangmod Area: WatBangmodSothararam, WatLuangPorOpasi, WatYairom and WatPuttabucha.

c) Community service around WatPuttabucha: Bangmod Massage Service Centre, Handmade Product by Government-Samaggi Housewife Group, Spots for freeing and feeding fish, Bangmod Cruise service.

d) Agricultural tourism spots: Mango garden of Uncle Praneet, Orchid garden of Auntie Saluay, Uncle Sawaeng, Orchid garden of Puttabucha, Orange orchard of Uncle Peed, Ideal orange orchard of Mr SupornWongjinda.

B. The Demands on WatPuttabucha Market for Agricultural Tourism

1) According to the survey on 50 King Mongkut's University of Technology Thonburi students,

It was found that there were 31 men or 62% and 19 women or 38%. The majority was in their first year (29 persons or 58%). It was found that the majority of the sampling group (28 persons or 56%) had never been to WatPuttabucha Market. However, the majority (47 persons or 94%) would like WatPuttabucha Market to be a site for agricultural tourism in Bangmod area.

The majority or 62% would like a retro style of market and this was followed by 22% of the sampling group who would like a floating market. The majority or 52% would like the market to be open mainly on Saturday and Sunday.

TABLE I. SHOWS THE BEHAVIOURS OF EXPOSURE TO MAIN MEDIA

Exposure to main media	Number persons	Percentage
Printing materials	32	34%
TV programmes	30	32%
Radio programmes	16	16.5%
Open area broadcasting	16	16.5%
Others	1	1%

TABLE II. SHOWS THE BEHAVIOURS OF EXPOSURE TO ONLINE SOCIAL NETWORK MEDIA OR ALTERNATIVE MEDIA

Exposure to online social network media and other alternative media	Number persons	Percentage
Internet	39	53.42%
Online social network such as facebook and twitter	26	35.62%
Community radio	5	6.85%
Others such as word of mouth	3	4.1%

TABLE III. SHOWS THE DEMANDS ON SPECIAL ACTIVITIES IN THE MARKET

Opinion	Number persons	Percentage
Food and product festivals	30	50.85%
Live bands	12	27.12%
Tourist attractions	16	20.34%
Others such as innovation	1	1.69%

Further Suggestions: 1.It was expected that there would be more vegetable, fruit and organic food stalls than gift shop and clothes stall. and 2. This was a good project and it should be developed seriously.

2) According to the survey on 50 WatPuttabucha Market and nearby community members,

It was found that the sampling group consisted of 30 men (60%) and 20 women (40%). The majority were aged between 41-50 years (15 persons or 30%). The majority or 56% earned less than 15,000 Baht per month. The majority (47 persons or 94%) would like WatPuttabucha Market to become a site for agricultural tourism and the majority or 42% would like it to be open mainly on Saturday and Sunday.

TABLE IV. SHOW THE BEHAVIOURS OF EXPOSURE TO MAIN MEDIA

Exposure to main media	Number persons	Percentage
Printing materials	20	20%
TV programmes	30	31%
Radio programmes	29	29%
Open area broadcasting	19	19%
Others	1	1%

TABLE V. SHOWS THE BEHAVIOURS OF EXPOSURE TO ONLINE SOCIAL NETWORK MEDIA OR ALTERNATIVE MEDIA

Exposure to online social network media and other alternative media	Number persons	Percentage
Internet	14	21%
Online social network such as facebook and twitter	8	12%
Community radio	37	56%
Others such as word of mouth	7	11%

TABLE VI. SHOWS THE DEMANDS ON SPECIAL ACTIVITIES IN THE MARKET

Opinion	Number persons	Percentage
Food and product festivals	31	53.45%
Live bands	7	12.07%
Tourist attractions	16	27.59%
Others such as innovation	4	6.89%

Further Suggestions: 1.WatPuttabucha Market should be developed in terms of hygiene and order. and 2. If there is a development plan, it should be done seriously and in a concrete manner.

C. The Marketing Communications Plan for WatPuttabucha to Promote Agricultural Tourism through Main Media and Online Social Network Media

a) Main Media could be classified into 7 kinds as follows:

1) Production of TVC about Longka Market at WatPuttabucha (duration: 15 minutes).

2) Production of radioSpot about Longka Market at WatPuttabucha (duration: 30 seconds).

3) Production and Design of Mobile Advertisement.

4) Production and Design of Booklet about Longka Market at WatPuttabucha.

5) Production and Design of Leaflet about Longka Market at WatPuttabucha.

6) Production and Design of Vinyl to promote Longka Market at WatPuttabucha.

7) Production and Design of Brochure to promote Longka Market at WatPuttabucha.

b) Samples of Main Media

Fig. 10. TVC aboutL Longka Market at WatPuttabucha.

c) Details regarding Check-In (Event)/special activities through online social network and alternative mediacould be classified into 5 kinds:

- Planning Check-in activitieson various Social Media networks. When visitors arrive at Longka Market at WatPuttabucha, they could use their mobile phone to confirm their arrival and registration process to get a souvenir (a miniature of giant doll for modern-day mobile phone users). This was a virus-based marketing type which makes use of online social network to

reduce the cost in accordance with the strategy called 'Above the Line'.

- Using Facebook to advertise main media such as TVC to invite visitors to come and to participate in the activities at the market.
- Using Facebook to announce the auspicious events such as paying homage to Buddha images, Buddhist Lent, Magha Puja Day, and Vesak.
- Using Facebook to announce other marketing promotion campaign for fruit season such as mango during the early year and orange during the end of the year.
- Organising a photo competition event about Rongka Market at WatPuttabucha on facebook.

Fig. 11. Booklet.

d) Samples of online social network media and alternative media.

Fig. 12. Online Social Network Media.

Fig. 13. Alternative Media.

e) Result from the integration of community research in the Marketing Communications course.

The majority of the students (mean score of 4.89 and standard deviation of 0.86) strongly agreed with the integration of community research in the Marketing Communications course because it allowed them to get more familiar with the communities near the campus and they would like this project to continue in the next year. Moreover, the Department submitted a report about the survey results, demands and a marketing communications plan to the governmental organization in the community in March 2013.

VI. Discussions

According to the research study, it was found that the sampling group looked forward to the development of WatPuttabucha Market through the collaboration from many relevant organisations. Such policy was in compliance with the Green idea proposed by Jacquelyn A. Ottman cited in WeeraManaruaysombat [3] in that the world is changing and so is the expense behaviour of the housewives. Therefore, there must be a campaign to raise awareness of environment. Moreover, internet has improved dramatically and with its high speed of data distribution, internet has become an interactive medium for people to share information and discuss various issues ranging from agriculture, tourism and the like. Therefore, all relevant bodies should be aware of this trend.

VII. Suggestions

A. Suggestions from Research Results

The research results show that both students and community members would like WatPuttabucha Market to become a site for agricultural tourism. Therefore, the relevant governmental sectors and the private organizations should collaborate to develop it intensely in the retro form or a floating market. Moreover, online social network should be considered along with main media for distribution of information.

B. Suggestions for Further Research

There should be a survey study on the environment and the demands of agricultural products through main media and online social network media in the communities behind Thonburi Rom Park and around King Mongkut's University of Technology Thonburi as a way to integrate it in the Marketing Communications course next year.

References

[1] Department of Educational Communications and Technology, Faculty of Industrial Education and Technology, [Online], Avaiable: http://edt.kmutt.ac.th//ectmoodle, 2013, [Retrieved 10 February, 2013].

[2] Department of Educational Communications and Technology, Faculty of Industrial Education and Technology, [Online], Avaiable: http://202.44.14.12/e-broadcast/eradio.html, 2012, [Retrieved 8 February, 2013].

[3] Weera Manaruaysombat, 2011, Green Marketing: Blueprint for Globalized World. ARIP: Bangkok.1st Imprint, pp.32, 38-39.

Draft dynamic student learning in design and manufacturing of complex shape parts

Ivana Kleinedlerová; Peter Kleinedler
STU MTF in Trnava
Detached workplace STU MTF Dubnica n/V
Dubnica nad Váhom, Slovakia

Alexander Janáč; Ivan Buranský
Slovak University of Technology in Bratislava
Faculty of Materials Science and Technology in Trnava
Trnava, Slovakia

***Abstract*—The contribution deals with the dynamic teaching of students through blended learning and teaching online distance teaching which can be considered nowadays to be a very effective and dynamic education of students. Content of the article is focused on the sphere of programming with CNC machines and use Cax systems for the production of a particular shape complex part - shearing knife. The article presented also proposed effective teaching resources. The motivation for solution of this project is that dynamic education leads students to gaining experience and skills, individual identification of the issue, creativity, suggestion of problem solving variations. The achieved way of education and its confirmed and verified positive results can be applied for various target groups of students and their fields of study.**

Keywords—dynamic education blended learning; e-learning; CA systems.

I. INTRODUCTION

Latterly, is recorded growth of the use of information technologies that can be considered as tools for improving the efficiency of teaching students. In this regard, the most suitable technology of education through e-learning, e.i. electronic education can be considered appropriate [1]. The multi-medial learning in the form of electronic teaching materials being available on the Internet has been concerned. One of the advantages of the e-learning way is a possibility of students to communicate with a teacher or other workers in a distance way what results in efficiency and speed of the education independently of the place of school [2]. Current trend in education has also been the so called blended learning – combined education which represents the conventional teaching students by a teacher in a classroom and the e-learning education [3].

The aim of this contribution is to present a proposal on-line dynamic teaching students of department Computer-aided manufacturing technologies for the production of a particular shape complex part - shearing knife, which is part of the rolling forming tool for the production of extrusion. Students propose a design and documentation process for the production by blended learning through classroom teaching and the realization of the knife follow the classroom through online distance teaching. In practical terms, it means to prepare for students e-learning instructional materials in the manufacturing of forming tools and work in specific CAD and CAM systems. Then use throughout the realization of shearing knife CAD and CAM systems - that automate the design and technological work and production, and ultimately use blended learning and on-line distance learning, in which students are able to follow the entire process of production shearing knife. The aim of teaching students is also achieved, to design a suitable method of making from the perspective of rationalization - that is, to design production of knife in achieving the in minimum time, in the required accuracy of product and minimize consumption of materials. In the dynamic e-learning and teaching is an advantage for students to have the opportunity to justify the steps taken with the possibility of asking questions of the real-time production knife.

The project is carried out at field offices of STU MTF Dubnica nad Váhom, that does not have a machine park. Students thus solving technical proposal knife through CAD and CAM systems and production of knifes follow classroom using web camera in the workplace STU Trnava. On the present belongs to the advanced manufacturing technology 5-axis machining. The 5-axis machining belongs at present to the most frequent used production methods for a single-part production as well as for a small-butch production. This is a progressive method which markedly reduces the production time and thereby the factory price. The 5-axis machining production requires qualified manpower from the point of the workshop programming as well as the CAM system programming. Therefore, the shearing knife production will also take place through the progressive machining methods.

II. TOOLS OF DYNAMIC EDUCATION FOR STUDENTS AND BASIS FOR ITS IMPLEMENTATION

Practical experiences confirm, that any information from internal and external school environment is necessary to consider, generalize, sort and analyze in the fastest possible way. Therefore the ground of dynamic education is to motivate students to adopt techniques of active work with informations, ergo searching process ,relevant information sorting and combining of knowledge, which leads to creation and vindication of own opinion. The main difference between traditional educational approach , based on passive acceptance of knowledge and active dynamic education is , that the traditional education in form of lectures and seminars gives students ,,ready-made ‘’ theoretical studying materials, while practical-dynamical exercises gives space for gaining skills, acknowledging principles of team work, resp. Solving of individually given tasks, when is necessary systematically search for and to gather the newest information about given

subject. Combination of this two educational approaches is preferred to gain effective dynamic education model. Techniques of effective dynamic education leads students to individual identification of the issue, creativity, experiments, suggestion of problem solving variations, reevaluation of solutions, visualization, outcome testing and feedback. It's implementation into educational process leads to transformation of student position from receivers of theoretical information to the problem solvers. Active action of students in education rise their motivation for gaining new knowledge and skills and experience and enable straight theory application on real conditions simulated in multimedia class [4].

Currently accepted and worldwide implemented basic trends of applied designed dynamic education for students were also reflected in our project and can be summarized in the following aspects [4]:

- Allover system of education and practical education of students for all parts of component production implementation.
- Education and practical education continuity throughout all the study on university.
- Combining of education and practical education from engineering companies point of view (classes realized by companies, specialized practice for students offers and so on) with self-education of students.
- "Learning" become a part of given tasks and projects solving for students and is adequately appreciated , what is for them important motivation factor.
- Application of modern educational and training methods (like e-learning, learning-by-doing, visual learning etc.) through multimedia and internet technologies.

Dynamic methods of education in general is possible to divide in three groups [4]:

1) Informational methods: Contains mainly lectures, seminars, conference, video projection, systematical observation, and instruction with computer assistance, creativity exercise.

2) Simulation methods: Contains examples, program group exercises.

3) Practical education: Involves practical education of students while real problem solving, e.g. Production proposition.

According to the authors, who conducted projects of dynamic teaching students, they considered as her effective and most used resources [4]:

1) Multimedia e-learning: Concept multimedia in this case express connection of image, text or visual information-educational texts. Virtual education offers in electronic way many studying materials and information and by this form of education is maximally used IT and internet.

2) Visualized education as part of e-learning : Visualized education might be defined as giving information via illustrations , photographs, graphs, symbols, pictures or other visual models. Goal and assignment of visualized education is to simplify and shorten the process of introduction of complex information, in other words, enable to understand the thought on first sight. Higher level of visualized education presents the presentation of dynamic visual information, for example instruction video, video-clips and animations, instead of static only visualization, as is defined above.

3) „On the job training" – OJT : Currently educationally promising developing area of teaching, is the use of on-line camera with high picture quality in solving of specific given tasks (projects), and troubleshooting. This is the solution of practical examples of manufacturing components in the presence of the teacher, providing advices to solve of given project, practical skills training, using the same techniques as in engineering practice, analysis of failure technique and the like. An on-line conference led by a teacher, team members communicate each other and suggest possible solutions to production of parts. These were used in our dynamic education for students of PPT proposition, and within were proposed and presented effective ways of education for reaching desired target – effective dynamic education for students of PPT (Fig. 1).

Fig.1. Illustration of Videoconferencing [4]

III. The State Education Department of Computer Aided Manufacturing Technologies for Field Offices Dubnica

On the present our Detached workplace (hereinafter DP) does not possess any machineries which could be used for practical teaching of the mentioned section students.

Most of such activity is substituted by a video-demonstration of production of selected components or visiting engineering factories. Students thus miss the integrated viewpoint and practical skill with the design and production of e.g. a specific component where they could have a possibility of the self-realization, verifying their knowledge acquired at the practical example as well as the possibility to suggest the more potential effective production. Teaching the subject: Computer support of production technologies has been a key subject of the section named Computer support of production technologies which is offered by Slovak University of Technologies, Faculty of Material Science and Technologies (hereinafter STU MTF). Therefore, is this problem solved by the creation of on-line learning taking place

in the online classroom, which is interconnected in collaboration with the Center of Excellence for the MTF STU Trnava. It is a workplace that has a modern machine park.

IV. Creating Training Materials for CAD Modeling and CAM Programming

Given the interest of teachers to provide students with high quality and up to date training materials for the teaching of the subject, the educational system has been oversaturated with technological (computer) information in the form of multimedial education texts trying to give students quality information and the latest knowledge for the concrete educational subject in the time as quickly as possible [5]. The offered educational materials in the framework of the subject: Computer support of production technologies alternate from each other depending upon their author, required tasks being solved, practical contribution, etc. That is why in the framework of soluting this project, the educational materials have been modified and reduced in such a way so that students can study the necessary problem of the 5-axis machining, modeling and programming in the relevant CA system and based on the obtained knowledge they are able to solve also given tasks within the framework of their self-study. Educational texts were necessary to create in regard to knowledge level of students and regarding their previous secondary school study or practical skills from the sphere of engineering production of components.

The educational materials for students were created:

1) Electronic textbooks : from time to time are actualized, which contains simulations, animations and presentations. These are presented to students on the official page of faculty, where students can download it anytime or they have been send to academic information system in section ,,documents'', where they can always check actualized materials and download it. Electronic textbooks are published mainly in hypertext form , and are appropriately elaborated even for self education of subject without a teacher. E- learning textbooks uses animations , voice guide, dictionary, text finder, cross reference related to the electronic publication theme on the internet.

2) *In the PowerPoint program:* in the form of slides which included basic information from the sphere production components, design and manufacture of forming tools, modelling and by means of CA system programming whereby the most important information was highlighted with bold letters (Fig. 2). The information was contentually balanced for the needs of soluting the given task. Materials are available to students on-line at a distance without physical contact and attendance at local schools, too.

Fig.2. The slide created in MS PowerPoint

3) In program "Notepad": was created the final test (Fig.3) in each teaching area to verify their own knowledge gaps and students. Its advantage is that it allows students to get immediate feedback on the ability to obtain new knowledge [6]. Test was created to positively motivate students to engage in self-study and the ability to understand the basic things that are expected of this test. That notepad is located on a server MTF - KAIA, and is available to students at any time and from anywhere (with Internet access), and outside the classroom, too. Testing of students in the program "Notepad - Notepad" took place at the beginning of each lesson to verify their knowledge acquired in previous hours of teaching [7]. Also the test was used in the final evaluation of the student.

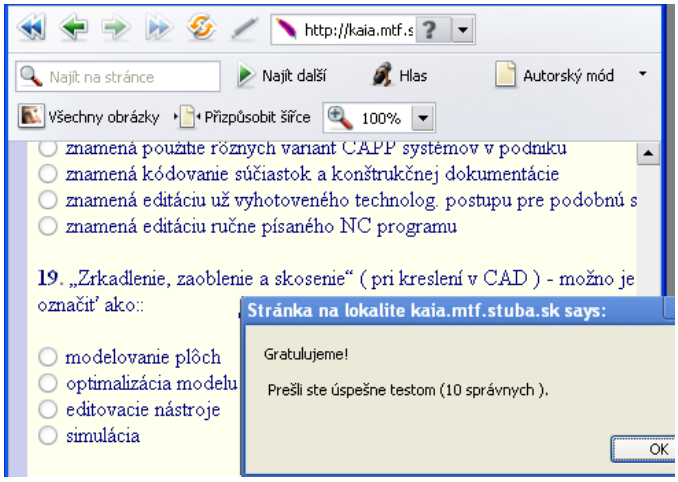

Fig.3. Test created using "Notepad" [11]

4) *In programs MS OFFICE*: were developed text-pictorial procedures for modeling (Fig. 4) and programming of the knife in the relevant CA system. These were created for all areas of modeling and programming steps of knife. Materials are available to students on-line at a distance without physical contact and attendance at local schools.

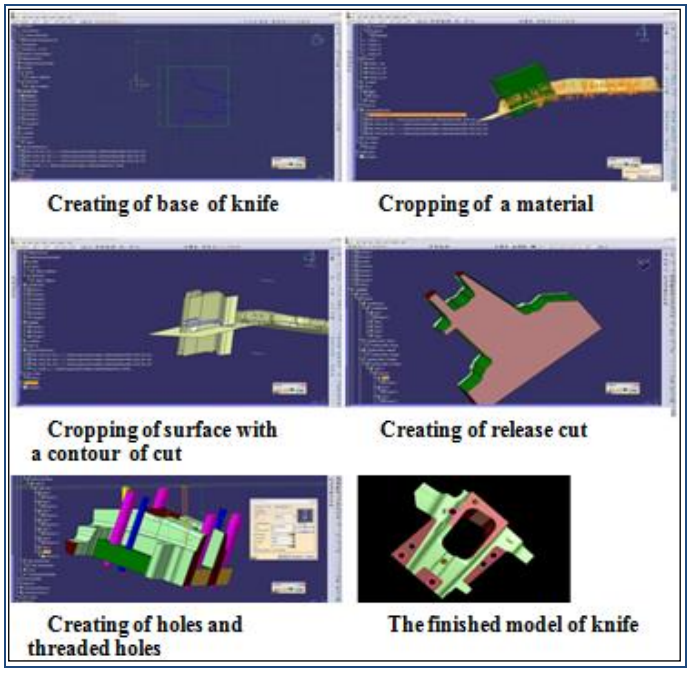

Fig.4. Text-pictorial procedures for modelling of knife

5) The video instructions: to create a text-pictorial procedures were created the video instructions (Fig. 5). As the component can be modeled several techniques - methods of modeling and programminng, were presented in video-all manual modeling techniques that offer a specific program design, in which the students drew. To enable students to understand the various techniques of painting. User-created video is also available to students on-line at a distance without physical contact and attendance at local schools.

Fig.5. . Video-manual for programming

6) Supplemental materials: since not all students solving the project had experiences with an engineering component manufacturing, it was necessary for them to create even more extensive teaching background. These have been addressed in the form of presentation materials in PowerPoint that contain text with Internet connections for graphics and video-examples of text from a given field of design shaping tools, design and manufacture of engineering components using the CA system and 5-axis machining. Materials are also available to students on-line.

V. Programming Production of Knife using CAM System

When creating a program in NC machining module used CAD / CAM system based on the model drawing knife. The first step for the realization of the production was the creation of the technological process. After finishing programming, were all programs sent like as CL data using a post processor Tebis been sent to the server, where the staff at MTF Trnava searched, downloaded to a CNC machine and used for machining. From an economic perspective and the time it starts out where the use of CAM system very convenient. Most major CAD / CAM systems can cover almost the entire production cycle from idea creation, through engineering design, creating NC programs and technological processes [8].

Using such a system, in our case, reduce the cost and time required, especially in the creation of NC programs on the grounds that, given the complexity of the shape produced a knife manual programming would be very difficult to impossible. Teaching students by PPT is realized in the so-called. multimedia classroom and focuses on teaching their own teaching methods for practical training in the field of engineering practice called. method OJT - on the job training.

This is the adaptation and development program for students who are preparing for target of specific job position or area of expertise in the field of drawing machine parts using CAD systems, programming and simulation of manufacturing parts using CAM system for the production and implementation of manufacturing machines using remote transmission via webcam from Centre of excellence of 5-axis machining in Trnava. Within the frame of the e-learning education, students were enabled to program the production of the knife on your personal computer in the classroom, in the presence of a teacher. There were two monitors in front of the students for better understanding of the programming procedures. The students could watch the teacher´s work and his/her visual demonstrations of the programming procedure on one monitor. On the other monitor, the students saw their own work and programming. The students thus could simultaneously understand the principle of the component programming by the teacher with their own activity whereby they could ask questions immediately and understand the principle of programming.

This way of learning has approved to be a very effective method for understanding the given problem.

After entering all necessary operations are generated graphical representation of machined with semi-attachment representation – simulation (Fig. 6).

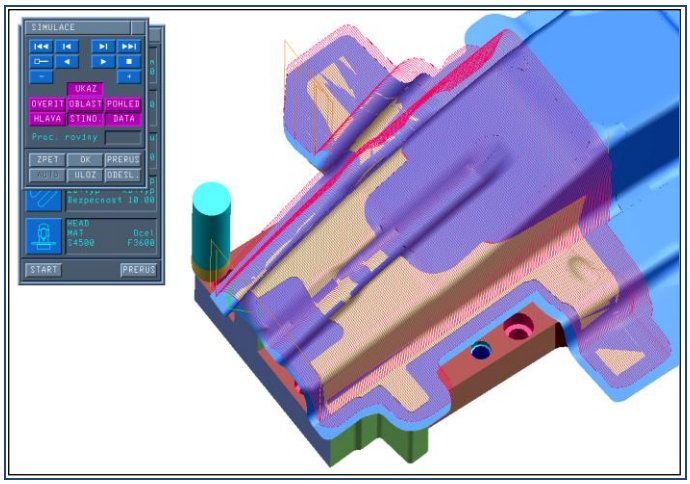

Fig.6. Graphic display during production knife - a simulation

VI. Implementation of Blade Production and its Evaluation

1) Production of knife 3-axis and 5-axis machining

Production of knife had to be carried out either directly on the machine tool. Since students have the opportunity to be directly in contact with the machine tools and directly see its production, this possibility was provided by them so. on-line learning in real time. On-line teaching students with software and hardware support to allow students to acquire required knowledge and skills at a distance without physical contact and attendance at local schools MTF in Trnava. Therefore, it can be seen in our case, a very effective and alternative way of teaching. Within this dynamic learning, students were provided a computer program Team Viewer (Fig.7).

Fig.7. On-line monitoring of production of knife on the computer

When it is activated on a computer student and computer teacher, to ensure video and audio data transmission over the Internet, in which students had the opportunity to see and hear

the teacher's instructions and work on their monitors. Since it was on track to manufacture blade machine tool, teachers connect to your computer web camera and directed it to the machine tool for students to see the whole process of programming and production knives. Teachers had the opportunity to explain to students adjust production machinery for manufacturing, and students could ask him any questions in real time. As part of the transfer was also simulated production knife with CNC and students to submit proposals to upgrade for innovation the programmed production. The aim of teaching students was the rationalization of work in the production of knife.

Therefore, the way the strategy of design documentation and production tool has been chosen so as to ensure a minimum of preparation and production times, subject to compliance with the required quality [9]. However, the acquisition of programming skills and a better understanding of production Engineering components were intentionally selected component complex shapes that can be produced 3-axis continuous cultivation methods (milling, drilling) and 5-axis cultivation methods. This work was completed on the shearing knife, which its production shifted to the heat treatment hardening shops. Since no work in Trnava lacks such technology, the students were introduced to the heat also working with video and on-line teaching of business component that worked. Students have a unique opportunity to monitor the progress of hardening the knife and practically familiar with this technology.

2) *Manual machining and assembly tool in unveiling*

After burring the piece should be ready for further manual processing (Fig. 8), which were also able to see the students using the on-line transmission and learning. The first act was carried burring sites, whereas the complexity of the blade shape and the lack of non-conforming areas, it was not possible to choose the option clamping in a vice or with magnetic clamping the machine working.

Fig.8. Removal base area – the burring

After burring was necessary to achieve a flatness of at least 90% of the area because poignancy perfect tool for folding and compacting reduction.

Placing a tool in the kit has been carried out by qualified personnel, who have long experience in this field; after subsequent machining of the mold tool, further by incorporation of different grain grinding stones. After incorporation of the upper OT and lower UT part, molds were taken to the press, where it was being worked on. For this

work to eliminate the remaining allowance 0.05 mm on both parts by qualified professionals, which it used in abrasive bodies clamped straight grinder. This operation was the most important to get right and precision moldings produced by crimping tool. The result was a production made knife that meets all the required parameters (Fig. 9). We can state that the selected way of machining the component has met the required aims. Based on the performed strategy of the production and character of the selected component, the students could understand the strategies of the programming procedure 3-axis and 5-axis machining. They could think forwards with reference to minimization of the production costs and working time.

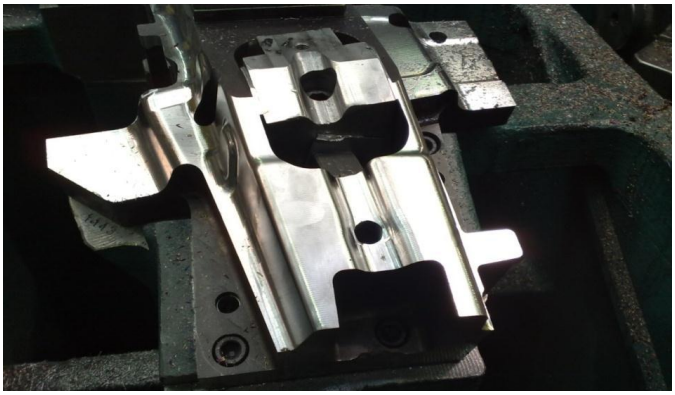

Fig.9. The final shape of manufactured knife

VII. CONCLUSION

Conventional methods of education currently adequately reflect the requirements of the labor market and practical information to gain knowledge and skills in the field of engineering technology in their teaching [10]. Theoretical knowledge that students acquire in traditional education are not be able to apply in practice and at the same time, these data largely short-term in nature. Therefore, it is necessary to apply innovative forms of education in this area. The contribution of the article was to present a dynamic learning design in the design and manufacture of complex shape parts, which in our view has brought efficiency in the acquisition of practical skills and the acquisition of new knowledge for students. The presented method of teaching has proved to be very beneficial in teaching effectiveness and meet our desired goals. Students expressed in solved project ambit rising interest in study. In comparison with classical way of education students showed their independence and creativity within production design of the component. They've gained practical experience, which they've wouldn't achieve with classical type of education. Through visual learning they can better connect informations and understand relations between them. By that they can better understand to the new concepts, confidently link to previously achieved knowledge and in other similar projects solving, they didn't have problem to solve individual tasks. We are convinced that given dynamic way of education is great motivation for students and good base for their adaptation in engineering practice.

This contribution is worked out in the frame of the KEGA 047STU-4/2012 project - Realisation of On-line classroom for dynamic education of secondary technical schol and university students focused on design and manufacturing of freeform surfaces.

REFERENCES

[1] Š. Svetský, I. Kleinedlerová and P. Kleinedler *"Počítačová podpora výučby technológií – galvanotechnika a obrábanie."* Zborník prednášok. 53. Medzinárodná galvanická konferencia. Kočovce, 2011, pp. 47-53.

[2] B. Divjak, N. Begičević "Imaginave acquisition of knowledge - strategic planning of E-learning". Cavtat, ITI 2006, 2006, pp. 36-43.

[3] N. Begičević, B. Divjak and T. Hunjak *"Development of AHP Based model for decision making on E-learning implementation".* Journal of information and organizational sciences, Vol. 31, 2007, pp. 13-24.

[4] I. Kleinedlerová, A. Janáč, P. Kleinedler, I. Buranský *"Dynamic Educational Process Efficiency Improvement for Students of Computer Production Technologies Support Subject".* IJECCE, Vol. 4, 2013, pp. 446-450.

[5] O. Moravčík, Š. Svetský, F. Hornák, D. R. D. Sobrino and J. Štefánková *"Experiences with the Personalised Technology Support for Engineering Education".* 21st Annual Conference of the Australasian Association for Engineering Education. Sydney, 2010, pp. 532-538.

[6] Ch. Adiele, E. D. Nwanze "*The Dynamics of Interactivity Modeling for e-learning*". Knowledge management and e-learning, Vol. 2, 2010, pp. 370-382.

[7] B. H. Khan *"A Framework for E-learning".* 2001. URL: http://bookstoread.com/framework. (18.12.2012).

[8] N. Buzađija „*Istrazivanje efikasnosti primjene Blended Learning sustava u nastavi inforrmatike u srednjem obrazovanju".* Život i škola, Vol. LV, No. 22. Studeni: 2009, pp. 50-61.

[9] P. Košč *"Implementation of e-learning Technologies in the workplace".* Kvalita inovácií a prosperita, Vol. 10, 2006, pp. 7-15.

[10] Š. Svetský, I. Kleinedlerová, P. Kleinedler *" Počítačová podpora výučby technológií - galvanotechnika a obrábanie".* 53. medzinárodná galvanická konferencia. Kočovce, 2011, pp. 47-53.

[11] A. Reháková, D. Rusková, Š. Svetský *"Modeling multilingual support systems for trainee teachers of technical branches via the use of ICT".* Problemy doksztalcania i doskonalenia zawodowego nauczycieli.om, 2009, pp. 219-223.

Genetic algorithms to optimize base station sitting in WCDMA networks

Najat Erradi
Laboratory Information Systems and Telecommunications
Faculty of Sciences. University Abdelmalek Essaadi
Tetouan 93000, Morocco.

Noura Aknin
Laboratory Information Systems and Telecommunications
Faculty of Sciences. University Abdelmalek Essaadi
Tetouan 93000, Morocco.

Fadoua Thami Alami
Laboratory Information Systems and Telecommunications
Faculty of Sciences. University Abdelmalek Essaadi
Tetouan 93000, Morocco.

Ahmed El Moussaoui
Laboratory Information Systems and Telecommunications
Faculty of Sciences. University Abdelmalek Essaadi
Tetouan 93000, Morocco.

***Abstract*—In UMTS network, radio planning cannot only be based on signal predictions, but it must also consider the traffic distribution, the power control mechanism as well as the power limits and the signal quality constraints. The present work aims to optimize the number of base stations used in the WCDMA radio network. In this paper, we propose a mathematical programming model for optimizing the base station locations considered for the uplink (mobile to BS) direction, and which considers the typical power control mechanism of WCDMA. The two contrasting objectives of the optimization process are the traffic coverage maximization and the installation costs minimization. A mimetic algorithm (AM) (genetic algorithm+ a local search) is proposed to find good approximate solutions of this NP hard problem. The Numerical results are obtained for reels instances, and generated by using classical propagation models.**

Keywords*—Ukumura-Hata model; UMTS; W-CDMA; Genetic Algorithms.

I. INTRODUCTION

Choosing the optimal location sites for WCDMA Network is a big challenge for a telecommunication vendor. Indeed, the deployment of a UMTS network represents a huge investment mainly related to infrastructure costs. In this context, an accurate and efficient optimization of radio access networks become essential to saving these investments, reduce the number of site deployed and to ensure a good quality of service to users [2].

Traditional models of planning adopted in TDMA cellular systems are based on the prediction of signal level and they do not take account of the effect of traffic on the capacity of a cell, or the impact of the control mechanism power on the overall interference level in the system. For UMTS, and due to technology CDMA access [6], the design takes into account the interference and tries to guarantee a certain quality target for each radio link. Although, the capacity will depend on the tolerable level of interference in the system because of strong correlation between coverage and capacity aspects, the choice of site locations must necessarily take into account both these aspects.

Modeling optimization problems are a key step before defining the appropriate methods for their resolution. The problem we deal with is to look for sites to install from a number of potential sites while starting propagation models and well-defined Traffic [1], [3]. The choice of sites WCDMA positions can be formulated mathematically as an optimization problem under constraints, an objective function that involves financial costs and other costs related to the amount of power transmitted in the system.

II. LOCATION MODEL FOR UPLINK DIRECTION

Consider a territory to be covered by UMTS service. A is a set of candidate sites, A = {1, ..., s} where the base stations can be installed and T a set of test point (TP), T = {1, ..., m}. TP is a relatively small region of the service area from which one or more connections can be initiated.

Each site j has an installation cost noted Cj. We denote by ni the number of simultaneous connections by TP. Thus, it can match the number of simultaneous active connections or by TP. This is a feature that can be refunded after the study and analysis of traffic requested in the study area. Information propagation are also known. Indeed, let F = {fij} 1 <= i <= m, 1 <= j <= s is the propagation gain matrix, where fij 0 <fij <1, is the propagation factor [3], the radio link between a TP i and j a potential site.

In the problem of locating sites WCDMA we wish to select a subset of the set A of potential sites where base stations will be installed, and assign the TPs suitable sites taking into account the requested traffic, quality of service terms of SIR and installation costs.

The problem of the location of base stations in the context of UMTS in the direction uplink is modeled by the following optimization problem:

$$\min \Sigma^{s}_{j=1} C_j a_j + \mu \Sigma^{m}_{i=1} \Sigma^{s}_{j=1} n_i (1/f_{ij}) b_{ij} \quad (1)$$

Under the constraints:

$$\Sigma^{m}_{i=1} b_{ij} = 1 \qquad i \varepsilon T \quad (2)$$

$$b_{ij} <= a_j \qquad i \varepsilon T ; j \varepsilon A \qquad (3)$$

$$b_{ij} , a_j \varepsilon \{0,1\} \qquad i \varepsilon T ; j \varepsilon A \qquad (4)$$

The first term of the objective function is the sum of the cost of installation sites. Thus, the ratio 1 / fij is proportional to the power emitted by a TP i assigned to the BS (Base Station) j, the second term corresponds to the total power emitted. $\mu > = 0$ is the parameter difference between the two objective functions. Constraint (2) ensures that TP can be connected to a single base station. Constraint (3) requires that the TPs are assigned only to sites where base stations are installed. Both decision variables, bij, aj, have binary values 0 or 1.

In UMTS, the mobile is much more limited in power than GSM network [6]. The constraint of limited power states that TP cannot be connected to a site with a power greater than it can deliver. Another fundamental aspect is the quality of the signal received by each BS that identifies the ability of a site [4]. It defines the number of connections supported by a base station (BS). The criterion adopted for a TP to communicate with such a base station is based on the value of the SIR. Indeed, a TP is connected to a particular site if the value of the SIR is greater than or equal to a minimum value. For each connection it embodies this constraint by the following inequality [3]:

$$SIR = SF * P_{reçue} / I_{intra} (1+f) >= SIR_{min} \qquad (5)$$

We assume that the interference caused by neighboring cells (I_{extra}) can be expressed by f factor interference caused by other connections of the same cell (I_{intra}). Received power $P_{received}$ by a base station j, for a TP assigned to this site, is equal to a power P_{target}. Our final model simplifies the problem of locating sites which is among NP-hard problems [1], [2], [7].

For the model more realistic, the interference must be explicitly extracellular and intracellular interference considered independently. However, for an uplink connection between TP i and base station j, there is no significant difference between the two types of interference [6]. With a received power based power control mechanism, the overall interference in the system for each potential site j ε A, has the following expression:

$$P_{target} / (\Sigma^{m}_{h=1} n_h f_{hj} \Sigma^{s}_{t=1} (P_{target}/f_{ht}) b_{ht} - P_{target}) >= SIR_{min} a_j \qquad (6)$$

Where the thermal noise is neglected. This constraint assumes that if a base station is installed at the site j (ie, j = 1), the value of the SIR resulting exceed the given value of SIR_{min}.

III. Optimization Methods And Some Computational Results

A. Basic principle of genetic algorithm

The problem of locating base stations of a UMTS network is an NP-hard problem [1-2]. To solve this problem we propose an algorithm memetic (AM) based on genetic algorithms methodology and local search.

Genetic algorithms rely heavily on a binary encoding string 0/1 fixed length s*m represents a configuration (the problem) solution called individual. Genetic operators: crossover, mutation and selection [7], are defined to operate on a random person or two to generate new configurations. GAs are generally sensitive to the distribution of the initial population. The adaptation of genetic operators in our problem and hybridization with local search makes our method can produce good quality results. Indeed, the two genetic operators allow the AM to exploit and explore the search space effectively guiding the search towards the most promising regions.

Rather than deterministically decide in favor of individuals best adapted, GAs do that by fostering probabilistic rules. This leaves little room for those less well to survive and reproduce. In order to better promote this principle, we have introduced the local search in each iteration of the genetic algorithm (Figure 1) with a probability pls.

The step of evaluating the fitness function allows selection of the best individuals created, by ordering the best fitness of the worst individual in the population size of 100. The search stops when the number of iterations limit is reached.

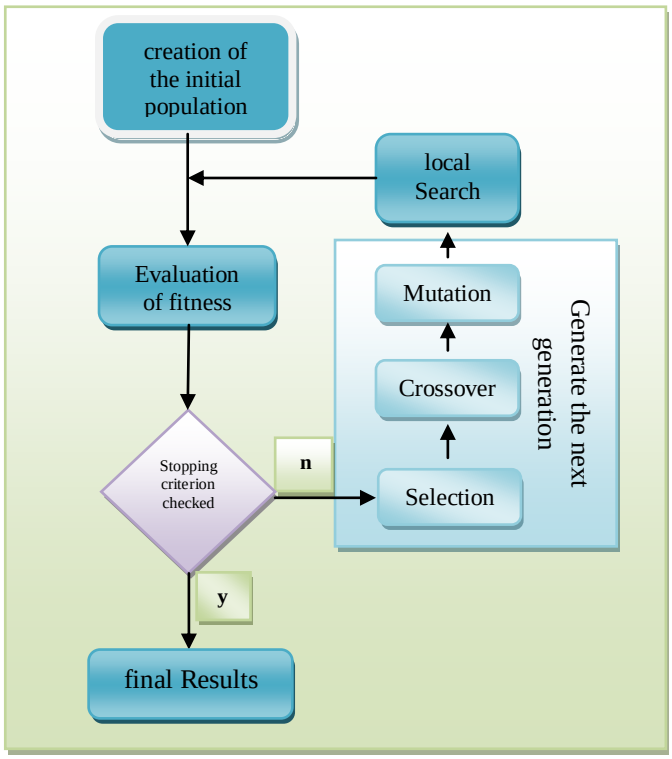

Fig.1. Optimization model using genetic algorithm and local search

B. Numerical results

In our simulation, we will focus on the basic model. The power control is important for the proper functioning of a WCDMA network. Indeed, it can meet the needs of users and minimize the overall interference in the network. For this, we assume that the power control mechanism is perfect and is based on the received power.

We studied the case of an urban environment and multi-service, voice service speed 12.2 kbps data service rate 64 kbps and 384 kbps. We model Okumara-Hata [3] as a model of propagation attenuation is given by the equation:

$$A_u = 69,55+26,16\log(F) – 13,82\log(H_b) – [(1,1\log(F) – 0,7)H_m – (1,56\log(F) – 0,8)] + [44,9 – 6,55\log(H_b)]\log(d) \qquad (7)$$

Where F is the frequency signal in megahertz, H_b and H_m are respectively the height of the base station and the height of the mobile in meters, d is the distance in kilometers.

For the simulation, we consider the following parameters shown in Table 1 [1]:

TABLE I. SIMULATION PARAMETERS

Parameters	values
frequency (en Mhz)	2000
height of TPs (in meters)	2
Height sites (in meters)	10
Power target TPs (in dBm)	-100
Maximum power of TPs (in dBm)	30
SIR_{target} for voice service (in dB)	6
SIR_{target} for data service 64 kbps (in dB)	3.2
SIR_{target} for data service 384 kbps (in dB)	1
Number of connections by TP	1

Distribution by a uniform law to location of TPs. The instances with medium-size are characterized by service area size of 400 * 400 m, m = 95 TPs and s = 22 potential sites. The cost of installation sites is constant Cj = C for all j of A. Minimum activated sites (Figure 2) among 22 potential sites are between 7 and 9 sites for 4 distributions ZU1 to ZU4 (urban area). Each ZUi is executed 20 times (Table 2). The required traffic is always satisfied.

The dissimilarity of the number of connections in each site installed by our metaheuristic algorithm, due to the random distribution of the potential number of TPs in the area to be covered. The aspect of the quality of the signal received by each BS for identifying the ability of a site defines the number of connections supported by a given base station. The criterion adopted for a TP to communicate with such a base station is based on the value of the SIR, the results obtained with the SIR model for the uplink case with real instances generated and granted propagation model. Noting that in uplink, the number of sites installed is much more important than in downlink. Indeed, in downlink intra interference is less significant than in uplink because each BS uses these orthogonality codes and the entire couvrement is still obtained with a minimum number of BSs. Otherwise, in downlink direction we consider a diversity of variable power received by the TPs, whereas in uplink it is sufficient to consider a single received power for each BS.

IV. CONCLUSION

We studied a model to optimize the location of base stations in the UMTS standard and in the uplink case. Indeed, the hybridization of genetic algorithm and local search has allowed us to install an optimal number of base stations while satisfying the constraints of quality of service, power, capacity and total network coverage on the zone concerned.

TABLE II. RESULTS OBTAINED FOR m = 95, s = 22

area	# of BSs	Execution time (mn)	# average
ZU-1	8	13	8.5
ZU-2	7	12	7.4
Z-U3	8	12	8.4
ZU-4	8	13	8.6

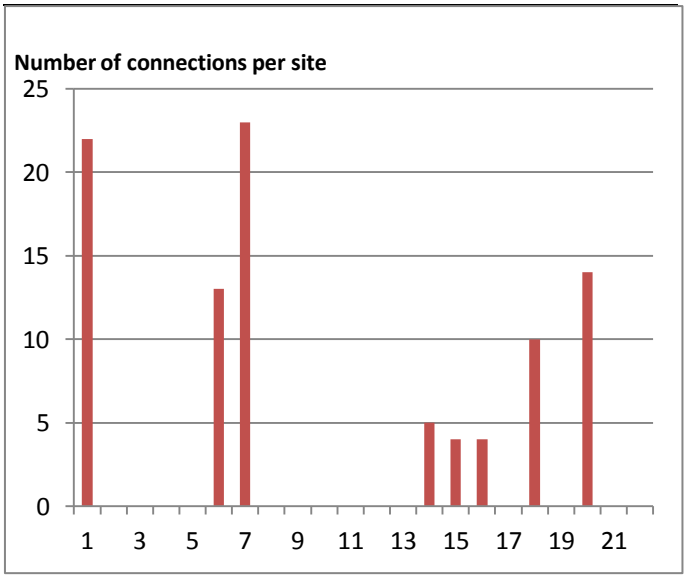

Fig.2. number of TP connected to each site j

The memetic algorithm has shown high efficiency in order to don't have a premature convergence and to avoid local optima. Our study focused on voice and data services with a classical propagation model. As perspective to this work, we aim to run simulations of larger instances, and study the same mathematical model with other algorithms.

References

[1] E. Amaldi, A. Capone, F. Malucelli. Optimization models and algorithms for downlink UMTS radio planning. Manuscript, (2003).
[2] E. Amaldi, A. Capone, F. Malucelli. Optimizing base station siting in umts networks. In Proceedings of IEEE VTC Spring (2001).
[3] M. Hata. Empirical formula for propagation loss in land mobile radio service. IEEE Trans. On Vehicular Technology, (29:317-325, 1980).
[4] R. Mathar and T. Niessen. Optimum positioning of base stations for cellular radio networks. Wirelless Networks, pages (421-428, 2000).
[5] C. Oliva. Techniques hybrides de propagation de contraintes et de programmation mathématique. Thèse, Université d'Avignon et des Pays de Vaucluse, (2003).
[6] J. Laiho, A. Wacker, T. Novasad. Radio network planning and optimization for UMTS. Copyright by John Wiley and Sons, (2002).
[7] J.Dréo, A.Pétrowski, P.Sinrry, E.Taillard. Metaheuristics for Hard Optimization, Springer (2006).

Algorithm to Match Ontologies on the Semantic Web

Alaa Qassim Al-Namiy
School of Science, Aston University
Oakville, Canada

***Abstract*—It has been recognized that semantic data and knowledge extraction will significantly improve the capability of natural language interfaces to the semantic search engine. Semantic Web technology offers a vast scale of sharing and integration of distributed data sources by combining information easily. This will enable the user to find the information easily and efficiently.**

In this paper, we will explore some issues of developing algorithms for the Semantic Web. The first one to build the semantic contextual meaning by scanning the text, extract knowledge and automatically infer the meaning of the information from text that contains the search words in any sentence and correlate with hierarchical classes defined in the Ontology as a result of input resources. The second to discover the hierarchical relationships among terms (*i.e.* discover the semantic relations across hierarchical classifications). The proposed algorithm will be relying on a number of resources including Ontology and WordNet.

Keywords—Semantic Web; Ontology matching; WordNet; Information retrieval; web service

I. INTRODUCTION

There are many different design methodologies for software development, each having several advantages and disadvantages. To determine the best suited methodology for this research, an analysis was performed based on research into the various design methodologies. From the results of the analysis, the methodology chosen was the Object Oriented Design (OOD) methodology [2].

This methodology provides a number of benefits. Firstly the OOD methodology takes a real world view a system and models it using objects. This provides a natural decomposition of a system into modules. In the OOD methodology, the analysis and design phases are closely coupled together which helps in developing a prototype of the problem domain a lot quicker compared to more traditional design approaches. The reason for this is that the initial foundation of the design phase will be the information developed in the analysis phase.

The object oriented approach focuses more on data specifications, including the relationships between objects. One of the most important parts of the automatic annotation tool is data and so by using a design methodology that is strongly focused on data, it is hoped that there will be a greater chance of developing a successful design. In addition designs created from OOD approaches map directly into implementations using object oriented programming languages such as Java or C#. Henderson-Sellers & Edwards (1990) believe that more flexible can be provided to a system based on object representation as modifications at the implementation level did not require any changes to the systems design itself due to the easily accomplished [2].

However, the traditional model for software development and the Object Oriented approaches are both suffered from the lack of identifying the role of Human Computer Interaction (HCI).The automatic annotation system clearly needs to provide interactivity for the user through a simple interface and so a significant part of the design will need to be focused on this aspect [11].

In addition, this paper describes how the methods of the system is developed for (i) a general algorithm to build the semantic contextual meaning by scanning the text, extract entity or knowledge and correlate with hierarchical classes defined in the Ontology as a result of input resources (ii) a specific algorithm to discover the hierarchical relationships among terms (*i.e*. discover the semantic relations across hierarchical classifications). The algorithms will be relying on a number of resources including Ontology and WordNet [9].

Knowledge Extraction can be used to automatically extract specific information from documents and this information could then be utilized to generate possible semantic annotations [10]. During the research stage of the author became aware of a powerful of WordNet component and Jena component which represent the foundation of the proposed system. This system was chosen to provide the Knowledge Extraction capabilities needed as it offered all of the features required including named entity recognition [4]. Another benefit of choosing WordNet and Jena components was that it has been designed to be easily incorporated into other applications and also there is a lot of documentation available explaining how to use it [12]. Figure 1 shows the layout of the main components of the system and also the input and output data.

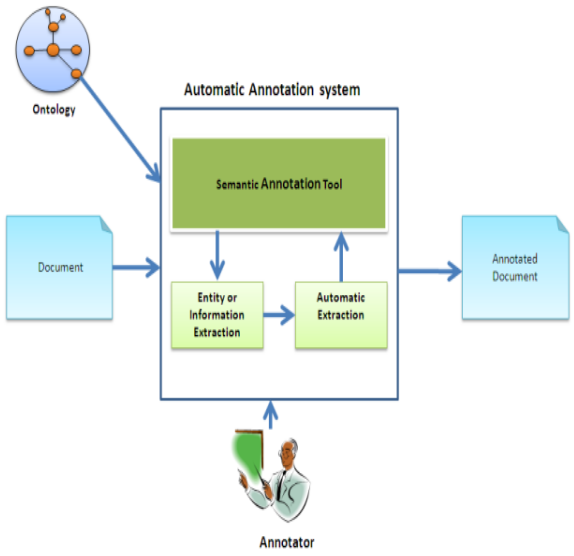

Fig.1. High level architecture of the system

The explanation of these components shown in figure 1is as follows:

1) *Semantic Annotation Tool*
This component is the foundation of the system. It provides all the functionality required to create annotations automatically. This will include viewing Ontologies and browsing web pages. This component developed as part of this research.

2) *Knowledge Extraction*
The knowledge Extraction component of the system will analyze web pages and extract specific information found within the text. This component developed using features provided by WordNet.

3) *Automatic Annotator*
This is the main component of the system. It will take the information extracted by the knowledge Extraction component and use it to generate possible annotations. These annotations will be presented to the user through a graphical user interface. This interface will also allow the user to create annotations in RDF and save annotations to a file.

In the remainder of this paper we will first talk about the methodology and approach in Sec. II and then about the Senses Algorithm in Sec. II. In Sec. IV we will present how to build the Semantic Contextual Meaning. In sec. V the process design is discussed. Finally, we conclude our work

II. Methodology and Approach

To move toward Semantic Coordination we proposed methodology based on the insight with the aim of managing conceptual structure and managing structures tag.

The proposed system gives the ability to use the semantic organization implicit with complex level in the client way that uses the language taken by the tag. In this work, three different levels of semantic information are considered (*i.e.* knowledge) which are required to annotate structures tagged semantically with language:

- **Lexical data (Knowledge):**

Information on certain words (*i.e.* concepts) used in the tags and the relationship among them such as the word 'right' can give a meaning of correct or opposite to left.

Structural data (Knowledge): deriving information from the tags which are given in a certain structure. For example, the Entity London can be used to classify city, and London name (people with the name London).

Domain: information concerning the relation among senses of tags in a specific domain. The sense term refers to meaning of a word in WordNet *i.e.* London represent both cities in South Western Ontario, Canada and a capital city of United King Dom.

In this methodology we consider the hierarchical classifications method used for classifying particular text. The proposed algorithms must be clearly enriched with particular structure and principle functions to determine the semantic relation between the entities. This will improve the current information retrieval search anomalies.

Ontologies also play an important role in research on computational linguistics, particularly for information extraction (IE) and natural language processing (NLP) [9]. In this application area, ontologies are used as knowledge bases which provide background information for machine processing of texts. They are usually not bound to a certain domain but capture universal knowledge, and thus resemble upper ontologies in this respect. Yet their focus is less on representing the essence of the world but on capturing linguistic behavior and lexical surroundings of concepts [7]. The structure of linguistic ontologies may differ from the typical structure of concepts, instances, relations and axioms as discussed for ontologies; although they typically use hyponymic structures as a backbone and enrich them with additional concept relations. Single linguistic ontologies have recently also been transferred to the OWL format.

Used in combination with information extraction systems, linguistic ontologies can be applied in order to gather factual data for the semi-automatic construction of other (domain) ontologies [7]. They may further be used as synonym collections and dictionaries or as a major mapping reference vocabulary. Some projects also focus on supporting machine translation.

Let us look at a further example, using the three semantic levels mentioned above, to determine the semantic relations tagged London as a capital city of England, and between the entity (*i.e.* node) London city in Ontario, Canada, we can account the relations are different. Consider the mapping properties between the entities London England and London Ontario.

The lexical data notifies that the sense of the two tags is similar and refers to city. Domain notifies, among other things, that London is a city in South-western Ontario region. Finally,

structural data derived the properties of the entities and intends meaning of the node. For example the structure knowledge of ” London” England will refer to all possible knowledge like: History, Middle Ages, Early modern, Local Government , Geography, Economy, Tourism, etc. while the structure of “London” Ontario may derive the following knowledge: Residents, Business, city Hall , City Life, E-Services, etc.

Example

The example shown in Figure 2 explains the category of the different levels of semantic information.

```
</owl:Ontology>
<owl:Classrdf:ID="Country">
<rdfs:subClassOf>
<owl:Classrdf:about="#UnitedKingdom "/>
</rdfs:subClassOf>
<rdfs:comment> United Kingdom of Great Britain
and Northern Ireland </rdfs:comment>
</owl:Class>
        <owl:ObjectPropertyrdf:ID=" London
        ">
        <rdfs:domainrdf:resource="#Capital
        City England"/>
        <rdfs:rangerdf:resource="#London
        England "/>
         <owl:Classrdf:ID=" History " />
         <owl:Classrdf:ID=" Middle Ages " />
         <owl:Classrdf:ID=" Local Government " />
         <owl:Classrdf:ID=" Geography " />
         <owl:Classrdf:ID=" Economy " />
         <owl:Classrdf:ID=" Tourism " />
        </owl:ObjectProperty>
```

Fig.2. Example of different levels of semantic information

```
<owl:Ontologyrdf:about="">
<owl:versionInfo>Version
0.1</owl:versionInfo>
<rdfs:comment>Countries Ontology,
</rdfs:comment>
</owl:Ontology>
<owl:Classrdf:ID="Country">
<rdfs:subClassOf>
<owl:Classrdf:about="#Canada"/>
</rdfs:subClassOf>
<owl:disjointWith>
<owl:Classrdf:about="#ProvincesandTerritories
"/>
</owl:disjointWith>
<owl:Classrdf:about="#AssociatedState"/>
</owl:disjointWith>
<rdfs:comment>No government body
exists</rdfs:comment>
</owl:Class>
<owl:ObjectPropertyrdf:ID=" Southwestern
Ontario ">
        <rdfs:domainrdf:resource="#London
        "/>
<rdfs:rangerdf:resource="#London Canada
"/>
<owl:Classrdf:ID=" Residents" />
<owl:Classrdf:ID=" Business " />
 <owl:Classrdf:ID=" city Hall " />
<owl:Classrdf:ID=" City Life " />
 <owl:Classrdf:ID=" E-Services " />
</owl:ObjectProperty>
```

Fig.3. Example of structure data (knowledge)

While structure data (knowledge) of ”London”, Canada could be represented as in figure 3.

The conclusion from above that the most important step is to find the word description, using WordNet which provides complex word descriptions.

III. SENSES ALGORITHM

As mentioned, to produce automatic annotation, the first phase is to create an algorithm that obtains a description about text automatically [8]. The algorithm will consider the description of a word as a textual definition, more general terms, more specific terms, or a definition in a specific language or domain. The primary source is the web text where the aim is to divide the text into sentences which enables the extraction process step by step.

To obtain the sense set for Ontology, the entire synonym words presenting in the text which are related to the semantics of the Ontology (*i.e.* concept)

will be extracted via the key functional requirements of WordNet. These main carriers of information will be analyzed based on lexical resource using the WordNet. The procedure below describes the system process manually of what WordNet needs to do, what synsets might be derived, and then how it will be annotated; our separate processes involved, namely:

A.Preliminary Analysis Of The Input Source,

This process will be the foundation phase of the system. It should provide all of the functionality required to create annotation, this will include:

1) *ESA system access web documents toallocate text sentence.*

2) *ESA system accessdomain knowledge,Ontology document and WordNet interface.*

3) *ESA systemestablishes characteristics of the sentence, such as case, number, time and gender, etc.*

B.Analysis Of The Sentence Structure,

4) *ESA system access Ontology and obtain related knowledge on syntax*

5) *ESA implements syntactical analysis, in order to classify the syntactical structure of the paragraph. The entities and how they are arranged within the text will be analyze and describe via synset methods.*

6) *ESA system parse the paragraph and sentences based on the syntactic patterns derived from the WordNet dataset. Prior to linguistic processing the extraction process will divide the web text into sentences; the tokenization take place once the text is loaded, then tokenizer split a web text into textual tokens.*

7) *The internal structure level will be analyze and describe the relations among entities via tokenization process and pointer method ;*

8) *At the sentence level, characteristics sentence structures will be analyze and describe via the scanner and lexer generator methods.*

9) *ESA system will declare synonyms using annotation property, for example*

```
<owl:AnnotationPropertyrdf:ID="synonyms" >
<rdf:typerdf:resource="http://www.w3.org/
2002/07/owl#DatatypeProperty"/>
</owl:AnnotationProperty>
```

From this process the text can be converted into a view tree after interpreting the structure of the text [1].

C. Analysis of semantic, analyzing a semantic is a method of describing syntactic structure of sentences, clauses and phrases.

10) *ESA system will access Ontology and obtain related knowledge on semantics*

11) *ESA system retrieves possible meanings of words and their proprieties from Ontology that generate a semantic descriptor of the sentence.*

12) *Entities will be represented as object using string of characters to identify the resource known as Uniform Resource Identifier (URIs). The advantage of using URI representation is that the object can be used to create inters relation. The word entity refer to the class of things and sub entity refer to sub class, for example "University" likely an entity.*

13) *ESA system will be able to indicate subclassOf relations between entities, such as department and people. This will allow detecting connections, for example employees in a specific department.*

14) *Semantic analysis of the entities will produce triples with two nodes. One to represent relations and terms and the other to represent the relation which describes the sort of connections among the nodes.*

15) *The triples produced can be nested – which means they can further be utilized as node of the further triples. This allows for the facilitation of complex interrelations representations where and each different type of relation will describe a different linguistic phrases or keywords in text. When the triples are combined into the knowledge base, the knowledge from the texts is also transferred resulting in the generation of a more refined structure.*

16) *Representing knowledge can be expressed by subtypeOf and subClassOfproperty which is relevant to RDF property Entity relationships are expressed by instanceOfrelations.*

17) *ESA system will identify all the necessary classification of entity which is required to determine whether the entity belongs to the main class or subclass. For example, to extract entities from the instance sentence "ASTON UNIVERSITY in the heart of BIRMINGHAM CITY" would refer to: ORGANIZATION situated in LOCATION, the outcome of extraction will be, "Aston University in Birmingham City". This process is generating an automatic annotation which can be stored in a separate RDF or XML document. Furthermore, annotation properties will be used to represent the category of annotation properties in an Ontology language.*

18) *The terms and concepts which have been extracted will be annotated since the ontology of original text is rolled bythem. The relations can be mapped in finer way and preserved due to using the ontology by the authors. It can also offer different levels of information details by creating an overview of the contents.*

19) *The word relations and symbol will be schematics at the bottom will be complete.*

D. Incorporation the acquired results (i.e. relevant information).The information will then be built-in as a knowledge which is consisted of terms, concepts, and their interrelations. The Jena framework will be used to manage and store the information [4]. Finally, the system will provide significant support for the agent server which has responsibility for retrieving data. Figure 43 explains the system definition phases for the proposed system.

IV. BUILDING THE SEMANTIC CONTEXTUAL MEANING

The core task of this sub-section is to introduce the independent part of the algorithm called EXTRACT–CONCEPT. The basis of this algorithm is to match the same topic in the sentence with entity / sub entity in the Ontology document

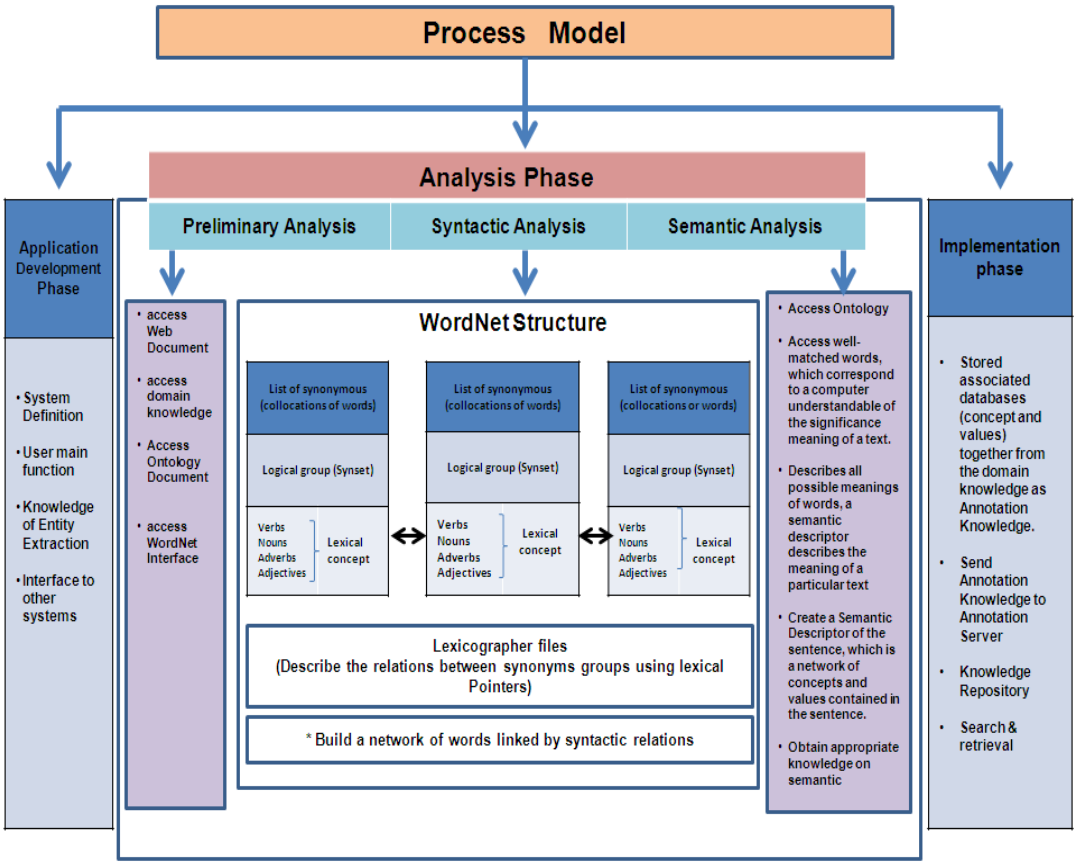

Fig.4. System Definition Phase Based Semantic Web

This algorithm designed to build the hierarchical relationships between words among concepts since the key elements of the knowledge is composed specifically an internal structure *IST*, an Ontology *GO* and a lexicon *LO*. The key input source of the algorithm is the context. The context will be analyzed based on lexical resource using the WordNet methods and will be enriched with specific functions required to scan the text, extracts knowledge and building semantic contextual meaning. The concepts expressed by a generic entity e (*i.e.* node) in a general text to match the hierarchical classifications [3]. In addition, the algorithm consists of functions that are necessary for retrieving information in terms of supporting user query.

In conclude the output will be the semantic relations among entity *e* and all terms belonging to internal structure. This relation represented as logical formulas (σ,ψ) that symbolize the relation among the individual concepts represented by entity and the other generic words in internal structure.

We observe that the use of WordNet as major resources allowed providing structured information relating to semantic relations among words. WordNet employ as Lexical Ontology that contains word and world knowledge which considers analyzing the text as in linguistics. The algorithm has many steps. Line 1 verifies the focus of entity *e* as a preliminary analysis of the input. The entities and how they are arranged within the text will be analyze and describe via synset methods [5]. This step is useful toextract the meaning of entity *e* as it determines whether the entity *e* in structure *IST* exists in structure *SUBF*.

Lines 2 and 3 *extract the sentence related to each entity in structure SUBF and* provide a link between each entity for the synsets found in the Lexicon. To obtain the sense set, the entire synonym words existing in the text which are related to the semantics of the Ontology (*i.e.* concepts) will be extracted via the key functional requirements of WordNet. Consequently, in support of the example mentioned the word 'London' in WordNet has two different meanings 'Capital city of United Kingdom' and 'City of Ontario, Canada'. These senses can be recorded by the array *SynSet*, so that, *SynSet* will have two different meanings as above. The array of senses *SynSet* must provide more attention before starting analysis of the corpus of the algorithm. The set of synonyms represented by synset is a collection of senses, such that concepts can be represented by expressions which use synset in a lexicon. In Lines 4 and 5 passes through a filter out the non-relevant concept associated to generic word in internal structure.

A formula approximating the meaning can assist in building the function INDIVIDUAL–CONCEPT to be expressed by entity e. The defined classes in the ontology will

be correlated with the entity e. The function returns the relationships between the Ontology concepts, entities and objects. The combination of both domain in input to the function and the linguistic interpretation with structural knowledge (*T*) can assist in doing this. Finally, build the formula (σ, ψ) which represents the relation among the individual concepts represented by entity and the *local relevant axioms* as shown in Fig.5.

Algorithm 1 EXTRACT–CONCEPT (*EXC*, *e*)
Context EXC = (IST, *LO*, GO), *where IST is a internal structure*
LO is a lexical Ontology – Lexicon
GO is a General Ontology Concepts - Ontology
Sentence finite list of words
entity e is a Generic Word

Variable Identifications
Sentence SynSet[ ][ ] Synset*Array of synonyms*
Structure *SUBF*
Formula σ, ψ

1 FIND- CONCENTRATE (*e*, IST) → *SUBF*;
*the*concentrate *SUBF is a substructure of IST*
2 **for** each entity *i*in*SUBF***do**
3 EXTRACT–CONCEPT(*i, LO*) → *SynSet*[*i*] ;
extract the sentence related to each entity in the structure SUBF
4 **for** each entity *i*in*SUBF***do**
5 NON-RELEVANT–CONCEPT(*SUBF*,*GO*, *SynSet*, *i*) → *SynSet*[*i*];
difficult to deal with sentence are redundant
6 INDIVIDUAL–CONCEPT (*e*, *SynSet*, *SUBF*, *GO*) → σ;
7 EXTRACT– RELEVANT-KNOWLEDGE (*SUBF*, *SynSet*, *GO*) → ψ;
8 **Return** (σ, ψ) ;

EXTRACT–CONCEPT ALGORITHM

V. PROCESS DESIGN

The automatic annotation system will allow an annotator to create new annotations for a specific web page automatically by using Knowledge Extraction techniques to generate possible annotations.

A. Proposed Implementation of the Algorithm

In this stage, the most important step is to find the word description, using WordNet which provides complex word descriptions that infer meaning thus minimizing any ambiguity. In this work the description of a word can be a textual definition, more general terms, more specific terms, or a definition in a specific language or domain.

To implement the suggested algorithm Ontology needs to be created. It could be produced using the Jena Framework as Jena is able to query and store Ontology and the Jena method of OntDocManageraddAltEntry enables [4] relationships between stored Ontologies, thus identifying the location of Ontology inside the database.

The procedure starts by reading a RDF/OWL document into a Jena model; that gives an API for handling the information [6]. Once the description of a word is recognized in the RDF document, the word available in a HTML document will be highlighted / underlined which in turn shows the description extracted from the RDF/OWL document. For example 'Dr Tony Beaumont' is identified in HTML page and the description of 'Dr Tony Beaumont' is available in RDF document as shown in Fig.6.

```
<rdf:RDF
xmlns:rdf="http://www.w3. org/1999/ 02/22-rdf-syntax-ns#"
xmlns:lib="http://keg.cs.aston.ac.uk/stfDtls/">
<rdf:Description about="Dr Tony Beaumont" >
<lib:creator>Alaa Al Naimy</lib:creator>
<lib:pages>10< /lib:pages>
</rdf:Description>
```

Fig.5. Example of Implementation Procedure

From the above example we deduce the following should be available:

- An HTML page P with some term T of interest.
- An RDF document R which describes the term T from a set of one or more RDF descriptions.

To find T of interest in P we have to parse P that says "the term T that appears on this page will be highlighted, italics, colour, and/or larger font *i.e.* Dr Tony Beaumont ".To find R of T if that term has RDF description, then it is possible to display the properties as annotation in a new page. Once parsing the HTML page to annotate 'Dr Tony Beaumont', it should:

- display the description of 'Dr Tony Beaumont', the author and date of creation for that page in a tab or new window
- produce a new HTML page which is P with T annotated
- store specific metadata in a specific Ontology which will be achieved by adding new annotation rules.

This work suggests the usage of Jena integrated with SPARQL [14] to create a rule-based system through GeneriRuleReasoner to store the derivation data. The reason for this is to answer user's queries about the derivation of derived statements.

The system will store the derivation data in the database as the reasoner run [13]. SPARQL is a query language for getting information from RDF graphs [14]. It provides the requirements for querying by triple designs, optional patterns, disjunctions, conjunctions and supports queries like "*show me all the projects on semantic annotation*". The *projects* will mapped by the semantic annotations. The resultant data from the project database related to the semantic annotation area will be used to identify only *projects.* The SPARQL queries results can be obtained and presented in several different forms [14].

Integrating semantic annotation within Ontology allows distinction between the same words in different contexts that give it different meanings e.g. the searching process will be easy to distinguish the word "Mississippi" the state, from "Mississippi" the river because the annotation will be with references to various concepts in the Ontology. This will improve the current information retrieval search anomalies.

This work proposes a user application which connects to an annotation server through a web site and annotates web pages of user choice. The proposed annotation server uses an Annotation engine with an embedded Jena repository, which then transfers the results of the annotation to the annotation server. The strength of this proposed work is to integrate a Knowledge Extraction platform and Ontology to provide flexibility for the formats and functions it uses. It will also support the HTML browser to display an integrated open APIs of the Ontology browser along with the documents**.** From looking back at the functional requirements**,** it is clear that the system will need to provide the following functionality:

VI. CONCLUSION

This paper provides a description of the design of the automatic annotation system. The design stage of any research is arguably the most crucial part as it describes how the system will be structured to meet the requirements. A carefully constructed design will hopefully make the system easier to implement and will minimise the number of problems encountered. Our method focuses on representing the documents succinctly and explicitly through extracting only the related resultant semantics from the document. The specific domain ontology will assist the extraction process. The guidance to the modelling process and decoupling of the knowledge base from the required documents is provided by the proposed framework.

This paper describes how the methods of the system is developed for (*i*) a general algorithm to build the semantic contextual meaning by scanning the text, extract entity or knowledge and correlate with hierarchical classes defined in the Ontology as a result of input resources (*ii*) a specific algorithm to discover the hierarchical relationships among terms (*i.e*. discover the semantic relations across hierarchical classifications). The algorithms will be relying on a number of resources including Ontology and WordNet.

REFERENCES

[1] Al-Namiy, Ala'a Qasim, "Annotation Approach for Sharing Deep Web Annotations Based on Ontology", International Conference on Internet and Multimedia Systems and Applications (IMSA 2009), August 17-19.

[2] B. Henderson-Sellers and J. M. Edwards, "BOOK TWO of Object-Oriented Knowledge: The Working Object.", Prentice Hall, 1994

[3] Bojars, U., Breslin, J. G., Finn, A., & Decker, S., "Using the Semantic Web for Linking and Reusing Data Across Web 2.0 Communities", Journal of Web Semantics, 2008,Vol.6, no.1,pp. 21– 28.

[4] Brian McBride, (2002). Jena: A Semantic Web Toolkit. Journal of IEEE Internet Computing, Vol.6, no.6, November /December 2002, pp. 55-59.

[5] David Milward, Marcus Bjäreland, William Hayes, Michelle Maxwell, Lisa Öberg, Nick Tilford, James Thomas, Roger Hale, Sylvia Knight, Julie Barnes, "Ontology-Based Interactive Information Extraction From Scientific Abstracts", Journal of Comparative and Functional Genomics, Feb-Mar, 2005,Vol.6, no1-2, pp. 67-71.

[6] Dietmar Jannach, Kostyantyn Shchekotykhin, Gerhard Friedrich, "Automated ontology instantiation from tabular web sources-The All Right system", Web Semantics: Science, Services and Agents on the World Wide Web, September, 2009 ,Vol.7, no.3, pp.136-153.

[7] Hepp, M., "Possible Ontologies: How Reality Constrains the Development of Relevant Ontologies", IEEE Internet Computing,2007, 11(1), pp. 90– 96.

[8] Hahn, U. & Romacker, M., (2000), Content Management in the SYNDIKATE system – How technical documents are automatically transformed to text knowledge bases", Data & Knowledge Engineering, November 2000, Vol.35, Issue 2, , pp. 137-159.

[9] Huang Xiao-xi and Zhou Chang-le, (2007); "An OWL-based WordNet. lexical ontology", Journal of Zhejiang University SCIENCE A, vol.8 ,no.6, pp. 864-870.

[10] Ishizuka, M. and Vranes S., "A Common Concept Description of Natural Language Texts as the Foundation of Semantic Computing on the Web", 2008 IEEE International Conference on Sensor Networks, Ubiquitous, and Trustworthy Computing 11-13 June, 2008, pp. 385 – 385.

[11] John M. Carroll, "Conceptualizing a possible discipline of human–computer interaction", Journal of Interacting with Computers, 2010, Vol. 22, Issue 1, pp. 3–12.

[12] Koji Murakami, Eric Nichols, Junta Mizuno, Yotaro Watanabe, Hayato Goto, Megumi Ohki, Suguru Matsuyoshi, Kentaro Inui, Yuji Matsumoto, "Automatic Classification of Semantic Relations between Facts and Opinions", Proceedings of the 2nd International Workshop on NLP Challenges in the Information Explosion Era (NLPIX 2010), August, Beijing, China, pp. 21-30.

[13] Petya Osenova and Kiril Simov,"Semantic Annotation for Semi-Automatic Positioning of the Learner", Proceedings of the 1st Workshop on Supporting eLearning with Language Resources and Semantic Data, LREC 2010, Valetta, Malta, May 2010, pp. 46-50.

[14] Stefan Bischof, Stefan Decker, Thomas Krennwallner, and Axel Polleres, "Mapping between RDF and XML with XSPARQL", Journal on Data Semantics, 2012, Vol.1, no.3, pp. 147-185.

Energy-Aware Fragmented Memory Architecture with a Switching Power Supply for Sensor Node

Harish H Kenchannavar
Department of CSEGogte Institute of Technology
VTU, Belgaum

M.M.Math
Department of IS E
Gogte Institute of Technology
VTU, Belgaum

Umakant P.Kulkarni
Department of CSE
SDMcollege of Engineering and Technology
Dharwad, VTU, Belgaum

***Abstract*—The basic sensor node architecture in a wireless sensor network contains sensing, transceiver, processing and memory units along with the power supply module. Because the basic sensor network application nature is surveillance, these networks may be deployed in a remote environment without human intervention. The sensor nodes are also battery-powered tiny devices with limited memory capacity. Because of these sensor node limitations, the architecture can be modified to efficiently utilise energy during memory accesses by dividing the memory into multiple banks and including a memory switching controller unit and a power switching module. This modification conserves energy, so power can be supplied only to the bank or part of the memory being accessed instead of powering the entire memory module, thus leading to efficient energy consumption. Simulations have been performed on fragmented memory architecture by incorporating the M/M/1 queuing model. When the packets get queued up, energy utilisation and a packet drop at the sensor node is observed. The energy consumption is reduced by an average of 70%, and there is significantly less packet drop compared to the normal memory architecture. This leads to increase in node and network lifetime and prevents information loss.**

Keywords—modified memory architecture; switching power supply; sensor node; energy conserve; idle energy

I. Introduction

A wireless sensor network is an essential networking component in applications, including fire surveillance, underwater experiments and robotic flying sensors. Wireless sensor networks contain sensor nodes, where each sensor node has sensing, transceiver, processing and memory units, as in figure 1.The limited memory capability and energy utilisation nature of the sensor nodes has compelled many researchers to explore this area. The memory architecture of a sensor node usually has RAM with less memory capacity, which is used to store programs for processing (32 KB – 128 KB). Modern flash-based micro-controllers contain between 1 KB and 512 KB of memory for program storage. This can be used as both program memory and for temporary data storage.

The flash memory design influences the sensor node life span. Flash memory has recently become a popular alternative storage for many portable devices. Constructing memory architecture in a wireless sensor network depends on the application type. The traffic data size also varies from small to large based on the application.

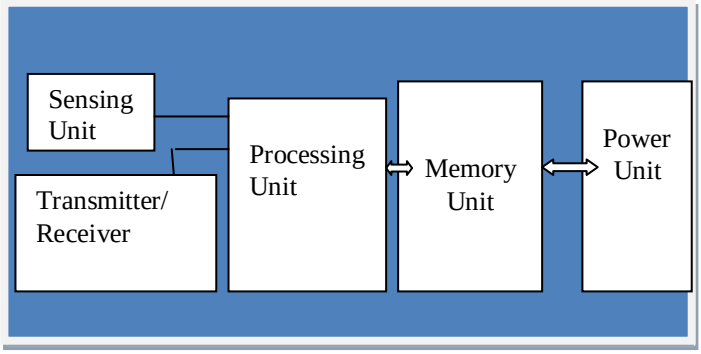

Fig.1. A typical Wireless Sensor Node

Transmitting scalar data, e.g., temperature, humidity or pressure, resort to a smaller traffic size over the WSN; transmitting captured images, videos or audio requires more information to be sent over the WSN. When the sensor nodes are deployed for a specific application within the network and are switched on, power is also supplied to the memory unit attached to the nodes even if the sensors are idle. The energy consumed in this state is known as idle energy, as the sensor is not performing any useful operation. There is thus a need to modify the sensor node architecture by incorporating efficient memory or buffer management schemes.

II. Literature Survey

The following section gives an insight into the work performed in this direction. The paper titled “Reducing Power Consumption for Mobile Multimedia Handsets” by authors Rong-Jaye Chen, Ting-Yu Lin, and Yi-Bing Lin [1] proposes 3 techniques called wake-up techniques that reduce battery power consumption in a mobile multimedia handset. Using these approaches, the system switches to sleep mode when the memory queue for packet arrivals is empty. Various wake-up mechanisms are considered based on these concepts. First among the approaches is the threshold approach mechanism. If the number of packets that have arrived in the memory queue is above a threshold, the system is switched on; otherwise, it remains in sleep mode. The second approach, called the vacation approach, switches on the system after completing vacation time. The third approach, called the hybrid approach, combines the above two approaches. In this approach, the system is turned on when either the memory queue length goes over the threshold level or at the end of vacation time. A comparative study of these approaches sheds light on some

important system performance parameters. The threshold approach also reduces the system switch-on rate, whereas the vacation approach has the lowest mean packet waiting time. The hybrid approach must he selected to maintain lower values for both the system switch-on rate and the mean packet waiting time. There is a possibility to obtain a set of threshold values and determine a small switch-on rate and the probability for packet dropping for a threshold approach, while such a possibility does not exist for the vacation approach to obtain the vacation time range.

The authors Tie Qiu, Lin Feng, Feng Xia, Guowei Wu, and Yu Zhou have published a paper titled "A Packet Buffer Evaluation Method Exploiting Queuing Theory for Wireless Sensor Networks". They focus on optimising the performance of a large-scale wireless sensor network for improved QoS transmission when the hardware consumption is limited. Their paper [2] proposes a novel evaluation scheme based on the packet buffer capacity of nodes using a queuing network model. The packet buffer capacity parameter for the queue is analysed for each node type when it is in the best working condition. This method expands the queuing network model into the equivalent queuing network model by adding holding nodes to the existing network to evaluate congestion within the queuing network and obtain effective arrival and transmission rates. This work establishes an M/M/1/N-type open queuing network model with WSN holding nodes; it includes designing approximate iterative algorithms to calculate arrival rates when the system reaches a steady state. Experimental results indicate that the model is consistent with real-world data. This paper discusses modelling for only a single-server WSN model and proposes a method to calculate the packet buffer capacity size for nodes. Recent research focuses on the convergence of multiple processor nodes that can be used for M/M/m/N queues, which are also multi-server queues. For large-scale WSNs, prioritised clusters can effectively improve WSN performance, which will be our follow-up research.

In the paper "Fundamental Lower Bound for Node Buffer Size in Intermittently connected Wireless Networks", the author analyse the fundamental lower bound for the node buffer size in intermittently connected wireless networks. Due to some external constraints, there is a possibility that node inactivity may occur, which is the main cause for intermittent network connectivity. In a static random network, each node keeps a constant message generation rate. The buffer occupation in each node does not approach zero despite having infinite network capacity and node processing speed. A detailed analysis has been performed on buffer occupation when the channel capacity is infinite, and the results can be viewed as a lower bound for networks with finite channel capacity. The analysis show that when the probability of node inactivity is below the critical value, the network state is supercritical, and the fundamental achievable lower bound of the node buffer size is $\Theta(1)$. The minimum node buffer size requirements are asymptotically independent of network size, and when the probability of node inactivity is greater than the critical value, the network state is subcritical and the achievable lower bound on node buffer size shoots up as the network expands in the order of $\Theta(\sqrt{n})$.

The paper "Limiting the Power Consumption of Main Memory" focuses [4][5] on the peak power consumption by the hardware components. This affects the power supply, packaging and cooling requirements of the system's hardware. Higher peak power consumption by the hardware leads to bulky and expensive systems. If the components and systems actually require peak power, it becomes necessary to limit the power consumption to a less-than-peak power budget. This leads to intelligent provisioning of the power supplies, packaging and cooling infrastructures for the hardware components. This paper studies dynamic approaches to limit the power consumption by the main memories. It proposes 4 techniques, i.e., Knapsack, LRU-Greedy, LRU-Smooth, and LRU-Ordered, in which the memory device power state are adjusted as a function of load on the memory subsystem. The simulations carried out from 3 benchmark applications prove that these techniques consistently limit the power to a pre-established budget accompanied by low performance degradation. The simulation results indicate that limiting power using these techniques has the same effect as the conservation approach used in state-of-the-art techniques exclusively designed for performance-aware energy management. Limitations of this work include addressing issues related to selecting an ideal power budget in different scenarios and studying the effect of greater concurrency in memory accesses in the context of chip multiprocessors in future.

Han-Lin Li, Chia-Lin Yang, and Hung-Wei Tseng have presented a paper titled "Energy-Aware Flash Memory Management in Virtual Memory System", which revisits the design of virtual memory system using flash memory [7][8][9] for many portable devices due to its improvements in storage capacity, reliability and lower power consumption. This paper concentrates on the energy efficiency aspect, as power is the first-order design consideration for embedded systems. Frequent writes into the flash memory lead to frequent garbage collection, thus incurring significant energy overhead. This is due to the write-once feature of the flash memory. To address this issue in increased energy consumption and prevent excess energy lost, the authors have proposed 3 methods to reduce the number of writes occurring in the flash memory. They are HotCache scheme, Subpaging technique and Duplication-aware garbage collection method. In the HotCache scheme, an SRAM cache is introduced to buffer frequent writes. In the subpaging technique, pages are partitioned into subunits and only dirty pages are written into the flash memory when a page fault occurs. The duplication-aware garbage collection method uses the data redundancy that exists between the flash and main memory to bring reduction in the writings that occur due to garbage collection. Intrapage locality, a type of data locality, is an inherent feature of flash memory and responsible for data allocation. This property of the flash memory should be carefully preserved while data are written from the storage buffer to flash memory. Destroying this property leads to increase in the energy consumption by the flash memory. Experiments have been performed using the 3 techniques and the results show an average energy reduction of 42.2% using the combination of the 3 techniques.

Several papers [11] [12] [13] address the basic issues involved in architectural design and the S used in sensor network applications. These papers present open issues in the hardware design and software components in wireless/multimedia sensor networks. Authors also classified the off-the-shelf hardware and the research prototype currently used in different forms sensor network. Much research has been performed in cluster–based WSN, focusing on energy efficiency and scalability related to clustering protocols. To select the cluster head in statistical techniques [14], all sensor nodes in the network equally share the role of cluster head, which adds to the life span of the sensor node. The HEED Clustering algorithm [15] implements a hybrid model to select the cluster head based on the residual energy of the node and its proximity to its neighbours - an additional parameter involved the selection process. The issues related to the power of balanced energy consumption among the cluster head nodes have been discussed in [16, 17]. The ACE clustering algorithm [18] partitions a network into uniformly dispersed clusters. Another clustering technique known as autonomous clustering and uses the coverage estimation parameter [19][20][21].

III. Memory Bank Architecture for a Wireless Sensor Node

In the heterogeneous network class, wireless sensor networks form the lower level of the Internet networking hierarchy, where energy utilisation due to various factors is the main issue that affects the lifespan of the wireless sensor network and must be considered during the design of the network architecture. One such energy-consuming factor is the memory access operations. Figure 2 shows the block diagram shows the modified sensor node along with Figure 3 modified memory architecture with switching power controller unit. Consider 128 KB flash memory that is equally divided into 4 blocks of 32 KB each and are known as memory banks. The architecture also contains a memory switching controller unit that will select the memory block and amount of memory needed by the sensor node based on the traffic flow. This leads to energy conservation by the memory unit in the sensor node where only that part of memory that is currently in use is powered.

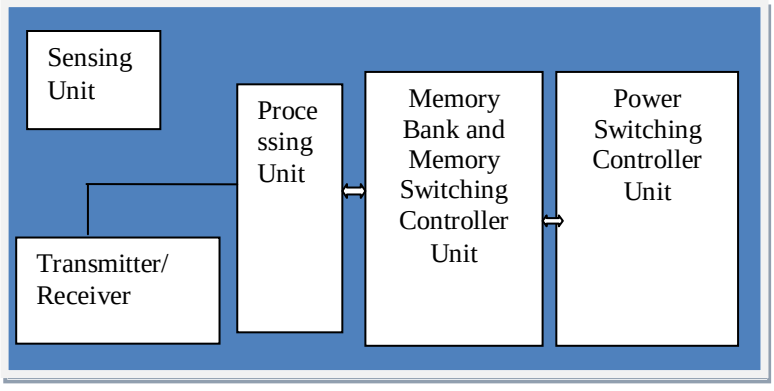

Fig.2. A typical Modified Wireless Sensor Node

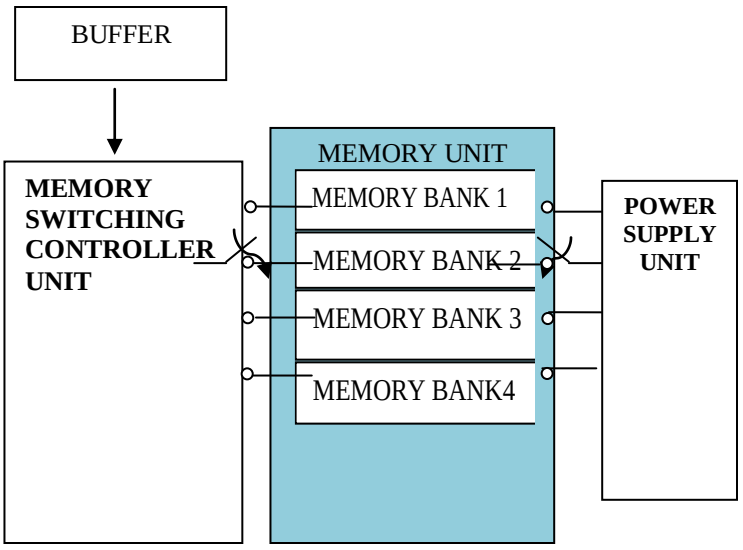

Fig.3. Block Diagram of Memory Bank Architecture of a Sensor Node

The amount of traffic flow is application-specific. Let us consider Aibe is following cues…

es.

Case I: Within the WSN, there are sensors that sense data, including temperature, humidity, and pressure. Such data require less storage.

Case II: WSN may also comprise multimedia sensors that capture multimedia information, such as images, video or audio, and process them. Processing of such data may include decision making, which is performed by the intelligent systems in the network. In such cases, the multimedia information requires large amounts of storage.

It is thus up to the sensor node to activate the number of memory banks required in the system based on the application for optimised energy utilisation.

In most wireless sensor network applications, we find variations in the traffic flow i.e., for some duration of the network operation the traffic flow is increased, while at some time the traffic flow is decreased. Thus an optimised way to achieve energy consumption is to divide the memory into a number of blocks and then use (power) only the part of the memory required for data storage. For example, let us say that amount of storage required for storing the data sensed by the node is only 20 KB out of total flash memory size of 256 KB. One approach is to consider the whole memory of 256 KB as one block and use only 20 KB. Though only 20 KB of space is being utilised but the power is supplied to the entire 256 KB memory. There is unnecessary wastage of excessive power in such a scenario, and this wastage can be avoided. Another alternative is to consider the memory unit consisting of a switching controller unit and divide the 256 KB memory into 8 banks of 32 KB each and use only 1 memory bank to store 20 KB of data; i.e., power is supplied to only 1 memory bank by the switching controller unit and the remaining 7 banks are switched off. Because less memory is being utilised, the power required will also be reduced thus leading to the

conservation of energy utilisation by the memory unit in the sensor node. The power consumption in different scenarios is given as follows:

Normal Scenario 1: power consumption in normal memory architecture as shown in FIG. 4

P_{normal} =Energy Dissipation (i.e., P_{read},P_{write}, $P_{process}$)for usage space + Idle Energy

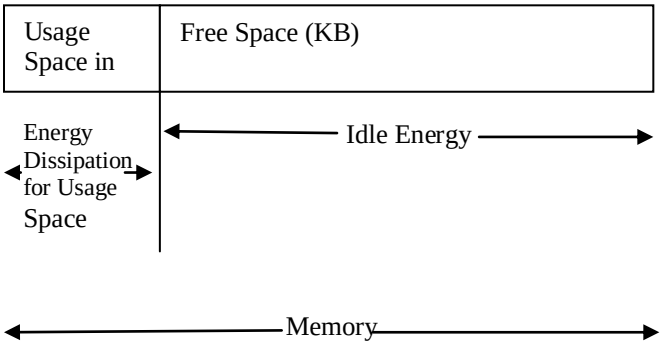

Fig.4. Energy Dissipation in normal memory architecture

Modified Scenario 2: power consumption in modified memory architecture from figure 5

P= {Number of Memory Bank} X Energy Dissipation (i.e., P_{read}, P_{write}, $P_{process}$)

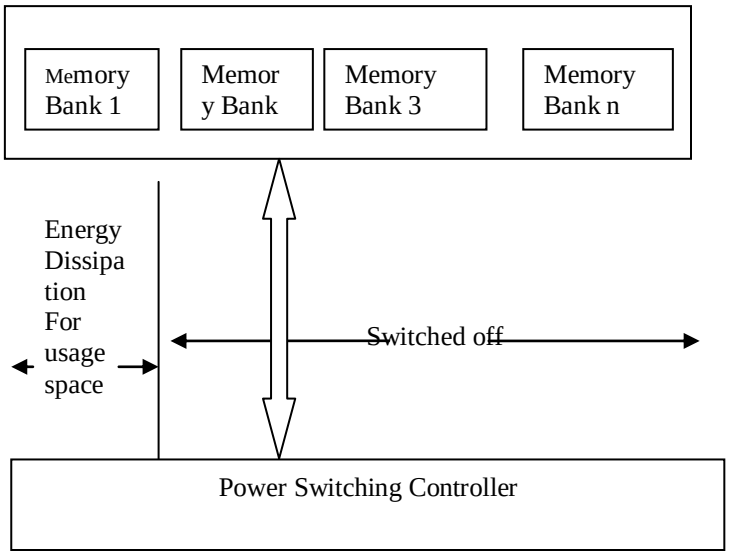

Fig.5. Energy dissipation in modified memory architecture

Figure 5 shows that ideal energy dissipation can be minimised, which conserves energy and leads to increases in the node lifetime.

IV. System Model for Memory Architecture

We have considered a simple queue system model in which packets arrive according to Poisson's model at rate λ, so the interarrival times are independent exponential random variable switch mean 1/ λ. In an M/M/1 model [10], the packet distribution is Poisson with rate λ or the interarrival time distribution is exponential using mean time 1/λ. Similarly, the service rate distribution is also based on a Poisson model with rate μ or is exponential with the mean time 1/μ. Interarrival and service times are independent variables. Assume that four packets, P_1 through P_4, arrive randomly and require service time S_1 through S_4. E_a is the energy dissipation for receiving the packet, E_s is energy dissipated during servicing the packet and E_q is energy dissipation when the packet is in queue, as in figure 6.

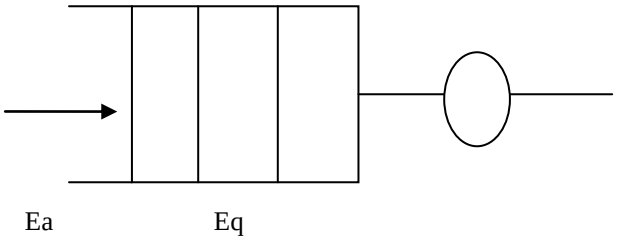

Fig.6. . Queuing Model

A. *Algorithm for modified memory architecture*

Input data:
$P_1,P_2,P_3 \ldots P_n$: Arriving Packets
$S_1,S_2,S_3 \ldots S_n$: Service Time for every Packet
Ea : Energy Dissipation for packet arrival
Es : Energy Dissipation for servicing the packet
Eq : Energy dissipation for queuing or Storing in buffer
n : Number of memory banks in use

Step 1: Traffic is generated i.e., interarrival and service times are generated using random processes for all incoming packets.
Step 2: if server is idle then
Packet is serviced
Else
Based on memory requirement by the arriving packets, memory banks are allocated by the memory controller and power switching controller unit will supply power to only the allocated memory banks.

Packet is stored in queue

End if

Total Energy Consumption = Ea + n* Eq +Es

Step 3: END

V. Simulation Environment:

We have considered the M/M/1 model to generate the traffic flow at the sensor nodes. In this process, the interarrival and service times are generated randomly using a Poisson distribution, and the total energy consumption is calculated for every event occurring in the sensor node. The analysis has been performed, varying both interarrival and service times. Figure 7 provides a sample snapshot with a graphical user interface created for the simulation.

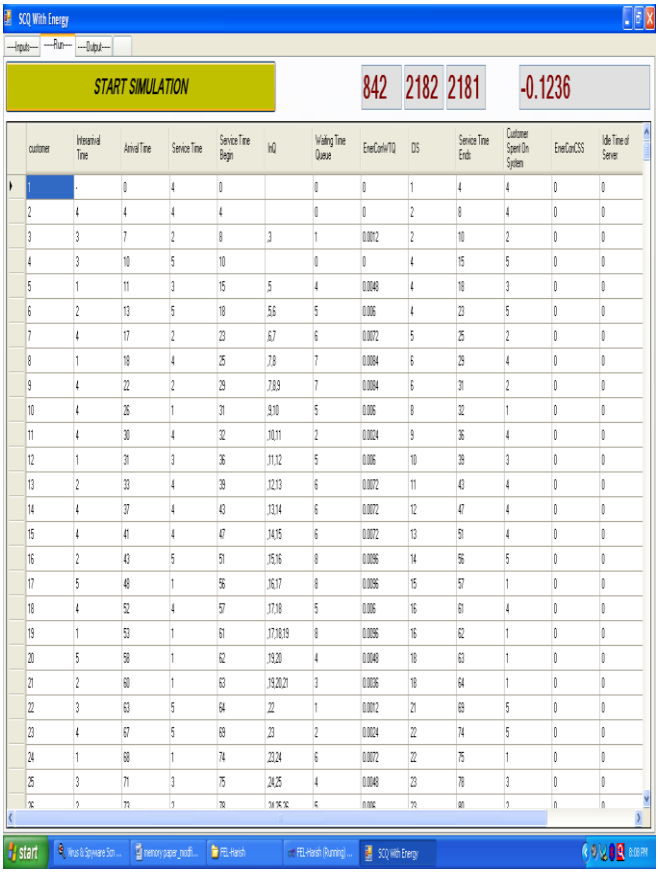

Fig.7. GUI Snapshot

VI. Result Analysis

In this section, we present the results obtained from simulations.

Table I lists the parameters and their corresponding values considered in the simulations.

Table I. Simulation Parameters:

Parameters	Value
Energy Threshold	200 Joules
Energy for Receiving	0.057 Joules
Energy for Transmitting	0.033 Joules
Idle Queue Energy	0.00012 Joules
Interarrival Time	1-7 sec
Service Time	1-7 sec
Number of Packets	1000 Packets
Queue Length	100 Packets

The graphs in Figures 8 - 10 are the plots of Service time (sec) on the X-axis and Energy Consumption (Joules) on the Y-axis.

Case I: Interarrival time: 1 sec
Service time : 1-5 sec

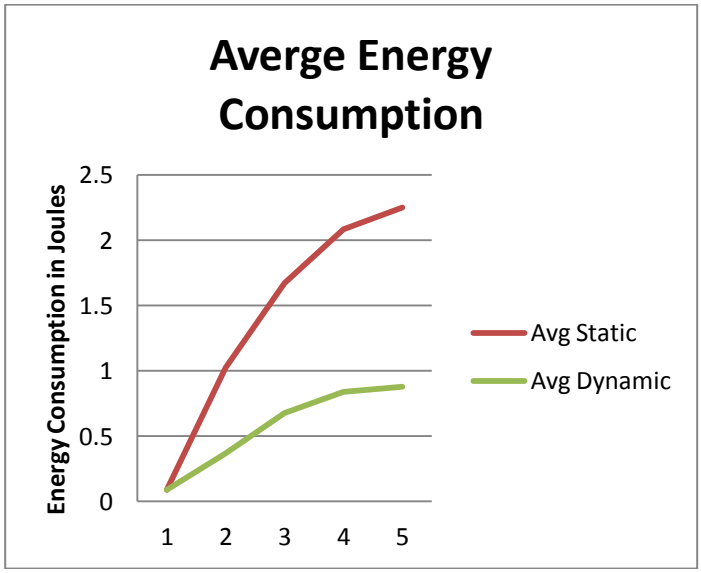

Fig.8. Comparing the average energy consumption normal memory (static) with modified memory architecture (Dynamic) for an interarrival time of 1 sec

Figure 8 shows that at service time 1 sec, there is a deviation in the energy utilisation curve for a memory-modified architecture (green curve) from the energy utilisation curve obtained for the normal memory architecture (red curve) without the memory banks. The energy utilisation by the modified architecture is significantly less than that of the normal architecture.

Case II: Interarrival time: 1-2 sec
Service Time: 1-5 sec

Figure 9 shows that the energy utilisation curves for both architectures are almost the same. At 2 sec of service time, the deviation occurs, i.e., the energy consumed during the memory operations in the normal memory architecture are much more than the modified memory architecture at the node.

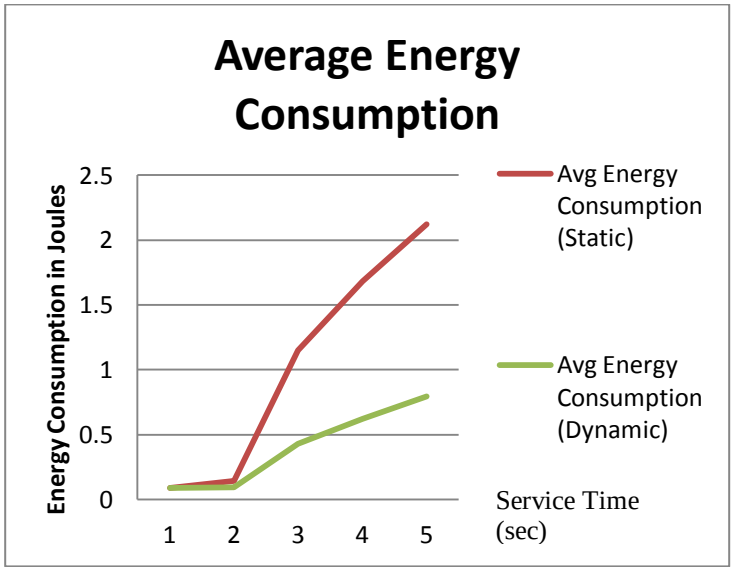

Fig.9. Comparison of average energy consumption normal memory(static) with modified memory architecture (Dynamic) for interarrival time between 1 -2 sec

Case III: Interarrival time: 1-5sec
Service time : 1- 5sec

Figure 10. Energy conservation is achieved using modified memory architecture.

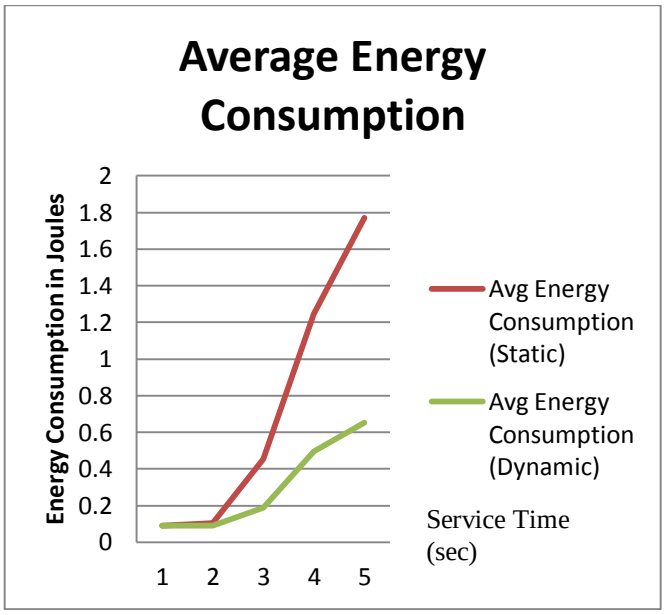

Fig.10. Comparing average energy consumption normal memory (static) with modified memory architecture (Dynamic); interarrival times between 1 and 5 sec

From Case-I to Case-III, the energy utilisation curve for the modified memory architecture clearly deviates from the normal curve. The energy consumed in the dynamic method is much lower than the original node memory architecture. During the simulations, this deviation occurs because the modified memory architecture increases in performance over the normal architect, as more packets get queued up to be serviced in the sensor node by consuming less energy during memory operations, which leads to energy saving and thus increases the network lifetime.

The graphs in Figures 11 to 13 plot of Service time (sec) on X-axis vs. Number of Packets dropped on Y-axis.

Case IV: Interarrival time: 1 sec
Service time: 1-5 sec
Case V: Interarrival time: 1-2 sec
Service Time: 1-5 sec
Case VI: Interarrival time: 1-5sec
Service time: 1-5sec

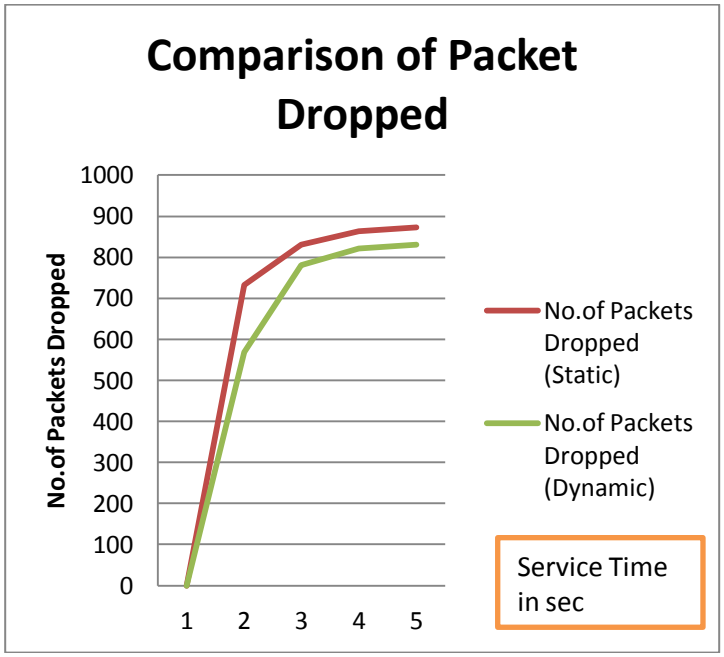

Fig.11. Comparing the number of packets dropped in normal memory (static) with modified memory architecture (Dynamic) with interarival time 1 sec.

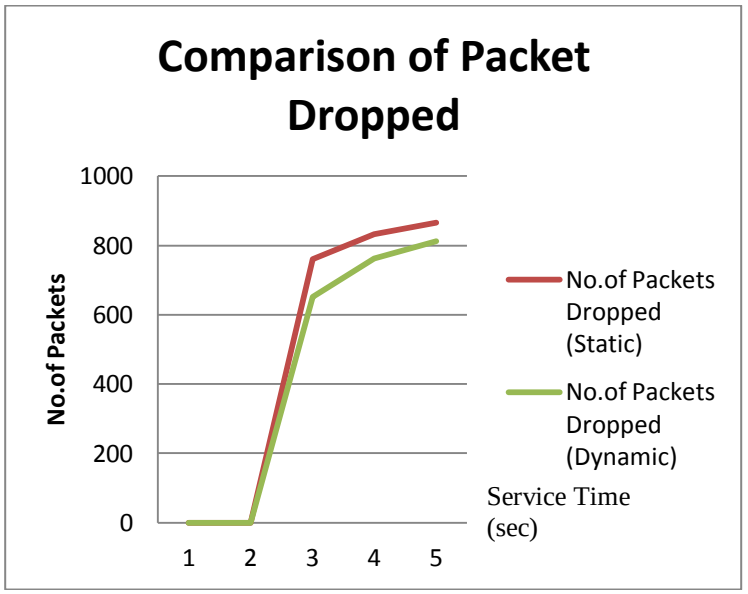

Fig.12. Comparing the number of packets dropped in normal memory (static) with a modified memory architecture (Dynamic) with interarrival between 1 and 2 sec

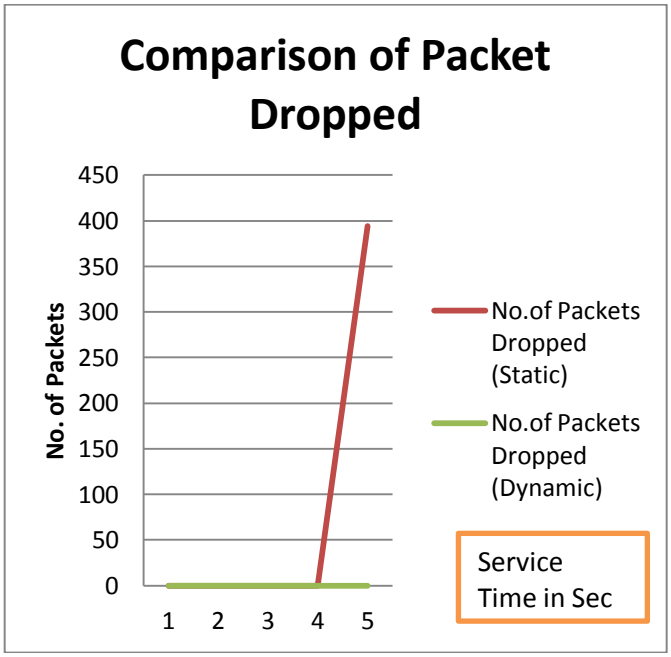

Fig.13. Comparing the number of packets dropped in normal memory (static) with modified memory architecture (Dynamic) with interarrival between 1 and 5sec

From Case-IV to Case-VI, the packet dropped in the dynamic method is less than the original node memory architecture. During the simulations, a variation in packet arrival is observed, i.e., interarrival time, where more packets get queued up to be serviced and the modified memory architecture show less packet drop in performance as against the normal architecture.

VII. Conclusion

This work proposes a modification of the memory architecture in the sensor node. In this architecture, the memory module is divided into several blocks known as memory banks that are activated by the memory controller unit and power-switching module. Depending on the amount of traffic flow the memory banks are activated. Simulations have been performed for varying interarrival and service times using the M/M/1 queuing model.

The graphs and simulations show a small difference in the energy utilisation at the initial stages when there are fewer packets in the queue and the service time is low. As the number of packets getting queued up and service time increase, the modified memory architecture performs significantly better than the normal memory architecture, considering the performance parameters energy consumption and packet drop. This increases the node lifetime and network lifetime.

References

[1] Rong-Jaye Chen, Ting-Yu Lin, and Yi-Bing Lin "Reducing Power Consumption for Mobile Multimedia Handsets", Tamkang Journal of Science and Engineering, Vol. 2, No. 3, pp. 133-141 (1999).

[2] Tie Qiu, Lin Feng, Feng Xia, Guowei Wu, and Yu Zhou "A Packet Buffer Evaluation Method Exploiting Queueing Theory for Wireless Sensor Networks" ComSIS Vol. 8, No. 4, Special 1028 Issue, October 2011

[3] Xinbing Wang, T. Yu, Y. Xu, "Fundamental Lower Bound for Node Buffer Size in Intermittently connected Wireless Networks" IEEE Transactions on Parallel and Distributed Systems, 2012.

[4] Yuanzhong Xu and Xinbing Wang "Limiting the Power Consumption of Main Memory", Infocom ,2011.

[5] Tajana ˇSimunic, Luca Benini, and Giovanni De Micheli, "Energy-Efficient Design of Battery-Powered Embedded Systems", IEEE Transactions On Very Large Scale Integration (Vlsi) Systems, Vol. 9, No. 1, February 2001.

[6] Han-Lin Li, Chia-Lin Yang, and Hung-Wei Tseng "Energy-Aware Flash Memory Management in Virtual Memory System" IEEE Transactions On Very Large Scale Integration (VLSI) Systems, Vol. 16, No. 8, August 2008.

[7] M. Chiang, P. Lee, and R. Chang, "Managing flash memory in personal communication devices," in *Proc.* 1997 Int. Symp. Consumer Electronics (ISCE'97), Singapore, Dec. 1997, pp. 177–182.

[8] Rulnick, J. M. and Bambos, N., "Mobile Power Management for Maximum Battery Life in Wireless Communication Networks," Proceedings of IEEE INFOCOM, Vol. 2, pp. 443-450, (1996).

[9] F. Douglis, F. Kaashoek, B. Marsh, R. Caceres, K. Li, and J. Tauber,"Storage alternatives for mobile computers," in *Proc. 1994* Symp. OperatingSyst. Design Implementation, Nov. 1994, pp. 25–37.

[10] Michael Baron "Probability and Statistics for computer Scientists" Chapman & Hall/CRC ,first Indian Reprint, 2010.

[11] Sanislava Soro and Wendi Heinzelman, "A Survey of Visual Sensor Networks" Advances in Multimedia Volume 2009, Article ID 640386, 21 pages.

[12] Youssef Chari, Bell Canada, Naoki Wakamiya,"Challenging Issues in Visual Sensor Networks", IEEE Wireless Communication, April 2009, page no 44-49.

[13] F.Akyildiz "A Survey on Sensor Networks", IEEE Communications Magzine., Vol.40, Aug.2002,pp. 102-114.

[14] F.Akyildiz, T.Melodia and K.R.Chowdhary, "A Survey on wireless Multimedia Sensor Networks", Elsevier, Computer Network, Vol.51, March 2007,pp.921-960.

[15] W.Heinzelman, A.Chandrakasan, Balakrishnan, "An application specific protocol architecture for Wireless micro sensor networks", IEEE Transactions on Wireless Communications 1 (4) 2002.

[16] O. Younis, S.Fahmy, Distributed Clustreing in ad-hoc sensor networks: a hybrid, energy efficient approach, IEEE Transaction on Mobile computing 3 (4) (2004).

[17] T.Shu, M.Krunz, S.Vrudhula, "Power balanced coverage-time optimization for clustered wireless sensor networks", in: proceedings of MobiHoc'05,2005.

[18] S.Soro, W.Heinzelman, Prolonging the lifetime of wireless sensor networks via unequal clustering, in: Proceeding of the Fifth International workshop on Algorithm for wireless, Mobile, Ad Hoc and Sensor Networks (IEEE WMAN'05), 2005.

[19] H.Chan , A.Perrig, ACE: "An emergent algorithm for highly uniform cluster formation", in Proceedings of EWSN, 2004.

[20] K.Bae, H.Yoon, "Autonomous Clustering Scheme for wireless sensor networks using coverage estimation self-pruning", IEICE Transcation on Communication E88-B (3) (2005).

[21] M.T. Thai, F.Wang, D.Du, "Coverage problems in wireless sensor networks- designs and analysis", International Journal of Sensor networks, Special Issue on Coverage Problems in Sensor networks, 2005.

[22] Stanislava Soro and Wendi Heinzelman, "Cluster head election techniques for coverage preservation in wireless sensor networks", Ad Hoc Networks,Elsevier, Sept 2008

Authors Profiles

Asst. Prof. Harish H. Kenchannavar received his Master's degree (M.E) from Shivaji University, Walchand College of Engineering & Tech, Sangli, Maharashtra. He has registered for Phd degree under Visvesvaraya Technological University, Belgaum. Research Center:- SDMCET, Dharwad, Karnataka under the guidance of Prof. Umakant P. Kulkarni. He is currently working as Assistant Professor in Computer Science Department, Gogte

Institute of Technology, Belgaum, Karnataka. He has presented and published papers at national and IEEE International conferences. His research interests include computer networking, simulation and modeling, visual sensor networks and queuing algorithms.

Assoc. Prof. M.M.Math received his Masters degree (M.S) from Birla Institute of Technology, Pilani, Rajasthan. He has registered for PhD degree under Graphics Era University, Deharadun. Research Center: - SDMCET, Dharwad, Karnataka under the guidance of Prof. Umakant P. Kulkarni. He is currently working as Associated Professor in Information Science Department, Gogte Institute of Technology, Belgaum, Karnataka. He has presented and published papers at national and IEEE International conferences. His research interests include autonomic computing, Persive computing and their applications and visual sensor network.

Prof. Umakant P. Kulkarni received his PhD degree from Shivaji University, Kolhapur. Research Center Walchand College of Engineering & Tech, Sangli, Maharashtra in Nov 2007 . He has completed his Masters degree (M.E) from PSG, Coimbatore. He is currently working as Professor in Computer Science Department, SDMCET, Dharwad, Karnataka. He has published and presented a number of papers in many reputed journals and at International IEEE conferences as well. He also has presented technical talks and tutorials on various aspects of Mobile Agents. His research interests include mobile agents, computer networking, and distributed networking.

A novel optical network on chip design for future generation of multiprocessors system on chip

M.Channoufi[1,3], P. Lecoy[1]
[1]ETIS(Research Team in Information Processing and Systems), ENSEA - University of Cergy-Pontoise - CNRS,France

S. Le Beux[2] , R. Attia[3]
[2]Lyon Institute of Nanotechnology, Central School of Lyon, France
[3]URCSE (Unité de Recherche Composants et Systèmes Electroniques), Ecole polytechnique de Tunisie

B. Delacressonniere[4]
[4]LaMIPS (Laboratoire de Microélectronique et de Physique des Semiconducteurs), CRISMAT-NXPSemiconductors-PRESTO engineering, CNRS UMR 6508, France

***Abstract*—The paper presents a novel Optical Network on Chip (ONoC) relying on the multi-level optical layer design paradigm and called "OMNoC". The proposed ONoC relies on multi-level microring resonator allowing efficient light coupling between superposed waveguides. Such microring resonator avoids using waveguide crossing, which contribute to reduce propagation losses. Preliminary experimental results demonstrate the potential of multi-level optical layer for reducing power consumption and increasing scalability in the proposed ONoC.**

Keywords—3D-Optical network on chip, multi-level optical layer, optical control.

I. INTRODUCTION

The constant progression in computer and smartphones architecture and the continuous growth of the number of transistors on a chip involve an increasing need of high-performance, low cost and low power consumption networks on chip. In the next future, electronic interconnections will no longer be able to fulfill these requirements.

The numerous advances in silicon photonic integration and the successful realization and fabrication of micro-optical devices such as photo-detectors[1,2,4] ,modulators [5,6,12], buffers [21] and optical switches [8,9,13,16,22] push the studies on future generation of multiprocessor systems-on-chip (MPSoC) using optical interconnections. Increasing importance is given to the architectures and topologies of optical networks on chip. Some of them use passive optical networks, such as Briere et al [7] and Vantrease et al[26]. This choice allows a 100% optical network using passive switches (preconfigured), but the challenge to overcome is to manage the complexity of static routing tables and to provide a large range of resonant wavelengths when increasing the number of cores. Others like A.Shacham et al. [10], Xu et al. [3], proposed the integration of active optical components, minimizing the number of optical resonators and waveguides, but requiring electrical command of the optical switches. In the same way, and in order to ensure reliable and efficient transmission of optical signals, many studies have been made to develop control protocols for packet routing that provide QoS [19] and synchronization or organization protocols of the optical traffic inside the network [18,19, 20].

The ONoC proposed in this paper relies on the multi-level optical layer design paradigm. As a main contribution, three waveguides level are used in order to implement two sub-networks without any waveguide crossing: a network is dedicated to payload data and the other is for control flow. The data network is realized through two superposed waveguides and is a combination between two modified Fat-H-Tree [11, 14].

Interactions between the waveguide levels are realized by a novel 3D microring resonator. The control network is Mesh-based and is located under the data network. In section II, the overall architecture, including the ONoC and the control network are presented. Results on optical power loss, design complexity, set up latency and power consumption are presented in Section III. Section IV concludes the paper and gives perspectives to this work.

II. NETWORK ARCHITECTURE

In this section, we present how multilayer can be used to design an effective ONoC. For this purpose, we exploit all the possibilities of optical structures such as superposed, crossing and curved waveguides.

A. Architecture Overview

The proposed 3D architecture is composed by a processing (electrical) layer and multi-level optical layer dedicated to data and control flow, as illustrated in Fig. 1. In this example, 8x8 processors are considered, resulting in 4x4 circuit interfaces (CI) and 3x3 control units (CU). The circuit-switched data network is implemented by two layers of superposed waveguides and adjacent to each other, as illustrated on the side view in fig. 1. The control network is composed by waveguides (implemented on a third dedicated layer) interconnecting control units located on the electrical layer. This optical network is efficiently implemented, without any waveguides crossing and realizing the shortest waveguide length between CU thanks to the multi-layer silicon deposit technology.

The electrical (i.e. processing) layer and both data payload network, and control networks interact with each other through Reduced Optical TurnArround Router (ROTAR).

B. ROTAR(Reduced Optical TurnAround Router)

Each ROTAR is composed by 4 waveguides superposed in two layers, 4 two-level switch (microring resonators), a Control Unit (CU) and 4 Circuit Interfaces (CI), as illustrated in fig.2. Since each circuit interface is shared by 4 processors, ROTAR manages communications for 16 cores. The CU is dedicated to the management of packets in the control network. If a source processor has to send data to a destination processor not sharing the same interface, the CU requests an access to the ONoC. For that, a setup packet P_{setup} is injected into the control network (i.e. in the waveguide located on the first level), following an XY static routing policy. Once the optical signal reaches the adjacent CU, it is converted in the electrical domain. If the destination is not reached, the control packet is re- converted in the optical domain and is transmitted to the next CU, depending on the availability of the optical resources, etc. Similarly to the networks proposed in [3,10,15], optical resources in the data flow network are reserved all along the setup packet path. Once the destination CU is reached, an optical acknowledgment packet P_{ack} is sent back to the source processor (it is transmitted similarly to P_{setup}). In order to avoid deadlock and to release optical resources as soon as possible, priority is given to acknowledgment packets. Once the P_{ack} is received by the source processor, payload data are injected in the data flow network; the optical signals will then propagate along the waveguides located on the first and second level, depending on the configuration of the circuit interface.

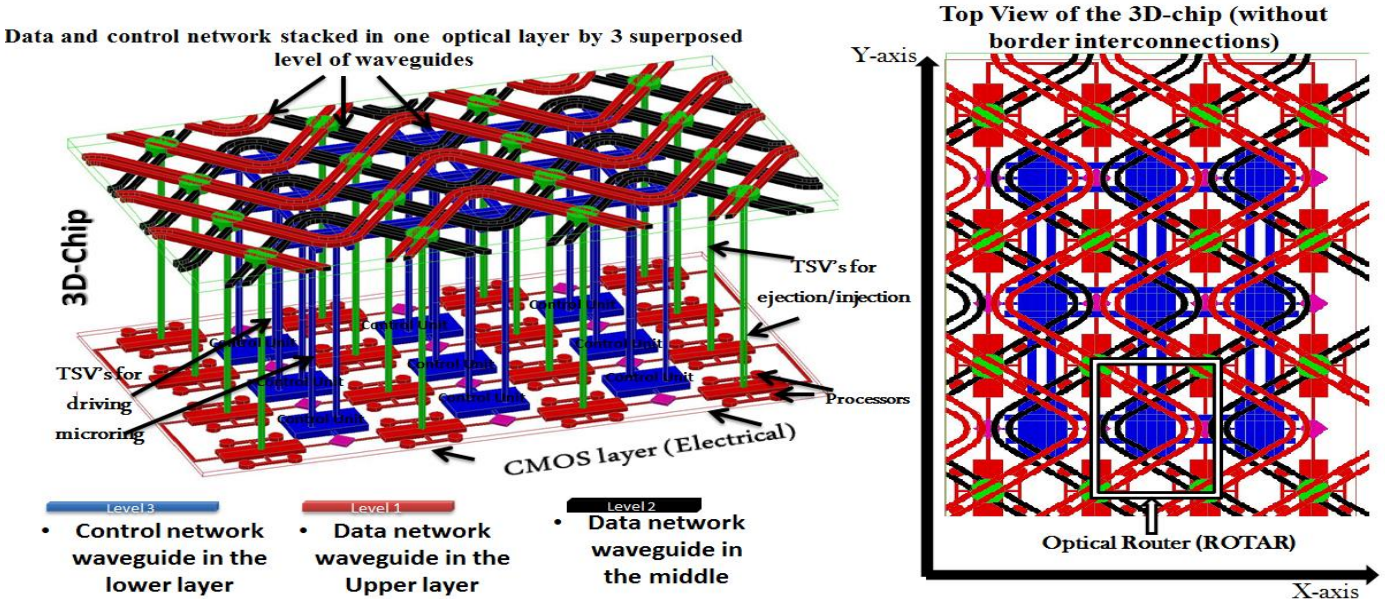

Fig.1. 4x4 3D optical network on chip (with a top view of optical network on chip) and Mesh-based control network on chip architecture

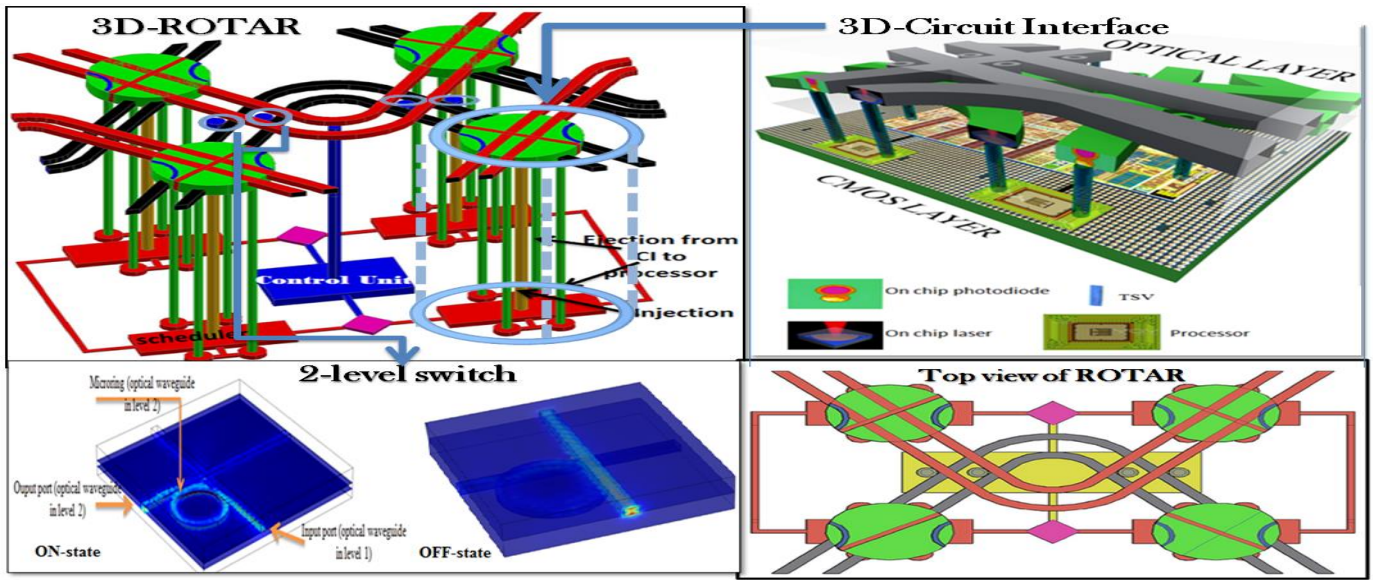

Fig.2. Reduced Optical TurnAround Router ROTAR

ROTAR is a reduced version of OTAR, the optical router proposed by Huaxi et al [3]. In order to simplify the topology, ROTAR consider only X-and Y-hops (does not allow diagonal communications) thus reducing the number of microrings by 30% compared to OTAR. This leads to a significant reduction of the power consumption, as detailed in the results section of the paper. The CI is formed by 6 superposed waveguides on 2 layers and 8 microring resonators to interconnect 4 cores (fig.2). One of the 8 microring resonator should be turned on in order to eject wave to its output port. To inject payload data, the processors send the signal through one of the 4 ports located in the CI (see fig.2). The configuration of each microring resonators is driven through TSV connected to the CU

Fig.3 illustrates a 2D view of the dataflow network layout with a chip size of 13mm×13mm, optical links between adjacent processors cores which are assumed to be 1mm by 1mm have an approximate length of 5 mm. This layout allows communication between 64 processors which need 64 lasers and 64 photodetectors to be fully interconnected.

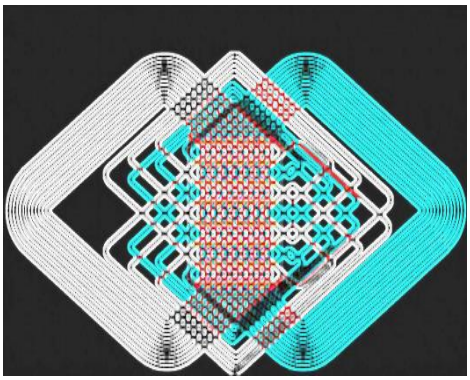

Fig.3. data payload ONoC (complete interconnections)

To achieve the high modulation speeds that would make on-stack interconnects practical (typically 10Gb/s data rate), one would need to use vertical cavity semi conductors lasers (VCSELs) for direct modulation. Since VCSELs are built using III-V compound semi-conductors, they cannot be easily integrated in a CMOS-compatible process. One stack mode locked lasers are an interesting separate modulation alternative. For that a one stack mode silicon locked lasers have been demonstrated [27].

C. 3D switch design (microring resonator)

In order to validate the interest of using multi-level optical layer for improving ONoC efficiency, a novel 3D implementation of the switching element (an active microring resonator) was realized using Comsol software. This switching element (fig. 4) is composed by two crossing and superposed waveguides (Si in SiO_2) with a width of 440 nm and a height of 300 nm, and a resonant ring of 3.4 µm diameter. The ring is located under the upper waveguide and adjacent to the lower one with a gap of 100 nm between ring and guides.

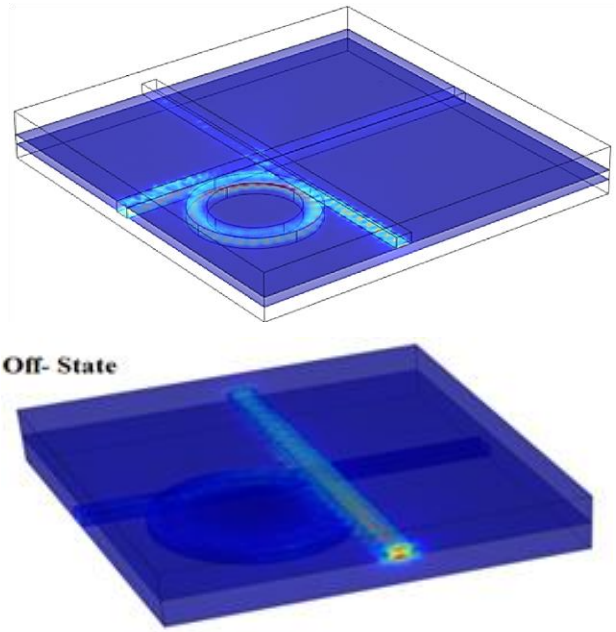

Fig.4. 2 waveguides levels based microring resonator (a) in ON state (b) in OFF state

The microrings resonators switches are configured to send the signal in the direction to be achieved. Basically, the configuration is achieved as follows:

-ON state in the case of horizontal hop: the optical signal is coupled from a waveguide to another;

-OFF state is configured otherwise: the optical signal propagates along the same waveguide.

D. Multi-path communications

Depending on the location of source and target processors in the network, the communications will occur through interlaced and external straight parts of waveguides (Fig.5). In order to reduce communication contention, each CI provides a dedicated ONoC access to its four attached processors P1, P2, P3 and P4. This is achieved by providing access to P1 and P2 (resp. P3 and P4) through the top (resp. bottom) optical layer and by allocating a given waveguide to each processor. Similarly, each processor can receive data independently from each other.

The waveguides located on the top (resp. bottom) layer are dedicated to propagate data from north to south (resp. south to north). Hence, data propagate along Y axis by using a same waveguide while communications along the X axis will require routing an optical signal from a waveguide to another.

E. Control unit

The control unit is one of the key elements to achieve a successful transmission; it is built from traditional CMOS transistors and it uses electrical signals to drive microring resonators; it deals only with control packets and it is formed by 4 optical/electrical converters, 4 multiplexers, 4 schedulers.

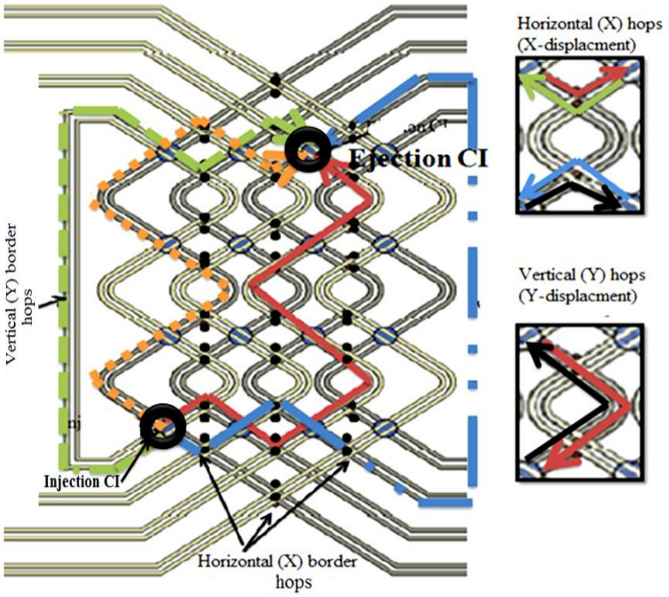

Fig.5. Possible communications paths between two different CI

The first scheduler for λ_{setup} uses FIFO algorithm for priority and the second gives priority always for λ_{acq} . Using optical waveguides in the control network affects directly the "End to End delay (ETE)" which will be much smaller than with the use of electrical buses The control unit is divided into two computing units, one for P_{setup} and the other for P_{acq}. This strategy has been adopted to decrease delay and packet queuing in CU, considering that each kind of control packet has a different wavelength so they can follow the same path simultaneously without any deadlock.

Each router is controlled by a control unit (CU) which processes electrical control packets. All control units are connected in an optical control network which commands microring resonators via TSV (through silicon via). The architecture of the control network for 256 cores is shown in fig.6.

The operation mode of the CU can be summarized as:

- Browsing of the table of "adjacent queue. Status" and synchronization of the control packets according to its content, update of the table by decrementing the current queue size and incrementing the queue size of the next control unit.
- Browsing the table of "path. Status", updating it according to the routing decision, decrement the field containing the number of displacements in the control packet P_{setup}.
- Command microrings at the slot time "T_n" if it is a horizontal hop, and increment the field of "time delay" in the control packet if the path is busy.

A study of set up latency and maximum queue size is done with Network Simulator NS-2 respecting the next rules:

- In each processor is implemented a routing protocol module developed with C++ due to its compatibility with NS-2.
- The processor generates a control packet according to this algorithm.
- The control packet is updated at each travel through a CU and is forwarded to the next CU until it reaches its destination.
- If it is an X hop, the CU switches the microring in the adequate time slot.

Results of this study is given in section III.

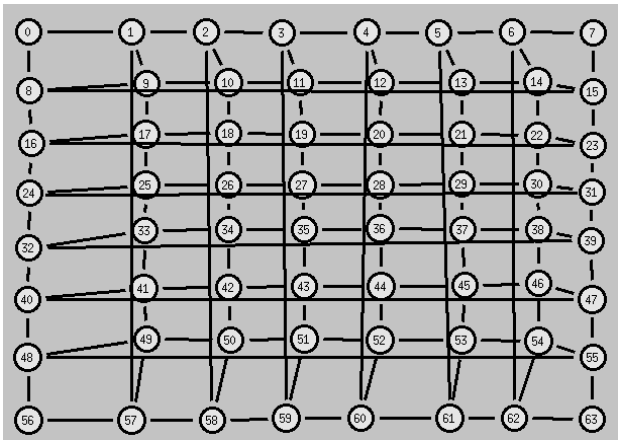

Fig.6. Control network architecture implemented in NS-2

F. *Circuit interface*

The circuit interface (CI) is the component interfacing the optical network layer for payload data and the CMOS electrical layer by EO-OE interfaces. The CI is formed by 6 superposed waveguides and 8 microrings to interconnect 4 cores, just one microring should be turned on in order to direct the wave to its output port. Top view of the CI is shown in Fig.7 while the complete 3D implementation is shown in Fig.2.

The CI processes only payload data, which means that after reserving path by control packets, the processor sends the payload data over the CI. The microrings in the CI are driven by the control unit and are switched on only if the current CI is linked to the processor's receiver of the final destination of the packet.

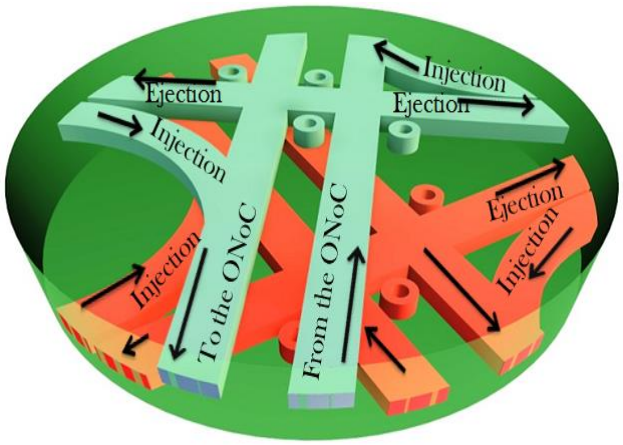

Fig.7. circuit interface

The connection between adjacent processors sharing a common CI is done electrically due to the short distance between them. Each processor has two ports, one for injection and a second for ejection. The injection is done directly through Y-waveguide while ejection requires driving on one of the microring resonators (Fig.8).

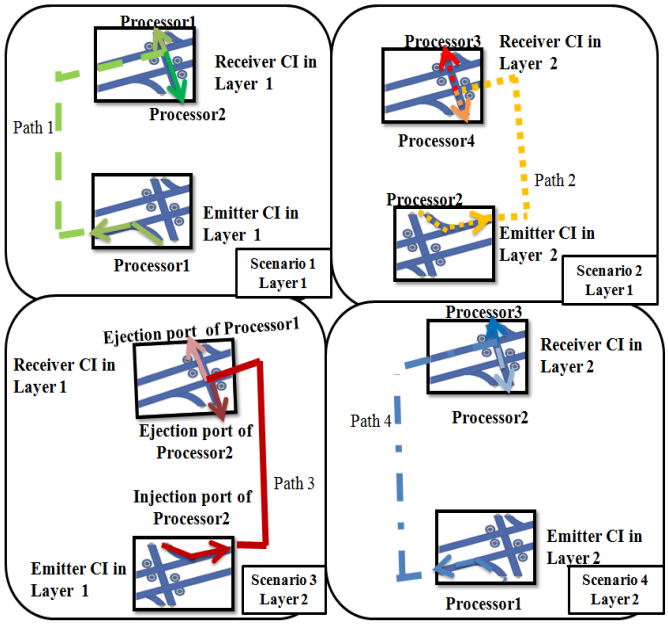

Fig.8. Wave injection and ejection in CI

Fig.8 shows the four possible paths that can be established between two different CI. Corresponding to injection port (processor 1, processor 2, processor 3, processor 4), the suitable path to the destination CI is defined (one of path 1, path 2, path 3, path 4). While in order to be driven to the corresponding processor , each time we command the microring resonator corresponding to the ejection port of this processor.(example from Fig.8 (scenario 1) ; for path 1, injection is from processor 1 in emitter CI and ejection is to one of processor 1 or 2 in receiver CI).

G. Discussions

Compared to the networks proposed by [3, 10, 15], the control flow is realized optically. In addition to allow a reduction of communication latency, WDM is used in order to concurrently propagate setup and acknowledgment signals, respectively through λ_{setup} and λ_{acq} wavelengths, which can help reducing contentions in the network. By using a single layer, the number of waveguides crossing would increase the propagation losses in the overall ONoC. With a two-level waveguide network, waveguides crossings are avoid and coupling losses as well as crosstalk can be minimized, leading to low latency and power efficient ONoC.

We believe that multi-level optical layer design paradigm opens new researches directions in ONoC topologies. Indeed, related works intend to decrease propagation loss by reducing the number of waveguides crossings. This has led to the use of ring topology and its associated serpentine like layout. However, optical signals propagate along with a single dimension, which negatively increase the distance between source laser and destination photodetector, thus impacting the power consumption. By reconsidering n-dimensional data routing network such as Mesh or Torus, shorter distances will be considering, leading to lower power consumption in ONoC.

III. EXPERIMENTAL RESULTS

Maximum optical power loss and crosstalk are two critical figures of merit for an optical network on chip, which determine the feasibility and scalability of this ONoC, as well as the power consumption of E/O interface to generate and detect the optical signal.

A. Optical Power Loss

The total optical loss in the network is the sum (in dB) of all waveguide losses and of the wave coupling losses with transmitters and receivers:

$$L_{TOTAL}=L_{EW}+L_{LW}+L_{BW}+L_{CW}+L_{MR}+L_{WR} \quad (1)$$

Where

- L_{EW} is the coupling loss from transmitter to waveguide through the Y-junction in CI (see figs 2 and 7).
- L_{LW} is the propagation loss of a straight waveguide expressed as : L_{LW} = α*waveguide length .
- L_{CW} is the loss due to waveguide crossings, proportional to the number of crossings over the path of signal.
- L_{BW} is the bending loss depending on radius and angle of curvature of the bent waveguide.
- L_{MR} is the loss due to the coupling between guides through the microresonators by evanescent field coupling; this loss is proportional to the number of switches over the path of signal.
- L_{WR}; the coupling loss from waveguide to receiver.

The main loss occurring in a straight waveguide is due to the sidewall roughness, exactly parameters such as roughness correlation length and it increases with the index contrast. The estimated optical losses using Comsol software of both single and multi-level implementations of elementary optical component are summarized in Table 1.

We first begin the performance evaluation study by demonstrating the potential of multi layer design in optimized standard network floorplans such as Mesh, Torus and passive lambda network. Analytical results of crossing waveguides number in longest path for M*N Mesh "CR_{mesh}" and optimized Torus "$CR_{optimized\_Torus}$" topologies based network are proposed by K.Feng et al[23]. While Le-Beux et al [24] give the number of crossing waveguides in multi stage lambda network "CR_{λ}":

$$CR_{mesh} = \frac{(M+N)}{3} \quad (2)$$

$$CR_{optimized\_Torus} = \frac{(3MN+8)(M+N)-4(M^2+N^2)}{2MN} \quad (3)$$

$$\cdot CR_{\lambda} = \frac{(M+N)}{2} \quad (4)$$

TABLE I. Optical Power Loss

Optical device loss parameter	Insertion loss
Waveguides propagation "L_{LW} "	6.5 dB/cm
Waveguides crossing " L_{CW} "	0. 5 dB
Waveguides bend " L_{BW} "	0,05 dB
Passing by ring (off)	0.5dB
Coupling in one level switch (On) " L_{MR} "	3.5 dB
Coupling in multi-level switch(On) " L_{MR} "	4.5 dB
loss via Y junction "L_{YW}"	0,5 dB
Crosstalk in one level crossing	-13dB
Crosstalk in two level crossing	-23 dB
Input coupling loss "L_{EW} "	3 dB
Output coupling loss "L_{WR} "	0,6 dB

Results shown in Fig.9 demonstrate that by using multi-layer design and so avoiding waveguides crossings, optical power of about 4dB is saved in lambda network and 6 to 8 dB are saved in Mesh and Torus networks.

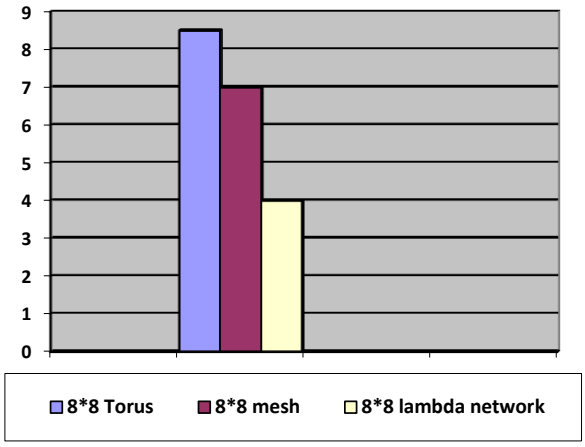

Fig.9. Optical power saved by using multi-layer design paradigm for different network architecture

For given photodetector and laser source devices, the maximum OMNoC size is limited by the worst case propagation loss L_{TOTAL}.

Assuming typical injected power of +5 dBm for on-chip integrable laser diodes and receiver sensitivity of -20dBm for 10 Gbit/s operation, the maximum insertion loss in any network size should be less than 25dB (available power budget) while crosstalk should be (in absolute value) much higher than this level in order to obtain a good reception quality.

Estimation of maximum optical power loss and crosstalk is done for different chip size in single and multi-layer implementations (Fig.10). In one level optical layer implementation, network scalability is limited to 64 cores, while by using superposed waveguides and so avoiding waveguides crossing loss, the cores number in one chip scales to 256.

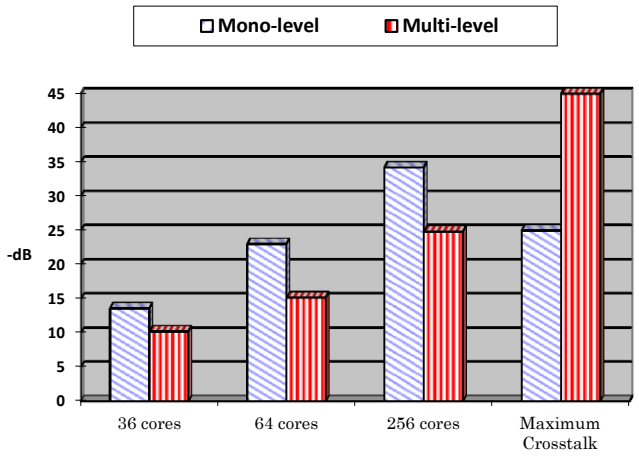

Fig.10. Worst case optical communications losses and crosstalk in our proposed multi-layer ONoC

The crosstalk in an overall communication is defined as the attenuation between the source processor and a processor which should not be the addressed processor. A higher crosstalk (in absolute value) involves less signal interference in the receivers. As shown in Fig.10, the use of the multi-layer design paradigm will satisfy this requirement with crosstalk 25dB lower than with single layer design.

B. Design complexity

Because all the constructed optical components are centrally symmetric, each waveguide in the ONoC satisfies the rules mentioned above. There are totally *4X+7Y-4* crossings for *X* horizontal and *Y* vertical hops number , Nr routers, $4((N_r)+(N/2))$ microrings and $2N/4$ waveguides for *N* lasers and N photodiode . For each optical link, only *(X+1)* Microrings are resonant at most, which can reduce the power consumption of the multi-level optical network on chip ONoC , and the details can be found in Table 2.

TABLE II. Merits of the constructed N multi level ONoC

Figure of merit	Value
Waveguide number	2N/4
CI number	√(N/4)
Microring number	$4((N_r)+(N/2))$
Waveguide crossings number	4X+7Y-4
Lasers number	N
Photodiode number	N

In table 3, a comparison is done between different ONoC topologies, one concerning the number of microrings in each router, including the microrings attached to injection and detection ports. The second parameter is the number of processors connected by optical waveguides in the route. Finally we calculate the number of driven microring resonators in the longest transmission scenario.

TABLE III. Number of microrings and processors required in OMNoC and related architectures

Top-logy	Number of microrings per router (Router+inj+eje)	Connected processor via router	Switched microrings in the longest path
Mesh [10]	14	1	6
Torus [19]	8	1	6
this work	36	16	5

According to parameters values given in Table 3, for mesh topology based network 14*8 microrings are needed to interconnect 8 processors. For Torus based networks 8*8 microrings are required for 8 processors too. While in our proposed multi-level ONoC, only 36 microrings are required to 16 processors (18 for 8 processors), leading to the lower number of used microrings. These results mean that OMNoC require lower chip area compared to Mesh and Torus based networks.

C. Maximum Queue size and packet set up delay

A study of packet set up latency and maximum queue size is done with network simulator NS-2. Contention may cause the packet to be blocked, leading to a path-setup latency on the order of tens of nanoseconds. For that the study of the maximum queue size is a key to avoid contentions in network. Once a path is acquired, the transmission latency of the optical data is very short, depending only on the group velocity of light in a silicon waveguide: approximately 6,6 10^7 m/s, or 300 ps for a 2-cm path crossing a chip .

We consider a traffic with 12 control units and each link between two CU supports a rate of 12.5Gb/s, we consider also 6 traffic generator that transmit 30 bits each 0.05ms during 1.5ms, this traffic share a common link, so we will focus on the maximum size of the queue in the common node in order to avoid packet drop.

The maximum queue size in the common traversed CU is found by comparing maximum queue size and queue lost and by decreasing each time data rate generating until reaching a curve of zero queue lost (without packet drop). According to that, the CU can deal with 19 packets without any network contentions (Fig.11).

The latency components are based on predicted individual latencies of electronic and silicon-photonic components in a future 45nm process. Results show a minimum set up latency of less than 50 ns for an offered load less than 0.2.While in overhead charge in the CU with an offered load up to 0.5, the set up latency increases to reach more than 350 ns per packet (Fig.12).

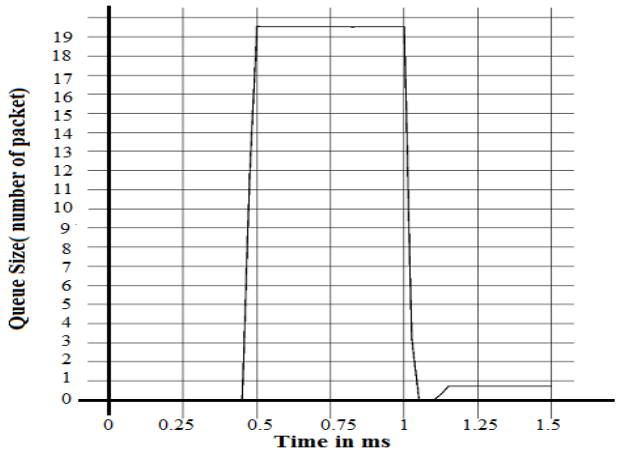

Fig.11. Maximum queue size

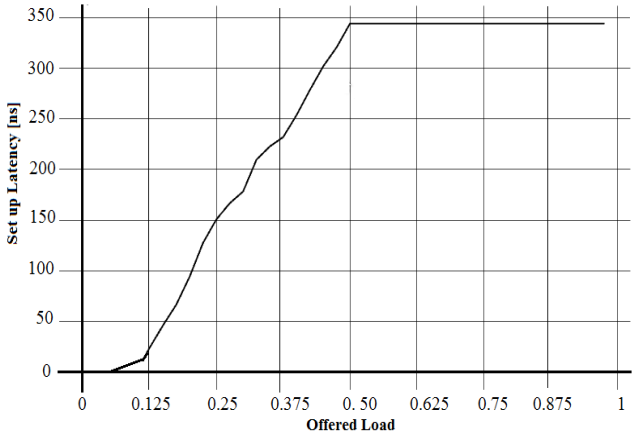

Fig.12. set up latency in control unit

D. Power consumption estimation

In order to evaluate the power consumption of our OMNoC, one must take into account the energy required by the control network ($E_{control}$) and by the data flow network ($E_{payload}$) for sending and receiving optical signals and by CU (E_{cu}) for saving data, scheduling packets, arbitration and storing CI configuration.

The total energy consumed to transmit a packet can be modeled analytically

$$E_{tot} = E_{payload} + E_{control} \quad (5)$$

$$E_{payload} = n * P_{mr}\left(\frac{L_{payload}}{R} + \frac{D_l}{v}\right) + E_{eo-oe}L_{payload} \quad (6)$$

$$E_{control} = E_{eo-oe} * L_{control} * J_p + E_{CU} * (J_p + 1) \quad (7)$$

$$E_{CU} = E_{buf} * 2L_{control} + E_{comp} + E_{scheduler} * 2L_{control} \quad (8)$$

Here n is the number of driven microring resonator in the network including those in the circuit interface. P_{mr} is the average power consumed by one microring resonator, in ON-state it consumes 20µW [17], $L_{payload}$ is the size of payload packet which is taken to be 1024 bits. R is the data rate transmitted by interfaces which taken to be 12,5Gb/s, D_l is the distance traveled by the optical packet in the ON-state, it depends on the processor core size which is taken here to 1mm by 1mm, and on the number of processor connected to each circuit interface. v is the light velocity. $E_{oe\text{-}eo}$ is the energy consumed for 1 bit oe-eo conversion which is assumed to be 1pJ/bit, J_p is the number of hops made in the control network. $L_{control}$ is the sum of the size of control and acknowledgment packets which is 28 bits. E_{CU} is the energy consumed by control unit, it was simulated by Cadence and is the sum of the energy consumed by buffers (0.003pJ/bit), the energy consumed by computation unit (1,5pJ) and by the schedulers using FIFO algorithm (0, 12 pJ/bit). For example, for a 256-core MPSoC and 128-byte packets, OMNoC consumes 1,032 nJ/packet in the payload data network and 0,187 nJ /packet in the control network using a control packet size of 28 bit.

IV. CONCLUSION

In this paper, we propose an ONoC that relies on the multi-level optical layer design paradigm. As a main contribution, three levels of waveguides are used in order to efficiently implement data flow and control networks. Interactions between the waveguides located on different levels are realized by a novel 3D microring resonator. Simulation results demonstrate the lower coupling loss of this 3D microring resonator compared to related works. The energy required by the resulting ONoC to send a packet is estimated to be 1,228 nJ, resulting in low power architecture.

REFERENCES

[1] L. Chen et al. High Performance Germanium Photodetectors Integrated on Submicron Silicon Waveguides by Low Temperature Wafer Bonding. In *Optics Express*, July 2008.

[2] S. Assefa, F. N. A. Xia , and Y. A. Vlasov, " Reinventing germanium avalanche photodetector for nanophotonic on-chip optical interconnects," Nature 464(7285), 80–84(2010)

[3] Huaxi Gu, Jiang Xu, Wei Zhang, « A Low-Power Fat Tree-based Optical Network-on-Chip for Multiprocessor System-on-Chip», Design, Automation Exhibition. DATE '09. 978-3-9810801-5-5.2009.

[4] S. Sahni et al. "Junction Field-effect-transistor based Germanium Photodetector on Silicon-on-Insulator" In *OpticsLetters*, May 2008.

[5] W. M. Green et al. « Ultra-compact, Low RF Power, 10Gb/sSilicon Mach-Zehnder Modulator". In *Optics Express*, Dec 2007.

[6] L. Gu et al. High Speed Silicon Photonic Crystal Waveguide Modulator for Low Voltage Application. In *Applied Physics Letters, 90, 071105*, 2007.

[7] M. Briere, B. Girodias, et al, "System Level Assessment and its capacity. of an optical NoC in an MPSoC Platform", Design, Automation & Test in Europe Conference & Exhibition, 2007.

[8] L. Martinez et al. High "Confinement Suspended Micro-ring Resonators in Silicon-on-Insulator". In *Optics Express*, June 2006.

[9] A. K. Okyay et al. « Silicon Germanium CMOS Optoelectronic Switching Device: Bringing Light to Latch". In IEEE Transactions on Electron Devices, Dec 2007.

[10] A. Shacham, Benjamin G. Lee,Aleksandr Biberman, Keren Bergman, Luca P. Carloni " Photonic NoC for DMA Communications in Chip Multiprocessors " in 15th IEEE Symposium on High-Performance Interconnects on Networks-on-Chips, *(NOCS 2007)*, Princeton, NJ, May 2007, paper 2.1

[11] M.Channoufi, P.Lecoy. R.Attia, B.Delacressonniere, "Study and modeling of a new configuration of an optical network on chip (ONOC) using FDTD" 6th International Workshop on Reconfigurable Communication-centric Systems-on-Chip (ReCoSoC), june 2011

[12] JuthikaBasak,LingLiao,AnshengLiu,Doren Rubin,Yoel Chetrit ,Hat Nguyen« developments in Gigascale Silicon Optical Modulators Using Free Carrier Dispersion Mechanisms »,Hindawi Publishing Corporation Advances in Optical Technologies, Volume 2008 ,article ID 678948.

[13] J. Van Campenhout, W. M. J. Green, S. Assefa, and Y. A. Vlasov, " Low-power, 2 x 2 silicon electro-optic switch with 110-nm bandwidth for broadband reconfigurable optical networks," Opt. Express 17(26), 24020–24029 (2009).

[14] Hiroki Matsutani, Michihiro Koibuchi, Hideharu Amano, "Performance, Cost, and Energy Evaluation of Fat H-Tree: A Cost-Efficient Tree-Based On-Chip Network," ipdps, pp.81, 2007 IEEE International Parallel and Distributed Processing Symposium, 2007.

[15] A. Biberman, K. Preston, G. Hendry, N. Sherwood-Droz, J. Chan, J. S. Levy, M. Lipson, K. Bergman, "Photonic Network-on-Chip Architectures Using Multilayer Deposited Silicon Materials for High-Performance Chip Multiprocessors," *ACM Journal on Emerging Technologies in Computing Systems* **7** (2) 7:1-7:25

[16] John Wiley &Sons, Chichester, UK, 2004. F. Xia, M.J. Rooks, L. Sekaric, and Y.A. Vlasov, "Ultra-Compact High Order Ring Resonator Filters Using Submicron Silicon Photonic Wires for On-Chip Optical Interconnects," Optics Express, vol. 15, no. 19, pp. 11934-11941, Sept. 2007.

[17] F. Xia, M.J. Rooks, L. Sekaric, and Y.A.Vlasov, "Ultra-Compact High Order Ring Resonator Filters Using Submicron Silicon Photonic Wires for On-Chip Optical Interconnects," Optics Express, vol. 15, no. 19, pp. 11934-11941, Sept. 2007.

[18] M.Channoufi, P.Lecoy. R.Attia, B.Delacressonniere, S.Garcia, "Toward All Optical Interconnections in Chip Multiprocessor (2)"Reconfigurable Computing and FPGAs (ReConFig 2011), Cancun, Mexico, Nov. 2011.

[19] Gilbert Hendrya, Eric Robinson, Vitaliy Gleyzer, Johnnie Chana, Luca P. Carloni, Nadya Bliss,Keren Bergman « Time-division-multiplexed arbitration in silicon nanophotonic networks-on-chip for high-performance chip multiprocessors » J. Parallel Distrib. Comput. 71 (2011) 641–650.

[20] Nicola Concer, Luciano Bononi, Michael Souli´e, Riccardo Locatelli, and Luca P. Carloni « The Connection-Then-Credit Flow Control Protocolfor Heterogeneous Multicore Systems-on-Chip » IEEE transaction on computer aided design of integrated circuit and systems, vol. 29, no. 6, june 2010.

[21] F. Xia, L. Sekaric, Y. Vlasov, Ultracompact optical buffers on a silicon chip,Nature Photonics 1 (2007) 65–71.

[22] Xi Xiao,* Hao Xu, Xianyao Li, Yingtao Hu, Kang Xiong, Zhiyong Li, Tao Chu, Yude Yu, and Jinzhong Yu "25 Gbit/s silicon microring modulator based on misalignment-tolerant interleaved PN junctions" OSA OPTICS EXPRESS 250930 January 2012 / Vol. 20, No. 3

[23] K.Feng, Y.Ye, J. Xu, "A Formal Study on Topology and Floorplan Characteristics of Mesh and Torus-based Optical Networks-on-Chip", Microprocessors and Microsystems, June 2012

[24] S.Le Beux, J.Trajkovic, I.O'Connor, G. Nicolescu, G. Bois and P. Paulin. Multi-Optical Network on Chip for Large Scale MPSoC. In IEEE Embedded Systems Letters, Vol. 2, Issue 3, Pages 77 - 80, Sept. 2010.

[25] Vantrease,D; Schreiber,R; Monchiero,M; McLaren,M; Jouppi N.P; Fiorentino,M; Davis, A; Binkert,N; Beausoleil,R.G; Ahn, J.H "Corona: System implication of emerging nanophotonic technology" 35th international symposium of computer architecture(ISCA), 2008.

[26] B.R Koch, A.W Fang, O.Cohen and J.E Bowers "Mode locked silicon evanescent lasers" Optics Express, 15(18), sep(2007).

[27] I.-W. Hsieh, X. Chen, J. I. Dadap, N. C. Panoiu, J. Richard M. Osgood, S. J. McNab, and Y. A. Vlasov. Ultrafastpulse self-phase modulation and third-order dispersion in si photonic wire-waveguides. Optics Express, 14(25):12380– 12387, Dec. 2006.

Toward Evolution Strategies Application in Automatic Polyphonic Music Transcription using Electronic Synthesis

Herve Kabamba Mbikayi
Département d'Informatique de Gestion
Institut Supérieur de Commerce
Kinshasa, The Democratic Republic of Congo

***Abstract*—We present in this paper a new approach for polyphonic music transcription using evolution strategies (ES). Automatic music transcription is a complex process that still remains an open challenge. Using an audio signal to be transcribed as target for our ES, information needed to generate a MIDI file can be extracted from this latter one. Many techniques presented in the literature at present exist and a few of them have applied evolutionary algorithms to address this problem in the context of considering it as a search space problem. However, ES have never been applied until now. The experiments showed that by using these machines learning tools, some shortcomings presented by other evolutionary algorithms based approaches for transcription can be solved. They include the computation cost and the time for convergence. As evolution strategies use self-adapting parameters, we show in this paper that by correctly tuning the value of its strategy parameter that controls the standard deviation, a fast convergence can be triggered toward the optima, which from the results performs the transcription of the music with good accuracy and in a short time. In the same context, the computation task is tackled using parallelization techniques thus reducing the computation time and the transcription time in the overall.**

Keywords—evolution strategy; polyphonic music transcription; FFT; electronic synthesis; MIDI; notes; frequency; audio; signal; fundamental frequency; pitch detection; F0; chords; monophonic; contours

I. INTRODUCTION

Automatic music transcription is the process that involves a computer in order to write partitures of a piece of music or an audio signal. In automatic music transcription, a piece of music or an audio signal is analysed in order to figure out the correspondent human representations of the perceived sound for a proper interpretation. As humans, we sense sound by noticing minute differences in the pressure of the air outside of our ears, hence these intensities can be reproduced by speakers and moreover they can be recorded by microphones.

The audio signal can be composed of a succession of monophonic sounds over the time which involves a set of notes played individually but not at the same time; or polyphonic sounds which are a succession of notes played at the same time from the same instrument or even from different instruments.

A music transcriber program should be able to analyse the audio signal in order to figure out the different elements composing the given signal. Transcribing music is a very difficult problem that still remains unsolved in a computational view, however even in a musical view this knowledge belongs only to experimented and skilled musicians who have not only learned to transcribe melodies but who have developed their internal skills over the time through their experiences or their predispositions. A formal way to transcribe music is to represent this information as universal sheets of music containing specific information on what notes are played at a given time without saying what the result will sound like. Using a computer, a way to represent music information is to use for instance MIDI files which abstract most of the information composing a piece of music in order to interpret it on a computer or in the real world. Music transcription mainly relies on the use of digital signal processing techniques, but current approaches are not able to capture the rich diversity found in audio signal [15], and some approaches propose the use of semi-automatic transcription to get better results [16].

The transcription problem can be also seen as a search space problem which consists to find optimal or acceptable representations of the music signal which are likely to be used directly or even as a starting point to find the optimal information. Due to the huge size of the search space, the use of evolutionary algorithms (EAs) in this context is the correct approach to deal with it since these algorithms start running with a small set of information going through the search space toward the optimal values.

We introduce in this paper a new approach for music transcription using evolution strategies (ES), which are considered as belonging to the class of EAs. Although in the literature, some reported works used genetic algorithms (GA) to tackle this problem, this process being complex due the size of search space some questions are raised on the time needed for a full convergence to the optimum when GA are used. GA use binary representations to encode the individuals of a population. Operations on the different individuals that include recombination and mutation are applied on the chromosomes by means of permuting the positions of bits randomly or modifying the value of bit when mutation is applied, and exchanging set of bits information or blocks between two individuals when it comes to recombination.

The use of ES can be more adapted for such problem since, the optimization process is done by evaluating information

which is presented in a way (frequencies, magnitudes, pitch, etc.) more adapted to deal with ES which contrarily to GA, use real-valued representations. Moreover, ES use self-adapting parameters which adapt themselves during the evolution process. The experiments showed that by tuning these parameters the time needed for convergence toward the optimal values can be significantly reduced while the obtained results still remain acceptable.

The rest of the paper is organized as follows: In section 2, an overview on ES is presented, in section 3 related work on the subject is discussed, in section 4 we discuss about the application of ES in music transcription, in section 5 we present and discuss about our experimental results while in section 6, we draw some conclusions talk about some future directions.

II. Evolution Strategies

ES are a sub-class of nature-inspired direct search methods belonging to the class of EAs which use mutation, recombination, and selection applied to a population of individuals containing candidate solutions in order to evolve iteratively better and better solutions [1]. They can be applied in all fields of optimization including continuous, discrete, combinatorial search spaces without and with constraints as well as mixed search spaces. A first type of strategy includes directly the mutation strength for each attribute of an individual inside the individual. This mutation strength is subject to evolution similarly to the individual in a classic genetic algorithm. The encoded individual for this type of ES must include a strategy parameter as part of the individual. Rechenberg [9] and Schwefel [10], was the first to introduce them for optimizing real-vectors. They are considered as belonging to the class of EAs. Contrarily to GAs, ES do not use a binary representations to encode a chromosome. They use real-valued vectors to encode an individual. The emphasis is given to the mutation operator which applies to the chromosome a random noise from a normal distribution.

ES abstract the evolution process by which genes are affecting the phenotype of individuals and are the external expression of those genes within an individual. The presumption for coding the variables in the ES is the realization of a sufficient strong causality (small changes of the cause must create small changes of the effect) [2]. Parameters in an ES self-adapt as the evolution process is happening. They use a particular formalism to denote their different types. The simplest form of ES can be expressed as (1+1)-ES in which we have one parent $x^{(t)}$ that will produce one offspring $x'^{(t+1)}$ by mean of mutation. Offspring need sufficient level of adaptability to survive to the next generation. A fitness value should be assigned to them in order to evaluate their adaptability level with respect to the problem we are dealing with. The individual with the best fitness value is selected for the next generation t+1 as the selection operation is deterministic. Equation 1 from [2], describes this process.

$$x^{(t)} = \begin{cases} x'^{(t+1)} & if\ fi\left(x'^{(t+1)}\right) \geq fi\left(x^{(t)}\right) \\ x^{(t)} & otherwise \end{cases} \quad (1)$$

Based on the way the selection operation is done, ES are differentiated as (1+ λ)-ES called "plus selection ES" in which the selection of best individuals is applied on both the parents and offspring, and (1, λ)-ES called "comma selection ES" in which the selection happens only on the offspring. The formalisms (μ/ρ, λ)-ES, (1+ λ)-ES, (1, λ)-ES are also used to describe ES. In the latter one, the symbol μ represents the total number of parents, ρ represents the number of parents that will be recombined and, and λ stands for the number of offspring.

$$x'^{(t+1)} = x^{(t)} + \sigma^{(t)} \cdot N(0,1) \quad (2)$$

The mutation operation is performed on $x^{(t)}$ using a random value $N\left(0, \sigma^{(t)}\right)$ from a normal distribution with a mean of zero by applying the 1/5th-rule based on the rate of successful mutations. Successful mutations happen only when the fitness of the produced offspring is better than its parent while the global step-size ($\sigma^{(t)} \in \mathcal{R}+$) used during the mutation is itself adapted (Eq(2)).

$$\sigma^{(t+1)} = \begin{cases} \sigma^{(t)} \cdot \alpha_{ES} & if\ fi\left(x'^{(t+1)}\right) \geq fi\left(x^{(t)}\right) \\ \sigma_{ES}^{-\frac{1}{4}} & otherwise \end{cases} \quad (3)$$

The normal distribution with a mean of zero and standard deviation of 1 is represented by N (0,1) whereas α_{ES} is the change rate of the global step-size. It is recommended to use values between $2^{1/n}$ and 2 for α_{ES} [2], where n is the dimension of the problem. Each element $x_i(t)$ should be initialized to a value $x_i(0)$ and $\alpha(t)$ to a constant value and $\alpha(0)$ the value for this constant depends on the problem. α_{ES} represents the changing rate of the step-size [2].

III. Related Work

In the literature many works addressing music transcription have been presented. They all use different approaches to address this issue. In [3], using a degenerative process, pitches was estimated by the subtraction of note estimate from the frequency spectrum at a time. Although this model presented good results, it suffers from Imperfections in terms of results obtained when it comes to dealing with small perturbations in the audio signal, as they result in the imperfect subtractions that cause problems with the whole transcription.

Masataka used an approach with every possible fundamental frequencies that could be guessed, and was able to transcribe a melody and the bass line among any numbers of instruments with good results [7]. In [8], Bayesian probability networks were used where bottom-up signal analysis could be integrated with temporal and musical predictions as polyphonic music can be addressed in a certain sense by considering the principles of human auditory organization. This probabilistic Bayesian networks was also used by Manuel Davy and Simon J. Godsill with variable-weight sound model as heuristic to transverse the large parameter space of music transcription [4]. This method however was only able to transcribe three simultaneous notes but could not do more.

The apparition of the first work applying evolutionary algorithms for music transcription was in 2001, in which Garcia [12], showed that polyphonic pitch detection can be

seen as a search space problem in which the goal is to find the pitches that compose an acoustic signal. He used GAs for this purpose and instead of decomposing the frequency lattice which is almost impossible to do, his approach was to reconstruct it, thus considering it as a search space problem.

Jorge dos Reis and Francisco Fernandez de Vega were able to successfully use GAs to transcribe polyphonic music with electronic synthesis [6]. However this approach suffers from its computationally intensive behaviour and the convergence time which is very long due to the application of GAs in the context of polyphonic music transcription. In [5], GAs was also used for polyphonic music transcription and moreover, they were applied to address multi-timbral music transcription.

Gustavo Reis et al. also used GAs for automatic polyphonic music transcription by addressing the multiple fundamental frequencies problem and tracking [14]. Their approach was restricted to three cases which are: estimation of active fundamental frequencies on a frame-by-frame basis; tracking of note contours on a continuous time basis; tracking of timbre on a continuous time basis.

IV. Technical Approach

Musical transcription is still an open challenge for researchers. Although there exists a lot of works that address this problem, most of them are trying to conceptualize this process which in reality is still unknown. There is no standard approach to transcribe music. Experimented musicians use rare internal skills that they possess and acquired over the time to tackle it whereas a formal way to develop them cannot be guaranteed as a lot of factors that are not likely to be totally abstracted, are involved in this process of developing internal abilities within a particular human. Standard methods are trying to quantify a process which is computationally unknown and even skilled musicians cannot provide formal methods to be used in order to transcribe music.

It is easy for a computer to go from a MIDI representation toward the synthesis of the specific audio signal; this representation can be understood by any program that can read a MIDI file. However going from an acoustic or an audio signal to a formal representation of that information raises concerns. This is a crucial issue that needs to be addressed in its context hence one has to discover who is playing what notes.

To tackle it, we developed a synthesizer that uses a particular MIDI-like representation to produce an audio signal during the transcription process. This synthesized audio signal is then compared with the original audio signal from a WAV file that needs to be transcribed. The ES takes as input this MIDI-like information containing standard midi numbers representing pitches to encode individuals of the population.

The evolution process then evaluates the level of adaptation of the population by comparing the synthesized signal with the original one from a Wav file.

In his work, Klapuri expressed the need for both a method for analysing the music and a mean of parameters for optimization [11]. A good optimization process applied to music transcription is likely to produce good results.

The fitness function comparing the two audio signals returns the results of the evaluation whereas the ES algorithm returns the improved hypotheses. With regards to the polyphonic music transcription, complex frequency lattice computationally infeasible to deconstruct is created. The benefit of this approach is that, this lattice will not need to be deconstructed but rather will be reconstructed. This reconstruction process will start from less fit individuals evolving toward fittest ones by means of ES operators applied to the population to get closer to ideal transcription of the music.

A. Indivuduals Encoding

To encode individuals as primitives for our ES, a real-valued vector is used. This latter one contains a set of randomly generated real numbers that are part of the chromosome. The transcription uses a set of three notes to compose a sound at a given time, thus forming a chord. In this approach we are not taking into account the timbre of the instruments that needs to be transcribed although this can be easily done by improving our algorithm in order to analyse the timbre information of the signal and generate the correct envelopes with a synthesizer. However, we investigate on what notes can reconstruct the played signal as well as their durations. Table 1 shows a generated individual encoded as a chromosome.

TABLE I. Encoded Chromosome for an Individual

59.98234	67.00242	64.03123	67.02345	71.36770	74.42356

The above example can be considered as a vector of 6 elements containing real values as they appear in the table. To encode a sound, we need three notes that should be played at the same time. Therefore, the example depicts a sequence of 2 sounds (each composed of three notes) played at different times. MIDI numbers are integers that represent pitches, the frequency of each pitches can be obtained using the formula given in equation 4. However a question is raised on the way ES would be applied in the context of evolving those chromosomes containing MIDI numbers which are integers.

The experiments have shown that by rounding the real number towards its closer midi integer gives very good and expected results. As per the example presented in Table 1, “59.9834” will be rounded to “60” and “67.00242” to “67”. This rounding process is done only after the ES completed the optimization process and sends back the results. However depending on the context, one may need the algorithm to return real values as results for purposes of analysis or for a manual rounding which in some cases may improve the precision, and in some cases it is important to use directly these real numbers without any rounding process for transcription of music from acoustic instruments.

The first 3 numbers are respectively representing notes “C (60)”, “G (67)”, “E (64)”. Played at the same time, they form a C major chord. The next three numbers respectively represent “G (67)”, “B (71)”, and “D (74)” and form a G Major when played at the same time.

$$Frequency = 6.875 \times 2^{\frac{3+\text{pitch}}{12}} \qquad (4)$$

Therefore, the optimization process will consist in finding the correct matching of notes to construct a signal that is closer to the target one from the WAV file.

B. Time Division

To deal correctly with our problem, we chose not to encode the timing information in the chromosome although it is possible to implement such approach.

To get the duration of individuals, the target audio signal is analyzed and split using notes onset detection algorithms. The resulting information is a set of time segments. The length of these particular segments represents the duration of each sound that will be synthesized at each corresponding time from the audio signal.

C. Fast Fourier Transform-FFT

Applying a straight comparison between two acoustic signals by measuring the difference between the samples is likely to result in similar sounds being rejected because of minute differences in small factors like phase [6]. It would be more convenient to work in the frequency domain. Therefore, phase will be thrown away by the power spectrum, thus enabling differences in the phase of the sine wave making up the signal to be not considered. During the submission of a particular segment of the sound to the ES process, the segment is split in smaller time slots and for each of these slots; a Fast Fourier Transform is applied to compare the magnitudes of all the frequencies with the corresponding slots in the original signal. This comparison happens during the evaluation process, to measure the level of adaptability of an individual.

D. Fitness Function

Our fitness function implements the process of comparing each individual with the original signal that needs to be transcribed. In order to do it, at the top level the original signal is first split according to the duration of each composing sound.

We address in this work equal length polyphonic sounds. Those segments are then submitted individually to ES algorithms instances. At the initialisation step, since the audio signal has been split in small segments representing a sound played in a certain interval of time, with our approach the ES will not need to use large size chromosomes, but rather will be constituted of a real-valued vector of only 3 elements or more depending of the number of notes composing a particular sound. These latter ones will enable the ES strategy to optimize only the related segment of the audio signal representing a sound played at a certain interval of time. Therefore, improving the accuracy of the results compared to others methods, which need to encode the full audio signal in a chromosome [5], [6]. At the end of the execution, the results from all ES which took as input each audio segment are returned in the correct order along with their durations.

Before calling the fitness function, the audio segment is again split in smaller time slots of approximately 93 ms by using a window size of 4096 with a samples rate of 44100, resulting in a set of smaller time slices (size 4096). Now, a FFT is applied to each of these time slices along with a Han windowing function to ensure that there are no artefacts of unwanted frequencies as per equation 5.

$$w(n) = 0.5\left(1 - \cos\left(\frac{2\pi n}{N-1}\right)\right) \quad (5)$$

The same process is applied to the original audio signal that we want to transcribe. The fitness function will then compute its value by summing the distance between each frequency in each time slice of the sound as per equation (6). Since we are minimizing the difference from the frequency magnitude of the original signal with the synthesized one, the closer it will get, the higher will be the level of adaptability.

$$Fitness = \begin{cases} \sum_{t=0}^{tmax} \sum_{f=27.5}^{fmax} \frac{O(t,f)}{X(t,f)}, & X(t,f) < O(t,f) \\ \sum_{t=0}^{tmax} \sum_{f=27.5}^{fmax} \frac{X(t,f)}{O(t,f)}, & X(t,f) \geq O(t,f) \end{cases} \quad (6)$$

The O(t, f) is the magnitude of frequency f at time slot t in the acoustic audio signal, and X(t, f) is the magnitude of the frequency f at time slot t for each of the synthesized individual. The fitness is computed from time slot t=0 to tmax, going through all times from the beginning to the end, and from fmin=27.5 to fmax=22050 which correspond respectively to the lowest frequency and the nyquist frequency of a 44100 HZ sample rate. The ES will adapt its parameters toward optimal values that will result in the correct transcription of the polyphonic sound.

V. Experiments & Results

The experiments were run using Matlab. We wrote the needed codes for this purpose using this latter one.

The identified constraints of our ES was that the results should be in the interval going from 21 to 108 corresponding to the lowest piano note (MIDI numbers) to 108 which is the highest note of the piano. In order to run our experiments, we synthesized a set of WAV files that we used as our target audio signals needing to be transcribed. We made some assumptions to ease our experiments as follow:

- The smallest duration of a note is 0.5 sec.
- The duration of a sound may be either 0.5 sec., 1 sec., 1.5 sec., 2 sec.
- Notes played at the same time should have the same length.

TABLE II. ES PARAMETERS VALUES

Parameters	Values
Population size	100
Offspring	80
Initialization strategy	[0.005, 0.05]
Max number of generations	300
Search space	[21, 108]

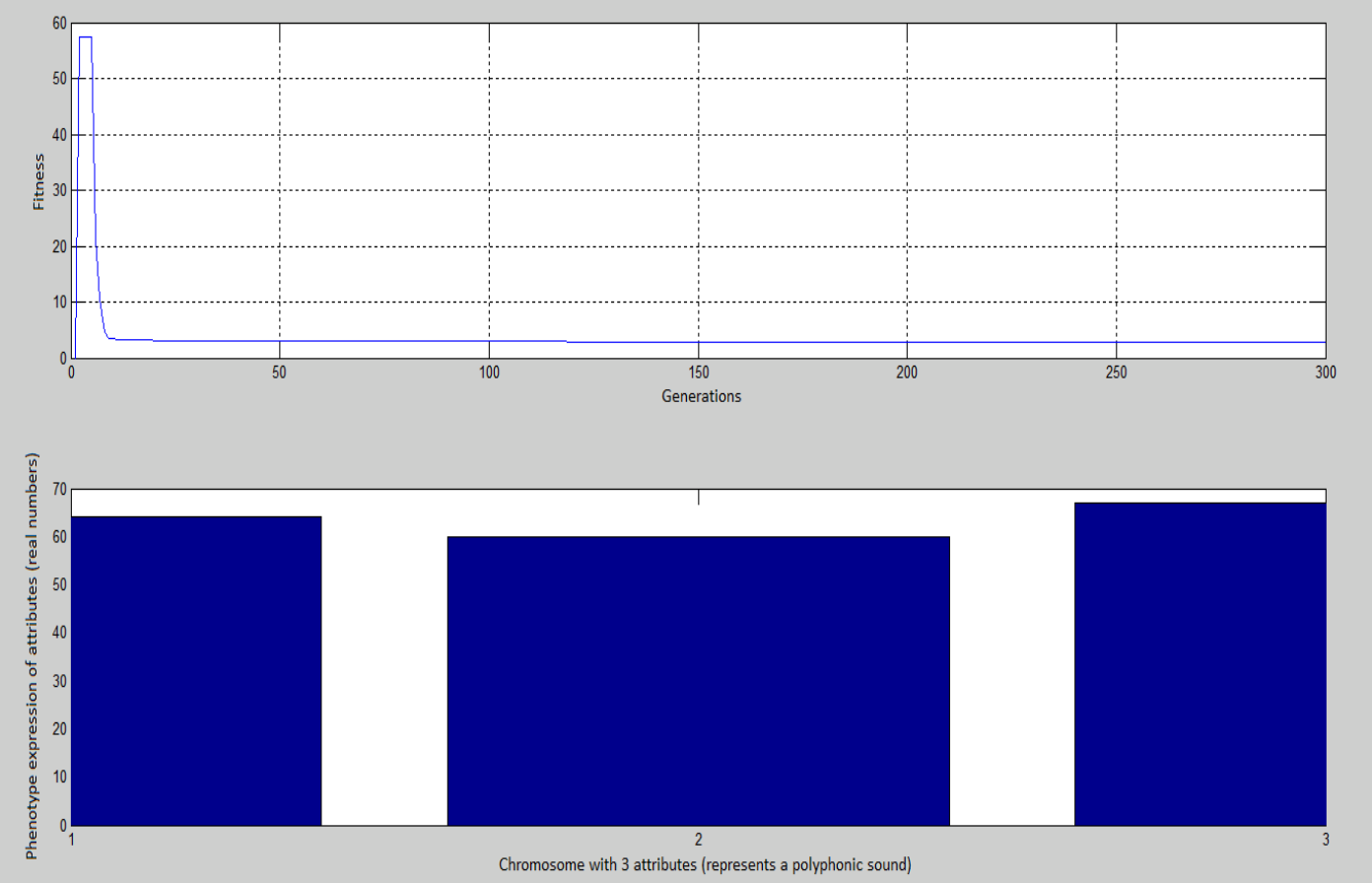

Fig. 1. Graphical Results of transcription of C major chord

Using ES with our approach, the first experiment run was to transcribe a C Major Chord synthesized with the notes C (60)", "G (67)", "E (64)". The transcription was perfectly done as Fig. 1 shows; we got the best results after 9 generations in about 1.5 minute. Figure 1 and Table III presents the best results returned by the ES although it was run for 300 generations without any further improvements of the results

As EA do not guarantee to return the same results even when run different times with the same parameters, it is important to run them many times in order to compare the results as they can produce better ones. Table IV shows the best results obtained after running a second set of tests for the transcription of the same chord (C Major). The results were obtained after 8 generations in approximately 1.5 min.

TABLE III. TRANSCRIPTION OF C MAJOR : SECOND RESULTS

	Note 1	Note 2	Note 3
Rounded numbers	64	60	60
Real values results	63.9985	60.1580	60.2356

We ran some other tests to transcribe a progression of 5 chords as shown in Table V. The ES took only 14 minutes to successfully transcribe them with good accuracy. Compared to others methods using evolutionary algorithms, these results are very interesting. In term of applying machine learning techniques to music transcription, our work clearly shows that ES are also good tools to deal with such problems.

In their work [6], Gustavo Miguel et al reported that the transcription of a progression of 5 chords took about 64 minutes to complete using GAs whereas using ES this shortcoming in term of computation time may be significantly reduced as our results shows.

By increasing the value of the initialization strategy parameter with our approach, a fast convergence with good accuracy can be triggered. Moreover, in our approach we do not submit the full audio signal to the ES which renders the computation very expensive, however we first identify using note onsets detection techniques the duration of each sound and then split the audio signal accordingly. Individual pieces of the audio signal are then submitted independently to ES instances which bring parallelization features to our approach, thus reducing the time for computation.

TABLE IV. CHORDS PROGRESSION OF A POLYPHONIC SOUND

Chord 1 (1 sec.)	Chord 2 (0.5 sec.)	Chord 3 (0.5 sec.)	Chord 4 (1.5 sec.)	Chord 5 (1 sec.)
60	55	69	64	60
64	59	76	67	64
67	62	72	71	67

Table VI presents the best results we obtained for the transcription of a 5 chords progression as returned by the ES without applying rounding process. The results are presented as real numbers. And as we can observe, the transcription process returns the results with a good accuracy. The experiments we have done on the application of ES in polyphonic music transcription show that these machine learning tools are good tools that can be applied in polyphonic music transcription. A tradeoff therefore on the value of the strategy parameters exists as in certain conditions, this latter one should be increased to obtained good results while on the other side some problems will need to decrease this value to obtain good results in term of optimization. Different values of this parameter should be tested and tuned to an acceptable one.

TABLE V. RESULTS OF TRANSCRIPTION PROGRESSION

Chord 1 (1 sec.)	**Chord 2 (0.5 sec.)**	**Chord 3 (0.5 sec.)**	**Chord 4 (1.5 sec.)**	**Chord 5 (1 sec.)**
60.0437	55.2045	68.8471	64.0000	60.3624
63.9456	59.1467	76.0000	66.9162	64.0132
66.8463	62.1978	72.4153	70.1457	66.2682

VI. CONCLUSION

We presented in this paper a novel approach for automatic polyphonic music transcription using evolution strategies. In this context, we showed through our experiments that the frequencies lattice of a perceived sound in an audio signal can be reconstructed by optimization procedures as the transcription of polyphonic sound can also be addressed as a search space problem. The application of ES as learning tools in automatic polyphonic music transcription has proven itself to be adapted for such problem in comparison to other state-of-the-art techniques. Moreover, using these machine learning tools, some shortcomings presented by other evolutionary algorithms approaches that include the long computation time and the high computation cost can be solved. As evolution strategies use self-adapting parameters for optimization, we showed that tuning the strategy parameter that controls the standard deviation, may trigger a fast convergence toward the optima while reducing the computation time. At the other side, the computation cost and time is addressed by mean of parallelization approach to ensure that the workload is distributed among the available resources, thus reducing the computation time.

An interesting and potential direction will be to investigate on the behavior of those machine learning tools when it comes to acoustic sounds. A question can be raised at this level as MIDI numbers are integer values that represent the pitches. However, knowing that it is hard for an acoustic instrument which is manually tuned by a human to sound exactly as the correspondent target frequency, but only, it can get near the ideal frequency. Investigating further on how ES can be improved to transcribe sounds from acoustic instruments constitute a potential challenge as its solution can only be seen in a search space that should include frequencies representations with their real values.

REFERENCES

[1] Herve Kabamba Mbikayi, "An Evolution Strategy Approach toward Rule-set Generation for Network Intrusion Detection Systems (IDS)," International Journal of Soft Computing and Engineering (IJSCE), vol. 2 Issue-5, pp. 201–205, 2012.

[2] Trung Hau Tran, Cédric Sanza, Yves Duthen, "Evolving Prediction Weights Using Evolution Strategy," Proceedings of GECCO conference companion on Genetic and evolutionary computation, pp. 2009-2016, 2008.

[3] Alain de Cheveigné, Hideki Kawahara, "Multiple period estimation and pitch perception model," Speech Communication 27, 175-185.

[4] Manuel Davy and Simon J. Godsill, "Bayesian Harmonic Models for Musical Signal Analysis Bayesian Statistics VII," Oxford University Press, 2003.

[5] G Reis, F Fernandez, A Ferreira, "Genetic algorithm approach to polyphonic music transcription for MIREX 2008," in Proc of the 4th Music Information Retrieval Evaluation eXchange (MIREX), 2008.

[6] Gustavo Miguel Jorge dos Reis, Francisco Fernandez de Vega, " Electronic Synthesis using Genetic Algorithms for Automatic Music Transcription," GECCO'07, July 7–11, 2007.

[7] Masataka Goto, "A Real-time Music-scene-description System: Predominant-F0 Estimation for Detecting Melody and Bass Lines in Real-world Audio Signals," Speech Communication (ISCA Journal), Vol.43, No.4, pp.311-329, September 2004.

[8] K. Kashino, K. Nakadai, T. Kinoshita, and H. Tanaka, "Organization of hierarchical perceptual sounds: Music scene analysis with autonomous processing modules and a quantitative information integration mechanism," In IJCAI, pp. 158-164, 1995.

[9] Rechenberg, I., "Evolutionsstrategie: Optimierung technischer Systeme und Prinzipien der biologische," Frommann-Holzboog, Stuttgart, 1973.

[10] Schwefel, H.-P. Numerical Optimization of Computer Models, Chichester: Wiley, 1981.

[11] A. P. Klapuri, "Automatic music transcription as we know it today," Journal of New Music Research, vol. 33(3), pp. 269-282, 2004.

[12] G. Garcia, "A genetic search technique for polyphonic pitch detection," In Proceedings of the International Computer Music Conference (ICMC), Havana, Cuba, 2001

[13] D. Lu, "music transcription using genetic algorithms and electronic synthesis," Computer Science Undergraduate Research, University of Rochester, New York, USA

[14] Gustavo Reis, Francisco Fernandéz, Annibal Ferreira, "A genetic Algorithm for polyphonic Transcription of Music," In proceeding of: Proceedings of the 2007 Doctoral Symposium on Artificial Intelligence, 2007

[15] Emmanouil Benetos, Simon Dixon, Dimitrios Giannoulis, Holger Kirchhoff, and Anssi Klapuri, 13th International Society for Music Information Retrieval Conference, 2012.

[16] H. Kirchhoff, S. Dixon, and A. Klapuri, Shift-variant nonnegative matrix deconvolution for music transcription, In ICASSP, 2012.

Hybrid Approach for Detection of Hard Exudates

Dr. H. B. Kekre
Computer Engineering
MPSTME, NMIMS University
Mumbai, India

Dr. Tanuja K. Sarode
Computer Engineering
TSEC
Mumbai, India

Ms. Tarannum Parkar
Computer Engineering
DBIT
Mumbai, India

***Abstract*—Diabetic Retinopathy is a severe and widely spread eye disease which can lead to blindness. Hence, early detection of Diabetic Retinopathy is a must. Hard Exudates are the primary sign of Diabetic Retinopathy. Early treatment of Diabetic Retinopathy is possible if we detect Hard Exudates at the earliest stage. The main concentration of this paper is to discuss techniques for efficient detection of Hard Exudates. The first technique, discusses Hard Exudates detection using mathematical morphology. The second technique, proposes a Hybrid Approach for Detection of Hard Exudates. This approach consists of three stages: preprocessing, clustering and post processing. In preprocessing stage, we resize the image and apply morphological dilation. The clustering stage applies Linde-Buzo-Gray and *k*-means algorithm to detect Hard Exudates. In post processing stage, we remove all unwanted feature components from the image to get accurate results. We evaluate the performance of the above mentioned techniques using the DIARETDB1 database which provides ground truth. The optimal results will be obtained when the number of clusters chosen is 8 in both of the clustering algorithms.**

Keywords— Diabetic Retinopathy; Hard Exudates; Clustering; Mathematical Morphology

I. INTRODUCTION

The term Diabetic Retinopathy (DR) consists of two words Diabetes and Retinopathy. Diabetes mellitus or simply diabetes, is a disease in which a person has high blood sugar, either because of low insulin production or low response to insulin produced. Retinopathy literally means damage to the retina. Hence, DR is a widely spread eye disease which is regarded as the manifestation of diabetes on the retina. DR is of two types. The first type is Non Proliferative Diabetic Retinopathy. In this condition, retinal capillaries get damaged and microscopic leaks form in these vessels. Leakage causes the retina to swell, which interferes with normal vision. The second type is Proliferative Diabetic Retinopathy. In this condition, the capillaries of retina shut down. This causes new blood vessel to grow in retina [1].

In order to study eye diseases like Diabetic Retinopathy ophthalmologists uses different retinal images, such retinal images are usually called as fundus images. One of the fundus image labeled, with various feature components of Diabetic Retinopathy is shown in Fig. 1. Microaneurysms are small saccular pouches caused by local distension of capillary walls and seen as small red dots. This may also lead to big blood clots called hemorrhage. Hard Exudates are yellow lipid deposits which appear as bright yellow lesions. The bright circular region from where the blood vessels emanate is called as optic disk. The fovea defines the center of the retina, and is the region of highest visual acuity [2]. For early detection of DR, detection of Hard Exudates plays an important role.

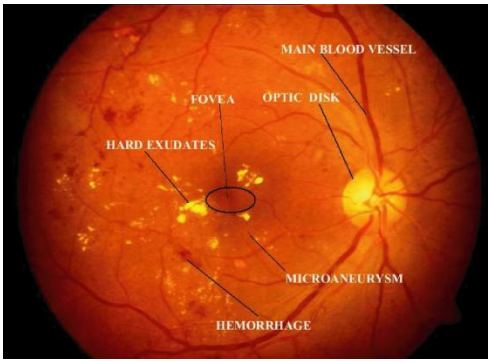

Fig. 1. Illustration of various features of a typical Retinopathy image

Over the past few years many techniques for detection of Diabetic Retinopathy are given in literature. V. Vijaya Kumari et al [1] uses mathematical morphology for extracting Exudates, optic disk and blood vessels. Here, Morphological opening and closing operations of different sizes are used to detect Hard Exudates, but one of the main drawbacks of morphological operation is the size of structuring element suitable for one image is not be suitable for another image. Saiprasad Ravishankar et al [2] also uses mathematical morphology to detect hard Exudates but it uses a linear classifier for classifying the patches based on their edge strength. Hussain F. Jaafar et al [3] introduced a pure splitting technique for detection of Exudates in retinal images. This technique uses an adaptive thresholding based on a novel algorithm for pure splitting of the image. S. Kavitha et al [4] uses mathematical morphology and pure splitting technique to detect faint Exudates. Sopharak et al [5] used a Naive Bayes classifier to detect Exudates. The main drawback of Naive Bayes classifier is it misses the faint Exudates. R. Vijayamadheswaran et al [6] proposed detection of Exudates using a combination of Contextual Clustering and Radial basis function. In this technique all the fundus images are transformed to a standard template image condition. Detection of Exudates is accurate when the fundus images are captured with good quality. Garcia et al [7] detects Hard Exudates using neural network (NN) approach. Here Three NN classifiers were investigated which includes multilayer perceptron (MLP), radial basis function (RBF) and support vector machine (SVM). This paper presents two techniques for detection of hard Exudates. The first technique discusses a modified

approach based on mathematical morphology. In the second technique a hybrid approach for detection of Hard Exudates is proposed. Here, mathematical morphology is combined with clustering approach to improve the accuracy of Exudates detection.

In this paper, a publicly available DIARETDB1 database is used to verify the result[8]. This Database is publicly available and it has the ground truth collected from several experts. The database consists of 89 color fundus images out of which 84 contain at least mild non-proliferative signs of the Diabetic Retinopathy and 5 are considered normal that do not contain any signs of the Diabetic Retinopathy according to all experts participated in the evaluation. The images were taken in the Kuopio University Hospital. It also has a strict evaluation protocol. The protocol is demonstrated with a baseline method included in the available tool kit. This study provides the means for the reliable evaluation of automatic methods for detecting Diabetic Retinopathy. In addition to this, the fundus images related to the Diabetic Retinopathy are evaluated by using sensitivity and specificity. Sensitivity is the percentage of abnormal fundus images classified as abnormal, and specificity is the percentage of normal funds classified as normal by the screening. The higher the sensitivity and specificity values, the better the diagnosis [8].

This paper is composed of five sections. Section II discusses Modified Morphology based Exudates detection. Section III presents the proposed method for Exudates detection. In section IV, Experimental Results are presented while Conclusion is included in Section V.

II. Modified Mathematical Morphology Based Hard Exudates Detection

Mathematical Morphology is a theory and technique for analysis and processing of geometrical structures (such as size, shape, and convexity), based on set theory, lattice theory, topology, and random functions [9]. The technique used here is a modification of morphology based technique given by Vijaya Kumari et al [1]. For detection of Hard Exudates three steps applied are extraction of the green channel, morphological processing, optic disk detection and removal.

A. Extraction of Green Channel

Here, Input image is initially resized to a standard size of 768×576 pixels. Resized image is RGB image. So, from resized image we extract only green channel image. We select the green channel because fundus images are almost always saturated in the red channel and have very low contrast in the blue channel [2].

B. Morphological processing

Exudates are the primary sign of Diabetic Retinopathy. Initially dilation is performed on the green channel extracted image across two disc shape structuring elements. Dilation is an operation that grows or thickens object in a binary image [1]. It is defined in terms of set operation as given by (1).

$$A \oplus B = A_1(X, Y) = \max_{i,j \in B} \left(A(X-i, Y-j) + B(i, j) \right) \quad (1)$$

Here, A is an input image, B is the structuring element used for dilation.

Once the Image is dilated across two structuring elements both the results are subtracted to get the boundary of Hard Exudates. In order to get exact boundaries the image is thresholded using Otsu's thresholding technique. Then Morphological filling is done to get the closed regions. Once closed regions are obtained, morphological opening is performed to remove small bright details. Thus, the regions which are possible candidates for Hard Exudates are obtained in this step.

C. Optic Disk Detection and removal

In the morphological processing step the regions corresponding to possible Hard Exudates are obtained. But it was observed, that normally Hard Exudates and Optic disk are of the same brightness, color and contrast [1]. Hence, optic disk is sometimes misclassified as Hard Exudates. Therefore, Optic disk must be eliminated from the possible candidates. Here, Circular Hough Transform is applied to detect the optic disk. Once detected, it is eliminated and the Hard Exudate regions are obtained.

III. Proposed Algorithm

The proposed Algorithm consists of three main stages, Preprocessing, Clustering and Post processing.

A. Preprocessing

The main purpose of this stage is to remove unwanted details from an image and make the image suitable for applying next step. Here, Input image is initially resized to fixed size of 256×256. Green channel is extracted from resized image and then morphological dilation is applied by using disk shape structuring element.

B. Clustering

Once the image is dilated, clustering algorithm is applied on image to get Hard Exudates. Here two different types of clustering algorithms are implemented.

1) Linde – Buzo – Gray Algorithm

The LBG Algorithm is an iterative clustering technique. For the purpose of explaining this algorithm, two dimensional vector space as shown in Fig. 2 is considered. In this figure each point represents two consecutive pixels. In this algorithm centroid is computed as the first code vector C1 for the training set. In Fig. 2 two vectors v1 & v2 are generated by adding constant error to the code vector. Euclidean distances of all the training vectors are computed with vectors v1 & v2 and two clusters are formed based on nearest of v1 or v2. The procedure is repeated for these two clusters to generate four new clusters. This procedure is repeated for every new cluster until the required size of the codebook is reached [10].

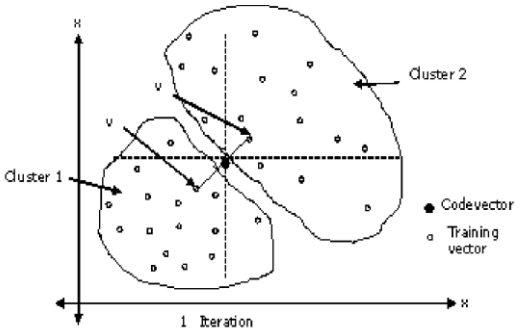

Fig. 2. LBG for two dimensional case

Modified LBG Algorithm derived from [10] is explained as follows

1. Start.
2. Read the input image A.
3. Resize image A to a fixed size of 256×256.
4. Divide the image into two 2×2 non overlapping blocks.
5. Represent each block in the form of training vector space. Each block is converted to the training vector $X_i = (x_{i1}, x_{i2}, x_{ik})$.
6. Consider entire training vector space as one cluster.
7. Find the centroid of the cluster. i.e. code vector of codebook.
8. Initialize error vector (E) which will be of the same size as codevector generated in step 7.
9. Add and subtract constant vector i.e. error vector from codevector generated in step 7 and get two new vectors as follows:

   C1=C+E

   C2=C-E
10. Find Euclidean distance by considering each training vector in training vector space with respect to C1 and C2 as follows:

    $d(X_i , C_j) = \sum_{p=1}^{k} (x_{ip} - c_{jp})^2$

    where,

    X_i is the training vector,

    C_j is the codevector of the codebook
11. If training vector is closed to C1 put it in cluster 1 else in cluster 2 and form clusters.
12. Repeat step 8 to 11 until codebook of the desired size is obtained.
13. Stop.

2) k-means Algorithm

k-means is an unsupervised clustering algorithm which is used to classify input image to *k* clusters based on the nearest mean.

The modified algorithm for *k*-means derived from [11] is explained as follows

1. Start.
2. Read the input image A.
3. Resize image A to a fixed size of 256× 256.
4. Divide the image into two 2×2 non overlapping blocks.
5. Represent each block in the form of a training vector space X. Each block is converted to the training vector $X_i = (x_{i1}, x_{i2}, x_{ik})$.
6. Select *k* random vectors from the training set and call it as initial codebook C.
7. Select training vector X_i from training vector space.
8. Calculate squared Euclidean distance of X_i with the codebook C as follows:

   $d(X_i , C_j) = \sum_{p=1}^{k} (x_{ip} - c_{jp})^2$

   where,

   X_i is the training vector,

   C_j is the codevector of the codebook
9. Calculate value of minimum Euclidian distance as follows:

   $d(X_i , C_{min}) = \min_{i \le j \le N} \{d(X_i, C_j)\}$
10. Insert X_i vector to cluster corresponding to C_{min}.
11. Repeat steps 7 to 10 for all training vectors in training vector space.
12. Compute the centroid for each cluster by taking column wise average of each codevector in the codebook.
13. Generate the codebook by inserting the centroids obtained in step 12 and give it as input to the next iteration.
14. Repeat steps 7 to 13 until codebook obtained in successive two iterations are same.
15. Stop.

C. Post processing

Once clustering Algorithm is applied to Dilated Image, Hard Exudates Regions are obtained in any of the one cluster from *k* clusters. It has been observed that normally Hard Exudates and Optic disk are of same brightness, color and contrast.

.So, sometimes optic disk is misclassified and must be eliminated from the Hard Exudates result obtained after applying a clustering algorithm to get accurate Hard Exudates. Here, Circular Hough Transform is applied to the result obtained by applying a clustering algorithm for detecting optic disk. Once the optic disk is detected it is eliminated and the Hard Exudates Result is obtained.

IV. Result And Discussion

For Evaluation of proposed technique we have used 89 Images provided in DIARETDB1 Database. This database is selected because this database is publicly available and it has the ground truth collected from several experts. This ground truth acts as a good mean for verifying the results of the proposed algorithm with the findings of ophthalmologists provided in DIARETDB1 database. All 89 Images were tested on Intel Core i5-2410M, 3GB RAM using Matlab R2011b. Image results were obtained in approximately 7 seconds. To evaluate performance of our proposed Algorithm values of the three parameters are calculated which includes Sensitivity, Specificity and Accuracy [12]. These parameters are calculated by using (2), (3) and (4) .

$$\text{Sensitivity} = \frac{TP}{TP+FN} \quad (2)$$

$$\text{Specificity} = \frac{TN}{TN+FP} \quad (3)$$

$$\text{Accuracy} = \frac{(TP+TN)}{(TP+FP+TN+FN)} \quad (4)$$

where, TP (true positive) is number of pixels classified as Exudates by both the ophthalmologist and the algorithm, FP (false positive) is number of non-exudates pixels which are wrongly detected as Exudates pixels by the algorithm, TN (True negative) is number of no Exudates pixels which are identified as non-Exudates pixels by both the ophthalmologist and the algorithm, FN (false negative) is number of Exudates pixels that are not detected by the algorithm but are considered as Exudates by ophthalmologist.

The result is optimal for highest sensitivity, sensitivity and accuracy's value. Initially Hard Exudates detection was done using modified morphological approach. The result of Exudates detection using mathematical morphology is as shown in Fig. 3. After implementing morphology based detection technique it is observed that out of three evaluation parameters the value of specificity and accuracy is less in this case. Hence same database images were tested using LBG Algorithm. The result of Exudates detection using LBG is as shown in Fig. 4. In this case it is observed that the value of specificity was increased as compared to morphology based approach but the value of sensitivity was largely reduced. So, *k*-means algorithm was implemented. Result of *k*-means is as shown in Fig. 5. Here, the result obtained is good as compare to morphology based detection and LBG.

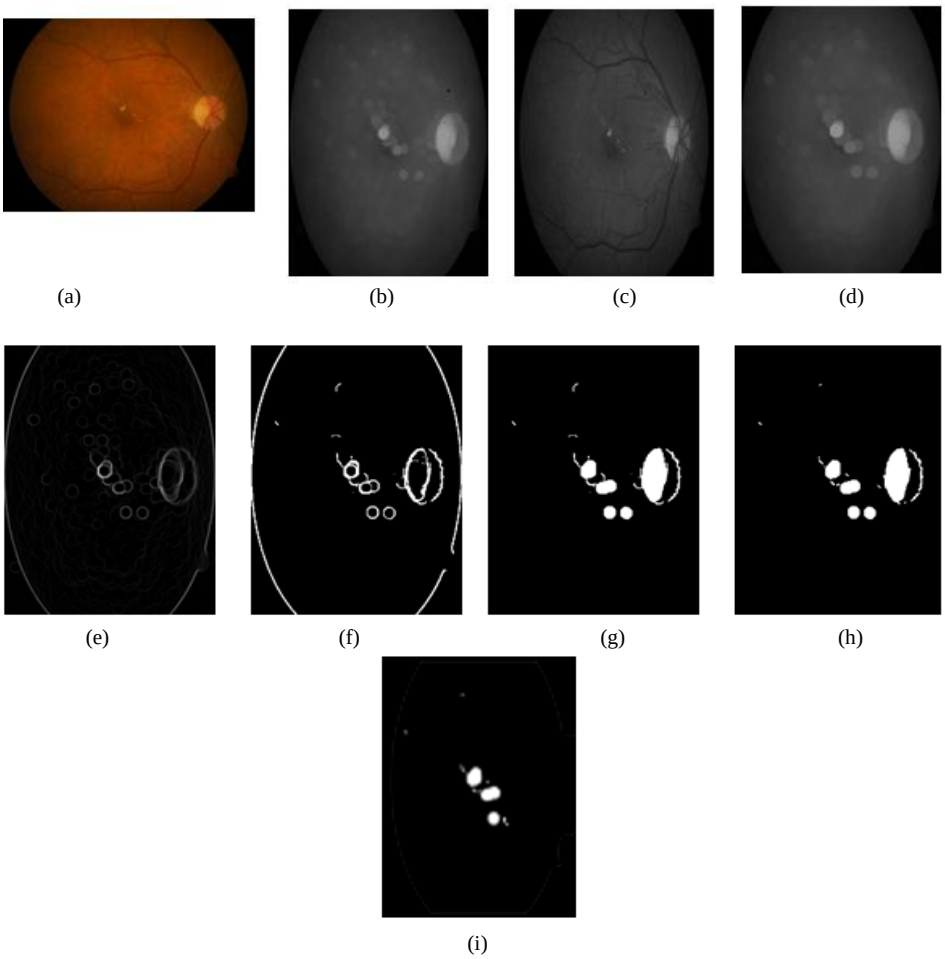

Fig. 3. Hard Exudates using Morphology (a) Original Image (b) Green Channel Extracted Result (c) Dilated Image1 (d) Dilated Image2 (e) Subtracted Image (f) Thresholded Result (g) Filled Image (h) Result after Open (i) Final Hard Exudates

Summary of results obtained after applying all the three algorithms is as shown in Table I. From Table I it is clear that *k*-means gives better result as compared to other two techniques.

One of the main parameters in clustering algorithm is choosing number of clusters which gives best result. Hence, here DIARETDB1 database is tested by considering the number of clusters as 4, 6 and 8 in *k*-means algorithm as shown in Fig. 6. It is observed that *k*-means with 8 clusters gives optimal results. Same Database is also tested by LBG algorithm with the number of clusters as 4 and 8 as shown in Fig. 7. Here, it is observed that for LBG best results are obtained when the number of clusters is chosen as 8. For both *k*-means and LBG clustering when the number of clusters increased more than 8 the Exudates were split into different clusters. Hence, the results are not accurate for more than 8 clusters.

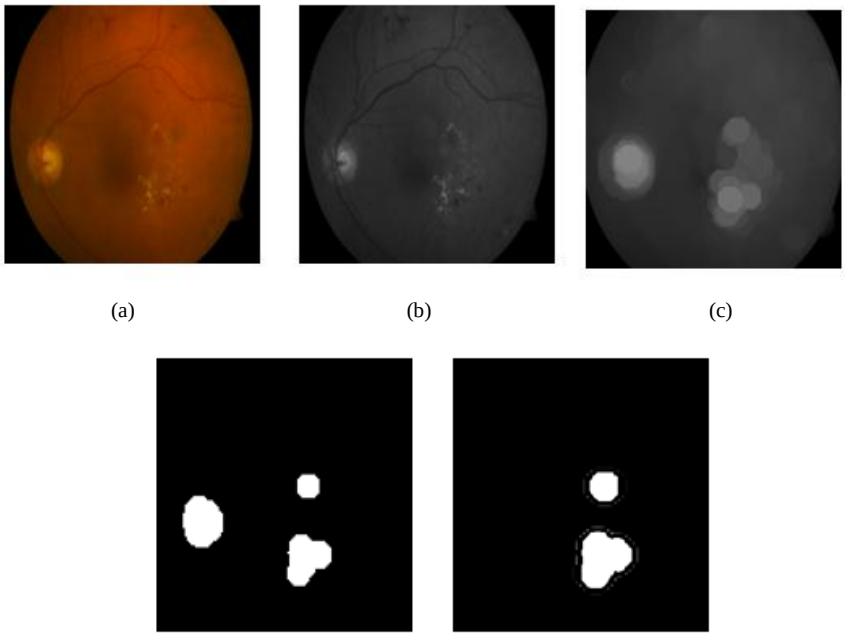

(a) (b) (c)

(d) (e)

Fig. 4. Hard Exudates using LBG (a) Original Image (b) Green Channel Extracted Result (c) Dilated Image (d) LBG Result (e) Hard Exudates

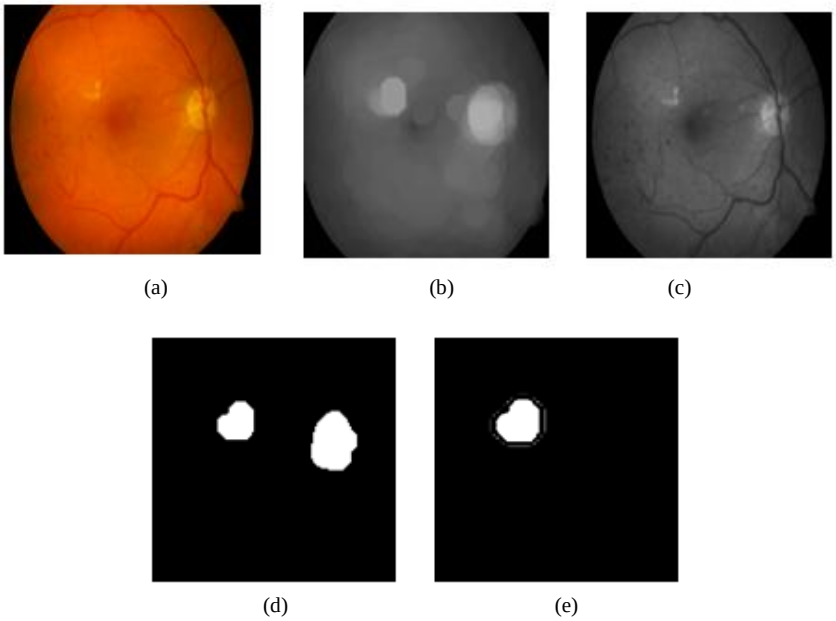

(a) (b) (c)

(d) (e)

Fig. 5. Hard Exudates using *k*-means (a) Original Image (b) Green Channel Extracted Result (c) Dilated Image (d) *k*-means Result (e) Hard Exudates

TABLE I. COMPARISION OF HARD EXUDATES RESULT

Algorithm	Evaluation Parameters		
	Sensitivity	*Specificity*	*Accuracy*
Morphology Based Approach	91%	39%	67%
LBG	80%	57%	68%
k-means	77%	76%	76%

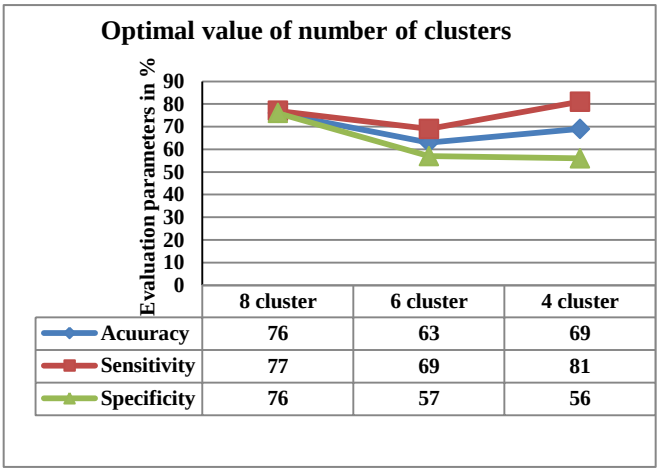

Fig. 6. Comparison Results for optimal value of number of clusters *k* in *k*-means

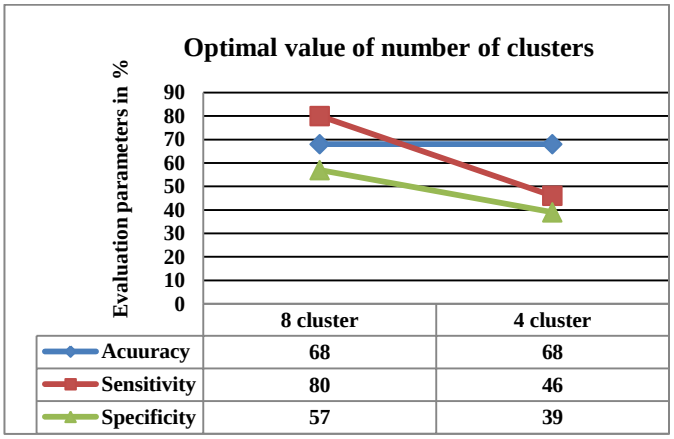

Fig. 7. Comparison Results for optimal value of number of clusters *k* in LBG

V. CONCLUSION

The main idea of detection of Diabetic Retinopathy is to detect Hard Exudates. In this paper, a fast method for detection of Hard Exudates is proposed. This method consists of three stages in the preprocessing stage image is brought to the form where clustering technique yields accurate results Second stage is clustering. Here, LBG and *k*-means clustering techniques are applied to detect Hard Exudates and third stage is Post processing where Optic Disk is removed from clustering results to get accurate Hard Exudates. The final results obtained from these techniques are compared with the results obtained from Morphology based detection and the ground truth provided in DIARETDB1 database. The performance of Algorithm is evaluated by calculating values of sensitivity, specificity and accuracy. Our result suggests that clustering using *k*-means produce best result as compared to other two techniques.

REFERENCES

[1] Vijaya Kumari, N. Suriyanarayanan, C.Thanka Saranya , "A Feature Extraction for Early Detection of Diabetic", International Conference on Recent Trends in Information Telecommunication and Computing, pp. 359 – 361, 2010.

[2] Saiprasad Ravishankar, Arpit Jain, Anurag Mittal, "Automatic Feature Extraction for Detection of Diabetic Retinopathy in Fundus Images", International Conference on Computer Vision and Pattern Recognition, pp. 210-217, 2009.

[3] Hussain F. Jaafar, Asoke K. Nandi and Waleed Al-Nuaimy, "Detection of Exudates in Retinal Images Using a Pure Splitting Technique", 32nd Annual International Conference of the IEEE EMBS Buenos Aires, Argentina, pp. 6745 - 6748, 2010.

[4] S. Kavitha, K. Duraiswamy, A. R. S. Sri Supreetha, "Detection of Exudates and macula in fundus images to estimate severity of Diabetic Retinopathy", International Journal of Communications and Engineering Vol.7, Issue: 01, pp. 24-29, March 2012.

[5] Sopharak, Akara, Dailey, Matthew N., Uyyanonvara, Bunyarit, Barman, Sarah, Williamson, Tom, Nwe, Khine Thet and Moe, Yin Aye, "Machine learning approach to automatic exudate detection in retinal images from Diabetic Patients", Journal of Modern Optics, Vol. 5, Issue 2, pp. 124-135, 2010.

[6] R. Vijayamadheswaran, Dr. M. Arthanari, Mr. M. Sivakumar, "Detection of Diabetic Retinopathy using Radial Basis Function", International journal of Innovative technology & creative Engineering, Vol.1, pp. 41-47, January 2011.

[7] María García, Clara I. Sánchez, María I. López, Daniel Abásolo, and Roberto Hornero, "Neural Network based detection of Hard Exudates in Retinal Images", Computer Methods and Programs in Biomedicine, Vol.93, Issue 1, pp. 9-19, January 2009.

[8] Tomi Kauppi, Valentina Kalesnykiene, Joni-Kristian Kamarainen, Lasse Lensu, Iiris Sorri, Asta Raninen, Raija Voutilainen, Hannu Uusitalo, Heikki K¨alvi¨ainen and Juhani Pietila, "DIARETDB1 Diabetic Retinopathy database and evaluation protocol", Technical report, Faculty of medicine, University of Kuopio, Finland, 2007.

[9] Ardimas Andi Purwita, Kresno Adityowibowo, Ashlih Dameitry, Made Widhi Surya Atman, "Automated Microaneurysm Detection Using Mathematical Morphology", International Conference on Instrumentation, Communication, Information Technology and Biomedical Engineering , pp. 117 – 120, November 2011.

[10] Dr. H.B. Kekre, Tanuja K. Sarode, Suchitra M. Patil, "2D Image Morphing With Wrapping Using Vector Quantization Based Colour Transition", International Journal of Computer Science and Information Security, Vol. 9, No. 7, pp. 75-82, 2011.

[11] Dr. H.B. Kekre, Tanuja K. Sarode, "Vector Quantized Codebook Optimization using K-Means" , International Journal on Computer Science and Engineering, Vol.1, No. 3, pp. 283-290, 2009.

[12] John Attia, "Moving Beyond Sensitivity And Specificity: Using Likelihood Ratios To Help Interpret Diagnostic Tests". Austral. Prescriber, Vol.26, No.5, pp. 111-113, 2003.

Extended Standard Hough Transform for Analytical Line Recognition

Abdoulaye SERE, Oumarou SIE
Laboratory of Information Processing and Communication
University of Ouagadougou
Ouagadougou, Burkina Faso
Email: abdoulaye.sere@Univ-Ouaga.bf, oumarou.sie@Univ-Ouaga.bf

Eric ANDRES
Laboratory XLIM-SIC
University of Poitiers
Poitiers, France
Email: andres@sic.sp2mi.univ-poitiers.fr

***Abstract*—This paper presents a new method which extends the Standard Hough Transform for the recognition of naive or standard line in a noisy picture. The proposed idea conserves the power of the Standard Hough Transform particularly a limited size of the parameter space and the recognition of vertical lines. The dual of a segment, and the dual of a pixel have been proposed to lead to a new definition of the preimage. Many alternatives of approximation could be established for the sinusoid curves of the dual of a pixel to get new algorithms of line recognition.**

***Index Terms*—hough, transform, recognition, discrete.**

I. Introduction

In an acquired (photography, satellite picture, scanner) or synthetic picture, we can be interested in different colored areas corresponding to the type of crops, extract the rivers or, in the case of scanner images, determine the contour of organs. To get these information, some manipulations are needed such as the segmentation in region, the recognition and the extraction of the geometric elements such as the border of regions and other kind of processing that may depend on human perception. In image processing, particularly in pattern recognition, we are interested in new extraction and reconstruction techniques in 2D, 3D or higher dimensional objects. Discretization is the transform that associates a discrete object to a continuous one. Reconstruction is the transform that associates a continuous object to a discrete one. There are various ways of considering points in discrete geometry. In this paper, where we focus on dimension two, we consider that a discrete point is represented by a continuous surface element (pixel). One of the question is how to recognize a discrete line.

The Hough Transform, initially defined by Paul Hough in 1962 is very used in lines recognition in a noisy picture. It uses an image space and a parameter space, associates a point in an image space to a line in a parameter space. A lot of methods [3], [4], [5], [6], [7], [8], [9] have been proposed to extend or to improve the Hough Transform in order to permit lines, circles, spheres recognition. An unified definition of the Hough Transform has also been proposed by Maître in [8]. In [5], Martine Dexet introduced the generalized dual space, that extends the Hough Transform to have analytical discrete hyperplane (naive or standard) recognition.

In this paper, we define a new method, which extends the standard hough transform for naive or standard discrete line recognition. The standard Hough transform is based on the polar coordinates of lines. It associates a point in an image space to a sinusoïd curve in a parameter space. The proposed method limits the size of the parameter space.

The starting point of this paper focus on basic notions as the generalized dual space, naive and standard hyperplane definitions and the standard Hough Transform, in the section II. In the section III, we present the extended standard Hough Transform : we define a new dual of a pixel and then the notion of preimage that allows us to establish a recognition algorithm. At the end of this paper, we discuss what still needs to be done in perpectives.

II. Preliminaries

In this section, we define some notions to facilitate the understanding of the next sections. These notions concern the generalized dual space, discrete hyperplane definitions and the Standard Hough Transform.

A. Generalized dual space

In 1962, Paul Hough introduced the Hough Transform. The method uses an image space and a parameter space and is able to recognize objects in noisy pictures. The method has also changed with improvements and extensions to the detection of arcs, circles or sphere.

We define the Hough Transform by :

Definition 1: (Hough Transform) Let M(X_0, Y_0) be a point in an image space($\subset\mathbb{R}^2$). The Hough Transform of M is a set of points(a,b) in a parameter space($\subset\mathbb{R}^2$) verifying b=Y_0-aX_0. Then, the Hough Transform of a point is a line. Let A(X_1, Y_{1a}), B(X_2, Y_2), C(X_3, Y_3) be three points on an euclidean line defined by the equation y=ax+b, where (a, b)$\in\mathbb{R}^2$, in an image space. Then, the coordinates of A, B, C verify respectively the equations

$$b = Y_1 - aX_1 \quad (1)$$

$$b = Y_2 - aX_2 \quad (2)$$

$$b = Y_3 - aX_3 \quad (3)$$

The system of equations (1), (2), (3) determines the line parameters (a,b) that crosses A, B, C. (see the below figure 1)

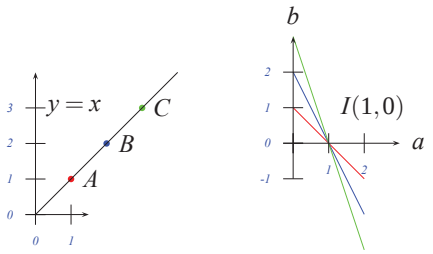

(a) points (b) Hough Transform

Figure 1: Hough Transform

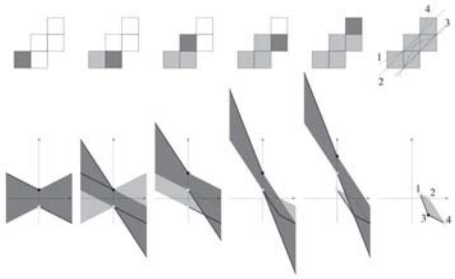

Figure 2: The preimage of five pixels *[5]*

As you see in the figure 1, the coordinates (1, 0) of the point I represent the value of the couple (a, b) with a=1 and b=0. The line equation correponding to the couple (a, b) is then obtained by substitution : y=ax+b with a=1 and b=0 $\Longleftrightarrow$ y=x. When a$\rightarrow\infty$, we notice the difficulties to realize vertical lines detection because of the problem to represent an infinity number (a) as a data type that leads to the increasing size of the parameter space. The recognition algorithm consists of the determination of the couples (a, b) in the parameter space.

The Hough transform according to the definition1 in a continuous space, can not be applied directly on analytical discrete lines recognition because in discrete domain, we work with $\mathbb{Z}^2$ points and a discrete line can be seen as a sequence of pixels that are squarre regions centered in $\mathbb{Z}^2$ point.

In [5], Martine Dexet extends the Hough transform with the generalized dual space that allows to establish analytical discrete hyperplane (naive or standard) recognition and is equivalent to analytical line recognition in 2D. That leads to build a reconstruction method to obtain a euclidean line from a discrete line .

Definition 2: **(**The dual of a point in 2D [5]) Let $P_\xi(x_1,x_2)\in \xi_2$ ($\subset\mathbb{R}^2$) an image space and $P_P(y_1,y_2)\in P_2$ ($\subset\mathbb{R}^2$) a parameter space be two points. The Dual of P_ξ (respectively P_P) is defined by Dual(P_ξ)=$\{(y_1,y_2)\in P_2 | y_2 = x_2 - x_1 y_1\}$ (respectively Dual(P_P)=$\{(x_1,x_2)\in P_2 | x_2 = y_2 + x_1 y_1\}$)

As we can see, the definition 2 is equivalent to the Hough transform one and it can be used to establish the dual of an object as follows :

Definition 3: **(**The dual of an object [6]**)** *Let O be an object of $\xi_n(\subset\mathbb{R}^n)$. The Dual of O is defined by Dual(O)=* $\bigcup_{p\varepsilon O} Dual(p)$

We conclude that the dual of a polytope[5] from the definition 3, particularly the dual of a pixel is the union of the dual of each point.

The preimage[5] is also defined by :

Definition 4: **(**The preimage of n pixels [5]) *Let $S=\{P_1,P_2,...,P_{n-1},P_n\}$ be a set of n pixels P_i in $\xi_2(\subset\mathbb{R}^2)$. The preimage of S is defined by* $P(S) = \bigcap_{1\leq i\leq n} Dual(P_i)$.

The following figure 2 illustrates the preimage of five pixels.

According to [5], we know that the preimage of n (n $\geq$ 2) pixels give a polygonal area representing a set of points whose coordinates determine the parameters of Naive or Standard lines. As we can see in the figure 2, the preimage of these pixels is a polygon.

If the pixels are vertical, their preimage will be an unlimited polygon [5]; we will need to have a wide size of the parameter space to represent the polygon because the values of the coordinates of the points in the polygon increase, particularly the vertices coordinates. The problem of data types representing these values happens.

One of the question is what is an analytical discrete line in order to build algorithms to recognize them.

B. Analytical hyperplane models

The analytical hyperplane has been defined by Reveillès [10], [11]. Many models of analytical hyperplanes have been proposed : The bresenham discrete line (Bresenham (1965) – Pitteway (1967)), Pythagorean hyperplanes, naive and standard hyperplanes [1], [2].

For this paper, we are interested in naive and standard hyperplane definitions.

Definition 5: **(**The Naive hyperplane [1], [2]) *The Naive hyperplane with the parameters $(c_0,...,c_n)\in R^{n+1}$ is the set of points $(x_1,...,x_n)\in Z^n$ verifying :*

$$-\frac{max_{1\leq i\leq n}\|c_i\|}{2} \leq c_0 + \sum_{i=1}^{n} c_i x_i < \frac{max_{1\leq i\leq n}\|c_i\|}{2}$$

where $c_1\geq 0$, $c_1 = 0$ and $c_2\geq 0$ or $c_1 = c_2 = ... = c_{n-1} = 0$ and $c_n \geq 0$.

If n=2, we will have the naive line definition from the definition 5. We obtains a naive line in considering the losange of each pixel, crossed by an euclidean line as we can see in the figure 3. The losange is also a squarre centered in $\mathbb{Z}^2$ point and can be seen as a pixel depending on the choice of the axes of the repere in the image space.

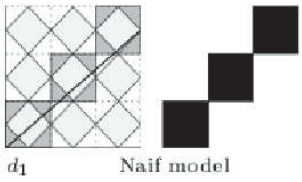

Figure 3: Naive discrete line

Definition : **(**The Standard hyperplane [1], [2]**)** *The* Standard *hyperplane with the parameters* $(c_0,...,c_n) \in R^{n+1}$ *is the set of points* $(x_1,...,x_n) \in Z^n$ *verifying :*

$-\frac{\sum_{i=1}^{n}\|c_i\|}{2} \leq c_0 + \sum_{i=1}^{n} c_i x_i < \frac{\sum_{i=1}^{n}\|c_i\|}{2}$

where $c_1 \geq 0$, $c_1 = 0$ *and* $c_2 \geq 0$ *or* $c_1 = c_2 = ... = c_{n-1} = 0$ *and* $c_n \geq 0$.

When n=2, we will obtain the standard line definition from the definition 6. We build a standard line in considering the pixels crossed by an euclidean line as we can see in the figure 4.

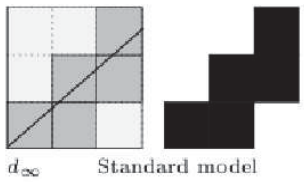

Figure 4: Standard discrete line

Previously in the section II-A, we discuss of vertical line detection problem in the euclidean space. The standard hough transform is a solution to this problem.

C. Standard ough Transform

The Standard Hough Transform uses the polar coordinates of lines. It associates a point in a image space to a sinusoïd curve in a parameter space [6].

Definition : *Let* ξ *and* $\square$ *be respectively an image space* ($\subset \mathbb{R}^2$) *and a parameter space*($\subset \mathbb{R}^2$) *in 2D dimension. Let* $\square(x, y)$ *be a point in* ξ *. The standard* ough *transform of* $\square$ *is the sinusoid curve* $S(\square)$ *in* $\square$ *defined by* $S(\square) = \{(\theta, r) \in \mathbb{R}^2 / r = x * cos\theta + y * sin\theta\}$.

The Standard Hough Transform is a sinusoïd curve with the periode 2π. That means, we can consider $\theta \in [0,2\pi]$ to analyze the function.

Let A(1, 3) be a point in $\mathbb{R}^2$. The standard Hough Transform of the point A is

$$r = cos\theta + 3 * sin\theta \quad (4)$$

According to the definition 7, as we can see in the following figure 5, the point A and its dual.

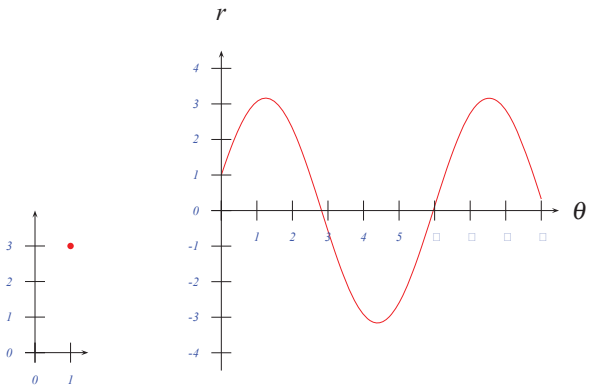

(a) point (1,3) (b) standard hough transform of the point(1,3)

Figure 5: Standard hough transform

The recognition algorithm consists to determine the coordinates of the intersection points in the parameter space. In the following figure 6a, we see the points A, B, C on a euclidean line, and in the 5b, their dual.

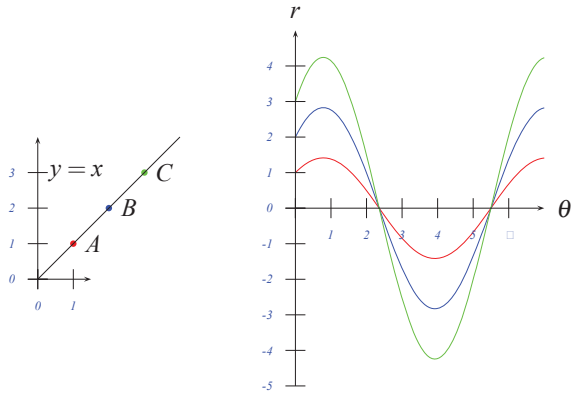

(a) points (b) Standard Hough Transform

Figure 6: Standard Hough Transform

If the point(θ_1, r_1) is an intersection point between two sinusoïd curves then the point ($\theta_1 + \pi$, $-r_1$) will be also an intersection point between them because we have :

$$r = x * cos(\theta) + y * sin(\theta) \Longleftrightarrow -r = x * cos(\theta + \pi) + y * sin(\theta + \pi) \quad (5)$$

Then finally, we can retain $\theta \in [0,\pi]$. That will be useful forward to optimize the computing of the preimage.

The detection of vertical lines is possible, because we can obtain x=α with $\alpha \in \mathbb{R}$ from $r = x * cos(\theta) + y * sin(\theta)$ with ($\theta = \frac{\pi}{2}$ modulo 2π) or ($\theta = \frac{3\pi}{2}$ modulo 2π).

We have extended the Standard Hough Transform into the discrete aspect. The idea is to conserve the power of the Standard Hough Transform and to have naive or standard line recognition in the proposed method.

III. Extended Standard Hough Transform

This section highlights the proposed method. Firstly, we will analyse how to compute the dual of a pixel, what can

be its approximation in order to build the preimage. At the end of this part, we will present an recognition algorithm, the advantages of the proposed method and some illustrations.

We consider here that the term Dual is equivalent to the standard Hough transform.

We conserve the definition 3 of the dual of an object in preliminaries that is the dual of an object O is the union of the dual of each point of O.

A. Dual of a segment

The dual of a segment is the union of the dual of each point on this segment. The introduced theorem 1 determines how to compute the dual of a segment.

Theorem 1: The dual of a segment is an area limited by the dual of its extremities

Proof:

Let us prove that. Let [AC] be a segment in an image space with C(x_c,y_c) and A(x_a,y_a). Let M(x_m,y_m) be a point ∈[AC]. We know that the Dual(A), Dual(C), Dual(M) are respectively a set of points (θ, r_a), (θ, r_c), (θ, r_m) verifying respectively the equations :

$$r_a = x_a \cos\theta + y_a \sin\theta \quad (6)$$

$$r_c = x_c \cos\theta + y_c \sin\theta \quad (7)$$

$$r_m = x_m \cos\theta + y_m \sin\theta \quad (8)$$

We have also

$$\overrightarrow{O\square} = \square * \overrightarrow{0A} + (1-\square) * \overrightarrow{OC} \quad (9)$$

where k∈ℝ, $0 \leq \square \leq 1$.

We obtain with (6) , (7) and (8) that

$$(9) \Rightarrow x_m = \square * x_a + (1-\square) * x_c \quad (10)$$

and

$$(9) \Rightarrow y_m = \square * y_a + (1-\square) * y_c \quad (11)$$

.

Then considering (10) and (11) we conclude $r_m = \square * (x_a \cos\theta + \square * y_a \sin\theta) + (1-\square) * (x_c \cos\theta + y_c \sin\theta)$

That implies $r_m = \square * r_a + (1-\square) * r_c$.

That means $r_a \leq r_m \leq r_c$ or $r_c \leq r_m \leq r_a$.

So, the curve of Dual(M) is between the curve of Dual(A) and the curve of Dual(C).

Inversely, suppose N(θ_1, r_1) a point between the curve of Dual(A) and the curve of Dual(C). We want to show that there exists a point M ∈[AC] such as the curve of Dual(M) passes through N.

We have $r_c(\theta_1) \leq r_1 \leq r_a(\theta_1)$ or $r_a(\theta_1) \leq r_1 \leq r_c(\theta_1)$

That means ∃k∈ℝ such as $0 \leq \square \leq 1$ such as

$$r_1 = \square * r_a(\theta_1) + (1-\square) * r_c(\theta_1) \quad (12)$$

As $r_a(\theta_1) = x_a \cos\theta_1 + y_a \sin\theta_1$ and $r_c(\theta_1) = x_c \cos\theta_1 + y_c \sin\theta_1$

Then, we obtain

$$(12) \Rightarrow r_1 = \square * (x_a \cos\theta_1 + y_a \sin\theta_1) + (1-\square) * (x_c \cos\theta_1 + y_c \sin\theta_1) \quad (13)$$

So

$$(13) \Rightarrow r_1 = (\square * x_a + (1-\square) * x_c) \cos\theta_1 + (\square * y_a + (1-\square) * y_c) \sin\theta_1 \quad (14)$$

.

Finally (14) implies the point of coordinates $((\square * x_a + (1-\square) * x_c), (\square * y_a + (1-\square) * y_c))$ is on the segment [AC]. ■

In the following figure 7, we see a segment [AC] with M∈[AC] in 7a, in7b, the dual of M between the dual of A and C and in 7c the equivalent surface of the dual of [AC].

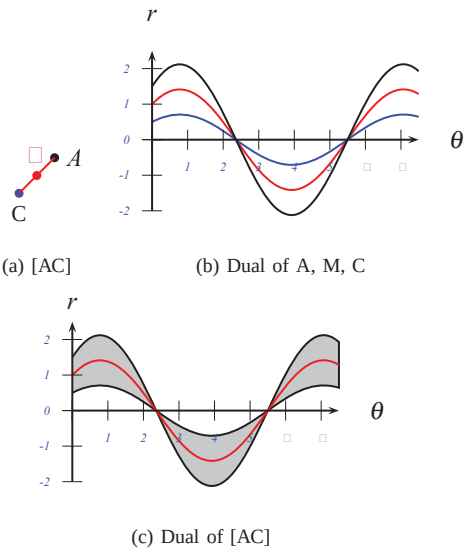

(a) [AC] (b) Dual of A, M, C

(c) Dual of [AC]

Figure 7: Dual of a segment

B. Dual of a pixel

A pixel is the unit squarre region centered in(p_1, p_2) a $\mathbb{Z}^2$ point : $\{(x,y) \in \mathbb{R}^2 \,|\, |x-p_1| \leq \frac{1}{2}, |y-p_2| \leq \frac{1}{2}\}$. The dual of a pixel is then the union of the dual of each point(x, y). Its definition is :

Definition □: Let p be a pixel centered in (p_1, p_2) in a image space ξ. The Dual of p is a set of points of the parameter space □, defined by Dual(p)=$\{(\theta, r) \in \square^2 / \forall(\alpha,\beta) \in [\frac{-1}{2}, \frac{1}{2}]^2, r = (p_1+\alpha)\cos\theta + (p_2+\beta)\sin\theta\}$.

The figure 8 shows the standard Hough transform of vertices of pixel (1,1) : Each colored vertex correspond to its colored curve image.

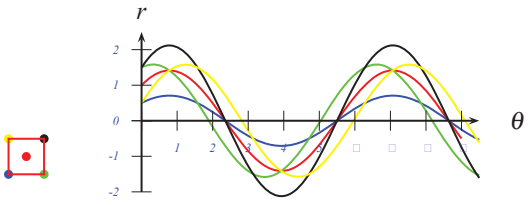

(a) *pixel(1,1)* (b) Standard hough transform of vertices

Figure 8: Extended standard hough tranform

Let A, B, C, D be the vertices of a pixel p as ilustrated in the figure 9. A pixel is a set of an infinity of vertical segments (9a) or an infinity of horizontal segments (9b). We have also the diagonal segments in (9c).

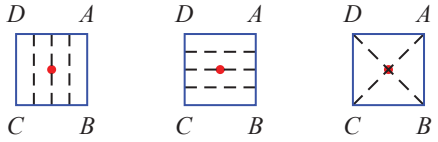

(a) (b) (c)

Figure 9: Sides of a pixel

Our aim is to determine the dual of a pixel in going with the dual of its segments (vertical, diagonal or horizontal).

We propose the following theorem 2.

Theorem 2: Let p be a pixel in $\xi_2(\subset\mathbb{R}^2)$. Its dual is a area limited by the curve of the duals of its vertical sides. This area is also limited by the curve of the duals of its horizontal sides or by the duals of its diagonals.

Proof: Let us prove that. Let p be a pixel with its vertices A, B, C, D in image space like in the figure 10.

Firstly, one shows that the dual of a pixel is an area limited by the dual of its vertical sides [AB] and [CD]. The dual of a segment is obtained by the theorem 1. Let N be a point in a pixel p with vertices A, B, C, D where N $\notin\{A,B,C,D\}$. There exists two points I, J such that N $\in$ [IJ] where I $\in$[CD], J$\in$[AB]. We notice that [IJ] is a segment. According to the theorem 1, the dual of N is a sinusoid curve between the duals of I and J. As I $\in$[CD], J$\in$[AB], the dual of I is between the duals of the points C and D. The dual of J is also between the duals of the points A and B. So, the dual of N is in the surfaces limited by the duals of [AB] and [CD]. Inversely, let N' be a point in the surface limited by the dual of [AB] and [CD]. N' is between two sinusoïd curves, the duals of two vertices X, Y with (X,Y) $\in\{A,B,C,D\}^2$. A pixel is convex, so [XY] $\subset$p. According to the theorem 1, there exists a point s $\in$[XY] in the pixel such as dual(s) is a sinusoïd curve that pass through N'.

Secondly, one shows that the dual of a pixel is an area limited by the dual of its horizontal sides [AD] and [BC]. By analogy to the first case, we define a point N in a pixel where N $\notin\{A,B,C,D\}$. There exists two points I, J such that N $\in$ [IJ] where I $\in$[AD], J$\in$[BC]. As I $\in$[AD], J$\in$[BC], the dual of I is between the duals of A and D. The dual of J is between the duals of B and C. So, the dual of N is in the surfaces limited by the duals of [AD] and [BC]. We can also notice that when we apply on the pixel p, a central symmetry by the center of the pixel, a horizontal side become a vertical side. Inversely, let N' be a point in the surface limited by the dual of [AD] and [BC]. N' is between two sinusoïd curves, the duals of two vertices X, Y with (X,Y) $\in\{A,B,C,D\}^2$. A pixel is convex, so [XY] $\subset$p. According to the theorem 1, there exists a point s $\in$[XY] in the pixel such as dual(s) is a sinusoïd curve that pass through N'.

Thirdly, we show that the dual of a pixel is a surface limited by the diagonals segments [AC], [BD]. There exists two points I, J such that N $\in$ [IJ] where I $\in$[AC], J$\in$[BD]. As I $\in$[AC], J$\in$[BD], the dual of I is between the duals of the points A and C. The dual of J is between the duals of the points B and D. So, the dual of N is in the surfaces limited by the duals of [AC] and [BD]. Inversely, let N' be a point in the surface limited by the duals of [AC] and [BD]. N' is between two sinusoïd curves, the duals of two vertices X, Y with (X,Y) $\in\{A,B,C,D\}^2$. A pixel is convex, so [XY] $\subset$p. According to the theorem 1, there exists a point s $\in$[XY] in the pixel such as dual(s) is a sinusoïd curve which pass through N'. ■

We present an illustration of this proof in the following figure 10 where we can see the points N, I, J in the different cases of sides and diagonals : in 10a, we have the vertical sides; in 10b, the horizontal sides, and in 10c, the diagonals.

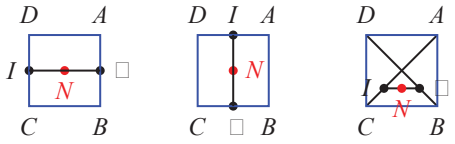

(a) [AB] , [CD] (b) [AD], [BC] (c) [AC], [BD]

Figure 10: Segments of pixels

Let p a pixel centered in (1,1) with the vertices A, B, C, D as in the figure 10. The following figures 11,12, 13 illustrate how we obtain the area of the dual of a pixel with the application of the previous theorem 2 : we compute the dual of sides and diagonals and we present their associated surface.

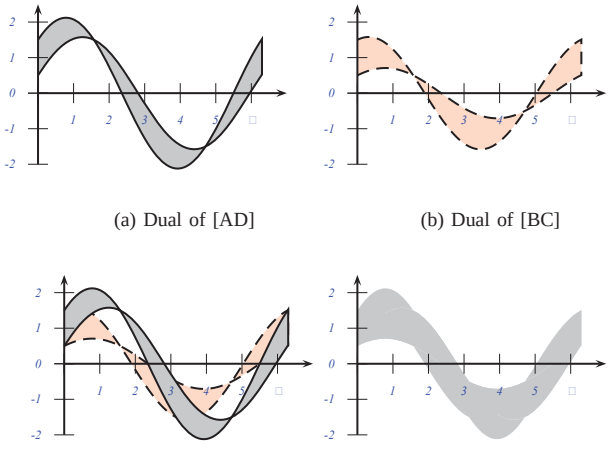

(a) Dual of [AD] (b) Dual of [BC]

(c) Dual of [AD] and [BC] (d) Surface

Figure 11: Horizontal sides

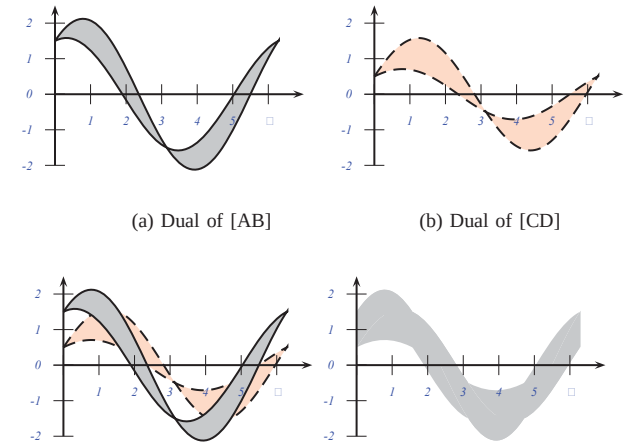

(a) Dual of [AB] (b) Dual of [CD]

(c) Dual of [AB] and [CD] (d) Surface

Figure 12: Vertical sides

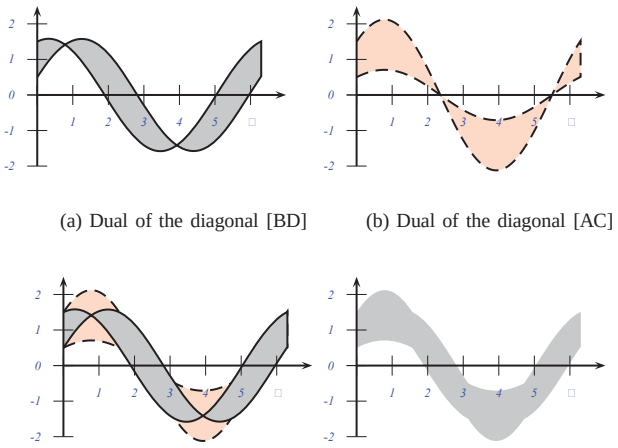

(a) Dual of the diagonal [BD] (b) Dual of the diagonal [AC]

(c) Union of duals (d) Surface

Figure 13: Diagonals

We observe that in the previous figure 13, there does not exist empty space between the dual of the diagonals. Then, the dual of pixel is easy to be computed by the following theorem 3.

Theorem 3: the dual of a pixel is the union of the dual of its diagonal segments.

Proof: Let us prove that. Let p be a pixel with its vertices A, B, C, D and its diagonals [AC] and [BD]. In the previous theorem 2, we proved that the dual of a pixel is a surface between the dual of its diagonals. We are going to show that this area is equivalent to the union of the dual of its diagonals. That means, for a point in the dual of a pixel, it must belong to the dual of [AC] or the dual of [BD]. [AC] and [BD] are a common point, the center O of the pixel. So, the dual of O is a sinusoïd curve in the Dual([AC]) and the Dual([BD]) according to the theorem1. With $\theta \in [0, 2\pi]$, we can classify the Dual(A), Dual(B), Dual(O), Dual(C), Dual(D) by the relation$\leq$ or $\geq$. Dual(O) is in the middle of the classification.

Then, we have Dual([AC])$\subset$ Dual([BD]) or Dual([BD]) $\subset$ Dual([AC])

As a conclusion, the set of points N verifying the proposition [N$\in$Dual(p) with N $\notin$ Dual([AC]) and N $\notin$ Dual([BD])] is ϕ. ■

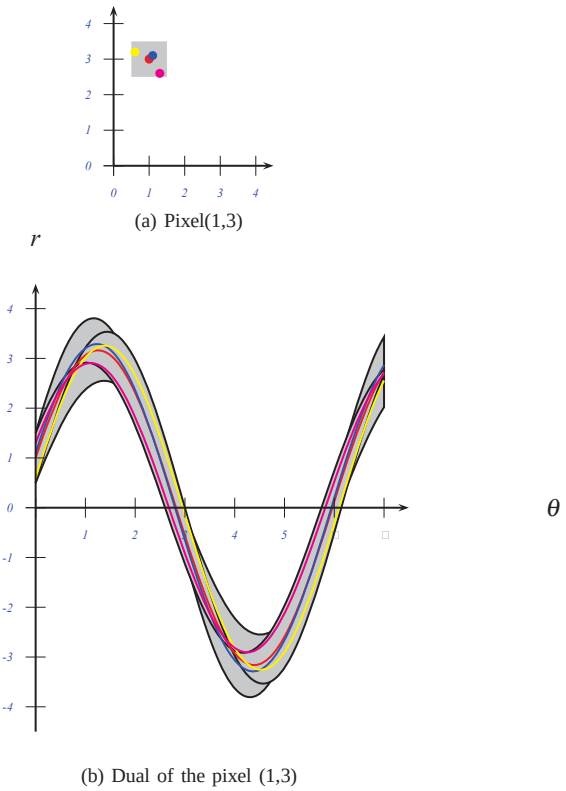

(a) Pixel(1,3)

(b) Dual of the pixel (1,3)

Figure 14: Extended standard hough tranform

We see in the figure 14, a pixel (1,3) and its dual : we can notice that the dual of some points in the pixel is in the area.

1) Analysis of the dual : The purpose of this section is to analyze the dual of a pixel and to obtain some remarkable points that can be useful for an approximation of the dual.

Let p (p_1, p_2) be a pixel with its vertices : A$(p_1+\frac{1}{2}, p_2+\frac{1}{2})$, B$(p_1+\frac{1}{2}, p_2-\frac{1}{2})$, C$(p_1-\frac{1}{2}, p_2-\frac{1}{2})$, D$(p_1-\frac{1}{2}, p_2+\frac{1}{2})$.

The Dual(A), Dual (C), Dual(B), Dual(D) are respectively given by:

$$Dual(A) : r_A = (p_1+\frac{1}{2})\cos\theta + (p_2+\frac{1}{2})\sin\theta \qquad (15)$$

$$Dual(C) : r_C = (p_1 - \frac{1}{2})\cos\theta + (p_2 - \frac{1}{2})\sin\theta \quad (16)$$

$$Dual(B) : r_B = (p_1 + \frac{1}{2})\cos\theta + (p_2 - \frac{1}{2})\sin\theta \quad (17)$$

$$Dual(D) : r_D = (p_1 - \frac{1}{2})\cos\theta + (p_2 + \frac{1}{2})\sin\theta \quad (18)$$

Considering (15), (17), (16), (18), with $\theta \in [0, 2\pi]$, we have the intersection points

$$Dual(B) \cap Dual(D) = \square, L \quad (19)$$

$$Dual(A) \cap Dual(C) = I, \square \quad (20)$$

$$Dual(A) \cap Dual(B) = O_1, \square_0, \square_1 \quad (21)$$

$$Dual(A) \cap Dual(D) = \square_1, \square_0 \quad (22)$$

$$Dual(B) \cap Dual(C) = \square_0, \square_1 \quad (23)$$

$$Dual(C) \cap Dual(D) = O_0, \square_1, \square_0 \quad (24)$$

The below table I gives more details on the coordinates of the points obtained in (19), (20), (21), (22), (23), (24).

Table I: Summary of intersections points

θ	**External points**
0	$O_0(0,\ p_1 - \frac{1}{2}),\ O_1(0,\ p_1 + \frac{1}{2})$
$\frac{\pi}{2}$	$\square_0(\frac{\pi}{2},\ p_2 - \frac{1}{2}),\ \square_1(\frac{\pi}{2},\ p_2 + \frac{1}{2})$
π	$\square_0(\pi,\ -(p_1 + \frac{1}{2})),\ \square_1(\pi,\ -(p_1 - \frac{1}{2}))$
$3\frac{\pi}{2}$	$\square_0(3\frac{\pi}{2},\ -(p_2 + \frac{1}{2})\ ),\ \square_1(3\frac{\pi}{2},\ -(p_2 - \frac{1}{2})\ )$
2π	$\square_0(2\pi,\ p_1 - \frac{1}{2}),\ \square_1(2\pi,\ p_1 + \frac{1}{2})$
θ	**Internal points**
$\frac{\pi}{4}$	K $(\frac{\pi}{4},\ (p_1 + p_2)\frac{\sqrt{2}}{2}\ )$
$3\frac{\pi}{4}$	I$(\frac{3\pi}{4},\ \frac{\sqrt{2}}{2}(p_2 - p_1))$
$5\frac{\pi}{4}$	L$(\frac{5\pi}{4},\ -(p_1 + p_2)\frac{\sqrt{2}}{2}\ )$.
$7\frac{\pi}{4}$	J $(\frac{7\pi}{4},\ \frac{\sqrt{2}}{2}(p_1 - p_2))$.

As we can see, in the figure 15, we have the points I, J of the intersection of the dual of A and C; in the figure 16, Those of the duals of B and D with the points K, L, the figure 17 show all the points.

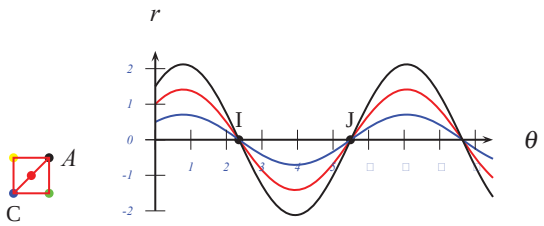

(a) [AC] (b) Dual of [AC]

Figure 15: Dual of segment

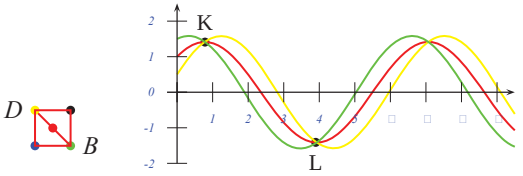

(a) [BD] (b) Dual of [BD]

Figure 16: Dual of segment

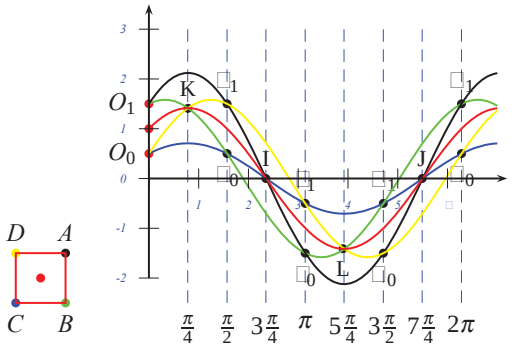

(a) Pixel(1,1) (b) Sinusoïd curves of a pixel (1,1)

Figure 17: Sinusoïd curves

When we follow the values of θ in [0 2π], we will establish the following tables II, III, IV, V that compare in each interval, the values of the dual of vertices.

Table II: $\theta \in [0, \frac{\pi}{2}\ ]$

θ	$0 \le \theta < \frac{\pi}{4}$	$\frac{\pi}{4} \le \theta < \frac{\pi}{2}$
relation	$r_C \le r_D \le r_B \le r_A$	$r_C \le r_B \le r_D \le r_A$

Table III: $\theta \in [\ \frac{\pi}{2},\ \pi\ ]$

θ	$\frac{\pi}{2} \le \theta < \frac{3\pi}{4}$	$\frac{3\pi}{4} \le \theta < \pi$
relation	$r_B \le r_C \le r_A \le r_D$	$r_B \le r_A \le r_C \le r_D$

Table IV: $\theta \in [\pi, \frac{3\pi}{2}]$

θ	$\pi \le \theta < \frac{5\pi}{4}$	$\frac{5\pi}{4} \le \theta < \frac{3\pi}{2}$
relation	$r_A \le r_B \le r_D \le r_C$	$r_A \le r_D \le r_B \le r_C$

Table V: $\theta \in [\frac{3\pi}{2},\ 2\pi]$

θ	$\frac{3\pi}{2} \le \theta < \frac{7\pi}{4}$	$\frac{7\pi}{4} \le \theta < 2\pi$
relation	$r_D \le r_A \le r_C \le r_B$	$r_D \le r_C \le r_A \le r_B$

When θ passes the values $\frac{\pi}{2}$, π, $3\frac{\pi}{2}$, 2π, we will observe that the exteriors r_i become the interiors $r_{i'}$ and inversely.

According to

$$r = x*cos\theta + y*sin\theta \Longleftrightarrow -r = x*cos(\theta+\pi) + y*sin(\theta+\pi) \quad (25)$$

we will work on an interval [0, π], with the tables II, III and the external or internal points of this interval. The others exterior or interior points and the tables IV, V are deductions.

2) Approximation of the dual : Here, we propose an approximation of the area of the dual of a pixel. In computational geometry, algorithms exists to compute the intersection of convex polygons. A lot of methods of approximation possibility could be studied forward.

In our method, we consider a polygonal approximation based on a few points of the dual in the way to obtain some parameters (θ, r) : the idea is that if an object O' is an approximation of an object O then Dual(O') will be also an approximation of Dual(O).

Moreover, if O'⊂O, we will have Dual(O')⊂Dual(O). Some points of the initial pixel are used to obtain its dual approximation.

Let p be a pixel centered in (p_1,p_2). The pixel p has the vertices A($p_1+\frac{1}{2}$, $p_2+\frac{1}{2}$), B($p_1+\frac{1}{2}$, $p_2-\frac{1}{2}$), C($p_1-\frac{1}{2}$, $p_2-\frac{1}{2}$), D($p_1-\frac{1}{2}$, $p_2+\frac{1}{2}$).

Let p^i be a pixel centered in (p_1,p_2) with its vertices $A^i(p_1+\frac{1}{2}-i*\delta,\ p_2+\frac{1}{2})$, $B^i(p_1+\frac{1}{2},\ p_2-\frac{1}{2}+i*\delta)$, $C^i(p_1-\frac{1}{2}+i*\delta,\ p_2-\frac{1}{2})$, $D^i(p_1-\frac{1}{2},\ p_2+\frac{1}{2}-i*\delta)$.

where i∈ ℕ and δ∈[0,1] with the contraints $i*\delta$∈{0,1}. The duals of the vertices of p^i are :

$$Dual(A^i) : r_{A^i} = (p_1+\frac{1}{2}-i*\delta)\cos\theta + (p_2+\frac{1}{2})\sin\theta \quad (26)$$

$$Dual(C^i) : r_{C^i} = (p_1-\frac{1}{2}+i*\delta)\cos\theta + (p_2-\frac{1}{2})\sin\theta \quad (27)$$

$$Dual(B^i) : r_{B^i} = (p_1+\frac{1}{2})\cos\theta + (p_2-\frac{1}{2}+i*\delta)\sin\theta \quad (28)$$

$$Dual(D^i) : r_{D^i} = (p_1-\frac{1}{2})\cos\theta + (p_2+\frac{1}{2}-i*\delta)\sin\theta \quad (29)$$

Then, p^i is an approximative pixel of p where $i*\delta$ is the difference with the real vertice coordinates of p. The maximal value of $i*\delta$ must be inferior to the maximal of the tolerance error.

We use the external points (see the table I) of the dual of the pixels p^0, p^1, p^2,... p^n to get a polygonal approximation of the dual of p with $p^0 = p^{n+1} = p$.

We know that

$$p^{n+1} = p \Longleftrightarrow (n+1)*\delta = 1 \quad (30)$$

Then (30) $\Longleftrightarrow \delta = \frac{1}{n+1}$.

Finally, we need to take $\delta = \frac{1}{n+1}$ to have the pixels p^0, p^1, p^2,...,p^n.

As we know, we work in [0, π]; we determine the approximation of the dual in this interval. We obtain the polygon O_1□$_1$□$_1$□$_0$□$_0O_0$. with the pixel p^0, (see the figure 17 for more details). The following figure 18 shows the polygon (in red color).

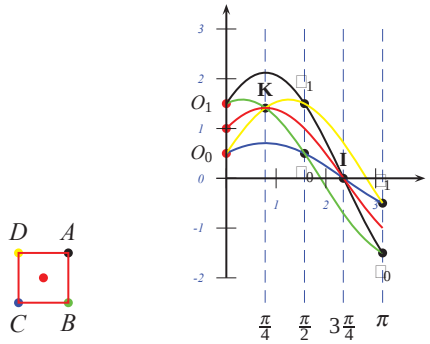

(a) Pixel(1,1) (b) Sinusoïd curves of a pixel (1,1)

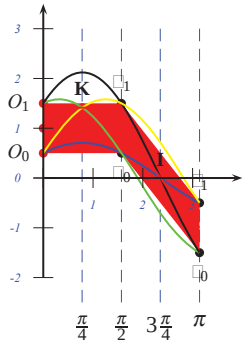

(c) Sinusoïd curves of p

Figure 18: Approximative pixels Sinusoïd curves

The intersection points of vertices, with i $\geq$ 1 are Dual(A^i)∩Dual(B^i)={O_1^i}, Dual(A^i)∩Dual(D^i)={□$_1^i$}, Dual(B^i)∩Dual(C^i)={□$_0^i$}, Dual(C^i)∩Dual(D^i)={O_0^i}.

As p^i is close of p, these intersections points are close of O_1, □$_1$, □$_1$, □$_0$, □$_0$, O_0 respectively.

The proposed polygon is then $O_1O_1^1...O_1^n$□$_1$□$_1^1$...□$_1^n$□$_1$ □$_0$□$_0^n$...□$_0^1$□$_0O_0^n$...$O_0^1O_0$.

Let S_n be the surface associated to this polygon. According to the tables II, III, we know that the surface of the dual of a pixel is :

$$I = \int_{[0,\frac{\pi}{2}]}(r_A - r_C)dx + \int_{[\frac{\pi}{2},\pi]}(r_D - r_B)dx = 4 \quad (31)$$

According to (31), the extimated error is then $I - S_n = 4 - S_n$ and the percentage will be $\frac{4-S_n}{4}$.

If $\delta = \frac{1}{4}$, we will obtain p^1= p'(p_1,p_2), p^2=p"(p_1,p_2), p^3=p"'(p_1,p_2) that are presented in the following figure 19.

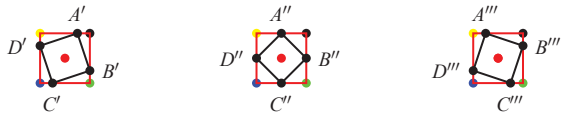

(a) pixel p' (b) pixel p" (c) pixel p"'

Figure 19: Approximative pixels

.

We illustrates step by step the proposed polygon in the following figures 20, 21

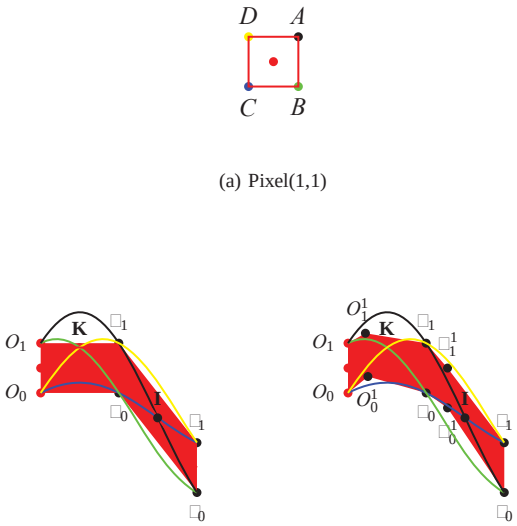

(a) Pixel(1,1)

(b) p (c) p^1

Figure 20: Sinusoïd curves

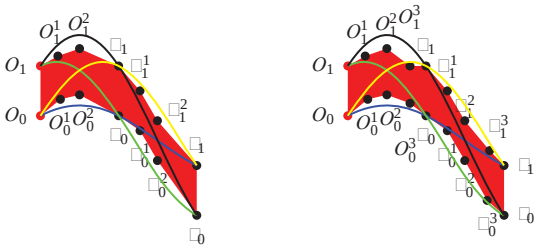

(a) p^2 (b) p^3

Figure 21: Sinusoïd curves

C. Preimage

We present a new definition of preimage of pixels. Here, the term Dual means the Standard Hough transform. The preimage of n pixels is an intersection of n sinusoïd surfaces and differs from the definition introduced in[**?**], by Martine Dexet in her thesis.

Definition □: *Let* $S=\{P_1,P_2,...,P_{n-1},P_n\}$ *be a set of n pixels* P_i *in* ξ_2. *The preimage of S is defined by* $Preimage(S) = \bigcap_{1\le i\le n} Dual(P_i)$.

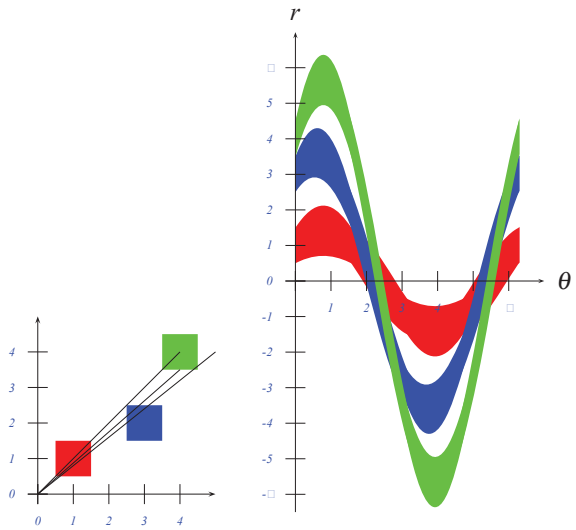

(a) pixels (b) Intersection of the Dual of pixels

Figure 22: Preimage of three pixels

In the figure 22, we see in 22a three colored pixels. In 22b, the corresponding colored dual of each pixel. The intersection of these three duals is a set of points representing the parameters (θ, r) of line that cross each pixel.

The parameters (-r, $cos\theta$, $sin\theta$) are equal to the parameters (c_0, c_1, c_2) of the analytical hyperplane in 2D dimension,

presented in the section II-B. As you can see in the figure 22 the preimage of n pixels give two areas because

$$r = x * cos\theta + y * sin\theta \Longleftrightarrow -r = x * cos(\theta + \pi) + y * sin(\theta + \pi) \quad (32)$$

D. Recognition algorithm

In this part, we recall that the term dual indicates the Extended Standard Hough Transform. We can see that when, the dual of the losange of each pixel is considered, we will be in the case of naive line recognition.

Moreover, according to the definition of the naive and standard hyperplanes introduced in preliminaries and the geometry construction of these models, we see that the preimage contains the parameters of analytical line that crosses the pixels.

We propose the following algorithm :

Algorithm 1 Naive, Standard line recognition

Data : A set S of n pixels P_1,..., P_n.
Begin
  Preimage←Dual(P_1)
  i←2
  while Preimage≠ Ø and i≤ n **do**
    Preimage←Preimage ∩ Dual(P_i)
    i←i+1
  End while
  if Preimage ≠ Ø **then**
    S belongs to a digital line
  else
    S does not belong to a digital line
  End if
End

The Dual(P_i) could be replaced by an approximation (polygon for example) in order to increase the performance of the algorithm.

The Extended Standard Hough Transform has its particularity to answer the question how can we recognize Naive and Standard by the standard Hough Transform. It conserves the properties of the Standard Hough Transform [6] as the size of the parameter space is limited [6]:$\theta \in [0, \pi]$ and r $\in[0, \sqrt{col^2 + row^2}\}$ with an image col x row. This leads to the vertical line detection.

IV. Dual of a triangle

We are interested in how to compute the dual of a triangle. In case of triangle grid, we need to know how to determine the dual of a triangle. We establish the following theorem 4.

Theorem 4: The dual of a triangle is the union of the dual of one of its two adjacent(consecutif) sides

Proof: Let [AC] and [AB] be two adjacents sides of a triangle (ABC) as we see in the following figure 23. Let N be a point in the triangle (if N is a vertex the proof is realized). There exists two point I and J such that I ∈[AC], J∈[AB] and N ∈[IJ]. By analogy with the proof of the theorem 2. We have two consecutif sides [AC] and [AB] that are secants on the vertex A of a triangle (ABC). Then, the surface between the dual of [AC] and [AB] does not contains empty space. Morover, we knows that the dual of I is between the dual of A and C like the dual of J is between the dual of A and B. As we know the dual of N is between the dual of I and the dual of J, then the dual of N is in the union of the dual of [AC] and [AB] . ■

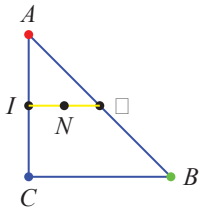

Figure 23: Triangle

The below figure 24 shows the dual of a triangle, it contains the dual of each point of the triangle : In 24b, the dual of the vertex of a triangle in 24a, and in 24c, the dual of a triangle.

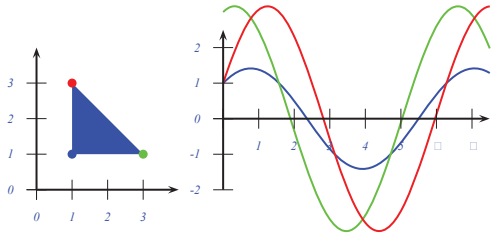

(a) Triangle (b) Dual of segments

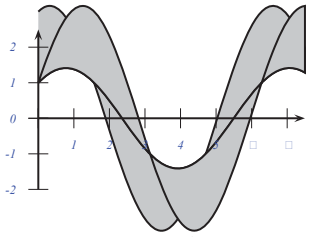

(c) Union of duals

Figure 24: Extended standard hough transform

V. Conclusions

This paper establishs a new method based on the Standard Hough Transform for the recognition of naive or standard lines in a noisy picture. We introduced a new definition of preimage that allows us to obtain an algorithm recognition. We obtained that the dual of a pixel is an non polygonal area. That leads

to propose an approximation. Others approximative methods could be studied deeply forward in the objectif to improve the algorithm. Some works still left to be done, particularly the implemention on concrete pictures. The dual of a triangle has been proposed. That could give interested perpectives in the others grids. One of the remaining question is to extend the method in 3D.

ACKNOWLEGDMENT

The authors would like to thank the organization “L’Agence Universitaire de la Francophonie”(AUF) for their help and support in making this work possible.

REFERENCES

[1] E. Andres. Discrete linear objects in dimension n : the standard model. Graphical Models, pages 65 :92–111, 2003.
[2] E. Andres, R. Acharya, C. Sibata, Discrete analytical hyperplanes, Graphical Model and Image processing, Volume 59, Issue 5, September 1997, Pages 302–309.
[3] D.H.Ballard. Generalizing the hough transform to detect arbitrary shapes. Pattern Recognition, Vol. 13, No. 2, pp. 111–112, 1981.
[4] M Bruckstein, N.Kiryati, Y.Eldar. A probabilistic hough transform. Pattern Recognition, 24(4) : 303–316, 1991.
[5] M.Dexet. Architecture d’un modéleur géometrique à base topologique d’objets discrets et methodes de reconstruction en dimensions 2 et 3. Thèse de Doctorat, Université de Poitiers, France, 2006.
[6] F. Dubeau, S.El mejdani, R.Egli. Champs de hauteur de la transformée de hough standard. Actes de 4ième Conférence Internationale en Recherche Opérationnelle, pages 133-144, 2005.
[7] J. Cha , R. H. Cofer , S. P. Kozaitis, Extended Hough transform for linear feature detection, Pattern Recognition, v.39 n.6, p.1034-1043, June, 2006
[8] H.Maître. Un panorama de la transformée de hough - a review on hough transform. Traitement du Signal, 2(4) :305–317, 1985.
[9] J. Matas, C. Galambosy and J. Kittler. Progressive probabilistic hough transform, Transform, Volume: 24, n.4, Pages: 303-316, 1991
[10] J. P Reveillès, combinatorial pieces in digital lines and planes, in Vision Geometry IV Proc. SPIE, Vol. 2573, San Diego, CA, 1995, pp. 23-24.
[11] J.P. Reveillès. Géométrie discrète, Calcul en nombres entiers et algorithmiques. Thèse d’état, Université Louis Pasteur, Strasbourg, France, 1991

k-Modulus Method for Image Transformation

Firas A. Jassim
Department of Management Information Systems
Irbid National University
Irbid 2600, Jordan
Email: firasajil@yahoo.com

***Abstract*—In this paper, we propose a new algorithm to make a novel spatial image transformation. The proposed approach aims to reduce the bit depth used for image storage. The basic technique for the proposed transformation is based of the modulus operator. The goal is to transform the whole image into multiples of predefined integer. The division of the whole image by that integer will guarantee that the new image surely less in size from the original image. The k-Modulus Method could not be used as a stand alone transform for image compression because of its high compression ratio. It could be used as a scheme embedded in other image processing fields especially compression. According to its high PSNR value, it could be amalgamated with other methods to facilitate the redundancy criterion.**

I. Introduction

Image transformations have received a significant consideration due to its importance in computer vision, computer graphics, and medical imaging [1]. The transformed images are information about the dissimilarities between input image and the output image and trying to make these dissimilarities as closely as possible [2]. Image transformations are the extremely significant process in image processing and image analysis. Image transforms are used in image enhancement, restoration, reconstruction, encoding and description. A spatial transformation is an image processing process that re-identifies the spatial relationship between pixels in an image. This procedure will make the manipulation of an image layout is easier concerning image size and shape. The mathematical concept of image transformation is a powerful procedure that is recruited in various fields in image processing disciplines and the most important one is image compression [3]. The pixels pattern in natural images is not random, but has a noticeable statistical regularity. This regularity is clearly may be touched at the single pixel level or the block of pixels [4]. Redundancy in data is exemplary reachable through transforming the original data from one representation to another [5]. The basic idea in image compression is that the new pixels are almost smaller than the original pixels. Alternatively, the decoder side enters the transformed pixels and reconstructs the original image by implementing the inverse transform procedure [3]. The image transformation could be imagined as a mapping from one coordinates to another transformed coordinates. It must be mentioned that, there are two types of image transformations according to the reversibility procedure. The first one is lossless transform and the other one is the lossy transform. In case of lossless transform, the original pixels are completely reversible. While in the lossy transforms, the genuine pixels could not be obtained because lossy transformations are fully irreversible [6]. In principle, the idea behind image transformation is the representation of the pixels in the original image in terms of fewer bit length than the original bit stream. Transformation of an image usually decreases the entropy of the original image by eliminating the redundancies of the image pixel sequence [5].

The remainder of the paper is organized as follows. Section II discusses the spatial transformation for image processing. The proposed k-Modulus Method (k-MM) has been introduced by details in section III. Section IV presents the experimental results when applying the proposed k-Modulus Method to a variety of test images. The conclusion of this paper was presented in section V.

II. Spatial Transformation Preliminaries

Spatial transformations are important in many aspects of functional image analysis [7]. The main concept in spatial transformation is to find a mapping for each pixel lies in the original integer lattice to a new grid used to resample the input pixels [1]. The relationship between the image and its corresponding mapping is depending on the structure of the images themselves [4]. Therefore, the selection of the suitable representation of image is only part of the solution for transforming the original image into a suitable mapping for ulterior processing [6]. According to [1], the geometric transformation is completely determined by the spatial transformation because analytic mapping is bijective, i.e. one-to-one and onto. The principle motivation behind transformation could be summarized in two aspects. The firs aspect is that, transformation yielding more efficient representation of the original samples. On the other hand, the transformed pixels must demand fewer bits [8]. Spatial transformation mappings may take different forms and this is depends on the type of application [1]. The choice of the mapping model is essential to obtain reliable results; this choice must be considered seriously and assessed before any processing. As mentioned above, the transformation functions depend on the nature of the scene and on the acquisition system used. However, under some assumptions, and before applying a complicated model, it may be useful to reach the idealistic mapping solicited by consecutive less and less 'rigid' mapping models [9].

The general mapping function can be given in the following form. Let f be the original image and g is the transformed image then there exist an operator T such that:

$$T : f \longrightarrow g, \qquad f, g \in R^{N \times M} \tag{1}$$

and

$$g(x, y) = T\left[f(x, y)\right] \tag{2}$$

where N and M are the image dimensions. It must be mentioned that the operator T is a one-to-one operator, i.e. for each pixel in f there exist a corresponding one and only one pixel is g. Moreover, the one-to-one transformation could be shown in figure 2.

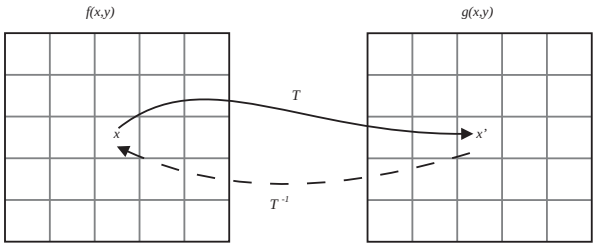

Fig. 1. Spatial one-to-one transformation

Fig. 2. Test Images (Lena,Peppers, Allah, Boy1, and Boy2)

III. Proposed Transformation

The proposed transform is actually a generalization of the Five Modulus Method (FMM) proposed by [10]. The basic idea behind FMM is to transform the original image into multiples of five only. Hence, it was called Five Modulus Method (FMM). Now, a question may arise and that is why not to generalize FMM into k-Modulus Method (kMM). In another words, instead of using number five only why not to use any integer according to the desired precision?. Therefore, the proposed transform has been established. According to [10], the human eye does not differentiate between the original image and the transformed FMM image. Moreover, for each of the Red, Green, and Blue arrays in the color image are consisting of pixel values varying from 0 to 255. The cardinal impression of k-Modulus Method is to transform the all pixels within the whole image into multiples of k. According to figure 4, it is clear that the k-Modulus Method transformation, up to the 10-Modulus Method, does not affect the Human Visual System (HVS). Now, to simplify the above idea, an illustrative example will be presented. Suppose k=2, then the original range of values 0 to 255 will be transformed as 0, 2, 4, 6,. . . , 254. Similarly, when k=3, the transformed range is 0, 3, 6, 9, 12, . . . , 255. The same previous procedure may be applied for any integer k. The k-Modulus method have been applied to k=2,3,4,. . . 20 have been calculated and presented in figure 3. Obviously, increasing k will lead to high distortion in the output image. Hence, by using try and error, we can see that up to k=10 the human eye could not differentiate between the original and the transformed images. According to figure 3, it can be seen that a selective k values (2, 3, 5, 7, 10, 15, 20) have been used to transform a random 6×6 block from Lena image using k-Modulus Method.

A. k-Modulus Method Bit Depth

Bit depth refers to the color information stored in an image. More colors could be stored in an image whenever there is high bit depth in the image. In the case of black and white, it contains one bit either 0 or 1. Hence, it can only show two colors which are black and white. Furthermore, an 8 bit image can store 2^8 which is equal to 256 possible colors, etc. It must be mentioned that, the bit depth specify image size. As the bit depth increase, image size also increases because each pixel in the image requires more information [6]. One way to think about bit depth is to consider the difference between having the capability to make measurements with a ruler that is accurate to the nearest millimeter, compared with one that can only measure to the nearest centimeter [11].

In this paper, a general formula to extract the exact bit depth for each of the k-Modulus Methods has been derived as:

$$n = \left\lfloor \frac{256}{k} \right\rfloor + 1 \tag{3}$$

where k is an integer number ($k = 2, 3, \ldots$).

As with resolution, bit depth determines file size. The higher the depth, the greater the file size. It must not be confounded with the amount of actual colors within an image. Therefore, an image with 25 colors may be created with 16 colors. Hence, we may have thousands instead of millions of possibilities. This would obviously lead to increase in file size and that may not be necessary. A versed understanding of bit depth is essential to any graphic or multimedia application [12].

IV. Experimental Results

In this article, five test images have been tested using the proposed k-Modulus Method. In figure 4, the implementation of the k-Modulus Method was applied using k=2,3,,20 for Lena image. It is clear that, the human eye could distinguish

Original 6×6 Block	175	192	203	211	215	220							
	179	195	205	210	214	220							
	181	198	207	211	217	221							
	188	201	208	215	218	219							
	194	203	212	215	215	218							
	193	204	212	215	217	217							
	197	209	213	216	216	218							
2-MM	174	192	202	210	214	220		87	96	101	105	107	110
	178	194	204	210	214	220		89	97	102	105	107	110
	180	198	206	210	216	220		90	99	103	105	108	110
	188	200	208	214	218	218	→	94	100	104	107	109	109
	194	202	212	214	214	218		97	101	106	107	107	109
	192	204	212	214	216	216		96	102	106	107	108	108
	196	208	212	216	216	218		98	104	106	108	108	109
3-MM	174	192	204	210	216	219		58	64	68	70	72	73
	180	195	204	210	213	219		60	65	68	70	71	73
	180	198	207	210	216	222		60	66	69	70	72	74
	189	201	207	216	219	219	→	63	67	69	72	73	73
	195	204	213	216	216	219		65	68	71	72	72	73
	192	204	213	216	216	216		64	68	71	72	72	72
	198	210	213	216	216	219		66	70	71	72	72	73
5-MM	175	190	205	210	215	220		35	38	41	42	43	44
	180	195	205	210	215	220		36	39	41	42	43	44
	180	200	205	210	215	220		36	40	41	42	43	44
	190	200	210	215	220	220	→	38	40	42	43	44	44
	195	205	210	215	215	220		39	41	42	43	43	44
	195	205	210	215	215	215		39	41	42	43	43	43
	195	210	215	215	215	220		39	42	43	43	43	44
7-MM	175	189	203	210	217	217		25	27	29	30	31	31
	182	196	203	210	217	217		26	28	29	30	31	31
	182	196	210	210	217	224		26	28	30	30	31	32
	189	203	210	217	217	217	→	27	29	30	31	31	31
	196	203	210	217	217	217		28	29	30	31	31	31
	196	203	210	217	217	217		28	29	30	31	31	31
	196	210	210	217	217	217		28	30	30	31	31	31
10-MM	170	190	200	210	210	220		17	19	20	21	21	22
	180	190	200	210	210	220		18	19	20	21	21	22
	180	200	210	210	220	220		18	20	21	21	22	22
	190	200	210	210	220	220	→	19	20	21	21	22	22
	190	200	210	210	210	220		19	20	21	21	21	22
	190	200	210	210	220	220		19	20	21	21	22	22
	200	210	210	220	220	220		20	21	21	22	22	22
15-MM	180	195	210	210	210	225		12	13	14	14	14	15
	180	195	210	210	210	225		12	13	14	14	14	15
	180	195	210	210	210	225		12	13	14	14	14	15
	195	195	210	210	225	225	→	13	13	14	14	15	15
	195	210	210	210	210	225		13	14	14	14	14	15
	195	210	210	210	210	210		13	14	14	14	14	14
	195	210	210	210	210	225		13	14	14	14	14	15
20-MM	180	200	200	220	220	220		9	10	10	11	11	11
	180	200	200	220	220	220		9	10	10	11	11	11
	180	200	200	220	220	220		9	10	10	11	11	11
	180	200	200	220	220	220	→	9	10	10	11	11	11
	200	200	220	220	220	220		10	10	11	11	11	11
	200	200	220	220	220	220		10	10	11	11	11	11
	200	200	220	220	220	220		10	10	11	11	11	11

Fig. 3. A random 6×6 block from Lena image (Left) k-Modulus Method ($k = 2, 3, 5, 7, 10, 15$, and 20) (Right) The division of block by the corresponding k

TABLE I. BIT DEPTH OF k-MODULUS METHOD

k-Modulus Method	Range	Binary representation	Length of pixel
2-MM	0..128	10000000	8
3-MM	0..85	1010101	7
4-MM	0..64	1000000	7
5-MM	0..51	110011	6
6-MM	0..42	101010	6
7-MM	0..36	100100	6
8-MM	0..32	100000	6
9-MM	0..28	11100	5
10-MM	0..25	11001	5
11-MM	0..23	10111	5
12-MM	0..21	10101	5
13-MM	0..19	10011	5
14-MM	0..18	10010	5
15-MM	0..17	10001	5
16-MM	0..16	10000	5
17-MM	0..15	1111	4
18-MM	0..14	1110	4
19-MM	0..13	1101	4
20-MM	0..12	1100	4

dissimilarities up to k=10. Higher k may produce noticeable distortion. Moreover, for more illustration, a magnified image of Lena for k=3,5,7,10,15,20 have been presented in figure 6. Also, according to figure 5, the image histogram for the same previous k values k=3,5,7,10,15,20 have been obtained. Here, the same assumption that was stated previously, and that is, up to k=10 the shape of the histogram is approximately similar to the original histogram. Finally, The Peak Signal to Noise Ratio (PSNR) [13] was used to measure the dissimilarities between the transformed and the original images, table (II).

TABLE II. PSNR VALUES OF k-MODULUS METHOD

k-MM	Lena	Peppers	Allah	Boy1	Boy2
2-MM	50.7787	50.4276	51.1058	50.9156	51.1518
3-MM	49.5941	49.1845	49.8984	49.6841	49.8853
4-MM	46.0309	45.7001	46.4233	46.1599	46.3588
5-MM	44.7639	44.4059	45.0469	44.9447	45.1021
6-MM	42.7984	42.4311	43.0906	42.9874	43.1331
7-MM	41.7680	41.4927	41.8433	41.9210	42.0895
8-MM	40.4774	40.0450	40.6093	40.6246	40.7477
9-MM	39.5383	39.2124	39.7726	39.9181	39.9031
10-MM	38.4859	38.1514	38.8397	38.7334	38.8230
11-MM	37.8295	37.4656	38.5854	38.2731	38.1404
12-MM	36.9491	36.7879	37.2798	37.0228	37.2974
13-MM	36.4654	35.8355	36.9229	36.5131	36.6772
14-MM	35.9254	35.3525	35.9268	35.9884	35.9164
15-MM	35.0014	34.8275	35.1099	35.4527	35.4560
16-MM	34.7193	34.4729	35.2276	34.6802	34.8957
17-MM	33.9161	33.7502	34.7368	34.3753	34.2375
18-MM	33.6590	32.9851	33.8404	33.7727	33.7870
19-MM	33.0598	32.7615	33.2398	32.9910	33.4654
20-MM	32.5316	32.3079	33.0107	32.8999	32.8903

According to [14][15], the typical values for the PSNR in lossy image and video compression are between 30 and 50 dB, where higher is better . Hence, it is clear that the PSNR values in table II are quite acceptable.

V. CONCLUSION

In this paper, a novel spatial image transform has been presented. The proposed transform use modulus operator in a way that transform the whole image array into multiples of one and only one integer k. As a main conclusion from this article is that, the k-Modulus Method could helps in image compression as a scheme but not as stand alone image compression technique. The graphical examples demonstrated that the k-Modulus Method produce better results when k is up to 10. Depending on the application used, the designer may control k. Therefore, higher k (more than 10) could be used whenever there is a need to a low resolution images.

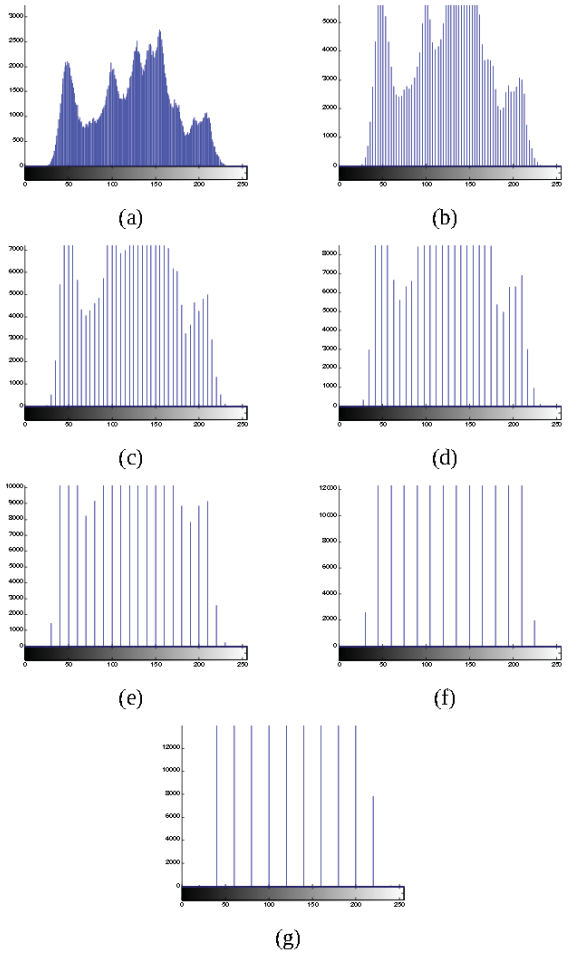

Fig. 5. Image Histogram (a) Original (b) 3-MM (c) 5-MM (d) 7-MM (e) 10-MM (f) 15-MM (g) 20-MM

REFERENCES

[1] G. Wolberg, "Geometric transformation techniques for digital images: A survey," *Technical report, CUCS-390-88*, 1988, new York, NY 10027.

[2] K. Kaczmarek, B. Walczak, and S. D. Jong, "Comparison of image transformation methods used in matching 2d gel electrophoresis images," *Acta Chromatographica*, vol. 13, pp. 7–21, 2003.

[3] D. Salomon, *Data Compression: The Complete Reference*. Springer-Verlag, 2007.

[4] R. Memisevic and G. E. Hinton, "Unsupervised learning of image transformations," in *IEEE Computer Society Conference on Computer Vision and Pattern Recognition CVPR*, Minneapolis, Minnesota, USA, 2007, pp. 18–23.

[5] T. Acharya and P.-S. Tsai, *JPEG2000 Standard for Image Compression: Concepts, Algorithms and VLSI Architectures*. Wiley-Interscience, 2004.

[6] R. C. Gonzalez and R. E. Woods, *Digital Image Processing*, 2nd ed. Boston, MA, USA: Addison-Wesley Longman Publishing Co., Inc., 2001.

[7] K. J. Friston, J. Ashburner, S. J. Kiebel, T. E. Nichols, and W. D. Penny, *Statistical Parametric Mapping: The Analysis of Functional Brain Images*. Academic Press, 2006.

Fig. 4. *k*-Modulus Method (First row) Original, 2-MM, 3-MM, 4-MM, 5-MM (Second row) 6-MM, 7-MM, 8-MM, 9-MM, 10-MM (Third row) 11-MM, 12-MM, 13-MM, 14-MM, 15-MM (Fourth row) 16-MM, 17-MM, 18-MM, 19-MM, 20-MM

[8] K. R. Rao, P. Yip, and V. Britanak, *Discrete Cosine Transform: Algorithms, Advantages, Applications*. Orlando, FL, USA: Academic Press, Inc., 2007.

[9] J. Chanussot, C. Collet, and K. Chehdi, *Multivariate Image Processing*. Wiley-ISTE, 2009.

[10] F. A. Jassim and H. E. Qassim, "Five modulus method for image compression," *Signal & Image Processing: An International Journal*, vol. 3, no. 5, pp. 19–28, 2012.

[11] M. Evening, *Adobe Photoshop CS5 for Photographers: A Professional Image Editor's Guide to the Creative Use of Photoshop for the Macintosh and PC*. Elsevier Science, 2010.

[12] W. Burger and M. Burge, *Principles of Digital Image Processing*. Springer-Verlag London, 2009.

[13] A. M. Eskicioglu and P. S. Fisher, "Image quality measures and their performance," *IEEE Transactions on Communications*, vol. 43, no. 12, pp. 2959–2965, 1995.

[14] S. Welstead, *Fractal and Wavelet Image Compression Techniques*. SPIE, 1999.

[15] M. Barni, *Document and Image Compression*. Taylor & Francis, 2006.

Fig. 6. Top left (3-MM) Top right (5-MM) Middle left (7-MM) Middle right (10-MM) Bottom left (15-MM) Bottom right (20-MM)

Analytical Solution of the Perturbed Oribt-Attitude Motion of a Charged Spacecraft in the Geomagnetic Field

Hani M. Mohmmed*, Mostafa K. Ahmed†, Ashraf Owis‡ and Hany Dwidar§
* Graduate Research Assistant, Department of Solar and Space Research, NRIAG, El Marsad st. Helwan 11421, Cairo, Egypt.
E-mail: hani.20@yahoo.co.uk
† Cairo University, 13126 (Egypt)
E-mail: mkahmed.g@gmail.com
‡ Cairo University, 13126 (Egypt)
E-mail: aowis@eun.eg
§ Cairo University, 13126 (Egypt)
E-mail: hrydwidar@gmail.com

***Abstract*—In this work we investigate the orbit-attitude perturbations of a rigid spacecraft due to the effects of several forces and torques. The spacecraft is assumed to be of a cylindrical shape and equipped with a charged screen with charge density σ. Clearly the main force affecting the motion of the spacecraft is the gravitational force of the Earth with uniform spherical mass. The effect of oblate Earth up to J_2 is considered as perturbation on both the orbit and attitude of the spacecraft, where the attitude of the spacecraft is acted upon by what is called gravity gradient torque. Another source of perturbation on the attitude of the spacecraft comes from the motion of the charged spacecraft in the geomagnetic field. This motion generates a force known as the Lorentz force which is the source of the Lorentz force torque influencing the rotational motion of the spacecraft. In this work we give an analytical treatment of the orbital-rotational dynamics of the spacecraft. We first use the definitions of Delaunay and Andoyer variables in order to formulate the Hamiltonian of the orbit-attitude motion under the effects of forces and torques of interest. Since the Lorentz force is a non-conservative force, a potential like function is introduced and added to the Hamiltonian. We solve the canonical equations of the Hamiltonian system by successive transformations using a technique proposed by Lie and modified by Deprit and Kamel to solve the problem. In this technique we make two successive transformations to eliminate the short and long periodic terms from the Hamiltonian.**

I. Introduction

The motion of a rigid spacecraft is specified by its position, velocity, attitude, and attitude motion. The first two describe the translational motion of the center of mass of the spacecraft, while the latter two describe the rotational motion of the body about the center of mass, In general the translational and attitude motions are independent as long as no resonance conditions are assumed between the orbital and rotational motions, where in this case attitude-orbit coupling results. A spacecraft is in general under the perturbation effect of gravitaional potential of the Earth, which includes both perturbations on the orbital and the attitude motion of the spacecraft. Other forces maybe added to the gravitational force, such as solar radiation pressure, which is investigated analytically in [11] and [2] . In this work we invesitgate analytically the perturbation effects of both the gravitational force up to J_2 and Lorentz force on both the orbital and attitude motion. Following the work of [2], this paper is organized as follows: we formulate the Hamiltonian of the motion of the spacecraft under the perturbing forces and torques, the problem is then tackled using the straight forward Lie technique. This technique was proposed by Lie and developed by Deprit and Kamel (see [1] and [5]). In this technique we perform two successive transformations to eliminate the short and long periodic terms from the Hamiltonian, and hence the new canonical equations are solved easily. The novelty of this work is that we obtain an analytical solution of the problem. Despite the numerical solution is accurate and can be applied in practise, analytical treatments can lead to closed form solutions, and enables us to analyze the problem.

II. Coordinate Systems and Systems of Canonical Variables

Before starting to formulate the problem we first define the coordinate systems and the canonical variables used to describe the motion. Let the inertial coordiante system $OXYZ$ with origin at the Earth's center and defined such that the $X-$axis is toward the Vernal Equinox, the $Y-$axis is normal to the $X-$axis and located in the equatorial plane and the $Z-$axis coincides with the rotational axis of the Earth. Three unit vectors $(\hat{i}, \hat{j}, \hat{k})$ are taken in the X, Y, Z directions respectively. The body coordinate System $O'X'Y'Z'$ is located at the center of mass of the spacecraft with $X'-$axis, $Y'-$axis and $Z'-$axis choosen along the principal axes of the spacecraft.The three unit vectors $(\hat{e_1}, \hat{e_2}, \hat{e_3})$ are taken in the X', Y', Z' directions respectively. The orbital coordinate system $O'\xi\eta\zeta$ is located at the center of mass of the spacecraft and with the $\xi-$axis

along the radius vector of the spacecraft from the geocenter, the η-axis is normal to the radius vector and in located in the orbital plane and ζ-axis is normal to the orbital plane.The three unit vectors $(\hat{R}, \hat{S}, \hat{T})$ are taken in the ξ, η, ζ directions respectively.

A. Sets of Canonical variables

There are two types of sets of canonical variables used, one for the description of the orbital motion , and the other describes the attitude motion. There are many sets of variables for both types. Two of the most famous sets are Delaunay and Andoyer sets of variables used to describe both orbital and attitude motion respectively.

B. Delaunay variables

Delaunay variables are usually used to describe the orbital motions of the Earth and of the Moon and Sun, assumed to produce measurable tidal effects. They are usually defined as :
l : Mean anomaly, g : Argument of perigee, h : Longitude of the node, $L = \sqrt{\mu a}$, $G = \sqrt{\mu a(1-e^2)}$ and $H = \sqrt{\mu a(1-e^2)}\cos I$. Where μ is the Earth's mass, a is the semi-major axis of the spacecraft, e is the eccenricity, and I is the inclination.

C. Andoyer variables

Andoyer variables are the most commonly used for the description of attitude motion. [3] performed transformation from the inertial frame to the body frame through the intermediate invariable plane using $3-1-3-1-3$ successive rotations.

The transformation matrix of this transformation is given in terms of Andoyer variables as:

$$R(h_a, I_a, g_a, J_a, l_a) = [\boldsymbol{V}_1 \quad \boldsymbol{V}_2 \quad \boldsymbol{V}_3] \tag{1}$$

where I_a is the inclination of the invariable plane on the reference plane, J_a is the angle between the invariable plane and the body plane. The column vectors $\boldsymbol{V}_1, \boldsymbol{V}_2$ and $\boldsymbol{V}_3$ are given as:

$$\boldsymbol{V}_1 = \begin{bmatrix} (c_{h_a}(c_{g_a}c_{l_a} - c_{J_a}s_{g_a}s_{l_a}) - s_{h_a}(-s_{I_a}s_{J_a}s_{l_a} \\ +c_{I_a}(c_{l_a}s_{g_a} + c_{g_a}c_{J_a}s_{l_a})) \\ c_{h_a}(-c_{J_a}c_{l_a}s_{g_a} - c_{g_a}s_{l_a}) - s_{h_a}(-c_{l_a}s_{I_a}s_{J_a} \\ +c_{I_a}(c_{g_a}c_{J_a}c_{l_a} - s_{g_a}s_{l_a})) \\ c_{h_a}s_{g_a}s_{J_a} - s_{h_a}(-c_{J_a}s_{I_a} - c_{I_a}c_{g_a}s_{J_a}) \end{bmatrix}$$

$$\boldsymbol{V}_2 = \begin{bmatrix} s_{h_a}(c_{g_a}c_{l_a} - c_{J_a}s_{g_a}s_{l_a}) \\ +c_{h_a}(-s_{I_a}s_{J_a}s_{L_a} + c_{I_a}(c_{l_a}s_{g_a} + c_{g_a}c_{J_a}s_{l_a})) \\ s_{h_a}(-c_{J_a}c_{l_a}s_{g_a} - c_{g_a}s_{l_a}) \\ +c_{h_a}(-c_{l_a}s_{I_a}s_{J_a} + c_{I_a}(c_{g_a}c_{J_a}c_{L_a} - s_{g_a}s_{l_a})) \\ s_{g_a}s_{h_a}s_{J_a} + c_{h_a}(-c_{J_a}s_{I_a} - c_{I_a}c_{g_a}s_{J_a}) \end{bmatrix}$$

$$\boldsymbol{V}_3 = \begin{bmatrix} c_{I_a}s_{J_a}s_{l_a} + s_{I_a}(c_{l_a}s_{g_a} + c_{g_a}c_{J_a}s_{l_a}) \\ c_{I_a}c_{l_a}s_{J_a} + s_{I_a}(c_{g_a}c_{J_a}c_{l_a} - s_{g_a}s_{l_a}) \\ c_{I_a}c_{J_a} - s_{I_a}s_{J_a}c_{g_a} \end{bmatrix}$$

Andoyer variables used in the previous transformation are defined as: $L_a \equiv Z'$ component of the angular momentum vector (i.e. that normal to the body plane), $G_a \equiv$ Total angular momentum vector, $H_a \equiv Z$ component of the angular momentum vector (i.e. that normal to the reference plane). The conjugate angle variables are :
$l_a \equiv$ the longitude of the X' axis (of the body frame) with respect to the node of the body plane on the invariable plane.
$g_a \equiv$ the longitude of the node N_3 with respect to N_2 (measured in the invariable plane).
$h_a \equiv$ longitude of the node N_2 with respect to the X axis (of the inertial frame).

III. FORMULATION OF THE HAMILTONIAN OF THE ORBIT-ATTITUDE MOTION

The Hamiltonian of the orbit-attitude motion of the spacecraft is formulated using the prescribed Delaunay and Andoyer variables. The total Hamiltonian consists of the Hamiltonian of the gravitational potential, the Hamiltonian of the torque free motion, and the Hamiltonian of the Lorentz torques.

A. Hamiltonian of the gravitational potential

As mentioned before the gravitational potential of oblate Earth will be considered affecting on a spacecraft of a cylindrical shape and consisting of only one single body. The gravitational potential of the Earth is given by [4] as

$$\begin{aligned} V_g \quad = \quad & -\frac{\mu m}{R_c}\{1 + \frac{1}{2}J_2(\frac{R_e}{R_c})^2(1 - 3\sin^2\phi_c)\}\Sigma_2) \\ & -\frac{\mu}{2R_c^3}\{(\Sigma_1 - 3 + \frac{3}{2}J_2(\frac{R_e}{R_c})^2 \times [(1 - 5\sin^2\phi_c)\Sigma_1 \\ & -5(1 - 7\sin^2\phi_c)\Sigma_2 + 2\Sigma_3 + 20\sin\phi_c\Sigma_4]\} \end{aligned} \tag{2}$$

where $\sin\phi_c = \sin I \sin(f + g)$, $J_2 = 1.083 \times 10^{-3}$ is the coefficient of the second harmonic of Earth's gravitational potential and

$$\Sigma_1 = \sum_{i=1}^{3} I_i \, , \Sigma_2 = \sum_{i=1}^{3} I_i c_{i3}^2 \, , \Sigma_3 = \sum_{i=1}^{3} I_i c_{ei3}^2 \, , \Sigma_4 = \sum_{i=1}^{3} I_i c_{i3} c_{ei3}$$

and I_i are the principle moments of inertia of the satellite, c_{i3} are the direction cosines between the principle axes and the unit vector $\hat{S}$ along the radius vector $\mathbf{R_c}$, and c_{ei3} are the direction cosines between the principal axes and the Earth's rotational axis.

The direction cosines c_{i3} and c_{ei3} need to be evaluated in terms of Delaunay and Andoyer variables. They were evaluated in [2] and [6] as:

$$c_{13} = \sum_{\substack{i,j,k=-1 \\ k \neq 0}}^{1} A_{ijk} \cos((f+g) + i(h_a - h) + jg_a + kl_a) \tag{3}$$

,

$$c_{23} = \sum_{\substack{i,j,k=-1 \\ k \neq 0}}^{1} B_{ijk} \sin((f+g) + i(h_a - h) + jg_a + kl_a) \tag{4}$$

and

$$c_{33} = \sum_{i,j=-1}^{1} C_{ij} \sin((f+g) + i(h_a - h) + jg_a) \tag{5}$$

where the coefficients A_{ijk}, B_{ijk} and C_{ij} are known functions of I, I_a and J_a arising from the transformations between frames. Now after evaluating the direction cosines c_{i3} we proceed in evaluating their squares c_{i3}^2. We have

$$c_{13}^2 = \sum_{i=0,2} \sum_{j,k,m=-2}^{2} P_{ijkm} \cos(i(f+g) + j(h_a - h) + kg_a + ml_a) \tag{6}$$

where

$$P_{0jkm} = P_{2jkm} = \sum_{\substack{\nu_1,\mu_1=-1 \\ \nu_1 \pm \mu_1 = j}}^{1} \sum_{\substack{\nu_2,\mu_2=-1 \\ \nu_2 \pm \mu_2 = k}}^{1} \sum_{\substack{\nu_3,\mu_3=-1,1 \\ \nu_3 \pm \mu_3 = m}} \frac{A_{\nu_1\nu_2\nu_3} A_{\mu_1\mu_2\mu_3}}{2}$$

,

$$c_{23}^2 = \sum_{i=0,2} \sum_{j,k,m=-2}^{2} Q_{ijkm} \cos(i(f+g) + j(h_a - h) + kg_a + ml_a) \tag{7}$$

where

$$\begin{aligned} Q_{0jkm} = Q_{2jkm} \quad = & \sum_{\substack{\nu_1,\mu_1=-1 \\ \nu_1 - \mu_1 = j}}^{1} \sum_{\substack{\nu_2,\mu_2=-1 \\ \nu_2 - \mu_2 = k}}^{1} \sum_{\substack{\nu_3,\mu_3=-1,1 \\ \nu_3 - \mu_3 = m}} \frac{B_{\nu_1\nu_2\nu_3} B_{\mu_1\mu_2\mu_3}}{2} \\ & - \sum_{\substack{\nu_1,\mu_1=-1 \\ \nu_1 + \mu_1 = j}}^{1} \sum_{\substack{\nu_2,\mu_2=-1 \\ \nu_2 + \mu_2 = k}}^{1} \sum_{\substack{\nu_3,\mu_3=-1,1 \\ \nu_3 + \mu_3 = m}} \frac{B_{\nu_1\nu_2\nu_3} B_{\mu_1\mu_2\mu_3}}{2} \end{aligned}$$

and

$$c_{33}^2 = \sum_{i=0,2} \sum_{j,k=-2}^{2} R_{ijk} \cos(i(f+g) + j(h_a - h) + kg_a) \tag{8}$$

where

$$\begin{aligned} R_{0jk} = R_{2jk} \quad = & \sum_{\substack{\nu_1,\mu_1=-1 \\ \nu_1 - \mu_1 = j}}^{1} \sum_{\substack{\nu_2,\mu_2=-1 \\ \nu_2 - \mu_2 = k}}^{1} \frac{C_{\nu_1\nu_2} C_{\mu_1\mu_2}}{2} \\ & - \sum_{\substack{\nu_1,\mu_1=-1 \\ \nu_1 + \mu_1 = j}}^{1} \sum_{\substack{\nu_2,\mu_2=-1 \\ \nu_2 + \mu_2 = k}}^{1} \frac{C_{\nu_1\nu_2} C_{\mu_1\mu_2}}{2} \end{aligned}$$

The direction cosines c_{ei3} are evaluated as:

$$c_{e13} = \sum_{\substack{i=0,\\ j=-1}}^{1} A_{eij} \sin(ig_a + jl_a)$$

$$c_{e23} = \sum_{\substack{i=0,\\ j=-1}}^{1} B_{eij} \cos(ig_a + jl_a) \tag{9}$$

,

$$c_{e33} = \sum_{i=0}^{1} C_{ei} \cos(ig_a)$$

Here A_{eij}, B_{eij} and C_{ei} are functions of I, I_a, and J_a. Their squares are also evaluated as:

$$c_{e13}^2 = \sum_{j=-1,k=-2}^{2} E_{jk} \cos(jg_a + kl_a) \tag{10}$$

where

$$E_{jk} = \sum_{\substack{\nu_1,\mu_1=0\\ \nu_1-\mu_1=j}}^{1} \sum_{\substack{\nu_2,\mu_2=-1\\ \nu_2-\mu_2=k}}^{1} \frac{A_{e\nu_1\nu_2}A_{e\mu_1\mu_2}}{2} - \sum_{\substack{\nu_1,\mu_1=0\\ \nu_1+\mu_1=j}}^{1} \sum_{\substack{\nu_2,\mu_2=-1\\ \nu_2+\mu_2=k}}^{1} \frac{A_{e\nu_1\nu_2}A_{e\mu_1\mu_2}}{2}$$

,

$$c_{e23}^2 = \sum_{j=-1,k=-2}^{2} F_{jk} \cos(jg_a + kl_a) \tag{11}$$

where

$$F_{jk} = \sum_{\substack{\nu_1,\mu_1=0\\ \nu_1\pm\mu_1=j}}^{1} \sum_{\substack{\nu_2,\mu_2=-1\\ \nu_2\pm\mu_2=k}}^{1} \frac{B_{e\nu_1\nu_2}B_{e\mu_1\mu_2}}{2}$$

and

$$c_{e33}^2 = \sum_{j=-1}^{2} G_j \cos(jg_a) \tag{12}$$

where

$$G_j = \sum_{\substack{\nu_1,\mu_1=0\\ \nu_1\pm\mu_1=j}}^{1} \frac{C_{e\nu_1}C_{e\mu_1}}{2}$$

The products $c_{i3}c_{ei3}$ are also evaluated as:

$$c_{13}c_{e13} = \sum_{j=-1}^{1} \sum_{k,m=-2}^{2} U_{jkm} \sin((f+g) + j(h_a - h) + kg_a + ml_a) \tag{13}$$

where

$$U_{jkm} = \sum_{\substack{\nu_1=-1,\\ \nu_1=j}}^{1} \sum_{\substack{\nu_2=-1,\\ \mu_2=0,\\ \nu_2+\mu_2=k}}^{1} \sum_{\substack{\nu_3,\mu_3=-1,\\ \nu_3\neq 0,\\ \nu_3+\mu_3=m}}^{1} \frac{A_{\nu_1\nu_2\nu_3}A_{e\mu_2\mu_3}}{2} - \sum_{\substack{\nu_1=-1,\\ \nu_1=j}}^{1} \sum_{\substack{\nu_2=-1,\\ \mu_2=0,\\ \nu_2-\mu_2=k}}^{1} \sum_{\substack{\nu_3,\mu_3=-1,\\ \nu_3\neq 0,\\ \nu_3-\mu_3=m}}^{1} \frac{A_{\nu_1\nu_2\nu_3}A_{e\mu_2\mu_3}}{2}$$

In the same way we get :

$$c_{23}c_{e23} = \sum_{j=-1}^{1} \sum_{k,m=-2}^{2} V_{jkm} \sin((f+g) + j(h_a - h) + kg_a + ml_a) \tag{14}$$

where

$$V_{jkm} = \sum_{\substack{\nu_1=-1,\\ \nu_1=j}}^{1} \sum_{\substack{\nu_2=-1,\\ \mu_2=0,\\ \nu_2\pm\mu_2=k}}^{1} \sum_{\substack{\nu_3,\mu_3=-1,\\ \nu_3\neq 0,\\ \nu_3\pm\mu_3=m}}^{1} \frac{B_{\nu_1\nu_2\nu_3}B_{e\mu_2\mu_3}}{2}$$

and

$$c_{33}c_{e33} = \sum_{j=-1}^{1} \sum_{k=-2}^{2} W_{jk} \sin((f+g) + j(h_a - h) + kg_a) \tag{15}$$

where

$$W_{jk} = \sum_{\substack{\nu_1=-1,\\ \nu_1=j}}^{1} \sum_{\substack{\nu_2=-1,\\ \mu_2=0,\\ \nu_2\pm\mu_2=k}}^{1} \frac{C_{\nu_1\nu_2}C_{e\mu_2}}{2}$$

B. Contribution of the gravitational potential to the total Hamiltonian

Considering the spacecraft is of a cylindrical shape and considering the dimensions of the cylinder to be of length $\approx 100m$ then $\frac{\rho}{R_E}$ is of order J_2, where ρ is the radius vector of any point on the spacecraft relative to its center of mass, and R_E is the Earth's radius. Now note that the principal moments of inertia I_i are directly proportional to the square of ρ, $\sin^2(\phi_c) = \sin^2(I)(\frac{1}{2} - \frac{1}{2}\cos(2g+2f))$ and $a = \frac{L^2}{\mu}$. We then have a new form of the gravitational potential written in terms of Delaunay and Andoyer variables as:

$$V_g = -\frac{\mu^2}{2L^2} + \frac{1}{4}\frac{A_2}{L^6}\left(\frac{a}{R_c}\right)^3 \left[(3s^2-2) - 3s^2\cos(2f+2g)\right] \tag{16}$$

$$- \frac{J_2^2}{2!}\frac{\mu^4 R_e^2}{2L^6}\left(\frac{a}{R_c}\right)^3 \left[\sum_{\substack{j,k,m=-2\\ i=0.2}}^{j,k,m=2} \widetilde{B}^{11}_{ijkm} \cos(i(f+g) + j(h_a-h) + kg_a + ml_a)\right]$$

$$- \frac{J_2^3}{3!}\frac{3\mu^6 R_e^4}{2L^{10}}\left(\frac{a}{R_c}\right)^5 \left[\sum_{\substack{j,k,m=-2\\ i=-2,0,2,4}}^{j,k,m=2} \widetilde{C}^{11}_{ijkm} \cos(i(f+g) + j(h_a-h) + kg_a + ml_a)\right] \tag{17}$$

where R_c is the distance from the center of Earth to the center of mass of the spacecraft, $s = \sin I$, $A_2 = \mu^4 R_e^2$ and the coefficients $\widetilde{B}^{11}_{ijkm}$ and $\widetilde{C}^{11}_{ijkm}$ are functions of I_a, J_a, I, I_i, R_e and J_2

C. Contribution of Lorentz force to the Hamiltonian

If we consider the spacecraft is equipped with a charged cylindrical sheet with surface charge density σ, the total charge of the spacecraft is $Q = \int_S \sigma dS$, where S is the surface area of the screen. It was shown by [**?**] that when the center of charge is off-center, the expression for Lorentz torque can be approximated by :

$$\mathbf{N}_l = Q\rho_\circ \times (\mathbf{v} \times \mathbf{B})_b \tag{18}$$

where $\rho_\circ$ is the radius vector of the center of charge and is given by in the body coordinate system

$$\rho_\circ = x_\circ \hat{e_1} + y_\circ \hat{e_2} + z_\circ \hat{e_3} = \frac{1}{Q}\int_S \sigma \rho dS$$

$\mathbf{v}$ is the velocity of the center of mass of the spacecraft relative to the ECEF (Earth Centered Earth Fixed) frame and $\mathbf{B}$ is the geomagnetic field intensity.

$$\mathbf{B} = -grad\ U_m \tag{19}$$

where U_m is the geomagnetic potential. We use here the inclined dipole model for the geomagnetic potential described in the Cartesian coordinates. [**?**]

$$U_m = \frac{R_e^3}{R_c^2}(g_0\frac{z}{R_c} + g_1\frac{x}{R_c} + h_1\frac{y}{R_c}) \tag{20}$$

where

$$g_0 = -29615, g_1 = -1728, h_1 = 5186$$

Evaluating equation (18) in terms of Delaunay and Andoyer variables takes long calculations. The final form of the Lorentz torque is then

$$\begin{aligned}
\mathbf{N}_l \;=\; & Q(\frac{R_E}{R_c})^3\Bigg[\Bigg(\sum_{\substack{i,j=0\\k=-2}}^{i,j=3,k=2}\ \sum_{\substack{m,n=-1\\r,s=-1}}^{1}\Big[X^0_{ijkmnrs} \\
& \times\cos(if+jg+kh+mg_a+nh_a+rl_a+sE) \\
& +\widetilde{X}^0_{ijkmnrs}\sin(if+jg+kh+mg_a+nh_a+rl_a+sE)\Big]\Bigg)\hat{e_1} \\
+\ & \Bigg(\sum_{\substack{i,j=0\\k=-2}}^{i,j=3,k=2}\ \sum_{\substack{m,n=-1\\r,s=-1}}^{1}\Big[Y^0_{ijkmnrs}\cos(if+jg+kh+mg_a+nh_a+rl_a+sE) \\
& +\widetilde{Y}^0_{ijkmnrs}\sin(if+jg+kh+mg_a+nh_a+rl_a+sE)\Big]\Bigg)\hat{e_2} \\
+\ & \Bigg(\sum_{\substack{i,j=0\\k=-2}}^{i,j=3,k=2}\ \sum_{\substack{m,n=-1\\r,s=-1}}^{1}\Big[Z^0_{ijkmnrs}\cos(if+jg+kh+mg_a+nh_a+rl_a+sE) \\
& +\widetilde{Z}^0_{ijkmnrs}\sin(if+jg+kh+mg_a+nh_a+rl_a+sE)\Big]\Bigg)\hat{e_3}
\end{aligned} \tag{21}$$

where E is the eccentric anomaly, and the coefficients $X^0_{ijkmnrs}, \widetilde{X}^0_{ijkmnrs}, Y^0_{ijkmnrs}, \widetilde{Y}^0_{ijkmnrs}$ $Z^0_{ijkmnrs}$ and $\widetilde{Z}^0_{ijkmnrs}$ are known functions of I, I_a and J_a and arise from the transformations between coordinate systems.

D. Potential like function

Since Lorentz force is not conservative, i.e not derived from a potential function, we introduce the potential like function to contribute to the Hamiltonian. The potential like function ϑ_l has the form

$$\vartheta_l = -\mathbf{N_l}.\mathbf{R_c} = -\mathbf{N_l}.R_c(c_{13}\hat{e_1} + c_{23}\hat{e_2} + c_{33}\hat{e_3}) \tag{22}$$

The potential like function is then evaluated in the form :

$$\vartheta_l = -Q\frac{R_E^3}{R_c^2}\Bigg(\sum_{\substack{i,j=4,k=3\\ i,j=-2\\ k=-3}} \sum_{\substack{s=1\\ m,n,r=2\\ m,n,r=-2\\ s=-1}} \Big[A^{11}_{ijkmnrs} \times \sin(if+jg+kh+mg_a+nh_a+rl_a+sE) + \widetilde{A}^{11}_{ijkmnrs}\cos(if+jg+kh+mg_a+nh_a+rl_a+sE)\Big]\Bigg) \tag{23}$$

According to [**?**], the magnitude of the Lorentz torque acting on a spacecraft is

$$|\mathbf{N}_l| = Q|\rho_\circ|R_c(\omega_\circ - \omega_E)|\mathbf{B}| \tag{24}$$

where $\omega_\circ$ is the angular velocity of the rotation of the orbital coordinate system relative to the inertial system and ω_E is the angular velocity of diurnal rotation of the Earth. Thus if we take a practical example in which $R_c = 7\times10^6\ m$, $S = 100\ m^2$, the electric potential $U = 3\times10^5 V$ and electric capacity $c_s = 10^{-11}$, so that the charge has a magnitude of 3×10^{-3}. $\omega_\circ = 1.1\times10^{-3}$ and if $|\rho_\circ| = 0.5\ m$ then the Lorentz torque is of order $\sim 10^{-5}$, i.e. the order of Lorentz torque is close to J_2^2. In terms of the small parameter J_2 the potential like function can be written as:

$$\vartheta_l = -\frac{J_2^2}{2!}\Bigg(\sum_{\substack{i,j=4,k=3\\ i,j=-2\\ k=-3}} \sum_{\substack{s=1\\ m,n,r=2\\ m,n,r=-2\\ s=-1}} \Big[A^{11}_{ijkmnrs}\sin(if+jg+kh+mg_a+nh_a+rl_a+sE) + \widetilde{A}^{11}_{ijkmnrs}\cos(if+jg+kh+mg_a+nh_a+rl_a+sE)\Big]\Bigg)\left(\frac{a}{R_c}\right)^2\frac{\widetilde{Q}\mu R_E^3}{L^2} \tag{25}$$

where $\widetilde{Q} = \frac{2!Q}{J_2^2}$.

E. Total Hamiltonian

Using the expressions of the gravitational potential and the potential like function, the total Hamiltonian is then written as:

$$\mathcal{H} = \sum_{n=0}^{3}\frac{J_2^n}{n!}\mathcal{H}_n \tag{26}$$

where

$$\mathcal{H}_0 = -\frac{\mu^2}{2L^2} + \frac{1}{2}\left(\frac{1}{I_3}-\frac{1}{I_1}\right)L_a^2 + \frac{1}{2I_1}G_a^2 \tag{27}$$

where the second and third terms in $\mathcal{H}_0$ belong to the Hamiltonian of the torque free motion.

$$\mathcal{H}_1 = \frac{1}{4}\frac{A_2}{L^6}\left(\frac{a}{R_c}\right)^3\left[(3s^2-2)-3s^2\cos(2f+2g)\right] \tag{28}$$

$$\mathcal{H}_2 = -\frac{\mu^4 R_e^2}{2L^6}\left(\frac{a}{R_c}\right)^3 \sum_{\substack{j,k,m=2 \\ j,k,m=-2 \\ i=0.2}} \widetilde{B}^{11}_{ijkm}\cos(i(f+g)+j(h_a-h)+kg_a+ml_a)$$

$$-\frac{\widetilde{Q}\mu R_E^3}{L^2}\left(\frac{a}{R_c}\right)^2\left(\sum_{\substack{i,j=4,k=3 \\ i,j=-2 \\ k=-3}}\sum_{\substack{s=1 \\ m,n,r=2 \\ m,n,r=-2 \\ s=-1}}\left[A^{11}_{ijkmnrs}\times \sin(if+jg+kh+mg_a+nh_a+rl_a+sE)\right.\right.$$
$$\left.\left.+\widetilde{A}^{11}_{ijkmnrs}\cos(if+jg+kh+mg_a+nh_a+rl_a+sE)\right]\right) \quad (29)$$

$$\mathcal{H}_3 = -\frac{3\mu^6 R_e^4}{2L^{10}}\left(\frac{a}{R_c}\right)^5\left[\sum_{\substack{j,k,m=2 \\ j,k,m=-2 \\ i=-2,0,2,4}}\widetilde{C}^{11}_{ijkm}\cos(i(f+g)+j(h_a-h)+kg_a+ml_a)\right] \quad (30)$$

From the above equations we note that $\mathcal{H}_0$ is a function of L, L_a and G_a, hence l, $l_a$and g_a are fast variables while the other variables are slow ones.

IV. PERTURBATION APPROACH

Let ϵ be the small parameter of the problem and let the canonical system of differential equations be written as :

$$\dot{u} = H_U^T \quad , \quad \dot{U} = -H_u^T$$

What is required is to construct two (or more) transformations $(u, U; \epsilon) \to (\grave{u}, \grave{U})$ and $(\grave{u}, \grave{U}; \epsilon) \to (\grave{\grave{u}}, \grave{\grave{U}})$ analytic in ϵ at $\epsilon = 0$ to eliminate in succession the short and long period terms from the Hamiltonian such that $\grave{\grave{U}}$ reduce to constants and $\grave{\grave{u}}$ become linear functions of time.

The old and new Hamiltonians and the Generators are assumed expandable as

$$\begin{aligned}
H &= H_0 + \sum_n \frac{\epsilon^n}{n!} H_n \\
H^*(-, \grave{u}_2, \grave{u}_3; \grave{U}; \epsilon) &= H_0^*(\grave{U}_1) + \sum_n \frac{\epsilon^n}{n!} H_n^*(-, \grave{u}_2, \grave{u}_3; \grave{U}) \\
H^{**}(-; \grave{\grave{U}}; \epsilon) &= H_0^{**}(\grave{\grave{U}}) + \sum_n \frac{\epsilon^n}{n!} H_n^{**}(-; \grave{\grave{U}}) \\
W(\grave{u}; \grave{U}; \epsilon) &= \sum_n \frac{\epsilon^n}{n!} W_{n+1}(\grave{u}; \grave{U}) \\
W^*(-, \grave{\grave{u}}_2, \grave{\grave{u}}_3; \grave{\grave{U}}; \epsilon) &= \sum_n \frac{\epsilon^n}{n!} W_{n+1}(-, \grave{\grave{u}}_2, \grave{\grave{u}}_3; \grave{\grave{U}})
\end{aligned} \quad (31)$$

Elimination of Short period terms

Using the transformation equations we have the following basic identities

$$\begin{aligned}
H_0^* &= H_0 \\
H_n^* &= \widetilde{H}_n + (H_0; W_n) \\
\widetilde{H}_n &= H_n + \sum_{j=1}^{n-1}\left\{\begin{pmatrix} n-1 \\ j-1 \end{pmatrix}(H_{n-j}; W_j) + \begin{pmatrix} n-1 \\ j \end{pmatrix} G_j H_{n-j}^*\right\}
\end{aligned} \quad (32)$$

Let u_1 be the fast variable in H . We choose H_n^* to be the average of $\widetilde{H}_n$ over u_1; i. e.

$$H_n^* = < \widetilde{H}_n >_{u_1} \quad (33)$$

So that the periodic term is

$$P_n = \widetilde{H}_n - H_n^* = (H_0; W_n) \tag{34}$$

from which

$$W_n = \left(\frac{\partial H_0}{\partial U_1^1}\right)^{-1} \int P_n d\grave{u}_1$$

After determining the generator, the elements of the transformation and its inverse are determined by

$$u = \grave{u} + \sum_{n=1}^{2} \frac{J_2^n}{n!} \grave{u}^{(n)} \quad , \quad U = \grave{U} + \sum_{n=1}^{2} \frac{J_2^n}{n!} \grave{U}^{(n)} \tag{35}$$

$$\grave{u} = u + \sum_{n=1}^{2} \frac{J_2^n}{n!} u^{(n)}(u, U) \quad , \quad \grave{U} = U + \sum_{n=1}^{2} \frac{J_2^n}{n!} U^{(n)}(u, U) \tag{36}$$

where

$$\grave{u}^{(1)} = \frac{\partial W_1}{\partial \grave{U}} \quad , \quad \grave{u}^{(2)} = \frac{\partial W_2}{\partial \grave{U}} + L_1 \grave{u}^{(1)} \tag{37}$$

$$\grave{U}^{(1)} = -\frac{\partial W_1}{\partial \grave{u}} \quad , \quad \grave{U}^{(2)} = \frac{\partial W_2}{\partial \grave{u}} + L_1 \grave{U}^{(1)} \tag{38}$$

and

$$u^{(1)} = -\grave{u}^{(1)} \quad , \quad u^{(2)} = -\grave{u}^{(2)} + 2L_1 \grave{u}^{(1)} \tag{39}$$

$$U^{(1)} = -\grave{U}^{(1)} \quad , \quad U^{(2)} = -\grave{U}^{(2)} + 2L_1 \grave{U}^{(1)} \tag{40}$$

where L_1 is the Lie derivative.
Note that in the last two equations the right hand sides are evaluated at $\grave{u} = u$ and $\grave{U} = U$.

A. *Elimination of Long period terms*

The second transformation to eliminate the long period terms proceeds in exactly the same way but replacing (u, U) by $(\grave{u}, \grave{U})$; $(\grave{u}, \grave{U})$ by $(\grave{\grave{u}}, \grave{\grave{U}})$; H by H^* ; H^* by H^{**} and W by W^*

V. SOLUTION OF THE TRANSLATIONAL ROTATIONAL MOTION

In this section the translational rotational motion is solved using the Lie technique. As discussed in the previous section, there will be two successive canonical transformations in order to eliminate the short and long period terms in succession. secular and periodic terms will be retained up to $O(J_2^3)$ and $O(J_2^2)$ respectively.

A. *Short Period transformation*

we proceed to eliminate the short period terms (those depending on l, l_a and g_a) from the Hamiltonian in equation (26)

1) Zero Order: Using equation (32) and equation (27) we find that :

$$\mathcal{H}_0^* = \mathcal{H}_0 = -\frac{\mu^2}{2L^2} + \frac{1}{2}\left(\frac{1}{I_3} - \frac{1}{I_1}\right) L_a^2 + \frac{1}{2I_1} G_a^2$$

where all the variables in the right hand side are understood to be single primed, but the primes are removed from now on for simplicity.

2) First Order: From equation (32) we have :

$$\mathcal{H}_1^* = \widetilde{\mathcal{H}}_1 + (\mathcal{H}_0; W_1) \tag{41}$$

and

$$\widetilde{\mathcal{H}}_1 \quad = \quad \mathcal{H}_1 = \frac{1}{4}\frac{A_2}{L^6}\left(\frac{a}{R_c}\right)^3 \left[(3s^2 - 2) - 3s^2 \cos(2f + 2g)\right]$$

we then choose $\mathcal{H}_1^*$ to be the secular part of $\widetilde{\mathcal{H}}_1$. Thus we take the average of $\widetilde{\mathcal{H}}_1$ over the fast angles.

$$\mathcal{H}_1^* = < \widetilde{\mathcal{H}}_1 >_{l, l_a, , g_a} = \frac{1}{8\pi^3} \int_0^{2\pi} \int_0^{2\pi} \int_0^{2\pi} \widetilde{\mathcal{H}}_1 dl_a dg_a dl \tag{42}$$

That is

$$\mathcal{H}_1^* = \frac{1}{4}\frac{A_2}{L^3 G^3}(1 - 3\frac{H^2}{G^2}) \tag{43}$$

The Periodic part is given as

$$P = \widetilde{\mathcal{H}}_1 - \mathcal{H}_1^* = (W_1; \mathcal{H}_0) = \frac{1}{4}\frac{A_2}{L^6}\left(\frac{a}{R_c}\right)^3\left[(1-3\frac{H^3}{G^3}) - 3s^2\cos(2f+2g)\right] - \frac{1}{4}\frac{A_2}{L^3G^3}(1-3\frac{H^2}{G^2}) \tag{44}$$

Since P is independent of l_a and g_a, we have only $\frac{\partial W_1}{\partial l}$ not vanishing.
thus

$$\begin{aligned} W_1 = \frac{L^3}{\mu^2}\int P dl &= \frac{1}{4}\frac{A_2}{\mu^2 G^3}\Big((1-3\frac{H^3}{G^3})(f - l + e\sin(f)) \\ &\quad -3s^2\Big[\frac{1}{2}\sin(2f+2g) + \frac{e}{2}\big(\frac{1}{3}\sin(3f+2g) + \sin(f+2g)\big)\Big]\Big) \end{aligned} \tag{45}$$

3) Second order: Again we use the perturbation equations.
The equations for the second order are :

$$\mathcal{H}_2^* = \widetilde{\mathcal{H}}_2 + (\mathcal{H}_0; W_2) \tag{46}$$

$$\widetilde{\mathcal{H}}_2 = \mathcal{H}_2 + (\mathcal{H}_1 + \mathcal{H}_1^*; W_1) \tag{47}$$

Where $\mathcal{H}_2$ is given in equation(29) and the bracket $(\mathcal{H}_1 + \mathcal{H}_1^*; W_1)$ is evaluated as:

$$\begin{aligned} (\mathcal{H}_1 + \mathcal{H}_1^*; W_1) &= -\frac{3A_2^2}{16\mu^2L^4G^6}\left(3s^2-2\right)^2 - \frac{3A_2^2(4-5s^2)}{16\mu^2L^3G^7}\sum_{i=1}^{3}K_{i,2}^2\cos(if+2g) \\ &+ \frac{9A_2^2s^2}{8\mu^2L^6G^4}(4-5s^2)(f-l)\left(\frac{a}{R_c}\right)^3\sin(2f+2g) \\ &+ \frac{A_2^2}{256e\mu^2L^{11}G^8}\left(\frac{a}{R_c}\right)^2\sum_{j=-1}^{2}\sum_{i=0}^{8}\widetilde{H}_{j,i}\cos(if+2jg) \end{aligned} \tag{48}$$

where f is the true anomaly, $K_{i,2}^2$ and $\widetilde{H}_{j,i}$ are functions of e and s. Now $\widetilde{\mathcal{H}}_2$ is easily obtained. Now we take $\mathcal{H}_2^*$ in equation (46) to be the average of $\widetilde{\mathcal{H}}_2$

$$\mathcal{H}_2^* = <\widetilde{\mathcal{H}}_2>_{l,l_a,,g_a} = \frac{1}{8\pi^3}\int_0^{2\pi}\int_0^{2\pi}\int_0^{2\pi}\widetilde{\mathcal{H}}_2 dl_a dg_a dl$$

In performing this averaging we use Hansen coefficients to express functions of the true and eccentric anomaly in terms of the mean anomaly.

$$\left(\frac{a}{R_c}\right)^n\cos(mf) = \sum_{k\geq 0}a_k^{-n,m}(e)\cos(kl) \tag{49}$$

and

$$\left(\frac{a}{R_c}\right)^n\sin(mf) = \sum_{k\geq 0}b_k^{-n,m}(e)\sin(kl) \tag{50}$$

where the coefficients a, b are Hansen coefficients that many procedures has been developed to evaluate[**?**].
Upon averaging of $\widetilde{\mathcal{H}}_2$ we have

$$\begin{aligned} \mathcal{H}_2^* &= \sum_{i=0}^{2}H_i^*\cos(ig) + \sum_{\substack{j=-2 \\ i=0,2,-2}}^{j=2}\widetilde{\widetilde{B}}_{0ij00}^{11}\cos(ig+j(h_a-h)) - \frac{\widetilde{Q}\mu R_E^3}{L^2}\times \\ &\sum_{\substack{j=-2 \\ k=-3}}^{j=4,k=3}\sum_{n=-2}^{n=2}\left[F_{jk0n00}^{11}\sin(jg+kh+nh_a) + \widetilde{F}_{jk0n00}^{11}\cos(jg+kh+nh_a)\right] \end{aligned} \tag{51}$$

and the generator W_2 is given as

$$W_2 = \sum_{i=-\infty}^{\infty} \sum_{\substack{j=-2 \\ k=-3}}^{j=4,k=3} \sum_{m,n,r=-2}^{m,n,r=2} \Big[F^{22}_{ijkmnr} \sin(il+jg+kh+mg_a+nh_a+rl_a) + \widetilde{F}^{22}_{ijkmnr} \cos(il+jg+kh+mg_a+nh_a+rl_a) \Big] \quad (52)$$

where $F^{11}_{jk0n00}, \widetilde{F}^{11}_{jk0n00}, F^{22}_{ijkmnr}$ and $\widetilde{F}^{22}_{ijkmnr}$ are functions of the action variables.

4) Third order:: The equations for the third order are

$$\mathcal{H}^*_3 = \widetilde{\mathcal{H}}_3 + (\mathcal{H}_0; W_3) \quad (53)$$

$$\begin{aligned} \widetilde{\mathcal{H}}_3 &= \mathcal{H}_3 + \sum_{j=1}^{2} \left\{ \begin{pmatrix} 2 \\ j-1 \end{pmatrix} (\mathcal{H}_{3-j}; W_j) + \begin{pmatrix} 2 \\ j \end{pmatrix} G_j \mathcal{H}^*_{3-j} \right\} \\ &= \mathcal{H}_3 + (\mathcal{H}_2; W_1) + 2G_1\mathcal{H}^*_2 \\ &\quad + 2(\mathcal{H}_1; W_2) + G_2\mathcal{H}^*_1 \\ &= \mathcal{H}_3 + (\mathcal{H}_2 + 2\mathcal{H}^*_2 - (\mathcal{H}^*_1; W_1); W_1) + (2\mathcal{H}_1 + \mathcal{H}^*_1; W_2) \end{aligned} \quad (54)$$

The bracket $(\mathcal{H}_2 + 2\mathcal{H}^*_2 - (\mathcal{H}^*_1; W_1); W_1)$ is evaluated as

$$\begin{aligned} (\mathcal{H}_2 + 2\mathcal{H}^*_2 - (\mathcal{H}^*_1; W_1); W_1) &= \sum_{i=-\infty}^{\infty} \sum_{\substack{j=-4 \\ k=-3}}^{j=4,k=3} \sum_{m,n,r=-2}^{2} Q^{11}_{ijkmnr} \times \\ &\quad \cos(il+jg+kh+mg_a+nh_a+rl_a) \\ &+ \widetilde{Q}^{11}_{ijkmnr} \sin(il+jg+kh+mg_a+nh_a+rl_a) \end{aligned} \quad (55)$$

and the bracket $(\mathcal{H}_1 + 2\mathcal{H}^*_1; W_2)$

$$\begin{aligned} (\mathcal{H}_1 + 2\mathcal{H}^*_1; W_2) &= \sum_{i=-\infty}^{\infty} \sum_{\substack{j=-4 \\ k=-3}}^{j=4,k=3} \sum_{m,n,r=-2}^{m,n,r=2} Q^{22}_{ijkmnr} \times \\ &\quad \cos(il+jg+kh+mg_a+nh_a+rl_a) \\ &+ \widetilde{Q}^{22}_{ijkmnr} \sin(il+jg+kh+mg_a+nh_a+rl_a) \Big] \end{aligned} \quad (56)$$

So that when using equation (30) we have

$$\mathcal{H}^*_3 = < \mathcal{H}_3 + (\mathcal{H}_2 + 2\mathcal{H}^*_2 - (\mathcal{H}^*_1; W_1); W_1) + (2\mathcal{H}_1 + \mathcal{H}^*_1; W_2) >_{l,l_a,g_a}$$

After performing the averaging we have

$$\begin{aligned} \mathcal{H}^*_3 &= -\frac{3\mu^6 R^4_e}{2L^{10}} \Big[\sum_{\substack{j=-2 \\ i=-2,0,2,4}}^{j=2} \widetilde{C}^{11}_{ij00} a_0^{-5,i} \cos(ig + j(h_a - h)) \Big] \\ &+ \sum_{\substack{j=-4 \\ k=-3}}^{j=4,k=3} \sum_{n=-2}^{2} \left(\widetilde{\widetilde{Q}}^{11}_{jkn} \cos(jg+kh+nh_a) + \widetilde{\widetilde{Q}}^{22}_{jkn} \sin(jg+kh+nh_a) \right) \end{aligned} \quad (57)$$

where $Q^{11}_{ijkmnr}, \widetilde{Q}^{11}_{ijkmnr}, Q^{22}_{ijkmnr}, \widetilde{Q}^{22}_{ijkmnr}, \widetilde{\widetilde{Q}}^{11}_{jkn}$ and $\widetilde{\widetilde{Q}}^{22}_{jkn}$ are all functions of the action variables and the previously computed coefficients.

B. Elements of Short Period transformation

The elements of the transformation are obtained following the same procedures used by Kamel[**?**]. The equations are :

$$\grave{u}_i^{(1)} = \frac{\partial W_1}{\partial \grave{U}_i} = W_{1i} \quad , \quad \grave{u}_i^{(2)} = \frac{\partial W_2}{\partial \grave{U}_i} + L_1 \grave{u}_i^{(1)} \qquad (i = 1, 2, 3) \tag{58}$$

$$\grave{U}_i^{(1)} = -\frac{\partial W_1}{\partial \grave{u}_i} = W_{1,3+i} \quad , \quad \grave{U}_i^{(2)} = -\frac{\partial W_2}{\partial \grave{u}_i} + L_1 \grave{U}_i^{(1)} \qquad (i = 1, 2, 3) \tag{59}$$

where

$$L_1 \grave{u}_i^{(1)} = \sum_{j=1}^{3} \left[\frac{\partial W_{1i}}{\partial \grave{u}_j} W_{1j} + \frac{\partial W_{1i}}{\partial \grave{U}_j} W_{1,3+j} \right] \tag{60}$$

$$L_1 \grave{U}_i^{(1)} = \sum_{j=1}^{3} \left[\frac{\partial W_{1,i+3}}{\partial \grave{u}_j} W_{1j} + \frac{\partial W_{1,i+3}}{\partial \grave{U}_j} W_{1,3+j} \right] \tag{61}$$

The derivatives of W_2 in the above expressions were already computed while evaluating Poisson brackets.

C. Long Period Transformation

In the new transformation we consider that the new Hamiltonian is expandable in powers of J_2 such that

$$\mathcal{H}^{**} = \mathcal{H}_0^{**}(\grave{\grave{L}}, \grave{\grave{G}}_a, \grave{\grave{L}}_a) + \sum_{n=1}^{2} \frac{J_2^n}{n!} \mathcal{H}_n^{**}(\grave{\grave{L}}, \grave{\grave{G}}, \grave{\grave{H}}, \grave{\grave{L}}_a, \grave{\grave{G}}_a, \grave{\grave{H}}_a) \tag{62}$$

and the generator W^* is expandable as

$$W^*(\grave{\grave{g}}, \grave{\grave{h}}, \grave{\grave{h}}_a, \grave{\grave{L}}, \grave{\grave{G}}, \grave{\grave{H}}, \grave{\grave{L}}_a, \grave{\grave{G}}_a, \grave{\grave{H}}_a) = \sum_{n=0}^{2} \frac{J_2^n}{n!} W_{n+1}^*(\grave{\grave{g}}, \grave{\grave{h}}, \grave{\grave{h}}_a, \grave{\grave{L}}, \grave{\grave{G}}, \grave{\grave{H}}, \grave{\grave{L}}_a, \grave{\grave{G}}_a, \grave{\grave{H}}_a) \tag{63}$$

We use the same equations of transformation but now to transform the system associated with $\mathcal{H}^*$ to $\mathcal{H}^{**}$

$$\begin{aligned} \mathcal{H}_0^{**} &= \mathcal{H}_0^* \\ \mathcal{H}_n^{**} &= \widetilde{\mathcal{H}}_n^* + (\mathcal{H}_0^*; W_n^*) \\ \widetilde{\mathcal{H}}_n^* &= \mathcal{H}_n^* + \sum_{j=1}^{n-1} \left\{ \begin{pmatrix} n-1 \\ j-1 \end{pmatrix} (\mathcal{H}_{n-j}^*; W_j) + \begin{pmatrix} n-1 \\ j \end{pmatrix} G_j \mathcal{H}_{n-j}^{**} \right\} \end{aligned} \tag{64}$$

but since W^* is a function of the slow variables only $(\grave{\grave{g}}, \grave{\grave{h}}, \grave{\grave{h}}_a)$ then the bracket $(\mathcal{H}_0^*; W_n^*)$ vanishes, and the last two of equations (64) can be written in a single equation as

$$\mathcal{H}_n^{**} = \mathcal{H}_n^* + \sum_{j=1}^{n-1} \left\{ \begin{pmatrix} n-1 \\ j-1 \end{pmatrix} (\mathcal{H}_{n-j}^*; W_j) + \begin{pmatrix} n-1 \\ j \end{pmatrix} G_j \mathcal{H}_{n-j}^{**} \right\} \tag{65}$$

Now we solve for different orders as before.

1) Zero Order:: The identity for the zero order is

$$\mathcal{H}_0^{**} = \mathcal{H}_0^*$$

thus

$$\mathcal{H}_0^{**} = -\frac{\mu^2}{2L^2} + \frac{1}{2}\left(\frac{1}{I_3} - \frac{1}{I_1}\right) L_a^2 + \frac{1}{2I_1} G_a^2$$

where we will be omitting the double primes from now on for simplicity.

2) First order: From equation (65) the identity for the first order is

$$\mathcal{H}_1^{**} = \mathcal{H}_1^*$$

from which

$$\mathcal{H}_1^{**} = \frac{1}{4} \frac{A_2}{L^3 G^3} (1 - 3\frac{H^2}{G^2}) \tag{66}$$

3) Second order: : From (65) the identity for the first order is

$$\begin{aligned}\mathcal{H}_2^{**} &= \mathcal{H}_2^* + \sum_{j=1}^{1}\left\{\begin{pmatrix}1\\0\end{pmatrix}(\mathcal{H}_1^*;W_1) + \begin{pmatrix}1\\1\end{pmatrix}G_1\mathcal{H}_1^{**}\right\}\\ &= \mathcal{H}_2^* + (\mathcal{H}_1^*;W_1) + G_1\mathcal{H}_1^{**}\\ &= \mathcal{H}_2^* + (\mathcal{H}_1^*;W_1) + (\mathcal{H}_1^*;W_1)\\ &= \mathcal{H}_2^* + 2(\mathcal{H}_1^*;W_1^*) \end{aligned} \tag{67}$$

so that

$$\begin{aligned}\mathcal{H}_2^{**} &= 2(\mathcal{H}_1^*;W_1^*) + \sum_{i=0}^{2} H_i^*\cos(ig) + \sum_{\substack{j=-2\\ i=0,2,-2}}^{j=2} \widetilde{\widetilde{B}}_{0ij00}^{11}\cos(ig+j(h_a-h)) - \frac{\widetilde{Q}\mu R_E^3}{L^2}\times\\ &\sum_{\substack{j=-2\\k=-3}}^{j=4,k=3}\ \sum_{n=-2}^{n=2}\left[F_{jk0n00}^{11}\sin(jg+kh+nh_a) + \widetilde{F}_{jk0n00}^{11}\cos(jg+kh+nh_a)\right]\end{aligned} \tag{68}$$

we perform the averaging over $\mathcal{H}_2^*$ and the secular part in the right hand side is then chosen to be $\mathcal{H}_2^{**}$ that is

$$\mathcal{H}_2^{**} = H_0^* + \widetilde{\widetilde{B}}_{00000}^{11} - \frac{\widetilde{Q}\mu R_E^3}{L^2}\widetilde{F}_{000000}^{11} \tag{69}$$

and then we evaluate W_1 from the remaining part as

$$W_1 = \sum_{\substack{j=-2\\k=-3}}^{j=4,k=3}\ \sum_{n=-2}^{n=2}\left[R_{jkn}^*\cos(jg+kh+nh_a) + \widetilde{R}_{jkn}^*\sin(jg+kh+nh_a)\right]$$

where as before the coefficients $H_i^*, \widetilde{\widetilde{B}}_{0ij00}^{11}, F_{jk0n00}^{11}, \widetilde{F}_{jk0n00}^{11}, R_{jkn}^*$ and $\widetilde{R}_{jkn}^*$ are functions of the action variables and the previously computed coefficients.

4) Third Order:: The equations of the third order are

$$\mathcal{H}_3^{**} = \widetilde{\mathcal{H}}_3^* + 3(\mathcal{H}_1^*;W_2^*) \tag{70}$$

$$\begin{aligned}\widetilde{\mathcal{H}}_3^* &= \mathcal{H}_3^* + \sum_{j=1}^{2}\left\{\begin{pmatrix}2\\j-1\end{pmatrix}(\mathcal{H}_{3-j}^*;W_j^*) + \begin{pmatrix}2\\j\end{pmatrix}G_j\mathcal{H}_{3-j}^{**}\right\}\\ &= \mathcal{H}_3^* + \frac{3}{2}(\mathcal{H}_2^* + \mathcal{H}_2^{**};W_1^*)\end{aligned} \tag{71}$$

the bracket $(\mathcal{H}_2^* + \mathcal{H}_2^{**};W_1^*)$ is evaluated as

$$(\mathcal{H}_2^* + \mathcal{H}_2^{**};W_1^*) = \sum_{\substack{j=-6\\k=-6}}^{j=8,k=6}\ \sum_{n=-4}^{n=4}\left(S_{jkn}^{*14}\cos(jg+kh+nh_a) + \widetilde{S}_{jkn}^{*14}\sin(jg+kh+nh_a)\right) \tag{72}$$

Proceeding, we then evaluate $\mathcal{H}_3^{**}$ as

$$\mathcal{H}_3^{**} =< \widetilde{\mathcal{H}}_3^* >_{g,h,h_a} = -\frac{3\mu^6 R_e^4}{2L^{10}}\left[\widetilde{C}_{0000}^{11}a_0^{-5,0}\right] + Q_{000000}^{11} + Q_{000000}^{22} + \frac{3}{2}S_{000}^{*14} \tag{73}$$

and

$$
\begin{aligned}
W_2^* &= -\frac{\mu^6 R_e^4}{2L^{10}} \sum_{\substack{k=-2 \\ j=-2,0,2,4}}^{k=2} \widetilde{C}_{jk}^{*22} \sin(jg + k(h_a - h)) \\
&+ \frac{1}{3} \sum_{\substack{j=-4 \\ k=-3}}^{j=4,k=3} \sum_{n=-2}^{2} \left[Q_{jkn}^{*44} \sin(jg + kh + nh_a) - \widetilde{Q}_{jkn}^{*44} \cos(jg + kh + nh_a) \right] \\
&+ \frac{1}{2} \sum_{\substack{j=-6 \\ k=-6}}^{j=8,k=6} \sum_{n=-4}^{n=4} \left[S_{jkn}^{*16} \sin(jg + kh + nh_a) - \widetilde{S}_{jkn}^{*16} \cos(jg + kh + nh_a) \right]
\end{aligned} \tag{74}
$$

D. Elements of Long Period transformation

The elements of the transformation and its inverse maybe obtained from the equations of short period transformation, but with the replacement of W_n by W_n^*, (u, U) by $(\grave{u}, \grave{U})$, L_n by L_n^* and $(\grave{u}, \grave{U})$ by $(\grave{\grave{u}}, \grave{\grave{U}})$.

E. Secular perturbations and the computation of position and velocity

The equations of motion are now reduced to

$$
\frac{d\grave{\grave{U}}}{dt} = -\frac{\partial \mathcal{H}^{**}}{\partial \grave{\grave{u}}} = 0 \quad , \quad \frac{d\grave{\grave{u}}}{dt} = \frac{\partial \mathcal{H}^{**}}{d\grave{\grave{U}}} = c \tag{75}
$$

where c are arbitrary constants so that they admit the solution

$$
\grave{\grave{U}} = \grave{\grave{U}}_0 \quad , \quad \grave{\grave{u}} = \grave{\grave{u}}_0 + ct \tag{76}
$$

where the constants $(\grave{\grave{U}}_0, \grave{\grave{u}}_0)$ are to be determined from the initial conditions.

Let the elements (u_0, U_0) be known at a given initial epoch t_0 then we can obtain the constants $(\grave{\grave{U}}_0, \grave{\grave{u}}_0)$ as follows:
1- From the elements of the transformation we can compute the initial values $(\grave{U}_0, \grave{u}_0)$ from

$$
\grave{u}_0 = u_0 + \sum_{n=1}^{2} \frac{J_2^n}{n!} u_0^{(n)} \quad , \quad \grave{U}_0 = U_0 + \sum_{n=1}^{2} \frac{J_2^n}{n!} U_0^{(n)} \tag{77}
$$

2- From the corresponding equations for the elements of the long period transformations

$$
\grave{\grave{u}}_0 = \grave{u}_0 + \sum_{n=1}^{2} \frac{J_2^n}{n!} \grave{u}_0^{(n)} \quad , \quad \grave{\grave{U}}_0 = \grave{U}_0 + \sum_{n=1}^{2} \frac{J_2^n}{n!} \grave{U}_0^{(n)} \tag{78}
$$

Now having determined $\grave{\grave{u}}_0$ and $\grave{\grave{U}}_0$ we can evaluate $\mathcal{H}^{**} = \mathcal{H}^{**}(\grave{\grave{U}})$, and in turn the constants c are now known.
To compute the position and velocity at any time t we compute

$$
\grave{u} = \grave{\grave{u}} + \sum_{n=1}^{2} \frac{J_2^n}{n!} \grave{\grave{u}}^{(n)} \quad , \quad \grave{U} = \grave{\grave{U}} + \sum_{n=1}^{2} \frac{J_2^n}{n!} \grave{\grave{U}}^{(n)} \tag{79}
$$

then

$$
u = \grave{u} + \sum_{n=1}^{2} \frac{J_2^n}{n!} \grave{u}^{(n)} \quad , \quad U = \grave{U} + \sum_{n=1}^{2} \frac{J_2^n}{n!} \grave{U}^{(n)} \tag{80}
$$

Having determined (u, U) at time t, we compute the position, velocity, attitude and attitude motion of the spacecraft.

VI. Conclusion

In this paper we have obtained an analytical solution for the orbit-attitude motion of a charged spacecraft under the effect of Earth oblateness (J_2) and Lorentz force through Hamiltonian framework. The problem is tackled by means of Lie perturbation technique. Two successive canonical transformations were performed in order to eliminate the short and long period terms in succession. secular and periodic terms were retained up to $O(J_2^3)$ and $O(J_2^2)$ respectively.

Acknowledgments

This project was supported financially by the Science and Technology Development Fund (STDF), Egypt, Grant No 1834.

References

[1] Deprit, A. 1969: Celest. Mech. 1,12
[2] Dwidar,H.R. 2007,: "Analysis of the attitude motion of a satellite of an oblate earth". Ph.D. thesis, Cairo University
[3] Gurfil, P. et al. 2007: Regular and Chaotic Dynamics, 12,389
[4] Hughes, P.C. 1986:"Spacecraft attitude dynamics", John Wiley
[5] Kamel, A.A. 1969: Celest. Mech. 1,190
[6] Mohammed,Hani.M. 2012: "Attitude analysis of a rigid spacecraft". M.Sc. thesis, Cairo University
[7] Plummer, H.C. 1918 :" An introductory treatise on Dynamical Astronomy",Dover
[8] Tikhonov, A. A. 2002 : Cosmic Research. 40,171
[9] Tiknonov, A.A. and Petrov, K. G. 2002 : Cosmic Research. 40,219
[10] Tikhonov, A.A. 2003 : Cosmic Research. 41,69
[11] Zanardi, M.C. and De Moraes, R. V. 1999: Celest. Mech. 75,227

AUTOMATIC SKIN CANCER IMAGES CLASSIFICATION

Mahmoud Elgamal
Institute of Hajii and umra., Um Alqura Uni.
Saudii Arabia
Email: mahmoud_40@yahoo.com

***Abstract*—Early detection of skin cancer has the potential to reduce mortality and morbidity. This paper presents two hybrid techniques for the classification of the skin images to predict it if exists. The proposed hybrid techniques consists of three stages, namely, feature extraction, dimensionality reduction, and classification. In the first stage, we have obtained the features related with images using discrete wavelet transformation. In the second stage, the features of skin images have been reduced using principle component analysis to the more essential features. In the classification stage, two classifiers based on supervised machine learning have been developed. The first classifier based on feed forward back-propagation artificial neural network and the second classifier based on k-nearest neighbor. The classifiers have been used to classify subjects as normal or abnormal skin cancer images. A classification with a success of 95% and 97.5% has been obtained by the two proposed classifiers and respectively. This result shows that the proposed hybrid techniques are robust and effective.**

Keywords: Skin cancer images, wavelet transformation, principle component analysis, feed forward back-propagation network, k-nearest neighbor classification.

I. Introduction

Skin cancer is a major public health problem in the light-skinned population. Skin cancer is divided into *non melanoma skin cancer* (NMSC) and *melanoma skin cancer* (MSC) figure (1.1). Non melanoma skin cancer (MMSC) is the most prevalent cancer among light-skinned population. It is divided into basal cell carcinoma (BCC) (75%), squamous cell carcinoma (SCC) (24%), and other rare types (1%) such as sebaceous carcinoma[19]. The critical factor in assessment of patient prognosis in skin cancer is early diagnosis. More than 60,000 people in the United States were diagnosed with invasive melanoma in recent years, and more than 8000 Americans died of the disease. The single most promising strategy to cut acutely the mortality rate from melanoma is early detection. Attempts to improve the diagnostic accuracy of melanoma have spurred the development of innovative in-vivo imaging modalities, including total body photography, dermoscopy, automated diagnostic system and reflectance confocal microscopy. The use of computer technology in medical decision support is now widespread and pervasive across a wide range of medical area, such as cancer research, gastroenterology, hart diseases, brain tumors etc. [10], [12]. Recent work [19] has shown that skin cancer recognition from images is possible via supervised techniques such as artificial neural networks and fuzzy systems combined with feature extraction techniques. Other supervised classification techniques, such as k-nearest neighbors ($k-NN$) also group pixels based on their similarities in each feature image [5], [8], [9] can be used to classify the normal/abnormal images. Therefore image processing become our choice for an early detection of the skin cancer, as it is non-expensive technique. The identification of the edges of an object in an image scene is an important aspect of the human visual system because it provides information on the basic topology of the object from which an interpretative match can be achieved. In other words, the segmentation of an image into a complex of edges is a useful prerequisite for object identification. However, although many low-level processing methods can be applied for this purpose, the problem is to decide which object boundary each pixel in an image falls within and which high level constraints are necessary. In this paper, supervised machine learning techniques, i.e., Feedforawd-Backpropagation Neural Network($FP-ANN$) used as a classifier. Also unsupervised classification techniques such as $k-NN$used as a classify images into normal/abnormal as will be discussed in the subsequent sections. Wavelet transform is an effective tool for feature extraction, because they allow analysis of images at various levels of resolution. This technique requires large storage and is computationally more expensive [12]. In order to reduce the feature vector dimension obtained from wavelet transformation and increase the discriminative power, the principal component

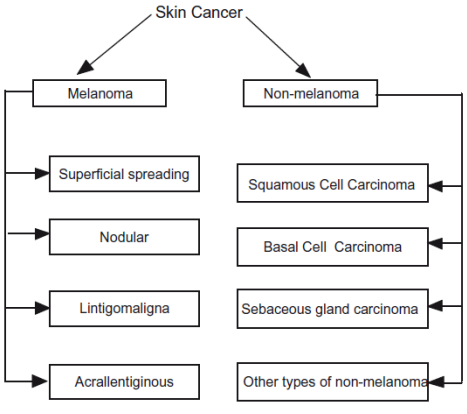

Fig. 1.1. Types of skin cancer.

analysis (PCA) has been used; PCA reduces the dimensionality of the data and therefore reduces the computational cost of analyzing new data.
This paper is organized as follows: a short description of the images preprocessing section (II), details of the proposed hybrid techniques sections (III) and (IV), section (V) contains simulation and results and finally the conclusion.

II. Skin Cancer Images Preprocessing

There are many types of the skin cancer, each type has a different color, size and features. Many skin features may have impact on digital images like hair and color, and other impacts such as lightness, and type of the scanner or digital camera. In the preprocessing step, the border detection procedure namely, color space transformation, contrast enhancement, and artifact removal, treated as follow [2]:

i) Color space transformation Dermoscopy images are commonly acquired using a digital camera with a dermoscope attachment. Due to the computational simplicity and convenience of scalar (single channel) processing, the resulting RGB (red-green-blue) color image is often converted to a scalar image using one of the following methods:
   - Retaining only the blue channel (lesions are often more prominent in this channel).
   - Applying the luminance transformation, i.e.

$$Luminance = 0.299 \times Red + 0.587 \times Green + 0.114 \times Blue.$$

   - Applying the *Karhunen-Love* (KL) transformation [18] and retaining the channel with the highest variance.

ii) Contrast enhancement Delgado et al. [6], proposed contrast enhancement method, based on *independent histogram pursuit* (IHP). This algorithm linearly transforms the original RGB image to a decorrelated color space in which the lesion and the background skin are maximally separated. Border detection is then performed on these contrast-enhanced images using a simple clustering algorithm.

iii) Artifact removal Dermoscopy images often contain artifacts such as such as black frames, ink markings, rulers, air bubbles, as well as intrinsic cutaneous features that can affect border detection such as blood vessels, hairs, and skin lines. These artifacts and extraneous elements complicate the border detection procedure, which results in loss of accuracy as well as an increase in computational time. The most straightforward way to remove these artifacts is to smooth the image using a general purpose filter such as the *Gaussian*(GF), *median*(MF), or *anisotropic diffusion filters*(ADF).

Images are processed to have the following starting features: same size, color segmentations to remove hair if any as discussed in the next subsection.

A. Segmentation

Segmentation refers to the partitioning of an image into disjoint regions that are homogeneous with respect to a chosen property such as luminance, color, texture, etc. ([3] and [20]). Segmentation methods can be roughly classified into the following categories:

- Histogram thresholding: These methods involve the determination of one or more histogram threshold values that separate the objects from the background.
- Clustering: These methods involve the partitioning of a color (feature) space into homogeneous regions using unsupervised clustering algorithms.
- Edge-based: These methods involve the detection of edges between the regions using edge operators.
- Region-based: These methods involve the grouping of pixels into homogeneous regions using region merging, region splitting, or both.
- Morphological: These methods involve the detection of object contours from predetermined seeds using the watershed transform.
- Model-based: These methods involve the modeling of images as random fields whose parameters are determined using various optimization procedures.
- Active contours (snakes and their variants): These methods involve the detection of object contours using curve evolution techniques.
- Soft computing: These methods involve the classification of pixels using soft-computing techniques including neural networks, fuzzy logic, and evolutionary computation. Figure (2.1) shows a segmentation of *Superficial Spreading Melanoma* (SSM) image.

III. The Proposed Hybrid Techniques

The proposed hybrid techniques based on the following techniques, discrete wavelet transforms DWT, the principle components analysis PCA, FP-ANN, and k-NN. It consists of the following phases: feature extraction, feature reduction, and classification phase as illustrated in Fig. (3.1).

(a) Original image.

(b) Filtered image.

(c) Black and white.

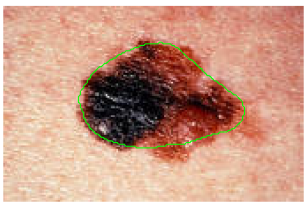

(d) Traced.

Fig. 2.1. Superficial spreading image segmentation.

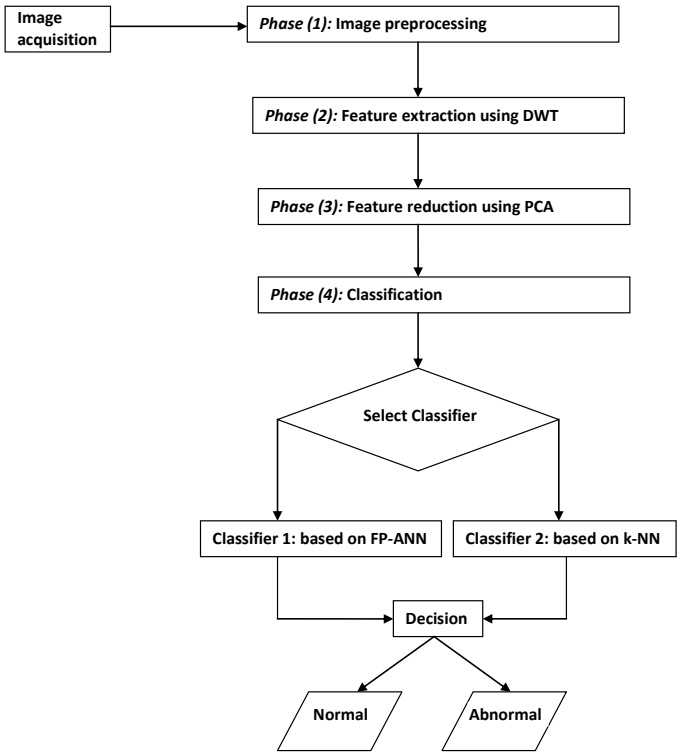

Fig. 3.1. Flow-diagram of the proposed technique.

A. DWT based feature extraction

The rationale of the approach proposed here implies two steps. In the first step, signals (tissue samples) are transformed into time-scale domain by DWT. In the second step features are extracted from the transformed data by a principle component analysis(PCA). The continuous wavelet transform of a signal $x(t)$ is defined as the sum over all time of the signal multiplied by wavelets $\psi_{ab}(t)$ (see Eq. (2)), the scaled (stretched or compressed) and shifted versions of the mother wavelet $\psi(t)$:

$$WT_x(a,b) = \frac{1}{\sqrt{a}} \int_{-\infty}^{\infty} x(t)\psi^*\Big(\frac{t-b}{a}\Big)dt, \qquad (1)$$

$$\psi_{a,b}(t) = \frac{1}{\sqrt{a}}\psi\Big(\frac{t-b}{a}\Big),\ a \in R^+,\ b \in R, \qquad (2)$$

where $\psi^*(.)$ represents the conjugated transpose of the wavelet function$\psi(.)$. The time-wavelet resolution depends on the scaling parameter a. For smaller c, $\psi_{ab}(t)$ has a narrow time-support and therefore a wider frequency support. When parameter a increases, the time support of $\psi_{ab}(t)$ increases as well and the frequency support becomes narrower. The translation parameter b determines the localization of $\psi_{ab}(t)$ in time. The DWT is defined taking discrete values of a and b. The full DWT for signal $x(t)$ can be represented as

$$x(t) = \sum_{k\in Z} \mu_{j_0,k}\phi_{j_0,k}(t) + \sum_{j=-\infty}^{j_0}\sum_{k\in Z} \omega_{j,k}\psi_{j,k}(t), \qquad (3)$$

where $\phi_{j_0,k}(t)$ and $\psi_{j,k}(t)$ are the flexing and parallel shift of the basic scaling function $\phi(t)$ and the mother wavelet function $\psi(t)$, and $\mu_{j_0,k}(j < j_0)$ and $\omega_{j,k}$ are the scaling coefficients and the wavelet coefficients, respectively. Generally, scales and positions are based on powers of 2, which is the dyadic DWT. Once a mother wavelet is selected, the wavelet transform can be used to decompose a signal according to scale, allowing separating the fine-scale behavior (detail) from the large-scale behavior (approximation) of the signal [1]. The relationship between scale and signal behavior is: low scale corresponding to compressed wavelet, and to rapidly changing details, namely high frequency; high scale corresponding to stretched wavelet, and to slowly changing coarse features, namely low frequency. Signal decomposition is typically done in an iterative fashion using the scales $a = 2, 4, 8, \cdots, 2^L$, with successive approx-

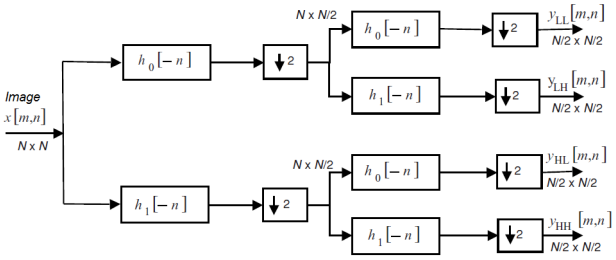

(a) forward 2D DWT.

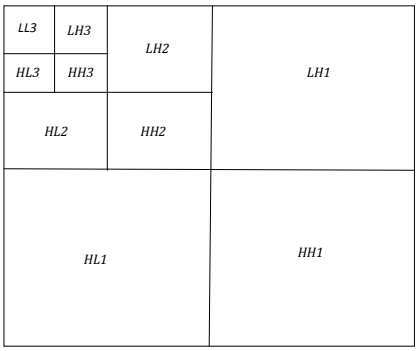

(b) approximation and detail coefficient placement.

Fig. 3.2. Computation of a three-level 2D DWT via subband coding scheme.

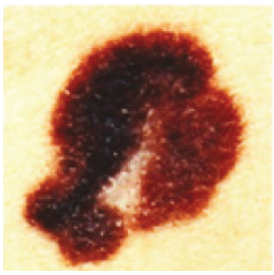

(a) Superficial spreading image.

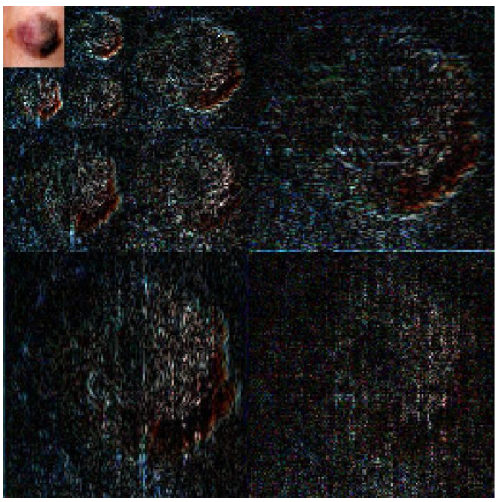

(b) DWT of the image.

Fig. 3.3. A three-level 2D DWT of the tissue image.

imations being split in turn, so that one signal is broken down into many lower resolution components. In practice, signal decomposition can be implemented in a computationally efficient manner via the fast wavelet transform developed by Mallat [15], behind which the basic idea is to represent the wavelet basis as a set of high-pass and low-pass filters in a filter bank, as shown in figure (3.2). Figure (3.3) shows the three-level DWT of SSM image. The first level consists of LL, HL, LH, and HH coefficients. The HL coefficients correspond to high-pass in the horizontal direction and low-pass in the vertical direction. Thus, the HL coefficients follow horizontal edges more than vertical edges. The LH coefficients follow vertical edges because they correspond to high-pass in the vertical direction and low-pass in the horizontal direction. As a result, there are 4 sub-band (LL, LH, HH, HL) images at each scale. The sub-band LL is used for the next 2D DWT. The LL subband can be regarded as the approximation component of the image, while the LH, HL, and HH subbands can be regarded as the detailed components of the image. As the level of the decomposition increased, we obtained more compact yet coarser approximation components. Thus, wavelets provide a simple hierarchical framework for interpreting the image information. In our algorithm, level-3 decomposition via Haar wavelet was utilized to extract features.

B. PCA based feature reduction

The Principal Component Analysis (PCA) is one of the most successful techniques that have been used in image recognition and compression. The purpose of PCA is to reduce the large dimensionality of the data space (observed variables) to the smaller intrinsic dimensionality of feature space (independent variables), which are needed to describe the data economically. This is the case when there is a strong correlation between observed variables. The jobs which PCA can do are prediction, redundancy removal, feature extraction, data compression, etc. Because PCA is a classical technique which can do something in the linear domain, applications having linear models are suitable, such as signal processing, image processing, system and control theory, communications, etc. Given a set of data, PCA finds the linear lower-dimensional representation of the data such that the variance of the reconstructed data is preserved ([13] and [14]). Using a system of feature reduction based on a combined PCA on the feature vectors that calculated from the wavelets limiting the feature vectors to the component selected by the PCA should lead to an efficient classification algorithm utilizing supervised approach. So, the main idea behind using PCA in our approach is to reduce the dimensionality of the wavelet coefficients. This leads to more efficient and accurate classifier. In figure(3.4) given below an outline of PCA-algorithm.

Input: Data set(matrix) $X_{m\times n}$, ($m \equiv$ # parameters and $n \equiv$ # samples).
Output: $Y = PX$, $P \equiv$ transformation matrix from X to Y; basis for X, s.t.,
the covariance matrix in this base is diagonalized.

Step 1: Calculate the covariance matrix in the new basis $C_y = \frac{1}{n-1}PAP^T$,
$A = XX^T$; A is symmetric.
Step 2: Diagonalize the cov. matrix, i.e., $A = EDE^T$.
Step 3: Find the eigenvalues and eigenvectors from the previous step;
$A = EDE^T$, where
D = diagonal matrix contains the eigenvalues of A,
E = matrix contains the eigenvectors of A.
Step 4: Dimension reduction:
- rearrange the eigenvectors and eigenvalues, i.e., sort the columns of the eigenvector matrix E and eigenvalue matrix D in order of decreasing eigenvalue.
- select a subset of the eigenvectors with higher values as basis vectors, project the data onto the new basis; of lower dimensions.

Fig. 3.4. PCA algorithm.

Therefore, the feature extraction process was carried out through two steps: firstly the wavelet coefficients were extracted by the DWT and then the essential coefficients have been selected by the PCA (see Fig. 3.5).

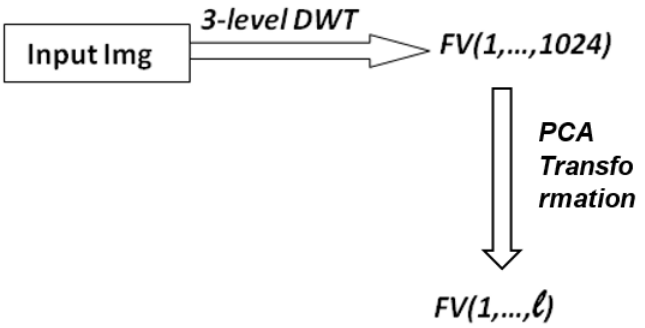

Fig. 3.5. Feature extraction of image using DWT and reduction using PCA(ℓ is new feature vector dimension).

IV. Supervised Learning Classification

Supervised machine learning is the search for algorithms that reason from externally supplied instances to produce general hypotheses, which then make predictions about future instances. In other words, the goal of supervised learning is to build a concise model of the distribution of class labels in terms of predictor features. The resulting classifier is then used to assign class labels to the testing instances where the values of the predictor features are known, but the value of the class label is unknown. In this paper two supervised learning algorithms are employed for classification, the first is *k-Nearest neighbors* and *Artificial neural network*, a details of both will be given below.

A. k-Nearest neighbors(k–NN):

One of the most straightforward instance-based learning algorithms is the nearest neighbor algorithm. *k–NN* is based on the principle that the instances within a dataset will generally exist in close proximity to other instances that have similar properties [4]. If the instances are tagged with a classification label, then the value of the label of an unclassified instance can be determined by observing the class of its nearest neighbors. The $k-NN$ locates the k nearest instances to the query instance and determines its class by identifying the single most frequent class label. Figure (4.1) shows a description of the algorithm. The training phase for $k-NN$ consists of simply storing all known instances and their class labels. A tabular representation can be used, or a specialized structure such as a kd-tree. If we want to tune the value of k and/or perform feature selection, n-fold cross-validation can be used on the training dataset. The testing phase for a new instance t, given a known set I is as follows:

1) Compute the distance between t and each instance in I.
2) Sort the distances in increasing numerical order and pick the first k elements.
3) Compute and return the most frequent class in the k nearest neighbors, optionally weighting each instance's class by the inverse of its distance to t.

Fig. 4.1. *k–NN* algorithm.

B. Artificial Neural Network (ANN):

An artificial neural network (ANN), usually called neural network (NN), is a mathematical model or computational model that is inspired by the structure and/or functional aspects of biological neural networks. A neural network consists of an interconnected group of artificial neurons, and it processes information using a connectionist approach to computation. In most cases an ANN is an adaptive system that changes its structure based on external or internal information that flows through the network during the learning phase [21]. The feed-forward neural network was the first and arguably simplest type of artificial neural network devised. In this network, the

information moves in only one direction, forward, from the input nodes, through the hidden nodes (if any) and to the output nodes figure(4.2). There are no cycles or loops in the network. The neural network which was employed as the

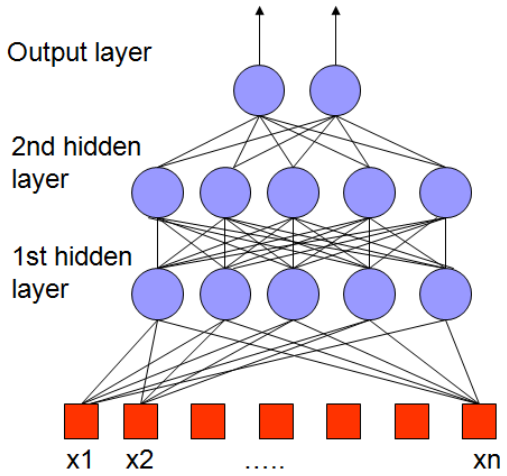

Fig. 4.2. Feed forward neural network.

classifier required in this study had three layers, as shown in figure (4.2). The first layer consists of eight input elements in accordance with the size of the feature vectors that selected from the wavelet coefficients by the PCA. The number of neurons in the hidden layer was five. The single neuron in the output layer was used to represent normal and abnormal tissue image (see Fig. 4.2). The most frequently used training algorithm in classification problems is the back-propagation (BP) algorithm, which is used in this paper too. The details of back-propagation (BP) algorithm are well documented in the literature [7]. The neural network has been trained to adjust the connection weights and biases in order to produce the desired mapping. At the training stage, the feature vectors are applied as input to the network and the network adjusts its variable parameters, the weights and biases, to capture the relationship between the input patterns and outputs [7]. The performance is measured by mean square error(MSE):

$$MSE = \frac{1}{n}\sum^{m}(y_t - y_o)^2, \tag{4}$$

here y_t is the target value, y_o is the actual output, and m is the number of training data, figure(4.3) shows ANN Back-propagation algorithm.

Initialize the weights in the network (often randomly).
Do For each example e in the training set:

a) O = neural-net-output(network, e) ; forward pass,
b) T = teacher output for e,
c) Calculate error $(T - O)$ at the output units,
d) Compute δ_{wh} for all weights from hidden layer to output layer ; backward pass,
e) Compute δ_{wi} for all weights from input layer to hidden layer ; backward pass continued,
f) Update the weights in the network.

Until all examples classified correctly or stopping criterion satisfied.
Return the network.

Fig. 4.3. ANN Back-propagation algorithm.

V. Simulation:

In this section the proposed hybrid techniques are used for the classification of malignant melanoma. The data set consists of total 40 images (20 normal and 20 abnormal) images downloaded from [11]. Figure (5.1) shows some samples from the used data. The proposed approach was implemented in Matlab 7.12[16], on a PC with the following configurations, processor 2GHz; 2 GB of ram; run under MSWin. 7 operating system. Figure (6.3) shows GUI of the implementation. The images resized to smaller size of pixels 8×8, Haar wavelet with the third level used, and the feature vector reduced to just eight components. With those settings, the hybrid classifiers; FP-ANN and KNN were run and an instance of the output shown in Fig. (6.3).

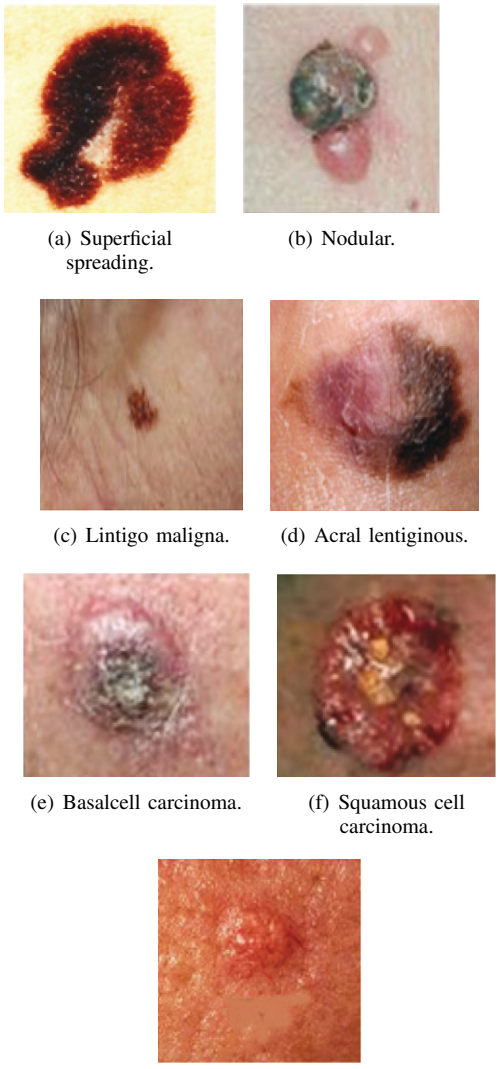

(a) Superficial spreading. (b) Nodular.

(c) Lintigo maligna. (d) Acral lentiginous.

(e) Basalcell carcinoma. (f) Squamous cell carcinoma.

(g) Sebaceous gland carcinoma.

Fig. 5.1. Samples of skin cancer.

A. Performance Evaluation

In this section, the performance of the proposed techniques are evaluated for the skin cancer images. The proposed techniques performance evaluated in terms of confusion matrix, sensitivity, specificity, and accuracy. The three terms defined as follow [17]:

a) Sensitivity(true positive fraction): the result indicates positively(disease).

$$Sen. = \frac{TP}{(TP + FN)}$$

b) Specificity(true negative fraction): the result indicates negatively(non-disease).

$$Spec. = \frac{TN}{(TN + FP)}$$

c) Accuracy: the probability that the diagnostic test is performed correctly.

$$Accur. = \frac{(TP + TN)}{(TP + TN + FP + FN)}.$$

Where,
TP (True Positives) ≡ Correctly classified positive cases,
TN (True Negative)≡ Correctly classified negative cases,
FP (False Positives) -Incorrectly classified negative cases, and
FN (False Negative)≡ Incorrectly classified positive cases.

Prop. Tech.	*TP*	*TN*	*FP*	*FN*	*Sen.(%)*	*Spec.(%)*	*Accur.(%)*
ANN	19	19	1	1	95	95	95
K-NN	20	19	1	0	100	95	97.5

Fig. 5.2. Performance of the used techniques.

VI. Conclusion

In this paper, an automated medical decision support system for skin cancer developed with normal and abnormal classes. First the discrete wavelet transformation were applied on the images to get the feature vectors, as the dimensionality of the vectors quite large, one needed to reduce it through the principle component analysis. The resulting feature vectors have a few components; means, less time and memory requirements. Afterwards, those vectors were used for classification either with feed-forward neural network or k-nearest neighbor algorithm. The results of the deployed techniques were promising as, we got 100% for sensitivity, 95% for specificity , and 97.5% for accuracy.

References

[1] L.M. Bruce, C.H. Koger, and J. Li, *Dimensionality reduction of hyperspectral data using discrete wavelet transform feature extraction*, IEEE Trans. Geosci. Remote Sensing 40 (10) (2002) 10.

[2] M. E. Celebi, H. Iyatomi, G. Schaefer, and W. V. Stoecker, *Lesion Border Detection in Dermoscopy Images*, Computerized Medical Imaging and Graphics 33 (2009).

[3] M. E Celebi, H. A. Kingravi, and H.Iyatomi, *Border detection in dermoscopy images using statistical region merging*, Skin Research and Technology, 2008;14(3):34753.

[4] T. Cover, P. Hart, *Nearest neighbor pattern classification*, IEEE Transactions on Information Theory, 1967; 13(1): 217.

[5] I. Daubechies, *Ten Lectures on Wavelets*, Regional Conference Series in Applied Mathematics, SIAM, Philadelphia, 1992.

[6] D. Delgado, C. Butakoff, BK. Ersboll, and WV. Stoecker,*Independent histogram pursuit for segmentation of skin lesions*, IEEE Trans on Biomedical Engineering 2008;55(1):15761.

[7] Jerome Feldman, *Neural Networks - A Systematic Introduction*, Springer-Verlag, Berlin, New-York, 1996.

[8] P.S.Hiremath, S. Shivashankar, and J. Pujari,Wavelet Based Features for Color Texture Classification with Application to CBIR, IJCSNS International Journal of Computer Science and Network Security, 6 (2006), pp. 124- 133.

[9] K. Karibasappa, S. Patnaik, *Face Recognition by ANN using Wavelet Transform Coefficients*, IE(I) Journal-CP, 85,(2004), pp. 17-23.

[10] F. Gorunescu, *Data Mining Techniques in Computer-Aided Diagnosis: Non-Invasive Cancer Detection*, PWASET Volume 25 November 2007 ISSN 1307-6884, PP. 427-430.

[11] Is it skin cancer? 38 photos that could save your life, *http://www.cbsnews.com/2300-204_162-10006772.html*.
[12] S. Kara, F. Dirgenali, *A system to diagnose atherosclerosis via wavelet transforms, principal component analysis and artificial neural networks*, Expert Systems with Applications 32 (2007), pp. 632-640.
[13] M. Kocionek, A. Materka, M. Strzelecki, and P. Szczypinski, *Discrete wavelet transform derived features for digital image texture analysis*, Proc. of Interational Conference on Signals and Electronic Systems, 18-21 September 2001, Lodz, Poland, pp. 163-168.
[14] F. Latifoglu, K. Polat, S. Kara, and S. Gunes, it Medical diagnosis of atherosclerosis from Carotid Artery Doppler Signals using principal component analysis (PCA), k-NN based weighting pre-processing and Artificial Immune Recognition System (AIRS), Journal of Biomedical Informatics 41 (2008), pp. 15-23.
[15] S.G. Mallat, *A theory for multiresolution signal decomposition: the wavelet representation*,IEEE Pattern Anal. Machine Intell. 11 (7) (1989) 674693.
[16] MatLab, *http://www.mathworks.com/*.
[17] K. Polat, B. Akdemir, S. Gnes, *Computer aided diagnosis of ECG data on the least square support vector machine*, Digital Signal Processing 18 (2008), pp. 25-32.
[18] Pratt WK. ,*Digital image processing: PIKS inside.*, Hoboken, NJ: John Wiley & Sons; 2007.
[19] B. Salah, M. Alshraideh, R. Beidas and F. Hayajneh, *Skin Cancer Recognition by Using a Neuro-Fuzzy System*, Cancer Informatics, 2011.
[20] M Sonka, V Hlavac, and R. Boyle, *Image processing, analysis, and machine vision*, Cengage-Engineering 2007.
[21] *http://en.wikipedia.org/wiki/Artificial_Neural_Network*, Wikipedia 2012.

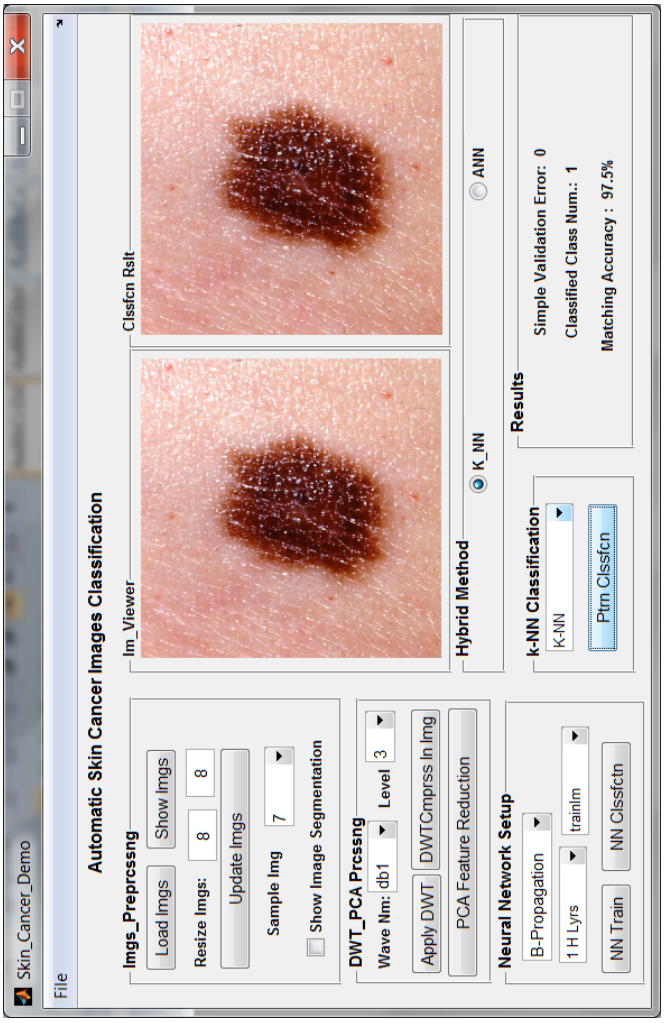

Fig. 6.3. GUI of the proposed techniques.